

# **Shape-Selective Catalysis**





# Shape-Selective Catalysis

## Chemicals Synthesis and Hydrocarbon Processing

**Chunshan Song**, EDITOR  
*Pennsylvania State University*

**Juan M. Garcés**, EDITOR  
*Dow Chemical Company*

**Yoshihiro Sugi**, EDITOR  
*Gifu University*



**American Chemical Society**  
American Chemical Society, Washington, DC  
**Library**

**1155 16th St., N.W.**

**Washington, D.C. 20036**

In Shape-Selective Catalysis, S. C. Colonna, Ed., ACS Symposium Series; American Chemical Society: Washington, DC, 1999.

**Shape-selective catalysis :  
chemicals synthesis and**



**Library of Congress Cataloging-in-Publication Data**

Shape-selective catalysis : chemicals synthesis and hydrocarbon processing / Cunshan Song, Juan M. Garcés, Yoshihiro Sugi, editors.

p. cm—(ACS symposium series : 738. ISSN: 0097-6156)

Includes bibliographical references and index.

ISBN 0-8412-3619-4

1. Catalysis Congresses.
2. Zeolites Congresses.
3. Organic compounds—Synthesis Congresses.
4. Petroleum—Refining Congresses. I. Song, Chunshan. II. Garcés, Juan M. III. Sugi, Yoshihiro. IV. Series.

TP156.C35S47 1999  
660'.2995-dc21

99-32010  
CIP

The paper used in this publication meets the minimum requirements of American National Standard for Information Sciences—Permanence of Paper for Printer Library Materials, ANSI Z39.48-94 1984.

Copyright © 2000 American Chemical Society

Distributed by Oxford University Press

All Rights Reserved. Reprographic copying beyond that permitted by Sections 107 or 108 of the U.S. Copyright Act is allowed for internal use only, provided that a per-chapter fee of \$20.00 plus \$0.50 per page is paid to the Copyright Clearance Center, Inc., 222 Rosewood Drive, Danvers, MA 01923, USA. Republication or reproduction for sale of pages in this book is permitted only under license from ACS. Direct these and other permissions requests to ACS Copyright Office, Publications Division, 1155 16th Street, N.W., Washington, DC 20036.

The citation of trade names and/or names of manufacturers in this publication is not to be construed as an endorsement or as approval by ACS of the commercial products or services referenced herein; nor should the mere reference herein to any drawing, specification, chemical process, or other data be regarded as a license or as a conveyance of any right or permission to the holder, reader, or any other person or corporation, to manufacture, reproduce, use, or sell any patented invention or copyrighted work that may in any way be related thereto. Registered names, trademarks, etc., used in this publication, even without specific indication thereof, are not to be considered unprotected by law.

PRINTED IN THE UNITED STATES OF AMERICA

**American Chemical Society  
Library**

**1155 16th St., N.W.**

In Shape-Selective Catalysis: Song, C. et al.;

ACS Symposium Series; American Chemical Society: Washington, DC, 1999.

# Advisory Board

## ACS Symposium Series

**Mary E. Castellion**  
ChemEdit Company

**Arthur B. Ellis**  
University of Wisconsin at Madison

**Jeffrey S. Gaffney**  
Argonne National Laboratory

**Gunda I. Georg**  
University of Kansas

**Lawrence P. Klemann**  
Nabisco Foods Group

**Richard N. Loeppky**  
University of Missouri

**Cynthia A. Maryanoff**  
R. W. Johnson Pharmaceutical  
Research Institute

**Roger A. Minear**  
University of Illinois  
at Urbana-Champaign

**Omkaram Nalamasu**  
AT&T Bell Laboratories

**Kinam Park**  
Purdue University

**Katherine R. Porter**  
Duke University

**Douglas A. Smith**  
The DAS Group, Inc.

**Martin R. Tant**  
Eastman Chemical Co.

**Michael D. Taylor**  
Parke-Davis Pharmaceutical  
Research

**Leroy B. Townsend**  
University of Michigan

**William C. Walker**  
DuPont Company

# Foreword

**T**HE ACS SYMPOSIUM SERIES was first published in 1974 to provide a mechanism for publishing symposia quickly in book form. The purpose of the series is to publish timely, comprehensive books developed from ACS sponsored symposia based on current scientific research. Occasionally, books are developed from symposia sponsored by other organizations when the topic is of keen interest to the chemistry audience.

Before agreeing to publish a book, the proposed table of contents is reviewed for appropriate and comprehensive coverage and for interest to the audience. Some papers may be excluded in order to better focus the book; others may be added to provide comprehensiveness. When appropriate, overview or introductory chapters are added. Drafts of chapters are peer-reviewed prior to final acceptance or rejection, and manuscripts are prepared in camera-ready format.

As a rule, only original research papers and original review papers are included in the volumes. Verbatim reproductions of previously published papers are not accepted.

ACS BOOKS DEPARTMENT

# Preface

Shape-selective catalysis is important for synthesis of organic chemicals and for processing of hydrocarbons and fuels. The pioneering study on shape-selective catalysis was first reported in 1960 by Paul Weisz and co-workers at Mobil. Since then shape-selective catalysis has rapidly evolved into an area of active research and development worldwide. Great strides have been made both in fundamental research and practical application in the shape-selective catalytic materials and chemical reaction processes in the past 40 years.

As we move into the 21st century shape-selective catalysis will continue to occupy an important position in catalytic research and development. Because of the need to develop new environmentally-benign catalytic reaction processes and to improve existing catalytic processes, shape-selective catalysis will continue to be applied, and further diversify into various branches of chemicals synthesis and hydrocarbon processing. To foster the research and development in this area, we organized a symposium on Shape Selective Catalysis in Hydrocarbon Processing and Chemicals Synthesis as a part of the 215th American Chemical Society (ACS) National Meeting in Dallas, Texas, March 29–April 2, 1998. This symposium was sponsored by the ACS Division of Petroleum Chemistry, Inc. This book was developed based on the ACS symposium. It is composed of peer-reviewed chapters from both contributing authors and invited authors.

This book is unusual in the area of shape-selective catalysis in that world-renowned pioneers (Paul B. Weisz, Nai Y. Chen, Paul B. Venuto, and Clarence D. Chang) provide accounts on both historical developments including the original discoveries and the current state of the art as well as insights into future research and development. The contributors of the chapters are active researchers and leaders in this area in the United States, Japan, China, India, and France. The review and original research articles covered a wide variety of topics including (1) introductory account and general overviews, (2) catalysis of organic reactions, (3) methanol conversion to gasoline and olefins, (4) paraffin cyclization and aromatization, (5) conversion of monocyclic hydrocarbons, (6) conversion of polycyclic hydrocarbons, and (7) new concepts and new catalytic materials.

Shape-selective catalysis is a closer analogue of enzymatic catalysis. A good fraction of the activity in shape-selective catalysis deals with the chemistry of acid catalysis for hydrocarbon conversion such as in Friedel–Crafts type reactions. Of course this is an important step that provides a pathway to the creation of new generations of catalysts that will incorporate shape selectivity and specific functionality. Recent research on ship-in-a-bottle (e.g., catalytically active metal complex inside the cage of molecular sieves) chemistry is perhaps a good example of such catalysts. Any book has a limit in coverage, but shape-selective catalysis is not limited to the reactions or applications that are discussed in the book. Shape-selective catalysis could lead to novel types of catalysts or processes that we can only imagine at this time, or applications that we have not thought about so far.

It is our hope that this book will serve as an important reference in the area of shape-selective catalysis for chemicals synthesis and hydrocarbon processing. The

structure and the contents of the book are such that it will be useful not only to scientists and engineers involved in related research and development, but also to researchers and graduate students who are new to this area. The chapters in this book should serve to activate the minds of current and future generations of chemists and engineers to expand the application of shape-selective catalysis.

We thank all the authors who contributed to the ACS symposium and to the ACS book, and all the peer reviewers whose helpful comments and suggestions on the individual chapters were important for improving the overall quality of the book. We are grateful to the invited authors and the pioneers in this area, whose review or original research articles greatly enhanced the depth and comprehensiveness of this book. We wish to acknowledge the sponsorship of ACS Division of Petroleum Chemistry, Inc. and the support from the division program, preprints, and executive committee members. We would also like to thank the general support to us for carrying out this project by the Pennsylvania State University, Dow Chemical Company, and Gifu University, and the skillful editorial assistance and support of Anne Wilson and her staff in the ACS Books Department.

CHUNSHAN SONG

Applied Catalysis in Energy Laboratory  
Department of Energy and Geo-Environmental Engineering  
Pennsylvania State University  
University Park, PA 16802

JUAN M. GARCÉS

Catalysis Laboratory  
Corporate Research and Development  
1776 Building  
Dow Chemical Company  
Midland, MI 48674

YOSHIHIRO SUGI

Department of Chemistry  
Faculty of Engineering  
Gifu University  
Yanagido, Gifu 501-11  
Japan

## Chapter 1

# Introduction to Shape-Selective Catalysis

Chunshan Song<sup>1,4</sup>, Juan M. Garcés<sup>2</sup>, and Yoshihiro Sugi<sup>3</sup>

<sup>1</sup> Applied Catalysis in Energy Laboratory, and Department of Energy and Geo-Environmental Engineering, Pennsylvania State University, 209 Academic Projects Building, University Park, PA 16802

<sup>2</sup> Corporate Research and Development, Catalysis Laboratory, 1776 Building, Dow Chemical Company, Midland, MI 48674

<sup>3</sup> Department of Chemistry, Faculty of Engineering, Gifu University, Yanagido, Gifu 501-11, Japan

Shape-selective catalysis is important for synthesis of organic chemicals and for processing of petroleum fractions and fuels. This article provides an introductory overview of the principles and applications of shape selective catalysis. It also discusses current areas of research on shape-selective catalysis.

According to a recent study conducted jointly by several professional societies and industrial associations summarized in "Technology Vision 2020" report, catalysis is used in making over 60% of the products and accounts for 90% of the manufacturing process in the U.S. chemical industry that generates 7,000 different products (1,2). Governmental studies also indicated that catalytic technologies contributed some 20-30% to gross domestic product in both the U.K. and the U.S. (3). This includes not only chemical industry but also other manufacturing sectors such as petroleum refining industry for making clean transportation fuels, and automobile industry where catalysts are used for control of emissions from exhaust gases.

Heterogeneous catalysis plays an important role in hydrocarbon processing, chemicals synthesis, and environmental protection. In 1992 over \$1.48 billion worth of catalysts were used in the U.S. chemical and petroleum industries; these catalysts resulted in the production of over \$890 billion worth of products, roughly equivalent to 18% of US GNP (4). For example, a single pound of catalyst can easily process 1,200-2000 pounds of gasoline. In 1993, U.S. catalyst sales market was \$1.93 billion, with a breakdown including chemicals (\$650 million), petroleum, (\$665 million), automotive (\$570 million), and other industrial catalysts (\$50 million) (4). In keeping with the above-mentioned "Technology Vision 2020" report, two major goals for catalysis in the next twenty-five years are accelerating new catalyst development and raising catalyst selectivity approaching 100% (5).

Shape-selective catalysis occupies a unique position in manufacturing industries for environmentally benign chemical processing, because it provides specific, desired pathways leading to desired products in hydrocarbon processing and chemicals

<sup>4</sup> Corresponding author. E-mail: [csong@psu.edu](mailto:csong@psu.edu); Fax: 814-865-3248; Telephone: 814-863-4466

synthesis. Paul B. Weisz and coworkers at Mobil discovered shape-selective catalysts about 40 years ago and published the first paper on shape selective catalysis in 1960 (6). Since then, shape-selective catalysis has stimulated great interest in many industrial and academic research laboratories in the world. Several reviews have been published on zeolite catalysis related to shape selectivity (7-15).

Here we provide an introductory review on shape-selective catalysis over molecular sieves. It starts with a discussion of basic concepts for those who need to understand the fundamental principles, then moves to the current areas of research interests, followed by a brief introduction to the technical contents and highlights of this book. One of us (CS) has been involved in teaching graduate and undergraduate courses on "Catalytic Materials" and on "Industrial Organic Chemistry" at the Pennsylvania State University. The students have expressed concerns for the lack of published information suitable for students on fundamental principles of shape-selective catalysis. Consequently, in this review the fundamental thermodynamics and kinetics for shape-selective catalysis are discussed, so that new researchers in this area and graduate students in chemical sciences can better understand and appreciate shape-selective catalysis. Historical developments, industrial applications, and current areas of research and developments are briefly mentioned below, and these subjects are covered broadly in this book by pioneers and active researchers.

## Principles of Shape-Selective Catalysis

**Thermodynamics and Kinetics.** All chemical reactions are subject to thermodynamic limitations such as equilibrium composition. For a simple reaction expressed by Eq. 1, when thermodynamics predicts that the reaction is favorable under certain conditions (i.e.,  $\Delta G < 0$ ) under given conditions of temperature and pressure, then the maximum yield of products C and D is determined by the thermodynamic equilibrium constant K (Eqs. 2-4).

What would happen if we now place a catalyst into the same reaction system under the same operation conditions? Textbooks (16,17) describe a catalyst as "a substance that increases the rate of approach to equilibrium of a chemical reaction without being consumed in the reaction", or "a substance that does not disturb the equilibrium composition of the reaction system, only the rate at which the equilibrium is attained". The statement implies that the catalyst can only speed up the reaction rate without changing the equilibrium composition.



$$K = [P_C P_D] / [P_A P_B] \quad 2)$$

$$\Delta G^\circ = \Delta H^\circ - T \Delta S^\circ \quad 3)$$

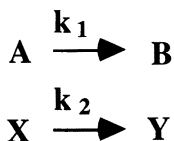
$$\Delta G^\circ = - RT \ln K \quad 4)$$

However, for a reaction expressed by Eq. 1, shape-selective catalysis can often lead to a product mix that differs from the equilibrium predicted composition. For example, the yield of a given product (e.g., C in Eq. 1) may be higher than that predicted by the equilibrium composition. Why is this possible? Heterogeneous catalysis begins with adsorption on the catalyst surface. As pointed out by Bond (16), the standard statements about equilibrium quoted above are valid only if the catalytic and noncatalytic reactions are truly the same, and yield identical products. Catalytic reactions are as much subject to the laws of thermodynamics as are noncatalytic reactions. However, it is rather difficult to find truly comparable pairs of catalytic and

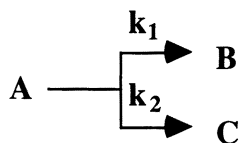


noncatalytic reactions that yield the same products in hydrocarbon processing and chemicals synthesis. The catalytic reactions inside the pore channel of a shape-selective catalyst can be substantially different from those that occur in homogeneous catalytic or noncatalytic reactions involving the same reactants.

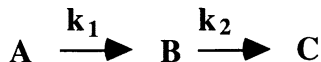
**General Types of Selectivity in Heterogeneous Catalysis.** Shape-selective catalysis belongs to the family of heterogeneous catalysis. Heterogeneous catalytic reactions generally involve three types of selectivity. Type I selectivity refers to that occurring when two reactions are taking place simultaneously (18). The selectivity may be defined as  $S = k_1/k_2$ . Examples of this type include the hydrogenation of benzene and toluene that are present as aromatics in naphtha or gasoline. When type I selectivity is involved, the more active the catalyst, the greater the effect that mass transport has on the reaction selectivity. The more rapid reaction will be influenced more by mass transport limitations. Conducting the reaction under those conditions in which mass transport is the limiting factor will lower the apparent selectivity of the catalyst. The same effect will be noted if the active sites on the catalyst is increased.



Type II selectivity involves the differentiation between two parallel reactions in which different products are formed by separate paths from the same starting material (18). Here the selectivity may be defined as  $S = \text{Yield of B}/\text{Conversion of A}$ . When both reactions are first order reactions,  $S = k_1/(k_1 + k_2)$ . An example is the hydrogenation of 1-methylnaphthalene to form either 1,2,3,4-tetrahydro-1-methylnaphthalene or 5,6,7,8-tetrahydro-1-methyl-naphthalene. Another example is the hydrogenation of crotonaldehyde  $\text{CH}_3\text{-CH=CH-CHO}$  to either butyraldehyde  $\text{CH}_3\text{-CH}_2\text{-CH}_2\text{-CHO}$  or crotonalcohol (2-buten-1-ol)  $\text{CH}_3\text{-CH=CH-CH}_2\text{-OH}$ . When both reactions are of the same kinetic order changes in mass transport will influence them both to the same extent and there will be no effect on reaction selectivity. When the reactions are of different kinetic orders, that one with the higher order will be more affected by mass transport limitation.



Type III selectivity is that found with serial reactions (18). Examples include the benzene hydrogenation to cyclohexene and then to cyclohexane; the hydrogenation of naphthalene first to tetrahydronaphthalene and then to decalin, and the hydrogenation of an  $\text{C}_2$  acetylene first to ethylene and then to ethane. When type III selectivity is involved, the transport of the organic substrate through the liquid/solid interface can have a significant impact on the reaction selectivity. For partial oxidation of ethylene into ethylene oxide over solid catalyst, type III selectivity is very important, because the further oxidation to  $\text{CO}_2$  is an easy reaction. In such a case, designing and making use of a catalyst having the active species present primarily on the particle surface (egg shell type, not microporous) could improve the selectivity to ethylene oxide (17).



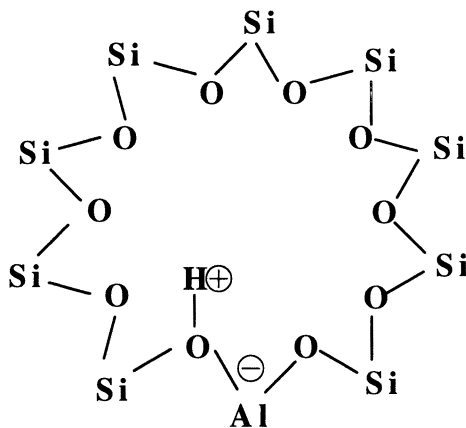
Two different types of reactions may be involved in Type III selectivity. For example, naphthalene can be alkylated over acidic catalysts with an alcohol or an olefin to form mainly 1-alkylnaphthalene, because 1-position is more reactive (kinetic control). However, once it has been produced, 1-alkylnaphthalene can isomerize into 2-alkylnaphthalene because the latter is more stable (thermodynamic control). It should be mentioned that type I and type II selectivity may also involve two or more competing reactions of different types.

**Definition of Shape-Selective Catalysis.** How do we define shape-selective catalysis? We will attempt to give a definition here. Shape-selective catalysis is the molecular-sieving function in action during a catalytic reaction that distinguishes between the reactant, the product or the transition state species in terms of the relative sizes of the molecules and the pore space where the reaction occurs. What is so special about shape-selective catalysis? It is different in principle from that in most other heterogeneous catalytic reactions where the selectivity originate mainly from the interactions between the catalyst surface and reacting molecules or intermediate species. Shape-selective catalysis involves the use of a special class of solid catalytic materials called molecular sieves, which impose space restrictions on the reactions based on the shape of reactants, products or transition states, in addition to the surface interactions that are common to all heterogeneous catalytic reactions on solid materials.

Table 1 lists some typical molecular sieves that have well-defined pore channels whose sizes are in the range of organic chemicals (8, 19-23). The most widely used molecular sieves for catalytic applications are zeolites which are crystalline aluminosilicates. Figure 1 gives a schematic presentation of a zeolite pore (with 10 tetrahedral atoms in a ring) with a Bronsted acid (proton), which is the catalytically

**Table 1.** Some Representative Molecular Sieves and Their Pore Dimensions

Structure Type	No of T Atoms	Pore Size	Pore Shape
Zeolite A	8	4.1 Å	Circular
Erionite	8	3.6 x 5.1 Å	Elliptical
Ferrierite	10	4.2 x 5.4 Å	Elliptical
ZSM-5	10	5.3 x 5.6 Å	Elliptical
ZSM-12	12	5.5 x 5.9 Å	Elliptical
Mordenite	12	6.7 x 7.0 Å	Elliptical
Faujasite (X, Y)	12	7.4 Å	Circular
Beta	12	7.6 x 6.4 Å	Elliptical
Linde L	12	7.1 Å	Circular
VPI-5	18	12.1 Å	Circular
MCM-41	> 18	15-100 Å	Circular



**Figure 1.** A schematic presentation of the zeolite pore and the Bronsted acid site in hydrogen zeolite with 10 tetrahedral atom in a ring.

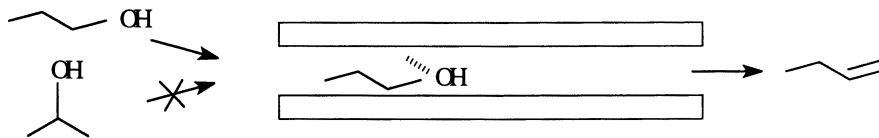
active site for acid-catalyzed reactions such as aromatics alkylation with olefins. Replacing one tetrahedral Si (+4 in its oxidation state) in the silicate framework with one Al (+3 in its oxidation state) creates one negative charge which must be balanced by a positive charge that is usually an alkali metal cation such as sodium. The subsequent ion-exchange with  $\text{NH}_4$  or protonic acid followed by thermal treatment can give proton-form zeolite illustrated in Figure 1. Partial substitution of tetrahedral Si or Al species in molecular sieve framework by other atoms (such as Ga, Fe, etc.) can form metallosilicates, which have also found some important catalytic applications in the past decade.

## Type of Shape Selectivity

There are three basic types of shape-selectivity, as described below, in which the first two of them are related to mass transfer limitations and the third concerns spatial limitation of transition state. The discussion below also briefly describes the characteristics of different types of shape selectivity and their dependence on diffusional characteristics of hydrocarbon species and the catalyst morphologies (crystal size, and particle size, etc.) as appropriate. Shape-selective reactions often involve configurational diffusion, a concept first proposed by Weisz (24), which occurs where the structural dimensions of catalyst pore channels approach those of molecules. More detailed descriptions and propositions for other types of shape-selectivity such as half-cavity model and molecular traffic control are given in a monograph by Chen and coworkers (12).

**Reactant Shape Selectivity.** There are often competitive reactions when the reactants include more than one type of molecules. Reactant selectivity is defined as the selective conversion of certain reactant molecules when there are other types of molecules in the feedstock but whose size is larger than the pore opening can allow, as illustrated in Figure 2. In this context, this type of selectivity depends on intra-pore diffusional characteristics of reacting molecules.

The simplest form of reactant selectivity is observed when some of the reactant molecules are excluded from the catalyst particles because they are too large to enter the pores, or when the relative diffusion rates of given reactants differ by orders of magnitude. In fact, the so-called reactant selectivity is the first recognized type of the shape-selective catalysis in the pioneering work by Weisz and his coworkers at Mobil (6). Classic examples of reactant selectivity are the selective dehydration of alcohols on CaA and CaX zeolites, and the selective cracking of linear and branched paraffins on CaA zeolite. Mixtures of primary and secondary butanol result in selective dehydration of n-butanol over CaA and non-selective dehydration over CaX that has a larger pore size than CaA (6). In mixtures of n-hexane and 3-methylpentane, n-hexane is preferentially cracked because 3-methylpentane is too bulky to enter the pores of CaA. An example involving 12MR zeolite is the hydrogenation of cyclohexene and cyclodecene over rhodium supported on carbon support and on Y zeolite support (18). In the former case, both reactions occur significantly. However, in the latter case, cyclohexene hydrogenation is dominant. In addition to zeolite and other metallosilicate molecular sieves, carbon molecular sieves have also been explored for shape-selective reactions. In 1971 Walker and his coworker (25) reported the selective hydrogenation of certain olefins among the mixture of olefinic reactants over platinum supported on carbon molecular sieve prepared by a unique method.



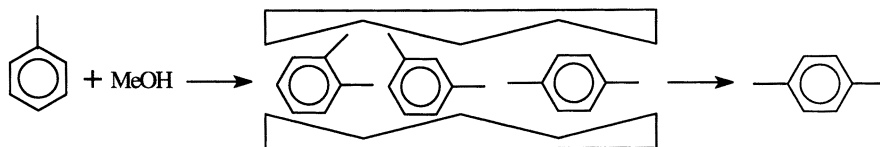
**Figure 2.** Reactant shape selectivity in the alcohol dehydration reactions.

The above-mentioned Type I selectivity corresponds to the reactant shape selectivity when shape-selective catalytic materials are involved. In practice, the reactant selectivity may be observed when the diffusion rate of one type of reacting molecules is substantially faster than that of the other type of molecules present in the reactant mixture. The diffusion of molecules into the pore channel also depends on the temperature for two reasons. First, the molecules may become more flexible at higher temperatures, since the molecular bending and stretching motions need energy. Second, the pore mouth of zeolites and other molecular sieves may have breathing motions which lead to pore diameters larger than those determined by crystallographic calculations or estimated based on adsorption measurements at room temperature. In fact, there are experimental evidence showing that some molecules can not diffuse into ZSM-5 at room temperature but become able to do so at elevated temperatures (26).

**Product Shape Selectivity.** Different products may originate from the same reactants in catalytic reactions, such as paraffin isomerization. Product shape selectivity refers to the selective formation of certain products when there are other potential products whose formation is also thermodynamically feasible but is limited because of their limited diffusion out of pore. Selective formation of certain products occurs when they are the small-sized molecules that can readily diffuse out of the pore channel and appear as the main observed products, as shown in Figure 3.

The methylation of toluene with methanol and isomerization of xylenes on ZSM-5 catalysts result in the preferential formation of *p*-xylene. Among the 3 xylene isomers, *p*-xylene is not thermodynamically favored, but its formation is favored

because the diffusivity of p-xylene is several orders of magnitude larger than those of m-xylene and o-xylene, as demonstrated by Chen and coworkers (27, 28).

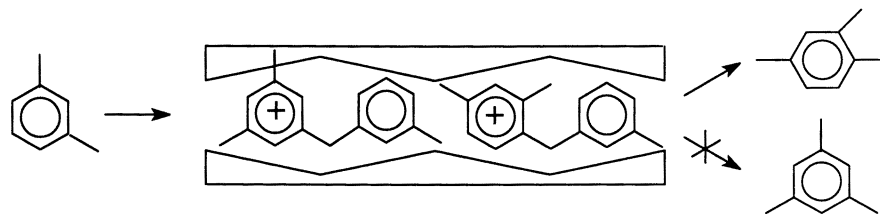


**Figure 3.** Product shape selectivity in toluene methylation reactions.

The product shape selectivity corresponds to the above-mentioned Type II selectivity in heterogeneous reactions. Designing a suitable catalytic material that can make use of the differences in diffusivity of the products could enhance the selectivity. For example, increasing the diffusion path length by increasing the crystallite size of ZSM-5 crystals can significantly increase the product selectivity (28, 29), as observed in the p-xylene selectivity from m-xylene isomerization or from toluene methylation. Alternatively, slightly reducing the size of the pore channel in zeolite structure could also increase the product selectivity, as observed for selectivity of p-xylene from xylenes by Kumar and Ratanasamy who noted increasing selectivity with switching zeolite structure from ZSM-5 to ZSM-48 to ZSM-22 and ZSM-23 (30).

For reactions over microporous molecular sieves, reactant and product molecules must diffuse in and out of the pore in a regime called configurational diffusion, where a very small changes in the relative size between pore channel diameter and molecular diameter can induce large differences in the diffusion coefficients, as shown by Weisz (7, 24). Product shape selectivity appears when there is a large difference in diffusion coefficients between two or more types of product molecules in a pore channel whose size is very close to those of the molecules. In other words, certain product molecules can be formed readily inside the pore, but their out-of-pore diffusion is very slow; thus the product molecules that can diffuse out of pore rapidly appear in higher percentage in bulk.

**Transition-State Shape Selectivity.** Homogeneous chemical reactions go through a transition state whose configuration is affected mainly by the nature of reacting molecules in the absence of external restrictions. However, when the reactions occur inside a confined micropore or channel within catalysts, the geometry of the pore around the active sites can impose steric restriction on the transition state. This is illustrated in Figure 4.

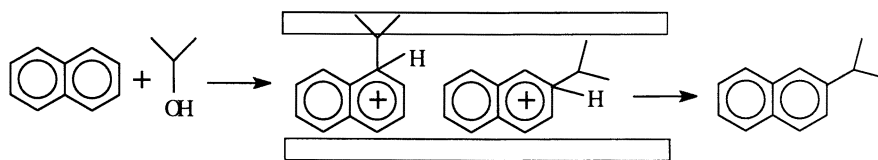


**Figure 4.** Transition-state shape selectivity in m-xylene disproportionation (transmethylation) reactions.

The acid-catalyzed disproportionation (or transalkylation) of dialkylbenzenes typically produces mono- and trialkylbenzenes over silica-alumina or large pore zeolites such as HY. At equilibrium the symmetrical 1,3,5-trialkylbenzenes are the main products, as is the case with HY. However, H-mordenite prevents the formation of the 1,3,5-trialkylbenzenes because the diphenylmethane-like transition state that leads to 1,3,5-isomer does not fit within the 12-ring channels of H-mordenite (31). Thus spatially restricted transition-state selectivity proposed by Csicsery (9, 31) occurs when certain (kinetically feasible) reactions are prevented because the corresponding transition state requires more space than is available. In such cases, the reactions requiring smaller sizes of transition states proceed unimpaired; and neither reactant nor potential product species are prevented from diffusing through the pores. For *m*-xylene disproportionation, 1,2,4-trimethylbenzene is formed but the formation of 1,3,5-trimethylbenzene is inhibited within the pore channel of H-mordenite (32). It should be mentioned that the positions of alkyl groups in the transition-state species that leads to 1,2,4-trimethylbenzene in Figure 4 are different from those for the transition-state species in the reviews by Csicsery (9).

How can we distinguish the transition-state selectivity from product selectivity? If the reaction products are governed by transition state selectivity, then the catalyst particle size or crystallite size does not affect the selectivity to any significant extent. However, the so-called product selectivity would be strongly influenced by the crystal size.

It should be mentioned that two types of selectivity may be involved simultaneously in some reaction systems. Shape-selective alkylation of naphthalene, as illustrated for isopropylation in Figure 5, may present an example of control of the reaction pathway by both the transition-state selectivity and the product selectivity in some large- and medium-pore zeolites (33, 34). The relative contribution of the two also depends on the size of the alkyl groups and the dimension of the pore channel. For example, formation of 1-isopropyl naphthalene (1-IPN) is dominant when HY zeolite is used. However, in the case of H-mordenite, formation of 2-isopropyl naphthalene becomes predominant. Formation of 1-alkylnaphthalene may be restricted in its transition state by the space availability. Even after 1-alkylnaphthalene is formed in low yields, its diffusion out of pore can be much slower than the 2-alkylnaphthalene because of its larger critical diameter (34).



**Figure 5.**  $\beta$ -selective naphthalene alkylation reactions may involve both transition-state shape selectivity and product shape selectivity, depending on alkyl group and catalyst pore dimension.

Restricted electronic transition-state selectivity was proposed recently by Song et al. (34) and refers to the two spatially feasible shape-selective reactions but one of the two is favored electronically. In the case of alkylation of 2-alkylnaphthalene, both 2,6- and 2,7-dialkylnaphthalene can be formed in similar yields inside the so-called  $\beta$ -shape-selective catalytic channel of certain zeolites, but only one of the two isomers is the desired product. It was found that dealumination of mordenite facilitates the

selective formation of 2,6-diisopropylanaphthalene (35). The quantum chemical calculation suggests that 2,6-isomer is favored electronically (34), and the “ $\beta$ -selective” catalysts with lower acidity favor 2,6-isomer against 2,7-isomer (35). The term restricted electronic transition-state selectivity was used to highlight the importance of electronic factor for selective PAH conversion and to distinguish it from the well-known spatial transition state selectivity.

**Other Types of Shape Selectivity.** There are other types of selectivity which are discussed in the book by Chen and coworkers (12). While most shape-selective reactions give more linear or more slim products, there are cases where bulkier products are formed. Hydrocracking of n-hexadecane results in more 2,3-dimethylbutane and less n-hexane over Pd-HSSZ-24 than over Pd-HZSM-5 or Pd-HY. This so-called inverse shape selectivity over the SSZ-24 zeolite and other zeolites with pores in the range of 7-8 angstroms favors the formation of the bulkier molecule, as reported by Zones and coworkers at Chevron (36). This is related to the reduced space limitation in zeolites with relatively large micropores. More bulkier products can be favored if they are not restricted by space limitation. The so-called secondary shape-selectivity has also been discussed by Khouw and Davis (13), which refers to the change in selectivity in reaction of a specific reactant (A) by the presence of a co-reactant (B), which can inhibit the adsorption of A, or affect the diffusion of A, thus affecting the shape selectivity of zeolite catalysts. It appears that secondary shape selectivity is related to competitive sorption or competitive diffusion of the various molecules in the pore channels of molecular sieves.

## Applications of Shape-Selective Catalysis

The main applications of shape selective catalysis are found in chemicals synthesis and hydrocarbon processing. The successful development of synthetic aluminosilicate molecular sieves at Union Carbide and at Mobil, most notably the synthesis of ZSM-5 type (ZSM stands for zeolite of SOCONY Mobil) high-silica zeolites and their unique catalytic properties, stimulated the dramatic growth in shape-selective catalytic applications of zeolites and other metasilicate molecular sieves (7-15, 26-32, 37-40). The current areas of shape-selective catalytic applications of molecular sieves include hydrocarbon processing and the synthesis of organic chemicals. Recent studies are covered by the reviews and original contributions throughout this book. Only a brief account is given below to illustrate the usefulness of shape-selective catalysis. In addition, the monograph published by Chen and coworkers (12) discusses industrial applications of shape-selective catalysis up to 1995. It should be noted that shape-selective catalysis is not limited to the use of molecular sieves alone. In fact, there are many applications that involve transition metal species that are supported inside or “synthesized (ship-in-bottle)” inside the cages or pores channels of molecular sieves that can be used for catalyzing many selective reactions such as hydrocracking, hydroisomerization, hydrogenation, and oxidation reactions.

**Chemicals Synthesis.** Shape-selective reactions for synthesis of organic chemicals using molecular sieve-based catalysts include alkylation, isomerization, disproportionation, transalkylation, oxidation, hydrogenation, ring-shift isomerization, conformational isomerization, and chlorination. Table 2 shows some examples of shape-selective processes for synthesis of organic chemicals that have been either commercialized or reported in open literature. Synthesis of chemicals over molecular sieves has attracted attention worldwide and explored by many research groups for making commodity chemicals such as isobutene and p-xylene, and specialty chemicals such as 2,6-dialkylanaphthalene.

**Table 2.** Some Selective Catalytic Processes for Synthesis of Organic Chemicals

Reaction Type	Typical Process	Principal Product	Catalyst & Process Status
Alkylation	Benzene Ethylation	Ethylbenzene	ZSM-5 Commercialized
Alkylation	Benzene Isopropylation	Cumene, p-Diisopropylbenzene	Mordenite Commercialized
Alkylation	Toluene methylation	p-Xylene	ZSM-5 Laboratory
Alkylation	Toluene Ethylation	p-Ethyltoluene	ZSM-5 Commercialized
Alkylation	Benzene polymethylation	1,2,4,5-tetramethylbenzene	Various, Laboratory
Alkylation	Ethylbenzene ethylation	p-Diethylbenzene	ZSM-5, Commercialized
Alkylation	Naphthalene isopropylation	2,6-Diisopropyl naphthalene	Mordenite, Laboratory
Alkylation	Naphthalene methylation	2,6-Dimethyl naphthalene	MFI type, Laboratory
Alkylation	Biphenyl isopropylation	4,4'-Diisopropylbiphenyl	Mordenite, Laboratory
Isomerization	Xylene isomerization	p-Xylene	MFI type, Commercialized
Isomerization	Sym-Octa-hydrophenanthrene	Sym-Octahydroanthracene	Mordenite, Y Laboratory
Isomerization	Cis-Decalin isomerization	Trans-decalin	Pd/HM, Pd/HY Laboratory
Disproportionation	Toluene disproportionation	p-Xylene	Coked ZSM-5 Commercialized
Transalkylation	Toluene and trimethylbenzene	Xylene	Various, Laboratory
Acylation	Toluene acylation	p-Oriented products	Acidic zeolites Laboratory
Benzoylation	Naphthalene benzoylation	2-Benzoylnaphthalene	Acidic zeolite Laboratory
MTO	Methanol conversion	Olefins	Me-SAPO Research
Oxidation	Phenol oxidation	Catechol, hydroquinone	TS-1 Commercialized
Oxidation	Benzene oxidation by N <sub>2</sub> O	Phenol	Modified MFI type Commercialized
Hydrogenation	Naphthalene hydrogenation	Cis-Decalin or trans-decalin	Pt/Y, Pd/M Laboratory
Dehydrocyclization	Lower Paraffins	Aromatics	Ga-MFI Commercialized,
Dehydrocyclization	Naphtha conversion	Gasoline and gas oil	Modified ZSM-5 Laboratory
Cyclodimerization	1,3-Butadiene cyclodimerization	Vinylcyclohexene	Cu-Y, Laboratory
Chlorination	Toluene chlorination	p-Chlorotoluene	Various zeolites, Laboratory
Chlorination	chlorination of substituted aromatics	p-Oriented Chloroaromatics	Various zeolites, Laboratory



Amongst the processes for hydrocarbon-based chemicals, the large-volume chemicals are currently derived from aromatic alkylation, isomerization and disproportionation over shape-selective catalysts. The conversion of light hydrocarbons to aromatics and paraffin isomerization over molecular sieve catalysts are receiving increasing attention in terms of both fundamental understanding and practical applications. Two general trends of research are to explore new reactions or new catalytic materials, and to develop new or improved processes using molecular sieve catalysts that replace existing processes using corrosive acids or generating wasteful byproducts.

A detailed, comprehensive review on organic zeolite catalysis has been published by Venuto (8). Specific organic synthesis reactions using zeolite catalysts have also been discussed by Holderich and coworkers (38), and more recently by Corma and Garcia (39a) and by Waal and van Bekkum (39b). Selective oxidations for chemicals synthesis over molecular-sieve catalysts have been reviewed by Notari (40a) for phenol oxidation to catechol and by Panov coworkers (40b) for direct benzene oxidation to phenol. Recently more research groups began to explore conversion of polycyclic hydrocarbons using zeolite catalysts as reviewed by Sugi and Kubota (41) and by Song (42). There are also some recent reports on shape-selective chlorination of aromatics such as toluene (43) and benzylation of naphthalene (44) over zeolites for making chemicals.

**Hydrocarbon Processing.** The principle driver for hydrocarbon processing is the conversion and refining of petroleum fractions into high-quality fuels and non-fuel products. Hydrocarbon processing involves fuel applications for making transportation fuels (gasoline, etc.), and refining specific feedstocks to meet fuel specifications, and non-fuel applications such as distillate processing for making lube oils. Specific reviews on hydrocarbon processing using zeolites have been published by Maxwell and coworkers (3, 45, 46). In terms of volume, the main application for zeolite catalysts in the refinery is fluidized catalytic cracking (FCC) using acidic molecular sieves such as USY with added ZSM-5 in some cases. Table 3 gives some examples of shape-selective processes for hydrocarbon processing over molecular sieve-based catalysts.

**Table 3.** Some Selective Catalytic Processes in Hydrocarbon Processing

Feedstock	Typical Process,	Principal reactants	Catalysts, Status
Lube Oil	Lube Dewaxing	n-paraffins	Small-pore Mol. sieves Commercialized
Distillate Oils	Hydrocracking	n-paraffins	Small-pore Mol. sieves Commercialized
Gas oil	Hydrocracking	n-Paraffins	Small-pore Mol. sieves Commercialized
Paraffins isomerization	Total isomerization	C5-C6 Paraffins	Small-pore Mol. sieves Commercialized
Paraffin-rich feed	Isomerization Hydroisomerization	n-paraffins	Small-pore Mol. sieves Commercialized
Methanol	Methanol to gasoline	methanol	ZSM-5 Commercialized
Paraffin-rich feed	Alkylation	paraffins	Acidic molecular sieves Laboratory research
Gasoline	Alkylation	Benzene in gasoline	Acidic molecular sieves Research

For shape-selective hydrocarbon processing, of great importance in refining are hydrocracking, hydroisomerization, cracking, dewaxing and paraffin isomerization which also use zeolites as catalyst components. For hydroprocessing applications transition metals are often supported on the molecular sieves. Paraffin alkylation over zeolite catalysts can also have potential application but the active and stable zeolite catalysts remain to be established. It appears that the reactant shape-selectivity has been widely used and continue to be applied for improving existing processes and for developing new processes for petroleum processing such as paraffin isomerization, paraffin hydrocracking, and conversion of methanol, lower olefins and lower alkanes.

**Separations.** Related to shape-selective processing is shape-selective separation by selective adsorption on molecular sieves. Separations based on zeolites or other molecular sieves share some common features of shape-selective processing with the above mentioned chemical processes. Since chemical processing often involves separation of product mixtures, molecular sieves have begun to play a role as shape-selective adsorbent (47). For example, some molecular sieves can be used as selective adsorbent for separation of p-xylene from its mixture with o- and m-xylene.

### Highlights of This Book:

At the American Chemical Society Symposium on Shape-Selective Catalysis held at ACS National Meeting in Dallas during March 29-April 2, 1998, 26 papers were accepted for presentation. This book contains the peer-reviewed manuscripts developed from the ACS symposium as well as the refereed manuscripts from invited contributors who did not attend the ACS symposium. This book consists of 27 chapters; the authors include not only active researchers worldwide, but also several well-known pioneers who laid the foundation of shape-selective catalysis in the 1960s and 1970s.

Paul B. Weisz, who first discovered shape-selective catalysts based on zeolites in the late 1950s, presents a historical overview of the emergence of shape-selective catalysis and the basic science and technology (Chapter 2). He published the first paper together with Friette in 1960 (6) and he may be called the father of shape-selective catalysis. The current status and recent advances of industrial applications of shape-selective catalysis are discussed in a comprehensive review by Nai Y. Chen (Chapter 3), a pioneer who made numerous original contributions and inventions and who published the first monograph on shape-selective catalysis with his colleagues (now in its second edition) (12).

The catalysis of organic reactions is reviewed by Paul B. Venuto (Chapter 4), who pioneered the shape-selective alkylation of benzene and alkylbenzenes over zeolites and published the first review on organic zeolite catalysis in 1968 (8b) and an updated comprehensive review in 1994 (8a). New development on regioselective cyclization over TS-1 molecular sieve is reported by Tatsumi and his coworker (Chapter 5). The catalytic properties of new octahedral molecular sieves for oxidation of alkanes are reported by Suib and coworkers (Chapter 6). Related to the topics in these chapters are recent reviews by Corma and Garcia (39a) and by Waal and van Bekkum (39b).

A mechanistic review on selective methanol conversion to hydrocarbons is provided by Clarence D. Chang (Chapter 7), who is a pioneer on conversion of methanol to gasoline (MTG) and a chief inventor of Mobil's MTG process. MTG is now well-known as one of the most important C-1 chemical processes for making alternate fuels and chemicals, since methanol can be produced from synthesis gas ( $\text{CO} + \text{H}_2$ ) that can be derived from coal, natural gas and biomass, and none of them depends on petroleum. The methanol to olefin research and the new development on selective methanol-to-ethylene conversion are reviewed by Tomoyuki Inui who has

made many important contributions to methanol conversion studies and recently found highly selective catalysts for ethylene from methanol (Chapter 8).

Cyclization and aromatization are among the most important processes for converting lower alkanes or for making high-octane gasoline. Alkane dehydrocyclization is an important reaction in catalytic reforming processes. Prasada Rao and coworkers presents a detailed report on the role of shape selectivity in n-heptane dehydrocyclization and aromatization reaction on modified ZSM-5 (Chapter 9). Davis and coworkers reports on shape selectivity for alkane dehydrocyclization with Pt-silicalite catalysts (Chapter 10).

Selective conversion of monocyclic aromatic hydrocarbons has been one of the main areas of shape-selective catalysis research for organic chemicals. Yashima and coworkers provide a selective review on MFI-type metallosilicates as useful tools to clarify what determines the shape selectivity of ZSM-5 zeolites for aromatics conversion (Chapter 11). Niwa and coworkers presents a case study on the para-selectivity and discuss the contributions of molecular diffusion and external-surface acidity (Chapter 12). Ramaswamy and coworkers reports on the importance of passivating external surface of ZSM-5 by silylation for para-selectivity in alkylation and isomerization (Chapter 13). Xie and coworkers illustrates the effectiveness of metal oxide dispersion on ZSM-5 for obtaining high para-selectivity in toluene methylation (Chapter 14). Wang and coworkers describe the performance of chemically modified HZSM-5 zeolites for shape-selective synthesis of para-diethylbenzene which led to commercialization (Chapter 15). Tian and coworkers reports on the interaction of P with HY zeolite and its influence on catalytic transformation of alkylbenzene (Chapter 16).

Significant advance has been made recently in the selective conversion of polycyclic hydrocarbons. Earlier publication on selective alkylation of naphthalene by Fraenkel and coworkers in 1986 (48) and on selective biphenyl alkylation by Lee, Garces and their coworkers in 1989 (49) were beneficial to the subsequent development. This subject has not been covered in previous monographs in this area. Some recent progress in selective catalytic conversion of polycyclic hydrocarbons over zeolite catalysts is briefly reviewed by Song (Chapter 17). Sugi and coworkers reports on the selective alkylation of biphenyl covering the influence of reagent bulkiness (Chapter 18) and the analysis of the encapsulated products inside mordenite pore channel (Chapter 19). Kikuchi and coworkers report on selective synthesis of 2,6-diisopropylnaphthalene by alkylation over modified mordenite catalysts (Chapter 20). Toba and coworkers discuss the catalytic performance of solid acids for isopropylation of naphthalene (Chapter 21). A computational analysis on shape-selective alkylation of naphthalene with MOPAC for the synthesis of 2,6-dialkylnaphthalene is presented by Song and coworkers (Chapter 22). Some shape-selective applications of Y zeolite have been reported in literature (50-53), and in this book Chen reports on the crystallinity of USY zeolites during hydrothermal dealumination (Chapter 23).

Recent development in new concepts and new catalytic materials is also reflected in this book. Guisnet and coworkers present a proposed new concept called tunnel shape selectivity to account for the shape selectivity they observed on monodimensional molecular sieves such as mesoporous MCM-41 (Chapter 24). Wang and coworkers discuss the shape-selective solid acid catalysts based on tungstophosphoric acid supported on mesoporous silica (Chapter 25). Okuhara and coworkers report on shape-selective catalytic behavior of platinum supported on porous heteropoly compounds in skeletal isomerization of n-butane (Chapter 26). Finally, Song proposes a new concept for design of sulfur-resistant noble metal catalysts based on shape-selective exclusion, hydrogen spillover and two types of sulfur resistance (Chapter 27).

## Concluding Remarks

The research and development on shape-selective catalysis have contributed greatly to hydrocarbon processing and chemicals synthesis in industry. This research area will continue to expand and diversify, even after 40 years since the pioneering study by Weisz and coworkers. It is expected that the basic principles and intrinsic advantages of shape-selective catalysis with molecular sieves will continue to stimulate further research to improve existing processes and to develop new applications in chemicals synthesis, hydrocarbon processing, separations, as well as in other sectors of broadly-defined manufacturing industries.

## Acknowledgments

One of the authors (CS) would like to thank Dr. Paul B. Weisz, Dr. Werner O. Haag, Dr. Nai Y. Chen, Dr. Ian E. Maxwell and Prof. Philip L. Walker Jr. for their encouragements and helpful discussions. He also wishes to acknowledge his colleagues and graduate students at the Pennsylvania State University whose comments and suggestions made this review more readable to young researchers who are new to the area of shape-selective catalysis.

## References

1. Special Report. Technology Vision 2020: The U.S. Chemical Industry. Washington D.C., **1996**, Prepared by American Chemical Society (ACS), American Institute of Chemical Engineers (AIChE), Chemical Manufacturers Association (CMA), Council for Chemical Research (CCR), and Synthetic Organic Chemical Manufacturers Association (SOCMA), 91 pp.
2. Office of Technology Policy, U.S. Department of Commerce. *Chemtech*, **1996**, 26, 46.
3. Maxwell, I. E. *CATTECH*, **1997**, 1, 5.
4. Armor, J. N. *Appl. Catal. A.*, **1996**, 139, 217.
5. News. *Ind. Catal. News*, **1998**, 1, 3.
6. (a) Weisz, P. B.; Frilette, V.J. *J. Phys. Chem.*, **1960**, 64, 382; (b) Weisz, P. B.; Frilette, V.J.; Maatman, R. W.; Mower, E. B. *J. Catal.*, **1962**, 1, 307; (c) Chen, N. Y.; Weisz, P. B. *Chem. Eng. Progr. Symp. Ser.*, **1967**, 73, 86.
7. Weisz, P. B. *Pure & Appl. Chem.*, **1980**, 52, 2091.
8. (a) Venuto, P. B. *Micropor. Mater.*, **1994**, 2, 297; (b) Venuto, P. B.; Landis, P. S. *Adv. Catal.*, **1968**, 18, 259.
9. (a) Csicsery, S. M. *Pure & Appl. Chem.*, **1986**, 58, 841; (b) Csicsery, S. M. *Chem. Brit.*, **1985**, 473; (c) Csicsery, S.M. *Stud. Surf. Sci. Catal.*, **1995**, 94, 1.
10. (a) Chen, N. Y.; Garwood, W. E. *Catal. Rev. – Sci. Eng.*, **1986**, 28, 185; (b) Dwyer, F. G. *Stud. Surf. Sci. Catal.*, **1991**, 67, 179.
11. (a) Haag, W. O. *Stud. Surf. Sci. Catal.*, **1994**, 84, 1375; (b) Olson, D.; Haag, W. O. *Am. Chem. Soc. Sym. Ser.*, **1984**, 248, 275.
12. Chen, N. Y.; Garwood, W. E.; Dwyer, F. G. *Shape-Selective Catalysis in Industrial Applications*. 2nd Edition, Marcel Dekker, New York, **1996**, 282 pp.
13. (a) Davis, M. E. *Acc. Chem. Res.*, **1993**, 26, 111; (b) Khouw, C. B.; Davis, M. E. *Am. Chem. Soc. Sym. Ser.*, **1993**, 517, 206.
14. (a) Suib, S. L. *Am. Chem. Soc. Sym. Ser.*, **1993**, 517, 1; (b) Suib, S. L. *Chem. Rev.*, **1993**, 93, 803.
15. Weitkamp, J.; Weiß, U.; Ernst, S. *Stud. Surf. Sci. Catal.*, **1995**, 94, 363.

16. Bond, G. C. *Heterogeneous Catalysis, Principles and Applications*. 2nd ed., Clarendon Press, New York, 1987, 176 pp.
17. Gates, B. C. *Catalytic Chemistry*. Wiley, New York, 1992, 458 pp.
18. (a) Augustine, R. L. *Heterogeneous Catalysis for the Synthetic Chemist*. Marcel Dekker, New York, 1996, Chpater 5, p.93; (b) Wheeler, A. *Adv. Catal.*, **1951**, 3, 249.
19. Breck, D. W. *Zeolite Molecular Sieves: Structure, Chemistry, and Use*. Wiley, New York, 1974, 771 pp.
20. van Bekkum, H.; Flanigen, E. M.; Jansen, J.C. *Introduction to Zeolite Science and Practice*. Elsevier, Amsterdam; 1991, 754 pp.
21. Bartholmeuf, D.; Derouane, E. G.; Hoelderich, W. *Guidelines for Mastering the Properties of Molecular Sieves*. Plenum Press, New York, 1990, 426 pp.
22. Bhatia, S. *Zeolite Catalysis: Principles and Applications*, CRC Press, Boca Raton, 1990, 291 pp.
23. Kresge, C. T.; Leonowicz, W. J.; Roth, W. J.; Vartuli, J. C.; Beck, J. S. *Nature*, **1992**, 359, 710.
24. (a) Weisz, P. B. *Chemtech*, **1973**, 3, 498; (b) Weisz, P.B. *Ind. Eng. Chem. Res.* **1995**, 34, 2692.
25. (a) Schmitt, J.L.; Walker, P. L. Jr. *Carbon*, **1971**, 9, 791; (b) Schmitt, J.L.; Walker, P. L. Jr. *Carbon*, **1971**, 10, 87.
26. Haag, W. O. personal communication. July 1998.
27. Chen, N. Y.; Garwood, W. E. *J. Catal.*, **1978**, 52, 453.
28. Chen, N. Y.; Kaeding, W.W.; Dwyer, F. G. *J. Am. Chem. Soc.*, **1979**, 101, 6783.
29. (a) Ratanasamy, P.; Rabu, G. P.; Chandwadkar, J.; Kulkarni, S. B. *Zeolites*, **1986**, 6, 98; (b) Beschmann, K.; Rieker, L.; Muller, U. *J. Catal.*, **1994**, 145, 243; (c)
30. Kumar, R.; Ratanasamy, P. *J. Catal.*, **1989**, 118, 68.
31. (a) Csicsery, S.M. *J. Org. Chem.*, **1969**, 34, 3338; (b) Csicsery, S.M. *J. Catal.*, **1970**, 19, 394; (c) Csicsery, S.M. *J. Catal.*, **1971**, 23, 124.
32. Weitkamp, J.; Nernst, S. *Catal. Today*, **1994**, 19, 107.
33. Song, C.; Kirby, S. *Micropor. Mater.*, **1994**, 2, 467.
34. (a) Song, C.; Ma, X.; Schmitz, A. D.; Schobert, H. H. *Appl. Catal. A: General*, **1999**, in press; (b) Song, C.; Ma, X.; Schobert, H. H. *Am. Chem. Soc. Sym. Ser.*, **1999**, in press.
35. (a) Song, C.; Schmitz, A. D.; Reddy, K. M. *Proc. 12<sup>th</sup> Int. Zeolite Conf., July 1998*, Baltimore, U.S., Vol. 2, p.1133; (b) Schmitz, A. D.; Song, C. *Catal. Today*, **1996**, 31, 19; (c) Schmitz, A. D.; Song, C. *Catal. Lett.*, **1996**, 40, 59.
36. Santilli, D. S.; Harris, T. V.; Zones, S. I. *Micropor. Mater.*, **1993**, 1, 329.
37. (a) Sachtler, W. M. H. *Acc. Chem. Res.*, **1993**, 26, 383; (b) Sachtler, W. M. H.; Zhang, Z. *Adv. Catal.*, **1993**, 39, 129; (c) Thomas, J. M.; Thomas, W. J. *Principles and Practice of Heterogeneous Catalysis*. VCH, Weinheim, Germany, 1997, p.608; (d) Thomas, J. M. *Sci. Am.*, **1992**, 266, 112.
38. Holderich, W.; Hesse, M.; Naumann, F. *Angew. Chem. Int. Ed. Engl.*, **1988**, 27, 226.
39. (a) Corma, A.; Garcia, H. *Catal. Today*, 1997, 38, 257; (b) Van der Waal, J. C.; van Bekkum, H. *J. Porous Mater.*, **1998**, 5, 289.
40. (a) Notari, B. *Stud. Surf. Sci. Catal.*, **1991**, 67, 243; (b) Panov, G. I.; Uriarte, A. K.; Rodkin, M. A.; Sobolev, V. I. *Catal. Today*, **1998**, 41, 365.
41. Sugi, Y.; Kubota, Y. *Catalysis-Specialist Periodical Report*, **1997**, 13, 55.
42. Song, C. *Stud. Surf. Sci. Catal.*, **1998**, 113, 163.
43. (a) Singh, A. P.; Kumar, S. B. *Appl. Catal. A: General*, **1995**, 126, 27; (b) Sharma, S.; Hedge, S. G.; Singh, A. P. *Appl. Catal. A: General*, **1997**, 162, 201; (c) Ratanasamy, P.; Singh, A. P.; Sharma, S. *Appl. Catal. A: General*, **1996**, 135, 25.
44. Bhattacharya, D.; Sharma, S.; Singh, A. P. *Appl. Catal. A: General*, **1997**, 150, 53.

45. Maxwell, I. E. and Stork, W. H. J. *Stud. Surf. Sci. Catal.*, **1991**, 58, 571.
46. John, C. S.; Clark, D. M.; Maxwell, I. E. New Insights into Zeolite Catalysis. in *Perspectives in Catalysis*, Ed. By J. M. Thomas and K. I. Zamaraev, Blackwell Scientific Publications, London, **1992**, p.387.
47. Nagy, J. B.; Bodart, P.; Hannus, I.; Kiricsi, I. *Synthesis, Characterization and Use of Zeolitic Microporous Materials*. DecaGen Ltd., Szeged, Hungary, **1998**, p.189.
48. Fraenkel, D.; Cherniavsky, M.; Ittah, B.; Levy, M. *J. Catal.*, **1986**, 101, 273.
49. Lee, G. S.; Maj, J. J.; Rocke, S. C.; Garces, J. M. *Catal. Lett.*, **1989**, 2, 243.
50. Yamaguchi, I.; Joh, T.; Takahashi, S. *J. Chem. Soc. Chem. Comm.*, **1986**, 1412.
51. Moreau, P.; Finiels, A.; Geneste, P.; Joffre, J.; Moreau, F.; Solofo, J. *Catal. Today*, **1996**, 31, 11.
52. Schmitz, A.; Bowers, G.; Song, C. *Catal. Today*, **1996**, 31, 45.
53. Creighton, E. J.; Downing, R. S. *J. Mol. Catal. A: Chemical*, **1998**, 134, 47.

## Chapter 2

# The Emergence of Shape-Selective Catalysis: Adventure, Basic Science, and Technology

Paul B. Weisz<sup>1</sup>

Department of Bioengineering, University of Pennsylvania,  
Philadelphia, PA 19104-6392, and Department of Chemical Engineering,  
Pennsylvania State University, University Park, PA 16802

Many publications, patents and books now exist that deal with shape-selective zeolite catalysis. This is an account of the adventure of its evolution. It recalls the basic interests that drove the exploration, the steps taken and the bridges crossed on the pathways from science to technology. It will also remind us of human and social elements that interplay, as always, in the evolution of any major technological innovation. This historical review serves furthermore to remind us of basic scientific elements that became recognized or evolved. It may stimulate thoughts toward more science and other technologies that may be sprung from these roots.

Scientific research generally explores vertically deeper down into one's specialty. The rarer form connects elements horizontally from different columns of experience and specialized knowledge. When such combination is made of several such basic elements, we have the makings for innovation and – if effectively developed – for the growth of new technologies for society. A past example is the transistor. It sprung from a seed in basic solid state physics at the Bell Telephone Laboratories. It led to the exponential growth of a multitude of new technologies for society. It began with smaller radios, but now embraces nearly all-human experience from information technology to space travel. There is an analogy here with the emergence of zeolite catalysis and zeolite technology. It grew exponentially from a laboratory experiment to embrace the major chemical industries world-wide, the energy supply system, the raw materials for polymers and fibers, the automobiles, the clothes we wear, the construction materials we use, and more. Molecular structure selectivity was the basic focus of the search and discovery and success surrounding shape-selective catalysis.

<sup>1</sup> Current address: Foxdale Village A-1, 500 East Marylyn Avenue, State College, PA 16801; E-mail: pweisz@aol.com

## The Personal Adventure

At age fifteen I passed a bookstore on the way to school. Two titles in the window mystified me. One was "Indigo". I learned much later about that early brilliant dye, a natural product imported from Asia, and about the time, art and skill it took for man to duplicate its molecular structure which nature's enzymes could tirelessly and continuously duplicate in *Indigofera tinctora*. The other title was "Catalysis". That, my teacher told me, is a substance that would cause transformations of chemical structures to proceed by "just being there". I was even more mystified.

After an earlier career as a physicist, I joined what is now Mobil Corporation. I was free to browse the tasks and the problems of the industry. In retrospect this was a most important circumstance, rarely duplicated in industry. I soon recognized that catalysis was clearly a major and key involvement. Moreover, I was impressed by the tremendous number of chemical species in petroleum oil, and the very limited "selectivity" that the man-made catalysts were able to exercise by "just being there". Why, even a single hydrocarbon component exposed to the catalyst would produce a plethora of products. What a contrast to nature's enzymes, the kind that could make indigo with precision!

Our working environment was that of acid catalysis on porous solids. You needed hundreds of square meters per gram of surface area on the particles. Crystals, even as small as 1 micron particle size could offer only some 3 m<sup>2</sup> of surface area per gram. Decades of research had evolved some porous clays and finally synthetic silica/alumina amorphous solids of sufficient porosity to provide sufficient surface area and acidity to operate catalytic cracking operations.

In the 1950's, synthetic zeolites 4A and 5A became available from the Linde Division of Union Carbide, for absorbing moisture. They also sorbed certain light gases, and did so reversibly. Could we build catalytic activity inside of these particles and then have catalysis, and have it specific to only those certain gases? Zeolites are crystals! And 4A and 5A are salts of Na (4A) and Ca (5A), not acids. The usual methods of generating acidity, using acids or ammonium salts with subsequent thermal decomposition to exchange the cations on the solids for protons proved to destroy the zeolites. Rather than quit outright we tried catalysis on the "salts" as is, anyway. We obtained observable catalytic activity on 5A, the Ca-zeolite (1,2,3): At 260°C it dehydrated 60 % of 1-butanol. Moreover, it, dramatically, did not convert iso-butanol or a secondary alcohol. It even cracked n-hexane but did not crack 3-methylhexane, and the activity was actually not much lower than that of a then prevailing industrial catalyst (Table Ia). Not only did we have charge selectivity but we clearly had molecular shape selectivity among the emanating products (Table I b). Conventional catalytic cracking of paraffins always yields a great deal more isobutane than n-butane. On cracking hexane, we saw *no* isobutane (2). It left us with excitement over witnessing the extraordinarily selective principle at work in our hands. But, even before resolving the question as to the possible usefulness of converting only linear molecules with extraordinary selectivity, we had to admit to having rather limited activity, thermal and acid stability of this zeolite. Two directions for progress were indicated: 1) exploring the potential for non-acid catalytic modifications of the zeolite, and 2) searching for other zeolites that may be more acid stable. We undertook both.



As to exploration of non-acidic catalysis on zeolites, could we include catalytic metal "sites" within the zeolites? Platinum ions were too large to penetrate A-zeolite channels. But we succeeded to incorporate some tenths of percents of platinum by including cationic platinum complex to the normal crystallization ingredients to create the A-zeolite. The catalyst did hydrogenate 1-butene while leaving isobutene entirely unconverted (1,2,3) from a mixture of both (Table IIa)!. Similarly we could hydrogenate linear pentadienes in admixture with isoprene (3,4) (Table IIb). Perhaps even more dramatically, this catalyst would catalytically burn n-butane or n-butene in admixture with air to carbon dioxide cleanly from a mixture with iso-butane, leaving the latter entirely untouched (3) (Table IIc)!

Looking beyond the one synthetic A-zeolite, there was always nature, but natural zeolites were rare minerals then. My partner in exploration Vincent Friette and I began a search for zeolite mineral samples and testing their capability to perform acid catalysis. The most exciting discoveries occurred with two particular samples: mordenite pebbles from the beaches of Newfoundland that Vince located, and a sample of gmelinite which I purchased (along with desmine, epistilbite and others) in a mineral store near the Sorbonne, on the west-bank of Paris. With these we obtained the highest acid catalytic activity we had ever seen, corresponding to rate constants near 10,000 times those of conventional silica/alumina cracking catalysts. We pronounced them "superactive" catalysts (5,6). In this process of exploration of natural zeolites, we learned that extraordinary acid and thermal stability could be had if the zeolite had a silicon-to-aluminum atom ratio of at least 2.0, preferably 3.0 or larger.

Another remarkable case of shape-selectivity occurred with mordenite. My early and long time co-explorer N.Y. Chen was able to introduce platinum by removing its sodium by conversion to H-mordenite, then introducing the Pt-ion and thereafter reloading sodium. To assure non-availability of Pt-sites to large molecules, "external" Pt was poisoned using a catalytic poison of large molecular size (7). Remarkably, this catalyst would hydrogenate ethylene but not propylene, in spite of its ability to sorb both (Table III). We learned that this "engineered" zeolite structure was unable to emit propane when or if it was produced; propane has a slightly wider effective diameter than propylene, inasmuch as propylene has one stiff double bond!

In 1966, the Encyclopedia of Chemistry (Reinhold Publ. Co.) decided to add a new entry "Catalysis, Shape-Selective" to their new edition (8). It was noteworthy from a historical perspective that in the Encyclopedia this now followed the entry "Catalysis" which ended with "...enzymes are part of such large molecules that they can probably best be classified as heterogeneous catalyst. They are characterized by an astonishing specificity....". It added drama to the step from enzyme to man-made catalyst for catalytic selectivity.

**The Path toward Technology.** We had shape-selective catalysis, a new capability at a very basic level. But where could this catalysis, selective to linear molecules, fit into our society, anyway? Furthermore, if such applications were identified, where would we find or produce such zeolite material, with thermal and acid stability and in sufficient quantity for industrial operation? And must we always be limited to selectivity toward strictly linear molecular structures? Any further progress clearly required a multidimensional effort.

**Table I. Shape selective paraffins cracking over Ca-A zeolite (as is)**  
 n-Hexane and 3-me-pentane, 500°C, 1 atm, t = 7 sec

(a) Activity:	% conversion	
	on Ca-A	on silica/alumina
n-hexane	9.2	12.2
3-me-pentane	<1.0	28.0

(b) From n-hexane:	iso/normal ratio	
	on Ca-A	on silica/alumina
butanes	<0.05	1.4
pentanes	<0.05	10.0

**Table II. Shape-selective conversions over Pt incorporated CaA zeolite**

	Conversion %
(a) Hydrogenation of olefins and diolefins 70°C, 9:1 H <sub>2</sub> /olefin, t = 1.6 sec	
n-butene	95
i-butene	<1
b) Hydrogenation of isoprene with 8 % pentadienes impurity 150°C, H <sub>2</sub> = 1 atm, t = 0.07 sec, mix at 0°C vap. press.	
trans-pentadiene	58.7
cis-pentadiene	36
isoprene	0.35
(c) Combustion of hydrocarbons in air, 1 atm (Ref. 3)	
n-butane	97
n-butene-2	98,6
propylene	98.6
i-butane	< 0.1
i-butene	<1.0

**Table III. "Engineered" shape selectivity in Pt-containing Na-mordenite**  
 Hydrogenation of 1:1 mixture of ethylene and propylene, 1 atm, 0.18 sec

	Conversion %	
	175°C	250°C
ethylene	18	29
propylene	<1	<1

Thanks to management wisdom and action, especially by R.W. Schiessler and S.L. Meisel, three different and important missions were initiated.

- 1) I was able to assemble an *ad hoc* multidisciplinary study group that included engineers with backgrounds from various sectors of our industry's technology. The purpose was to study the chemical characteristics of the petroleum resources and of the industry's varied products, and the relationships of their chemical constituents to traditional measures of their quality. This would hopefully enable us to identify *potential utilities* of our new capability.
- 2) The company's geology arm was alerted to our potential interest in zeolite mineral resources as to *potential varieties, availability, and quantity*.
- 3) The talents and efforts in the existing catalyst development group, with its inorganic chemical, analytical and crystallographic skills were to be expanded to include *study and synthesis of zeolites*.

In retrospect, these three undertakings proved symbiotically important and successful.

**Early Identification of Potentials for the Industry.** The exploration group identified two major potentials for the shape-selective conversion of linear hydrocarbon components. One was the removal of (ca. C<sub>5</sub> - C<sub>10</sub>) normal paraffins from gasoline to thereby gain octane number quality. The other was the removal of higher molecular weight normal paraffins from heavier oil fractions, especially lubricating oil, to provide the essential low temperature fluidity requirements. The chemical basis was the fact that long-chain paraffins begin to associate to waxy aggregates at low temperatures. In view of our laboratory experience with the lower molecular weight paraffins, the gasoline upgrading potential was closer at hand, if only we had a suitable zeolite catalyst, sufficiently stable and in large quantity of supply.

**A First Commercial Shape-Selective Process Using a Natural Zeolites.** It was in the late 1950's, that the existence of zeolites in large sedimentary deposits became gradually recognized. This fortunate progression in geological knowledge, and the vigilance of our alerted Mobil geology group pointed to a potential source of zeolite, in the desert of Nevada: An extensive deposit of erionite and clinoptilolite. We obtained and tested samples of the previously "rare" erionite (9). To our delight we found that it had a 3:1 Si/Al ratio and was therefore expected to be acid and thermally stable. Indeed we found it to be transformable to a superactive n-paraffin selective acid catalyst.

The large scale mining presented new problems. One difficulty was the intermingling of the erionite deposits with the poorly and non-shape-selective offretite or clinoptilolite. A young post doctoral engineer, Paul Rys, who had just joined us from Switzerland promised to come up with a simple spot field-test over the weekend and did. It involved a drop of a solution of methylene blue, which visibly would penetrate into offretite but be excluded by the target erionite. To this day he remembers his shape-selective research in the Nevada desert, performed in high boots to protect against rattlesnakes. (Paul is presently Chairman of Chemical Engineering at ETH – the Swiss Federal Institute of Technology, in Zurich).

Thus a natural zeolite helped realize the first shape-selective commercial process. The process would upgrade the octane-quality of gasoline by removing n-paraffins from gasoline to boost its octane number quality. Since it was an adjunct to

the existing gasoline “reforming” process, we named it “Selectoforming” (10, 11, 12). Incorporation of nickel provided hydrogenation of olefins without converting aromatics and prevented deposit formation. Continuous operation was achieved for many weeks without regeneration (12). The commercial development involved many diverse skills and contributions, from laboratory R & D, zeolite mining and preparation, to engineering design and process development, economic evaluations, and geographic strategies. It demanded cooperation and contributions by our exploration group, the geological field research, diverse catalyst development, process development, process design, economic evaluation and other groups of the Mobil organization. Since the major product of paraffin cracking was propane, with an impact on the resulting ratio of gasoline and LPG production, marketing conditions led to the commercial initiation of the process at a Mobil refinery in France, and later in Venezuela.

The concept of extending shape-selective paraffin conversion to heavier petroleum fractions, especially for a continuous catalytic lubricating oil dewaxing capability had to rest. The narrow channel zeolite catalysts did not function well enough at high molecular weights. We also learned in the process that for higher carbon number petroleum fluids, the methyl paraffins still have a linear chain long enough to lead to coalescence at lower temperature (the initial step to wax formation) because the majority of methyl groups of the isoparaffins in petroleum are in 2-position. This is pictured symbolically in Figure 1. It demonstrates the fluidity improvement obtained for a typical paraffinic oil by removal of only the n-paraffins as compared to removal of the isoparaffins also.

**Emergence of New Synthetic Zeolites.** Meanwhile the zeolite synthesis research effort wisely instituted by Mobil’s management was growing in size and success. The use of quaternary ammonium ions in place of inorganic ions in the customary zeolite synthesis procedures instituted by G.T. Kerr initiated a new phase of successive zeolite discoveries. Among the first new structures (13, 14), in the ZK designated series, there were now zeolites (ZK4, ZK20) with A-sized pore structures available that had the desired 2:1 Si/Al atom ratios. Then followed the ZSM designated series. Excitement began when my colleague N.Y. Chen found that ZSM-5 (15, 16) was able to convert iso-paraffins, and routine sorption characterization showed its ability to sorb cyclohexane also. He wrote that it “has more open structure than any of the erionite samples tested”.

### The Rise of New Technologies

In retrospect, at that moment we had a zeolite of an ultra stable silica structure of multiple utility. The Si/Al atomic ratio was extremely high. Potentially it could approach infinity, except, as it turned out, the minute levels of Al items were the essential catalytic acid sites! Within little more than a year, exploratory work ascertained its ability to react waxy paraffins (n- and monomethyl paraffins) from nearly any boiling range of petroleum, from jet fuel, heating oil to lubricating oils. Many reactions proceeded with remarkably long periods of time on stream without activity loss. This was “a first” for a catalyst without a Pt-hydrogenation component. One of our colleagues, W.E. Garwood, later commented to me about a period of

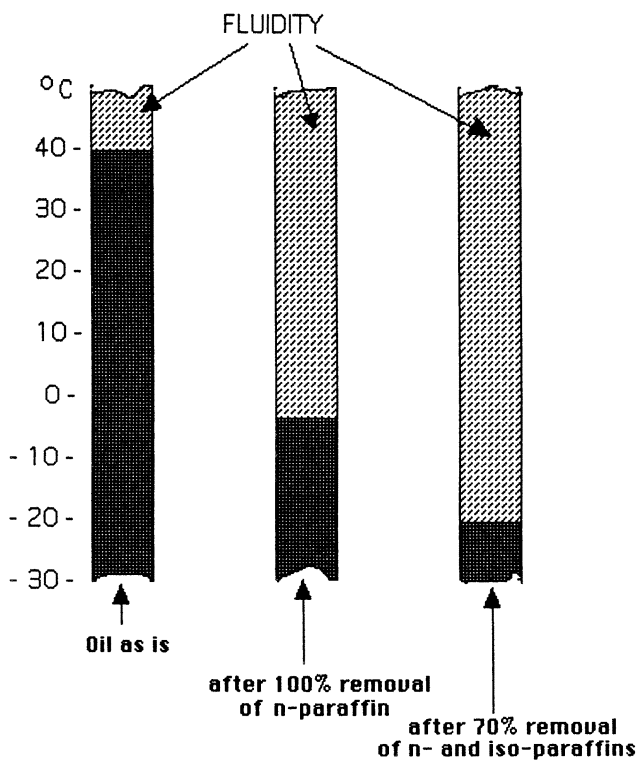
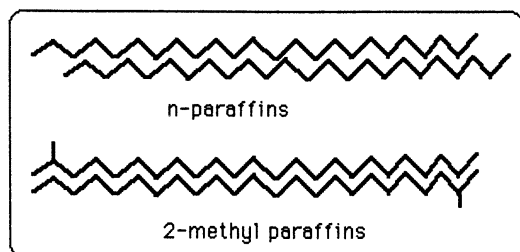


Figure 1. Low temperature limit for acceptable fluidity of a typical paraffinic petroleum fraction (boiling range 350<sup>0</sup> to 450<sup>0</sup>C).

exploratory work in 1968: "This was a very exciting period. It worked on everything!"

For this ZSM-5 zeolite structure (17), the shape-selective cut-off size was somewhere near the effective diameter of di- or certain trimethyl benzenes (18). For aromatic hydrocarbons this corresponds to near the boiling end point of a gasoline. It also meant that there was no room for condensation to larger products, including what is commonly referred to as "coke". Yet n- and most branched aliphatics of petroleum would pass the size requirements for diffusional penetration.

This revived the sleeping giant potential of dewaxing petroleum fractions to gain fluidity. To illustrate the importance of such capability, Figure 2 is a sketch of the boiling ranges (carbon-number ranges) of the major "premium products" (the cross-shaded area). They comprise Diesel and jet fuel, and also home heating oils. Catalytic normal and isoparaffin removal allows extending the boiling range (end point). This implies the ability of including of higher boiling heavy petroleum fractions into premium products, or to improve the fluidity quality of a given product, or both. In the same manner, it allows conversion of still higher molecular weight fractions into useful lubricating oils. Moreover, it makes available crude sources which, because of high paraffin contents, had not been eligible for lubrication oil production.

Processes for the upgrading of higher boiling distillates ("MDDW") (19,20) were introduced commercially in 1978. There are now at least 27 licensed processes in 10 countries. Lubricating oil dewaxing ("MLDW") was first introduced in 1981 in Australia and at least seven additional units have been placed in operation.

The other major branch of novel processes derives from the shape selectivity towards specific isomers of aromatics, in particular the specificity for para-substituted aromatics. They include para-xylene production by isomerization, or disproportionation or transalkylation. At this time, it is safe to assume that more than one of three readers of this paper is wearing polyester apparel for which the monomer raw material para-xylene was created on the shape selective zeolite catalyst. Shape selective properties have also led to selective processes for cumene and ethyl benzene production. The latter is practiced in at least twenty-five units in ten countries around the world.

The new processes have created new capabilities and flexibility for entire petroleum and petrochemical refinery systems. They have had broad and worldwide impact. They allowed new choices for crude resources; changed the relative value of petroleum crude sources previously penalized by high paraffin contents; they provided greater total utilization of the raw materials, and flexibility in accommodating product markets, geography, etc. The polyester based industry, a major resource to our fiber and clothing sector relied on a limited resource of para-xylenes. That constraint was lifted. As regards a future "alternative fuels" capability, one such alternative was demonstrated in New Zealand using ZSM-5 catalyst to convert methanol made from off-shore natural gas directly to high octane gasoline for to-days automobiles, when the use of that only domestic hydrocarbon resource was preferred to importation (21,22).

The relatively rapid development of numerous new and large-scale technologies was largely enabled by a well-coordinated management and team effort involving a large variety of skills. It is interesting to observe that the development and use of basically novel technology can and does encounter resistance by

“specifications” that had long been accepted by society as necessary and inviolate, based on decades of past experience. Examples are the “pour points” and “end points” jointly dictated by long accepted product specifications in fuel oils, or, in the case of jet fuels, the pair “freeze point” and “end point”. In each case, both parameters had to conform to specification. However, the new chemical capability of selective removal of the paraffin group of constituents decoupled the interdependence of these two parameters. Fluids extending to much higher “end points” could now satisfy the *real* operating requirements as regards low temperature fluidity. The realignment of “tradition” to a new reality took and still takes time and education. That condition, in itself is proof of a *fundamental* change having been made to a chemical technology!

### The Science - Technology Symbiosis

**Shape Selectivity and Diffusion.** The selectivity difference that was first demonstrated for n- vs. iso-paraffins on the narrow pore zeolites such as zeolite A, gmelinite, or erionite depended on a near infinite difference in diffusion capability of the respective molecules: The n-paraffin did enter, the iso-paraffin was fully excluded. In contrast, for somewhat larger channel diameters such as in ZSM-5, shape-selective differentiation is accomplished by very large but finite differences in molecular diffusivities  $D$  for the species, say  $D_A \gg D_B$  for discrimination of species A against B. However, this is a necessary but *not sufficient* condition for obtaining process shape selectivity. In order to understand, or to manage diffusion controlled shape selectivity, it is necessary to understand the basic chemical engineering fundamentals of diffusion control of the catalytic rate (23).

If shape selectivity for A against B is to be attained it is NOT sufficient that  $D_A \gg D_B$ . It is necessary that in addition the intrinsic reaction turn-over time  $\tau_{B(\text{reaction})} = 1/k$  of the catalytic reaction be shorter (i.e. the intrinsic rate be faster) than the characteristic diffusion time of B,  $\tau_{B(\text{diffusion})} = R^2 / D_B$ , where  $k$  is the first order reaction rate constant of the reaction and  $R$  is the particle (the zeolite crystallite) radius. In the engineering science discipline, this condition is expressed by the Thiele modulus of the species B, which means that  $R (k / D_B)^{1/2} \gg 1$ . This case is pictured in Figure 3, for  $D_A / D_B = 400$ . Thiele modulus is assumed to be near 10 for the species B for the prevailing reaction condition. It is in the region of inhibition, while the modulus for species A is still at a position where reaction rate is nearly uninhibited. In simple operational terms, we can approximate that important condition by stating that B will be shape selectively inhibited if

$$R^2 / D_B \gg T / f, \quad (1)$$

where  $f$  is the fractional conversion attained for the species A, and  $T$  is the reactor residence time employed. This assumes that the *intrinsic* reaction rate constant of A and B (for its conversion or its generation) are of similar magnitude which is true for most cases of practical interest.

It will be seen that we can have diffusivity differences between the species like the case above, but can attain great, little or no effective shape selectivity if we operate at low per-unit-catalyst conversion. By way of an example, we can obtain

para-xylene shape selective toluene-methanol addition at high temperature (and small catalyst volume), or obtain little shape selectivity at lower temperature and larger catalyst volume!

**Shape Selectivity by “Clogging”.** Another means of achieving shape selectivity relies on *decreasing* the diffusion rate  $D/R^2$  of both A and B. This moves the bar that represents the ratio  $D_A / D_B$  in Figure 3 from a position too far on the left on the Thiele modulus abscissa to the position indicated (or even further to the right). It is generally understood that such is accomplished by increasing crystallite size R, thus effecting A as well as B. However, it is not generally understood that partial clogging of entry by chemical agents such as phosphates, borates, various oxides, silylation or by “coking” can also accomplish this process of *reducing the transport rates of both components* (24,25). This has been demonstrated for this entire variety of modifiers. E.g. the para-xylene selectivities achievable correlated only with a measurement of diffusion time only, regardless of which chemical agent was used (26) or whether particle size was changed. The modifications thus are not due to chemical modifications but to *physical* alteration of diffusion rate, by either “clogging” of pores or path length (particle size) variation.

**Measurement of “Diffusivity”.** We learned very soon that diffusivity values derived by standard uptake (sorption), i.e. transient procedures provided us with magnitudes inconsistent with observations in catalysis. In the transient methods, rapid equilibration occurs between the applied mobile (and diffusing) phase and adsorption to an immobilized portion of the species that does not participate in diffusion. In the catalytic process, we deal with the steady state, where this equilibrium has long been established. Nevertheless the traditional treatment of the sorption rate curve reflects the entire added time required to fill the volume elements with both the diffusing as well as the much larger amount of immobilized participants. The proper steady state and actual diffusivity D is obtained (27, 28, 29) by correcting the apparent diffusivity  $D_{app}$  by

$$D = (C_a/C_o) D_{app} ,$$

where  $C_a$  is the equilibrium volume concentration adsorbed on the zeolite for the externally applied concentration  $C_o$  in the sorption technique. The resulting magnitudes of D are then consistent with those that are operative during steady state catalysis (30).

In any pursuit of determining diffusivities, it is also important to recognize that at certain low temperatures and pressure conditions a process equivalent to capillary condensation will occur near the surface followed by capillary migration of the ‘condensate’; and this is not equivalent to diffusive mass transport (27,28). Thus many non-equilibrium, i.e. “uptake” measurements taken at low temperature are not valid as a means to determine the diffusivity D or even of  $D_{app}$  !

**Shape selectivity due to Size of Reaction Complex.** A second major mechanism of shape selective conversion can be operative when the intracrystalline dimensions cannot accommodate the size of the *reaction complexes* that must be formed (31,32). Thus, bimolecular reactions such as, for example, disproportionation reactions



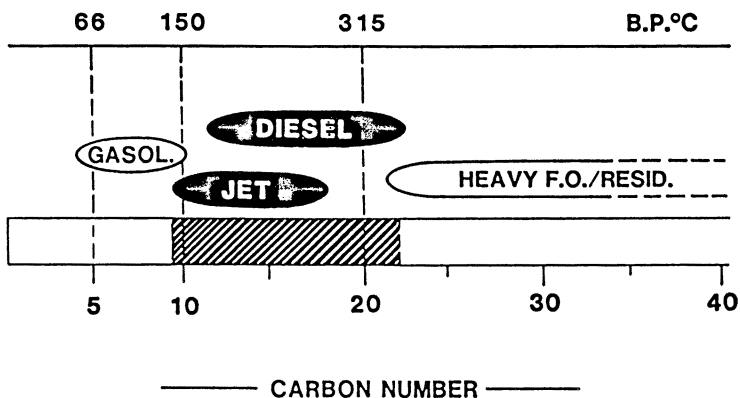


Figure 2. Boiling and approximate carbon number ranges of typical gasoline and premium products (shaded black) from petroleum.

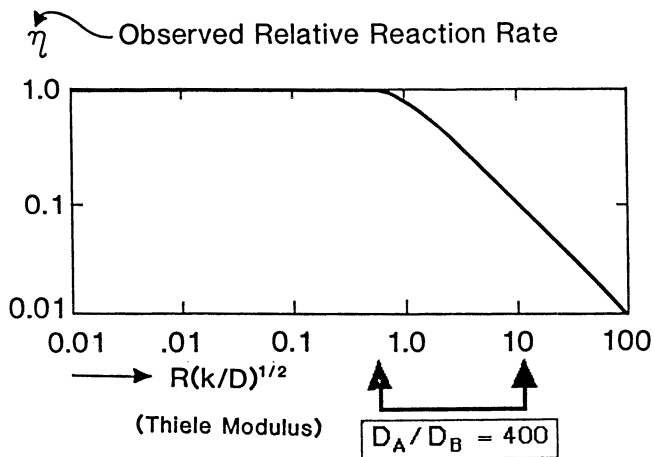


Figure 3. The relationship between the Thiele Modulus and the effectiveness factor  $\eta$  (the reduction of catalyst activity from diffusion uninhibited conversion). The bar marks the ideal operating position for maximum attainable shape selectivity for  $D_A/D_B = 400$ .

involving two aromatic molecules can be impeded or prevented. This may apply to certain isomeric configurations of several possible ones, or to all.

The inhibition may not only involve the accommodation of two bimolecular reactants at the catalytic site. It may involve complexing a single reactant with a complex such as a propyl carbenium ion on the catalytic site (33). Figure 4 illustrates the difference in minimum molecular dimension between the complex formed with the site associated propyl carbenium ion with n-hexane and with 3-methyl pentane. This turned out to be the inhibitory effect of shape utilized in the use of what we called the "Constraint Index" (= cracking rate of n-hexane/cracking rate of 3-methyl pentane). Like any of the effects of *size of the reaction complexes*, the effect is *not* dependent on crystallite size. (This was fortunate in the early days of exploration of ZSM-5 type zeolites, since no routine control of size was available when comparing or testing numerous samples). It is to be remembered, however, that, even when shape-selectivity due to the size of the reaction complex is operative, the mass transport effects that depend on the Thiele modulus can and will be *additionally* superposed (30, 34). This will be the case for conditions of sufficiently large particle size and/or high conversion rate operation.

**The Window Effect.** Remarkably large and near periodic down and up variations of diffusivities for n-paraffins with systematically increasing carbon number (length) were reported by Gorrington for zeolite-T (35) and in chabazite (36). Various rather sophisticated explanations have been discussed (37,38). We must note that the reported diffusion measurements were carried out by conventional uptake rate evaluation. The reported data  $D_{app}$  therefore contain information concerning any possibly variations in the degree of immobilization (adsorption) of the hydrocarbons of varying lengths in the zeolite structure. A revisitation of data with the correction for absorption (see above) to obtain the true transport diffusivity  $D$  would seem indicated. Beyond this, it would appear important to consider the basic fact that a n-paraffin is not a linear and stiff rod, but each bond is subject to rotation events. Thus, in a periodic lattice of smaller ports, a molecule while traveling toward the next port may undergo a segment rotation that now hinders penetration at the next "gate", until further rotations occur. Figure 5 crudely illustrates shapes after segment rotations that go beyond a fixed "port" dimension, and lists typical classical and elementary parameters of distance and time of passage for a port to port passage in a zeolite structure. These magnitudes of time appear to us consistent with Raman wave numbers of segment rotation. The frequency of rotation events for any one bond is dependent on the mass of the particular segment. Such process can therefore be expected to be subject to "periodic" events dependent on the length of the molecule. This seems worthy of further consideration.

**Internal Events on an Acid Catalytic Surface.** Upon the emergence of ZSM-5 as a shape selective catalyst, many investigators at Mobil studied the conversion of different reactants, and at various degrees of reaction severity. It was an eye opening experience to observe the generation from methanol of products that, beginning with dimethyl ether and further progressing to olefins and paraffins and aromatics would produce a mixture of products nearly identical with that in a high grade gasoline (39,40).

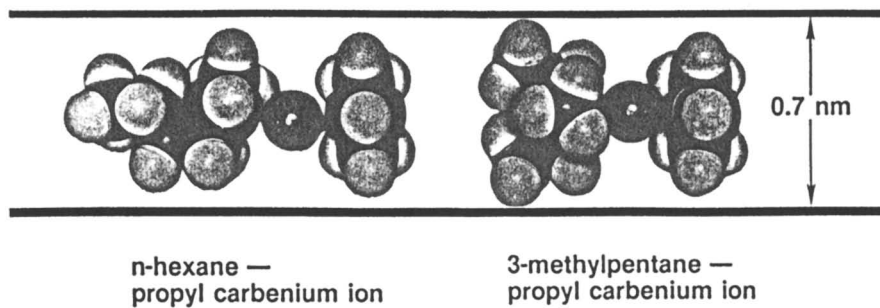
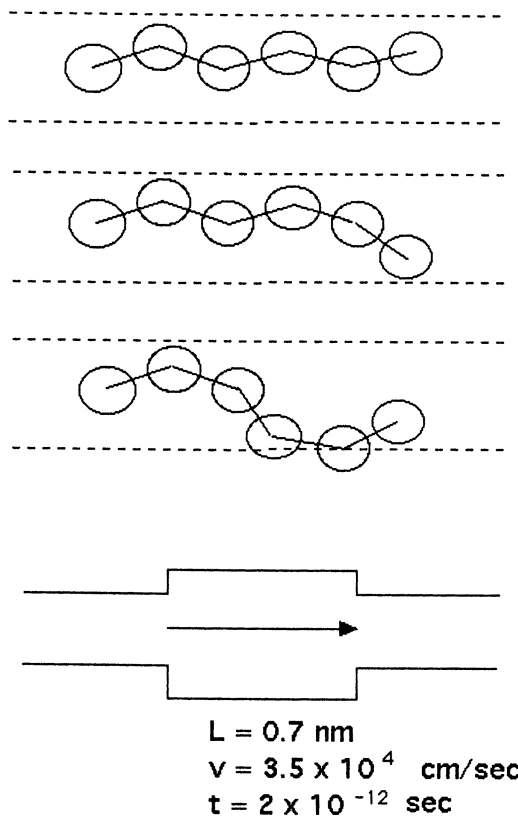


Figure 4. Relative size (molecular model) of the n-hexane vs the 3-methylpentane complexes with propyl carbenium ion.



Corresponds to a Raman wave number of

$$R = c/t = 3 \times 10^{10} / 2 \times 10^{-12} = 150$$

Figure 5. Illustration of configurational changes of a n-paraffin chain due to segment bond rotation. Typical kinetic parameters, time of travel between zeolite "gates" and comparison with Raman wave number.

It seemed logical to inquire as to why such an important conversion was not observed before on classical acid catalysts. Was the intrinsic nature of the acid sites different? A careful investigation with methanol over a conventional acid catalyst was revealing. As summarized in Figure 6, ZSM-5 catalyst produced gasoline range products for 5000 hours. Yes, acid montmorillonite, for example, also produced hydrocarbons, but only within the first tenth of an hour, with products tending toward progressively higher molecular weights. After about 1 hour conversion diminished as molecular condensation progressed to “coke” to “kill” the catalyst.

It was a clear demonstration that intrinsic acid activity was initially available in both materials. The chain building and re-cracking processes via ionic species were taking place in both catalysts. The shape inhibition in ZSM-5 allowed aromatics condensation up to the size of di- and tri-methyl benzenes but could not accommodate larger condensation products that would deactivate (“coke”) the catalyst. Here we have a case of drastic reaction complex size limitation (see above) turning an undesirable catalytic chain process into a technologically useful process of aromatization.

It furthermore became clear that the internally cycling acid catalyzed processes would yield nearly the same product mix from any aliphatic hydrocarbon molecule that could enter the ZSM-5 shape-constrained acid environment, as demonstrated (41) by the product distributions from six very different reactant charges, from methanol to peanut oil! See Figure 7.

### Gazing toward the Future

Thus there are now new principles of structure selectivity available and an infinite amount of chemistry where they may be practiced. We published the first paper on shape-selective catalysis in 1960. The last 10 years have produced 600 papers on the subject (API Literature Abstracts), and 260 patents (Derwent World Patent Index). The major impact so far has been on the hydrocarbon industry, petroleum and petrochemicals. The latter have been oriented toward monomer starting materials for polymer products and commodities.

**Other Chemical Industries.** I have seen enough of the chemical industry to see large numbers of new potentials ahead for applications of the new capabilities for molecular selectivity in catalysis. It will take time and some abandonment of custom and habit. For example, in many sectors of the chemical and pharmaceutical industry, it will require a fresh look at the use of *heterogeneous* catalysis, of adopting continuous flow *in place of batch reactor* approaches, and deserting reliance on old standby “proven” catalyst bases like activated carbon. There exist convictions that continuous reactor equipment does not provide sufficient operating flexibility comparable to batch operations. This is a misconception based on familiarity of old and unfamiliarity of the new.

**Other than Chemical Objectives.** It is interesting to explore not just new applications to other chemistries but to realize that there are potentials for objectives connected with other branches of technologies that do not have production of a specific chemical as their objective.


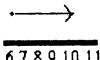
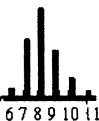
	CATALYST:		
	Montmorillonite Clay		ZSM-5
Time on Stream	0.1 hr	1.5 hrs	0 - 5000 hrs
% Methane Conversion to C4+ Products	<70	< 8	80
Aromatics Distribution (Carbon number)		COKE 	

Figure 6. Methanol conversion. Comparison of amorphous acid clay catalyst and ZSM-5.

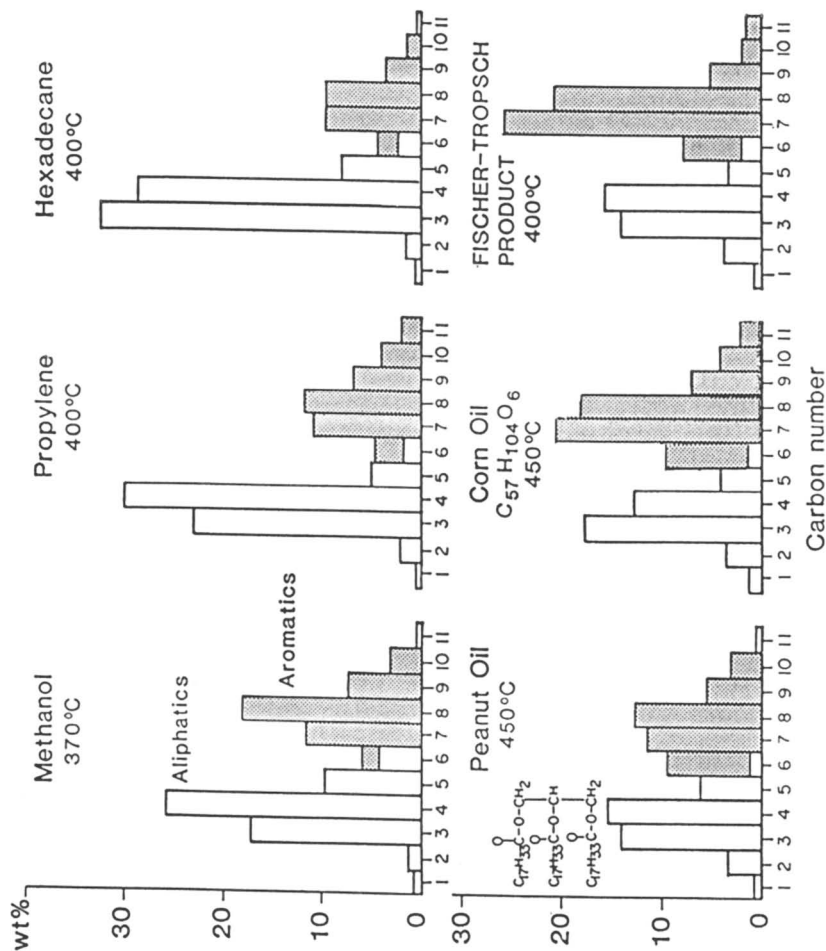


Figure 7. Comparison of product distributions obtained for ZSM-5 catalyzed conversion of a wide variety of charge molecules, by carbon number. Shaded area are aromatics; white area are aliphatics.

For example, we saw it possible (see above) to introduce catalytic oxidation sites in a narrow pore zeolite structure accessible to O<sub>2</sub>, CO, CO<sub>2</sub>, H<sub>2</sub>O, CH<sub>4</sub>, but inaccessible to larger reactant molecules. It was possible to thereby carry out controlled oxidation for internal reactor heat production along with an otherwise endothermic reaction progressing on other catalyst (7) within the same reactor volume. It constitutes basically a method of homogeneous heat production, with sources distributable at will according to need, and controllable by controlled feed of a suitable low molecular weight "fuel" component.

There exists a range of technology objectives in the field of chemical sensors, for various purposes such as are related to analytical, safety, drug detection, etc. We can illustrate this by a potential example: A narrow pore zeolite such as erionite or zeolite T may distinguish between ethanol and acetone (Figure8a). It could distinguish between ethanol and the acetone metabolite in a breath test for alcohol, as may be appropriate in the case of a diabetic. Detection may be done via the heat produced via internal catalytic combustion, as just noted above.

There exists a large potential for selective chemical *detection* technologies. It is interesting to consider combinations of zeolite and transistor chip technology. As illustrated in Figure9, it is conceivable to take a silicon chip with a p/n-junction, to oxidize a limited portion of surface across the junction, transform that portion of SiO<sub>2</sub> into a zeolite. Selective adsorption of a species can then be expected to result in an electronic signal across the p/n- device.

Needless to say, molecular structure selectivity plays a key role everywhere, in life, biology, the world. To mention one other example of shape differentiation in environmental science: it is not generally known that the dioxin family of toxins shows the very high toxicity only for the isomer with chlorine atoms in the 2,3,7,8 positions (42) (Figure8b) but not for the isomers having a Cl atom in lateral substitution. Judging from our analogous experience with the 1- vs. 2-methylnaphthalenes, only the notorious dioxin would probably enter a zeolite such as ZSM-5.

We noted at the outset a general analogy between the rise and versatility of the transistor technology and the shape-selective catalysis technology. It is remarkable that the former arose and exists based on pure silicon "doped" with aluminum atoms to provide the required key electrical property. The shape selective zeolite technology is based on pure silicon dioxide "doped" with aluminum atoms to provide the key catalytic property.

## Acknowledgement

The development of shape-selective catalytic technology has involved a very large number of contributors. I wish to name at least a few that were involved in the earliest discovery stages. In early and science exploration: N.Y. Chen, V.J. Frilette, W.E. Garwood, R.L. Golden, W.O. Haag, G.T. Kokotailo, R.M. Lago, J.N. Miale, E.B. Mower, R. J. Moyola. In early development: G.T. Kerr, A.J. Argauer, F.G. Dwyer, J.R. Landolt, J. Mazuik, D.H. Olson, A.B. Schwartz. As consultants: Prof. M. (John) Hassialis (Columbia University), Prof. R.M. Barrer (Imperial College, London), Prof. Walter Meier (Swiss Federal Institute of Technology, Zuerich). Imperfections in memory will inevitably omit others. It is important to acknowledge



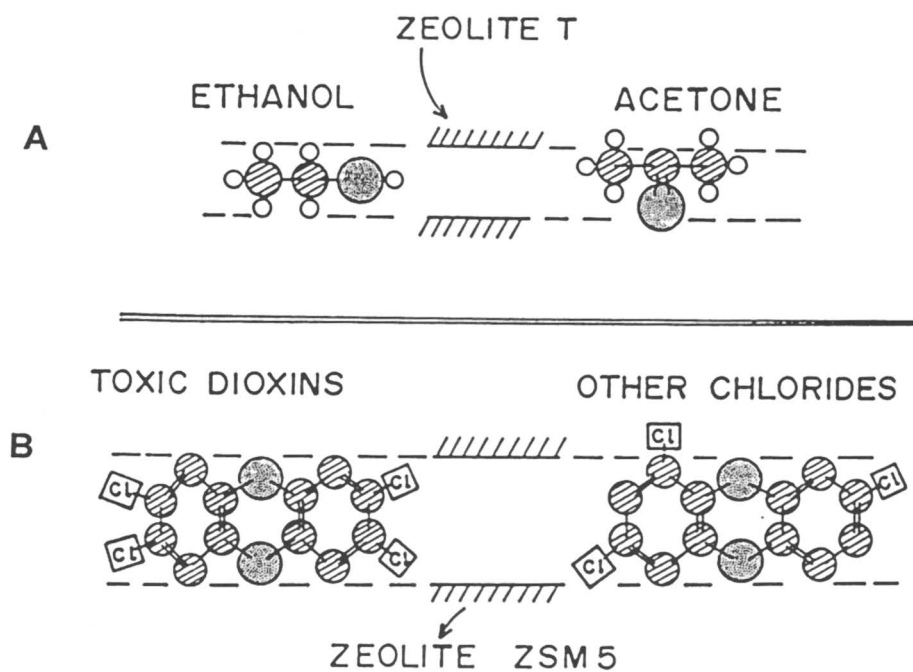


Figure 8. Effective diameter of molecules relative to a zeolite channel width. A) acetone vs ethanol in zeolite T; B) major toxic dioxin vs other dioxin isomers in ZSM-5.

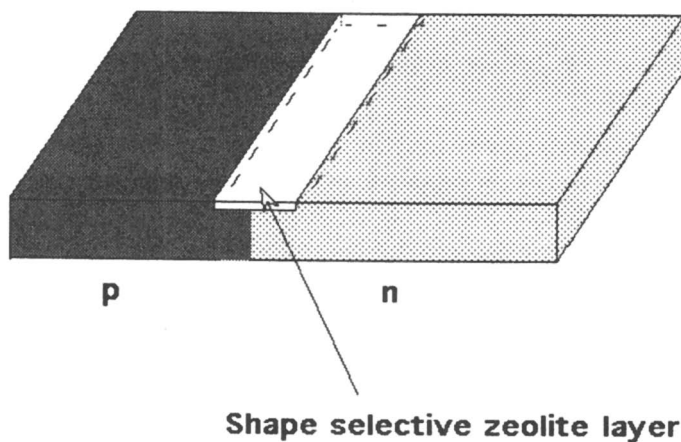


Figure 9. Conceptual chemical-detecting silicon chip with a p/n junction across a section of oxidized Si that has been transformed to a zeolite.

key decisions and wisdom by management, particularly Drs. R.W. Schiessler and S. L. Meisel, and the general spirit of support of innovation by the Mobil Corporation.

### Literature Cited:

- (1) Weisz, P.B; Frilette, V.J *J. Phys. Chem.* **1960**, *64*, 382
- (2) Weisz, P.B; Frilette, V.J; Maatman, R.W; Mower, E.B *J. Catalysis* **1962**, *1*, 307
- (3) Weisz, P.B *Erdoel und Kohle* **1965**, *18*, 525
- (4) Chen, N.Y; Lucki, S.J Hydrogenation of 1,3-Pentadiene over Zeolite Supported Platinum Catalysts", Am. Chem. Soc; Nat. Mtg. Chicago, Sept. 1967
- (5) Weisz, P.B; Miale, J.N *J. Catalysis* **1965**, *4*, 527
- (6) Miale, J.N; Chen, N.Y; Weisz, P.B *J. Catalysis* **1966**, *6*, 278
- (7) Chen, N.Y; Weisz, P.B *Chem. Eng. Progress Symp. Ser.* **1986**, *63*, 86
- (8) *Encyclopedia of Chemistry, 2<sup>nd</sup> Edition*, p. 191, N.Y. Reinhold Publ. Co. 1996
- (9) Staples, L.W; Gard, J.A; *Mineral. Mag.* **1959**; *32*, 261
- (10) Weisz, P.B; U.S.P. 3,395,094, 1968
- (11) Chen, N.Y., Mazuik, J., Schwartz, A.B., Weisz, P.B. *Oil & Gas J* **1968.**, *66*, 154
- (12) Chen, N.Y., Garwood, W.E., U.S.P. 3,379,640, 1968
- (13) Kerr, G.T. *Science* **1963**, *140*, 1412
- (14) Kerr, G.T. *Inorg. Chem.* **1966**, *5*, 1537
- (15) Chen, N.Y., Lucki, S.J., Garwood, W.E., U.S.P. 3,700,585, 1972
- (16) Argauer, R.J., Landolt, G.R., U.S.P. 3,702,886, 1972
- (17) Kokotailo G.T., Lawton, S.L., Olson, D.H., Meier, W.M. *Nature* **1978**, *272*, 437
- (18) Chen, N.Y., Garwood, W.E. *J. Catalysis* **1978**, *52*, 453,
- (19) Chen, N.Y., Gorring, R.L., Ireland, H.R., Stein, T.R. *Oil Gas J.* **1977** *75*, 165
- (20) Meisel, S. L., McCullough, J.P., Lechthaler, C.H., Weisz, P.B. Leo Friend Symposium, 174<sup>th</sup> American Chemical Society Meeting, Chicago, Ill., 1977
- (21) Meisel, S.L., McCullough, J.P., Lechthaler, C.H., Weisz, P.B. *Chemtech* **1976**, *6*, 86
- (22) Fox, J.M., *The Fixed-Bed Methanol-To-Gasoline Process Proposed for New Zealand*, Austral. Inst. Petr., Coal Gasification Conf., Adelaide, Mar. 2, 1982
- (23) Weisz, P.B. *Pure & Appl. Chem* **1980.**, *52*, 2091
- (24) Chen, N.Y., Kaeding, W.W., Dwyer, F.G. *J. Am. Chem. Soc.* **1979**, *101*, 6783
- (25) Kaeding W.W., Chu C., Young, L.B., Butter, S.A. *J. Catalysis*, *69*, 392, 1981
- (26) Olson, D.H., Haag, W.O. *ACS Symposium Series* *248*, 275, 1984
- (27) Garcia, S., Weisz, P.B. *J. of Cat* **1990**, *121*, 294; *ibid.* **1993** *142*, 69; *ibid* **1993**, *144*, 109
- (28) Weisz, P.B. *Ind. and Eng. Chem. Res.* **1995**, *34*, 2692
- (29) Liang, W., Chen S., Peng S. *Ind. and Eng. Chem. Res* **1997**, *36*, 1882
- (30) Haag, W.O., Lago, R.M., Weisz, P.B. *Faraday Disc. Chem. Soc.* **1981**, *72*, 317
- (31) Csicsery, S.M. *J. Catalysis* **1971**, *23*, 124
- (32) Csicsery, S.M. *Pure and Appl. Chem.* **1986**, *58*, 841
- (33) Haag, W.O., Zeolites and Related Microporous Materials: State of the Art 1994, *Studies in Surface Science and Catalysis* **1994**, *84*, 1375, Elsevier Science B.V.
- (34) Voogd, P., Van Bekkum H. *Appl. Cat.* **1990** *59*, 311

- (35) Goring, R.L. *J. Catalysis* **1973**, 31, 13
- (36) Goring, R.L., Daniels, R.H. *ACS Symposium Series* **1984**, 248, 51
- (37) Ruckenstein, E., Lee, P.S. *Phys. Letters* **1976**, 56A, 423
- (38) Nitsche J.M., Wei. J. *AIChE Journal* **1991**, 37, 661
- (39) Chang, C.D. *Cat. Rev. Sci. Eng.* **1983**, 25, 1
- (40) Chang, C.D., Chu C.T.-W., Socha, R.F. *J. Catalysis* **1984**, 86, 289
- (41) Weisz, P.B., Haag, W.O., Rodewald, P.G. *Science* **1979**, 206, 57
- (42) Safe S. *Chemosphere* **1983**, 12, 447

## Chapter 3

# Recent Advances in Shape-Selective Catalysis and Its Industrial Applications

Nai Y. Chen

Technical Consultant, 4 Forrest Central Drive, Titusville, NJ 08560-1310

Presented herein is a general review of the advancement of a selected list of industrial applications and selected potential opportunities in shape selective catalysis. Also included is a review of the advances in the understanding of the catalytic properties of other useful molecular sieves than the traditional medium pore zeolites and the advanced practical catalyst modification methods. Molecular sieves covered in this paper include four major classes: (1) Intersecting channels of different size openings (2) Non-intersecting channels (3) Two, non-intersecting pore systems, such as MCM-22 and (4) Mesoporous molecular sieves, or the MCM-41S family.

Since writing the 2nd Edition of the book, *Shape Selective Catalysis in Industrial Applications*, first published in 1989 by Marcel Dekker, co-authored by me and my co-workers, Bill Garwood and Frank Dwyer at Mobil, was completed in 1995 after we retired from Mobil (published in 1996 by Marcel Dekker), three years have passed and a surprisingly large group of molecular sieves, mostly zeolites, established their commercial importance. Chemical modification of the molecular sieve catalysts also led to second and third generation catalysts for quite a few petrochemical processes.

This paper is written to briefly review the advances in the following four areas:

1. The chemical and physical characteristics of useful molecular sieves with respect to their catalytic properties.
2. Practical methods in the modification of molecular sieves to improve activity, stability and selectivity in shape selective catalysis.

3. Advances in industrial applications
4. New opportunities in shape selective catalysis

### New Useful Molecular Sieves

The crystal structure of a molecular sieve is defined by the specific order in which a network of tetrahedral units are linked together to form a set of open pores and channels. The closeness of the pore size of these materials to the size of many organic molecules of practical interest, gave birth to a new type of catalysis known as "shape selective catalysis". Beginning in the late fifties with the original discovery of the selective conversion of straight chain hydrocarbons using small pore (8-membered oxygen ring systems) zeolites, led to the first commercialized process known as the "Selectoforming" process in the mid-60's (1).

This was followed by the discovery in 1967 of the unusual catalytic properties of ZSM-5 (2,3), the first medium pore (MFI, 10-membered oxygen ring systems) zeolite, and extended the application of shape selective catalysis to organic reactions involving not only linear and branched paraffins and olefins, but also aromatics, naphthenes and non-hydrocarbons. By now, not only we have quite a number of medium pore molecular sieves but also have learned many sophisticated physical and chemical techniques of selecting and/or modifying the catalyst to achieve the desired activity and selectivity in practical applications.

In addition to classical medium pore molecular sieves (MFI, MFL), industrial application of shape selective catalysis has extended to four new classes of molecular sieves:

- 1) Molecular sieves possessing intersecting channels of different size openings with examples shown in Table 1 (4).

Table 1. Intersecting Channels Of Different Size Openings

IZA Code	Name	Intersecting Channels	Pore size, Å
EMT	EMC-1, CSZ-1, ECR-30, ZSM-20	12, 12	7.4 x 7.6
BEA	Zeolite Beta	12, 12	7.6 x 6.4 ↔ 5.5
DFO	DAF-1	12, 10, 8	7.3 ↔ 3.4 x 5.6 ↔ 6.0 ↔ 5.4 x 6.4
CON	CIT-1, SSZ-33, SSZ-36	12, 10	6.4 x 7.0 ↔ 6.8 ↔ 5.1
GME	Gmelinite	12, 8	7.0 ↔ 3.6 x 3.9
MOR	Mordenite	12, 8	6.5 x 7.0 ↔ 2.6 x 5.7
OFF	Offretite, Linde T, LZ-217	12, 8	6.7 ↔ 3.6 x 4.9
BPH	Linde Q	12, 8	6.2x6.7 ↔ 3.0x3.2
MEI	ZSM-18	12, 7	6.9 ↔ 3.2 x 3.5
MFI	ZSM-5, Silicalite	10, 10	5.3 x 5.6 ↔ 5.1 x 5.5
FER	Ferrierite, FU-9, ISI-6, NU-23, ZSM-35	10, 8	4.2 x 5.4 ↔ 3.5 x 4.8
HEU	Heulandite, Clinoptilolite	10, 8	2.6 x 4.7 ↔ 3.0 x 7.6. 3.3 x 4.6
MFS	ZSM-57	10, 8	5.1 x 5.4 ↔ 3.3 x 4.8

Source: Meier and Olson (1996) (4).

- 2) Non-intersecting channel system molecular sieves, with examples shown in Table 2 (4).

Table 2. Non-Intersecting Channel System Molecular Sieves

IZA Code	Name	Channels	Pore size, Å
AFI	SAPO-5, SSZ-24	12	7.3
LTL	Linde Type L, LZ-212	12	7.1
MAZ	Mazzite, LZ-202, Omega, ZSM-4	12 8	7.4   3.4 x 5.6
ATS	MAPO-36	12	6.5 x 7.5
VET	VPI-5	12	5.9
MTW	ZSM-12, CZH-5, NU-13, Theta-3, VS-12, TPZ-12	12	5.5 x 5.9
ATO	SAPO-31	12	5.4
TON	Theta-1, ISI-1, KZ-2, NU-10, ZSM-22	10	4.4 x 5.5
MTT	ZSM-23, EU-13, KZ-1, ISI-4	10	4.5 x 5.2
EUO	EU-1, TPZ-3, ZSM-50	10	4.1 x 5.7
LAU	Laumontite	10	4.0 x 5.3
AEL	SAPO-11	10	3.9 x 6.3

Source: Meier and Olson (1996)(4).

- 3) An unusual two, non-intersecting pore system molecular sieve such as MCM-22 (MWW).
- 4) Mesoporous molecular sieves, including the MCM-41S family.

Following is a brief review of their chemical and physical characteristics with respect to their catalytic properties:

- 1) Molecular Sieves Possessing Intersecting Channels Of Different Size Openings

Zeolite Beta (BEA), which is a high silica zeolite with one unidimensional large 12-membered oxygen ring channel (7.6 x 6.4Å) intersecting a two dimensional puckered 12-membered oxygen ring channel system (5.5Å) has some unusual catalytic characteristics compared to other 12-membered oxygen ring zeolites such as the faujasites (FAU). In the hydrocracking of gas oils, for example, metal supported faujasite catalysts selectively convert the non-paraffinic fraction while zeolite Beta selectively convert the

paraffinic fraction by hydroisomerization in the presence of aromatics. This technology in hydroisomerization has extended to the conversion of Fischer-Tropsch waxes to low pour point distillates with high cetane number and high viscosity index (VI) lubricating oil basestocks (5). The combination of hydrocracking over an amorphous catalyst with hydroisomerization over a low acidity metal supported zeolite Beta followed by a third step to dewax the lubricating oil fraction over the MLDW catalyst further improves the conversion of petroleum waxes to a high VI, low pour point lubricants (6).

Similar properties were identified in mono-functional catalytic cracking of gas oils. Chen et al. (7) studied catalytic cracking a waxy gas oil, the catalyst yielded a higher octane gasoline and a lower pour point distillate fuel than a commercial FCC catalyst. Its commercialization depends on the reduction of the cost of its synthesis.

Mordenite (MOR), a dual pore zeolite with intersecting channels of puckered 12 and 8-membered oxygen ring openings and Ferrierite (ZSM-35, FER), a dual pore zeolite with interconnecting channels of elliptical 10 and 8-membered oxygen ring openings are also used in commercial processes. Their chemical and physical characteristics with respect to their catalytic properties have been reviewed in 1995 (8).

## 2) Non-Intersecting Channel System Molecular Sieves

### Paraffin Hydroisomerization

Non-intersecting unidimensional channel medium pore structures, such as TON, MTT, EUO and AEL have potential industrial applications as dual functional paraffin hydroisomerization catalysts with unusually high yield and product selectivity when compared to the traditional medium pore zeolites (MFI, MEL) or zeolite Beta. For example, Chevron commercialized their ISODEWAXING<sup>®</sup> Process (9) for lube dewaxing by wax isomerization. It could be based on a bifunctional SAPO-11 (AEL) catalyst (10). Furthermore, we also found that noble metal loaded zeolites of this group with proper acid-metal balance can even hydroisomerize paraffins of a raw gas oil without prior hydrotreating to remove the nitrogen and sulfur impurities (11).

In pure component studies Campelo et al. (12) compared the hydroisomerization of *n*-heptane over Pt/SAPO-5 (AFI) and Pt/SAPO-11 (AEL), both unidimensional molecular sieves containing 0.5 wt% Pt. As shown by the data in Table 3, the difference in their channel size gave major differences in the C<sub>7</sub> isomer distribution at 1 atm. SAPO-11, a 10-membered oxygen ring system produced nearly all monobranched isomer, very low dibranched and zero tribranched isomer.

Table 3. Product Distribution (Wt%)

Temp. °C	SAPO-5	SAPO-11	
	350	350	425
2,2-DiMePentane	1.60	–	0.06
2,4-DiMePentane	2.27	0.05	0.64
2,2,3-TriMeButane	0.29	–	–
3,3-DiMePentane	1.10	–	0.05
2,3-DiMePentane	3.60	0.07	0.99
2-MeHexane	14.34	4.90	19.91
3-MeHexane	15.62	3.43	19.59
3-EtPentane	1.44	–	–
<i>n</i> -heptane	44.12	89.45	43.70

Source: Campelo et al. (1995) (12)

Martens et al. (13,14) studied the alkane conversions relevant to the catalytic dewaxing of diesel with ZSM-22 (TON) and SAPO-11 (AEL). Their results were quite different from those reported by Campelo et al. (12) and Miller (10). They showed a substantial level of *n*-C<sub>8</sub>-C<sub>11</sub> alkane isomerization to multibranching isomers and proposed that the catalytic reactions occur at the external crystal surface and named it “Pore mouth and key-lock catalysis” (or cage or window effect). This selective “Pore mouth and key-lock catalysis” was further confirmed by Souverijns et al. on Pt/ZSM-22 (TON) on the hydro- isomerization of *n*-C<sub>8</sub>-C<sub>11</sub> alkanes (15) and the hydro- isomerization of *n*-heptadecane (*n*-C<sub>17</sub>) at 3.5 atm total pressure and 350/1 H<sub>2</sub>/alkane at 180-260°C (16). As shown in Figure 1, the yield of multibranching C<sub>17</sub> isomers increased at high conversion to as high as 64 wt % with little hydrocracking compared to the data obtained with a Pt/H-Y (FAU) zeolite.

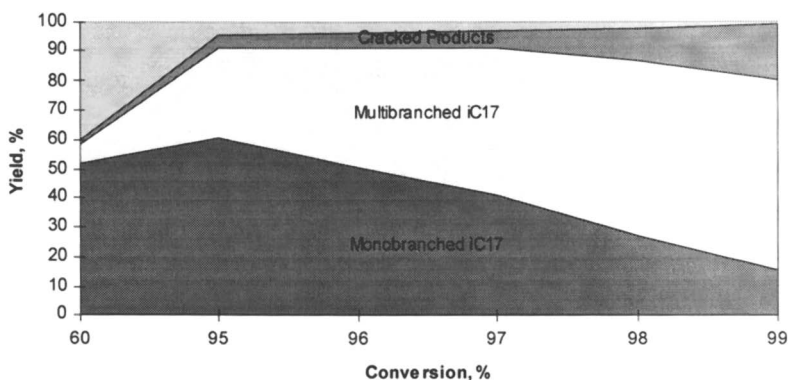


Figure 1 Product Distribution, Wt %. Source: Souverijns et al. (1998)(16).



Table 4 shows the percent of the key isomer, dimethyl-branched, obtained under similar reaction conditions (15).

Table 4. "Pore mouth and key-lock catalysis"

Feed	Key Isomer	Content, %
<i>n</i> -C <sub>11</sub>	2,8-DM C <sub>9</sub>	50
<i>n</i> -C <sub>10</sub>	2,7-DM C <sub>8</sub>	88
<i>n</i> -C <sub>9</sub>	2,6-DM C <sub>7</sub>	62
<i>n</i> -C <sub>8</sub>	2,5-DM C <sub>6</sub>	75

Source: Souverijns et al. (1997) (15).

Selective Skeletal Butene Isomerization - Butene isomerization over MFI, FER, TON, and EU-1 at 350°C was studied by Guisnet et al. (17). They observed the presence of primary products including propene and pentenes on all the fresh catalyst and suggested that the skeletal butene isomerization operates at least partly through oligomerization-isomerization-cracking steps (bimolecular mechanism). Earlier Guisnet et al. (18) found high selectivity of isobutene for partially coked Ferrierite (FER) catalyst and proposed a new monomolecular mechanism (not involving primary carbenium ions), involving carbocations formed with benzylic carbocations and *n*-butene to secondary carbenium ions which isomerize through hydride and methyl shift to form isobutene selectively instead of dimerization-cracking mechanism over the uncoked catalyst to form C<sub>3</sub>-C<sub>5</sub> olefin isomers.

Suib's group, Xu et al. (19,20) earlier found similar result with fresh Ferrierite, and ZSM-23 (MTT) and they also found that coke formation has a profound effect on the shape selectivity of zeolites with intersecting channels of 10 and 8-membered oxygen ring openings.

Houzvicka and Ponc (21) studied the same reaction over SAPO-11 (AEL), another unidimensional molecular sieve with non-intersecting, 10-membered ring channels and were convinced that the prevailing mechanism of skeletal isomerization of butene is monomolecular. The bimolecular mechanism, which is responsible for the formation of byproducts, is suppressed when using the unidimensional 10-ring molecular sieve.

The unusual catalytic properties of these non-intersecting medium pore molecular sieves bring back an old story on a non-intersecting 12-membered oxygen ring zeolite MAZ (ZSM-4, Mazzite) in light paraffin disproportionation (22,23). Compared to other 12-membered oxygen ring zeolites such as the unsteamed REX, liquid phase reaction with *n*-pentane was studied under autogenous pressure at 215°C. Not all superactive zeolites were found to be the same. Among all the catalysts tested, only ZSM-4 showed a remarkably high activity (over 80 times higher than the

next catalyst) for isomerization and disproportionation reactions, the latter made a substantial amount of hexanes from pentanes. Because of its low octane rating, *n*-pentane had a product value as low as natural gas. Upgrading it to isopentane, which has a good octane rating and C<sub>6</sub> hydrocarbons could have a significant impact on refining economics. Furthermore, the C<sub>6</sub> hydrocarbons made from *n*-pentane were in chemical equilibrium with all the high octane branched isomers (Table 5).

Table 5. Distribution of Hexane Isomers from *n*-Pentane

	Observed	Equilibrium
<i>n</i> -hexane	20	18
2,2-dimethylbutane	15	19
2,3-dimethylbutane + 3-methylpentane	44	42
2-methylpentane	22	21

Source: Chen (1986) (23).

The uniqueness of ZSM-4 for this reaction was attributed to its non-intersecting 12-membered oxygen ring channels. Unfortunately, ZSM-4, the only one of its kind available in the early 70's, was not stable enough for industrial application and the subject has been neglected ever since. Other members of this group such as ZSM-12 (MTW), SAPO-5 (AFI), Linde Type L (LTL), MAPO-36 (ATS) and SAPO-31 (ATO) are potentially attractive candidates for this reaction.

Another interesting reaction is the dehydrocyclization of *n*-hexane over Pt/BaKL, which has already been commercialized. In view of its extreme sensitivity to sulfur (24), it is well known that the feedstock must be hydrodesulfurized. Nash et al. (25) investigated whether other impurities such as a trace amount of oxygenates in the hexane produced by the Fischer-Tropsch synthesis could have similar adverse effect. Fortunately, they found that their Pt/KL catalyst could tolerate up to 1% of oxygenates without losing activity and selectivity and they identified CO to be the deactivator.

3) An unusual two, non-intersecting pore system molecular sieve -- MCM-22 (MWW).

MCM-22 is a unique zeolite first synthesized by Rubin and Chu (26), using hexa-methyleneimine (HMI) as the directing agent. The synthesized product of unknown structure is identified as MCM-22 precursor or MCM-22(P). MCM-22(P) after calcination at 538°C, undergoes a change in its structure to produce MCM-22, which has a 2-dimensional framework topology and some unique and unusual structural features. It is a layered thin platelet zeolite comprised of two, non-intersecting pore systems: (1) within each

thin platelet layer, there is a 2-dimensional sinusoidal 10-membered oxygen ring channels, (approximately  $6.5 \times 6.0 \text{ \AA}$ ) and (2) the layers are bonded by 12-membered oxygen supercages (approximately  $7.1 \times 7.1 \times 18.2 \text{ \AA}$ ) as schematically represented in Figure 2. Thus, the external surface of the zeolite has opened supercages, which could play a significant role in catalysis (27). Its IZA Code: MWW was approved by the IZA Structure Commission on April 30, 1997 (28).

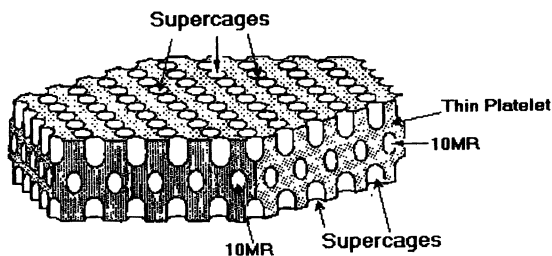


Figure 2 MCM-22

It reminded us the “nest effect” speculated by Fraenkel et al. (29) that the acid sites located in the “half cavities” on the external crystal surface of ZSM-5 could be active for a second type of shape selective reaction.

Corma et al. (30) repeated the synthesis of MCM-22 using hexamethyleneimine (HMI) as the directing agent and did an interesting catalytic diagnostic study of MCM-22 compared to ZSM-5 and zeolite Beta based on the isomerization/disproportionation of *meta*-xylene and *n*-decane hydroisomerization over these zeolites containing 0.75 wt% Pt. From the distribution of the trimethylbenzene isomers in xylene disproportionation, MCM-22 appeared to have larger pore volume than that of ZSM-5. On the other hand, in *n*-decane hydroisomerization, MCM-22 showed some of the ZSM-5's shape selectivity in the distribution of monobranched isomers. They concluded by assuming the presence in the structure of the 10-membered oxygen rings MCM-22 some larger cavities which would give it the typical 12-membered oxygen ring properties.

More recently, Cheng, et al. (31) observed the selective production of *ortho*-diethyl benzene at short contact times in the ethylation of benzene reaction. They concluded that the reaction must be occurring on the external surface because sterically *ortho*-diethyl benzene fits the “half cavities” best among the three isomers. They proved this point further by poisoning all the external acidity with molecules of a large nitrogen poison, 2,4,6-collidine, and then found that the initial diethylbenzene produced was the *para*-isomer, as could be expected from the 2-dimensional sinusoidal 10-membered oxygen ring channels. The structural studies on MCM-22 (32) support the presence

of “half cavities” and possibly the importance of the “nest effect” proposed more than 20 years ago.

MCM-22 has found many potential applications, including olefin isomerization, aromatics alkylation to ethylbenzene, cumene; catalytic cracking, and hydrocracking among others (30).

Zeolite MCM-49 (33) is a directly synthesized MCM-22 type zeolite without going through the precursor step. It uses the same directing agent (HMI, and other organic amines such as cycloalkylamine, piperidine, etc.) as is used in the synthesis of MCM-22 except that its synthesis uses a different ratio of organic directing agent to inorganic cations in the synthesis mixture.

MCM-36 (27,34) is the first pillared molecular sieve with zeolitic properties. It is produced by first reacting the MCM-22(P) wet cake with a swelling reagent, hexadecyl-trimethyl-ammonium hydroxide ( $C_{16}TMA-OH$ ) for 96 hours in a steambox to produce a swollen material, and then pillared with tetraethylorthosilicate or tetramethylammonium silicate solutions. Thus the thin MCM-22 platelet layers are separated by  $\sim 25$  Å thick interlayer strata with mesopores ranging between 30 and 35 Å.

#### 4) Mesoporous Molecular Sieves

Ultra large pore molecular sieves, M41S (35,36,37), represent a family of mesoporous molecular sieves having uniform large pores ranging from 16 to  $100^+$  Å. Notable members include MCM-41, MCM-48 and MCM-50. They can be synthesized in a variety of chemical compositions including Si, Al, Fe, W, Ti, Zr, etc.

By reacting their silanols with a variety of compounds such as  $(CH_3)_3SiCl$  and  $((CH_3)_3Si)_2O$ , it is possible to reduce the pore volume and change their hydrophobicity.

Tatsumi et al. (38) reported the increase in the activity of titanium containing MCM-41, MCM-48 by trimethylsilylation in the liquid phase oxidation of cyclohexene by  $H_2O_2$  at  $50^\circ C$ . The large pore mesoporous molecular sieves also allow the anchoring of homogeneous catalyst (39).

## Modification Of Molecular Sieves

Many methods have been developed over the years to modify the activity, stability and selectivity in shape selective catalysis. Following is a list of several new methods:

- 1) The improvement of the activity and hydrothermal stability of zeolites as FCC catalysts was achieved by incorporating phosphorus in its formulation (40).
- 2) A new FCC catalyst for the production of light olefins is formulated to contain a rare earth ZRP (MFI) zeolite, modified by aluminum phosphate (41).
- 3) Significantly higher activity, selectivity and catalyst stability in the Beckmann rearrangement of cyclohexanone oxime to  $\epsilon$ -Caprolactam was achieved by the selective dealumination of zeolite Beta via dicarboxylic acid treatment to eliminate all the external surface activity (42).
- 4) Product selectivity during the light olefin oligomerization reaction is improved by the use of molecules of a large nitrogen compound, 2,4,6-collidine, to reduce the surface activity of a medium pore zeolite catalyst (43).
- 5) A shape selective intracrystalline sulfonic acid catalyst is made by first covalently linking phenethyl groups to the framework silicon of a pure-silica zeolite Beta followed by sulfonation (44).
- 6) The pore diameter is reduced and the functionality of a mesoporous MCM-41 added by introducing organic groups of desired sizes to obtain alkyl, alkylamine and alkylamide bonded phases (45).

## Advances in Industrial Applications

### 1. High Energy High Density Fuels

High energy high density fuels have the potential value to boost the energy of conventional jet fuels and for military applications, such as rocket fuels. Jet fuels are a special type of distillate fuels high in flash point ( $>170^{\circ}\text{C}$ ) to reduce fire hazard during refueling; high in heating value for long flying range; and low in freeze or pour point for high altitude. For example, the commercial jet fuel, Jet A, has a boiling range of 170 to 270  $^{\circ}\text{C}$  and a freeze point of  $-40^{\circ}\text{C}$ , and the premium military jet fuel, JP-7, specifies an even narrower boiling range because it also requires a minimum heating value of 34,280 MJ/m<sup>3</sup> or 123,000 BTU/Gal., which limits its aromatics content to 5 vol % maximum.

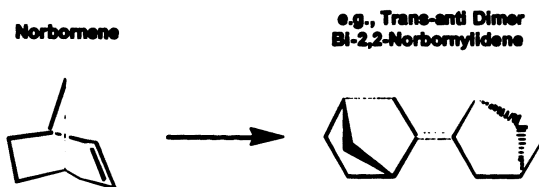
Earlier, by catalytic dewaxing using ZSM-5 (MFI), we found that the supply of Jet A could be increased by more than 25% by the inclusion of higher boiling range kerosene and meet all the quality requirements. The manufacture of high energy jet fuels, such as the premium military jet fuel, JP-7, is possible by dewaxing waxy crudes over ZSM-5. Since then, with the discovery of the non-intersecting one dimensional channel medium pore structures, such as the Theta-1 (TON, ZSM-22), ZSM-23 (MTT) and SAPO-11(AEL), catalytic dewaxing by dual functional hydroisomerization was found to be an effective system to produce even higher

quality  $-40^{\circ}\text{C}$  freeze point high energy high density jet fuels ( $>34,500\text{ MJ/m}^3$  or  $123,934\text{ BTU/Gal}$ ,  $0.79$  specific gravity, and  $6.58\text{ lb./gal}$ ) (46).

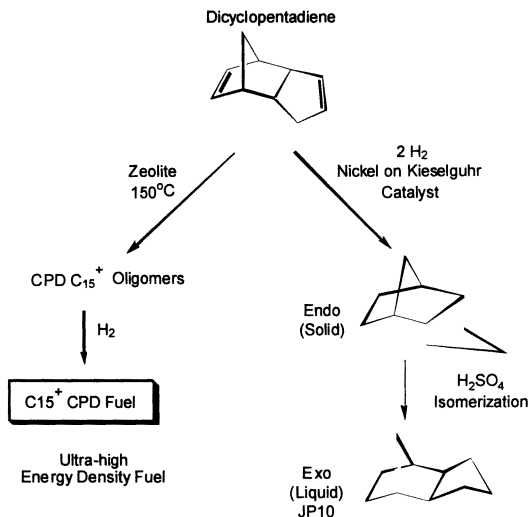
The current commercial military rocket fuel, JP-10 ( $39,580\text{ MJ/M}^3$  or  $142,000\text{ BTU/Gal}$ ,  $0.94$  specific gravity, and  $7.83\text{ lb./gal}$ ), is an expensive fuel. This much higher density product is prepared by the synthesis of *exo*-3, 4, 8, 9-tetrahydro-dicyclopentadiene. The synthesis starts with the hydrogenation of an endo-dicyclopentadiene to a solid endo-tetrahydrodicyclopentadiene, which is then isomerized to the *exo*-tetrahydro-dicyclopentadiene liquid over sulfuric acid or  $\text{AlCl}_3$ .

Similar high density high energy fuels meeting or exceeding the specifications of JP-10 could be produced using the medium pore zeolite catalyst. For example, liquid phase oligomerization of norbornene over ZSM-5 produces an oligomer (about 80% dimers and 20% trimers) which has a  $-45^{\circ}\text{C}$  pour point and a heating value of  $41,780\text{ MJ/M}^3$  ( $149,900\text{ BTU/Gal}$ ,  $1.0$  specific gravity, and  $8.33\text{ lb./gal}$ ) (47). Norbornene has a cyclic "bridged" structure which is known to have high fluid densities, and therefore, high volumetric heats of combustion, but it is unsuitable as a high-energy fuel because its melting point is above room temperature ( $45^{\circ}\text{C}$ ). Although norbornene is not commercially available, it may be synthesized by reacting commercially available dicyclopentadiene with ethene via a thermal Diels-Alder condensation reaction (48).

Analysis of the oligomer indicated the presence of four dimers as *trans*-anti (as shown below), *cis*-anti, *cis*-syn and *trans*-syn bi-2,2-norbornylidenes, all having two-fold symmetry. The double bonds on the dimers are tetra-substituted and further shielded by two methylene bridges, making them less reactive toward further oligomerization, thereby promoting termination of the oligomerization at the dimer stage.



Direct liquid phase oligomerization of dicyclopentadiene over ZSM-5 produces  $\text{C}_{15}^+$  polycyclopentadienes which can be hydrogenated to a low viscosity liquid having a specific gravity of  $1.044$ , a freeze point of  $-34^{\circ}\text{C}$  and a heating value of  $43,260\text{ MJ/M}^3$  or  $155,000\text{ Btu/Gal}$  (49).



As of now, these new research findings still require additional process development for their commercialization.

## 2. Styrene Technology

The styrene monomer, for the polystyrene industry comes from ethylbenzene by its oxidative dehydrogenation. The estimate of the annual worldwide ethylbenzene production capacity has increased from more than 5.7 million metric tons in 1991 (50) to over 20 million metric tons in 1997 (31).

The first zeolite based environmentally friendly ethylbenzene process by alkylating benzene in the vapor phase with ethene was commercialized as the Mobil/Badger Ethylbenzene process using the ZSM-5 catalyst in 1976 (51.52), gradually replacing the low temperature liquid phase process using the Friedel-Crafts type catalysts.

Despite the higher energy recovery efficiency of the vapor phase process over the classical liquid phase process, the ability of utilizing dilute ethene as the feed stream, and long catalyst life, the higher temperature of the gas phase process cannot avoid completely the acid catalyzed interconversion of ethylbenzene to xylenes to produce <1000 ppm of xylenes impurities in the ethylbenzene product. In the 90's UOP introduced a zeolite USY (FAU) based liquid phase alkylation process which produces less than 10 ppm of xylenes in the ethylbenzene product, a feature welcomed by the polymer industry. Unfortunately, the large pore USY (12-membered oxygen ring system) fouls more rapidly and produces as expected, a larger amount of polyalkylbenzenes as the by-product than ZSM-5. Interestingly, UOP's Van Opdorp and Wood (53) found that catalyst fouling can be mitigated by the continuous addition of water.

Mobil continued to improve the vapor phase process. For example, in 1990 a 3rd Generation Ethylbenzene Process was commercialized which has two reactors operating at different temperatures, one for alkylation and the other for the transalkylation of the recycled effluent diethyl benzenes with benzene to increase the total yield of ethylbenzene.

The liquid phase alkylation technology also received significant research and development effort to improve yield, product purity, energy recovery, and catalyst stability. Mobil and Badger developed the liquid phase EBMax<sup>SM</sup> process based on a new zeolite MCM-22, in 1994 (54) and commercialized in Japan in 1995 (55). UOP and Lummus commercialized a zeolite beta based process in 1996 (56). Both processes carried out the transalkylation step also in the liquid phase. UOP stayed with the USY catalyst, while Mobil has developed TRANS-4 catalyst based on a proprietary zeolite.

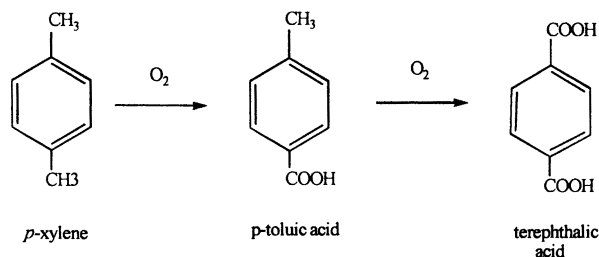
### 3. *Para*-Diethyl Benzene

Another *para*-selective alkylation product of commercial importance is *para*-diethyl benzene which is used in a sorption-desorption process, known as UOP's PAREX process, serving as the desorbing agent in removing the *para*-xylene from the adsorption tower. The diethyl benzene supplied by UOP comes from conventional refinery aromatic streams by physical separation of diethylbenzene isomers.

It is interesting to note that quite a number synthetic processes has now been commercialized in the Orient. Wang (57) reported a lower cost of the production of *para*-diethylbenzene via a one-step catalytic process. In this process, ethylbenzene is disproportionated over a zeolite catalyst modified by an in-situ silica deposition technology. Product selectivity higher than 99% has been achieved. Another *para*-diethylbenzene synthesis process was commercialized in the People's Republic of China by alkylating ethylbenzene with ethene (58), and in India a similar process was developed by alkylating ethylbenzene with ethanol (59).

### 4. Aromatic Polyester Technology

Polyethene terephthalate, the principal ingredient of polyester fibers, derives from terephthalic acid which is produced by the oxidation of *para*-xylene.





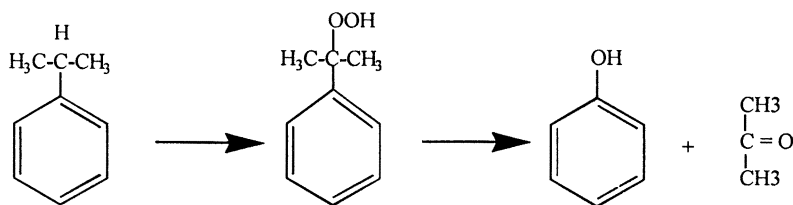
The discovery of the outstanding ability of ZSM-5 to isomerize xylenes with a minimum of side reactions, such as disproportionation to toluene and trimethylbenzenes (60,61) and the discovery of *para*-selectivity in the shape selective catalysis over ZSM-5 (62,63) revolutionized the *para*-xylene industry.

Over the last 25 years, Mobil developed a variety of industrial processes, including xylene isomerization, selective toluene disproportionation, and the selective alkylation of toluene with methanol. In 1997, a new process known as Mobil TransPlus<sup>sm</sup> process was co-developed and commercialized by the Chinese Petroleum Corporation (CPC) of Taiwan, ROC, using a new proprietary catalyst. This process effectively transalkylates C<sub>9</sub><sup>+</sup> heavy aromatics and toluene to mixed xylenes and simultaneously disproportionates toluene to additional mixed xylenes and high purity benzene (64).

## 5. Phenol Technology

Phenol is the basic material used in the production of a large variety of commercial products including the polyamides, such as nylon 6,6, a copolymer formed from 1,6-diaminohexane and adipic acid; nylon 6, a polymer of a cyclic amide,  $\epsilon$ -caprolactam. It is also the starting material for the production of phenolic resins and other plastics and polymers.

It is currently produced from cumene (isopropylbenzene) by its hydroperoxidation to cumene hydroperoxide (CHP) followed by cleavage to phenol with acetone as the major co-product. The usual catalyst is concentrated sulfuric acid.



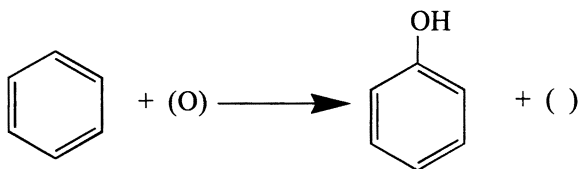
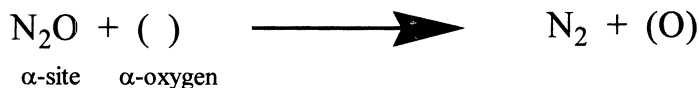
The annual world production capacity of cumene is estimated to be about 8 million metric tons and nearly 90% of it is used for the production of phenol and acetone (65,66). Zeolite was first used by Dow Chem. in 1992 by adding a modified dealuminized mordenite (3-DDM) as a transalkylation catalyst in their existing solid phosphoric acid (SPA) unit. Mobil and Badger developed a liquid phase cumene process first commercialized in 1996. This new technology employs a proprietary zeolite catalyst to produce very high yields of high purity cumene at low equipment

and operating costs, ready to replace the traditional process based on the SPA catalyst.

Perego et al. (67,68) reported the demonstration on a commercial scale at the Eni-Chem's plant in Porto Torres, Italy, a liquid phase benzene alkylation with propene using a new zeolite Beta catalyst with better catalyst stability, activity, yield and product purity than the traditional supported phosphoric acid catalyst. UOP also announced their zeolite based process (69).

More recently, Solutia, a new chemicals company which was spun off from Monsanto in 1997, announced the commercialization of a one-step phenol technology (70) based on the discovery of scientists in Russia's Boreskov Institute of Catalysis.

Kharitonov et al. (71) found that iron containing steamed ZSM-5 (MFI) or ZSM-11 (MEL) selectively catalyzes the oxidative hydroxylation of benzene to phenol by nitrous oxide ( $N_2O$ ), a rather expensive oxidant. At 100% phenol selectivity, one mole of nitrous oxide is consumed per mole of benzene converted and of course more nitrous oxide is consumed at lower phenol selectivity.

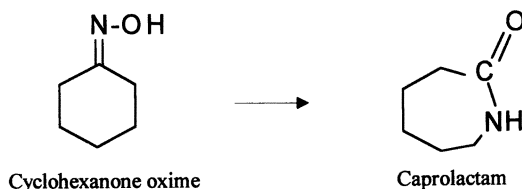


Chemistry Of The Oxidation Of Benzene To Phenol - it was proposed by the Russian scientists (72,73) that  $N_2O$  decomposes on the active sites (referred to as  $\alpha$ -sites) in Fe-ZSM-5 to generate a new type of surface  $\alpha$ -oxygen (O) which oxidizes benzene to phenol.

## 6. $\epsilon$ -Caprolactam Technology

$\epsilon$ -Caprolactam is the monomer for nylon 6 and is currently produced by liquid phase Beckmann rearrangement of cyclohexanone oxime using fuming sulfuric acid or concentrated sulfuric acid as a catalyst. Large amount of ammonia is used to neutralize the acid and co-produce ammonium sulfate as a fertilizer. It is possible that the commercialization of the one-step phenol technology discussed above could be synergistic to this type of fuming sulfuric acid process which could provide the expensive oxidant, nitrous oxide, for the benzene oxidation process. According to

Solutia's Weidhas (70) their new phenol technology fits the company's strategy of reducing the cost of making nylon 6,6.



Chemistry Of Beckmann Rearrangement Of Cyclohexanone Oxime To  $\epsilon$ -Caprolactam Over Zeolites - Using a zeolite to catalyze Beckmann rearrangement of cyclohexanone oxime to  $\epsilon$ -caprolactam was first reported in 1966 using 12-membered oxygen ring system zeolites (74). Considerable research studies have since been made by Haag and his coworkers at Mobil (75,76) to achieve higher activity, selectivity and catalyst stability by using low acidity steamed ZSM-5 or ZSM-11, and then by eliminating external surface activity with oxalic acid (Table 6).

Table 6. Effect of Acidity on Catalyst Performance

Catalyst: HZSM-5  
 Feed: 5% Cyclohexanone oxime in Benzene Solution (dried with NaA)  
 Feed rate: 1 LHSV of solution and 645 GHSV  $N_2$   
 Temperature: 300°C; Pressure: 1 atm.

Acidity, $\alpha$	105		1.5	
Hrs. on stream	2	54	1	68
Oxime Conv. Wt%	99.5	37.7	96.1	93.1
Caprolactam Selectivity, wt%	58.5	83.0	67.1	94.8

Source: Bell and Haag (1990) (75).

On the other hand, in view of the fact the reaction converts a 6-membered ring oxime to a larger 7-membered ring caprolactam, Sato et al. (77) concluded in their study of the same reaction over ZSM-5 that the reaction occurs on the external surface acidic sites. To resolve these controversial interpretations, Yashima and his group (78,79) extended their studies to a variety of zeolites of different pore sizes. They found that even CaA (LTA), and H-ferrierite (FER or ZSM-35) have better selectivity to  $\epsilon$ -caprolactam than HZSM-5 (Table 7), and led to the same conclusion that the reaction must be catalyzed by the external surface of the zeolites.

However, this conclusion is arguable because when they killed all the external acidity of H-ferrierite with 2,4-dimethyl quinoline, which killed all the activity to the cracking of 1,3,5-triisopropylbenzene, but still retained essentially all the activity and selectivity for  $\epsilon$ -caprolactam. Nevertheless, in view of the activity of CaA for the Beckmann rearrangement of cyclohexanone oxime to  $\epsilon$ -caprolactam, it

would be reasonable to conclude that the external surface sites of a zeolite, if not removed or deactivated, must be participating in this reaction.

Table 7. Performance of Various Zeolites

Feed: 15% Cyclohexanone oxime in Benzene and He, 4/35/61 mol ratio  
 Feed Rate: 0.098 Mols feed per hr per gm cat.  
 Temperature: 320°C; Pressure: 1 atm.

Zeolite	H-ferrierite		CaA		HZSM-5 (Si/Al=20)	
Hrs. on stream	0.25	1.75	0.25	1.75	0.25	1.75
Oxime Conv. Wt%	50	32	32	14	50	20
Caprolactam Selectivity, wt%	90.2	92.9	94.5	96.1	62.6	60.9

Source: Yashima, et al. (1994) (78).

They also compared the activity and selectivity of these zeolites with silicalite-1 (MFI, a high silica, low acidity HZSM-5). Their data (Table 8) confirmed the findings of Haag's group that significantly higher activity, selectivity and catalyst stability can be achieved by using low acidity and eliminating the external surface acidic sites.

Effect Of Solvent On The Beckmann Rearrangement Of Cyclohexanone Oxime To  $\epsilon$ -Caprolactam Over Zeolites - Benzene was used as the co-fed solvent in all the experiment studies conducted by these investigators. Yashima et al. (79) also assessed the effect of the type of solvent for cyclohexanone oxime on the selectivity for caprolactam formation. Under the same reaction conditions, ethanol was found to increase the  $\epsilon$ -caprolactam selectivity of all the zeolites tested, but ethanol depressed the activity of low Si/Al zeolites and accelerated the activity of high Si/Al zeolites (Table 9). Any zeolite will be more and more hydrophobic as its framework aluminum concentration is decreased, therefore the activity and selectivity could be influenced by the hydrophilic/hydrophobic property of the solvent in the desorption of reactants and products from the active sites.

Table 8. Performance of Various Zeolites

Feed: 15% Cyclohexanone oxime in Benzene and He, 4/35/61 mol ratio  
 Feed Rate: 0.098 Mols feed per hr per gm cat.  
 Temperature: 320°C  
 Pressure: 1 atm; Time on Stream: 1.75 Hr.

Zeolite	Si/Al	Oxime Conv. Wt%	Caprolactam Selectivity, wt%
Silicalite-1 (MFI)	>1000	66	93
HZSM-5 (MFI)	24	46*	40*
H-Ferrierite (FER)	10	76*	61*
CaA (LTA)	1	34*	89*

Source: Yashima, et al. (1997); \*values different from their 1994 data (78,79).

Table 9. Benzene vs. Ethanol as the Solvent

Feed: 15% Cyclohexanone oxime in Solvent and He, 4/35/61 mol ratio  
 Feed Rate: 0.098 Mols feed per hr per gm cat.  
 Temperature: 320°C; Pressure: 1 atm; Time on Stream: 1.75 Hr.

Zeolite	Solvent	Oxime Conv. Wt%	Caprolactam Selectivity, wt%
Silicalite-1 (MFI)	Benzene	66	93
Silicalite-1 (MFI)	Ethanol	80	98
HZSM-5 (MFI)	Benzene	46	40
HZSM-5 (MFI)	Ethanol	82	88
H-Ferrierite (FER)	Benzene	76	61
H-Ferrierite (FER)	Ethanol	54	84
CaA (LTA)	Benzene	34	89
CaA (LTA)	Ethanol	34	91

Source: Yashima, et al. (1997) (79).

## New Opportunities in Shape Selective Catalysis

### 1. Linear Alkylbenzenes

Long chain linear alkylbenzenes are currently produced by the HF technology. The discovery of new molecular sieves offers an opportunity to selectively produce the desired 2-phenyl linear C<sub>10</sub> to C<sub>14</sub> alkylbenzenes for the detergent industry.

### 2. Alkylation of Naphthalene and Biphenyl

Advanced polymers such as polyethylene naphthalate (PEN) and polybutylene naphthalate (PBN) requires 2,6-dialkyl naphthalenes (2,6-DAN) for making the monomers. Shape selective alkylation of naphthalene and biphenyl over molecular sieves catalysts to produce the desired isomer has attracted some attention as recently reviewed by Song (80).

Compared to monocyclic hydrocarbons, it is more difficult to achieve high selectivity because of the larger number of possible isomers. With the availability of a large number of new molecular sieves, it is quite possible that the shape selective alkylation and/or transalkylation to obtain the desired isomer can be achieved.

### 3. Update of In Vivo "Shape Selective Catalysis" at Body Temperatures

Since 1994, Visek and Mangian at the College of Medicine, University of Illinois (81,82) first reported the beneficial effects of adding less than 0.5 wt % (equivalent to about 10 lbs/ton of feed) of NaZSM-5 to the diet of Sprague Dauley rats such as binding ammonia (NH<sub>3</sub> + NH<sub>4</sub><sup>+</sup>) and adsorbing dimethylamine which could lead to the formation of N-nitroso-dimethylamine, a known carcinogen. formed in the gastrointestinal tract. Their study has extended to the diet of chickens. There is suggestive evidence that NaZSM-5 has similar benefits.

The estimated annual quantity of NaZSM-5 required based on the production of animals in the U.S. alone could be as high as 5.5 million tons, much higher than its current use as industrial catalysts, if the cost of NaZSM-5 could be reduced to less than \$1.50 per lb. This cost estimate is derived from the relative dosage and the cost of other feed additives such as antibiotics.

Many years ago, with the objective of reducing the cost of zeolite synthesis, Chen et al. (83) studied the continuous crystallization of ZSM-5 by maintaining a steady state rate of rapid synthesis of the zeolite at below 100°C. Rollmann and Valyocsik (84) followed with the design of a continuous up-flow ZSM-5 crystallizer. Recently, Slangen et al. of the Netherlands (85) reported the continuous synthesis of zeolites, including ZSM-5 using a tubular reactor. Additional effort in this area would certainly reduce the cost of the synthesis of NaZSM-5 and make it possible to use it as a feed additive.

#### 4. Aromatization Of Natural Gas Under Non-Oxidative Condition

The aromatization of light paraffins ( $C_3^+$ ) over the ZSM-5 was discovered by me in the late 60's, now known as the M-2 Forming to produce BTX aromatics (86,87). It was extended to the upgrading of ethane in the 70's during the Middle East Oil Crisis (88,89) using metal loaded ZSM-5, but the aromatization of methane was not achieved until researchers at the Dalian Institute of Chemical Physics reported in 1993 (90) the production of 100% benzene and hydrogen using a Mo/ZSM-5 at 700°C in the laboratory. Methane conversion increased at higher pressures. At 2 atm. and employing a 50/1  $SiO_2/Al_2O_3$  ratio Mo/ZSM-5, methane conversion of 7.2% was observed.

In a more recent paper, Lunsford's group attempted to characterize the active sites of a Mo/ZSM-5 catalyst for the conversion of methane to benzene (91). They found that the exposure of a 2 wt% Mo/ZSM-5 ( $SiO_2/Al_2O_3 = 50$ ) catalyst to  $CH_4$  or  $CH_4/H_2$  at 700°C causes reduction of Mo ions to  $Mo_2C$ , rather than to metallic Mo. Benzene selectivity has an induction period. It increases with on stream time and after the reaction reaches steady state, about 60-80% of Mo species are present in the form of  $Mo_2C$  while the rest remain present as  $Mo_4^+$  and  $Mo_5^+$  and are not reduced even when the catalyst is treated in  $CH_4/H_2$  at 700°C for many hours. It is believed that the clean surface of  $Mo_2C$  may be too reactive to form higher hydrocarbons and a "coked modified  $Mo_2C$ " may be the actual active species in the formation of ethylene as the reaction intermediate.

#### 5. Hydrogen Fuel Cells For Transportation

The U.S. Department of Energy (DOE) manages a National Hydrogen Program. In this role, DOE acts as a catalyst through partnerships with industry. This program has set a goal for 25% of all new vehicles sold in the United States in 2010 to be hydrogen powered, either as hybrids or as fuel cell vehicles. This will result in an important reduction in  $NO_x$ , CO, and  $CO_2$  emissions.

A consortium that includes the City of Palm Desert, California, the Schatz Energy Research Center, and E.I. DuPont de Nemours & Co. among other activities, is currently working on a hydrogen-fueled, Proton Exchange Membrane (PEM) fuel cell for the future hydrogen-based transportation vehicles, including the test of more conductive membrane, such as the Nafion<sup>®</sup> 1135 experimental membrane.

Daimler-Benz AG, Ford Motor Company, and Ballard Power Systems jointly own DBB Fuel Cell Engines GmbH, which is responsible for fuel-cell systems. They announced in August 1998 (92) a joint enterprise -- Ecostar Electric Drive Systems Company to put high-volume fuel-cell production vehicles on the road by 2004. These fuel-cell vehicles could either powered directly by stored high-pressure hydrogen or methanol using an onboard steam reformer (93).

On board production of hydrogen by steam reforming of gasoline fuel was first patented by Newkirk and Abel (94) in 1972. A pre-engine converter concept (95) presented the data of attaching a ZSM-5 catalytic reactor to an internal combustion engine to convert a low octane liquid fuel to a high octane gas/liquid fuel in 1974. Since then, the chemistry of converting light paraffins to hydrogen and aromatics over metal loaded medium pore zeolites has advanced to the stage that at least in the laboratory, it is already possible to convert methane directly to benzene and hydrogen (90,91). My opinion is that instead of converting a hydrocarbon fuel to hydrogen and CO<sub>x</sub> by steam reforming, additional research and development effort in paraffin aromatization could lead to a pre-engine converter designed to convert a hydrogen rich fossil fuel to co-produce hydrogen for the fuel cells and aromatic petrochemicals which could be recovered during refueling the vehicle. For example, 2 mols of propane could yield 3 mols of hydrogen and 1 mol of benzene.

## Conclusions

The commercial application of shape selective catalysis continues to blossom with advanced technologies in petroleum refining and petrochemical industries since its inception in the late 1950s. Its extension to other industries may include the fine chemicals and pharmaceuticals (80,96), the automobile engines, the upgrading of natural gas and the production of animal feed additives. We welcome innovations and scientific understandings in selective hydroisomerization reactions, alkylation of polycyclic aromatics and the selective oxidation chemistry; similar activities in the synthesis of new molecular sieves and in the modification and formulation of industrial catalysts.

However, the general de-emphasis of fundamental research by the energy industries in recent years is worrisome to me. By leaving all the fundamental research to the academic researchers will open wider the gap between knowing the basic principles governing shape selective catalysis and understanding the practical but often proprietary applications. The establishment of the rationality of the practical innovations is not only important to the advancement of the science of

catalysis but also crucial to future discoveries. This review paper will provide (I) a reasonable interpretation of some of the new shape selective catalytic processes and (II) our understanding and our confusion in terms of theories and basic principles. I hope it will alert the academic and industrial researchers to work toward closing the gap for the sake of science and technology.

## References

1. Chen, N. Y.; Maziuk, J.; Schwartz, A. B.; Weisz, P. B. *Oil Gas J.* **1968** *66* (47), 154.
2. Chen, N. Y.; Lucki, S. J.; Garwood, W. E., U.S. Pat. 3,700,585, Oct. 24, 1972, Filed on Oct. 10, 1969.
3. Chen, N. Y.; Garwood, W. E. *J. Catal.* **1978**, *52*, 453.
4. Meier, W. M.; Olson, D. H.; Baerlocher, Ch. *Atlas of Zeolite Structure Types*, 4th Revised Edition, Intern. Zeolite Assoc. Elsevier, Boston, MA, 1996.
5. Borghard, W. S.; Hanlon, R. T.; Schramm, S. E., U.S. Pat. 5,362,378, Nov. 8, 1994.
6. Borghard, W. S.; Degnan, T.,F. Jr.; Mazzone, D. N., U.S. Pat. 5,643,440, Jul. 1, 1997.
7. Chen, N. Y.; Degnan, T. F. Jr.; Kennedy, C. R.; Ketkar, A. B.; Koenig, L. R.; Ware; R. A., U.S. Pat. 4,911,823, Mar. 27, 1990.
8. Chen, N. Y.; Garwood, W. E.; Dwyer, F. G. *Shape Selective Catalysis in Industrial Applications; Second Ed., Revised and Expanded*; Chemical Industries v. 65; Marcel Dekker, NY, 1996, Chapter 1-5 pp 13-190.
9. O'Rear, D. J.; Scheuerman, G. L. paper presented at Div. Petrol. Chem. 214th Nat. Mtg., Am. Chem. Soc. Las Vegas, NV, Sep. 7-11, 1997.
10. Miller, S. J. *Microporous Materials* **1994**, *2*, 439.
11. Chen, N. Y.; Garwood, W. E.; McCullen, S. B. U.S. Pat. 4,814,543, Mar. 21, 1989.
12. Campelo, J. M.; Lafont, F.; Marinas, J. M., Cordoba, U. *J. Catal.* **1995**, *156*, 11.
13. Martens, J. A.; Parton, R. F.; Uytterhoeven, L.; Jacobs, P. A. *Appl. Catal.* **1991**,*48*, 95.
14. Martens, J. A.; Souverijns, W.; Verrelst, W.; Parton, R. F.; Froment, G. F.; Jacobs, P.A. *Angew. Chem. Int. Ed.* **1995**, *34*, 2528.
15. Souverijns, W.; Froment, G. F.; Martens, J. A.; Uytterhoeven, L.; Jacobs. P. A. *Stud. Surf. Sci. Catal.* **1997**, *105B*, 1285.
16. Souverijns, W.; Martens, J. A.; Froment, G. F.; Jacobs, P. A. *J. Catal.* **1998**, *174*, 177.
17. Guisnet, M.; Andy, P.; Gnep, N. S.; Benazzi, E.; Travers, C. paper A27, 12th Intern. Zeolite Conf. Baltimore, MD, Jul. 5-10, 1998.



18. Guisnet, M.; Travers, C.; Andy, P.; Gnep N. S.; Benazzi, E. *Stud. Surf. Sci. Catal.* **1997**, *105B*, 1365.
19. Xu, W. Q.; Yin, Y.G.; Suib, S. L.; O'Young, C. L.; *J. Catal.* **1994**, *150*, 34.
20. Xu, W.Q.; O'Young, C. L.; Yin, Y.G.; Suib, S. L. *J. Phys. Chem.* **1995**, *99*, 758.
21. Houzvicka, J.; Ponec, V. *Ind. Eng. Chem. Res.* **1997**, *36*, 1424.
22. Chen, N. Y.; Lucki, S. J., U.S. Pat. 3,812,199, May 21, 1974..
23. Chen, N. Y. "Disproportionation of Paraffins I. Pentanes", *Proc. 7th Intern. Zeolite Conf.* Kodansha Ltd. Tokyo, Japan, 1986, pp.653-60.
24. Derouane, E. G.; Vanderveken, D. *Appl. Catal.* **1988**, *45*, L15.
25. Nash, R. J.; Dry, M. E.; O'Connor, C. T. "The Effect Of Oxygenates On The *n*-Hexane Aromatization Activity Of Pt/KL", paper A24, 12th Intern. Zeolite Conf. Baltimore, MD, Jul. 5-10, 1998.
26. Rubin, M. K.; Chu, P., U.S. Pat. 4,954,325, Sep. 4, 1990.
27. Leonowicz, M. E.; Lawton, J. A.; Lawton, S. L.; Rubin, M. K. *Science* **1994**, *264*, 1910.
28. IZA web site: <http://www.iza-sc.ethz.ch/IZA-SC/updates/Updates.html> Sep. 1998.
29. Fraenkel, D.; Cherniavsky, M.; Levy, M. *Proc, 8th Intern. Congr, Catal.* **1984**, *4*, 545.
30. Corma, A.; Corell, C.; Llopis, F.; Martinex, A.; Perez-Pariente, *J. Appl. Catal. A: General* **1994**, *115*, 121.
31. Cheng, J. C.; Beck, J. S.; Mazzone, D. N.; Venkat, C. R.; Degnan, T. F. "EBMax<sup>sm</sup> - A New Process For Ethylbenzene Production" paper IL-4, 3rd Tokyo Conf. on Advan. Catal. Sci. and Tech., Tokyo, Japan. July 19 - 24, 1998.
32. Kennedy, G. J.; Lawton, S. L.; Rubin, M. K. *J. Am. Chem. Soc.* **1994**, *116*, 11000.
33. Lawton, S. L.; Fung, A. S.; Kennedy, G. J.; Alemany, L. B. Chang, C. D.; Hatzikos, G. H.; Lissy, D. N.; Rubin, M. K.; Timkin, H. C.; Steuernagel, S.; Woessner, D. E. *J. Phys. Chem.* **1996**, *100*, 3788.
34. Roth, W.J.; Kresge, C. T.; Vartuli, J.C.; Leonowicz, M. E.; Fung, A. S.; McCullen, S. B. *Stud. Surf. Sci. Catal.* **1995**, *94*, 301.
35. Beck, J. S.; Vartuli, J. C.; Roth, W. J.; Leonowicz, M. E.; Kresge, C. T.; Schmitt, K. D.; Chu, C. T-W. *J. Am. Chem. Soc.* **1992**, *114*, 10834.
36. Kresge, C. T.; Leonowicz, M. E.; Roth, W. J.; Vartuli, J. C.; Beck, J. S. *Nature* **1992**, *359*, 710.
37. Roth, W.J., U.S. Pat. 5,595,715, Jan, 21, 1997.
38. Tatsumi, T.; Koyano, K. A.; Igarashi, N. "Activity enhancement by trimethylsilylation in liquid phase catalyzed by titanium containing mesoporous molecular sieves", paper presented at the 9th Republic of China - Japan Joint Symp. on Catal. Taiwan, ROC, Feb. 8-10, 1998.

39. Krijnen, S.; Abbenhuis, H. C. L.; Hanssen, R. W. J. M.; van Hooff, H. C.; van Santen, R. A. "Heterogenization Of A Novel Epoxidation Catalyst: Phase Immobilization Of A Titanium Silsesquioxane In An MCM-41 Molecular Sieve", paper A37, 12th Intern. Zeolite Conf. Baltimore, MD, Jul. 5-10, 1998.
40. Absil, R. P. L.; Degnan, T. F.; Hatzikos, G. H.; Kowalski, J. A.; Mebrahtu, T.; Yokomizo, G. H., U.S. Pat. 5,457,078, Oct. 10, 1995.
41. Shi, Z.; Shi, W.; Ye, S.; Ge, X.; Cao, P.; Liu, S.; Yang, X.; Fu, W.; Zhou, M.; He, M., U.S. Pat. 5,380,690, Jan. 10, 1995.
42. Apelian, M. R.; Degnan, T. F.; Fung, A. S.; Kennedy, G. J. *J. Phys. Chem.* **1996**, *100*, 16577.
43. Chen, C. S. H.; Bridger, R. F. *J. Catal.* **1996**, *161*, 687.
44. Jones, C. W.; Tsuji, K.; Davis, M. E. "Shape selective catalysis with organic-functionalized molecular sieves", paper B33, 12th Intern. Zeolite Conf. Baltimore, MD, Jul. 5-10, 1998.
45. Jaroniec, M.; Jaroniec, C. P.; Kruk, M.; Sayari, S. "Surface Modification Of Mesoporous Ordered Silicates With Organosilanes", paper A56, 12th Intern. Zeolite Conf. Baltimore, MD, Jul. 5-10, 1998.
46. Chen, N Y.; Garwood, W. E., U.S. Pat. 4,717,465, Jan. 5, 1988.
47. Audeh, C. A.; Boulton, J. R.; Kremer, R. A.; Xiong, Y. U.S. Pat. 5,461,181, Oct. 24, 1995.
48. Venuto, P. B. *Microporous Materials*, **1994**, *2*, 319.
49. Kremer, R. A.; Boulton, J. R., U.S. Pat. 5,446,222, Aug. 25, 1995.
50. Dwyer, F. G.; Ram, S. "Development and Commercialization of the Mobil/Badger Ethylbenzene Process," paper presented at the AIChE Spring Nat. Mtg., Houston, Apr. 7-11, 1991.
51. Dwyer, F. G.; Lewis, P. J.; Schneider, F. M. *Chem. Engr.* **1976**, *83*(1), 90.
52. Dwyer, F. G. *Catalysis of Organic Reactions*, W. R. Moser, ed., Chemical Industries v. 5; Marcel Dekker, NY, 1981, p 39.
53. Van Opdorp, P. J.; Wood, B. M., U.S. Pat. 5,177,285, Jan. 5, 1993.
54. Chu, P.; Landis, M. E.; Le, Q. N., U.S. Pat. 5,334,795, Aug. 2, 1994.
55. Maerz, B.; Chen, S. S.; Venkat, C. R.; Mazzone, D. N. *Hydrocarbon Tech. Intern.* **1996**, *21*.
56. Narsolis, F.; Woodle, G.; Gajda, G.; Ganghi, D. "High Performance Catalyst for Liquid Phase EB Technology," *Petroleum Technology Quarterly*, summer 1997, pp 77-81.
57. Wang, I. "Disproportionation and Transalkylation of alkylbenzenes over Zeolite", paper presented at the 9th Republic of China - Japan Joint Symp. on Catal. Taiwan, ROC, Feb. 8-10, 1998.

58. Gao, Z. "Recent Advances in Zeolite-based Catalytic Process in People's Republic of China", paper IL-9, 3rd Tokyo Conf. on Advan. Catal. Sci. and Tech. Tokyo, Japan, July 19 - 24, 1998.
59. Halgeri, A.B.; Das, J. "Design of Pore Size Regulated MFI Zeolite Catalysts and Development of Ecofriendly Process for para-dialkyl benzenes", paper IL-12, 3rd Tokyo Conf. on Advan. Catal. Sci. and Tech., Tokyo, Japan, July 19 - 24, 1998.
60. Haag, W. O.; Olson, D. H., U.S., Pat. 3,859,871, Dec. 24, 1974.
61. Haag, W. O.; Dwyer, F. G. "Aromatics Processing with Intermediate Pore Size Zeolite Catalysts," paper presented at the AIChE 8th Nat. Mtg., Boston, Aug. 19, 1979.
62. Chen, N. Y., U.S. Pat. 4,002,697, Jan. 11, 1977.
63. Chen, N. Y.; Kaeding, W. W.; Dwyer, F. G. *J. Am. Chem. Soc.* **1979**, *101*, 6783.
64. Absil, R. P. L.; Han, S.; Marler, D. O.; Shihabi, D. S.; Vartuli, J. C.; Varghese, P., U.S. Pat. 5,030,787, Jul. 9, 1991.
65. Meima, G.R.; van der Aalst, M. J. M.; Samson, M. S. U., Garces, J. M.; Lee, J. G. *Erdoel, Erdgas, Kohle* **1996**, *7/8*, 315.
66. Meima, G.R. *CATTECH* **1998**, *2* (No.1), 5.
67. Perego, C.; Amarilli, S.; Millini, R.; Bellussi, A. G.; Girotti, G.; Terzoni, G. *Microporous Materials* **1996**, *6*, 395.
68. Perego, C.; Amarilli, S.; Bellussi, G.; Cappellazzo, O.; Girotti, G. "Development and Industrial Application of a New Beta Zeolite Catalyst for the Production of Cumene," paper A34, 12th Intern. Zeolite Conf. Baltimore, MD, Jul. 5-10, 1998.
69. Jeanneret, J.; Greer, D.; Ho, P.; McGehee, J.; Shakir, H. *1997 Dewitt Petrochem. Rev. Houston, TX Mar. 1997*, pp G1-27.
70. Solutia Inc. Company Press Release, Mar. 10, 1998.
71. Kharitonov, A. S.; Panov, G. I.; Sheveleve, G. A.; Pirutko, L. V.; Voskresenskaya, T. P.; Soblev, V. I., U.S. Pat. 5,672,777, Sep. 30, 1997.
72. Soblev, V. I.; Dubkov, K. A.; Paukshtis, E. A.; Panov, G. I.; Pirutko, L. V.; Rodkin, M. A.; Kharitonov, A. S.; Panov, G. I. *Appl. Catal. A: General* **1996**, *141*, 185.
73. Panov, G. I.; Kharitonov, A. S.; Soblev, V. I. *Appl. Catal. A: General* **1993**, *98*, 1.
74. Venuto, P. B.; Landis, P. S. *J. Catal.* **1966**, *6*, 245.
75. Bell, W. K.; Haag, W. O., U.S. Pat. 4,927,924, May 22, 1990.
76. Apelian, M. R.; Bell, W. K.; Fung, A. S.; Haag, W. O.; Venkat, C., U.S. Pat. 5,292,880, Mar. 8, 1994.
77. Sato, H.; Hirose, K.; Kitamura, M.; Nakamura, Y. *Stud. Surf. Sci. Catal.* **1989**, *49*, 1213.

78. Yashima, T.; Miura, K.; Komatsu, T. *Stud. Surf. Sci. Catal.* **1994**, *84*, 1897.
79. Yashima, T.; Oka, N.; Komatsu, T. *Catal. Today* **1997**, *38*, 249.
80. Song, C. *Stud. Surf. Sci. Catal.* **1998**, *113*, 163.
81. Chen, N. Y.; Garwood, W. E.; Dwyer, F. G. *Shape Selective Catalysis in Industrial Applications; Second Ed., Revised and Expanded*; Chemical Industries v. 65; Marcel Dekker, NY, 1996, Chapter 8, pp 253-6.
82. Garwood, W. E.; Chu, P.; Visek, W. J.; Mangian, H. J. "Relationship of In Vitro Properties of Medium Pore Zeolite ZSM-5 to in Vivo Performance," Paper 326, Inorganic Div., Am. Chem. Soc. 207th Nat. Mtg., San Diego, Mar. 12-17, 1994.
83. Chen, N. Y.; Miale, J. N.; Reagan, R. J., U. S. Pat. 4,112,056, Dec. 14, 1978.
84. Rollmann, L. D.; Valyocsik, E. W., U. S. Pat. 4,374,093, Feb. 15, 1983.
85. Slangen, P. M.; Jansen, J. C.; Van Bekkum, H.; Hofland, G. W., van der Ham, F.; Witkamp, G. J. "Continuous Synthesis Of Zeolites Using A Tubular Reactor" paper B28, 12th Intern. Zeolite Conf. Baltimore, MD, Jul. 5-10, 1998.
86. Chen, N. Y., U.S. Pat. 3,767,568, Oct. 23, 1973.
87. Chen, N. Y.; Yan, T. Y. *Ind. Eng. Chem. Process Des. Dev.* **1986**, *25*, 151.
88. Chen, N. Y.; Haag, W. O., U.S. Pat. 4,100,218, Jul. 11, 1978.
89. Chen, N. Y.; Haag, W. O.; Huang, T. J., U.S. Pat. 4,260,839, Apr. 7, 1981.
90. Wang, L.; Tao, L.; Xie, M.; Huang, J.; Xu, Y. *Catal. Lett.* **1993**, *21*, 35.
91. Wang, D.; Lunsford J. H.; Rosynek, M. P. *J. Catal.* **1997**, *165*, 347.
92. EV world, "Ecostar Lights the Way for Fuel-Cell Vehicles," Internet "www.evworld.com" Aug. 18, 1998.
93. Thomas, C. E.; James, B. D. Hydrogen vs. Methanol: A Comparative Assessment for Fuel Cell Vehicles. Argonne National Laboratory Report ANL-94/44, Jul. 1995, Supplement 1 by Directed Technologies, Inc.
94. Newkirk, M. S.; Abel, J. L., U.S. Pat. 3,682,142, Aug. 8, 1972.
95. Chen, N. Y.; Lucki, S. J. *Approaches to Automotive Emissions Control*; R. W. Hurn, ed., Am. Chem. Soc. Symp. Ser. 1; Am. Chem. Soc.: Washington, D.C. 1974, pp 69-77.
96. Weitkamp, J.; Weiss, U.; Ernst, S. *Stud. Surf. Sci. Catal.* **1995**, *94*, 363.

## Chapter 4

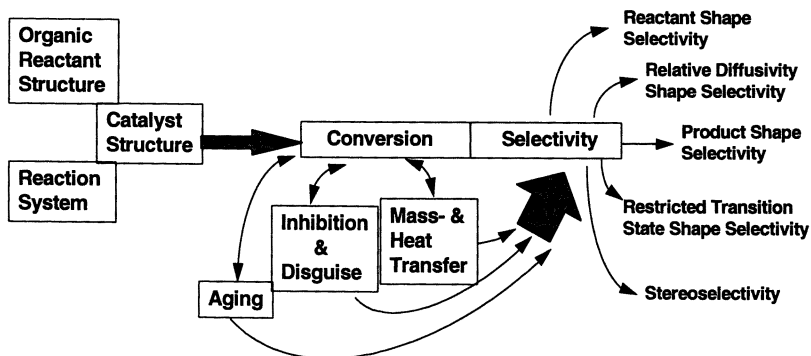
# Organic Catalysis over Zeolites and Other Molecular Sieves: Shape-Selective Effects in Catalytic Transformations

Paul B. Venuto

Consultant, 1073 Princeton Drive, Yardley, PA 19067

With the discovery of the ZSM-5 family of medium pore zeolites, there evolved a remarkable capability for *shape selective control* of reaction selectivity in zeolite catalysis. Recently, there has been steady expansion of organic catalysis into synthesis of fine chemicals, pharmaceuticals and the environmental area. Much of this effort involves *refined shape-selective applications* of medium pore zeolites and exploits the potentials of the growing number of new zeolites. The focus of such activity includes regiospecific aromatic substitutions, halogenation of aromatics, nucleophilic substitution over Cu zeolites, dehydrocyclization, selective catalytic hydrogenation, heterocyclic synthesis, selective partial oxidations, base catalysis, carbonyl condensation reactions, olefin oligomerizations, diverse isomerizations and some stereoselective reactions.

Structure-reactivity-selectivity effects in “classical” organic chemistry in solution or fluid phases---in the *absence* of the perturbing influence of zeolite micropores---are enormously complex in themselves. Variations in molecular structure are associated with steric, inductive, field, electronic and other effects which, under diverse reaction conditions, profoundly affect reaction selectivity. And when the situation is perturbed by conducting organic transformations within the micropores of a crystalline zeolite or other molecular sieve, many new dimensions of complexity are added to the reaction system. As shown in Figure 1, these new dimensions offer great opportunity for control of reaction pathways and selectivity, but the added considerations of diffusion and mass transfer effects must be carefully assessed.



**Figure 1.** Interaction of organic reactant, catalyst structure and reaction system in zeolite-catalyzed transformations: the genesis of shape selectivity.

From the 1960's through the early 1980's, numerous commercially important applications of zeolites as petroleum, petrochemical and synthetic fuels catalysts became well established. These included fluid catalytic cracking and hydrocracking using synthetic faujasite catalysts, reforming of light straight run naphtha with Pt/KBaL and paraffin isomerization over Pt/mordenite. But it remained for the discovery of ZSM-5 and other medium pore, high silica-alumina zeolites to enable a remarkable capability for *shape-selective control* of reaction selectivity. As illustrated in Table 1, this has led to significant industrial applications in aromatics processing (e.g., xylene isomerization, ethylbenzene synthesis and selective toluene disproportionation), catalytic dewaxing, ZSM-5 octane-enhancing additives in cracking, the methanol-to-gasoline process and other developments.

The potentials of shape-selective catalysis have also been greatly amplified by the added dimension of isomorphous substitution and the availability of a large variety of  $\text{AlPO}_4$ -, SAPO- and MeAPO-type compositions. Shape selectivity by mass transport discrimination includes at its extreme boundaries, complete *reactant* shape selectivity and *product* shape selectivity, but includes many subtle variations between these boundaries that are based on *relative diffusivities*. Spatioselectivity or *restricted transition state selectivity* can occur within zeolite microchannels when the pore size is insufficient to allow formation of the required transition states or intermediates (Figure 1). And there are many other variations that may involve pore mouth or external surface effects. A number of excellent reviews on shape-selectivity can be found in the literature, (e.g., 1-3). In the last 10 to 15 years moreover, there has been steady expansion of organic catalysis using zeolites, including significant thrusts into the synthesis of fine chemicals and intermediates, pharmaceuticals, and the environmental area. This is extensively documented in a,

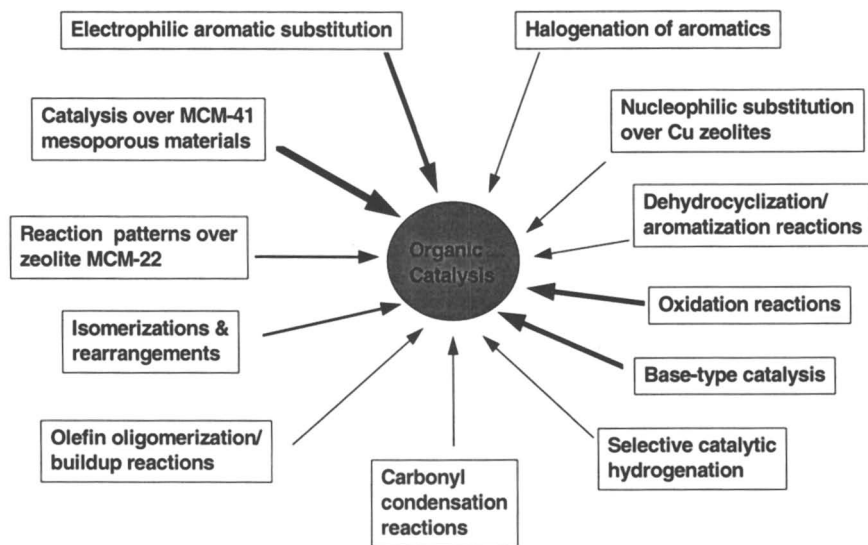
**Table 1**  
**Some Commercial Applications Utilizing Shape Selective Zeolites**

Process	Description
Fluid catalytic cracking	ZSM-5 as additive for octane-enhancement and generation of light olefins
Selectoform.	Octane-enhancement after reforming by selective paraffin cracking (erionite)
M-Forming	Post reforming process for octane-enhancement and benzene reduction via selective paraffin cracking and aromatic alkylation via cracking fragments
M2-Forming	High temperature conversion of paraffins and other aliphatics to BTX aromatics and light gas byproducts
MLDW, MDDW	Dewaxing of lube base stocks or distillates via selective cracking of <i>n</i> - and singly-branched paraffins, with preservation of essential lube molecules
MOGD	Processing of C <sub>2</sub> - C <sub>10</sub> olefins to gasoline and distillate via oligomerization, disproportionation and aromatization
MTG	Conversion of methanol to gasoline-range (C <sub>4</sub> - C <sub>10</sub> ) isoparaffins and aromatics
MTO	Conversion of methanol to C <sub>2</sub> - C <sub>5</sub> olefins but not aromatics
MVPI, MHTI, MHAI, MLPI	Xylene isomerization to give high yields of <i>p</i> -xylene; various catalytic systems and process modes
MTDP	Disproportionation of toluene to produce benzene and xylene with long cycle life and minimal side reactions
MEB	Synthesis of ethylbenzene in high yield with minimal side reactions
MBR	Reduction of benzene in reformat with octane boost by alkylation with light olefins and cracking of low octane paraffins
ISOFIN	Isomerization of <i>n</i> -butene/ <i>n</i> -pentene to corresponding <i>iso</i> -olefins; useful for ether synthesis

number of comprehensive recent reviews (4-10). Among others, commercial processes for manufacture of substituted pyridines, *tert*-butylamine, and 4-methylthiazole have been implemented, and, using the remarkable titanium zeolite material TS-1, mild oxidations for synthesis of hydroquinone from phenol and ammoxidation of cyclohexanone have been reported.

There is continuing aggressive exploration and scoping of the potentials for organic catalysis over zeolites in a variety of areas as shown in Figure 2, with continued progress in exploiting the potentials of the steadily increasing arsenal of new zeolites and molecular sieves (including the MCM-41 family of mesoporous materials and related compositions), and in understanding reaction mechanisms and the subtleties of structure-reactivity-selectivity relationships (11) in these complex systems.

Many of these explorations comprise refined and finely-tuned shape-selective applications of the ZSM-5 family of medium pore zeolites and even larger pore materials, often with emphasis on conversion of molecules with polar and/or multiple functional groups or other sensitive structural configurations.



**Figure 2.** Scope of recent activity in organic catalysis over zeolites. from a survey of the recent literature (11); thickness of arrows denotes relative intensity of effort.

A number of specific examples in organic catalysis over zeolites that demonstrate various aspects of shape-selective catalytic behaviour are worth noting: In the nucleophilic aromatic substitution of chlorobenzene with ammonia to form aniline over a variety of Cu-exchanged zeolites, improved selectivity for monoamination, i.e., formation of aniline rather than diphenylamine, was greater with Cu-mordenite and Cu-ZSM-5, probably from spatioselective inhibition effects (12). In the highly *para*-selective bromination of toluene to form bromo-toluenes at 25°C. in the presence of propylene oxide as promoter, a bulky Br<sub>2</sub>-oxirane complex was thought to increase steric restrictions favoring *para*-selectivity (13). In the dimerization of styrene over HY and H-beta at 72° C., a mixture of the *cis*- and *trans*- isomers of 1-methyl-3-phenyl indane was formed (14). A small but meaningful degree of *cis*-selectivity was observed with H-beta (*cis/trans* ratio ~ 1.3-1.4). Possible involvement of spatioselectivity, product selectivity by relative diffusion rates, or even external surface effects may explain this observation. Restricted transition state selectivity may also underly the stereoselective reduction of 4-*tert*-



butylcyclohexanone to *cis*-4-*tert*-butylcyclohexanol over zeolite beta in a Meerwein-Ponndorf-Verley reduction (*iso*-C<sub>3</sub>H<sub>7</sub>OH as reducing agent) as recently reported by the Delft group (15). Catalytic reaction patterns diagnostic of both 10-ring and 12-ring micropores have been observed in recent studies over zeolite MCM-22; the 10-ring behavior comprised tendencies toward shape selectivity (as in ZSM-5). Among a number of possible explanations for the 12-ring behavior, the proposal that reaction occurs in half-supercage "pockets" on the external surface is an interesting possibility (16).

A broad spectrum of selective catalytic oxidations have been reported under mild conditions using TS-1(Ti-ZSM-5) (e.g., see References 6 and 10). Product distributions in many of these reactions are enhanced via restricted transition state selectivity, i.e., *para*- and/or 1,2,4-substitution are favored, as well as minimization of coke and gas formation because of the negligible acidity. An interesting example in this area is the mild oxidation of aniline to azoxybenzene with H<sub>2</sub>O<sub>2</sub> over TS-1. In this reaction, which shows high selectivity for azoxybenzene (17), conversion was highly dependent on crystallite size. Mechanistically, however, it was thought that reactions with the mononuclear aromatics occurred *inside* the zeolite channels (e.g., the key catalytic step for transfer of reactive oxygen from the titanium-peroxo complex of TS-1 to aniline), while formation of the bulkier azobenzene and azoxybenzene probably occurred on the *external* surface. Also in the oxidation area, "ship-in-the-bottle" Fe phthalocyanine complexes occluded in NaY have been used as catalysts for the selective partial oxidation of cyclohexane to adipic acid with *tert*-butyl hydroperoxide (18). In synthesizing the catalyst, the constituents of the complex are brought into the ~12Å supercage of zeolite Y, and assembled *in situ*; after synthesis, the complex is entrapped (much like product shape selectivity), thus allowing reasonably effective "site isolation" and selective oxidation.

A question that has interested the catalytic community for some time is the reason for the highly effective light paraffin aromatization activity of Pt/KBaL zeolite. Although a number of interesting mechanistic explanations have been proposed (e.g., see Reference 10), there still remained a number of significant inconsistencies. A recent study (19) proposed that the high dehydrocyclization activity/selectivity of Pt/KBa L derives from intrinsic but *structure sensitive* catalytic properties inherent in large, clean (i.e., unblocked) Pt ensembles, whether these are within or outside zeolite channels. Apparently spatioselective inhibition of formation of coke precursors is provided by the protective environment of the one-dimensional L-zeolite channels, thus preserving a *clean* Pt surface for 1,6-diadsorption and aromatization. Also involving a Pt containing zeolite, selective catalytic hydrogenation of cinnamaldehyde can be cited as an example where interaction of the dimensions of the organic reactant, the metal particle and the zeolite pore lead to structure-sensitive reaction and controlled selectivity (20). Specifically, over Pt-containing beta catalysts prepared by different methods of activation, high selectivity for the *unsaturated* alcohol was obtained with beta containing large (> 20Å) Pt clusters, while both the *saturated* aldehyde and alcohol were obtained with compositions with small (< 10Å) Pt clusters.

Considering some early classical work (21), the abrupt cut-off at about C<sub>10</sub> with ZSM-5 and ZSM-11 in the methanol-to-gasoline reaction, with generation of essentially no A<sub>11+</sub> aromatics, can be related to restrictive transition state control dictated by the 10-membered ring zeolite, as can the unique resistance of ZSM-5 to coke formation in this reaction. Also, in the classical work of Olson and Haag on selective toluene disproportionation (22), there was a unique interplay and coupling of chemical and diffusion kinetics over coke-modified ZSM-5. The coke plugged a significant fraction of pores on the ZSM-5 surface, thus increasing channel tortuosity and lengthening the intracrystalline diffusion path. This allowed the competitive diffusion advantage of *p*-xylene over the *ortho*- and *meta*-isomers ( $D_{para} / D_{meta, or ortho} \sim 10^3 - 10^4$ ) to be enhanced significantly, while the longer intracrystalline residence time allowed rapid isomerization of the *ortho*- and *meta*- isomers to the *para*-isomer. This is an example of shape selectivity by relative diffusion rates that is of such great magnitude that it mimics shape selectivity by product exclusion.

Turning briefly to mesoporous materials, a moderately acidic MCM-41[30 Å] (Si/Al=95) was effective in the synthesis of the extremely bulky 6,8-di-*tert*-butyl-2-phenyl-2,3-dihydro[4,*H*]benzopyran from two very large reactants, (2,6-di-*tert*-butyl phenol and cinnamyl alcohol) (23); zeolite Y was ineffective even after introduction of some mesoporosity by controlled steaming. A pure silica MCM-41 [30Å] on which 40% heteropoly acid (H<sub>3</sub>PW<sub>12</sub>O<sub>40</sub>, size ~ 12 Å) was dispersed comprised a large-pore mesoporous catalyst that now had very strong protonic acid activity, but could still handle bulky organic molecules (24). This composition was effective in the synthesis of 2-(1-phenylethyl)-4-*tert*-butyl phenol from reaction of 4-*tert*-butyl phenol and styrene. However, even in this large mesoporous channel system, spatioselective constraints inhibited formation of the even bulkier di-alkylated product.

### Literature Cited

1. Weisz, P.B. *Pure Appl. Chem.*, **1980**, 52, 2091.
2. Chen, N.Y.; Garwood, W.E.; Dwyer, F.G. *Shape Selective Catalysis in Industrial Applications*, Marcel Dekker: New York, N.Y., Basel, **1989**, pp.1-303.
3. Weitkamp, J.; Ernst, S.; Dauns, H.; Gallei, E. *Chem. Ing. Tech.*, **1986**, 58, 623.
4. Chang, C.D.; Lang, W.H.; Bell, W.K. in *Catalysis of Organic Reactions*, Moser, W.R., Ed.; Marcel Dekker: New York, N.Y., Basel, **1981**, pp. 73-94.
5. van Bekkum, H.; Kouwenhoven, H.W. *Stud. Surf. Sci. Catal.*, **1988**, 41, 45.
6. Hoelderich, W.F.; Hesse, M.; Naumann, F. *Angew. Chem. Int. Ed. Engl.*, **1988**, 27, 226
7. Hoelderich, W.F.; van Bekkum, H. *Stud. Surf. Sci. Catal.*, **1991**, 58, 631.
8. Parton, R.F.; Jacobs, J.M.; Huybrechts, D.R.; Jacobs, P.A. *Stud. Surf. Sci. Catal.*, **1988**, 46, 163.
9. Dartt, C.B.; Davis, M.E. *Catalysis Today*, **1994**, 19, 151-186.

10. Venuto, P.B. *Microporous Mater.*, **1994**, 2, 297-411.
11. Venuto, P.B. *Stud. Surf. Sci. Catal.*, **1997**, 105, 811-852.
12. Burgers, M.H. W.; van Bekkum, H. *Stud. Surf. Sci. Catal.*, **1994**, 84, 1981.
13. de la Vega, F.; Sasson, Y.; Huddersman, K. *Zeolites*, **1993**, 13, 341.
14. Benito, A.; Corma, A.; Garcia, H.; Primo, J. *Appl. Catal. A: General*. **1994**, 116, 127-135.
15. Creighton, E. Thesis: *New Applications of Zeolite Beta in Selective Catalytic Hydrogenations*, (with Prof. H. van Bekkum), Delft Univ. Press: Delft. **1996**.
16. Ravishankar, R.; Bhattacharya, D.; Jacobs, N.E.; Sivasanker, S. *Microporous Mater.*, **1995**, 4, 83.
17. Selvam, T.; Ramaswamy, A.V. *Catal. Letters*, **1995**, 31, 104.
18. Parton, R.F.; Huybrechts, D.R.C.; Buskens, Ph.; Jacobs, P.A. *Stud. Surf. Sci., Catal.*, **1991**, 65, 47.
19. Iglesia, E.; Baumgartner, J.E. *Proc. 9th Int. Zeol. Conf.*, von Ballmoos. R.. Ed.: Butterworth-Heinemann: Boston, MA, **1993**, pp.421-431.
20. Gallezot, P.; Blanc, B.; Barthomeuf, D.; Pais da Silva, M.I. *Stud. Surf. Sci. Catal.*, **1994**, 84, 1433.
21. Chang, C. D. *Hydrocarbons From Methanol*, Marcel Dekker: New York. N.Y., Basel, **1983**, pp. 1-129.
22. Olson, D.H.; Haag, W.O. *ACS Symp. Ser.*, **1984**, 248, 275.
23. Armengol, E.; Cano, M.L.; Corma, A.; Garcia, H.; Navarro, M.T. *J.Chem. Soc., Chem. Commun.*, **1995**, 519.
24. Kozhevnikov, I.V.; Sinnema, A.; Jansen, R.J.J.; Pamin, K; van Bekkum. H. *Catal. Letters*, **1995**, 30, 241.

## Chapter 5

# Highly Efficient and Regioselective Cyclization Catalyzed by TS-1

Asim Bhaumik and Takashi Tatsumi

Engineering Research Institute, The University of Tokyo, Yayoi, Tokyo 113, Japan

Unsaturated alcohols **1**, having general formula  $R_1CH=CH(CH_2)_nCHR_2OH$  (where  $R_1, R_2 = H$  or  $CH_3$  and  $n = 1 - 3$ ) have been efficiently cyclized to the corresponding hydroxytetrahydrofuran or hydroxytetrahydropyran over medium pore titanium silicate molecular sieve, TS-1, in one pot at mild liquid phase reaction conditions using dilute hydrogen peroxide as oxidant. When there is a choice of the attack of the hydroxy nucleophile to either of the activated carbon atoms to lead to tetrahydrofuranol and tetrahydropyranol, the former exclusively formed regioselectively. When  $R_1$  / or  $R_2 = CH_3$ , between the diastereoisomeric products *trans* predominates over *cis*. In this cyclization reaction TS-1 epoxidizes the olefin and successively catalyzes the opening of the oxirane ring via intramolecular attack of hydroxy oxygen, being bifunctional in nature.

Widespread occurrence of the substituted tetrahydrofuran and tetrahydropyran rings in many classes of natural products made them valuable in the building blocks for the synthesis of various biologically active organic target molecules (*1*). Thus, a new method for the synthesis of these oxacyclic compounds is an important area of research. The convenient route for the stereoselective synthesis of these compounds involves an electrophilic activation of the double bond (*2,3*) in **1** followed by intramolecular nucleophilic attack of the oxygen atom of the terminal hydroxyl group. Ring closure of substituted 4-penten-1-oxy and 5-hexen-1-oxy radicals (*4,5*) is also a useful tool for the preparation of these compounds. Titanium silicate molecular sieve, TS-1 (*6*) having the medium pore MFI topology

has been used as an efficient, clean and selective oxidation catalyst over a decade under liquid phase heterogeneous reaction conditions in the presence of dilute hydrogen peroxide (7). Until this date various TS-1 / H<sub>2</sub>O<sub>2</sub> catalyzed organic transformations (8-13) have been reported, some of which have been commercialized or tested in a large pilot plant and the aim of the recent research is to find out its applicability to other transformations. Here, we report a highly efficient regioselective cyclization of such olefinic alcohols over TS-1, under mild reaction conditions using dilute hydrogen peroxide as oxidant.

### Synthesis and Characterization of TS-1

TS-1 used in the present study was synthesized by modifying the standard literature procedure (6) and thoroughly characterized through XRD and FT IR and UV-Vis spectroscopies. The liquid phase reaction was carried out in a two-necked glass reactor fitted with water condenser under inert N<sub>2</sub> atmosphere at the required temperature (298 K and 333 K) with vigorous stirring. In a typical reaction the following constituents were employed : 0.02 mole substrate, 0.02 mole H<sub>2</sub>O<sub>2</sub> (30 wt % aqueous), catalyst (TS-1, Si / Ti = 29) 20 wt % with respect to the substrate, 10 g acetone, 2-butanol or H<sub>2</sub>O (in the three phase system). At various reaction times products were analyzed by a capillary gas chromatograph (Shimadzu 14 A, OV-1 and Chiraldex G-TA with Flame Ionization Detector). Products were identified through GC retention times and GC-MS splitting patterns of the authentic samples. When authentic samples were unavailable identification was done through <sup>1</sup>H NMR spectroscopy.

### Cyclization of Unsaturated Alcohols

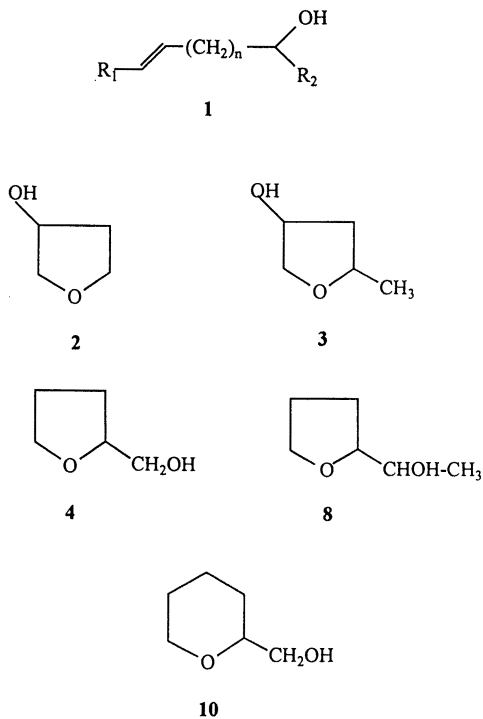
**3-buten-1-ol.** Cyclization of the simplest molecule of this series, 3-buten-1-ol, occurs at room temperature over the TS-1 / H<sub>2</sub>O<sub>2</sub> system. In 2-butanol solvent the reaction rate is slow and it takes 18 h to reach yield of 82 %, 3-hydroxy-tetrahydrofuran **2**, being the sole product (Scheme 1). However, in the presence of water as the dispersion medium (solid catalyst, aqueous H<sub>2</sub>O<sub>2</sub>, organic substrate initially forms three distinct three phases) (14) the reaction proceeds at a faster rate (93.6 % conversion after 6h) and selectivity towards **2** decreases to 75.5 %. In this case the oxirane ring opening via attack of external H<sub>2</sub>O molecules of the medium competes with intramolecular cyclization process leading to dihydroxylation (1,2,4-butanetriol, selectivity 24.5 %). Interestingly, increasing the reaction temperature to 333 K in the latter case decreases the yield of **2** to 2.5 % with selective dihydroxylation (15). Unlike phenylsulfenyl chloride system (3) the cyclization of 3-butene-1-ol is quite efficient over the present TS-1 / H<sub>2</sub>O<sub>2</sub> system (16). Another important aspect of the TS-1 catalyzed cyclization is that different from radical addition reaction, the products are hydroxy- substituted oxacyclic compounds.

(±) **4-penten-2-ol**. The tetrahydrofuran derivative 2-methyl-4-hydroxy-tetrahydrofuran **3** (*trans* : *cis* ratio 70 : 30) was formed from (±) 4-penten-2-ol using acetone solvent (yield 80 % at room temperature after 18 h reaction time) over TS-1 / H<sub>2</sub>O<sub>2</sub> system. In water medium at room temperature selectivity for **3** drops to 70 % with *trans* : *cis* ratio 67 : 33 after 12 h reaction time. At higher temperature using water dispersion medium the dihydroxylation product predominates in a similar manner to 3-buten-1-ol. Interestingly, here also the intermediate epoxide is highly reactive and undergoes very rapid oxirane ring opening either via intramolecular cyclization or dihydroxylation. However, using 2-butanol as solvent **3** forms as the sole product in 84 % yield (*trans* : *cis* ratio 72 : 28). High *trans* selectivity among the diastereomers of **3** may be due to the higher stability of the transition state at the active site. In Scheme 2 the reaction sequences at 298 K and 333 K are shown for (±) 4-penten-2-ol using water as dispersion medium.

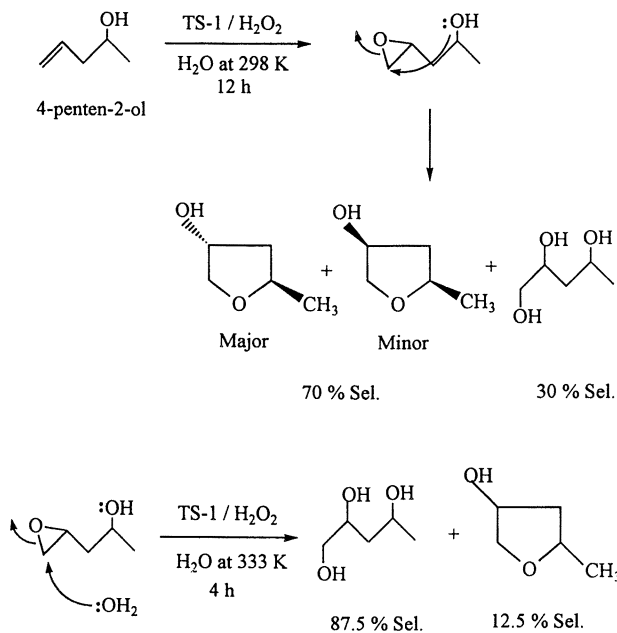
**4-penten-1-ol**. The cyclization of 4-penten-1-ol occurred regioselectively to the 5-exo product tetrahydro-2-furanmethanol **4**. Attack of the hydroxyl nucleophile absolutely does not take place on the carbon atom at the 5-position of the intermediate oxirane ring. Reaction medium has no effect, in 2-butanol, acetone and water, in all cases **4** was obtained in 98-99 % yield. This is quite interesting, since, 2,4,4,6-tetrabromo-1,5-cyclohexadienone (**2**) induced cyclization leads to a mixture of tetrahydropyran to tetrahydrofuran at a mole ratio of 3 : 1. In water medium at high temperature (333 K) also no dihydroxylation product is formed.

**Cis-4-hexen-1-ol**. In the case of *cis*-4-hexen-1-ol **6** (Scheme 3) between the two possibilities of the intermediate oxirane (**7**) ring opening the 5-exo product, tetrahydro-2-furan-1-ethanol **8**, forms exclusively in 92 % yield in acetone at 333 K. The 6-endo product 2-methyl-3-hydroxy-tetrahydropyran, **9** does not form at all although it would have given more stable carbocation intermediate. As shown in Scheme 3, the titanium hydroperoxo species **5** protonates the oxirane **7** and thus activates it for the nucleophilic attack of the OH groups at C<sub>4</sub>. One possible explanation for the 5-exo product formation from 4-penten-1-ol would be of the acidic nature of TS-1 / H<sub>2</sub>O<sub>2</sub> system ; if the oxirane ring opening follows S<sub>N</sub>1 pathways (involving initial protonation), more preferential attack would be on to the more substituted carbon atom. The hydroxyl group would attack preferentially at the more substituted carbon atom due to higher stability of the corresponding carbocation. On the contrary, alkyl group substitution at C<sub>5</sub> does not cause any change in the regioselectivity of cyclization.

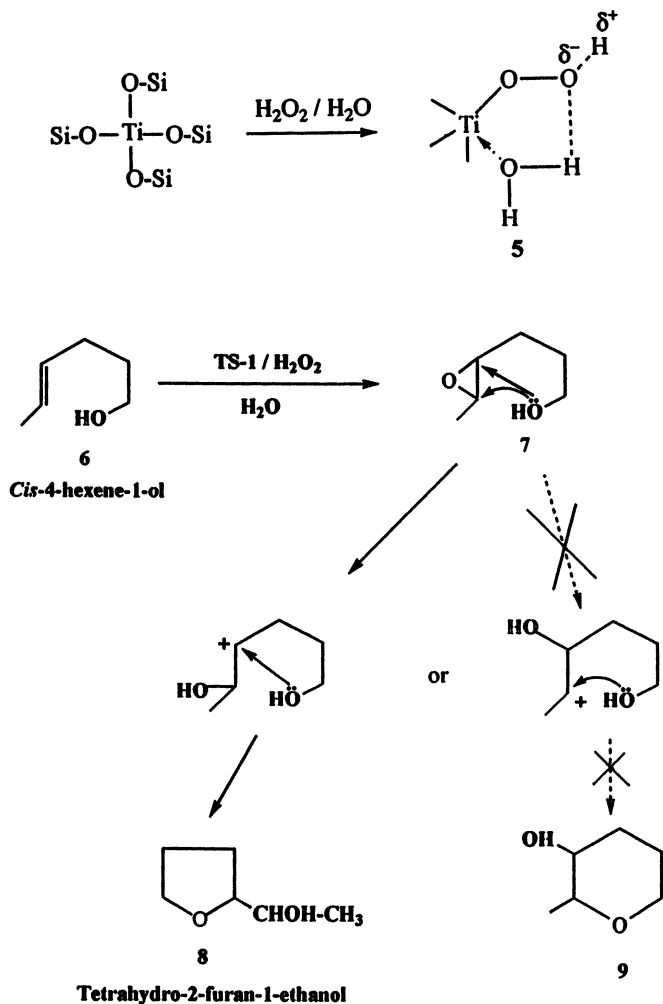
**5-hexen-1-ol**. In the case of 5-hexen-1-ol, where two products are possible, either tetrahydropyran or its 7-membered regioisomer tetrahydrohomopyran derivative, tetrahydro-2-pyranmethanol **10** only forms in 90 % yield in acetone at 333 K (Scheme 1).



Scheme 1. Unsaturation alcohols and their cyclized products.



Scheme 2. Reaction sequences for 4-penten-2-ol at 298 K and 333 K.



**Scheme 3.** Generation of titanium hydroperoxo species in TS-1 / H<sub>2</sub>O<sub>2</sub> system and the proposed reaction scheme for the cyclization of *cis*-4-hexen-1-ol.



## Mechanistic aspects

Although theoretical calculation on the transition state energies for 4-penten-1-oxyl radical (**4**) indicates the 5-exo product is strongly favored, in the TS-1 / H<sub>2</sub>O<sub>2</sub> system oxidation is believed to occur through titanium hydroperoxo species **5** (**17**) (Scheme 3) and thus essentially ionic in nature. Restricted geometry inside the TS-1 channel (the MFI topology with intersecting 10-member rings of 5.3 × 5.6 Å and 5.1 × 5.5 Å pore diameters and 0.10 cc/g internal void volume helps in bending the chain) might play a crucial role in the regioselective cyclization. The decreasing trend of the ratio of tetrahydropyrans to tetrahydrofurans from mesoporous MCM-41 (internal void volume very high 0.95 cc/g) to large pore Beta (**18**) followed by exclusive formation of tetrahydrofuran rings over medium pore TS-1 supports the above proposition. However, preferential formation of tetrahydrofuran derivatives is in line with the greater stability of 5-membered heterocycles.

In the oxidative cyclization (bifunctional behavior, epoxidation followed by acid catalyzed cyclization) observed in the oxidation of linalool (**18**) over Al-Ti-Beta and Al-Ti-MCM-41 the acidity at the Al sites was responsible for the oxirane ring opening leading to cyclized product. Since TS-1 employed here contains no Al, protonic character of the titanium hydroperoxo species **5** seems to promote the cyclization. In the transition state of the acid-catalyzed S<sub>N</sub>2 cleavage of the oxirane ring, bond-breaking proceeds faster than bond-making, and the carbon has acquired a considerable positive charge. Thus the reaction has considerable S<sub>N</sub>1 character and the nucleophilic attack is easy at the crowded carbon atom that can best accommodate the positive charge. However, for 3-buten-1-ol and (±) 4-penten-2-ol, the attack of the OH group on such a carbon leading to the four membered ring is unfavorable. The attack on the less crowded carbon occurs instead. Thus at high temperatures the attack of water predominates over the attack of the intramolecular OH group. In contrast, for 4-penten-1-ol the attack of the OH group on the crowded carbon to produce **4** is favorable, excluding the occurrence of dihydroxylation even at high temperature.

In the case of products **2** and **3** where the dihydroxylation product predominates at higher temperature in water medium this can be accounted by higher probability of the formation of titanium hydroperoxo species **5**, which protonates the oxirane oxygen fast. This promotes the hydrolysis due to easy access of water molecules of the medium. Interestingly, no intermediate epoxide is detected either while studying the kinetics of various constituents of the reaction mixture by GC, indicating that TS-1 catalyzed the present cyclization process at a very fast rate and ring closure takes place inside the cages of the zeolite immediately after the epoxidation.

## Conclusions

In the presence of aqueous  $H_2O_2$ , TS-1 generates titanium hydroperoxo species **5**, which not only efficiently epoxidizes the double bond of the unsaturated alcohols of type **1**, but catalyzes the oxirane ring opening via intramolecular attack of hydroxy nucleophile leading to oxacyclic ring formation. The reaction sequence indicates that when there is a choice of hydroxy tetrahydrofuran and tetrahydropyran, the former exclusively produced under the present reaction conditions. However, when there is no possibility of smaller oxacycles other than 6-membered one, hydroxy-tetrahydropyran forms exclusively.

**Acknowledgments.** A.B. thanks Japan Society for the Promotion of Science for a postdoctoral fellowship.

## Literature Cited

- (1) Lord, M.D., Negri, J.T.; Paquette, L.A. *J. Org. Chem.* **1995**, *60*, 191.
- (2) Ting, P.C.; Bartlett, P.A. *J. Am. Chem. Soc.* **1984**, *106*, 2668.
- (3) Tuladhar, S.M.; Fallis, A.G. *Tetrahedron Lett.* **1987**, *28*, 523.
- (4) Hartung, J., Stowasser, R., Vitt, D.; Bringmann, G. *Angew. Chem. Int. Ed. Engl.* **1996**, *35*, 2820.
- (5) Trost, B.M.; Li, C.J. *J. Am. Chem. Soc.* **1994**, *116*, 10819.
- (6) Taramaso, M., Perego, G.; Notari, B. *U. S. Patent* **1983**, 4410501.
- (7) Tatsumi, T., Nakamura, M., Negishi, S.; Tominaga, H. *J. Chem. Soc. Chem. Commun.* **1990**, 476.
- (8) Huybrechts, D.R.C., DeBruycker, L.; Jacobs, P.A. *Nature* **1990**, *345*, 240.
- (9) Tatsumi, T., Yako, M., Nakamura, M., Yuhara, Y.; Tominaga, H. *J. Mol. Catal.* **1993**, *78*, L41.
- (10) Clerici, M.G.; Ingallina, P. *J. Catal.* **1993**, *140*, 71.
- (11) Tatsumi, T.; Jappar, N. *J. Catal.* **1996**, *161*, 570.
- (12) Reddy, J.S.; Jacobs, P.A. *J. Chem. Soc. Parkin Trans. 1* **1993**, 2665.
- (13) Reddy, R., Reddy, J.S., Kumar, R.; Kumar, P. *J. Chem. Soc. Chem. Commun.* **1992**, 84.
- (14) Bhaumik, A.; Kumar, R. *J. Chem. Soc. Chem. Commun.* **1995**, 349.
- (15) Bhaumik, A.; Tatsumi, T. *J. Catal.* **1998**, *176*, 305.
- (16) Bhaumik, A.; Tatsumi, T. *J. Chem. Soc. Chem. Commun.* **1998**, 463.
- (17) Bellussi, G., Carati, A., Clerici, M.G., Maddinelli, G.; Millini, R. *J. Catal.* **1992**, *133*, 220.
- (18) A. Corma, Iglesias, M.; Sanchez, F. *J. Chem. Soc. Chem. Commun.* **1995**, 1635.

## Chapter 6

# Oxidation of Alkanes Catalyzed by Different Octahedral Molecular Sieves

Guan-Guang Xia <sup>1</sup>, Jin-Yun Wang <sup>2</sup>, Nian-Gao Duan <sup>2</sup>, Ying Ma <sup>2</sup>,  
and Steven L. Suib <sup>1-3</sup>

<sup>1</sup> Institute of Materials Science and <sup>2</sup> Departments of Chemistry and <sup>3</sup> Chemical Engineering, University of Connecticut, Storrs, CT 06269-3060

A series of manganese oxide based octahedral molecular sieves (OMS) with different pore openings were used as catalysts to study the oxidization of three organic substrates with different sizes or shapes. The catalysts used are ramsdellite (with 1x2 MnO<sub>6</sub> units as tunnel opening), cryptomelane (with 2x2 opening), todorokite (with 3x3 opening), and a 2x4 tunnel structure material. The organic substrates are cyclohexane, hexane, and decalin with tertiary butyl hydrogen peroxide (TBHP) as oxidant and its reduced state tertiary butyl alcohol (TBA) as solvent. The conversions of organic substrates, efficiencies of TBHP, and the rates of organic substrate conversions and rates of TBHP disappearance were systematically studied. The results show that OMS-2 and cyclohexane are the best combination to produce the highest reaction rate among all the catalysts and organic substrates. OMS-2 was also found to be the best catalyst to decompose TBHP. Results show that radicals were partially responsible for the reaction. The reaction pathway in this system was controlled by shape selectivity of OMS-2 catalyst to activation of cyclohexane and to decomposition TBHP (to produce radicals).

Saturated hydrocarbon functionalization in liquid phase has received much attention in the past decades because of great industrial importance and environmental friendly processes. The inertness of saturated hydrocarbons have also posed a challenge. (1-4) A great deal of work has been done using organometallic complexes(5-17), and reaction mechanisms based on different reaction systems have been proposed. (4,18-23) A radical mechanism for hydrocarbon oxidation has been widely accepted. (4,10)

Liquid phase hydrocarbon oxidation catalyzed by heterogeneous catalysts has been intensively studied in the past few years. Titanium silicate(24-28), titanium borolites(29),  $V_2O_5/TiO_2$ (30), vanadium silicate(31-33), chromium silicate(34),  $Mn^{2+}$  exchanged clay(35), and vanadium-substituted MCM-41 zeolite(36) have been employed as catalysts. Metal (Ti, V, and Cr) silicates, which have small pore sizes, show good activities for the oxidation of linear alkanes,(25,27,33-38) but much lower activities for the oxidation of cycloalkanes.

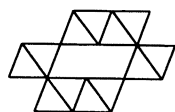
A new class of materials, manganese oxide based octahedral molecular sieves (OMS), have been recently synthesized.(39) The OMS materials used in this study have a microporous tunnel structure. These synthetic materials are based on natural manganese nodules, and they are mixed valent systems. The basic building blocks of these materials are  $MnO_6$  octahedra that are interconnected by edges and corners. These materials can be systematically doped with various transition metals (TM) in the framework of  $MnO_6$  octahedra to form  $TMO_6$  units, which are interconnected, with  $MnO_6$  octahedra. Exchangeable cations in the tunnels of these materials can readily be replaced by transition metals with ion-exchange methods.

Four different OMS materials (see Fig. 1) are OMS-1 (with todorokite structure)(40), OMS-2 (with cryptomelane structure)(39), synthetic ramsdellite (OMS-4), and a 2x4 structure (OMS-5) were used. OMS-1 possesses an edged-shared 3x3  $MnO_6$  octahedral tunnel with a tunnel opening of about 6.9 Å x 6.9 Å. OMS-2 possesses a 2x2 tunnel structure with an opening of about 4.6 Å x 4.6 Å. OMS-4 possesses a 1x2 tunnel structure with a tunnel opening of about 2.3 Å x 4.6 Å. OMS-5 possesses a 2x4 tunnel structure with a tunnel opening of about 4.6 Å x 9.2 Å.

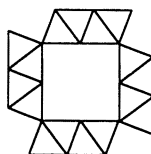
Our previous work has shown that both OMS-1 and OMS-2 has good catalytic activities toward cyclohexane oxidation with TBHP as oxidant.(41,42) Cyclohexanone and t-butyl cyclohexyl peroxide were found to be stable products, while cyclohexyl hydrogen peroxide was produced as an intermediate for cyclohexanone. Here we extend our investigation to the four catalysts with different tunnel openings, and organic substrates with different sizes and shapes (such as hexane and cis-decalin) in addition to cyclohexane. TBHP was used as oxidant, and TBA was used as solvent. The goal of this work is to understand relationships between the tunnel sizes of the catalysts and the conversions and selectivities of reactants in this catalytic system.

## Experimental Section

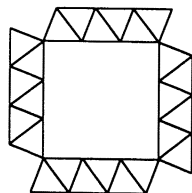
**Synthesis of Catalysts.** The preparation(40) of OMS-1 was done in the following way: 60 mL of 5.0 M NaOH solution was added dropwise to a vigorously stirred 40 mL mixture of 0.5 M  $MnCl_2$ , 0.1 M  $MgCl_2$  to form a suspension in a plastic flask at room temperature. After that, 40 mL of 0.2 M  $KMnO_4$  solution was added dropwise to the vigorously stirred suspension, and stirring was stopped upon completion. The plastic flask was sealed and aged at 35°C for 2 days before filtration and the solid powder was washed with distilled



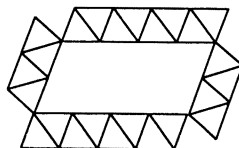
(a) OMS-4



(b) OMS-2



(c) OMS-1



(d) OMS-5

Figure 1. Scheme of Octahedral Molecular Sieves (OMSs). The materials are built up by edge and corner shared  $\text{MnO}_6$  octahedral ( $\nabla$ ) units. (a) OMS-4 (1x2), (b) OMS-2 (2x2), (c) OMS-1 (3x3), (d) OMS-5 (2x4).

deionized water (DDW). The filtered residue was ion-exchanged by using 200 mL of 1.0 M  $\text{MgCl}_2$  overnight at room temperature, and the exchanged material was filtered and washed with DDW. The mixture was transferred to an autoclave at  $150^\circ\text{C}$  for 2 days. The final product was filtered and washed, and then dried at  $110^\circ\text{C}$  overnight.

OMS-2 was prepared by refluxing method. In a 500 mL of round bottom flask with a condenser, a 225 mL of potassium permanganate solution (0.4 M) was added to a mixture 67.5 mL of volume of manganese sulfate solution (1.75 M) and 6.8 mL concentrated nitric acid. The dark-brown slurry was refluxing for 24 hours, then filtered and washed by DDW. The catalyst was dried at  $120^\circ\text{C}$  overnight before use.

OMS-4 was synthesized by refluxing a sodium permanganate solution under acidic conditions. The resulted brownish slurries were washed thoroughly with DDW using a centrifuge. The final product was dried at  $120^\circ\text{C}$  overnight.

OMS-5 was prepared using permanganate and manganese salt in a basic media, and aging the suspension for a few days to produce birnessite-type manganese oxide. Then the precipitation was ion-exchanged with  $\text{Na}^+$  and autoclaved at ca.  $210^\circ\text{C}$  for a few days. The solid was washed and dried before use. The structural properties of these materials have been characterized with XAS(44), TEM(40,45), XRD(39-45), BET and PSD(43).

**Catalytic Reactions.** All the catalytic reactions were performed in a batch reactor at autogenous pressure. The typical reaction compositions were 12.5 mmole of organic substrate, 10 mmole of TBHP, 25 mmole of TBA as solvent, and 20 mg of catalysts. The typical reaction temperature was  $60^\circ\text{C}$  with stirring rate of 600 rpm, at which diffusion effect can be minimized.(41,42) The reaction products were qualitatively identified by GC-MS (HP) and quantitatively analyzed by GC HP-5890 with a Supelcowax-10 capillary column (30m) and a thermal conductivity detector (TCD).

## Results

**Oxidation of Cyclohexane with Different Catalysts.** Cyclohexane oxidation was performed at  $60^\circ\text{C}$  for 24 hours. Four different products were identified, which were cyclohexanol (A), cyclohexanone (K), t-butyl cyclohexyl peroxide (P), and cyclohexyl peroxide (CHP). The results are listed in Table I. The order of cyclohexane conversions is:  $2\times 2 > 1\times 2 > 3\times 3 > 2\times 4$ , and the TBHP efficiencies show a reverse order. The order for selectivities of K and P is the same as that of cyclohexane conversion. The order of CHP selectivities is the same as that of TBHP efficiencies, but the ratio of K/A shows the same order as that of the conversions.

Table I. Cyclohexane Oxidation over Different Catalysts

	Conv.%. 7.8	Effic.%* 28.5	%S.A 32.3	%S.K 39.0	%S.CHP 20.5	%S.P 8.2	K/A 1.21
1x2	7.8	28.5	32.3	39.0	20.5	8.2	1.21
2x2	11.9	27.4	29.1	45.5	3.3	11.7	1.56
3x3	4.1	34.4	21.1	18.6	59.4	0.9	0.88
2x4	2.3	36.1	21.5	16.4	60.8	1.3	0.76

\*Efficiency of TBHP is calculated based on the moles of products per mole of TBHP consumed.

A=cyclohexanol, K=cyclohexanone, CHP= cyclohexyl hydrogen peroxide, P= t-butyl cyclohexyl peroxide.

**Oxidation of n-Hexane with Different Catalysts.** Catalysts with different pore openings were also used to catalyze the oxidation of n-hexane at 60°C for 24 hours, and the results are shown in Table II. Four different kinds of products are produced, alcohols (A), ketones (K), hexyl hydrogen peroxides (HP), and dialkyl peroxides (P). For the three possible alcohol products, the selectivities of primary hexanol are less than 1% for the catalysts studied. There was no aldehyde detected, and no peroxide functional groups were formed at primary carbon of hexane. Therefore, only functional groups in the second or third position of hexane were reported.

The selectivities of products with functional groups in the second position were higher than those in the third position. The selectivities of ketones were generally higher than those of alcohols, and selectivities to dialkyl peroxides were the smallest except for the reaction with 2x2 as catalyst. The selectivities of hexyl hydrogen peroxides (HP) were the highest among products except for OMS-2, where the total selectivities to HP were the smallest. The selectivity of 3-hexyl tertiary butyl peroxide was almost zero when the 1x2 material was employed as a catalyst.

**Oxidation of Decalin with Different Catalysts.** Oxidation of cis-decalin was performed at 60°C for 24 h with four different catalysts. The products were only classified as “alcohols”, “ketones”, and “others”. The experimental results are shown in Table III. The order of decalin conversion is 2x2 > 1x2 > 3x3 > 2x4. The order for selectivities to ketones is the same order as that of conversion, but the order of selectivities to other products (peroxides) except alcohols and ketones is the reverse of that for decalin conversion. The selectivities to alcohols are not very different for different catalysts. Alcohols are the main products for all the catalysts. The ratios of K/A show the same order as that of the conversions, but all are less than 1.

The overall conversions of organic substrates (or total yields of oxidation products) and efficiencies of TBHP were summarized in Table IV. OMS-2 leads to the highest conversions for all organic substrates. Cyclohexane shows the

Table II. Catalytic Oxidation of Hexane over Different Catalysts

Cat.	Conv. Effic*		Selectivity,%							
	%	%	K <sub>3</sub>	K <sub>2</sub>	A <sub>3</sub>	A <sub>2</sub>	HP <sub>3</sub>	HP <sub>2</sub>	P <sub>3</sub>	P <sub>2</sub>
1x2	4.4	29.1	11.1	12.9	8.2	9.5	20.2	34.5	0	3.6
2x2	8.9	28.2	28.8	36.5	10.6	10.2	1.4	1.0	4.9	6.6
3x3	3.4	35.6	15.1	16.3	9.4	5.6	14.2	31.9	3.6	4.0
2x4	2.5	36.2	13.6	16.9	16.6	12.8	14.2	21.6	1.8	2.4

\* Efficiency of TBHP is calculated based on the moles of products per mole of TBHP consumed.

K<sub>2</sub>= 2-hexanone, K<sub>3</sub>=3-hexanone, A<sub>2</sub>=2-hexanol, A<sub>3</sub>=3-hexanol,  
 HP<sub>2</sub>=2-hexyl hydrogen peroxide, HP<sub>3</sub>=3-hexyl hydrogen peroxide,  
 P<sub>2</sub>= 2-hexyl t-butyl peroxide, P<sub>3</sub>=3-hexyl t-butyl peroxide.

Table III. Catalytic Oxidation of Decalin over Different Catalysts

Cat.	Conv. %	Effic. %*	%S.A	%S.K	%S.	
					Others	K/A
1x2	3.6	29.8	49.1	41.8	9.1	0.85
2x2	8.4	28.7	47.6	45.8	6.6	0.96
3x3	1.2	33.7	52.6	27.4	20.0	0.52
2x4	0.8	35.2	45.3	15.2	39.5	0.34

\*Efficiency of TBHP is calculated based on the moles of products per mole of TBHP consumed.

A=decalols, K=decalones, Others=peroxide products.



highest conversion among the three organic substrates, followed by hexane and cis-decalin.

The trend for efficiencies of TBHP is different from that of conversions. The TBHP efficiency is the lowest for OMS-2 catalysts. However, efficiency differences between different organic substrates are small compared to the differences of conversions, especially for the catalysts other than OMS-2. In addition, the efficiency is generally smaller for small pore opening catalysts (OMS-2 and OMS-4) than that for large pore opening catalysts (OMS-1 and OMS-5).

Table IV. Conversions of Organic Substrates and Efficiencies of TBHP over Different Catalysts

	1 x 2		2x2		2x3		2x4	
	Conv.	Effic.	Conv.	Effic.	Conv.	Effic.	Conv.	Effic.
Cyclohexane	7.8	28.5	11.9	27.4	4.1	34.4	2.3	36.1
Hexane	4.4	29.1	8.9	28.2	3.4	35.6	2.5	36.2
Decalin	3.6	29.8	8.4	28.7	1.2	33.7	0.8	35.2

**Product Distribution with Different Catalysts.** Cyclohexane was chosen to study relationships of oxidation reactions and pore openings of the catalysts because cyclohexane had the highest conversion among the organic substrates studied. The conversions of cyclohexane were controlled at 10 % for all four different catalysts by adjusting reaction conditions. The selectivities to different products are given in Table V.

Table V shows that the product distribution varies between different catalysts. OMS-2 produced the highest K/A and P/A ratios, and the selectivity to CHP was less than 7%. The order of K/A and P/A ratios for the four different catalysts are in the order of 2x2 > 1x2 > 3x3 > 2x4, and the selectivities to CHP are the reverse order for that of K and P. At the conversion of 10%, selectivities to K and A are the first and second among the products, and the selectivity to CHP is third for all catalysts except OMS-2, which has the smallest selectivity to CHP.

**Relationships of Rates and Catalysts.** Initial reaction rate was obtained by measuring the slope of a conversion-time plot at time equal to zero. The initial reaction rates of the three organic substrates for different catalysts, which are normalized with surface area of catalysts, are shown in Table VI. The order of catalytic activities toward all the organic substrates is 2x2 > 3x3 > 1x2 > 2x4. The rate of cyclohexane conversion is the highest for all organic substrates and catalysts. The order of reaction rates of different organic substrates is cyclohexane > cis-decalin > n-hexane.

Interestingly, the combination of cyclohexane and 2x2 catalyst shows a remarkable high normalized reaction rate.

Table V. Selectivities of Products at 10% Conversion of Cyclohexane over Different Catalysts

	1x2	2x2	3x3	2x4
K (%)	45.8	50.3	43.0	42.9
A (%)	31.9	30.5	33.8	34.6
CHP (%)	13.4	6.8	14.9	16.9
P (%)	8.9	12.4	8.3	5.6
K/A	1.44	1.65	1.27	1.25
P/A	0.28	0.41	0.25	0.16

Table VI. Initial Reaction Rates of Different Organic Substrates over Different Catalysts

	1x2 (mole·h <sup>-1</sup> · M <sup>-2</sup> ) x 10 <sup>8</sup>	2x2 (mole·h <sup>-1</sup> · M <sup>-2</sup> ) x 10 <sup>8</sup>	3x3 (mole·h <sup>-1</sup> · M <sup>-2</sup> ) x 10 <sup>8</sup>	2x4 (mole·h <sup>-1</sup> · M <sup>-2</sup> ) x 10 <sup>8</sup>
Cyclohexane	3.2	34.1	9.0	1.2
Hexane	1.1	5.0	4.1	0.6
Decalin	2.0	7.6	6.3	0.6
Surface Area (M <sup>2</sup> /g)	44.9	59.8	28.9	26.4

Table VII lists the initial disappearance rates (normalized with surface area of catalysts) of TBHP with or without the presence of organic substrates. The OMS-2 catalyst has the highest activity to decompose TBHP no matter whether there is organic substrate or not. The disappearance rates of TBHP toward all catalysts decrease in the presence of organic substrates to a degree from ca. one-half to one-tenth of the decomposition rate without the presence of organic substrates.

**The Radical (TEMPO) Effects on Cyclohexane Oxidation.** TEMPO radical was added to the reaction system with OMS-2 as catalyst and cyclohexane as organic substrate to examine the effects of radicals in the reaction. TEMPO (ca. 8 % amount of TBHP) was introduced to the reaction mixture, and a parallel reaction was run without adding TEMPO. The reaction products and their selectivities are listed in Table VIII. The conversion of cyclohexane was significantly decreased in the presence of TEMPO to ca. 65% of the conversion without TEMPO.

Table VII. Initial Disappearance Rates of TBHP over Different Catalysts

	1x2 (mole•h <sup>-1</sup> •M <sup>-2</sup> ) x10 <sup>7</sup>	2x2 (mole•h <sup>-1</sup> •M <sup>-2</sup> ) x10 <sup>7</sup>	3x3 (mole•h <sup>-1</sup> •M <sup>-2</sup> ) x10 <sup>7</sup>	2x4 (mole•h <sup>-1</sup> •M <sup>-2</sup> ) x10 <sup>7</sup>
No substrate	8.1	44.0	4.8	1.7
Cyclohexane	3.3	13.9	2.5	0.3
Hexane	1.4	4.3	1.3	0.2
Decalin	1.6	6.7	1.6	0.2

Table VIII. Radical Trap (TEMPO) Effect on Cyclohexane Oxidation Using OMS-2 as Catalyst

Conv. (%)	Effic. (%) TBHP	S. (%)		S. (%)		S. (%) others
		A	K	CHP	P	
8.1*	18.2	24.9	58.2	0	6.4	10.5
11.9**	27.4	29.1	45.5	3.3	11.7	0

\* Reaction was done with TEMPO.

\*\* Reaction was done without TEMPO.

The initial rate of cyclohexane conversion, in the presence of TEMPO, was ca. 75% of the initial rate without TEMPO. In addition, there was 35% TEMPO left over after the reaction had been running for 24 hours. The efficiency of TBHP was decreased in the presence of TEMPO to ca 65% compared to experiments with no TEMPO. The selectivities to K and P did not have an obvious change, but the selectivity to A was decreased to ca. 65%. No CHP was detected in the reaction products in the presence of TEMPO. A selectivity of 11.9% to other products (derivatives of cyclohexane and TEMPO) was found.

## Discussion

**Oxidation of Cyclohexane.** From Table I it is obvious that OMS-2 is an outstanding catalyst among the four catalysts studied here. Although it is difficult to compare selectivities at different conversions, it may be possible to compare different catalysts with conversions between 5-20%. Data for selectivities at a constant conversion are shown in Table V.

OMS-2 produces the highest conversion of cyclohexane, the highest K/A ratio, the highest selectivity to product P, and the lowest selectivity of CHP, as well as the lowest TBHP efficiency. Catalysts with 2 X 4 pore opening gave lowest cyclohexane conversion.

Our previous work (41,42) has demonstrated that CHP is an unstable intermediate, which may transform to K by dehydration, and alcohol could slowly transfer to P or K either at high reaction temperature or with active catalysts, such as OMS-2.

Research by Neumann et al. (36) also indicates that alkyl hydrogen peroxide can form ketones. OMS-2 is the most active catalyst among the catalysts studied in this system, which is supported by data in Table VI. That is why the system with OMS-2 as catalyst possesses the highest K/A and K/CHP, as well as P/A ratios because deep oxidation can be expected with the active catalyst under the same conditions. The least active catalyst causes the least extent of oxidation; therefore catalyst with 2 X 4 pore opening catalyst shows worse activity than OMS-2 catalysts.

**Oxidation of Hexane.** As far as the four different kinds of products are concerned, data in Table II has the similar patterns in terms of K/A, P/A, and K/HP ratios with OMS-2 as catalyst as shown in Table I. These show that OMS-2 is more active than other catalysts in hexane oxidation. The other three catalysts do not show significant difference in terms of hexane conversion, and selectivities to different products. Catalysts with 1 x 2 tunnel opening are the second most active in terms of hexane conversion.

There were only trace (<1 %) amounts of primary functionalized products produced in these reaction systems. This indicates that primary carbons are more inert than non-primary carbons. The selectivities of the functional groups at secondary carbons are higher than those in the third carbon positions. This may be attributed to the fact that the second carbon has less stereo hindrance than the third carbon because methyl groups are much smaller than ethyl group.

**Oxidation of cis-decalin.** Reactions of cis-decalin with OMS-2 as catalyst has the highest conversion and K/A ratios. The results are similar to data for oxidation of cyclohexane and hexane. The obvious difference of cis-decalin oxidation from cyclohexane and hexane oxidation is that alcohols instead of ketones or alkyl hydrogen peroxides, are the main products. This may be attributed to the fact that the tertiary carbons are more active than secondary carbons. Therefore, tertiary carbons are functionalized more readily than in other positions. Since no double bond is allowed to form without breaking the C-C bond for tertiary carbons, ketones can not be formed in tertiary carbon positions. In addition, there is strong steric hindrance of large organic groups, such as tertiary butyl groups in cis-decalin.

Data in Table IV indicate that cyclohexane has the highest conversion among all organic substrates, especially for OMS-2 as catalyst. OMS-2 produces the highest conversions for oxidation of all organic substrates. In addition, the efficiency of TBHP strongly depends on the nature of the catalyst under reaction conditions. Data for TBHP efficiencies in Table IV suggest that systems with high conversions of the organic substrates (i.e. OMS-2) generally have low TBHP efficiency. These data imply that cyclohexane is more readily activated by OMS-2 catalysts. Hexane and decalin are oxidized at lower conversion than cyclohexane (see Table IV). All other catalysts besides OMS-2 (2x2) and OMS-4 (1x2) have high TBHP efficiencies, however, they show much lower

conversions. The fact that TBHP efficiencies of the 1x2 catalyst are not much higher than the 2x2 catalyst but have markedly lower conversion suggest that the 2x2 material is unique and may give higher conversion due to shape selective or other effects. The fact that there is no major difference in TBHP efficiencies among the substrates for one particular catalyst indicates that kinetic effects, such as oxidation rate and TBHP decomposition rate, may play an important role which will be discussed below.

**Rates of Organic Substrates Conversion and Disappearance of TBHP.** Data in Table VI show that there are differences in activities of a specific catalyst toward different organic substrates, and that these are also differences in activities of a specific organic substrate toward different catalysts under same reaction conditions. This clearly indicates that differences of the pore openings of the catalysts and properties of organic substrates, such as size or shape, are responsible for reaction activities. The exact differences in reaction rate are difficult to understand. However, it is clear that the largest tunnel sizes (3x3, 2x4) and smallest tunnel size(1x2) are least active and the intermediate tunnel material (2x2) is most active by far for all catalysts. This unique behavior of the 2x2 system is most likely due to shape selective effects.

The initial disappearance rates of TBHP in the presence of organic substrates are more than twice, even more than ten times, the rates of organic substrate conversion. This means that oxidation processes are the rate-controlling steps in the reaction and that the decomposition rate of TBHP is fast. This is why the efficiencies of TBHP for all the reactions studied are less than 50 %. The ratios of the disappearance rate of TBHP over the conversion rates of substrates for 1x2 and 2x2 materials are similar (8.5-12.5) for all substrates with an exception of the cyclohexane/OMS-2 system, which is 4. On the other hand, the ratios for the 3x3 and 2x4 catalysts are rather small for all substrates, which range from 2.5-3.4. These data suggest that the differences in TBHP efficiencies among the substrates for one particular catalyst are rather small and that these efficiencies might be related to the ratios. The disappearance rates of TBHP in the presence of organic substrate are much slower than the rates of TBHP decomposition over the catalysts without substrates. This might be attributed to the competition of adsorption on the surface of catalysts between TBHP and organic substrate, and that the active sites to decompose TBHP were partially occupied by organic substrates.

The pore diameter of OMS-2 is 4.6 Å, but the pore opening along its diagonal direction is about 6.4 Å, which can fit both TBHP(3.8-4.1 Å) and cyclohexane (4.7-6.2 Å) well. (38) This can explain why the decomposition rate of TBHP toward OMS-2 is the highest, and why the OMS-2 has the highest activity toward different organic substrates, especially toward cyclohexane, among different catalysts.

**Effects of TEMPO Radicals.** The decrease of both the conversion of cyclohexane and the efficiency of TBHP in the presence of TEMPO indicates that the radical trap affects the oxidation of cyclohexane. The decrease of TBHP efficiency also means that the presence of TEMPO promotes the decomposition of TBHP. Therefore, radicals are involved in this reaction. However, the amount of TEMPO was only 8.1 % (mole) of TBHP in the reaction mixture, and 35 % of TEMPO was left over after the reaction. This might indicate that the radical reaction pathway is only partially responsible for these reaction systems. The shape selectivities to both organic substrates and TBHP (which produces radical upon decomposition) of the catalyst control the reaction in this system.

## Overview

We expect that differences in the pore sizes and shapes of the manganese oxide materials may give rise to differences in activity and selectivity. In addition, it is clear that there is a relationship between the rate of disappearance of TBHP and the conversion. Leaching experiments (42) show that no species leach into solution and the solution phase is not active. There are clearly differences in selectivity for the 2x2 catalyst with respect to all other catalysts when the conversion is held constant at 10%. In fact, the rates of reaction over the 2 x 2 catalyst are at least 1 order of magnitude greater for the 2 x 2 catalyst than any other system we have studied. We believe that the diagonal distance of the tunnel diameter of 6.4 Å of the 2 x 2 system affords an intermediate pore size, not unlike that of ZSM-5 and this may lead to unusual activity and selectivity of the 2 x 2 system. Surface area normalized activities show that there is no relationship between surface area and activity.

## Acknowledgments

We thank the Department of Energy, Office of Basic Energy Sciences, Division of Chemical Sciences and Texaco, Inc., for support of this research.

## Literature Cited

1. Shilov, A. E.; *Activation of Saturated Hydrocarbons by Transition Metal Complexes*; Reidel Publishing Co.; Dordrecht, **1984**, Chapter 4.
2. Sheldon, R. A.; Kochi, J. R. *Metal-Catalyzed Oxidation of Organic Compounds*; Academic Press, New York, **1981**, Chapter 11.
3. Leising, R. A.; Kim, J.; Perez, M. A.; Que, L. *J. Am. Chem. Soc.*, **1993**, *115*, 9524-9530.
4. Hill, C. L. *Activation and Functionalization of Alkanes*, ed. Hill, C. L. John Wiley & Sons, **1989**, p. 243.
5. Neumann, R.; Gara, M. *J. Am. Chem. Soc.* **1994**, *116*, 5509-5510.

6. Inchley, P.; Smith, J. R., Lower, R. J. *New J. Chem.* **1989**, *13* (10-11), 669-76.
7. White, R. E.; Coon, M. J. *Ann. Rev. Biochem.* **1980**, *49*, 315-318.
8. Herron, N.; Tolman, C. A.; Stucky, G. D. *J. Chem. Soc., Chem. Commun.*, **1986**, 1521-2.
9. Herron, N. *Inorg. Chem.*, **1986**, *25*, 4714-17.
10. Cofre, P.; Richert, S. A.; Sobkowiak, A.; Sawyer, D. T. *Inorg. Chem.*, **1990**, *29* (14), 2645-51.
11. Barton, D. H. R.; Beviere, S. D.; Chavasiri, W.; Doller, D.; Hu, B. *Tetrahedron Lett.* **1993**, *34* (12), 1871-4.
12. Barton, D. H. R.; Cshuai, E.; Doller, D. *Tetrahedron Lett.* **1992**, *48* (42), 9195-9206.
13. Schuchardt, U.; Krahembuhl, C. E. Z.; Carvalho, W. A. *New J. Chem.* **1991**, *15* (12), 955-8.
14. Banfi, S.; Maiocchi, A.; Moqqi, A.; Montanari, F.; Quici, S. *J. Chem. Soc., Chem. Commun.* **1990**, 1794-6.
15. Barton, D. H. R.; Doller, D. *Acc. Chem. Res.*, **1992**, *25*, 504-512.
16. Balavoine, G.; Barton, D. H. R.; Boivin, J.; Gref, A. *Tetrahedron Lett.* **1990**, *31* (5), 659-62.
17. Haber, J.; Iwanejko, R.; Mlodnicka, T. *J. Mol. Catal.* **1989**, *55* (1-3), 268-75.
18. Barton, D. H. R.; Beviere, S. D.; Chavasiri, W.; Cshuai, E.; Doller, D.; Liu, W.-G. *J. Am. Chem. Soc.* **1992**, *114*, 2147-2156.
19. Sawyer, D. T.; Kang, C.; Liobet, A. *J. Am. Chem. Soc.* **1993**, *115* (13), 5817-5818.
20. Sheu, C.; Sobkowiak, A.; Jeon, S.; Sawyer, D. T. *J. Am. Chem. Soc.* **1990**, *112* (2), 879-81.
21. Mahroof-Tahir, M.; Karlin, K. D. *J. Am. Chem. Soc.* **1992**, *114*, 7599-7601.
22. Menege, S.; Vincent, J. M.; Lambeaux, G.; Chottard, G.; Grand, A.; Fontecave, M. *Inorg. Chem.* **1993**, *32*, 4766-4773.
23. Sheu, C.; Richert, S. A.; Cofre, P.; Ross, B., Jr.; Sobkowiak, A.; Sawyer, D. T.; Kanofsky, J. R. *J. Am. Chem. Soc.* **1990**, *112* (5), 1936-42.
24. Lu, G.-X.; Gao, H.-X.; Suo, J.-S.; Li, S.-B. *J. Chem. Soc., Chem. Commun.*, **1994**, 2423-4.
25. Sudhakar Reddy, J.; Sivasanker, S.; Ratnasamy, P. *J. of Mol. Catal.*, **1991**, *70*, 335-342.
26. Camblor, M. A.; Corma, A.; Martinez, A.; Perez-Pariente, J.; Primo, J. *Stud. Surf. Sci. & Catal. Heterogeneous Catalysis and Fine Chemicals III*, Elsevier, Amsterdam, **1993**, 393-399.
27. Corma, A.; Camblor, M. A.; Esteve, P.; Martinez, A.; Perez Pariente, J. *J. Catal.* **1994**, *145*, 151-158.
28. Corma, A.; Navarro, M. TPerez Pariente, J. *J. Chem. Soc., Chem. Commun.* **1994**, 147-148.

29. Trong On, D.; Kappoor, M. P.; Bonneviot, L.; Kaliaguine, S.; Gabelica, Z. *J. Chem. Soc., Faraday Trans.* **1996**, *92*, 1031-1038.
30. Matralis, H. K.; Papadopoulou, Ch.; Kordulis, Ch.; Aguilar Elguezabal, A.; Cortes Corberan, V. *Appl. Catal. A* **1995**, *126*, 365-380.
31. Rao, P. R. H. P.; Ramaswamy, A. V.; Ratnasamy, P. *J. Of Catal.* **1993**, *141*, 604-611.
32. Neumann, R.; Levin-Elad, M. *Appl. Catal. A* **1995**, *122*, 85-97.
33. Rao, P. R. H. P.; Ramesh Reddy, K.; Ramaswamy, A. V.; Ratnasamy, P. *Stud. Surf. Sci. Catal.: Heterogeneous Catalysis and Fine Chemicals III*, **1993**, 385-92.
34. Slagh, A. P.; Selvom, T., *J. Mol. Catal. A* **1996**, *113*, 489-497.
35. Tateiwa, J-I.; Horiuchi, H.; Uemura, S. *J. Chem. Soc., Chem. Commun.* **1994**, *22*, 2567-8.
36. Neumann, R.; Khenkin, M. *Chem. Commun.* **1996**, 2643-4.
37. Sudhakar Reddy, J.; Sivasanker, S.; Ratnasamy, P. *J. Mol. Catal.* **1991**, *70*, 335-342.
38. Tatsumi, Takashi; Nakamura, Makoto; Negishi, Shigeki; Tominaga, Hiroo. Fac. Eng., *J. Chem. Soc., Chem. Commun.* **1990**, Issue 6, 476-7.
39. Suib, S. L. In *Recent Advances and New Horizons in Zeolite Science and Technology, Studies in Surface Science and Catalysis* **1996**, *102*, 47-74.
40. Shen, Y. F.; Zerger, P. R.; DeGuzman, R. N.; Suib, S. L.; McCurdy, L.; Potter, D. I.; O'Young, C. L. *Science* **1993**, *260*, 511-515.
41. Wang, J.-Y.; Xia, G.-G.; Yin, Y.-G.; Suib, S. L.; O'Young, C.-L. *J. Catal.* **1998**, *176*, 275-284.
42. Xia, G.-G.; Wang, J.-Y.; Yin, Y.-G ; Suib, S. L. *Catalysis of Organic Reactions*, Marcel Dekker, Inc., Ed. Herces, F., **1998**, 615-620.
43. O'Young, C.-L.; Sawicki, R. A.; Suib, S. L. *Micr. Mater.* **1997**, *11*, 1-8.
44. Wasserman, S. R.; Carrado, K. A.; Yuchs, S.; Shen, Y. F.; Cao, H; Suib, S. L. *Physica B* **1995**, *209*, 674-676.
45. DeGuzman, R. N.; Shen, Y. F.; Neth, E. J.; Suib, S. L.; O'Young, C. L.; Levine, S.; Newsam, J. M. *Chem. Mater.* **1994**, *6*, 815-821.
46. Madon, R. J.; Boudart, M. *Ind. Eng. Chem. Fundam* **1982**, *21*(4), 438-447.



## Chapter 7

# The Methanol-to-Hydrocarbons Reaction: A Mechanistic Perspective

Clarence D. Chang

Strategic Research Center, Mobil Technology Company, Paulsboro, NJ 08066

Mobil's Methanol-to-Gasoline (MTG) Process was one of the first major commercial applications for the synthetic zeolite ZSM-5. Shape-selectivity of ZSM-5 was critical for maximizing the yield of gasoline-range hydrocarbons. The hydrocarbon formation reaction itself was one of the most-studied in the past several decades. Mechanistic questions abound and remain unresolved. This Chapter presents a concise survey, highlighting current research and opinion.

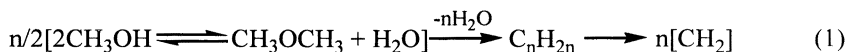
The conversion of methanol to hydrocarbons is one of the most remarkable reactions catalyzed by zeolites (1), most notably the zeolite ZSM-5. Discovered in the early 1970's, this chemistry was the basis of Mobil's MTG (Methanol-to-Gasoline) Process (2-5), that became the first viable alternative to the celebrated Fischer-Tropsch Process. Commercialized in New Zealand in 1985 (6), the MTG Process converted offshore natural gas to methanol and then to premium gasoline, at the rate of 14,500 barrels per day, and was the cornerstone of New Zealand's strategy to attain a measure of energy independence during the "oil crisis" of the 70's and 80's. At the time, the MTG Process met a third of New Zealand's total gasoline requirements. At present, due to prevailing low crude prices, the gasoline unit is mothballed, however methanol continues to be produced at the site and marketed worldwide.

What has not been idled is research on the diverse mechanistic aspects of the reaction. The focus of widespread attention following discovery, the reaction mechanism continues to be of interest to researchers to the present day. In particular the intriguing question of how the initial C-C bond is created from a C<sub>1</sub> starting material was much debated, and has remained a mystery. It will not be possible to present a

full account of the early history, but occasional reference will be made to select points for background. Extensive reviews of MTG chemistry and process are available in the Literature (5,7-9,83,93), to which the Reader is referred for detailed information.

### The Methanol-to-Hydrocarbon Reaction

**General Characteristics.** The overall methanol-to-hydrocarbon stoichiometry and reaction path is well established (1), and may be represented by equation 1:



As shown in the equation, dimethyl ether (DME) and olefins are reaction intermediates, and the end product is a mixture of aromatics and paraffin of average formula  $[\text{CH}_2]$ . The aromatics are mostly methyl-substituted, while paraffins are predominantly propane and isobutane. No hydrogen is produced in the main reaction. With ZSM-5, the hydrocarbon distribution cuts off sharply at around  $\text{C}_{10}$  due to catalyst shape-selectivity. This very fortunately coincides with the normal end-point of gasoline. The  $\text{C}_6$ - $\text{C}_{10}$  fraction is essentially aromatic, but contains little benzene.

With suitable adjustments of reaction conditions, the olefin formation step can be decoupled from aromatization, and the reaction exploited for light olefin synthesis. a process often referred to as MTO (Methanol-to-Olefins) (10-12). Alternatively, small pore zeolites have the potential for selective MTO reaction, and a number of such catalysts have been examined (see below). Because of the large amount of water produced in the reaction, it is essential to use zeolites with the highest framework Si/Al consistent with catalytic activity, in order to maintain steam-stability. Catalysts other than zeolites, most notably the silicoaluminophosphate SAPO-34 (chabazite structure) are reportedly active and steam-stable for MTO conversion (13), though little detailed information has been published to date.

The reaction is highly exothermic ( $-\Delta H_R = 1.67 \text{ kJ g}^{-1}$ ) (1), and autocatalytic (14-16).

**Zeolite Shape-Selectivity.** The influence of zeolite pore geometry on product selectivity is most clearly evident in the aromatics distribution. This is illustrated in Figure 1 (5) for methanol reaction over ZSM-5 (10-ring), ZSM-12 (non-planar 12-ring), and mordenite (planar 12-ring). As already noted, aromatics distribution with the 10-ring pore ZSM-5 terminates at around  $\text{C}_{10}$ . The distribution peaks at around  $\text{C}_8$ . Mordenite, with 12-ring pores, readily accommodates the larger polymethylbenzenes, and indeed these tend to be the main products. In the intermediate case of ZSM-12, its highly non-planar 12-rings define a smaller effective pore diameter, resulting in a somewhat more constrained access to sorbates than the planar mordenite 12-ring. As seen, this is reflected in broader aromatic distributions.

The bulkiest  $\text{C}_{10}$  aromatic that can readily diffuse out of ZSM-5 is 1,2,4,5-tetramethylbenzene (durene), whose critical dimensions closely match those of the zeolite pores. Durene is therefore the major tetramethylbenzene produced even

though it is not the thermodynamically preferred isomer. The bulkier isomers of durene are often observed in laboratory MTG experiments with freshly calcined catalyst. Assuming no zeolite crystal imperfections, this is largely due to secondary isomerization of durene on non-shape-selective acid sites on the external surface of the crystals (88,89). Though the external acid sites are fewer in number than in the bulk, and possibly of lower acid strength, they nevertheless can have significant activity for the relatively facile 1,2-alkyl shifts. However these sites deactivate readily due to the deposition of coke and other poisons, resulting in an improvement in catalyst shape-selectivity. This is strikingly demonstrated in Table 1 (17), with MTG pilot plant data taken at 11 and 645 hours on stream.

Here isomer distributions of the tri- and tetramethylbenzenes are compared with their equilibrium values. Selectivity for the 1,2,4- and 1,2,4,5-isomers are seen to increase with time on stream to 99.0% and 97.3%, respectively, compared with equilibrium values of 66.3% and 33.0%. Indeed techniques have been devised to enhance shape-selectivity by passivation of the external sites (18). These treatments will also impose diffusion barriers, which can further enhance selectivity according to classical principles established by Weisz (19).

Zeolite structures with limiting 8-ring apertures such as erionite and chabazite are capable of converting methanol selectively to light olefins (10). Aromatics, if formed, would be trapped in the supercages possessed by most of these small ring zeolites, and unable to escape. This is known as "ship-in-a-bottle" or "inverse" shape-selectivity. The accumulation of trapped aromatics can lead to catalyst deactivation.

### Mechanistic Considerations

It will be convenient to divide the following discussion into two parts. The first part concerns the sorption and activation of methanol, with formation of DME, culminating in the forming the initial C-C bond; the second, the autocatalysis and formation of intermediate olefins; and ensuing complex reactions.

**How Is The "First" C-C Bond Formed?** Early researchers were preoccupied with the question of how the initial C-C bond is formed from methanol. The origin and electronic structure of the purported C<sub>1</sub> reactive intermediate was vigorously debated. A wide variety of initiation mechanisms were proposed. These may be broadly classified as carbene-carbenoid, carbocationic, oxonium-ylide, or radical in nature. Consequently the proposed C<sub>1</sub> active species has been variously regarded as nucleophilic, electrophilic, or electroneutral. Unfortunately techniques for direct *in situ* observation of the reaction intermediates did not, and do not exist, and spectroscopic observation could only be conducted under conditions far from reaction conditions. As a result, much imaginative experimentation, including isotopic labeling and modeling of the active site or hypothetical intermediates with chemical surrogates, was undertaken to support or contradict the various proposals. The original evidence and arguments pro and con have been reviewed (7,8,93), and will

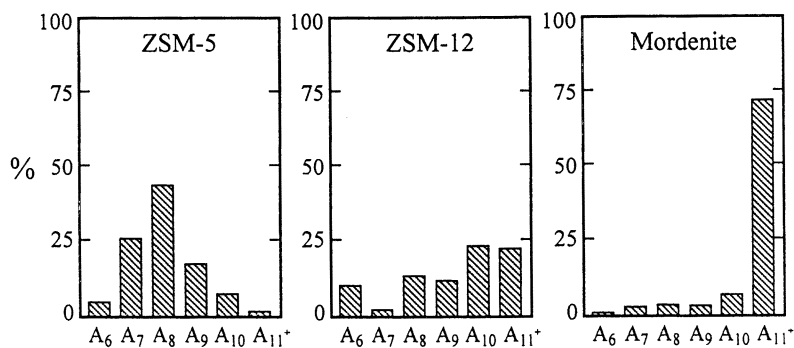


Figure 1. Influence of zeolite pore geometry on MTG aromatics distribution.

Table 1. Shape-Selectivity in Tri- and Tetramethylbenzenes from MTG

<b>T<sub>max</sub>, K</b>	670		687	
<b>WHSV, hr<sup>-1</sup></b>	1.6		1.6	
<b>TOS, hr</b>	11		645	
	<b>Equil</b>	<b>Exp</b>	<b>Equil</b>	<b>Exp</b>
<b>Tri-Me-Benzenes</b>				
<b>123</b>	8.1	2.2	8.2	0.3
<b>124</b>	66.3	90.9	66.6	99.0
<b>135</b>	25.6	6.9	25.4	0.7
<b>Tetra-Me-Benzenes</b>				
<b>1245</b>	33.0	67.6	32.8	97.3
<b>1235</b>	50.4	24.0	50.3	1.1
<b>1234</b>	16.6	8.4	16.9	1.6

not be repeated here. However the general hypotheses are sketched below for background.

**Carbene-Carbenoid Mechanisms.** As indicated by Equation 1, the key step or steps in the reaction is elimination of water.  $\alpha$ -Elimination would directly generate a carbene,  $\text{CH}_2$ . Elimination would be mediated by the cooperative action of acidic and basic centers in the zeolite. The carbene may be stabilized through interaction with the non-bonding electrons of the framework oxygen atoms in the zeolite to generate carbenoid species (isoelectronic with surface-bonded methylide as discussed later). Alternately, deprotonation of the methyl group of methanol or DME by a suitably basic site would generate a carbenoid species. These superactive  $\text{C}_1$  species would engage in C-C bond formation by  $\text{sp}^3$  C-H insertion.

**Carbocationic Mechanisms.** Carbocationic schemes are based on the assumption that the zeolite environment is superacidic in nature. Protonation of methanol in such a medium would generate methylium ions,  $\text{CH}_3^+$ , which would react by electrophilic attack on a C-H  $\sigma$ -bond to form the C-C bond, possibly through a pentavalent transition state.

**Oxonium-Ylide Mechanisms.** Methylation of DME would afford a trimethyloxonium (TMO) ion,  $(\text{CH}_3)_3\text{O}^+$ , associated with the zeolite conjugate base. Deprotonation of TMO would yield dimethyloxonium methylide,  $(\text{CH}_3)_2\text{O}^+-\text{CH}_2^-$ . The latter would undergo either an intramolecular Stevens-type rearrangement to form methyl ethyl ether, or an intermolecular reaction with an adjacent TMO to form dimethylethyloxonium,  $(\text{CH}_3)_2(\text{C}_2\text{H}_5)\text{O}^+$ . In another variation, deprotonation of a surface methoxyl generates a surface-bound nucleophilic methylide,  $\text{Z}-\text{OCH}_2^-$ , which can engage in C-C bond formation with electrophilic carbons in their vicinity. It has been noted that the surface-bound methylide is isoelectronic with surface-stabilized carbene (8). These mechanisms have attracted a great deal of attention, both theoretically and experimentally.

**Radical Mechanisms.** Radicals can readily be formed from DME by thermal decomposition, or by interaction with paramagnetic centers in the zeolite or on coke overlays. These radicals would interact with feed molecules as well as surface-bound species and the Brønsted site, leading to various  $\text{C}_1$  intermediates, including carbenoid.

Common to all the proposed reaction schemes, is the critical step of ultimately removing a proton from the methyl group. The timing of this event on the reaction coordinate, as well as its mechanism and energetics, is the crux of the debate. Deprotonation would presumably require a strongly basic site in the zeolite, and much of the mystery surrounding this reaction stems from this problem. If it is assumed that H-zeolites are strong Brønsted acids, then their conjugate base must be relatively weak. In fact it has been found that the HZSM-5 conjugate base is nucleophilic rather than basic towards the TMO cation (84). Radical initiation would circumvent this problem, however the experimental evidence thus far has eliminated this possibility (20).

Despite a prodigious amount of experimental work through the years, definitive answers to the question have remained elusive. In the last decade, computational methods have taken center-stage thanks to rapid advances in computer power and computational methodology, especially techniques based on density-functional theory (DFT). This has made possible an examination of the elementary processes of methanol activation on a molecular level, in unprecedented detail. A serious limitation to the theoretical approach however has been the necessity of working with relatively small clusters as models of the zeolite active site (21), in lieu of the extended structure. While the use of cluster models can provide an accurate picture of local H-bonding interactions, long-range forces are neglected. Significant progress has been made, however, in recent DFT calculations (22) with the relatively small (36 atoms) unit cell zeolite chabazite. In this work, use was made of periodic boundary conditions. In contrast, the unit cell of ZSM-5 has 288 atoms, an aggregate that is beyond the capability even of present-day massively parallel computers. Nevertheless the mechanistic insights afforded by computational methods, frequently complemented by spectroscopic data, have been quite remarkable. Most importantly, computational methods uniquely provide access to transition state structures.

The most elementary of the processes in methanol activation is chemisorption. Its initial interaction with zeolitic protons has now been analyzed in detail, and theoretical predictions compared with experimental data where possible. Earlier observations using  $^1\text{H}$  MASNMR, in conjunction with IR and TGA, indicated that the methyloxonium ion  $[\text{CH}_3\text{OH}_2]^+$  is formed as a stable cation through methanol protonation, at low coverages (23). At higher coverage, protonated clusters of H-bonded molecules were observed, with attendant fast proton exchange. This system was later simulated using small clusters of T-sites as models of the zeolite Brønsted site, and applying traditional quantum mechanical (Hartree-Fock, Møller-Plesset) as well as DFT methodology. These studies revealed that the methyloxonium ion is actually a transition state, while methanol is present mostly as a neutral, but strongly H-bonded molecule, rapidly exchanging protons (faster than the NMR time scale) with the zeolite host (24-26). Nevertheless, this interaction with the zeolite framework will polarize the C-O bond, resulting in an enhancement of the electrophilicity, and thus reactivity, of the carbon center (27) (however *vide infra*, ref. 85). In the early stages of reaction, the most abundant nucleophilic species present are "oxygenates" including water, or the framework oxygens, so that DME is the first observable product. Interaction with another methanol molecule yields DME, while interaction with framework oxygen would form surface methoxyl groups, which can be considered the final step of chemisorption. The presence of surface methoxyls is corroborated by extensive spectroscopic evidence (28-33). Their participation as reaction intermediates is supported by the fact that their appearance generally coincides with the first appearance of hydrocarbons.

Several detailed mechanisms have been proposed for DME formation. These proposals, which originally regarded  $[\text{CH}_3\text{OH}_2]^+$  as a stable intermediate, include that of Bandiera and Naccache (34) invoking the condensation of surface species  $[\text{CH}_3\text{OH}_2]^+$  and  $[\text{CH}_3\text{O}]$ , and Kubelková et al (35) where  $[\text{CH}_3\text{OH}_2]^+$  dehydrates to a

surface methoxyl, two of which condense to form DME. By means of DFT calculations, Blaszkowski and van Santen (36) examined the energetics of two parallel routes to DME. In the first route, a surface methoxyl reacts with a second molecule of adsorbed methanol; in the second, two methanol molecules interact while coadsorbed at the active site. In the second route, the calculations predicted an  $sp^2$  hybridization for central methyl group in the transition state. It is interesting to note that this is totally consistent with results of an earlier triple quadrupole MS study of gas phase ion-molecule reactions of methanol and methyloxonium ions. This study, carried out using isotopic labeling, revealed that the mechanism of DME-formation in the gas phase was  $S_N2$  (37). Blaszkowski and van Santen found the activation barrier of the second route to be 70 kJ/mol lower than the first, and therefore more favorable for DME formation. However the activation barrier is likely to vary with zeolite structure as demonstrated by Sinclair and Catlow (38). These workers also calculated the reaction path for surface methoxyl formation (39), discovering a product-like transition state with early proton transfer, thus raising the possibility that DME formation is a side reaction in equilibrium with methanol, rather than a sequential step as previously thought (1). Shah et al (22), in their DFT study with chabazite, considered surface methoxyl involvement, as well as the possibility of two methanols directly interacting in the channel. For the latter case, the aluminosilicate framework was regarded as a solvent-acid that stabilizes the reaction complexes through solvation. The direct reaction of two methanols was also found to be a favorable route, differing from other work only in the placement of the proton. The location of the transition state (in chabazite) according to this scenario was recently determined by Sandré et al (94).

As already mentioned, computational methods are being deployed to decipher the puzzle of initial C-C bond formation from methanol. Sinclair and Catlow (40) carried out a DFT study of carbene generation from methanol at aluminosilicate Brønsted sites. It was determined that carbenes from acid-catalyzed methanol deprotonation will be surface-stabilized with an activation barrier of 215-232 kJ/mol. This is in good agreement with the experimental value of 195 kJ/mol (41). Gas phase carbenes, on the other hand, are unlikely to be intermediates. Furthermore, the deprotonation of the methyl group to form a surface ylide would likely be the rate-limiting step of the MTG reaction. Shah et al (22) monitored the fate of a carbene in the 8-ring window of chabazite. The  $CH_2$  moiety, whether generated by deprotonation of surface methoxyl or initially placed in the middle of the channel, migrated to a framework oxygen where it inserts into OH or abstracts a proton from the zeolite to revert back to a methyl group. Thus the carbene does not correspond to a local minimum on the potential energy surface (PES). However the possibility of a transition state with carbenic character cannot be ruled out.

Using DFT, Blaszkowski and van Santen compared the heats of adsorption and activation barriers of a large number of possible reaction sequences culminating in the early C-C bond formation (42). It was concluded that ethanol and methyl ethyl ether are the first  $C_2$  products, and that these are formed from surface methoxyl. Subsequent dehydration of these products yields ethylene. It was further determined that trimethyloxonium, while it can exist as an intermediate on the PES, does not have

a direct role in C-C bond formation because of a high-energy barrier. The formation of all of these initial products has now been directly observed by *in situ*  $^{13}\text{C}$  NMR (43). Trimethyloxonium was detected upon adsorption of DME on HZSM-5 at 173 K, however its  $^{13}\text{C}$  NMR signal disappeared on warming to room temperature, before the appearance of hydrocarbons (44). This is consistent with Blaszkowski and van Santen's conclusion. Trimethyloxonium could not be observed in the presence of methanol. Shah et al (22) in their DFT study removed a proton from TMO, and upon optimizing the ylide, followed by optimizing the whole system, found that the proton migrated back from the framework to the  $(\text{CH}_3)_2\text{O}^+-\text{CH}_2^-$  without activation energy. This showed that ylide is unlikely to be a local minimum on the PES, at least in chabazite.

A recent paper of Stich et al (85) describes an *ab initio* molecular dynamics simulation of methanol activation in chabazite and the 8-ring of ferrierite. It was concluded that protonation of a single methanol does not lead to activation (as reflected in lengthening of the C-O bond). Higher methanol loadings are necessary. In addition, dynamical effects, and zeolite topology must be taken into account for any explanation of zeolite catalytic action.

In a recent landmark paper, with possible implications for MTG mechanism, Kramer et al (45) demonstrated the activation of  $\text{CH}_4$  by zeolitic protons. The rate of H-D exchange with  $\text{CD}_4$  in HZSM-5 was followed by IR, and proceeded with an activation energy of 130 kJ/mol. Using the cluster approximation, *ab initio* calculations were performed on the ground and activated states. The calculated transition state geometry for the reaction appears in Figure 2 (21,45).

The transition state is more covalent than ionic in character. By varying jointly the SiH bond distances of the peripheral (cluster terminating) groups it was possible to change the proton affinity (PA) of both oxygens equally. A change of this bonding distance between 0.12-0.17 nm causes a change in the PA of ~60 kJ/mol. The barrier height was found to be unchanged, due to the covalent sharing of partial OH bond strengths. In a second calculation, the PA of only the proton-accepting oxygen was lowered. In this case the barrier was seen to increase proportional to the PA difference between proton donor and acceptor by  $\Delta E_{\text{act}} \approx 0.7\Delta E_{\text{deprotonation}}$ .

To form a carbonium ion, it would be necessary to deform  $\text{CH}_4$ . In the adsorbed state  $\text{CH}_4$  is H-bonded with the zeolitic proton but with an energy of only about 10 kJ/mol. Thus no stable  $\text{CH}_5^+$  intermediate (local minimum on the PES) was found, and therefore this carbonium ion would be a transition state. However the short calculated bond distances indicate that the transition state is covalent rather than ionic.

According to this picture, the departing deuteron bonds to a lattice oxygen different than the one from which the attacking proton originated. The activation energy of the process was strongly dependent on the *difference* of the PA's between the two bonding oxygens rather than the absolute energy of deprotonation. This difference controls the effective acidity of the zeolite Brønsted site.



There is established a picture of dynamical bifunctional Lewis base-assisted Brønsted acidity, which could also provide a *modus operandi* for the elusive mechanism of deprotonation and “first” C-C bond formation in MTG. It should be noted however that this requires site heterogeneity, which is in contradiction to previous assumptions that the Brønsted sites in HZSM-5 are chemically homogeneous (83).

**Autocatalysis and Beyond.** The first evidence of autocatalysis in MTG was from reaction kinetics (14-16). Experimental verification soon followed in the observation of rate accelerations achieved by co-addition of olefins (or olefin precursors) (46,47), and interestingly, aromatics (48,49). It became quickly apparent that the reaction path of equation 1 is an idealization, and that the MTG mechanistic vista was becoming increasingly clouded.

There ensued a spirited debate around the question: “is ethylene the ‘first’ olefin?” The uncertainty surrounding ethylene origins was increased with publication of a study by Dessau and LaPierre (50), who reported that  $^{13}\text{C}_3\text{H}_7\text{OH}$ , co-reacted with unlabeled propylene over HZSM-5, gave high concentrations of singly-labeled ethylene. Dessau and LaPierre concluded that essentially all of ethylene is a secondary product of cracking of higher olefins, which had been formed from lower homologues through electrophilic methylation (51,52). Additional evidence was presented by Dessau (90) in experiments co-reacting  $^{13}\text{C}_3\text{H}_7\text{OH}$  and unlabeled 1-heptene, which gave similar results. Dessau’s interpretation was challenged by Mole (53), who cited his own results with  $^{13}\text{C}$  and deuterium-labeled feeds (46), where product isotope distributions showed that a significant fraction of ethylene must be produced by direct reaction of two methanol molecules.

The formation of higher olefins by step-wise methylation (47,51) was disputed by Dahl and Kolboe (54), based on  $^{13}\text{C}$  labeling experiments with methanol/ethanol mixtures reacting over SAPO-34. Isotope distributions revealed that only a minor fraction of  $\text{C}_3\text{H}_6$  resulted from  $\text{C}_2\text{H}_4$  methylation. Dahl and Kolboe proposed a “carbon pool mechanism” for methanol conversion, shown in Scheme 1.

According to these workers “the hydrocarbon pool  $(\text{CH}_2)_n$  represents an adsorbate which may have many characteristics in common with ordinary coke, and which might easily contain less hydrogen than indicated.” The  $(\text{CH}_2)_n$  adsorbate is methylated by methanol and eliminates olefins. Although the nature of this carbonaceous species was not further defined, the concept is intriguing, and we will return to it later. A similar study, but co-feeding  $^{13}\text{C}_3\text{H}_7\text{OH}$  and  $^{12}\text{C}_3\text{H}_7\text{OH}$ , was carried out by Dahl et al (55) over HZSM-5. Results supported their carbon pool hypothesis. Additionally isotope distributions showed that  $\text{C}_2\text{H}_4$  was essentially a primary, though parallel, product from methanol.

In a subsequent study on the mechanism of autocatalysis in the presence of aromatics, Mole et al (49) co-reacted  $^{13}\text{C}$ -labeled aromatics with unlabeled methanol, as well as  $^{13}\text{C}_3\text{H}_7\text{OH}$  with unlabeled aromatics. In both cases scrambling of  $^{13}\text{C}$  occurred as evidenced by formation of singly labeled ethylene. Therefore even ring carbon is incorporated into product ethylene. Mole et al sought to explain this finding by

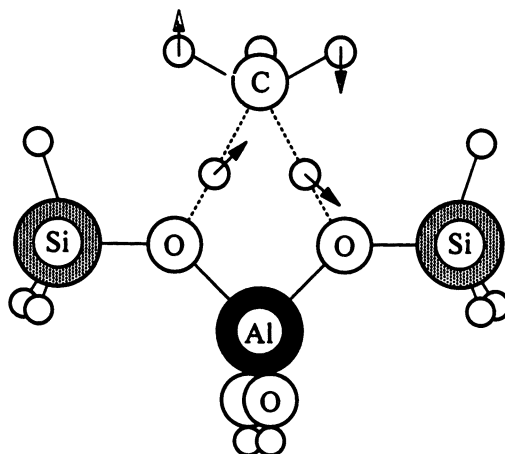
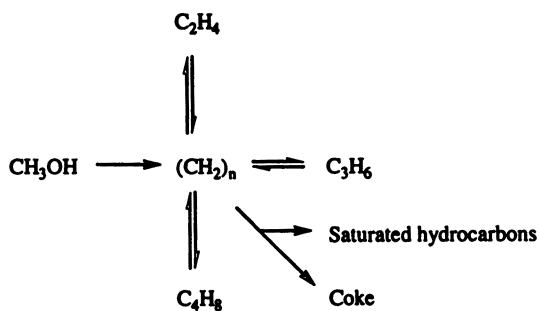


Figure 2. Calculated transition state geometry for H-D exchange between methane and an acid zeolite cluster. Arrows indicate main components of the displacement vectors along the reaction coordinate (adapted from ref. 45).

### Scheme 1



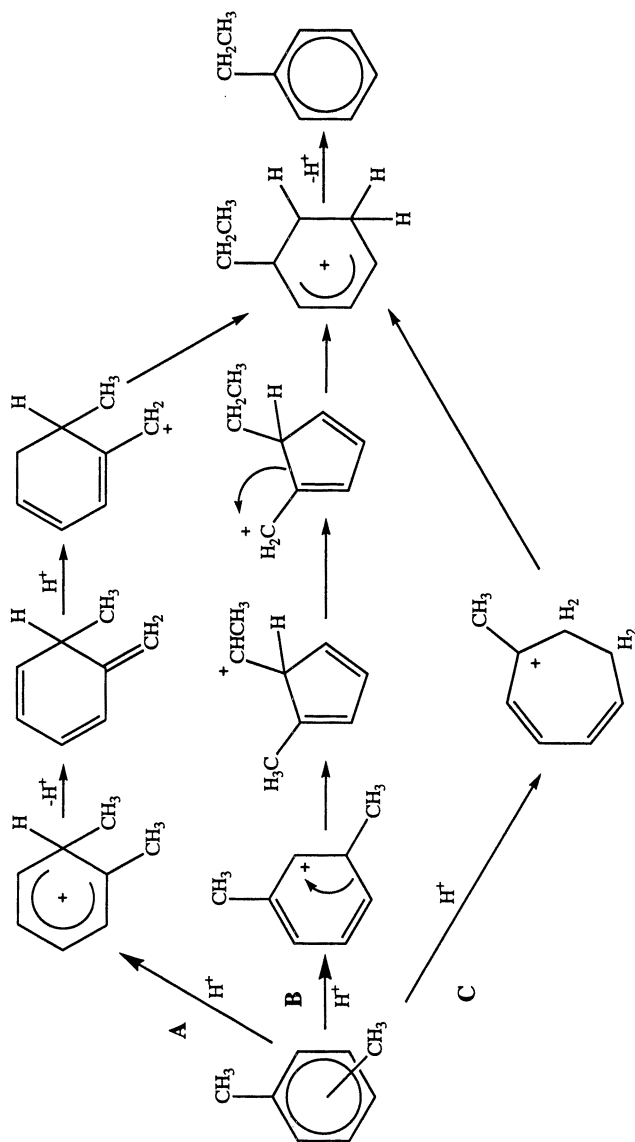
invoking an initial ring methylation followed by prototropic H-shift in the protonated aromatic to form an *exo*-methylene intermediate, which suffers electrophilic methylation (Path A, Scheme 2) to form the C-C bond. An alternate mechanism involving a 6,5-ring contraction was favored by Pines (56) (Path B, Scheme 2), while yet another involving a 6,7-ring expansion was proposed by Isagulyants et al (57) (Path C, Scheme 2).

The results of these model experiments may be especially significant in view of the fact that aromatics are detectable in very early stages of the reaction, at low (0.2%) conversion (58). However the intrusion here of diffusion disguise (50,59) cannot be discounted. These low conversion conditions would be conducive to the polymethylation of the benzene ring, owing mainly to the high local concentration of unconverted methanol and DME (15). Thus the ZSM-5 pores become quickly occupied by aromatics, and will remain so through the course of reaction due to diffusional and shape-selective constraints. Schulz et al (60,86) dissolved samples of equilibrium MTG catalysts with HF, and found the organic residue to consist of bulky polyalkyl aromatics, which had been entrapped in the zeolite. From geometric considerations these aromatics are likely to reside in the cages formed by intersecting channels of ZSM-5. A dynamic equilibrium with smaller aromatics will be established through alkyl transfers.

Unraveling MTG mechanism has proven to be a formidable task due to complex kinetics and diffusion disguise. An incomplete understanding of the bonding interactions of the organics with the catalyst surface further complicates the issue. The picture of the active site as a simple Brønsted acid may not be entirely adequate (91,92), at least for the post-initiation steps. It is becoming increasingly likely that the post-initiation working catalyst is some form of organic moiety working in concert with the framework protonic site. The organic moiety may be regarded in this sense as a co-catalyst. Derewinski et al (61) reported a most interesting result where HZSM-5, poisoned by pyridine, became active for MTO upon addition of a small amount of ethanol to the feed. The effect was completely reversible. These workers attributed the phenomenon to a selective poisoning of strong Brønsted sites, which are responsible for initiation and hydride transfer, and to ethanol enabling the by-passing of initial C-C bond formation. The propagation in presence of ethanol was assumed to be mediated through an ethoxyl moiety coordinated to a "weak" acid site, with bond formation concurrent with back-donation of a proton to a framework oxygen. Kolboe (62) reported similarly that fresh HZSM-5 is inactive for hydrocarbon formation below 523 K unless adsorbed hydrocarbons are present. Kolboe depicted the active site as a dual acid/base site consisting of a carbenium ion and an induced basic framework oxygen site.

Let us return now to Kolboe's "carbon pool" concept. It will be instructive first to consider the overall stoichiometry of oxygenates conversion over HZSM-5. Because ZSM-5 is an excellent H-transfer catalyst, little molecular hydrogen is formed during the conversion of oxygenates to hydrocarbons. In the latter stages of reaction three molecules of hydrogen are transferred to produce paraffins for every aromatic ring generated. For the general reaction stoichiometry

Scheme 2





where  $(C_xH_{y-2z})$  is the average composition of the hydrocarbon product, if  $(y-2z) < 2$  then coke or coke-like residues (and/or  $CO_2$  in the case of carboxylates) will be formed. Interestingly, for “H-deficient” feeds such as  $CH_3COOH$  as an extreme case,  $(y-2z)/x = 0$ , the deficiency can be partially remedied by adding methanol as a hydride source (63). Instead of producing  $CO_2$ , deoxygenation increasingly shifts over to  $H_2O$  with increasing methanol co-feed. This catalyst is in effect a “nanoscale Waring blender”, and regardless of feed stoichiometry gives product of very similar yield structure (Table 2), but with lower H-content feeds tending to give a more aromatic product.

The results in Table 2 could be attributable in part to diffusion disguise, but may also imply that there is a common intermediate or reaction path. Haag (64) postulated that this common “intermediate” is an equilibrium pool of olefins. Once formed, these olefins convert to aromatics, and to lower paraffins through H-transfer (1). This may be compared with the “carbon pool mechanism” of Dahl et al (54), who considered that the pool can be H-deficient, or coke-like. These pool mechanisms, while descriptive, are nevertheless “black box” schemes, and comprehension of the actual structure of the intermediate or intermediates at steady-state seemed beyond grasp.

Recent advances in laboratory heterogeneous catalytic reactor methodology, in conjunction with solid state NMR, promise to bring the ideal *in situ* experiment a step closer to realization. Goguen et al (65) have described a pulse catalytic flow reactor with the capability of being cooled from a reaction temperature of 643 K to 298 K in 200ms. Prior to the rapid quench, volatile products are continuously analyzed by GC-MS, so that the entire reaction sequence can be followed down to very low contact times. The cooled catalyst is transferred to a MAS rotor and sealed in a glovebox, and  $^{13}C$  MASNMR spectra immediately acquired. This technique effectively “freezes” the reaction in time, while providing a fossil record of reaction intermediates on the catalyst. This technique was used for studying the MTO reaction (65). After a 2s induction period, during which DME and traces of ethylene were detected, abundant hydrocarbons began to form. In the next 4s the usual MTO products were observed, but significantly the NMR spectrum showed the early presence of alkyl substituted cyclopentenyl carbenium ions similar to **1** in the catalyst.

These species had been previously found by Haw et al (66-68) to be readily formed from olefins on zeolites. Their significance rests on the facility with which they can undergo 5,6 ring rearrangements, as well as equilibrate with acyclic intermediates, suggesting a possible central role in the reaction. There is clearly an analogy with classical Friedel-Crafts, as well as sulfuric acid isoparaffin-olefin alkylation catalysis. These reactions are characterized by an induction period, during which complex organics known variously as “red oils”, “conjunct polymers”, or “sludge hydrocarbons” are built up. Indeed it was early-recognized (69-71) that alkylation performance was associated with the presence of red oil, i.e., poor quality alkylate is

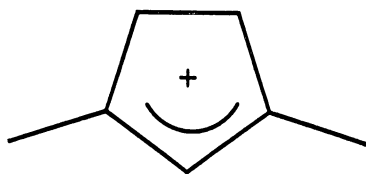
**Table 2. Hydrocarbon Product Distributions from Various O-Compounds over HZSM-5**

T = 644 K; P = 1 atm; LHSV = 1 hr<sup>-1</sup>

	Methanol (J)	1-Heptanol (J)	Acetone (J)	Acetic Acid (a) (62)	1 Acetic Acid 4 Methanol (b) (62)
C <sub>1</sub>	1.0	0.0	0.1	0.1	1.2
C <sub>2</sub>	1.1	0.4	2.6	1.7	1.7
C <sub>3</sub>	17.2	16.6	9.4	5.4	6.4
C <sub>4</sub>	25.6	30.4	11.5	7.5	5.4
C <sub>5</sub> +	13.9	13.3	12.8	0.7	6.2
A <sub>6</sub>	1.7	3.4	2.6	1.5	1.9
A <sub>7</sub>	10.5	14.3	13.0	12.3	11.1
A <sub>8</sub>	18.0	12.8	25.0	29.3	27.9
A <sub>9</sub>	7.5	5.3	20.2	20.2	26.0
A <sub>10</sub>	3.3	2.9	2.8	21.3	10.3
A <sub>11</sub> +	0.2	0.6	0.0	0.0	1.9
CO <sub>2</sub> yield, mol%	0.0	0.0	6.3	19.6	3.0

(a) 672 K; 95.3% conversion.

(b) 71.4% conversion.

**1**

produced in its absence. In sulfuric acid, isobutane/butene alkylation can be initiated by the addition of small amounts of pre-formed red oil (69). In addition to their catalytic function, red oils are believed to enhance the solubility of isobutane in the acid. Red oils are also formed in HF alkylation, but have no comparable catalytic effect (72), due to the greater solubility of isobutane in the HF acid phase. The red oils are a product of olefin polymerization plus H-transfer and, according to Pines (73), are "cyclic unsaturated hydrocarbons consisting predominantly of five-membered mono- or polycyclic rings and having an average of two to three double bonds per molecule". Deno et al (74) had previously studied the fate of the *t*-butyl cation in 96% H<sub>2</sub>SO<sub>4</sub>, and observed the predominance of cyclopentenyl cations similar to 1 in the complex product. The "red oil cation" (75) forms a complex with the acid component, and in addition to serving as an excellent source of hydride, it is active for hydride abstraction (69,76). All of the foregoing properties serve to justify its characterization as a co-catalyst.

Cyclopentenyl cations are therefore signature intermediates of olefin condensation reactions in many acidic environments including zeolites. Because of spatial restrictions, medium pore zeolites such as ZSM-5 cannot accommodate the high molecular weight components of red oils. Walsh and Rollmann (77-79) showed that coke formation in zeolites is controlled by zeolite shape-selectivity, and because of size-exclusion, ZSM-5 is exceptionally resistant to internal coke build-up. The most spacious cavities in ZSM-5 are the cages formed by channel intersections. From computer modeling (80) the maximum volume of the cage is 0.15 nm<sup>3</sup>. This would suffice to host a single aromatic nucleus comfortably, which is in agreement with the results of sorption measurements (81). Xu et al (87) have recently succeeded in preparing a stable benzenium ion in HZSM-5, which they believe to be formed in the channel intersection, with steric constraints accounting for its alkyl substitution pattern. Thus the (CH<sub>2</sub>)<sub>n</sub> "carbon pool" of Dahl et al may prove in the final analysis to have an exceedingly simple structure, a "low molecular weight red oil", as it were. Finally it seems likely that this organic moiety, in addition to being a precursor to aromatics, has a co-catalytic role, particularly for H-transfer, and is present in the form of a cycloalkenyl cation Lewis base complex.

## Conclusions.

While the mystery of initial C-C bond formation from methanol remains unsolved, a reasonable hypothesis has emerged in the bifunctional Lewis base- assisted Brønsted acid catalysis mechanism of Kramer et al (45). This hypothesis provides the theoretical underpinning for some earlier intuitive notions (1). Significant progress has been made in understanding the mechanisms of succeeding steps, owing largely to advances in experimental methodology, in conjunction with DFT calculations (82). Much of this new understanding may also be generally applicable to hydrocarbon reactions in zeolites. Finally, there are some workers who have maintained that since MTG is an autocatalytic reaction, the mechanism of initial C-C bond formation is of negligible interest. But this is tantamount to saying conception is less interesting than birth, a viewpoint with which this Author disagrees.



## Literature Cited

1. Chang, C. D.; Silvestri, A. J. *J. Catal.* **1977**, *47*, 249.
2. Kam, A. Y.; Schreiner, M.; Yurchak In *Handbook of Synfuels Technology*; Meyers, R. A., Ed.; McGraw-Hill: New York, 1984, Ch. 2-3.
3. Yurchak, S. *Stud. Surf. Sci. Catal.* **1988**, *36*, 251.
4. Penick, J. E.; Lee, W.; Maziuk, J In *Chemical Reaction Engineering-Plenary Lectures*, Wei, J.; Georgakis, C., Eds.; ACS Symposium Ser. 226; American Chemical Society: Washington, DC, 1983, Ch. 2.
5. Chang, C. D. In *Handbook of Heterogeneous Catalysis*, Ertl, G.; Knözinger, H.; Weitkamp, J., Eds.; Wiley-VCH: Weinheim, Germany, 1997, Vol. 4; Ch. 3.7.
6. Maiden, C. J. *Stud. Surf. Sci. Catal.* **1988**, *36*, 1.
7. Chang, C. D. *Catal. Rev.-Sci. Eng.* **1983**, *25*, 1.
8. Hutchings, G. J.; Hunter, R. *Catal Today* **1990**, *6*, 279.
9. Krohn, D. E.; Melconian, M. G. *Stud. Surf. Sci. Catal.* **1988**, *36*, 679.
10. Chang, C. D. *Catal. Rev.-Sci. Eng.* **1984**, *26*, 323.
11. Socha, R. F.; Chang, C. D.; Gould, R. M.; Kane, S. E.; Avidan, A. A. In *Industrial Chemicals via C<sub>1</sub> Processes*, Fahey, D. R., Ed.; ACS Symposium Ser. 328; American Chemical Society: Washington, DC, 1987, Ch. 3.
12. Keim, K. H.; Krambeck, F. J.; Maziuk, J.; Tönnemann, A. *Erdöl Kohle-Erdgas Kohle* **1987**, *103*, 82.
13. Barger, P. T.; Lesch, D. A. *Arabian J. Sci. Eng.* **1996**, *21*, 263.
14. Chen, N. Y.; Reagan, W. J. *J. Catal.* **1979**, *59*, 123.
15. Chang, C. D.; Lang, W. H.; Smith, R. L. *J. Catal.* **1979**, *56*, 169.
16. Ono, Y.; Imai, E.; Mori, T. *Z. Phys. Chem. NF* **1979**, *115*, 99.
17. Yurchak, S.; Voltz, S. E.; Warner, J. P. *Ind. Eng. Process Des. Dev.* **1979**, *18*, 527.
18. Olson, D. H.; Haag, W. O. In *Catalytic Materials: Relationship Between Structure and Reactivity*, Whyte, T. E., Jr.; Dalla Betta, R. A.; Derouane, E. G.; Baker, T. T. K., Eds.; ACS Symposium Ser. 248; American Chemical Society: Washington, DC, 1984, Ch. 14.
19. Weisz, P. B. *Pure Appl. Chem.* **1980**, *52*, 2091.
20. Hunter, R.; Hutchings, G. J. *J. Chem. Soc., Chem. Commun.* **1987**, 377.
21. van Santen, R. A.; Kramer, G. J. *Chem. Rev.* **1995**, *95*, 637.
22. Shah, R.; Gale, J. D.; Payne, M. C. *J. Phys. Chem. B* **1997**, *101*, 4787.
23. Lercher, J. A.; Anderson, M. W.; Klinowski, J. *J. Chem. Soc., Farad. Trans.* **1990**, *86*, 3039.
24. Blaszkowski, S. R.; van Santen, R. A. *J. Phys. Chem.* **1995**, *99*, 11728.
25. Zocovich-Wilson, C. M.; Viruela, P.; Corma, A. *J. Phys. Chem.* **1995**, *99*, 13224.
26. Sauer, J.; Ugliengo, P.; Garrone, E.; Saunders, V. R. *Chem. Rev.* **1994**, *94*, 2095.
27. Gale, J. D.; Catlow, C. R. A.; Cheetham, A. K. *J. Chem. Soc., Chem. Commun.* **1991**, 178.
28. Salvador, P.; Fripiat, J. *J. Phys. Chem.* **1975**, *79*, 1842.

29. Derouane, E. G.; Gilson, J. P.; B.Nagy, J. *Zeolites*, **1982**, *2*, 42.
30. Nováková, J.; Kubelková, L.; Dolejšek, Z. *J. Catal.* **1987**, *108*, 208.
31. Forester, T. R.; Howe, R. F. *J. Am. Chem. Soc.* **1987**, *109*, 5076.
32. Bosáček, V. *J. Phys. Chem.* **1993**, *97*, 10732.
33. Gregory Oliver, F.; Munson, E. J.; Haw, J. F. *J. Am. Chem. Soc.* **1992**, *96*, 8106.
34. Bandiera, J.; Naccache, C. *Appl. Chem.* **1991**, *69*, 139.
35. Kubelková, L.; Nováková, J.; Nedemová, K. *J. Catal.* **1990**, *124*, 441.
36. Blaszkowski, S.; van Santen, R. A. *J. Am. Chem. Soc.* **1996**, *118*, 5152.
37. Tedder, J. M.; Stewart Walker, G. *J. Chem. Soc., Perkin Trans. 2* **1991**, 317.
38. Sinclair, P. E.; Catlow, C. R. A. *J. Chem. Soc., Faraday Trans.* **1996**, *92*, 2099.
39. Sinclair, P. E.; Catlow, C. R. A. *J. Chem. Soc., Faraday Trans.* **1997**, *93*, 333.
40. Sinclair, P. E.; Catlow, C. R. A. *J. Phys. Chem. B* **1997**, *101*, 295.
41. Jayamurthy, M.; Vasudevan, S. *Catal. Lett.* **1996**, *36*, 111.
42. Blaszkowski, S. R.; van Santen, R. A. *J. Am. Chem. Soc.* **1997**, *119*, 5020.
43. Munson, E. J.; Kheir, A. A.; Lazo, N. D.; Haw, J. F. *J. Phys. Chem.* **1992**, *96*, 7740.
44. Munson, E. J.; Haw, J. F. *J. Am. Chem. Soc.* **1991**, *113*, 6303.
45. Kramer, G. J.; van Santen, R. A.; Emeis, C. A.; Novak, A. K. *Nature*, **1993**, *363*, 529.
46. Mole, T. *J. Catal.* **1983**, *84*, 423.
47. Wu, M. M.; Kaeding, W. W. *J. Catal.* **1984**, *88*, 478.
48. Mole, T.; Whiteside, J. A.; Seddon, D. *J. Catal.* **1983**, *82*, 261.
49. Mole, T.; Bett, G.; Seddon, D. *J. Catal.* **1983**, *84*, 435.
50. Dessau, R. M.; LaPierre, R. B. *J. Catal.* **1982**, *78*, 136.
51. Anderson, J. R.; Fogar, K.; Mole, T.; Rajadhyaksha, R. A.; Sanders, J. V. *J. Catal.* **1979**, *58*, 114.
52. Anderson, J. R.; Mole, T.; Christov, V. *J. Catal.* **1980**, *61*, 477.
53. Mole, T. *J. Catal.* **1987**, *103*, 524.
54. Dahl, I. M.; Kolboe, S. *Catal. Lett.* **1993**, 329.
55. Dahl, I. M.; Kolboe, S.; Rønning, P. O. *Stud. Surf. Sci. Catal.* **1995**, *98*, 176.
56. Pines, H. *J. Catal.* **1985**, *93*, 205.
57. Isagulyants, G. V.; Kovalenko, L. I.; Dubinskii, Yu. G. *Izvest. Akad. Nauk. SSSR, Ser. Khim.* **1987**, *11*, 2443.
58. Chang, C. D. *Chem. Eng. Sci.* **1981**, *35*, 789.
59. Rys, P. *Acc. Chem. Res.* **1976**, *9*, 345.
60. Schulz, H.; Barth, D.; Zhao, S. *Stud. Surf. Sci. Catal.* **1991**, *68*, 783.
61. Derewinski, M.; Dzwigaj, S.; Haber, J. *Zeolites*, **1984**, *4*, 214.
62. Chang, C. D.; Chen, N. Y.; Koenig, L. R.; Walsh, D. E. *Prep. Pap.-Am. Chem. Soc., Div. Fuel Chem.* **1983**, *28*, 146.
63. Kolboe, S. *Stud. Surf. Sci. Catal.* **1988**, *36*, 189.
64. Haag, W. O. In *Proc. Int. Zeolite Conf.*, **6<sup>th</sup>**; Olson, D. H.; Bisio, A. Eds.; Butterworth: UK; **1984**; p. 466.
65. Goguen, P. W.; Xu, T.; Barich, D. H.; Skloss, T. W.; Song, W.; Wang, Z.; Nicholas, J. B.; Haw, J. F. *J. Am. Chem. Soc.* **1998**, *120*, 2650.

66. Haw, J. F.; Richardson, B. F.; Oshiro, I. S.; Lazo, N. L.; Speed, J. A. *J. Am. Chem. Soc.* **1989**, *111*, 2052.
67. Xu, T.; Haw, J. F. *J. Am. Chem. Soc.* **1994**, *116*, 7753.
68. Oliver, F. G.; Munson, E. J.; Haw, J. F. *J. Phys. Chem.* **1992**, *96*, 8106.
69. Hofmann, J. E.; Schriesheim, A. *J. Am. Chem. Soc.* **1962**, *84*, 957.
70. Doshi, B.; Albright, L. F. *Ind. Eng. Chem., Proc. Des. Dev.* **1976**, *15*, 53.
71. Kramer, G. M. ACS Symp. Ser. 55; American Chemical Society: Washington, DC, 1977; Ch. 1.
72. Hutson, T., Jr.; Hays, G. E. ACS Symp. Ser. 55; American Chemical Society: Washington, DC, 1977; Ch. 2.
73. Pines, H. *The Chemistry of Catalytic Hydrocarbon Conversions*; Academic Press: New York, NY, 1981; pp. 39-41.
74. Deno, N. C.; Boyd, D. B.; Hodge, J. D.; Pittman, C. U., Jr.; Turner, J. O. *J. Am. Chem. Soc.* **1964**, *86*, 1745.
75. Albright, L. F.; Li, K. W. *Ind. Eng. Chem., Proc. Des. Dev.* **1970**, *9*, 447.
76. Albright, L. F.; Spalcing, M. A.; Faunce, J.; Eckert, R. E. *Ind. Eng. Chem. Res.* **1988**, *27*, 391.
77. Walsh, D. E.; Rollmann, L. D. *J. Catal.* **1977**, *49*, 369.
78. Rollmann, L. D.; Walsh, D. E. *J. Catal.* **1979**, *56*, 139.
79. Walsh, D. E.; Rollmann, L. D. *J. Catal.* **1979**, *56*, 195.
80. Nagy, T. F.; Mahanti, S. D.; Dye, J. L. *Zeolites* **1997**, *19*, 57.
81. Hill, S. G.; Seddon, D. *Zeolites* **1991**, *11*, 699.
82. Haw, J. F.; Nicholas, J. B.; Xu, T.; Beck, L. W.; Ferguson, D. B. *Acc. Chem. Res.* **1996**, *29*, 259.
83. Venuto, P. B. *Microporous Materials* **1994**, *2*, 297.
84. Hellring, S. D.; Schmitt, K. D.; Chang, C. D. *J. Chem. Soc., Chem. Commun.* **1987**, 1320.
85. Stich, I.; Gale, J. D.; Terakura, K.; Payne, M. C. *Chem. Phys. Lett.* **1998**, *283*, 402.
86. Schulz, H.; Lau, K.; Claeys, M. *Appl. Catal. A: General* **1995**, *132*, 29.
87. Xu, T.; Barich, D. H.; Goguen, P. W.; Song, W.; Wang, Z.; Nicholas, J. B.; Haw, J. F. *J. Am. Chem. Soc.* **1998**, *120*, 4025.
88. Farcasiu, M.; Degnan, T. F. *Ind. Chem. Res.* **1988**, *27*, 45.
89. Fraenkel, D.; Levy, M. *J. Catal.* **1989**, *118*, 487.
90. Dessau, R. M. *J. Catal.* **1986**, *99*, 111.
91. Medin, A. S.; Yu, V.; Kazansky, V. B.; Pelmentschikov, A. G.; Zhidomirov, G. M. *Zeolites*, **1990**, *10*, 668.
92. Fajula, F. *Stud. Surf. Sci. Catal.* **1995**, *97*, 133.
93. Chang, C. D. ACS Symp. Ser. 368, American Chemical Society, Washington, DC, 1988, Ch. 39.
94. Sandré, E.; Payne, M. C.; Gale, J. D. *J. Chem. Soc. Chem. Commun.* **1998**, 2445.

## Chapter 8

# Highly Selective Synthesis of Light Olefins from Methanol Using Metal-Incorporated Silicoaluminophosphate Catalysts

Tomoyuki Inui

Corporate Center for Gas and Chemical Research, Daido Hoxan Inc., 6-40,  
Chikko Shinmachi 2-Cho, Sakai, Osaka 592-8331, Japan  
(fax: +(81)-722-44-8085; e-mail: inui-tom@spk1.dhi.co.jp)

Development of zeolitic catalysts for light olefin synthesis for the past two decades is reviewed. Change in the trend of the research for olefin synthesis on the zeolite catalyst always involved the terms of selectivity, structure of zeolites, their acidic properties, and deactivation owing to coke formation. In the first decade, the kind of zeolite targeted has been shifted from the narrow pore-size zeolites such as chabazite, to the medium pore-size zeolite such as H-ZSM-5 and then metallosilicates having the pentasil structure. In the latest decade, the main target has been concentrated to SAPO-34 and MeAPSO-34, which possess a chabazite-like structure but weaker acidity than chabazite. The former converts methanol to C<sub>2</sub> - C<sub>4</sub> olefins more than 95%, and the later, especially Ni-APSO-34 converts methanol to ethylene as high as 90%. The unique catalytic property of Ni-APSO-34 is ascribed to the properly weak acidity. The most recent studies on this type of catalyst are elucidating the controlling factors for catalytic performance in detail. Beside the proper acid strength, the sharp size-distribution of the crystals around 0.8-0.9 μm is preferable. In order to realize these optimum properties, it has been recognized that the crystallization procedure is essentially important. The effect of several post-modifications on the catalytic performance are also described.

Light olefins such as ethylene and propylene are the indispensable building blocks for petrochemical industry, and major parts of them are producing by cracking of naphtha, especially in European and east Asian countries. Since this production method is sensitively reflected by the price of petroleum as practically occurred in the period of Oil Crises, alternative routes have been investigated thereafter (1-2). On the other hand, dehydrogenation of ethane, which is contained in natural gas, is operating mainly in USA and Canada, and a considerable part of ethylene demand is compensated by this method. This method is cheaper than the naphtha cracking, however, since other valuable light olefins, such as propylene and butenes must be obtained separately, whole olefins supply cannot be depended on this production route exclusively.

Investigations for the alternative route of light olefin synthesis done after the

Oil Crisis are roughly classified to three categories (3). One is the conversion of syngas, which can be obtained by various ways from alternative fossil resources, by using Fischer-Tropsch (FT) type Fe-, Co-, Ru-, or Rh-based catalysts. In fact, a considerable number of studies on the improvement of FT-type catalyst for the purpose of selective olefin synthesis had been done, however, since this synthesis route is essentially restricted by Shultz-Flory (SF) law in the carbon number distribution of the products, the objective could not be achieved (4). Some deviation from SF law could be observed in a condition of lower conversion level (5), however, most probably, at a higher conversion level this deviation would be canceled, and after all, the product distribution is apt obey in SF law.

Second one had been an ambitious challenge that oxidative coupling of methane to synthesize ethylene directly, and a variety of trials had been done in 1980's concentratedly (6). However, the consistent contradiction, appeared in a conflicted relationship between selectivity and conversion, prevented selective and effective synthesis of ethylene. The main reason is that this reaction essentially involves the homogeneous combustion process owing to the higher reaction temperature around 750 - 800°C, and moreover, durability of the catalyst cannot be easily guaranteed at that high temperature level.

The third route is methanol conversion using the shape-selective zeolitic catalysts. This route is regarded as an indirect olefin synthesis from the view point of syngas conversion or conversion of natural gas or associated gas (2). In spite of that, as pointed out through the feasibility study on olefin production from methanol, if the selectivity is high enough at a high conversion level of the feed materials, even such an indirect synthesis, the potential to realize the practical application for olefin synthesis would be much higher than other simple direct syntheses (2).

The difficulty accompanied with zeolitic catalysts is consistently in the problem of deactivation of the catalyst owing to coke formation. Therefore, always one of the focuses of these studies has been concentrated to prevent or minimizing the coke formation. However, judging from the selectivity and yield, methanol to olefin (MTO) route is considered to be the most promising way. In fact, most recently UOP/HYDRO process has started its operation in Norway using methanol synthesized from natural gas via reforming into syngas (7 - 8). However, still further improvement in catalyst performance, especially selectivity to aimed olefins is requested.

On this occasion, it would be important to review the progress of researches on MTO from the view point of the relationship between selectivity and characteristics of various kinds zeolite and zeolite-family catalysts.

### **Change in Trend of Research on Methanol-to-Olefin Conversion Using Zeolitic Catalysts**

**Catalytic Performance of Narrow-Pore Size Zeolites.** In the early stages of the study, narrow pore size zeolites, which have pore mouths of eight-oxygen-member ring, such as erionite, chabazite, and ZSM-34 or offretite-erionite intergrowth zeolite (1 - 3, 9 - 15), were adopted as the catalyst for this purpose. Simply because, it had been considered that the size of pore mouth around 3.8 Å is likely to fit the size of light olefinic molecules. In fact, these catalysts exhibited a higher selectivity to ethylene and propylene in methanol conversion reaction, however, always suffered from serious coke formation, resulting the rapid deactivation. The coke formation easily occurs mainly in the space of large cavities of these zeolites. Many trials had been done, such as moderation of the too strong acidity by adding basic materials, regulation of crystalline size and its distribution to minimize consecutive reactions, and combination of metallic ingredients such as Ru to reduce the coke deposit by oxidation.

However, these improvements could not give the essential solution, although they exhibited the extension of catalyst life at most several times (15).

**Catalytic Performance of Modified H-ZSM-5.** The focus of the study was then shifted to the medium pore size zeolite, ZSM-5, which has the ten-oxygen-member ring, and does not have the cavity at the intersect of pore channels. Protonated ZSM-5 (H-ZSM-5) had shown the prominent feature in the less coke formation in methanol conversion to gasoline range hydrocarbons (3, 16 - 18). In order to moderate its too strong acidity, which is responsible for the olefins to aromatic-rich gasoline conversion, was modified with various basic metal oxides, expecting the change to appropriate strength of acid sites just for light olefin synthesis (19 - 21).

Since by these treatments the activity decreased, in order to compensate it, the reaction must be carried out much higher temperature range around 550 - 600°C. Under these condition, hydrocarbons having longer C-C bonds once grown accepted  $\beta$ -fission, resulting the major olefin produced became propylene, and the selectivity of the most valuable ethylene was low.

Furthermore, formation of some aromatics could not be avoided at those high temperatures, and catalyst deactivation, owing to aromatic coke, occurred. Moreover, by the high concentrated steam come from the dehydration of methanol has a high potential to enhance dealumination from the framework and phase transformation, resulting permanent deterioration of the catalyst.

Steady retardation against the activity come from the too strong acidity of H-ZSM-5 was also tried (22) by adding a basic organic compound such as quinoline in the feed gas, and considerably high selectivity to ethylene (41%) beside propylene (40%) on an H-ZSM-5 was obtained continuously at a fairly lower temperature (295°C). However, in this case, methanol conversion must be sacrificed at a lower level such as 13%.

The reason of the strong acidity of H-ZSM-5 caused by the existence of Al in the framework would be elucidated by computer simulation applying Monte Carlo method, and it strongly suggested that the hydrogen shift property of H-ZSM-5 depends on the extremely localized acid sites, almost concentrated at one special location in each unit cell (23 - 24). Every reactant and product must be adsorbed on the vicinity of this strong acid site, and therefore, hydrogen atom or molecule formed by aromatization cannot be released from this site and immediately shifts to the hydrogen acceptors, i.e., lower olefins, and hydrogenates them into corresponding paraffinic hydrocarbons.

**Catalytic Performance of Metallosilicates Having MFI Structure.** As acid strength is strictly proportional to the content of aluminium in H-ZSM-5 (25), one cannot change the intrinsic acidic or catalytic property by merely varying the content of Al in the framework of ZSM-5 crystals.

In order to overcome this disadvantage of H-ZSM-5, isomorphous substitution of transition metal ions for the aluminium ion had been investigated (3, 26). By applying the intrinsic rapid crystallization method, the substitution was achieved certainly, especially in the cases of Fe, Ga, and Zn. These so called metallosilicates have not hydrogen shift function as H-ZSM-5 has (27). In the cases of H-Ga-silicate and H-Zn-silicate possess rather distinct property of hydrogen repulsion, and consequently they have a strong aromatization function for olefin, methanol, and even paraffins (28, 29).

In the case of H-Fe-silicate, which has a weaker acidity than H-ZSM-5 and H-Ga-silicate, exerted a high selectivities to ethylene (55%) and propylene (42%) exclusively at a lower temperature condition around 300°C (27). Other a few percents of products consist of butenes and pentenes, and almost no methane, paraffins, and aromatics were obtained. As a result, space-time yield of  $C_2 - C_4$

olefins amounted to 375 g/l·h with 98% selectivity without coke formation. Only one insufficiency of this catalyst is its not so high space-time yield of olefins due to its fairly weak acidity.

Trend of the research in recent one decade has then shifted to the use of silicoaluminophosphate family as the catalyst, which have zeolite-like pore structure but have weaker acid property than the corresponding zeolite structure has.

### Surveys of the Recent Studies on MTO and Its Related Reactions Using SAPOs and MeAPSOs as the Catalysts

**Catalytic Performance of SAPO-34 and its Homologues.** The crystalline aluminophosphate AlPOs family, which was first synthesized by UCC (31), has analogous pore-structures of zeolites. However, as AlPOs have almost no acidic properties, they scarcely exhibit catalytic activity. Silicon atom was then incorporated into the framework (SAPOs) to possess the acidic property due to unbalance of valencies of Al- and Si-ions (32). The acidity thus introduced is still weaker than that of zeolite having corresponding crystal structure (32).

This intrinsic weak acidic property based on the crystal structure was expected to have a high potential to produce light olefins from methanol without the serious coke formation, which could not be avoided in the case of narrow pore size zeolites such as chabazite, erionite, ZSM-34, and offretite, in spite of various post-modifications to reduce acid strength (3). The main reason must be ascribed to the coke formation on the strong acid sites located in the space of large cavities on these zeolites (33), and those acidic sites could not be reduced selectively by merely ordinary post-treatments for neutralization using compounds having basicity.

Some trials of methanol conversion had been done using SAPO-34 as the catalyst (34 - 37), because the crystalline structure is similar to a zeolite chabazite, which had been tried as the catalyst for MTO on the most beginning stage of this field of study, as mentioned above.

Simultaneously (35) and consecutively (38), some other SAPOs were tried for the same purpose and similar reason; those were SAPO-17 (erinite-type structure) (35) and SAPO-44 (-34 structural type homologues) (38). However, in the case of SAPO-17, the product of methanol conversion contained aromatics and light paraffins, and consequently, it showed lower selectivities to C<sub>2</sub> - C<sub>4</sub> olefins than those of SAPO-34. The reason was considered as that the mingle of a different phase, maybe SAPO-5, which is mordenite-like one-dimensional wider pore structure, with SAPO-17 during the synthesis occurred, and it allowed to form aromatics. In the case of SAPO-44, which was used as the reference catalyst in the comparative study on the performance of various MeAPSO-44s, as mentioned later, and the measurement of catalytic performance was compared by means of temperature programmed desorption (TPD), but only unconverted CH<sub>3</sub>OH, and produced (CH<sub>3</sub>)<sub>2</sub>O, ethylene and H<sub>2</sub>O were focused to measure. A higher selectivity to ethylene on SAPO-44 was observed than that on SAPO-34, but both were lower than those observed by the continuous flow reactor (35 - 37).

**Catalytic Performance of MeAPSO-34 and Its Homologues.** On the other hand, Inui et al. had studied isomorphous substitution of various kinds of transition metals for aluminium in ZSM-5 zeolite by adopting the rapid crystallization method (14), which enables the incorporation into the framework of pentasil-type structure more easily and reliably, and had found out that, among those various kinds of incorporated ions, iron-group metals, Fe, Co, and Ni, give metallosilicates having weaker acidity than H-ZSM-5 has, and consequently, C<sub>2</sub> -

C<sub>2</sub> olefins selectivities in MTO reaction increase markedly (14, 27). Therefore, the incorporation of these metallic ions into the framework of SAPO-34 was carried out (35), and furthermore, on the most effective Ni-incorporated SAPO-34 (Ni-APSO-34), more detailed investigation was done, and as a result, a Ni-APSO-34 containing a larger concentration of Ni exhibited the highly selective ethylene formation as high as 88% from methanol was observed without any deactivation at least during the period of durability test for 13h (39). The ethylene selectivity increased from 29 to 88% with an increase of Ni-incorporation as expressed by Si/Ni atomic ratio changed from infinity to 40, respectively. These were also corresponded to the decreased in the acidity, which were reflected to their NH<sub>3</sub>-TPD profiles in both the low and high temperature peaks. These facts indicate that the most proper acid strength, which fits to just only consecutive reactions from methanol to ethylene via formation of dimethyl ether as the intermediate was settled by the nickel incorporation.

This unique selectivity to ethylene formation on Ni-APSO-34 was reconfirmed by Thomas et al. (40), and then studies on the methanol conversion reaction and related reactions using MeAPSO-34 (41 - 43), SAPO-34 (44 - 46), MeAPSO-44 (38) (analogous structure of MeAPSO-34), and MAPO-18 (47) (corresponding to MAPO-34 family), have been done, extensively.

Thomas et al. (40, 41) observed that Ni in Ni-APSO-34 can be incorporated only a small degree like as Al/Ni atomic ratio 58.7, however, it is totally incorporated into the framework with tetrahedrally bonded state, and the loosely bound extra framework protons are thought to be the key components of the catalyst for such a highly selective conversion of methanol to ethylene with a level of 90% selectivity even at more than 90% conversion condition. They also pointed out that Ni-APSO-34 is much more thermally stable than the Co-substituted analogue (41). Although they tried methanol conversion using other MAPO catalysts such as CoAPO-5, Co-APO-11, and Co-APO-25, the major product was dimethyl ether owing to their too low acidity, and only in the case of Co-APO-5, at higher temperature range 350°C up to 450°C, dimethyl ether formed successively converted to higher hydrocarbons and the selectivity to vital ethylene became very low.

On the other hand, O'Connor et al. (46) studied MTO reaction on SAPO-34s with some modifications, and obtained the results of high selectivity of C<sub>2</sub> - C<sub>4</sub> olefins up to 92%, however, they concluded that there was no evidence that nickel could be easily incorporated into the framework of SAPO-34, and neither the addition of cobalt nor nickel enhanced the performance of the catalyst. Their conclusion seems to be contradiction against the results obtained by Inui et al. (27, 48) and Thomas et al. (40, 41), and it will be examined in more detail later.

Separately, Hočevár et al. Studied on MeAPSO-34 (43) and MeAPSO-44 (-34 structural type homologues) (38), by means of TPD measurement in detail for methanol dehydration reaction, and observed that ethylene selectivity on SAPO-44 is higher than that on SAPO-34, and the incorporation of metallic ions such as Co, Zn, or Mn increases ethylene selectivity, in this order. However, more precise catalytic performance for methanol to olefin conversion is not clear, because the reaction was not conducted by an ordinary continuous flow method.

More recently, Chen and Thomas (47) reported that MAPO-18 (M≡Mg, Zn, Co; structurally very similar to AlPO<sub>4</sub>-34) is a new family of catalysts for the conversion of methanol to light olefins, and they showed the results that incorporation of Zn, Co, or Mg into AlPO<sub>4</sub>-18, generates 65 to 70% light olefin (ethylene and propylene) products with the total conversion of methanol in the range of 350 to 400°C.

As shown above, the high selectivity to C<sub>2</sub> - C<sub>4</sub> olefins from methanol on SAPO-34 and MeSAPO-34 consistently coincides among researchers, however, ambiguous points and discrepancies still remain in the catalytic performance and



the structural feature of MeAPSO-34, and then most recently more detailed sequential experiments have been done by Inui and Kang et al. (49 - 52) as described below.

### Highly Selective Ni-APSO-34 Catalyst in Methanol to C<sub>2</sub>, C<sub>3</sub> Olefins Conversion and Control Factors of Its Performance

**Controlling Factors to Prepare the High Performance Catalyst.** From the synthetic procedures to the reaction methods and conditions, there are so many factors which affect to the results of the reaction. Especially, in order to obtain the extraordinary high selectivity, as now discussing, the catastrophic change to an ordinary selectivity, which would be more stable state than the extraordinarily high selectivity as high as 90% must be avoided. In other words, such a catalysis must be very sensitive to the properties of the catalyst, and then to the preparation procedures. As mentioned above, some discrepancies between the results obtained by Inui et al. and Thomas et al., and O'Connor et al. However, their synthetic methods were different each other. For example, different nickel sources, nickel nitrate, nickel chloride, and nickel acetate were used by those researchers, respectively. Synthetic procedures and compositions were different, and consequently, the resulting materials were also different, even though they showed the X-ray diffraction patterns of the same as SAPO-34. The most apparent difference is shown as follows.

O'Connor et al. (46) synthesized by the conventional slow crystallization method, which is apt to give fairly large size crystals and wider crystal-size distribution, i.e., 5 - 50  $\mu$  m in SAPO-34 and ca. 1  $\mu$  m, in Ni-APSO-34 and Co-APSO-34, which indicates that at least those metallic ions exhibited an evident effect upon the nucleation stage of crystallization. Moreover, the products contained a considerable ratio of a different crystalline phase (SAPO-5), which possesses a wider pore diameter and has a high potential to suffer from coke deposition just as they observed. In these circumstances the effect of Ni or Co would become ambiguous.

On the other hand, Inui et al. (35, 39, 48, 49) always adopted the rapid crystallization method, (14, 35) to promote the crystallization rate processes and to make easier incorporation of transition-metal ions, resulting the smaller and uniform size-distribution, single phase crystals, and a higher activity than that of crystals synthesized by slow crystallization methods (14).

**Reliable Procedure for the Synthesis of Ni-APSO-34 Catalyst.** In order to make more clear on these points, Inui and Kang examined in detail (49 - 53), especially, focusing on the uniformity of the mixed gel formation as the precursor for the crystallization (49). Six kinds of Ni-APSO-34 were prepared by different methods, and their physical properties and catalytic performances are summarized in Table I. As a result, as shown in Table I and Figure 1, one of the standard synthetic procedure, which gives a uniform crystalline size and its distribution of 0.8 - 0.9  $\mu$  m, and a good performance of ethylene selectivity of 86%, propylene 5%, and C<sub>2</sub> - C<sub>4</sub> olefins totally 91% was obtained at 425°C and the methanol conversion of 95%. However, this result is somewhat different from the results obtained in our previous work (39) that methane formed 6.9% in selectivity and unconverted dimethyl ether remained in the product by 0.8% in selectivity, whereas in the previous data, selectivity of methane was only 0.61 and 1.50% at 400 and 450°C, respectively, and no unconverted dimethyl ether was detected in the products. Therefore, the catalyst prepared by the procedure shown in Figure 1 was still delicately different from the best catalyst. However, through this study, very significant relationships between the acid density of internal surface of the crystals vs ethylene selectivity, and the acid density of external surface of

**Table I. Various Ni-APSO-34 Catalysts Prepared by Different Procedures and Their Physical and Catalytic Properties**

Procedure shown in Fig. 1	Cat. 1	Cat. 2	Cat. 3	Cat. 4	Cat. 5	Cat. 6
(2) Addition of seed crystal	None	None	None	0.5 wt%	2.0 wt%	5.0 wt%
(4) Milling	None	Done	Done	Done	Done	Done
(5) Ultrasonic wave	None	0.5 h	2 h	2 h	2 h	2 h
BET-surface area ( m <sup>2</sup> /g)	552	498	530	549	565	504
Crystallinity (%)	87	53	92	95	100	58
Size of crystals ( μ m)	1.0-1.5	0.3-0.5	0.7-0.8	0.7-0.8	0.8-0.9	1.0-1.5
Composition of the crystals	P	0.63	0.71	0.71	0.73	0.50
(Al=1)	Si	0.26	0.27	0.28	0.27	0.21
	Ni	0.0028	0.0027	0.0029	0.0029	0.0030
Amount of acid	Total <sup>a)</sup>	9.06	6.32	5.88	4.62	6.51
( μ mol/m <sup>2</sup> )	External surface <sup>b)</sup>	0.41	0.40	0.40	0.39	0.50
	Internal surface <sup>c)</sup>	7.65	5.89	5.46	4.22	6.01
Conversion of methanol (%)	94.5	100	100	100	94.50	100
Selectivity						
Ethylene	64.0	72.5	78.3	82.5	85.7	73.9
Propylene	22.7	2.80	4.83	3.78	4.86	9.29
Butene	2.18	1.00	0	0	1.71	7.40
C <sub>2</sub> -C <sub>4</sub> olefins	88.9	76.3	83.1	86.3	90.6	90.6
C <sub>5</sub>	0.79	0.20	0.43	1.32	0.46	1.85
Methane	2.61	20.7	14.7	10.9	6.85	6.47
C <sub>2</sub> -C <sub>4</sub> paraffin	4.36	1.42	1.65	1.56	1.31	1.10
Dimethyl ether	3.22	0	0	0	0.77	0
Amount of coke deposited (wt%)	3.33	3.42	3.28	3.09	2.59	3.55

a) Estimated by NH<sub>3</sub>-TPD. b) Estimated by 4-methylquinoline-TPD. c) Difference between a) and b).  
 Reaction conditions MeOH 15% - Ar 85%, GHSV 1000h<sup>-1</sup>, 425°C, Time on stream 1 h.  
 Reprinted with permission from ref. 49. Copyright 1997.

## Procedure

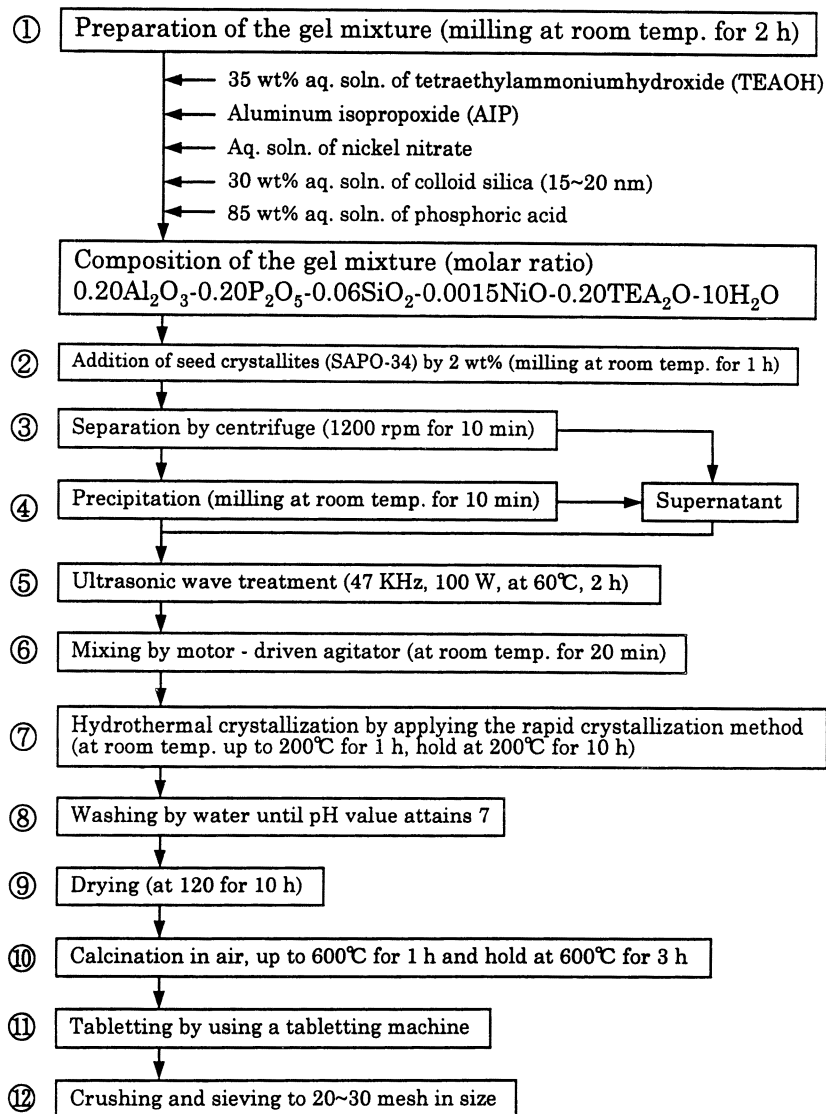


Figure 1. Preparation procedure of the Ni-APSO-34 in case of Cat. 5, which exhibited the best performance among the six catalysts. (Reproduced with permission from ref. 49. Copyright 1997 Elsevier Science B.V.)

crystals vs amount of coke deposited during the reaction for the same time on stream, were obtained as shown in Figures 2 and 3, respectively. The extrapolation of the relationship shown in Figure 2, indicates that when the acid density of internal surface of crystals is mostly proper like as  $3 \mu \text{mol/m}^2$ , the quantitative conversion of methanol to ethylene could be achieved. In this figure, a deviated point from the relation (Cat. 2) must be omitted, because the crystallinity of this sample was considerably low compared with others (49) as shown in Table I (49).

The coke formation was affected sensitively by the acid density of the external surface of crystals, it is very rationally understandable, because at the external surface of crystals received no restriction of the growth of fused-ring aromatics as the precursor of the coke.

**Post Modifications to Improve the Catalytic Performance.** The coke formation mentioned above could be markedly decreased by adopting the mechanochemical neutralization (54, 55) of acid sites located on the outer surface of the crystal particles (50). Crystals of Ni-APSO-34 was physically mixed with the insoluble basic oxide, such as BaO supported on non-porous fine spherical silica powder having very small diameter of ca  $0.5 - 2 \mu \text{m}$ , in a ceramic mortar for a definite period. Marked improvement, in the retardation of the deposit of coke due to the selective neutralization of the acid sites, was confirmed as same as the other cases, in 2,6-dimethyl ether formation (54), and aromatization of paraffins (55) using pentasil type zeolite catalysts.

As for the decrease in methane selectivity, since the reason of methane formation was considered as that Ni located at the extra framework has an activity of the decomposition of methanol into hydrogen and carbon monoxide, and these successively react to form methane, the deactivation of this Ni part was tried by using a low concentration of hydrogen sulfide in the feed (51). Evident result was found by this method that not only the decrease of methane formation, the selectivity to ethylene markedly increased due to the proper modification for the environment of the nickel deposited.

Fortunately, at higher temperature like as the reaction temperature around  $300 - 450^\circ\text{C}$ , SAPO-34 is stable against the existence of steam (44), however, as the catalyst it is always exposed under a hydrothermal condition due to the partial pressure of steam, which comes from the dehydration of methanol, to know the effect of the steam is considered to be important, especially from the view point of durability of the catalyst. The effect of the addition of steam in the feed was then examined for a Ni-APSO-34 catalyst (52). A sharp contrast was obtained between the conditions with and without steam. With the adding steam by 10 mol% in the feed, the selectivity of ethylene was maintained at a 80% level during a duration test for 5 h, whereas the condition without addition of steam the selectivity to ethylene gradually decreased, and in place of this the selectivity of propylene increased. The role of the water had to investigate furthermore, however, maybe it enhances the desorption of ethylene formed and promotes the instantaneous desorption of ethylene from the adsorbed sites resulting the protection of consecutive reactions to form higher olefinic hydrocarbons by oligomerization or other carbon-chain growth reactions. From this context, the mechanism of the highly selective formation of ethylene on Ni-APSO-34 seems to be the successive reaction routes after ethylene formation in the consecutive-type mechanism (45) is prevented by the promoted desorption of ethylene by an appropriate partial pressure of water molecules. However, on the mechanism of such a quantitative synthesis needs much more concentrated investigation in the future.

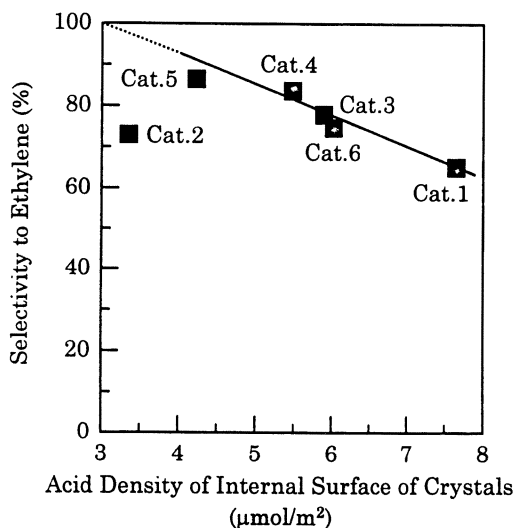


Figure 2. Correlation between the acid density of internal surface of crystals and the selectivity to ethylene.

Reaction conditions: MeOH 15 mol%, Ar 85 mol%, GHSV 1000  $\text{h}^{-1}$ , 425°C, Time on stream 1h.

Catalyst numbers in the figure correspond to those in Table I.

(Reproduced with permission from ref. 49. Copyright 1997 Elsevier Science B.V.)

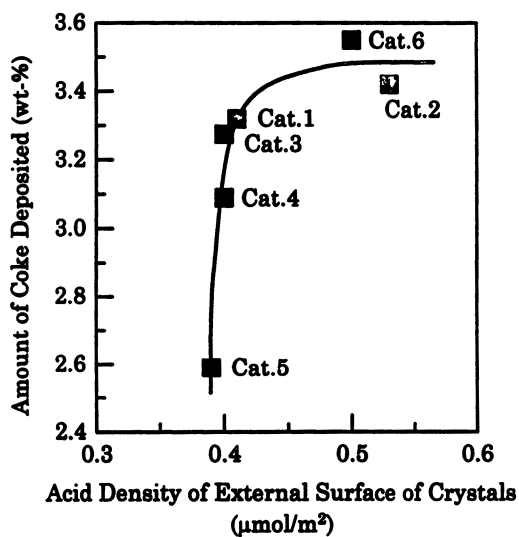


Figure 3. Correlation between the acid density of external surface of crystals and the amount of coke deposited.

Notes are same as those shown in Figure 2.

(Reproduced with permission from ref. 49. Copyright 1997 Elsevier Science B.V.)

## Conclusion

Light olefin synthesis via alternative routes is increasing its importance (56, 57). The feasibility of the process depends on the catalytic performance, especially, selectivity of aimed olefins and their space-time yields.

In this review, the trends of studies on this field for the past two decades were summarized from the viewpoints of the relationships between the structural features of catalysts and their selectivities, of course always considering the problem of minimization of the coke formation. It is concluded that, as a result, Me-APSO-34 and its family have a high potential to be realized as the practical catalyst. Therefore, further investigations to establish more reliable results are needed.

## Literature Cited

- (1) Anthony, R.G.; Shingh, B.B. *Hydrocarbon Process* **1981**, *3*, 85 - 88.
- (2) Inui, T.; Takegami, Y. *Hydrocarbon Process* **1982**, *11*, 117 - 120.
- (3) Inui, T. *Sekiyu Gakkaishi* **1992**, *35*, 33 - 40.
- (4) Inui, T. *Hyomen* **1985**, *23*, 518 - 527.
- (5) Madon, R.J. *J. Catal.* **1979**, *57*, 183 - 186.
- (6) Lunsford, J.H. *Stud. Surf. Sci. Catal.* **1994**, *81*, 1 - 12.
- (7) Eng, C.N.; Arnold, E.C.; Vora, B.V.; Fuglerud, T.; Kvisle, S.; Nilsen, H. *Proc. AIChE Spring National Meeting, New Orleans, 1998*, paper 45a.
- (8) Barger, P.T.; Wilson, S.T. *Abstracts, 12th Intern. Zeolite Confer., Baltimore, 1998*, A 33.
- (9) Chang, C.D.; Silvestri, A.J. *J. Catal.* **1977**, *47*, 249 - 259.
- (10) Whittam, T.V.; Spencer, M.S. *UK Patent Appl.*, GB, 1061999A.
- (11) Lin, F.N.; Anthony, R.G. *Oil & Gas J.* **1978**, March, 92 - 111.
- (12) Mobil, Jpn. *Kokai Tokkyo Koho*, **1978**, Jp 53 - 58, 499.
- (13) Inui, T.; Araki, E.; Sezume, T.; Ishihara, T.; Takegami, Y. *React. Kinet. Catal. Lett.* **1981**, *18*, 1 - 5.
- (14) Inui, T. *ACS Symposium Series*, **1989**, *398*, 379 - 492.
- (15) Inui, T.; Ishihara, T.; Morinaga, N.; Takeuchi, G.; Matsuda, H.; Takegami, Y. *Ind. Eng. Chem., Prod. Res. Dev.* **1983**, *22*, 26 - 30.
- (16) Dejaifue, P.; Aroup, A.; Gravelle, P.C.; Vedrin, J.C.; Gabelica, Z.; Derouane, E.G. *J. Catal.* **1981**, *70*, 123 - 136.
- (17) Langner, B.E. *Appl. Catal.* **1982**, *2*, 289 - 302.
- (18) Cormerais, F.X.; Perot, G.; Guinsnet, M. *Zeolites* **1981**, *1*, 141 - 144.
- (19) Kaeding, W.W.; Butter, S.A. *J. Catal.* **1980**, *61*, 155 - 164.
- (20) McIntosh, R.J.; Seddon, D. *Appl. Catal.* **1983**, *6*, 307 - 314.
- (21) Okado, H.; Shoji, H.; Kawamura, K.; Kohtoku, Y.; Yamagaki, Y.; Sano, T.; Takaya, H. *Nippon Kagaku Kaishi* **1987**, 25 - 30.
- (22) Inui, T.; Fukuda, K.; Morinaga, N.; Takegami, Y. *Sekiyu Gakkaishi* **1984**, *27*, 188 - 192.
- (23) Inui, T. *Trans. Mat. Res. Soc. Jpn.* **1994**, *14A*, 135 - 140.
- (24) Inui, T.; Matsuba, K.; Tanaka, Y. *Catal. Today* **1995**, *23*, 317 - 323.
- (25) Haag, W.O.; Lago, R.M.; Weisz, P.B. *Nature* **1984**, *309*, 581 - 591.
- (26) Inui, T.; Yamase, O.; Fukuda, K.; Itoh, A.; Tarumoto, J.; Morinaga, N.; Hagiwara, T.; Takegami, Y. *Proc. 8th Intern. Confer. Catal., Berlin (1984)*, Vol. III, 569 - 579.
- (27) Inui, T.; Matsuda, H.; Yamase, O.; Nagata, H.; Fukuda, K.; Ukawa, T.; Miyamoto, A. *J. Catal.* **1986**, *98*, 491 - 501.
- (28) Inui, T.; Makino, Y.; Okazumi, F.; Nagano, S.; Miyamoto, A. *Ind. Eng. Chem. Res.* **1987**, *26*, 647 - 652.

- (29) Inui, T.; Kim, J.; Takeguchi, T.; Nagata, H. *Appl. Catal. A*, **1993**, *106*, 83 - 95.
- (30) Inui, T.; Mtasuda, H.; Takeguchi, T.; Chaispakitsin, M. *Proc. 2nd Japan-Korea Symp. Catal.* **1989**, 19 - 22.
- (31) Higgin, J. *Chem. Eng. News* **1983**, June 20, 36.
- (32) Lok, B.M.; Messina, C.A.; Patton, R.L.; Gajek, R.T.; Cannar, T.R.; Flanigan, E.M. *J. Am. Chem. Soc.* **1984**, *84*, 6092 - 6093.
- (33) Anderson, J.R.; Chang, Y.-F.; Western, R.J. *J. Catal.* **1990**, *124*, 259 - 267.
- (34) Wilson, S.T.; Lok, B.M.; Flanigan, E.M. *US Patent*, **1982**, 4310440.
- (35) Inui, T.; Matsuda, H.; Okaniwa, H.; Miyamoto, A. *Appl. Catal.* **1990**, *58*, 155 - 163.
- (36) Liang, J.; Li, H.; Zhao, S.; Gus, W.; Wang, R.; Ling, M. *Appl. Catal.* **1990**, *64*, 31 - 40.
- (37) Xu, Y.; Grey, C.P.; Thomas, J.M. *Catal. Lett.* **1990**, *4*, 251 - 260.
- (38) Hočevar, S.; Batista, J.; Kaučič, V. *J. Catal.* **1993**, *139*, 351 - 361.
- (39) Inui, T.; Patanasry, S.; Matsuda, H. *J. Chem. Soc. Chem. Commun.* **1990**, 205 - 206.
- (40) Thomas, J.M.; Xu, Y.; Catlow, C.R.A.; Couves, J.W. *Chem. Mater.* **1991**, *3*, 667 - 672.
- (41) Xu, Y.; Couves, J.W.; Jones, R.H.; Richard, C.; Catlow, A.; Greaves, G.N.; Chen, J.; Thomas, J.M. *J. Phys. Chem. Solids* **1991**, *52*, 1229 - 1234.
- (42) Chen, J.; Sanker, G.; Thomas, J.M.; Xu, R.; Greaves, G.N.; Waller, D. *Chem. Mater.* **1992**, *4*, 1373 - 1380.
- (43) Hočevar, S.; Levec, J. *J. Catal.* **1992**, *135*, 518 - 532.
- (44) Vomscheld, R.; Briend, M.; Peltre, M.J.; Massiani, P.; Man, P.P.; Barthomeuf, D. *J. Chem. Soc. Chem. Commun.* **1993**, 544 - 546.
- (45) Dahl, I.M.; Kolboe, S. *J. Catal.* **1994**, *149*, 458 - 464.
- (46) Van Niekerk, M.J.; Fletcher, J.C.Q.; O'Connor, C.T. *Appl. Catal. A: General*, **1996**, *138*, 135 - 145.
- (47) Chen, J.; Thomas, J.M. *J. Chem. Soc., Chem. Commun.* **1994**, 603 - 604.
- (48) Inui, T. *Stud. Surf. Sci. Catal.* **1991**, *67*, 233 - 242.
- (49) Inui, T.; Kang, M. *Appl. Catal. A: General* **1997**, *164*, 211 - 223.
- (50) Kang, M.; Inui, T. *Catal. Lett.* **1998**, *53*, 171 - 176.
- (51) Kang, M.; Inui, T. *J. Mol. Catal., A: Chemical* **1998**, in press.
- (52) Kang, M.; Inui, T. *J. Mol. Catal., A: Chemical* **1998**, in press.
- (53) Inui, T.; Kang, M.; Nomura, Y. *Proc. 12th Intern. Zeolite Confer., Baltimore*, **1998**, in press.
- (54) Inui, T.; Pu, S.; Kugai, J. *Appl. Catal.* **1996**, *146*, 285 - 296.
- (55) Inui, T.; Yamada, T.; Matsuoka, A.; Pu, S. *Ind. Eng. Chem. Res.* **1997**, *36*, 4827 - 4831.
- (56) Layman, L. *Chem. Eng. News* **1989**, August 14, 7 - 11.
- (57) Haggin, J. *Chem. Eng. News* **1989**, August 14, 25 - 27.



## Chapter 9

# Role of Shape Selectivity in *n*-Heptane Cracking and Aromatization Reaction on Modified ZSM-5

T. S. R. Prasada Rao, N. Viswanadham, G. Murali Dhar, and N. Ray

Indian Institute of Petroleum, Dehra Dun 248 005, India (iipddn@del2.vsnl.net.in)

Cracking and aromatization reaction of *n*-heptane was carried out on ZSM-5 modified by three methods: They are

- (i) Extra framework alumina obtained by steaming at high temperature,
- (ii) Altering the pore size by coke deposition as a function of time on stream, and
- (iii) Presence of amorphous material in the zeolite.

The effect of these modifications on the shape selective product *p*-xylene is investigated. In all the cases the shape selective properties are profoundly influenced. The presence of extra framework alumina, and coke increased the concentration of *para* xylene in the product. In the case of ZSM-5 containing amorphous material obtained by synthesizing the zeolite without the aid of template, the *para* xylene in the product was higher than that obtained over zeolite synthesized using the template. In all the cases the increase in shape selective product may be resulted by decrease in channel dimensions due to the presence of the extraneous materials in the channel. Pore size distribution studies on deactivated catalyst provided evidence for the operation of molecular traffic control (MTC) mechanism in the case of *n*-heptane aromatization reaction.

Ever since weisz and co-workers from Mobil coined the word shape selectivity and demonstrated its commercial potential using small pore molecular sieves, shape selective properties of zeolites have been studied with great interest [1]. The availability of MFI type medium pore zeolites of ZSM family with pore sizes compatible with molecules in gasoline range has opened up new vistas in hydrocarbon transformations [2,3]. Based on their acidic and shape selective properties a number of processes were developed in the recent past [2]. Xylene isomerization, Methanol to gasoline, Distillate and lube dewaxing, M-forming, Mobil selective toluene disproportionation, manufacture of *para* diethyl benzene are

some of the many applications where shape selectivity concept has commercially exploited.

Various types of shape selectivities that can be considered in ZSM-5 system are the reactant shape selectivity, this type of selectivity is observed when only part of the feed molecules are small enough to diffuse through the zeolite pores. Mobil middle distillate dewaxing and selecto-forming are good examples in this context. Another important type of shape selectivity is the product shape selectivity. The product shape selectivity occurs when some of the products formed within the pores are too bulky to diffuse out to be observed as products. They are either converted to less bulky molecules or eventually deactivate the catalysts by pore blocking. Xylene isomerization, toluene methylation etc. are good examples in this connection. Yet another type of shape selectivity is transition-state shape selectivity, where certain reactions are prevented because corresponding transition-state would require more space than that is available in the zeolite pores or intersections. Since, neither reactant nor potential product molecules are prevented from diffusing, the reactions that proceed with smaller transition-state proceeds unhindered to alter the selectivity. Another variant of shape selectivity is molecular traffic control, which occurs in zeolites with more than one type of pore system [4]. The reactant molecules here may preferentially enter the catalyst through one of the pore systems, while the products diffuse out through the other type. Thus counter diffusion is minimized to maximize the selectivity.

There have been extensive research efforts to understand the nature of shape selectivity in industrially important reactions like xylene isomerization, alkyl benzene disproportionation and alkylation, in spite of such extensive efforts the phenomenon is not well understood. The para selectivity is influenced by transition-state, product selectivities, non selective reactions on external surface and, also by variations in the acidity and acid strength distribution. In addition higher quantities of shape selective products can be obtained by altering the pore dimensions by modification of the zeolite by extraneous matter present in the pores like extra framework alumina includes P, B, Mg or by altering the pore mouth by depositing silica by silylation. Yet another way of pore modification that is common in hydrocarbon transformations is by coke. The deposited coke can reduce the channel dimensions and thereby increase the shape selectivity in favor of faster diffusing molecule. Amount of acidity and the distribution of acid strength of the sites, in both internal and external surface of the zeolite crystal is another factor that alters the shape selectivity by controlling side reactions or by non shape selective transformations on acid sites present on the external surface.

There are numerous examples in this well studied area, a few examples relevant to the work presented will be discussed here. Kaeding et. al. [5] studied disproportionation of ethyl benzene, alkylation of toluene and ethyl benzene where they found that modification of the channels of ZSM-5 with oxides of P and B improves the selectivity for para isomer. They attributed this to the significantly higher diffusivity of para isomer due to decrease in channel dimensions. The diffusivity of para isomer in ZSM-5 is thousand times faster than other two isomers [6]. However, Chandawadker et. al. [7] reported that the presence of B, P and organic bases enhanced para selectivity by suppressing isomerization of primary product, para ethyl toluene. Kim et. al. [8] studied alkylation of ethyl benzene with

ethanol on MFI and MEL zeolites, and found that zeolites modified by steam, or coking or modified by oxides, exhibited much higher para selectivity.

Toluene ethylation was also studied by Lonyi et. al. [9] on modified ZSM-5 containing oxides of P, B, Mg etc. and observed higher para selectivities and concluded that both change in diffusivity due to decrease in channel dimensions as a result of modifications, and alteration of acidity and acid strength distribution play an important role. Prasada Rao and co-workers reported increased selectivity for isomer, p-diethyl benzene in alkylation of ethyl benzene on silylated ZSM-5 [10]. It can be seen that both diffusivity modified by channel dimensions and change in acidity play important role in altering the shape selectivity. In some cases the presence of amorphous material in the zeolite may also effect the concentration of shape selective products due to promotion of side reactions. In this investigation the effect of extra framework alumina obtained by steaming the zeolites at different temperatures, coke formed during time-on-stream, and presence of amorphous materials in the zeolites, on n-heptane aromatization reaction are presented. The studies on deactivated catalysts also provided evidence for operation of molecular traffic control mechanism in the case of n-heptane aromatization reaction.

## Experimental

ZSM-5 was synthesized following well known literature procedures [11]. The steam treatment of  $\text{NH}_4$  ZSM-5 was carried out in a fixed shallow bed reactor, the steaming was carried out with 100% water vapour, with water flow rate of 76ml/hr at different temperatures 300-600 $^{\circ}$ C for 3h. The extra framework aluminum was removed by acid leaching with 1N HCl at 100 $^{\circ}$ C for 2h. The samples after calcination at 480 $^{\circ}$ C for 12 hours were used for activity evaluation studies. The n-heptane aromatization reaction was carried out in a fixed bed down flow reactor at 773 $^{\circ}$ K, LHSV : 2h $^{-1}$ ,  $\text{N}_2/\text{HC}$  : 2, pressure : 10 kg/cm $^2$  TOS : 12h [4].

The pore volume and pore size distributions of the fresh and deactivated catalysts were evaluated on micromeritics equipment using argon adsorption and Harvath and Kawazoe method. Both micro and mesopores were brought into single display by using density function theory.

## Results and Discussion

Effect of foreign materials on shape selectivity has been examined by several investigators. Chen, Kaeding and Dwyer observed higher para xylene selectivities by modifying the ZSM-5 by phosphoric acid, boron compounds or coating the surface with a polymer [1,2]. Kaeding et. al. [15] observed increased selectivity for para isomer by modifying the ZSM-5 with B, Mg and Silicon. They have also observed increase of p-ethyl toluene as a function of coke deposition. Kim et. al. [8] modified the ZSM-5 and ZSM-11 with coke or by steaming and found that the presence of coke or extra framework alumina increased para isomer in alkylation of ethyl benzene with ethanol. In this investigation the zeolite material was modified by steaming and mild coking, and the effect of these modifications on shape selectivity is studied.

ZSM-5 zeolites containing three types of foreign materials viz. extra framework alumina, coke and amorphous materials were used in this investigation.

The extra framework alumina was obtained by steaming ZSM-5 at different temperatures under specified conditions mentioned in the experimental section. Fresh as well as samples steamed at different temperatures were analyzed by chemical analysis,  $\text{Si}^{29}$  NMR for evaluation of framework alumina, and total alumina. These results are presented in Table-I. The extra framework alumina was confirmed by  $\text{Al}^{27}$  NMR, spectra also. The coke on the catalyst was increased as a function of time on stream and the amount of coke deposited was analyzed.

**Table-I Dependence of the Concentration of the Aluminum Types on the Steaming Severity of ZSM-5**

Samples (1)	Steaming Severity (2)	Concentration of Al Species Per Unit Cell				
		ALF (3)	ALEF (4)	ASEFAL (5)	AIEFAL (6)	Al <sub>TOT</sub> (7)
Z-35	0°C	4.5	-	-	-	4.4
S <sub>1</sub> Z-35	300°C/3hr	4.3	0.2	0.1	0.1	4.4
S <sub>2</sub> Z-35	400°C/3hr	2.6	1.9	1.4	0.5	3.1
S <sub>3</sub> Z-35	500°C/3hr	2.1	2.4	2.0	0.4	2.5
S <sub>4</sub> Z-35	600°C/3hr	1.4	3.1	2.8	0.3	1.7

- (1) Zeolite samples : Z-35 (ZSM-5, SAR=35), and S<sub>1</sub>Z-35 to S<sub>4</sub>Z-35 are the samples steamed at different temperatures
- (2) Samples treated with steam at different temperatures
- (3) Framework atoms per unit cell calculated from  $^{29}\text{Si}$  MAS NMR
- (4) Extra framework alumina per unit cell
- (5) Acid soluble extra framework alumina per unit cell
- (6) Acid insoluble extra framework alumina per unit cell
- (7) Total alumina per unit cell after the steaming and acid treatments

The synthesis without the aid of organic template resulted in formation of ZSM-5 zeolites with lower-crystallinity due to the presence of amorphous material, which is deduced by comparing the XRD crystallinity with the corresponding templated zeolite material containing same Si/Al ratio. The n-heptane aromatization reaction carried out in a fixed bed down flow reactor at 773<sup>0</sup>K, LHSV: 2h<sup>-1</sup>, N<sub>2</sub>/HC : 2 and pressure 10 kg/cm<sup>2</sup>. A typical product distribution in n-heptane aromatization reaction is shown in Table-II. It can be seen that LPG range products and aromatics are obtained by a series of cracking, hydrogen transfer, oligomerization and cyclization reactions. The effects of shape selectivity were followed by detailed analysis of various xylenes formed.

**Effect of Extra Framework Alumina (EFAL) On Shape Selectivity.** The distribution of xylene isomers as a function of amount of extra framework aluminum in ZSM-5 is presented in Table-III. It can be noted that selectivity for p-xylene increases and selectivity for m-xylene and C<sub>9+</sub> aromatics decreases which indicate that in addition to the enhanced shape selectivity, the side reactions also decreased due to acidity modification by dealumination. It is also clear that increase in extra framework alumina indeed increases para selectivity. Table-IV gives the amount of alumina in the channels of zeolite, and product distributions in n-heptane aromatization on ZSM-5 unsteamed, steamed and acid treated zeolites ZSM-5.

**Table – II Typical Product Distribution in n- Heptane Aromatization Reaction**

Product Component	Yields (wt. %)
C <sub>1</sub> Methane	1.8
C <sub>2</sub> Ethane	4.5
C <sub>3</sub> Propane	35.0
C <sub>4</sub> Butanes	22.8
C <sub>5</sub> + Paraffins	7.4
Aromatics	28.5
Benzene	1.7
Toluene	10.2
Xylenes	13.6
C <sub>9+</sub> Aromatics	3.0

Reaction conditions : Temperature = 500<sup>o</sup>C, WHSV = 6 hr<sup>-1</sup>, Pressure = 10 kg/cm<sup>2</sup>, N<sub>2</sub>/HC = 2, Catalyst = H-ZSM-5 (4.5 Al/U.C)

The conversion decreased on steamed zeolites as expected since the decrease of aluminum ions in the framework decreases the aromatization activity. The aromatic yields are also decreased in a similar manner. In steamed zeolite containing extra framework alumina and the same zeolite where extra framework aluminum is removed by acid treatment, both showed similar conversion and aromatic yields Table-IV. It is interesting to see how the aromatic distribution, particularly para xylene yield varies in these three cases. It can be noted that the para xylene concentration is more in the steamed zeolite, where in extra framework alumina (EFAL) is present, compared to either unsteamed or acid treated zeolite and o- xylene and m - xylene yields varied exactly in the opposite way. The fact that the unsteamed and acid treated zeolites have comparable xylene selectivities indicates that the enhanced para selectivity obtained is indeed due to the presence of extra framework alumina.

**Table - III Effect of Extra Framework Alumina (EFAL) on Shape Selectivity**

EFAL / Unit Cell	0.0	1.9	2.4	3.1
<i>Selectivity (wt %)</i>				
p- Xylene	21.4	28.6	34.0	39.8
m - Xylene	18.6	17.5	16.0	15.5
C <sub>9+</sub> Aromatics	23.5	22.0	18.6	16.0
Total	100.0	100.0	100.0	100.0

**Table - IV Effect of Extra Framework Alumina (EFAL) on Shape Selectivity**

Catalysts	Unsteamed	Steamed	Acid treated
Conversion	96.0	86.2	87.1
Aromatics Yield	29.0	25.6	24.3
<i>Aromatic Distribution (wt%)</i>			
Benzene	7.2	5.5	6.6
Toluene	28.0	26.7	29.7
Ethyl Benzene	1.8	2.1	1.9
P - Xylene	13.5	19.0	14.0
m - Xylene	23.0	29.0	18.7
O - Xylene	11.7	10.3	16.2
C <sub>9+</sub> Aromatics	23.5	22.0	18.6

**Effect of Coke Formation on Shape Selectivity.** Formation of coke is inevitable in hydrocarbon reactions even on the ZSM-5 zeolite which is known for its coke resistance especially in aromatization reactions. We have examined the effect of coke on ZSM-5 zeolite which is on stream for several hours. The aromatic distribution as a function of time on stream is analyzed and the selectivity to p-xylene is taken as a scale to measure the shape selectivity change due to coke formation. It can be seen from the data Table-V, that the p-xylene concentration in the product increases a function of time-on-stream. It can also be seen that ortho and meta isomer concentration decreases simultaneously. It is clearly indicated that isomerisation of ortho, meta xylenes into para isomer is indeed happening due to their lower diffusivities. The presence of coke on the catalyst is confirmed at the end of the experiment and the carbon analysis showed that there is 6 wt% coke on the catalyst at the end of the run. It appears that the coke reduces the channel dimensions by its presence and in fact this decrease is responsible for the enhanced para selectivity.

**Table - V Presence of Coke on Shape Selectivity**

Time - on - Stream (TOS)	6 hr	12 hr	24 hr
<i>Aromatic Distribution (wt%)</i>			
Benzene	8.0	5.0	5.6
Toluene	30.0	28.5	25.0
Ethyl Benzene	1.5	2.5	2.0
P- Xylene	14.2	17.5	21.0
M- Xylene	22.5	23.0	21.0
o - Xylene	11.0	10.0	9.5
C <sub>9+</sub> Aromatics	12/8	13.8	15.9
Total	100	100	100

To verify whether the pore dimensions are reduced due to coke formation, the pore size distributions of the coked catalysts were evaluated by gas adsorption, and the data is treated using density functional theory. Results showed that median pore diameter of the zeolite pore is 6.4 Å<sup>0</sup> for the fresh catalysts and the same for the deactivated catalysts is 5.7 Å<sup>0</sup>. This clearly shows there is in fact decrease of pore diameter which has definitely contributed to the enhanced para selectivity.

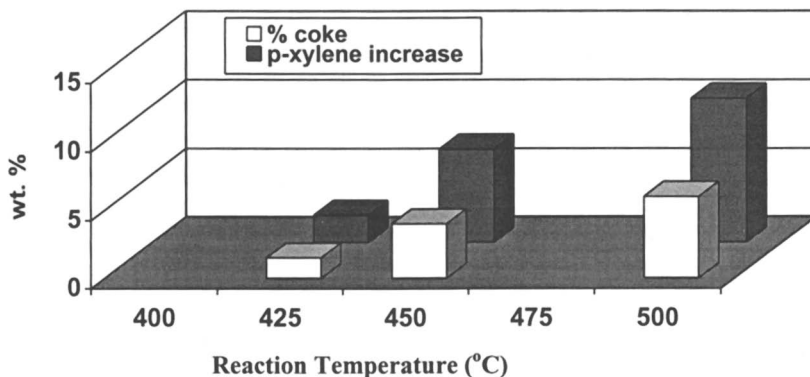
In order to understand the enhanced shape selectivity as a function of coke formation, three spent catalysts that were used in n-heptane cracking reaction were analysed to determine the amount of coke formed. Table VI provides the relevant data on product distribution as function of reaction severity.

The catalyst was on stream for 24 hrs at 425, 450 and 500°C, and the amount of coke and p-xylene formed at each condition are given in Table-VI. The incremental increase in p-xylene selectivity is calculated from the selectivities at the start of the run and those at the end of the run (24 hrs). As the reaction temperature increases coke formation increased and so does para xylene selectivities. To further appreciate the increase in para selectivity with increase of coke, the incremental increase of p-xylene selectivity as a function of amount of coke formed is shown in Figure-1. One can clearly see the effect of coke on p-xylene selectivity.

**Table-VI Effect of Reaction Severity on Coke Amount and Enhanced p-Selectivity**

Reaction Temp. (°C)	425		450		500	
*Wt% of coke	1.54.0		6.0		6.0	
Aromatic Distribution (wt%)	Start of run	End of run	Start of run	End	Start of run	End of run
B	4.0	3.5	8.0	5.6	10.0	8.0
T	28.0	25.0	30.0	25.6	25.0	20.0
EB	2.0	2.0	1.5	2.0	1.2	2.0
p-xylene	13.0	15.0	14.2	21.0	15.0	25.5
o-xylene	24.0	20.0	22.5	21.0	12.0	12.0
m-xylene	17.0	17.5	11.0	9.5	16.0	11.5
C <sub>9+</sub>	13.0	16.0	12.8	15.9	20.0	22.0
<b>Total</b>	<b>100</b>	<b>100</b>	<b>100</b>	<b>100</b>	<b>100</b>	<b>100</b>

\* Percent of coke formed (based on catalyst wt) after 24 hrs TOS



**Figure 1. Enhanced Shape Selectivity Due to Coke Formation**

**Effect of Amorphous Material in Zeolites.** The ZSM-5 zeolite was synthesized without the aid of template and also with the use of template in order to compare the relative performance of these materials, as a function of preparation method in n-heptane aromatization reaction. The formation of ZSM-5 by both the methods is confirmed by X-ray diffraction method and percent crystallinity was also evaluated which showed that the zeolites synthesized without the aid of template are of lower crystallinity indicating that some amorphous silica-alumina is indeed present, probably inside the pores. In order to understand the effect of presence of this amorphous material on n-heptane conversion and aromatic distribution and particularly on the xylene products, a comparative data on zeolites prepared by both the methods, is presented in Table-VII. It can be seen that conversions are lower on the zeolite containing amorphous material.

**Table – VII Effect of Presence of Amorphous Material**

Catalysts	H-ZSM-5 templated	H-ZSM-5 Without Template
Percent Crystallinity	99.0	89.0
<i>Aromatic Distribution (wt. %)</i>		
Benzene	7.2	3.5
Toluene	28.0	22.5
Ethyl Benzene	1.8	2.0
p – Xylene	13.5	16.0
m– Xylene	23.0	16.0
o – Xylene	11.7	8.0
C <sub>9+</sub> Aromatics	23.5	32.0
Total	100	100



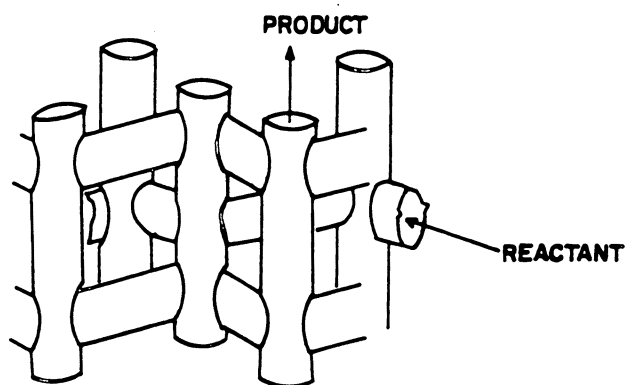
The para xylene selectivities are higher on ZSM-5 containing amorphous material resulted by synthesizing without the aid of template. In this case it is difficult to attribute the enhanced selectivity to pore dimension modification alone, since the ZSM-5 prepared by the two methods differ considerably in acidity and also the presence of amorphous material promotes formation of C<sub>9+</sub> aromatics [12]. In spite of these complications this can be taken as an example for alteration of shape selectivity due to presence of extraneous material.

In all the cases above discussed viz extra framework alumina, coke or amorphous materials, the shape selectivity is enhanced and this is manifested in the form of increased p-xylene selectivity, one of the main reason for such an observation is decrease in the channel dimensions and tortuosity due to the presence of such materials. However as pointed out by several authors [7,9], there are several other factors such as external acidity and change in internal acid strength distribution of ZSM-5, which also alters shape selective product formation. Most of the factors that decrease the channel dimensions such as extraneous materials like P, Al<sub>2</sub>O<sub>3</sub>, MgO, amorphous material, polymers, silylation alter both internal and external acidity. From this data presented here it is not possible to choose between the two without further investigating the role of acidity. However it appears from the pore size data obtained on coked catalysts that pore size is indeed decreased. Similar thing is expected in the case of extra framework Al<sub>2</sub>O<sub>3</sub> and amorphous material. It is our assessment that decrease in pore diameter is a major factor, while the effects due to acidity can not be ignored, in increasing the para selectivity in the products observed in n-heptane aromatization.

**Evidence for Molecular Traffic Control Mechanism.** It is well known that ZSM-5 crystalline framework consists of two types of intersecting channel systems made up of ten membered ring openings. One channel system is sinusoidal and has 5.1 x 5.5 Å<sup>0</sup> cross section. The other channel system has 5.3 x 5.6 Å<sup>0</sup> openings which run straight and perpendicular to the first system [13] Figure 2. Investigations by Derouane and co-workers group [4] suggested :

1. Linear aliphatic molecules diffuse freely in ZSM-5 framework and can be adsorbed in both the channels.
2. Isoaliphatic compounds experience steric hindrance effects, which may restrict their diffusion in sinusoidal channel system.
3. Aromatic compounds and methyl substituted aliphatic compounds have strong preference for diffusion and / or adsorption in the linear elliptical channels. Implying that flat and large molecules will prefer to diffuse in wider elliptical channels.

n-Heptane aromatization reaction on ZSM-5 catalyst consists of cracking, oligomerization, cyclization and other hydrogen transfer reactions. Applying the above mentioned observations by Derouane et. al. to the present reaction, it is clear that the reactant and/or the olefins formed by cracking, preferentially travel through sinusoidal channels and reach the intersections, where they undergo above mentioned reactions. Whereas, the aromatics and other bulkier products formed, diffuse out through linear channels of ZSM-5 catalyst. The experimental results that furnished an evidence for molecular traffic control in ZSM-5 during n-heptane aromatization reaction are discussed in the following.



**ZIG-ZAG CHANNELS = 5-1 X 5-5 Å**

**STRAIGHT CHANNELS = 5-3 X 5-6 Å**

**Figure 2. Molecular traffic control (MTC) in ZSM-5 channels (adapted from reference 1).**

The n-heptane aromatization reaction was carried out at 500°C, 10 kg/cm<sup>2</sup> pressure with LHSV = 2h<sup>-1</sup> in a micro catalytic reactor containing 5g of the catalyst, which is a mixture of ZSM-5 (4.5 Al/U.C) and alumina in 60:40 ratio. Synthesis, characterization and activity evaluation methods were described elsewhere [12]. Ultra pure nitrogen was used as carrier gas with N<sub>2</sub>/HC = 2. With a view to understand the effect of coke on pore volume and pore size distribution, the fresh H-ZSM-5 catalyst and the H-ZSM-5 catalyst that was 12 hrs on stream, were examined for pore size distribution using Argon adsorption and Harvath and Kawazoe method. Both micro and meso pore size distributions were brought onto single display by using density functional theory. The differential pore volume plot showed two peaks corresponding to sinusoidal channels and straight channels. In the case of used catalyst also similar display was observed, but the integrated areas of the peaks are smaller indicating loss of pore volume due to coke formed during the reaction Figure 3. From the data obtained using density functional theory shown in Tables-VIII & IX, the decrease in pore volumes and pore areas of zeolitic as well as non zeolitic portions were evaluated.

**Table-VIII Effect of Coke on Pore Size Distribution**

Properties	Fresh Catalyst	Used Catalyst	Percent Decrease
Maximum Pore Volume At Relative Pressure 0.30267	0.1503 cc/g	0.1131 cc/g	24.7 %
Median Pore Diameter	6.4 A <sup>0</sup>	5.7 A <sup>0</sup>	11.4 %

Analysis adsorptive = Argon at 87.05<sup>0</sup>K

**Table-IX Effect of Coke on Pore Size Distribution of ZSM-5 Catalyst**

Properties	Fresh Catalyst	Used Catalyst	Percent Decrease
Volume in ZSM-5 pores (< 5.6 A <sup>0</sup> )	0.05165 cc/g	0.05069 cc/g	2 %
Area in ZSM-5 pores (< 5.6 A <sup>0</sup> )	300.562 cc/g	287.213 m <sup>2</sup> /g	4.4 %
Total volume in pores (< 300 A <sup>0</sup> ) (Including binder)	0.32127 cc/g	0.20627 cc/g	35.8 %
Total area in pores (< 300 A <sup>0</sup> ) (Including binder)	32.872 m <sup>2</sup> /g	30.453 m <sup>2</sup> /g	7.4 %

Analysis Gas : Argon @ 87.29<sup>0</sup>K

The data indicates that the non zeolitic pore volume decreased by 35.8%, while the zeolitic pore volume decreased only 7.4% in the case of zeolitic pores indicating significant portion of zeolite is not occupied by coke. Figure 4 shows the display of

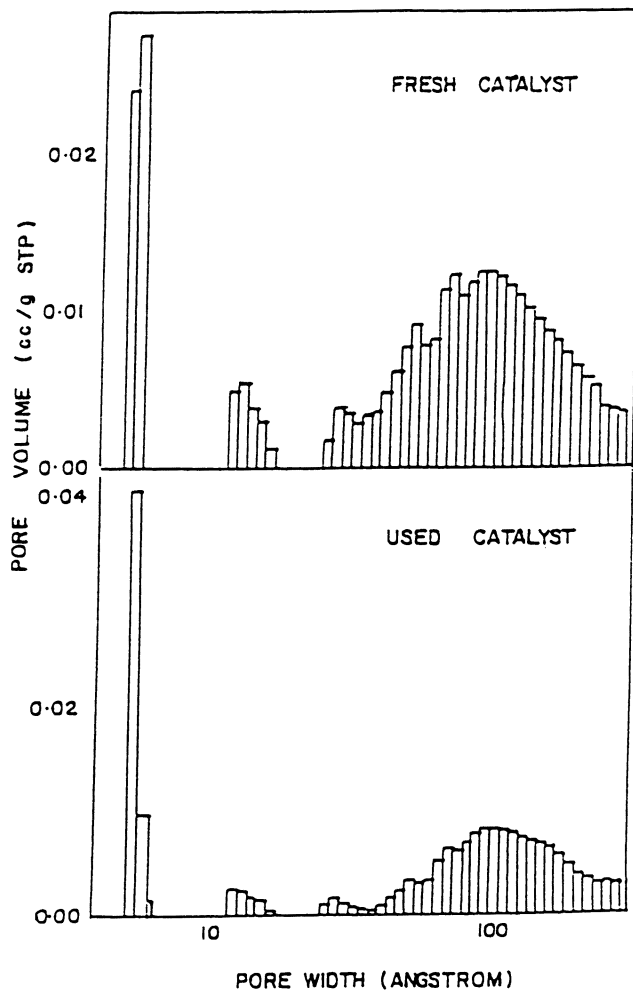
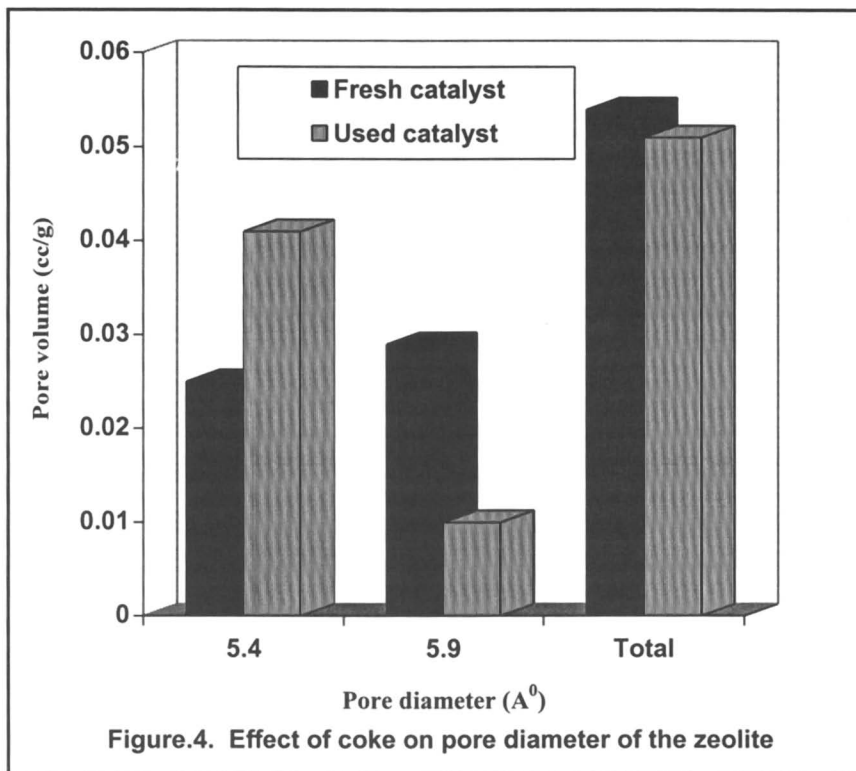


Figure 3. Effect of coke formation on the pore size distribution of the catalyst. (Reproduced with permission from reference 16, copyright 1999 Elsevier)

incremental pore volume versus pore width plots. It can be seen that both micropores and mesopores are brought into the graph in Figure 3, using density functional theory, undergo significant changes as a result of coke formation. It is interesting to see that total pore volume in zeolite channels is more or less intact. However, the individual pore volume of the two channels change significantly Figure 4. In the fresh catalyst, the volume of large pores, viz straight channels is higher than that of the sinusoidal channels. In the case of used catalyst, the reverse is observed to be true. The change in volume of the two zeolite channels, observed in fresh and used ZSM-5 catalyst, without change in total zeolite pore volume suggests that, what ever pore volume lost in one type of pores is transferred to the other. How did this happen? this can be understood by realizing that pore size distributions are evaluated using gas adsorption. The gas adsorption measures the diameter of the pores through which it enters. Therefore, in the fresh catalysts, where both the pores are accessible to gas adsorption, gives the real volume of the individual channels. The higher pore volume in linear channels compared to those of sinusoidal channels obtained in this study is in agreement with the earlier reports [4,14], where, based on the structure of ZSM-5 and Silicalite, it was determined that the total length of the pore system per unit cell is 8.8nm and, the individual length of the linear and elliptical channels is 5.9nm and 2.9nm respectively. In the case of used catalyst, the pore volume of straight channels decreased from 0.029 cc/g (in fresh catalyst) to 0.0095 cc/g (in the used catalyst) with a simultaneous increase in pore volume of sinusoidal channels from 0.025 cc/g (in the fresh catalyst) to 0.041 cc/g (in the used catalyst). No significant change in total zeolitic pore volume also can be seen from Figure 4. From these observations it is clear that, in the deactivated catalysts, the sinusoidal channels are predominantly accessible for gas adsorption. This also suggests that majority of straight channels are blocked by coke. It appears that the total gas is entering through sinusoidal channels and filling up the poremouth - blocked straight channels through intersections, and this is keeping the total pore volume more or less intact. Guisnet and Magnoux in an excellent review on deactivation of MFI zeolites by coke formation with special reference to n-heptane cracking [15]. They have discussed that the deactivation is primarily due to three causes at various stages of deactivation (i) limitation of access of reactant molecules to the active site (ii) blockage of access to the active sites at intersection in which coke molecules are situated and (iii) blockage of access to the sites of the pores in which no coke molecules are present. In our case, since that total pore volume and area is more or less intact, it appears that these pores are blocked at the pore mouths. Since there is a small (2%) reduction in pore volume a small amount of blockage in the internal structure such as intersections cannot be completely ruled out. By similar argument we can say that most of the sinusoidal pores are still open after deactivation.

Now, considering the aromatization reaction, the n-heptane reactant molecules and/or the olefins generated from them, enter the zeolite through small sinusoidal pores and these molecules undergo reaction at channel intersections, and aromatics produced preferentially travel through straight channels. Since, these



aromatics and other bulkier products are also coke precursors, they can preferentially block these pores. It is also known that the pore blockage in ZSM-5 zeolites is likely to occur at or near pore mouths [15]. This pore blockage is occurring preferentially in linear channels, which means that large aromatic molecules and other coke precursors prefer to travel in the channels. By similar argument one can explain why the sinusoidal channels are not blocked. This result, in our opinion, can be taken as evidence for molecular traffic control (MTC) mechanism.

## References

1. Csicsry, S. M.; *Zeolites* **1984**, *4*, 202.
2. Chen, N.Y.; and Garwood, W.E.; *Catal. Rev. Sci. Eng.*, **1986**, *28* (2&3).
3. N. Y. Chen, W. W. Kaeding and F. G Dwyer, *J. Am. Chem. Soc.* **1979**, *101*, 6783.

4. Derouane, E.G.; and Gabelica, Z.; *J. Catal.*, **1980**, *65*, 486.
5. Kaeding, W. W.; *J. Catal.*, **1985**, *95*, 512.
6. Chen, N.Y.; Garwood, W.E.; *J. Catal.*, **1978**, *52*, 453.
7. Chandawadker, K. H.; Kulkarni, S. B.; and Ratnasamy, P.; *Appl. Catal.*, **1982**, *4*, 287.
8. Kim, J. W.; Namba, S.; and Yashima, T.; *Stud. Surf. Sci. Catal.*, **1989**, *46*, 71.
9. Lonyi, F.; Engelhardt, J.; and Kallo, D.; *Zeolites*, **1991**, *11*, 169.
10. Halgeri, A. B.; Bhat, Y. S.; Unnikrishnan, S.; and Rao, T. S. R. Prasada.; *ACS, Div. Pet. Chem. Preprints*, **1991**, *36(4)*, 772.
11. Viswanadham, N.; Ph.D. Thesis, Roorkee University, India, **1996**.
12. Pradhan, A. R.; Viswanadham, N.; Suresh, S.; Gupta, O. P.; Ray, N.; Murali. Dhar G.; Uma Shanker,.; and, Prasada. Rao T. S. R.; *Catal. Lett.*, **1994**, *28*, 231.
13. Szostak, R.; in "Introduction to Zeolite Science and Practice" H. Van Bekkum, E. M. Flanigen, J. C. Hensen (Editors) **1991**, 153.
14. Derouane, E. G.; in B. Imelik et. al. (Eds.) *Catalysis by Zeolites*. Elsevier, Amsterdam, **1980**, p 5.
15. Guisnet, M.; and Magnoux, P.; *Appl. Catal.* **1989**, *54*, 1.
16. Viswanadham.N; Murali Dhar.G; and Prasada Rao, T.S.R; *J.mol.Catal* **1997**, *125*, L87-L90.

## Chapter 10

# Shape Selectivity for Alkane Dehydrocyclization with Pt Silicalite Catalysts

Yuguo Wang<sup>1</sup>, Fred L. Tungate<sup>2</sup>, George Kokotailo<sup>3</sup>, and Burtron H. Davis<sup>1</sup>

<sup>1</sup> Center for Applied Energy Research, University of Kentucky,  
2540 Research Park Drive, Lexington, KY 40511

<sup>2</sup> United Catalyst Inc., 1600 Hill Street, Louisville, KY 40210

<sup>3</sup> University of Pennsylvania, Tonne Boulevard, Philadelphia, PA 19104

In agreement with an earlier report we find that dehydrocyclization of *n*-octane and 3-methylheptane with a Pt-silicalite catalyst selectively forms ethylbenzene. In the earlier report a pulse reactor was utilized whereas a continuous flow reactor was used in this study. The slow rate of diffusion of aromatic products in the Pt-silicalite catalyst leads to the formation of significantly more hydrogenolysis to produce benzene and toluene than occurs on a support containing meso- and macro-porosity.

The dehydrocyclization of C<sub>6</sub>-C<sub>10</sub> alkanes is an important reaction for naphtha reforming. The reaction can be catalyzed by either monofunctional or polyfunctional catalysts (1-3). Recently, Mériaudeau et al. (4) used a pulse reactor to study the possible role of shape selectivity of a Pt-zeolite catalyst during dehydrocyclization of *n*-octane and 3-methylheptane. They reported that ethylbenzene comprised 90% or more of the C<sub>8</sub>-aromatic products. In agreement with others, Mériaudeau et al. found about equal amounts of ethylbenzene and *o*-xylene were produced when they used a Pt-silica catalyst to effect the dehydrocyclization reaction.

The aromatic selectivities with the Pt-silicalite catalyst were obtained from products generated during exposure of the catalyst to a pulse of the reactant for two minutes (4). It is possible that the slower diffusion of *o*-xylene in the silicalite pore system may allow ethylbenzene to appear as a dominant C<sub>8</sub>-aromatic product because of shape selective diffusion, and not because of shape selectivity in the ring forming step. We present results for aromatic selectivities obtained using a Pt-silicalite catalyst which was operated in a continuous flow reactor.



## Experimental

A silicalite catalyst support, provided by United Catalyst Inc., was calcined in air at 500°C overnight and then crushed to 325 mesh size. The zeolite powder was exchanged by dispersing it in an aqueous sodium nitrate solution with stirring at 70°C overnight. The zeolite was collected by filtration, dried at 120°C and then impregnated with an aqueous solution of  $\text{Pt}(\text{NH}_3)_4\text{Cl}_2$  to produce a material containing 0.9 wt.% Pt. The catalyst was calcined in air at 300°C for about 4 hours and is designated an acidic Pt-silicalite catalyst (PtSi-1-A) in the following description. A similar catalyst was prepared except that it contained 0.5 wt.% Pt. After this Pt-containing material was dried in air, it was reduced overnight in flowing hydrogen at 300°C. After reduction, the catalyst was placed in water and sufficient KOH was added as needed so as to maintain a pH of 10 during several hours. The solid was then collected and calcined in air at 300°C for 4 hours (PtSi-1-B). The heating rate for calcination and reduction in the preparation of PtSi-1 catalysts was rapid (ca. 20°C/min).

Another sample was prepared using the United Catalyst Inc. silicalite. In this preparation 50 grams of the 325 mesh powder was dispersed by stirring in 1 L of distilled water and then a sufficient amount of 0.05 M  $\text{Pt}(\text{NH}_3)_4(\text{NO}_3)_2$  was added so that the sample would contain 0.5 wt.% Pt, assuming complete exchange, and the sample was stirred overnight at 70°C. After washing four times with distilled water, the powder was dried overnight at 80°C. The sample was loaded into a reactor and heated in high-purity oxygen at 0.2°C/min from 100°C to 460°C, the oxygen flow was then replaced by a high-purity helium flow for 30 min., the helium flow was replaced by hydrogen and the temperature was increased at 0.5°C/min to 620°C and held at this temperature for 4 h. The sample was then cooled to room temperature (PtSi-2-A). A portion of this sample was suspended in 200 ml of 0.025 M KOH, stirred overnight, collected by filtration and dried at 100°C overnight (PtSi-2-B). A third sample (Pt-Si-3-B) was prepared using the procedure for sample Pt-Si-2B except that the catalyst was heated in oxygen from 100°C to 350°C and in hydrogen from 350°C to 482°C.

About 1 gram of catalyst was placed in a Quartz fixed bed reactor. About 6 cm of glass beads filled the space above the catalyst and the top of the reactor to serve as a preheater. The reactor was fitted with a thermowell that extended to the middle of the catalyst bed. Prior to a run, PtSi-1 was rapidly ramped (10 to 15 min) to 482°C and held at this temperature overnight in flowing hydrogen whereas PtSi-2 catalysts were activated in hydrogen flow at a ramp rate of 2°C/min. The reactor feed was a 3:1, 18.5:1 or 50:1 molar ratio of hydrogen:hydrocarbon and the conversion was effected at 1 atm. and 482°C or 620°C. Liquid product was collected in a trap held at 0°C. Gas and liquid samples were analyzed by g.c. using either a DB-5 or Bentone column.

X-ray diffraction patterns were recorded using a Philips XRG 3100 instrument, scanning at steps of  $2\theta = 0.02$ .

## Results and Discussion

At 482°C, much of the *n*-octane underwent cracking with the acidic catalyst (PtSi-1-A) that had not been exchanged with base following hydrogen reduction. It is apparent that the silicalite possessed sufficient acidity to effect bifunctional catalysis. Thus, the gaseous effluent contained only about 50 mole% hydrogen; the majority of the hydrocarbon products making up the remaining 50 mole % were C<sub>3</sub> and C<sub>4</sub> hydrocarbons. The aromatic composition of the liquid products for the *n*-octane and 3-methylheptane reactants are shown in Table I. With the acidic catalyst, the aromatic

Table I  
Distribution of aromatic products from the conversion of *n*-octane and 3-methylheptane over acidic Pt-silicalite catalyst PtSi-1-A at 482°C, atmospheric pressure, and H<sub>2</sub>:hydrocarbon = 3:1 molar

Reactant	Benzene	Toluene	EtBz <sup>a</sup>	PX + MX <sup>a</sup>	OX <sup>a</sup>	C <sub>9+</sub> Aromatic
<i>n</i> -octane	7.3	37.1	6.0	28.8	8.2	12.6
3-methylheptane	14.3	53.5	6.2	23.0	6.8	6.4

<sup>a</sup>EtBz = ethylbenzene; PM+MX = *p*- + *m*-xylene; OX = *o*-xylene; percentages are wt.% of liquid product.

distribution is determined by isomerization of the reactant prior to cyclization and of the aromatic products, hydrogenolysis of the products, and trans-alkylation. Thus, there is not a significant difference between the aromatic products obtained with the two reactants. With this catalyst, ethylbenzene is not the dominant C<sub>8</sub>-aromatic product and the xylene composition is approximately an equilibrium mixture.

The aromatic products obtained from the conversion of *n*-octane and 3-methylheptane with the non-acidic catalyst (Pt-Si-1-B) are presented in Table II. With this catalyst cracking of the feed was a very minor factor; the exit gas contains 95 molar% hydrogen or greater. For the *n*-octane reactant, the dominant products are the C<sub>8</sub>-aromatics, and about equal amounts of ethylbenzene and *o*-xylene are formed. These are the C<sub>8</sub>-aromatic products that are predicted for a mechanism that includes direct six-carbon ring formation. The products obtained from *n*-octane are the same as the ones obtained with a typical Pt-silica catalyst, and there is no evidence for the porosity of the zeolite impacting the aromatic products when a continuous flow reactor is used. Likewise, the aromatic products from the conversion of 3-methylheptane are mainly C<sub>8</sub>-aromatics and these are comprised of about equal amounts of the three isomers allowed by direct six-carbon ring closure - ethylbenzene, *p*-xylene and *o*-xylene. With this reactant, there is also no evidence for the pore structure of the

silicalite zeolite impacting the aromatic product - neither in the ring closure step nor in diffusion of the products.

Table II  
Distribution of aromatic products from the conversion of *n*-octane and 3-methylheptane over the nonacidic Pt-silicalite Pt-Si-1B catalyst at 482°C and atmospheric pressure ( $H_2$ :hydrocarbon = 3:1 molar).

Reactant	Time (Conv.)	Benzene	Toluene	EtBz <sup>a</sup>	PX + MX <sup>a</sup>		OX <sup>a</sup>
<i>n</i> -octane	30(20)	0.3	3.7	50.5	0.5		43.3
	45(16)	---	4.7	50.6	---		43.2
	60(14)	---	5.3	50.0	---		43.4
	105(8.7)	---	---	51.4	---		48.6
3-methylheptane	25(25)	5.0	8.2	26.7	32.5	6.9	20.9
	55(19)	8.3	10.3	27.6	26.7	7.9	19.2
	100(13)	11.8	10.0	24.9	24.9	10.4	20.3

<sup>a</sup>EtBz = ethylbenzene, PX = *p*-xylene, MX = *m*-xylene, OX = *o*-xylene.

X-ray diffraction (XRD) techniques have been used to obtain considerable information regarding the structure of crystalline materials, including such factors as their structure, identity, phase and crystallite size. The XRD pattern of a mixture of two or more crystalline materials is the superposition of their individual patterns. In the case of a crystalline material admixed with an amorphous material the intensity of the XRD pattern is a function of the crystalline concentration. The change in the XRD background reflects the presence of amorphous material. When the crystalline material is a porous zeolite, the presence of sorbate material in the pores changes the relative intensity of the lines in the XRD pattern with a reduction of the low-angle, high *d*-spacing lines. This change occurs because the sorbed molecules are scattering out of phase with the framework atoms to which they are coordinated. A comparison of the intensities of low-angle peaks to higher-angle peaks provides a simple and reliable technique to demonstrate the presence of sorbate material in the channels of the zeolite. The presence of highly dispersed Pt within the pore structure of a zeolite would therefore be expected to decrease the intensity of the low-angle lines relative to the higher angle lines in the XRD pattern. The data for PtSi-1-A was consistent with this but not to the extent shown below for PtSi-2-A.

It has been demonstrated that about equal amounts of ethylbenzene and *o*-xylene are formed from the conversion of *n*-octane over Pt on non-acidic alumina or silica supports (1-8). The products from the conversion of 3-methylheptane are about equal amounts of the three C<sub>8</sub>-aromatics expected from a direct six carbon ring formation:

ethylbenzene, *o*-xylene and *p*-xylene. Thus, the products shown in Table II are those expected from the conversion by Pt on a non-acidic support, and provide no indication of shape selectivity in the formation of aromatics. The aromatic selectivities for PtSi-1-B are consistent with the Pt being present in particles that are predominantly located on the exterior of the non-acidic zeolite support.

The amounts of benzene and toluene that are formed with PtSi-1-A and PtSi-1-B are significantly different. In both cases the amount of toluene is greater than that of benzene, indicating that benzene and toluene are formed by hydrogenolysis of C<sub>8</sub>-aromatics, and not by acid catalyzed dealkylation where benzene would be expected as the dominant product compared to toluene. The amount of benzene and toluene formed with the acidic (PtSi-1-A) catalyst is about equal to the amount of C<sub>8</sub>-aromatics. In contrast, benzene plus toluene are less than 5% of the total aromatics produced using the nonacidic support (PtSi-1-B). The results obtained with PtSi-1-B are very similar to those obtained with Pt supported on noncrystalline silica or nonacidic alumina (2,7). The difference between the two PtSi-1 catalysts implies that the Pt is located within the pores of PtSi-1-A but is on the exterior of PtSi-1-B.

Pt-Si-3B was used for the conversion of *n*-octane and 3-methylheptane at 482°C, 1 atm., hydrocarbon flow 6.2 mol/g, and H<sub>2</sub>/hydrocarbon molar ratio of 24.5. During 85 minutes 3-methylheptane was converted with the results shown in Table III. For this

Table III  
Conversion of 3-Methylheptane with Pt-Si-3B at 482°C, 1 atm,  
H<sub>2</sub>/Hydrocarbon = 25.4

Time, Min.	n-C <sub>8</sub> Conv., Wt. %	Aromatic Distribution, Mole %						
		Bz <sup>a</sup>	TOL <sup>a</sup>	Eb <sup>a</sup>	Px <sup>a</sup>	Mx <sup>a</sup>	Ox <sup>a</sup>	STY <sup>a</sup>
25	40	14.8	37.1	25.6	13.4	4.2	4.4	0.4
45	36	15.1	36.9	25.7	13.3	4.3	4.2	0.5
65	34	15.8	36.3	26.0	13.0	4.4	4.0	0.5
85	32	15.6	36.0	26.5	13.0	4.0	4.0	0.6

<sup>a</sup>BZ, benzene; TOL, toluene; EB, ethylbenzene; PX, *p*-xylene; MX, *m*-xylene; OX, *o*-xylene; STY, styrene.

reactant the aromatics that are predicted for a direct six-carbon ring formation are: ethylbenzene, *p*-xylene and *o*-xylene. The dominant products are ethylbenzene and *o*-xylene, isomers expected from a direct six-carbon ring formation, and the ratio ethylbenzene:*p*-xylene is 2. *o*-Xylene is formed but in a much smaller amount. The aromatic product distributions in Table III differ significantly from the ones obtained

with Pt-silica or Pt-nonacidic alumina catalysts where about equal amounts of ethylbenzene, *o*-xylene and *p*-xylene are formed. After converting 3-methylheptane, the catalyst was treated with only hydrogen at 482°C for 40 minutes. After this 40 minute period, *n*-octane flow was started ( $H_2$ :*n*-octane = 24.5). The conversion data (Table IV) include the aromatic product distribution and the distribution within the  $C_8$  aromatics (values given in the parentheses). The products differ significantly from those obtained with Pt-Si-1B and with Pt-SiO<sub>2</sub> and Pt-nonacidic alumina, and contain nearly 70% ethylbenzene plus styrene. The styrene/ethylbenzene ratio is about 0.02, essentially the ratio expected for the equilibrium condition.

Table IV  
Conversion of *n*-Octane with Pt-Si-3B at 482°C, 1 atm,  
 $H_2$ /Hydrocarbon = 25.4

Time, Min.	<i>n</i> -C <sub>8</sub> Conv., Wt.%	Aromatic Distribution, Mole %						
		Bz <sup>a</sup>	TOL <sup>a</sup>	Eb <sup>a</sup>	Px <sup>a</sup>	Mx <sup>a</sup>	Ox <sup>a</sup>	STY <sup>a</sup>
20	42	9.6	28.0	42.7	4.3	5.2	9.1	1.0
40	39	10.6	30.0	38.4	5.0	5.6	9.2	1.0
60	35	10.8	26.8	42.2 (67.6)	4.2 (8.0)	4.3 (8.8)	9.6 (14.5)	1.0
80	36	10.4	27.7	41.6	4.3	5.4	9.7	1.0
100	32	10.1	26.6	43.3	3.8	5.0	10.1	1.1

<sup>a</sup>BZ, benzene; TOL, toluene; EB, ethylbenzene; PX, *p*-xylene; MX, *m*-xylene; OX, *o*-xylene; STY, styrene.

An equimolar mixture of *n*-octane and 3-methylheptane was converted with the Pt-Si-3B catalyst. If adsorption at the pore opening was rate determining the conversion of *n*-octane/3-methylheptane should be about one since the conversion of each isomer was about the same under similar reaction conditions. The experimental ratio for *n*-octane/3-methylheptane is about 2.7. Thus, it appears the methyl group does inhibit the penetration of 3-methylheptane, relative to *n*-octane, into the internal pore volume.

2-Methylheptane was also converted under the same reaction conditions as was used for *n*-octane (Table III) and 3-methylheptane (Table IV). The aromatic distribution from 2-methylheptane (Table V) differ from those of 3-methylheptane; furthermore, the conversion is only about 75% of 3-methylheptane or *n*-octane. One of the direct six-carbon ring cyclization pathways leads to 1,1-dimethylcyclohexane. This structure cannot lead directly to an aromatic. The conversion of 1,1-

dimethylcyclohexane is very dependent upon the catalyst, ranging from predominantly isomerization to produce *o*-xylene and lesser amounts of xylenes to primarily dimethylation to produce toluene. With the Pt-Si-3B catalyst, more toluene is produced than with either *n*-octane or 3-methylhexane, indicating that demethylation is occurring. However, the isomerization pathway differs from that of the non-zeolitic supports since the meta isomer is the dominant product, and *p*-xylene is the next dominant isomer. *m*-Xylene is the only product that can form by direct six-carbon formation, and this is the experimental observation. Two isomers not allowed by a direct six-carbon ring formation, ethylbenzene and *p*-xylene are formed as major products. The formation of these isomers in much greater amounts than with the non-zeolitic support and implies that there is a steric effect imposed by the pore structure, and most likely in the transition state.

Table V  
Conversion of 2-Methylheptane with Pt-Si-3B at 482°C, 1 atm,  
 $H_2/\text{Hydrocarbon} = 25.4$

Time, Min.	n-C <sub>8</sub> Conv., Wt.%	Aromatic Distribution, Mole %						
		Bz <sup>a</sup>	TOL <sup>a</sup>	Eb <sup>a</sup>	Px <sup>a</sup>	Mx <sup>a</sup>	Ox <sup>a</sup>	STY <sup>a</sup>
25	31.2	13.2	45.0	13.3	8.8	17.1	2.2	0.3
45	28.2	13.2	42.6	13.2 (30.3)	8.9 (20.1)	19.5 (44.1)	2.4 (5.5)	0.2
65	25.4	11.5	39.9	13.3	9.2	23.0	2.9	0.2
85	23.4	9.7	37.3	13.4	9.7	26.6	3.0	0.2

<sup>a</sup>BZ, benzene; TOL, toluene; EB, ethylbenzene; PX, *p*-xylene; MX, *m*-xylene; OX, *o*-xylene; STY, styrene.

Because of the use of an improper thermocouple, some runs were conducted at 620°C. The conversion of *n*-octane at 620°C at two hydrogen:hydrocarbon ratios (3.0 and 50) with PtSi-2-B exhibits a selectivity for ethylbenzene and its dehydrogenation product, styrene, among the C<sub>8</sub>-aromatics (Table VI). About 50 wt.% of the aromatics are benzene and toluene for the lower H<sub>2</sub>:hydrocarbon ratio, and hence the lower flow rate, but these two aromatics still account for 40-45 wt.% of the aromatics at the higher flow rate. The XRD data clearly show that the lower angle peaks are much reduced in intensity for the PtSi-2-B catalyst from that of the original silicalite sample (Figure 1). Thus, the intensities of the low-angle peak at about  $2\theta = 8$  relative to the peak at about  $2\theta = 23$  are 0.93 for the silicate and the ratio decreases to about half this value (0.51) for the calcined, acid form (PtSi-2-A) (Table VII). Following ion exchange with

Table VI  
 Conversion of *n*-Octane with PtSi-B-2 at 620°C, 1 atm., hydrogen:*n*-octane = 3

Time, Min.	Conv., %	H <sub>2</sub> / <i>n</i> -C <sub>8</sub>	SV, g/g/hr	Benzene	Toluene	EB	Para-xylene	Meta-xylene	Ortho-xylene	Styrene	Styrene x 100/ (styrene + ethylbenzene)
25	24.2	3	7.1	33.8	22.2	15.1	3.8	1.7	11.0	12.5	45
40	20.9	3	7.1	38.8	31.4	13.8	3.7	1.1	6.5	4.7	25
55	20.4	3	7.1	40.7	24.4	13.8	4.0	1.4	7.2	8.5	38
70	19.5	3	7.1	37.2	34.1	12.3	3.5	1.0	5.6	6.3	34
90	17.2	3	7.1	40.2	27.8	13.5	4.0	1.2	6.5	6.8	34
110	16.9	3	7.1	41.3	27.9	13.0	3.9	1.2	6.3	6.5	33
30	20.5	50	5.6	20.2	39.0	24.5	4.5	2.5	8.1	14.5	
60	19.2	50	5.6	20.5	31.7	27.4	2.8	1.4	6.9	16.1	33
90	21.7	50	5.6	22.1	30.4	24.8	2.1	1.1	5.4	14.1	36
120	21.6	50	5.6	22.5	30.8	24.5	2.1	1.1	4.8	14.2	37
150	21.5	50	5.6	22.9	30.9	24.4	2.1	1.1	4.5	14.3	37
200	21.2	50	5.6	24.7	31.3	23.2	2.0	0.8	4.0	13.9	39
260	22.7	50	5.6	25.3	31.6	22.4	2.1	1.0	3.9	13.7	38
320	22.9	50	5.6	24.5	31.8	23.2	2.1	0.9	3.8	13.8	37

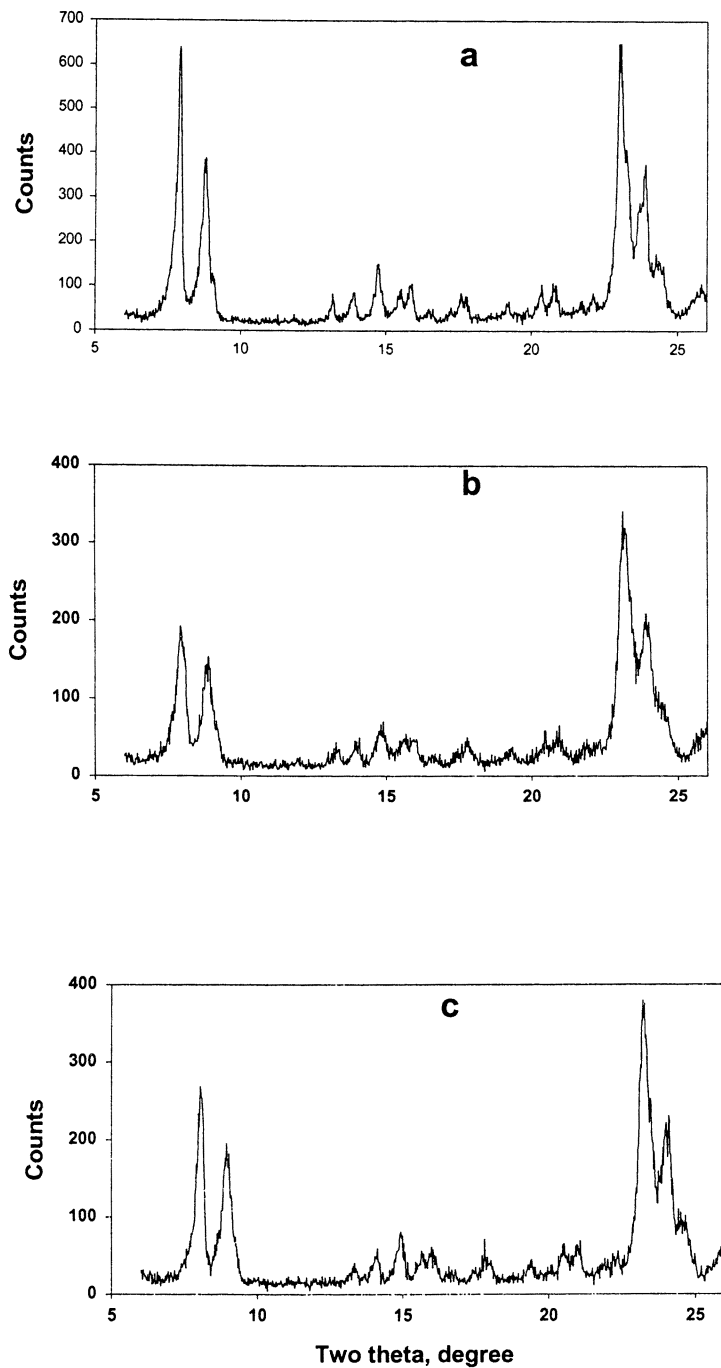


Figure 1. XRD of (a) silicalite, (b) PtSi-2-A and (c) PtSi-2-B.



potassium and reduction, the relative intensity of the  $2\theta = 8$  is 0.71. Based upon these relative intensities, it is concluded that the platinum is much better dispersed within the zeolite pores in the acidic catalyst than it is in the basic catalyst. Furthermore, it is apparent that platinum is much better dispersed, both in the acid and basic form, in PtSi-2 catalysts than in PtSi-1 catalysts.

Table VII  
The relative intensities of the  $2\theta = 8$  to the  $2\theta = 23$  peaks  
for silicalite and the PtSi-2 catalysts

Catalyst	Relative intensity, $2\theta=8/2\theta=23$
Silicalite	0.98
PtSi-2-A	0.51
PtSi-2-B	0.71
PtSi-1-A	0.91

Dessau (9), for example, describes the ability to prepare catalysts with platinum dispersed in the channels of ZSM-5 and the use of mild heating programs. Platinum migration and agglomeration during hydrogen reduction has been attributed to the formation of a neutral Pt(II)(NH<sub>3</sub>)<sub>2</sub>H<sub>2</sub> complex when Pt(NH<sub>3</sub>)<sub>4</sub>(NO<sub>3</sub>)<sub>2</sub> was used in the catalyst preparation (9,10). The data in Table III indicate that the platinum mobility during hydrogen reduction is not limited to instances of the formation of the neutral ammine containing complex. PtSi-2-A, the precursor of PtSi-2-B, has already been calcined and reduced and the ammonia would be lost during these procedures. Thus, the replacement of the H<sup>+</sup> by K<sup>+</sup> and subsequent hydrogen treatment led to platinum agglomeration, presumable through mobility of Pt atoms or small Pt clusters. This result implies that either the initial reduction of platinum to a zero valence state to produce PtSi-2-A was incomplete or that the proton retards migration of platinum atoms and/or very small clusters of platinum during hydrogen reduction.

The feed rate of *n*-octane was essentially the same for the two runs in Table VI with H<sub>2</sub>:*n*-octane ratios of 3 and 50; thus, the contact time is lower for the 50 ratio run and we would expect a lower conversion of *n*-octane. However, the conversion, expressed as percentage of feed (or per Pt atom), is essentially the same for the two ratios. This implies that the pores of the zeolite contain essentially the same concentration of *n*-octane for the partial pressures of *n*-octane used in the two runs; however, more data are required before this implication can be more conclusively demonstrated.

The C<sub>8</sub>-aromatics produced using PtSi-2-B even at 620°C (Table VIII) are consistent with the dehydrocyclization step being shape selective. At the lower H<sub>2</sub>/*n*-octane ratio, ethylbenzene plus styrene accounts for about 63% of the C<sub>8</sub>-aromatics. *o*-Xylene accounts for about 20% of the C<sub>8</sub>-products. *m*- and *p*-Xylenes should not be

formed by a six-carbon ring formation mechanism and the *m*-isomer is present in low (about 4%) amounts; however, the *para* isomer is a significant product (about 12%), implying that it is formed by isomerization of the initially formed *o*-xylene and appears in larger amounts because of its rapid diffusion from the interior of the silicalite crystal. Thus, *p*-xylene would be a shape selective product; however, the shape selectivity would not be due to the influence of shape selectivity on the cyclization step but because of the secondary shape selectivity factor of diffusional effects within the pore structure.

Table VIII  
C<sub>8</sub> Aromatic Distribution for aromatic products from *n*-octane conversion with PtSi-2-B (conversion data are in Table VI)

Time, min.	H <sub>2</sub> /C <sub>8</sub>	Ethylbenzene + Styrene	Para-xylene	Meta-xylene	Ortho-xylene
25	3	62.6	8.6	3.9	24.9
40	3	62.1	12.4	3.7	21.8
55	3	63.9	11.5	4.0	20.6
70	3	64.8	12.2	3.5	19.5
90	3	63.4	12.5	3.8	20.3
110	3	63.1	12.6	3.9	20.4
30	50	77.2	4.5	2.5	15.9
60	50	79.7	5.2	2.6	12.6
90	50	81.9	4.4	2.4	11.3
120	50	83.0	4.5	2.3	10.2
150	50	83.6	4.5	2.3	9.6
200	50	84.4	4.5	1.9	9.2
260	50	83.8	4.8	2.3	9.1
320	50	84.5	4.7	2.1	8.6

For both runs shown in Table VI, styrene accounts for about 33% of the styrene + ethylbenzene fraction. At 620°C, styrene should be about 35% of the ethylbenzene plus styrene fraction, and this is the amount obtained experimentally.

The conversion of 3-methylheptane with PtSi-2-B at  $H_2$ :3-methylheptane = 50 (Table IX) was only about half that of *n*-octane under the same conditions. Either the methyl group inhibits the diffusion of 3-methylheptane into the pore structure, the saturation concentration of 3-methylheptane in the pores of silicalite is only about half that of *n*-octane, or the rate of conversion of 3-methylheptane is about half that of *n*-octane. Based upon conversion data for *n*-octane and 3-methylheptane with Pt on nonacidic supports, it is anticipated that *n*-octane will be converted more rapidly than 3-methylheptane. Thus, at least a significant fraction of the lower conversion for 3-methylheptane is due to the relative reaction rates for the conversion of these two hydrocarbons, and not to shape selectivity of the transition state or of saturation concentration.

Table IX  
Distribution of Products from the Conversion of 3-Methylheptane over Pt-Si-2B at 620°C, 1 atm,  $H_2$ /Hydrocarbon = 50

Time, Min.	3-methylheptane conv., Wt. %	Aromatic Distribution, Mole %						
		Bz <sup>a</sup>	TOL <sup>a</sup>	EB <sup>a</sup>	PX <sup>a</sup>	MX <sup>a</sup>	OX <sup>a</sup>	STY <sup>a</sup>
40.0	10.0	15.4	37.5	18.6	14.4	1.7	10.0	8.7
80	11.1	17.2	35.6	17.8	12.1	1.7	6.7	8.5
120	10.7	18.2	36.6	17.8	11.8	1.6	5.5	8.2
160	10.7	18.5	38.0	17.6	11.5	2.1	4.7	8.0
200	11.4	19.0	38.9	17.1	11.4	2.2	4.5	7.5
260	11.5	19.4	39.4	17	11.3	2.0	3.9	7.5

<sup>a</sup>BZ = benzene, TOL = toluene, EB = ethylbenzene, PX = para-xylene, MX = meta-xylene, OX = ortho-xylene, STY = styrene.

Benzene and toluene account for about 50-60% of the total aromatic products. Thus, the amount of hydrogenolysis products from the conversion of *n*-octane and 3-methylheptane under the same conditions is about the same. That more *o*-xylene formed from 3-methylheptane over Pt located in the silicalite zeolite pore system than was formed for Pt on a meso- or macro-porous support implies that the dominant fraction of the benzene and toluene is produced by the hydrogenolysis of ethylbenzene.

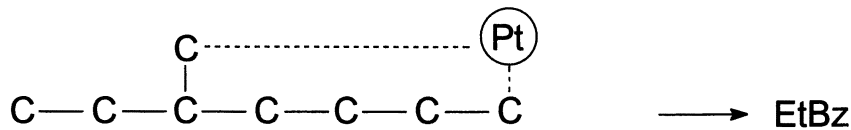
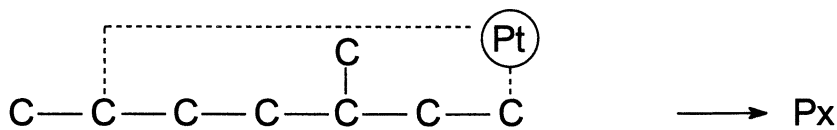
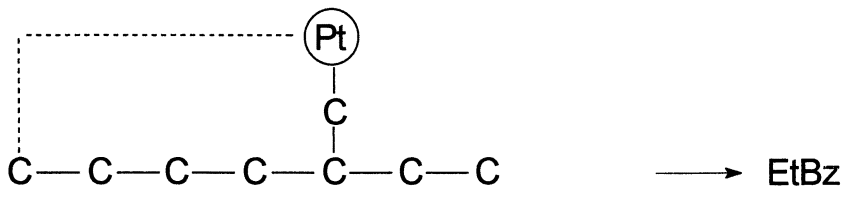
The aromatic selectivity from the conversion of 3-methylheptane with Pt on noncrystalline silica or nonacidic alumina support is ethylbenzene:*o*-xylene:*p*-xylene = about 1:1:1. At 620°C, for PtSi-2-B the aromatic selectivity is ethylbenzene +

styrene:p-xylene:o-xylene = about 6:3:1 (Table IX) and a similar ratio is obtained at the lower temperature (482°C). Thus, ethylbenzene is the dominant product. If, as seems likely, the benzene and toluene arise mainly from hydrogenolysis of ethylbenzene, 80-85% of the aromatics formed from dehydrocyclization are ethylbenzene.

Based only on the C<sub>8</sub>-aromatic product distribution, our results are in qualitative agreement with those of Mériaudeau et al (4) and the product distribution obtained using a pulse reactor agree with those obtained in a continuous flow reactor. If benzene and toluene are derived mainly from ethylbenzene hydrogenolysis, then 80% or more of the initial product from dehydrocyclization of n-octane and from 3-methylheptane is ethylbenzene. Based on results from the conversion of n-octane with platinum on graphitized carbon containing only very large pores from packing of large carbon particles, hydrogenolysis of ethylbenzene is more rapid than for xylene isomers (12). Furthermore, the rate of hydrogenolysis increases as the metal loading and the metal particle size increases (13). The platinum located within the porosity of silicalite must be present as atomic platinum or very small clusters. By analogy with the non-zeolite support, products from hydrogenolysis should be low (less than 5%) rather than 40-60% that is observed. It therefore appears that the hydrogenolysis is due to the multiple adsorptions of ethylbenzene as it diffuses to the gas-solid interface, and is therefore a selectivity based upon diffusion rather than on pore geometry that impacts the cyclization step. The formation of larger amounts of ethylbenzene compared to o-xylene cannot be due to pore diffusion and therefore must be due to some impact upon the cyclization transition state that alters the product distribution from that of platinum supported on non-zeolitic materials.

The aromatization of hexane can be carried out with a high selectivity with Pt-KL zeolite catalysts (14,15). One of the reasons proposed for this selectivity is that the n-hexane is required to adsorb on the platinum particle at the 1-carbon position as n-hexane diffuses along the pore channel and that the geometry of the cavity allows only the six-carbon ring to form (16-18). Based just on the products from the dehydrocyclization of n-octane with PtSi-2-B, one could explain the high selectivity for ethylbenzene by the mechanism described above for selective adsorption of the 1-carbon position. However, it is difficult to account for the preferred formation of ethylbenzene from 3-methylheptane with this mechanism. As illustrated below, ethylbenzene formation can occur only by a direct six-carbon ring formation that involves the methyl side chain.

There does not appear to be a reason to favor 3-methylheptane diffusing deep within the silicalite pore structure to encounter a platinum atom or particle that would result in structure I, leading to the formation of ethylbenzene, and not form structure II that would lead to the formation of p-xylene. Both ethylbenzene and p-xylene should be uninhibited by diffusional effects and we should therefore expect to obtain about equal amounts of ethylbenzene and p-xylene as products. Furthermore, since ethylbenzene should undergo hydrogenolysis more rapidly than p-xylene, we should expect to observe more p-xylene than ethylbenzene, and this is not the experimental result. Only if the methyl group inhibits cyclization in the formation of a ring by adsorption as shown in structure II and subsequent C-H rupture should result in the conversion of the structure in II into that shown in III would we expect to obtain a large excess of ethylbenzene product. The results require that the cyclization step be impacted by shape selectivity but it is not apparent what factors require this to be the case.

**Structure I****Structure II****Structure III****References**

1. Srinivasan, R., Sparks, D. and Davis, B. H. *J. Mol. Catal.*, **1994**, 88, 325.
2. Srinivasan, R. and Davis, B. H. *J. Mol. Catal.*, **1994**, 88, 343.
3. Srinivasan, R., Sparks, D. and Davis, B. H. *J. Mol. Catal.*, **1994**, 88, 359.
4. Mériaudeau, P., Thangaraj, A., Naccache, C. and Narayanan, S. *J. Catal.*, **1994**, 146, 579.
5. Davis, B. H., Westfall, G. A., Watkins, J. and Pezzanite, J. *J. Catal.*, **1994**, 42, 247.
6. Davis, B. H. *J. Catal.*, **1976**, 42, 376.
7. Davis B. H., in "Proceedings, 10th International Congress on Catalysis, Budapest, 1992" (L. Guzzi, F. Solymosi, P. Tétényi, Eds.), p 889, Akadémiai Kiado, Budapest, 1993.

8. Davis, B. H. and Venuto, P. B. *J. Catal.*, **1969**, 15, 363.
9. Dessau, R. M. *J. Catal.*, **1984**, 89, 520.
10. DellaBetta R. A. and Boudart, M. in "Proceedings, 5th International Congress on Catalysis, Palm Beach, 1972 (J. W. Hightower, Ed.), Vol. 2, p. 1329, North-Holland, Amsterdam, 1973.
11. Stull, D. R., Westrum, Jr., E. F. and Sinke, G. C. "The Chemical Thermodynamics of Organic Compounds," John Wiley & Sons, Inc., New York, 1969.
12. Westfall, G. A., Naylor, R. W. and Davis, B. H. *J. Catal.*, **1976**, 42, 238.
13. Westfall, G. A., Naylor, R. W. and Davis, B. H. *J. Catal.*, **1976**, 42, 238.
14. Hughes, T. R., Jacobson, R. and Tamm, P. *Catalysis* 87, (J. W. Ward, ed.), Elsevier, Amsterdam, **1987**, 317.
15. Hughes, T. R., Buss, W. C., Tamm, P. W. and Jacobson, R. L. in "New Developments in Zeolite Science and Technology," (J. Murakami, A. Iijima and J. W. Ward, eds.), Kodansha, Tokyo, 1986, pg. 725 and discussion CA-33.
16. S. J. Tauster and J. T. Steger, *J. Catal.*, **125** 387 (1990).
17. Manninger, I., Lun, X., Tétényi, P. and Páal, Z. *Appl. Catal.*, **1989**, 51, 7.
18. Gao, Y., Jiang, X., Ruan, Z. and Xy, Y. *Catal. Lettr.*, **1993**, 19, 81.

## Chapter 11

# MFI-Type Metallosilicates as Useful Tools to Clarify What Determines the Shape Selectivity of ZSM-5 Zeolites

T. Komatsu, J.-H. Kim <sup>1</sup>, and T. Yashima

Department of Chemistry, Tokyo Institute of Technology, Meguro-ku,  
Tokyo 152-8551, Japan

Ethylation of ethylbenzene and methylation of 2-methylnaphthalene on HZSM-5 are controlled by restricted transition state shape selectivity in the pore, yielding target molecules, *p*-diethylbenzene and 2,6-dimethylnaphthalene, respectively, as primary products. Weakening the acid strength and/or poisoning acid sites on the external surface of zeolite crystallites suppress the secondary isomerization of these primary products to improve the final selectivity to the target molecules. MFI-type metallosilicates having weaker acid strength than HZSM-5 and similar pore tortuosity to ZSM-5 are of great advantage to differentiate the effects of acid strength and pore tortuosity on the shape selectivity.

Shape selectivity of zeolite catalysts is essentially determined by the relation between the sizes of zeolite pore and molecules of reactants, products and intermediates. In the case of alkylation of aromatic hydrocarbons, products such as dialkylbenzene and dialkylnaphthalene consist of isomers with different molecular dimensions, often resulting in the shape selective formation of the smaller isomers on zeolite catalysts. However, the isomerization of such smaller isomers into larger ones will sometimes make the shape selective catalysis ambiguous. Because the acid strength necessary for the alkylation and isomerization is different, that is, weak acid sites only catalyze the alkylation, the selectivity in the alkylation strongly depends on the acid strength of zeolites. Though modification of zeolites by the addition of metal oxides has been used to improve the shape selectivity, it will change the pore dimension and acid strength of zeolites, simultaneously. On the other hand, metallosili-

<sup>1</sup>Current address: Department of Chemical Technology, Chonnam National University, Kwangju 500-757, Korea.

cates, whose acid strength is controlled by changing the metal cation in their framework, ideally possess the same structure as their aluminum analogue in zeolites, which accordingly provides the same diffusivity to the molecules inside the pore. Therefore, metallosilicates would be an effective tool to clarify the reason for the shape selectivity in the alkylation on zeolite catalysts. In this report, we used MFI-type metallosilicates as analogues to ZSM-5 in the ethylation of ethylbenzene and methylation of 2-methylnaphthalene to obtain the details in shape selectivity.

## Ethylation of Ethylbenzene

Alkylation of alkylbenzene is one of the commercially important processes because *para*-dialkylbenzene is one of the industrially useful chemicals. This reaction has been carried out using HZSM-5 zeolites modified with some metal oxides (1-6) to obtain high selectivity to *para*-isomers. Though many researchers have studied the factors governing the high *para*-selectivity of the modified HZSM-5 zeolites, a definite conclusion is not established yet.

Kaeding et al. (3) have proposed that the high *para*-selectivity of modified HZSM-5 zeolites for alkylation is due to so-called 'product selectivity', that is, the intracrystalline diffusivity of *para*-isomer is much higher than that of the other two isomers. In the report on the alkylation of toluene with ethanol (7), *para*-isomer was formed selectively inside the ZSM-5 channels, while isomerization of the *para*-isomer proceeded on the external surface of zeolite crystallite. Therefore, the improvement in *para*-selectivity by the modification with metal oxides was thought to result from the deactivation of acid sites on the external surface.

On the other hand, we have proposed that the primary product in the alkylation of alkylbenzene is only *para*-isomer because of so-called 'restricted transition-state selectivity' inside the ZSM-5 pore and that the other isomers are produced through the secondary isomerization of the primarily produced *para*-isomer (4,5). The modification by metal oxide would reduce the strength of acid sites, on which the secondary isomerization is accelerated. The influence of the secondary isomerization on the strong acid site has been discussed previously (8-11).

**Experimental.** NaZSM-5 with Si/Al atomic ratio of 96 was prepared hydrothermally and transformed into HZSM-5 by  $\text{NH}_4^+$ -exchange and subsequent calcination in air (2). Metallosilicates with MFI structure, expressed as Me-MFI (Me=Ga, Fe and B), were prepared in a similar manner to HZSM-5 and had Si/Ga=64 (12), Si/Fe=56 (13), and Si/B=70 (14), respectively. Antimonosilicate (Sb-MFI, Si/Sb=120) and arsenosilicate (As-MFI, Si/As=92) were prepared by the atom-planting method using MFI silicalite (Si/Al>1000) and  $\text{SbCl}_3$  and  $\text{AsCl}_3$ , respectively (15,16). HZSM-5 and Me-MFI modified with Mg, P or B oxide were prepared by an impregnation method (4,5,17), and expressed as Mg(x)HZSM-5, where x was the amount of Mg in wt%.

The ethylation of ethylbenzene with ethanol was carried out with a



continuous flow reactor at 673 K under atmospheric pressure. Partial pressures of ethylbenzene and ethanol in helium carrier were both 20 kPa. Conversion and yield were calculated based on the amount of ethylbenzene reacted. The *para*-selectivity is defined as the fraction of *para*-isomer in diethylbenzene produced. For the selective poisoning of acid sites on the external surface of zeolite crystallites, the ethylation of ethylbenzene with ethanol was carried out under the same reaction conditions with 2,4-dimethylquinoline (2,4-DMQ, 0.075 ml h<sup>-1</sup>) co-fed with the reactant (18). The cracking of 1,3,5-triisopropylbenzene (1,3,5-TIPB) was performed in the presence or absence of 2,4-DMQ to know the extent of poisoning on the external surface (19).

The effective pore dimension of each catalyst was estimated from the relative adsorption velocity of *o*-xylene. The catalyst (0.1 g) was set on a highly sensitive microbalance and evacuated at 823 K for 2 h. The gravimetric measurement was performed at 393 K with the vapor of *o*- or *p*-xylene (0.48 kPa). The acid properties of catalysts were examined by temperature-programmed desorption of ammonia (NH<sub>3</sub>-TPD). The measurement of NH<sub>3</sub>-TPD was conducted, using a conventional static adsorption system connected to a quadrupole mass spectrometer through a high vacuum line. The catalyst was evacuated at 823 K for 1 h and exposed to 20 kPa of ammonia at 423 K for 30 min. After the evacuation at 423 K for 1 h, TPD was carried out by raising the temperature in vacuo from 298 to 823 K at a constant rate of 10 K min<sup>-1</sup>.

**Para-Selectivity in Ethylation of Ethylbenzene.** Products in the reaction of ethylbenzene with ethanol on various HZSM-5 and Me-MFI catalysts were *p*- and *m*-diethylbenzene as main products, benzene in a considerable amount, and *o*-diethylbenzene in a trace amount, indicating that the ethylation as well as the dealkylation of ethylbenzene occurred under the reaction conditions. As shown in Table I, the *para*-selectivity of the catalyst was obtained at an almost constant yield of diethylbenzene (15-20%) by adjusting W/F.

In the case of HZSM-5, the *para*-selectivity increased by the addition of B-, P- and Mg-oxide though the catalytic activity decreased significantly. It is clear that all the Me-MFI catalysts exhibited the higher *para*-selectivity than HZSM-5. In particular, As-MFI gave the highest *para*-selectivity of 94% among the unmodified catalysts. The *para*-selectivity of Me-MFI catalysts was also improved by the modification with metal oxides. As a result, B(10)HZSM-5, B(5)Ga-MFI, B(1)Sb-MFI and B(3)Sb-MFI exhibited the perfect *para*-selectivity of 100%.

**Primary Product in Ethylation.** In order to clarify the primary product in the ethylation, reactions were carried out on HZSM-5 with various W/F at 673 K. The distribution of diethylbenzene isomers is plotted against W/F as shown in Figure 1, where the yield of diethylbenzene was in the range of 3-26%. As W/F decreased to approach zero, the fraction of *p*-diethylbenzene increased to 100%, while that of *m*- and *o*-isomer decreased to 0%. This clearly indicates that the primary product in the ethylation on HZSM-5 is *p*-

**Table I. Ethylation of Ethylbenzene with Ethanol on MFI Catalysts**

No.	Catalyst	Diethylbenzene Yield /%	Para-Selectivity /%
1	HZSM-5	19.8	43.2
2	B(1)HZSM-5	17.9	48.9
3	B(3)HZSM-5	18.8	55.3
4	B(10)HZSM-5	17.8	100.0
5	P(1)HZSM-5	20.1	49.3
6	P(5)HZSM-5	16.3	89.8
7	Mg(18)HZSM-5	19.9	72.4
8	Ga-MFI	16.9	59.6
9	Fe-MFI	16.5	61.0
10	B-MFI	16.6	70.3
11	Sb-MFI	15.0	90.4
12	As-MFI	15.3	94.1
13	B(0.5)Ga-MFI	18.5	67.1
14	B(1)Ga-MFI	17.5	77.3
15	B(3)Ga-MFI	16.7	94.3
16	B(5)Ga-MFI	17.1	100.0
17	B(1)Sb-MFI	15.2	100.0
18	B(3)Sb-MFI	15.6	100.0

SOURCE: Adapted with permission from reference 6. Copyright 1991 Elsevier.

diethylbenzene. The primary products on HY, which does not have significant shape selectivity for this reaction, were *o*- and *p*-diethylbenzene, as was explained by ortho/para orientation (4). Therefore, at the initial stage of the reaction, HZSM-5 shows 'restricted transition-state selectivity' to depress the formation of *o*-diethylbenzene. The increase in the fraction of *m*-isomer and the decrease in that of *p*-isomer with increasing W/F indicate the secondary isomerization of *p*-isomer into *m*-isomer. Although the molecular dimension of *o*-isomer is almost the same as that of *m*-isomer, only a trace amount of *o*-isomer was observed even at high W/F values. These results suggest that HZSM-5 has active sites for the isomerization of diethylbenzene and that it does not have 'product selectivity' due to the difference in diffusion of diethylbenzene isomers. From these results, it is obvious that the suppression of secondary isomerization will be effective to achieve the higher *para*-selectivity on HZSM-5. As shown in Table I, Me-MFI and modified HZSM-5 gave higher *para*-selectivity than HZSM-5. Therefore, they must have low activity for the secondary isomerization compared with HZSM-5. In the following sections, we try to clarify the reason for the very high *para*-selectivity of Me-MFI and modified HZSM-5 resulting from this low activity for the isomerization; the effects of acid sites on the external surface, pore tortuosity and acid strength are discussed.

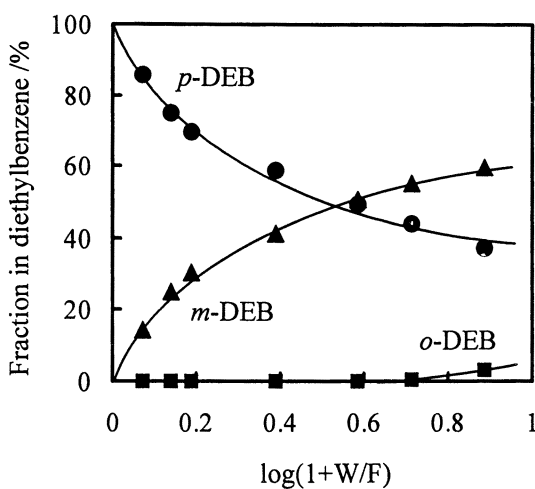


Figure 1. Effect of contact time on the fraction of diethylbenzene isomer in ethylation of ethylbenzene on HZSM-5.

(Adapted with permission from reference 4. Copyright 1988 Chemical Society of Japan.)

**Effect of Acid Sites on External Surface.** Acid sites on the external surface of zeolite crystallites usually decrease the shape selectivity because they do not have significant steric effect by pore walls. In order to clarify the effect of the acid sites on the external surface on the *para*-selectivity, the ethylation of ethylbenzene with ethanol was carried out with co-feeding 2,4-DMQ. This base molecule selectively poisons the acid sites on the external surface of HZSM-5 because its molecular dimension is too large to enter the pores of ZSM-5 (18). The results are summarized in Table II. The complete poisoning of the acid sites on the external surface was confirmed by the complete deactivation of the catalysts for the cracking of 1,3,5-TIPB, which is too large to enter the pore of ZSM-5 and will be cracked only by the acid site on the external surface (19). HZSM-5 and Me-MFI poisoned with 2,4-DMQ were completely inactive for the 1,3,5-TIPB cracking, indicating the complete poisoning of external surface. Although the selective poisoning improved the *para*-selectivity of HZSM-5 and Me-MFI to some extent, the effect of oxide modification was much stronger to achieve 100% *para*-selectivity (Table I). These results indicate that the weak activity for secondary isomerization, which leads to the very high *para*-selectivity, is not caused mainly by the poisoning of the external surface but predominantly by the suppression of the isomerization activity inside the pores of ZSM-5.

**Table II. Poisoning of acid sites on the external surface with 2,4-dimethylquinoline (DMQ)**

Catalyst	2,4-DMQ	Diethylbenzene Yield /%	Para-Selectivity /%	TIPB <sup>a</sup> Conversion /%
HZSM-5	without	26.3	39.2	51.1
	with	16.9	57.2	0.0
Ga-MFI	without	33.1	36.7	22.9
	with	29.9	40.2	0.0
Fe-MFI	without	25.6	35.5	41.0
	with	19.2	50.9	0.0
B-MFI	without	16.6	70.3	5.5
	with	8.7	83.0	0.0
Sb-MFI	without	15.0	90.4	0.7
	with	7.2	92.4	0.0

<sup>a</sup>1,3,5-Triisopropylbenzene

**Effect of Pore Tortuosity.** Micropores of MFI structure often influences the internal diffusion of specific molecules, which may generate molecular shape selectivity. In order to clarify the effect of the pore tortuosity on the *para*-selectivity in the ethylation of ethylbenzene, the adsorption measurements of *o*-

and *p*-xylenes were carried out at 393 K, where these adsorbates did not react by itself. Figure 2 shows the typical *o*-xylene uptake curves for the modified HZSM-5 and Me-MFI catalysts. The initial rate of adsorption depended on the catalyst and the equilibrium was not achieved for every catalyst within 200 min of the adsorption. This adsorption behavior must reflect the pore tortuosity of each catalyst. The pore tortuosity was estimated by comparison with the adsorption rate of *p*-xylene, which has a smaller molecular size than that of *o*-xylene. The adsorption of *p*-xylene on every catalyst reached the equilibrium within 30 min. The amount of *p*-xylene adsorbed at the equilibrium may correspond to the pore volume.

From the results of *o*- and *p*-xylene adsorption experiments (5,16,17,20, 21), we determined 'time to reach 30% of amount of *o*-xylene adsorbed in infinite time',  $t_{0.3}$ , as a parameter of the pore tortuosity, as used by Mobil's researchers (22). Furthermore, we determined 'relative *o*-xylene adsorption velocities',  $V_{ROA}$ , as another parameter of the pore tortuosity obtained from the amount of *o*-xylene adsorbed in 180 min divided by that of *p*-xylene adsorbed in infinite time, where the amount of *p*-xylene adsorbed in infinite time may correspond to the pore volume. In the case of disproportionation of toluene, *para*-selectivity, fraction of *p*-xylene, decreased monotonously with  $V_{ROA}$ , suggesting the product selectivity (23).

The relation between the *para*-selectivity in ethylation of ethylbenzene and the pore tortuosity,  $t_{0.3}$  and  $V_{ROA}$ , is shown in Figures 3 and 4, respectively. In the cases of parent (solid circle, No. 1) and modified (open circle, No. 2-7) HZSM-5, a close relation was observed both in Figures 3 and 4, that is, the *para*-selectivity increased with  $t_{0.3}$  and decreased with  $V_{ROA}$ . The *para*-selectivity of each parent (solid symbols, No. 8-12) and modified (open symbols, No. 13-18) Me-MFI was always higher than that of HZSM-5 catalysts when compared at the similar pore tortuosity. It is clear that a close relation between the *para*-selectivity and the pore tortuosity was never found for all the MFI catalysts examined here. It is doubtful that the *para*-selectivity in the ethylation of ethylbenzene on MFI catalysts is directly governed by the diffusivity of product molecules. Therefore, it would be concluded that the product selectivity is not the reason for the high *para*-selectivity in the ethylation of ethylbenzene on MFI catalysts.

**Effect of Acid strength.** The effect of acid strength of MFI catalysts is finally examined because strong acid sites will be necessary for the isomerization of dialkylbenzenes but even weak acid sites will catalyze the alkylation of alkylbenzenes. TPD of adsorbed ammonia was used to estimate the acid strength of the MFI catalysts. In general, the peak temperature in an  $NH_3$ -TPD profile corresponds intrinsically to the acid strength of the catalyst. However, it sometimes shifts to higher temperatures because of the readsorption of desorbed ammonia and/or the diffusion limitation (24). In this study, though every catalyst has the same MFI structure, its Si/metal ratio varies in the range of 56-120, indicating that the acid concentration differs significantly

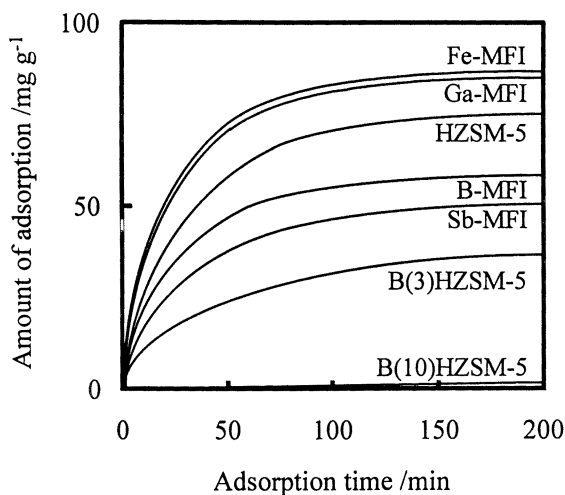


Figure 2. Change in the amount of *o*-xylene adsorbed on catalysts. (Adapted with permission from reference 20. Copyright 1991 Elsevier.)

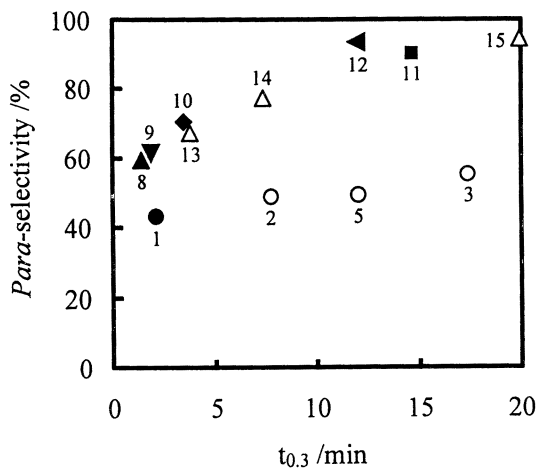


Figure 3. Relation between *para*-selectivity in ethylation of ethylbenzene and pore tortuosity,  $t_{0.3}$ , of catalysts. Number: see Table I. (Adapted with permission from reference 6. Copyright 1994 Elsevier.)

depending on the catalyst. Therefore, the peak temperature may not absolutely correspond to the acid strength.

$\text{NH}_3$ -TPD measurements were carried out in vacuo by using a very small amount (18 mg) of catalyst to minimize the effect of readsorption. We used the peak temperature in  $\text{NH}_3$ -TPD,  $T_{\text{max}}$ , as a parameter of the acid strength of catalysts. Figure 5 shows the typical profiles of  $\text{NH}_3$ -TPD for HZSM-5 and Me-MFI. The peak in the profile for all the Me-MFI catalysts appeared at a temperature lower than that for HZSM-5. As was expected, the modification of HZSM-5 and Me-MFI with oxide lowered the peak temperature. It is clear that the acid strength of Me-MFI and that of the modified zeolites are weaker than that of HZSM-5.

The relation between the *para*-selectivity in the ethylation of ethylbenzene and the acid strength,  $T_{\text{max}}$ , is shown in Figure 6. A close relation is observed for all the catalysts, that is, the weaker the acid strength, the higher the *para*-selectivity. This indicates that the *para*-selectivity in the ethylation on catalysts with MFI structure is strongly governed by their acid strength.

**Generation of Para-Selectivity.** The primary product in the ethylation of ethylbenzene on catalysts with MFI structure is *p*-diethylbenzene because of the restricted transition-state selectivity. Secondary isomerization of *p*-isomer into *m*-isomer lowers the *para*-selectivity of the catalysts. Only strong acid sites catalyze this isomerization, while the ethylation readily occurs on weak acid sites. Metallosilicates with MFI structure and H-ZSM-5 modified with metal oxides have weak acid strength compared with H-ZSM-5. Therefore, on these catalysts, primarily produced *p*-isomer does not suffer the isomerization to obtain high *para*-selectivity. It is concluded that the *para*-selectivity is caused by the restricted transition-state selectivity and the absence of strong acid sites.

### Methylation of 2-Methylnaphthalene

As was revealed above, metallosilicates are useful tools to clarify what generates the shape selectivity of zeolite catalysts. Next we studied on the shape selective formation of dimethylnaphthalene (DMN) again using MFI type metallosilicates. Naphthalene derivatives having substituents at C-2 and C-6 positions are important raw materials for manufacturing sophisticated polymers of special functions. Methylation of naphthalene (25-27) and transalkylation of methylnaphthalene (28-30) at these positions, therefore, have been studied using shape-selective zeolite catalysts in industrial prospects as well as for the further understanding of shape selective nature of zeolite catalysis. Fraenkel et al. (25,26) have carried out the methylation of naphthalene and 2-methylnaphthalene (2-MN) with methanol on various zeolites and found that HZSM-5 is highly selective for the alkylation at  $\beta$ -position to form 2,6- and 2,7-dimethylnaphthalene (DMN) compared with HY and H-mordenite. They attributed the high selectivity of HZSM-5 to the shape-selective sites called 'half-cavities' located on the external surface of HZSM-5 crystallites. On the other hand, Weitkamp and Neuber (27) have studied the methylation of 2-MN

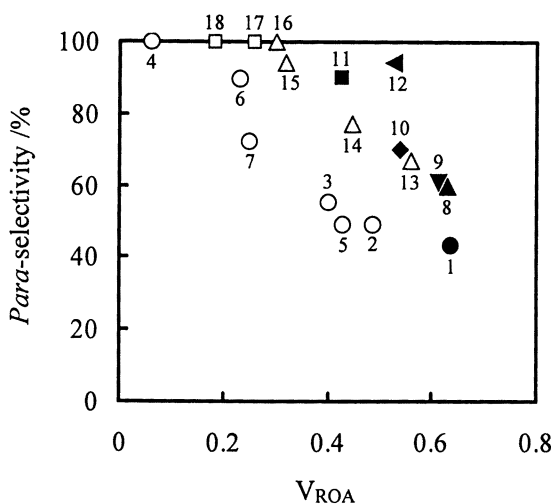


Figure 4. Relation between *para*-selectivity in ethylation of ethylbenzene and pore tortuosity,  $V_{ROA}$ , of catalysts. Number: see Table I. (Adapted with permission from reference 6. Copyright 1994 Elsevier.)

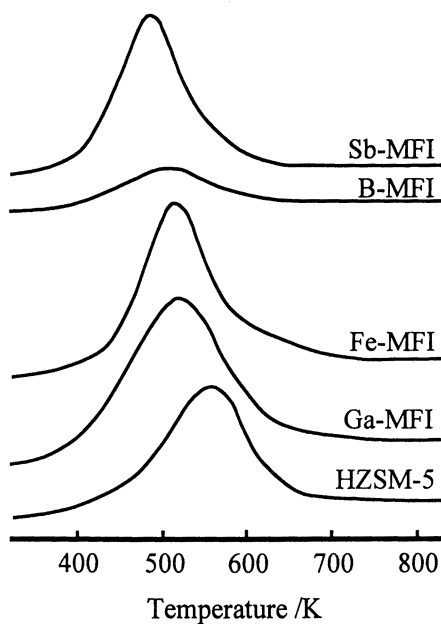


Figure 5.  $NH_3$ -TPD profiles.



on HZSM-5 and HZSM-11, and proposed that the high selectivity to 2,6- and 2,7-DMN is caused by the product shape selectivity, that is, the reaction occurs inside the pore of these zeolites. In the case of the transalkylation of 2-MN, Matsuda et al. (30) have claimed that the high selectivity to 2,6- and 2,7-DMN on dealuminated HZSM-5 is caused by its shape selectivity inside the pore.

We have carried out the methylation of 2-MN with methanol using HZSM-5 and MFI-type metallosilicates as catalysts to obtain 2,6-DMN (31). The reaction path was first examined taking account of the contribution of the acid sites inside and outside the zeolite crystallites. Then we will discuss on the factors determining the selectivity and a possible way to obtain 2,6-DMN with high selectivity.

**Experimental.** ZSM-5 (Si/Al=43), Ga-MFI (Si/Ga=42), Fe-MFI (Si/Fe=37) and B-MFI (Si/B=70) were prepared by hydrothermal synthesis. Sb-MFI (Si/Sb=120) was prepared by the atom-planting method (15). These were transformed into proton type by the usual ion-exchange technique. Boron oxide added HZSM-5 was prepared by the impregnating HZSM-5 with an aqueous solution of boric acid followed by the calcination in air.

The methylation of 2-MN with methanol was carried out with a continuous flow reactor under atmospheric pressure at 723 K. Partial pressures of 2-MN and methanol in helium carrier were 6.2 and 14.1 kPa, respectively. Conversion and selectivity were calculated based on the amount of 2-MN reacted. Similar techniques were taken for the selective poisoning of the acid sites on the external surface, the adsorption of *o*-xylene, and NH<sub>3</sub>-TPD.

**Methylation of 2-MN on HZSM-5.** Main products in the reaction of 2-MN with methanol on HZSM-5 at 723 K were isomers of DMN and 1-MN though small amounts of naphthalene, ethylnaphthalene and trimethylnaphthalene were observed. Among ten isomers of DMN, 2,6- and 2,7-DMN were produced with relatively high fractions. Other DMNs produced were 1,2-, 1,3-, 1,6-, 1,7- and 2,3-isomers. The high fractions of 2,6- and 2,7-DMN imply the shape selective catalysis of HZSM-5 as was reported for the alkylation of naphthalene derivatives on HZSM-5 (25-27). Data obtained at 30 min on stream were discussed hereafter because of the gradual deactivation.

**Reaction path.** As shown in Figure 7, the effect of contact time on the fraction of DMN isomers was examined to clarify the reaction path. When W/F was extrapolated to zero, only four isomers of DMN were observed, i.e., 2,6- (initial fraction of 50%), 2,7- (39%), 2,3- (6%) and 1,2-DMN (5%), indicating that these are the primary products in DMN. As W/F increased, the fractions of 2,6- and 2,7-DMN decreased and those of 1,6-, 1,7- and 1,3-DMN increased in the opposite manner. This can be explained by the secondary isomerization of the initially produced 2,6- and 2,7-DMN into the latter isomers. The slight increase in the fractions of initially produced 1,2- and 2,3-DMN indicate the secondary isomerization of 2,6- and 2,7-DMN also into these isomers. Figure 7 indicates that the reaction rate of methylation is much faster

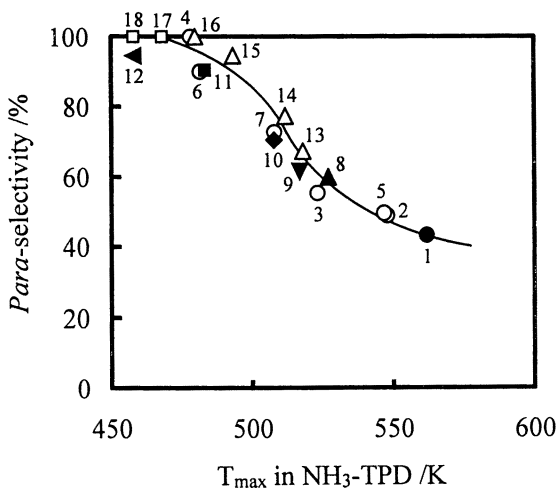


Figure 6. Relation between *para*-selectivity in ethylation of ethylbenzene and acid strength,  $T_{\max}$ , of catalysts. Number: see Table I. (Adapted with permission from reference 6. Copyright 1994 Elsevier.)

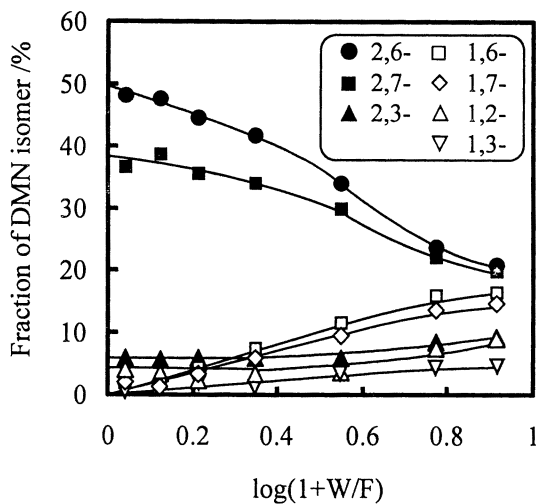


Figure 7. Effect of contact time on the fraction of DMN isomer in methylation of 2-MN on HZSM-5. (Adapted with permission from reference 31. Copyright 1991 Elsevier.)

than that of isomerization, suggesting the restricted transition state selectivity instead of the product selectivity in the early stage of the reaction. It has been known that the isomerization of DMN occurs predominantly between  $\alpha$  and  $\beta$  positions (32). Therefore, among the isomerizations mentioned above, those from 2,6- into 1,6-DMN and from 2,7- into 1,7-DMN should occur much easier than the others. From Figure 7, it is clear that the suppression of such isomerizations would increase the fraction of 2,6-DMN up to 50% (the initial value).

**Effect of Acid Sites on External Surface.** For the effective control of the isomerization of the initial products, it is necessary to know where the isomerization occurs. On the external surface of ZSM-5 crystallites, larger molecules like the isomerization products (1,6-, 1,7- and 1,3-DMN) would be formed from the lack of steric effect. 2,4-DMQ was co-fed in the reactant to clarify the reaction occurring inside and outside the crystallites in a similar manner to the ethylation of ethylbenzene mentioned above. The results on HZSM-5 with and without 2,4-DMQ are shown in Tables III and IV, respectively, together with the results on Me-MFI catalysts. In the case of HZSM-5, the complete disappearance of 1-MN in the presence of 2,4-DMQ indicates that the isomerization of 2-MN into 1-MN takes place solely on the external surface. On the other hand, the yield of DMN did not decrease greatly by 2,4-DMQ, suggesting that the methylation of 2-MN took place mainly inside the crystallites.

Figure 8 shows the effect of W/F on the fraction of DMN isomer in the presence of 2,4-DMQ. From the extrapolated values, the initial products formed inside the crystallites were 2,6-, 2,7- and 2,3-DMN with the fractions of 56, 38 and 6%, respectively. It should be noted that they are DMN with methyl groups only at  $\beta$ -positions. With increasing W/F, the fractions of 2,6-DMN decreased slightly and those of 2,3- and 1,2-DMN increased, while only negligible amounts of 1,3-, 1,6- and 1,7-DMN were produced. These results indicate that inside the crystallites the isomerization of 2,6-DMN occurs only slightly into 1,2- and 2,3-DMN. Thus, poisoning the external surface effectively increased the selectivity to 2,6- and 2,7-DMN. It should be noted, however, that the fractional ratio of 2,6-/2,7-DMN obtained on HZSM-5 did not increase significantly (from 1.21 to 1.22) by the addition of 2,4-DMQ.

From the above results, we summarize the reaction paths as shown in Figure 9, where bold-faced products are formed inside the pore of zeolite. At the initial stage, the methylation into 2,6-, 2,7- (**1a**) and 2,3-DMN (**1b**) occurs inside the pore, while on the external surface of the crystallite, the methylation into 1,2-DMN (**1c**) and the isomerization into 1-MN (**2**) occur with the minor formations of naphthalene and ethylnaphthalene (**3**). These primary products further react into secondary products. 2,6- and 2,7-DMN are transformed into 1,6-, 1,7- and 1,3-DMN (**4a**) through the secondary isomerization on the external surface. Inside the pore, only the slight isomerization into 2,3- and 1,2-DMN (**4b**) occurs. Poisoning the external surface will suppress the reactions **1c**, **2** and **4a** effectively to increase the selectivity to 2,6- and 2,7-DMN.

**Table III. Methylation of 2-Methylnaphthalene on MFI Catalysts**

Catalyst	HZSM-5	Ga-MFI	Fe-MFI	B-MFI	Sb-MFI
2-MN Conversion /%	25.1	16.9	13.4	4.5	4.5
1-MN Yield /mol%	13.9	6.0	1.1	0.5	0.1
DMN Yield /mol%	9.9	9.7	11.0	3.7	3.9
DMN Fraction /%					
1,2-	5.5	2.1	2.9	4.7	3.0
1,3	4.8	4.9	1.8	2.2	0.5
1,6	17.4	12.6	4.8	3.7	0.4
1,7	13.9	9.5	2.9	3.2	0.5
2,3	5.9	7.5	9.9	7.7	7.8
2,6	26.2	34.5	49.2	47.5	51.4
2,7	21.6	27.4	28.4	31.0	36.6
$T_{\max}$ /K	565	530	520	510	490
$T_{0.3}$ /min	0.8	0.5	1.0	5.3	29.5

SOURCE: Adapted with permission from reference 31. Copyright 1991 Elsevier.

**Table IV. Effect of 2,4-DMQ on the Methylation of 2-MN**

Catalyst	HZSM-5	Ga-MFI	Fe-MFI	B-MFI	Sb-MFI
2-MN Conversion /%	9.4	9.6	10.5	3.4	3.8
1-MN Yield /mol%	0.0	0.0	0.0	0.0	0.0
DMN Yield /mol%	8.6	8.6	9.5	3.1	3.6
DMN Fraction /%					
1,2-	5.2	1.7	0.9	0.9	2.1
1,3	0.6	0.8	0.6	0.4	0.3
1,6	0.1	0.1	0.1	0.0	0.0
1,7	0.2	0.2	0.2	0.3	0.2
2,3	10.3	10.7	10.9	7.9	7.3
2,6	46.0	49.5	56.0	55.5	52.5
2,7	37.7	36.9	31.4	35.0	37.7
2,6-/2,7-DMN Ratio	1.22	1.34	1.78	1.59	1.39

SOURCE: Adapted with permission from reference 31. Copyright 1991 Elsevier.

**Effect of Acid Strength.** The undesirable isomerization of 2-MN into 1-MN and that of initially produced 2,6-DMN into other DMNs might be retarded also by weakening the acid strength of zeolites similarly to the case of the ethylation of ethylbenzene. Table III shows the results on Me-MFI catalysts for the methylation of 2-MN together with  $T_{\max}$  in  $\text{NH}_3$ -TPD and  $t_{0.3}$  in *o*-xylene adsorption.  $T_{\max}$  values suggest that the acid strength decreases in the order

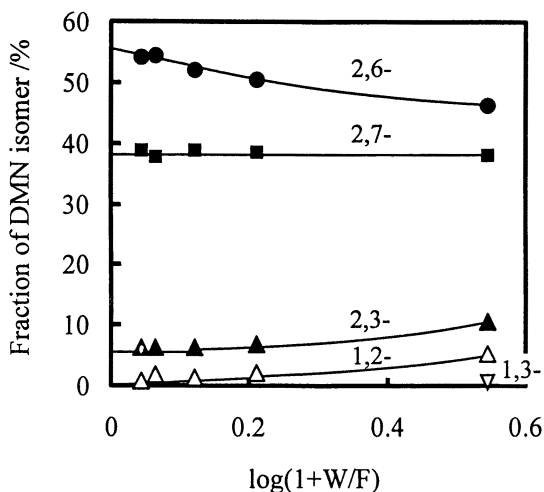


Figure 8. Methylation of 2-MN on HZSM-5 in the presence of 2,4-DMQ. (Adapted with permission from reference 31. Copyright 1991 Elsevier.)

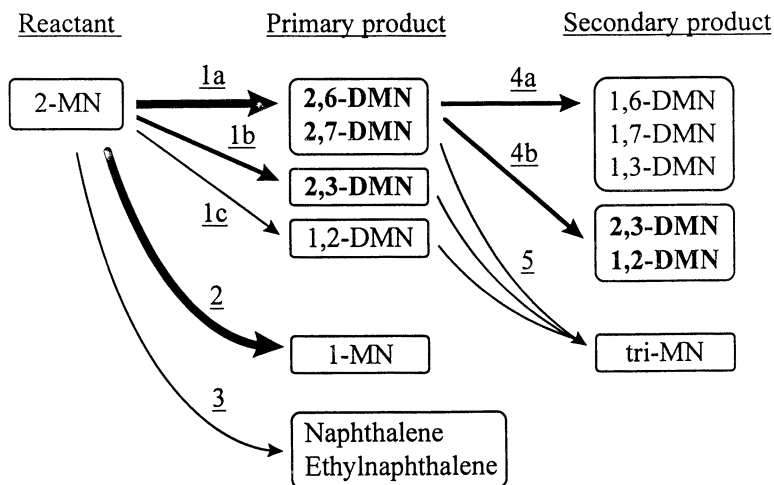


Figure 9. Reaction paths in methylation of 2-MN. Products in boldface are formed mainly inside the zeolite pore.

(Adapted with permission from reference 31. Copyright 1991 Elsevier.)

HZSM-5 > Ga-MFI > Fe-MFI > B-MFI > Sb-MFI. Ga-MFI and Fe-MFI gave similar DMN-yield to that on HZSM-5. The selectivity, however, changed with acid strength, that is, the yield of 1-MN drastically decreased and the fraction of 2,6-DMN increased with decreasing the acid strength. The isomerizations of 2-MN into 1-MN (Figure 9, 2) and of 2,6-DMN into 1,6, 1,7 and 1,3-DMN (4a), which occur on the external surface, were both suppressed by weakening the acid strength. However, the extent of suppression was slightly low compared with the poisoning of the external surface by 2,4-DMQ. It should be noted that the pore tortuosity ( $t_{0,3}$ ) shown in Table III did not change significantly among HZSM-5, Ga-MFI and Fe-MFI. Therefore, the steric effect of zeolite pore is not the reason for the changes in selectivity of these three catalysts.

**Selective Formation of 2,6-DMN.** Because 2,6-DMN is the target product, suppression of the formation of 2,7-DMN is the next step to improve the selectivity to 2,6-DMN. Acid strength of HZSM-5 would affect the selectivity between 2,6- and 2,7-DMN, if there is any difference between the reactivities of C-6 and C-7 positions of 2-MN. Me-MFI catalysts were again used as shown in Table IV, where the influence of the non-selective external surface was eliminated by 2,4-DMQ for the simple comparison of their shape selective properties. The fraction of 2,6-DMN increased with decreasing the acid strength, reached the highest value (56.0%) for Fe-MFI and decreased for B- and Sb-MFI. As shown at the bottom of Table IV, the fractional ratio of 2,6-/2,7-DMN increased markedly from HZSM-5 (1.22) to Fe-MFI (1.78). As can be expected from Figure 8, the isomerization of 2,6-DMN into 2,7-DMN would not occur inside the pore of HZSM-5. In fact, the reaction of 2,6-DMN on HZSM-5 gave the yield of 2,7-DMN only 3.3 mol% under the conditions of  $P(2,6\text{-DMN})=18$  kPa and  $W/F=1.0$  g h mol<sup>-1</sup>. This yield corresponds to at most 1% of the fraction of 2,7-DMN during the methylation. Accordingly, the low fraction of 2,7-DMN on Fe-MFI should not result from the low activity for the secondary isomerization but from the low fraction of 2,7-DMN in the primary products compared with HZSM-5. It is suggested that weaker acid sites prefer to produce 2,6-DMN to 2,7-DMN. This may be caused by the slight difference between the reactivities of C-6 and C-7 positions of 2-MN. In the case of electrophilic substitution such as alkylation studied here, the electron density of HOMO is a measure of reactivity at a specific position. For 2-MN, our calculation showed that the electron density at C-6 is significantly higher than that at C-7, which indicates the higher reactivity of C-6 position.

In Table IV, however, B-MFI and Sb-MFI exhibited contradictory results, that is, the 2,6-/2,7- ratio decreased with decreasing the acid strength. In the cases of these metallosilicates, larger values of  $t_{0,3}$  (Table III) indicate the increase in the pore tortuosity probably by the deposited boron oxide or antimony oxide. We speculate that the narrower the pore dimension of MFI catalysts, the easier the formation of 2,7-DMN.

To obtain the evidence for the effect of pore dimension on the selectivity

to 2,6-DMN, HZSM-5 impregnated with boron oxide was examined with 2,4-DMQ co-fed in the reactants. Figure 10 shows the change in the fraction of DMN,  $t_{0.3}$  and  $T_{\max}$  with the amount of boron added to HZSM-5.  $T_{\max}$  decreased gradually with the amount of boron, indicating the poisoning effect of boron oxide on acid sites. It should be noted that HZSM-5 with 3 wt% of boron still possessed acid strength comparable to Fe-MFI. This means that as far as acid strength is concerned, the addition of boron would enhance the formation of 2,6-DMN as in the case of Ga- and Fe-MFI. Figure 10, however, shows the increase in the fraction of 2,7-DMN as the amount of boron increased and that 2,7-DMN dominated over 2,6-DMN at higher boron content. This result can not be explained by the change in acid strength. On the other hand,  $t_{0.3}$  increased with increasing the amount of boron, which indicates the gradual increase in pore tortuosity by the boron impregnation. Therefore, it is again suggested that the narrower the pore dimension, the easier the formation of 2,7-DMN than that of 2,6-DMN. In the case of boron-impregnated HZSM-5, the influence of pore tortuosity on the selectivity between 2,6- and 2,7-DMN must be much greater than that of acid strength, resulting in the low 2,6-/2,7-DMN ratio.

From the above discussions, we conclude that to obtain 2,6-DMN in high selectivity, it is effective to weaken the acid strength keeping the pore dimension of MFI structure constant (or, if possible, slightly wider), which can be

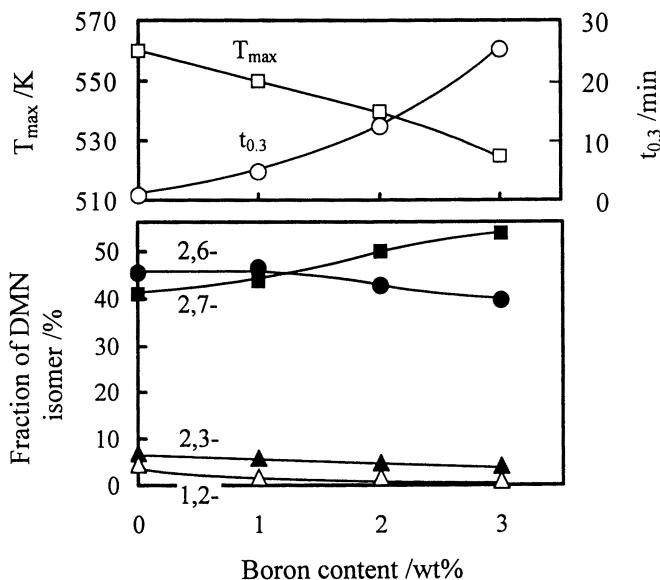


Figure 10. Effect of boron added to HZSM-5 on methylation of 2-MN in the presence of 2,4-DMQ, acid strength, and pore tortuosity.

(Adapted with permission from reference 31. Copyright 1991 Elsevier.)

achieved by using Fe-MFI as a catalyst. For example, 51 mol% selectivity to 2,6-DMN with its fraction in DMN of 56% was obtained at the conversion of 11% on Fe-MFI modified with 2,4-DMQ.

### Literature Cited

1. Chen, N.Y.; Kaeding, W.W.; Dwyer, F.G. *J. Am. Chem. Soc.* **1979**, *101*, 6783.
2. Yashima, T.; Sakaguchi, Y.; Namba, S. *Stud. Surf. Sci. Catal.* **1981**, *7*, 739.
3. Kaeding, W.W.; Chu, C.; Young, L.B.; Weinstein, B.; Butter, J. *J. Catal.* **1981**, *67*, 159.
4. Kim, J.-H.; Namba, S.; Yashima, T. *Bull. Chem. Soc. Jpn.* **1988**, *61*, 1051.
5. Kim, J.-H.; Namba, S.; Yashima, T. *Stud. Surf. Sci. Catal.* **1989**, *46*, 71.
6. Namba, S.; Kim, J.-H.; Yashima, T. *Stud. Surf. Sci. Catal.* **1994**, *83*, 279.
7. Papparatto, G.; Moretti, E.; Leofanti, G.; Gatti, F. *J. Catal.* **1987**, *105*, 227.
8. Lonyi, F.; Engelhardt, J.; Kallo, D. *Stud. Surf. Sci. Catal.* **1989**, *49*, 1357.
9. Lonyi, F.; Engelhardt, J.; Kallo, D. *Zeolites* **1991**, *11*, 169.
10. Parikh, P.A.; Subrahmanyam, N. *Catal. Lett.* **1992**, *14*, 107.
11. Chandevkar, K.H.; Hegde, S.G.; Kulkarni, S.B.; Ratnasamy, P.; Chitlangia, G.; Singh, A.; Deo, A.V. In *Proc. 6th Intern. Zeolite Conf.*; Olson, D.; Bisio, A. Eds.; Butterworths: Guildford, UK, 1984; pp. 325-330.
12. Argauer, R.J.; Landolt, G.R. *U.S. Pat.* **1972**, 3 702 886.
13. Bibby, D.M.; Aldridge, L.P.; Mileston, N.E. *J. Catal.* **1981**, *72*, 373.
14. Taramasso, M.; Manara, G.; Fattore, V.; Notari, B. *Ger. Pat.* **1989**, 2 924 915.
15. Yamagishi, K.; Namba, S.; Yashima, T. *Stud. Surf. Sci. Catal.*, **1989**, *49*, 459.
16. Kim, J.-H.; Yamagishi, T.; Namba, S.; Yashima, T. *J. Chem. Soc., Chem. Commun.* **1990**, 1793.
17. Kim, J.-H.; Namba, S.; Yashima, T. *Appl. Catal. A: General* **1993**, *100*, 27.
18. Namba, S.; Nakanishi, S.; Yashima, T. *J. Catal.* **1984**, *88*, 505.
19. Namba, S.; Inaka, A.; Yashima, T. *Zeolites* **1986**, *6*, 107.
20. Kim, J.-H.; Namba, S.; Yashima, T. *Zeolites*, **1991**, *11*, 59.
21. Namba, S.; Ohta, H.; Kim, J.-H.; Yashima, T. *Stud. Surf. Sci. Catal.* **1993**, *75*, 1685.
22. Olson, D.H.; Haag, W.O. In *Catalytic Materials*; Whytes, T.H. Ed.; ACS Symp. Ser. 248; ACS: Washington, D.C., 1984, pp 275-307.
23. Kim, J.-H.; Namba, S.; Yashima, T. *Appl. Catal. A: General* **1992**, *83*, 51.
24. Niwa, M.; Iwamoto, M.; Segawa, K. *Bull. Chem. Soc. Jpn.* **1986**, *59*, 3735.



25. Fraenkel, D.; Cherniavsky, M.; Ittah, B.; Levy, M. *J. Catal.* **1986**, *101*, 2673.
26. Fraenkel, D. *J. Mol. Catal.* **1989**, *51*, L1.
27. Weitkamp, J.; Neuber, M. *Stud. Surf. Sci. Catal.* **1991**, *60*, 291.
28. Domitrov, C.; Popova, Z.; Tuyen, M. *React. Kinet. Catal. Lett.* **1978**, *8*, 101.
29. Solinas, V.; Monaci, R.; Rombi, E.; Forni, L. *Stud. Surf. Sci. Catal.* **1987**, *34*, 493.
30. Matsuda, T.; Yogo, K.; Mogi, Y.; Kikuchi, E. *Chem. Lett.* **1990**, 1085.
31. Komatsu, T.; Araki, Y.; Namba, S.; Yashima, T. *Stud. Surf. Sci. Catal.* **1994**, *84*, 1821.
32. Suld, G.; Stuart, A.P. *J. Org. Chem.* **1964**, *29*, 2939.

## Chapter 12

# What Preferentially Determines the *para* Shape Selectivity: Diffusion of Molecules or External Surface Acidity

Miki Niwa <sup>1</sup>, Takehisa Kunieda <sup>1</sup>, and Jong-Ho Kim <sup>2</sup>

<sup>1</sup> Department of Materials Science, Faculty of Engineering, Tottori University, Koyama, Tottori 680-8552, Japan

<sup>2</sup> Department of Chemical Technology, Chonnam University, Kwangju 500-757, Korea

In this short review, we will summarize our recent investigations on the generation of shape-selectivity of *p*-xylene formation. ZSM-5 zeolites modified by a method of CVD (Chemical Vapor Deposition) with silicon alkoxides as well as those synthesized under the hydrothermal conditions were comprehensively characterized; the obtained characterization parameters were correlated with the selectivity to form *p*-xylene. It was found that the pore size is a preferential parameter, except for a special case.

The formation of *para* alkylaromatics is the most important reaction in which the shape selectivity of zeolites is utilized. Because the selectivity on the usual ZSM-5 is insufficient, the enhancement of the selectivity is required. In order to enhance the shape-selectivity, the generation of *p*-xylene formation should be understood correctly; and based on the correctly explained mechanism, the selective catalyst is to be designed.

The generation of selectivity was first elucidated based on a concept of reactant shape-selectivity by Mobil researchers (1). However, much attention is recently focused on another idea (2), *i.e.*, the shape-selectivity on a zeolite ZSM is based upon the transition state selectivity due to the restricted pore space, and the selectivity will be deteriorated, if *p*-xylene undergoes isomerization on the external surface. In other words, the selectivity is, in the former concept, controlled by the diffusion of molecule, however, in the latter concept, it is by the external acidity. This is a controversial problem which allows us to study comprehensively.

Adsorption property and external surface acidity are usually correlated each other, because both parameters depend on the size of crystal; it is thereby so difficult to study the effect of these parameters on the reaction selectivity, independently. To solve the problem, characterization experiments which are carefully, systematically and comprehensively carried out is only an effective way to

reach a conclusion. In this communication, two kinds of investigations to study the generation of selectivity not only on the silica-deposited ZSM-5 but also on the synthesized ZSM-5 will be elucidated.

### Enhancement of *p*-xylene formation by CVD with silicon alkoxides

We have already reported the extremely high selectivity of *p*-xylene formation on the silica deposited HZSM-5, modified by the CVD of silicon tetramethoxide. The high selectivity of *p*-xylene formation, nearly 100 %, was first noticed in the xylene isomers formed during the conversion of methanol (3), and later confirmed in the alkylation and disproportionation of toluene as well (4). In each case, the yield of *p*-xylene increased at the expense of *o*- and *m*-xylenes. The degree of selectivity depends on the amount of deposited silica, but not on the type of reaction, such as methanol conversion and alkylation of toluene.

In this modification technique, silica is deposited only on the external surface because of the bulkiness of silicon compound, and the inside of zeolite is not modified at all (5). The deposited silica not only controls the pore-opening size, but also inactivates the external surface acidity. Namely, both the diffusion of molecule and the non-selective reaction on the external surface are controlled due to the deposited silica, but the reaction on acid site inside the zeolite pore can proceed in a same manner before the modification.

The extent of modification depends on the amount of silica deposited. The amount of silica required for the modification of pore-opening size is affected by the composition of a zeolite; the higher the silica to alumina molar ratio of the zeolite, the larger amount of deposited silica is required. On the other hand, the extent of inactivation of external surface acidity does not depend on the composition of a zeolite. These remarks have been experimentally observed in our previous studies using  $\text{Si}(\text{OCH}_3)_4$  (6,7). As long as silicon tetramethoxide is used, therefore, the factors affecting the shape selectivity, diffusion and external acidity, cannot be varied independently. Then, other kinds of silicon alkoxide with 1, 2 or 3 methoxide and methyl groups, *i.e.*,  $\text{Si}(\text{OCH}_3)_x(\text{CH}_3)_{4-x}$ , ( $x=1,2,3$ ) were utilized for the modification (8).

The degree of control in pore-opening size was evaluated from the adsorption of *o*-xylene at 373 K, and the external surface acidity was measured from the cracking of 1,3,5-triisopropylbenzene which was too large to enter the pore. As shown in Figure 1, the pore-opening size thus controlled was not affected by the deposited silicon compound. In other words, any molecule of silicon compounds controls the pore-opening size in the same degree, which is related to the amount of deposited silica. On the other hand, the inactivation of external acidity depends on the selected molecule, as shown in Fig. 2.  $\text{Si}(\text{OCH}_3)(\text{CH}_3)_3$ , shown as Mono in Figure, a typical reagent for silylation of  $\text{SiO}_2$ , was effective in the inactivation, and a smaller amount silica was required than that for  $\text{Si}(\text{OCH}_3)_4$ , Tetra. The most effective reagent found in the investigation was MTPS,  $\text{Si}(\text{OCH}_3)(\text{C}_3\text{H}_7)_3$ . The degree and manner of modification was thus varied by choosing the molecule and the amount of deposited silica; we were thus able to obtain various SiHZSM-5 with different property as for the pore opening size and the external surface acidity.

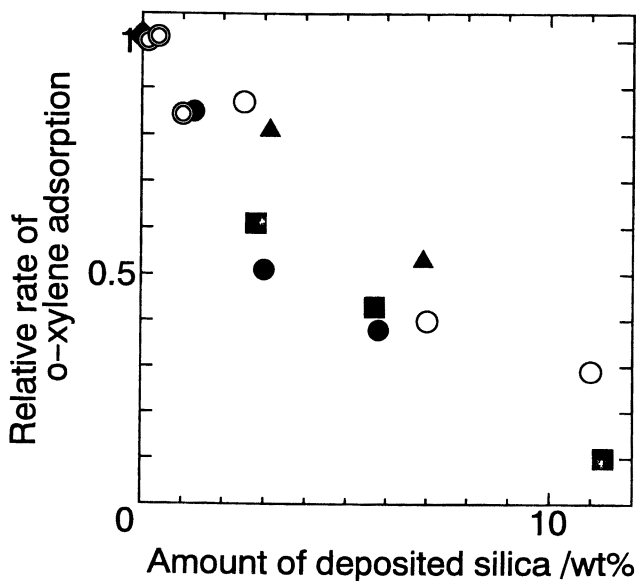


Fig. 1. Control of pore-opening size by depositing silica from various silicon compounds. Symbols referred to in Fig. 2.

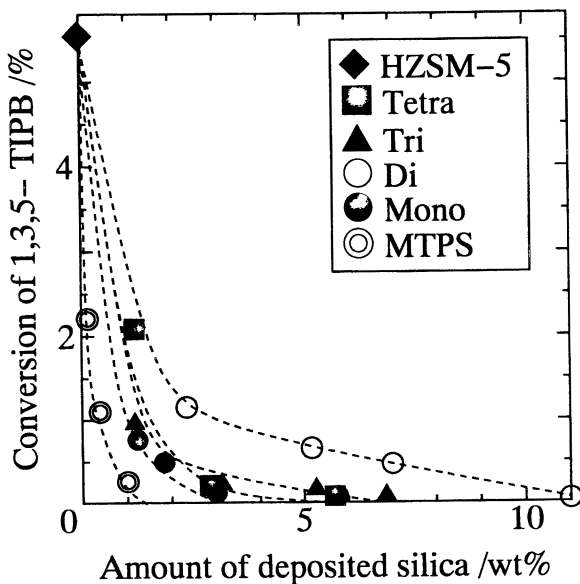


Fig. 2. Inactivation of external surface acidity by depositing silica from various silicon compounds. Tetra to Mono means number of methoxide group in  $\text{Si}(\text{OCH}_3)_x(\text{CH}_3)_{4-x}$ , and MTPS,  $\text{Si}(\text{OCH}_3)(\text{C}_3\text{H}_7)_3$ .

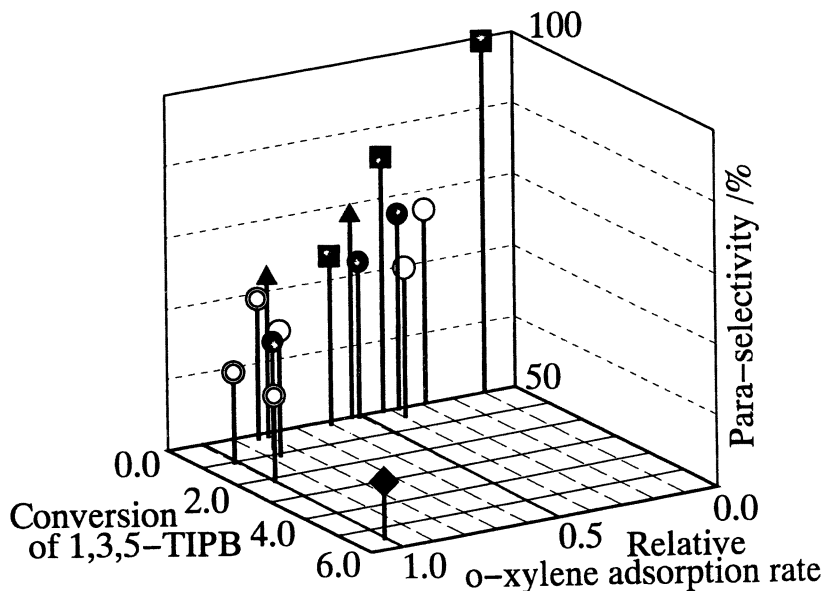


Fig. 3. Three dimensional plot of selectivity against the external surface acidity and the pore-opening size. Symbols referred to in Fig. 2.

The selectivity usually depends on the conversion; *i.e.*, the larger the conversion, the smaller the selectivity. The selectivity is therefore to be evaluated at a constant conversion. Alkylation of toluene with methanol was performed at 673 K by varying the amount of catalyst; and the selectivity to form *p*-xylene was measured at a constant conversion, 20 %. Actually, it was measured from a plot of selectivity vs conversion. Because we have two parameters simultaneously varied, *i.e.*, the pore-opening size and the external surface acidity, a simple two dimensional plot is insufficient to look at the behavior precisely. Thus, Fig. 3 shows the three dimensional plot of the selectivity against the rate of adsorption and the external surface acidity. The selectivity was enhanced gradually by depositing silica, and finally attained almost 100 %. Note that, in the first, the external surface acidity was inactivated to increase the selectivity up to *ca.* 70 %. Then, it increased steeply by narrowing the pore-opening size. This indicated that the extremely high selectivity of *p*-xylene formation was generated effectively by adjusting the pore-opening size to the size of molecule. In other words, it was found that diffusion was a prevailing factor in generating the shape-selectivity.

### Shape-selectivity on the synthesized ZSM-5

Subsequently, we used the synthesized ZSM-5 to study the generation of selectivity (9), because the conclusion obtained with the CVD modified ZSM-5 could not always be applied to the usual zeolite. More than 20 kinds of ZSM-5 were prepared under different conditions of synthesis. We obtained various samples of

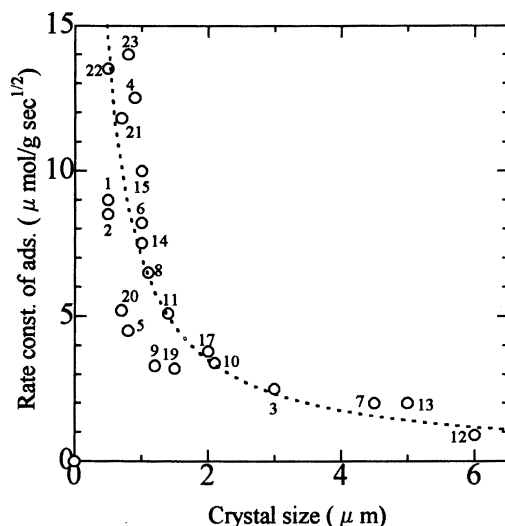


Fig. 4. Relationship between rate constant of adsorption of *o*-xylene and crystal size. Sequential number is added to the ZSM-5.

ZSM-5 with *ca.* 70 - 90 Si/Al<sub>2</sub> ratio, and only two of them contained too small aluminum so that these were excluded in following experiments. In this study, we characterized these synthesized zeolites comprehensively. Measured property in the investigation were crystal size by SEM, chemical composition by ICP, N<sub>2</sub> adsorption capacity at 77 K, XRD, its diffraction pattern and *d*-spacing, adsorption property of *o*-xylene, and external surface acidity. Finally, the selectivity of *p*-xylene formation was determined at the constant conversion of toluene, 20 %, as above mentioned.

Diffusion constant for *o*-xylene adsorption was correlated simply with the size of zeolite crystal, as shown in Fig. 4. This is an important confirmation that these experiments were properly carried out. Morphology of the synthesized ZSM was usually a sphere crystal, but some of them were a rod-like crystal or an apparently large one consisted of primary small crystals. On the other hand, the external surface acidity was not simply correlated with the reciprocal of crystal radius,  $1/r$ , which could be proportional to the external surface area, as shown in Fig. 5. It was thereby found that the distribution of acid sites along the crystal size was not homogeneous. Acid site was enriched on the external surface of such species as No. 15 and 23, whereas inside the pore of such species as No. 5 and 20. The adsorption of *o*-xylene was not affected by the distribution of acid sites, but by the size of crystal.

By comparing the obtained selectivity with these parameters, a simple relationship between the selectivity and the adsorption rate constant was obtained,

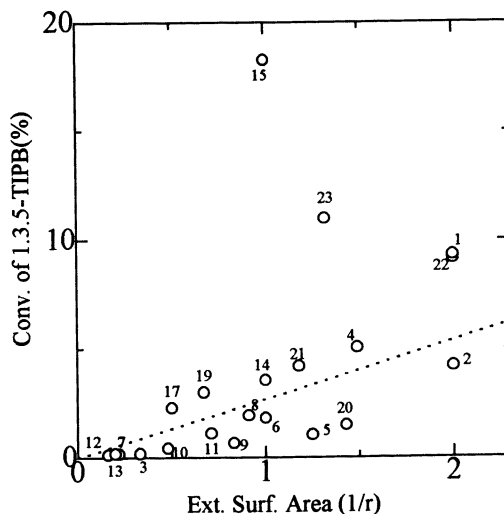


Fig. 5. Plot of external surface acidity against the external surface area

as shown in Fig. 6. The selectivity increased with decreasing the rate constant of adsorption, except for only one sample of No. 15. On the No. 15 sample, there was exceptionally a large amount of external surface acid sites, as mentioned above.

Further study of characterization by temperature programmed desorption (TPD) of ammonia showed existence of the very strong acid site on the No. 15 (10); the strong site was generated due to the interaction of non-framework aluminum atom with usual acid site in the framework. The extra-framework Al sites enhanced the Lewis type character, as found from *ir* measurements. It was the very strong acid site that enriched on the external surface and deteriorated the selectivity. However, except for the special case, the selectivity was simply explained due to the difference in rates of diffusion of molecule.

## Conclusion

It was experimentally confirmed not only on silica deposited but also synthesized ZSM-5 that the diffusion property is a prevailing parameter to decide the selectivity in the *p*-xylene formation. Exceptional case was observed on a special species with the very strong acid site enriched on the external surface, where the selectivity was deteriorated due to the non-selective reaction. Enhancement of the selectivity was thereby possible by controlling the diffusion property. Chemical vapor deposition of silica was an elegant and powerful method to control the diffusion property and thus to enhance the selectivity extremely.

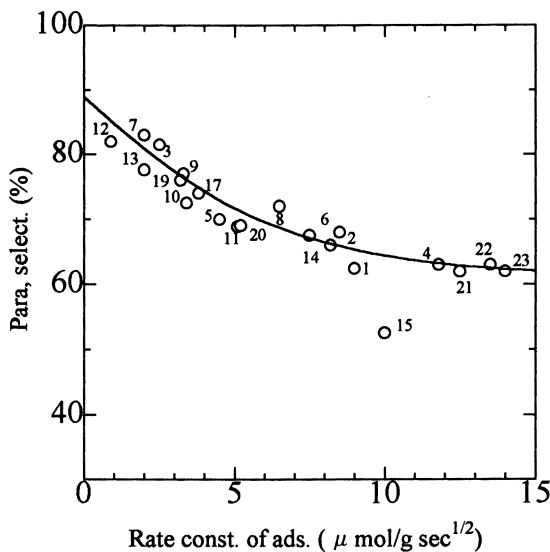


Fig. 6. Selectivity on the synthesized HZSM-5 plotted against the rate constant of *o*-xylene adsorption.

## References

1. Haag, W. O.; Lago, R. M.; Weisz, P. B., *Disc. Faraday Soc.*, **72**, 317 (1981).
2. Paparatto, G.; Moretti, E.; Leofani, G.; Gatti, F., *J. Catal.*, **105**, 227 (1987).
3. Niwa, M.; Kato, M.; Hattori, T.; Murakami, Y., *J. Phys. Chem.*, **90**, 6233 (1986).
4. Hibino, T.; Niwa, M.; Murakami, Y., *J. Catal.*, **128**, 551 (1991).
5. Niwa, M.; Kato, S.; Hattori, T.; Murakami, Y., *J. Chem. Soc., Faraday Trans. I*, **80**, 3135, (1984).
6. Hibino, T.; Niwa, M.; Kawashima, Y.; Murakami, Y., "Chemistry of Micro Porous Crystals", Eds by Inui, T., Namba, S., and Tatsumi, T., pp.151-158, Kodansha, Tokyo, (1991).
7. Hibino, T.; Niwa, M.; Murakami, Y., *Zeolites*, **13**, 518 (1993).
8. Kim, J. H.; Ishida, A.; Okajima, M.; Niwa, M., *J. Catal.*, **161**, 387 (1996).
9. Kim, J. H.; Kunieda, T.; Niwa, M., *J. Catal.*, **173**, 433 (1998).
10. Kunieda, T.; Katada, N.; Niwa, M., Oral presentation A23 in 12<sup>th</sup> International Zeolite Conference, Baltimore, 1998.



## Chapter 13

# Dispersion of Oxides on HZSM-5 and Threshold Effect on Shape-Selective Methylation of Toluene

Youchang Xie, Biying Zhao, Xiangyun Long, and Youqi Tang

Institute of Physical Chemistry, Peking University,  
Beijing 100871, Peoples Republic of China

A series of oxide-supported HZSM-5 catalysts have been studied. The results show that  $B_2O_3$ , MgO,  $Sb_2O_3$ , ZnO and  $P_2O_5$  can disperse onto the surface of HZSM-5 on an atomic scale. Their dispersion thresholds on HZSM-5 have been determined by XRD and XPS. For all these catalysts, with increase of oxide loading, para-selectivity of methylation of toluene increases rapidly and reaches a maximum at the dispersion threshold, and hereafter does not change any more. This phenomenon is termed 'threshold effect'. The decrease in activity, specific surface area and surface acidity of the catalyst also show the similar threshold effect, which reveals the internal relations between the structure and the behavior of this kind of catalysts.

The shape-selective catalytic alkylation of toluene with methanol is a process of much practical interest because of the great industrial demand for paraxylene. The selective preparation of paraxylene can be achieved by means of appropriately modified acidic zeolite, in particular, HZSM-5 zeolites(1-4). Among a variety of modification methods, modifying HZSM-5 with oxides has been proved to be an effective method for improving the para-selectivity of methylation of toluene over HZSM-5(1,3,5). It was widely reported that paraxylene in xylene produced over HZSM-5 modified with some oxides, such as  $Sb_2O_3$ ,  $P_2O_5$ ,  $SiO_2$ ,  $B_2O_3$ ,  $La_2O_3$ , MgO, CaO and etc., can be up to above 95%(5-12). Although continuing efforts have been made to explore the essence of this catalytic reaction, there are still some controversies about the explanation of high para-selectivity over HZSM-5 modified with oxides. It seems to be generally recognized that added oxides may reduce the dimensions of the pores

and channels of zeolite(1,2), and/or weaken or cover surface acid sites, in particular, those on the external surface(9,10). However, there are still divergences on some aspects such as the dominant factor leading to high para-selectivity, the state and distribution of oxides on HZSM-5. It seems very necessary to explore the internal relations between these factors and to find out some common rules which take effect on shape-selective catalysis over zeolite modified with oxide.

We have reported that many oxides and salts can spontaneously disperse onto surfaces of supports with highly specific surface area to form a monolayer or submonolayer, and each system has a certain utmost dispersion capacity termed the dispersion threshold(13,14). For a compound with not too high melting point, its monolayer dispersion on a support can be done by heating the compound mixed with the support at a suitable temperature well below its melting point. For compounds with high melting points, although their monolayer dispersion on supports can not be done by just heat dispersion, it can be done by impregnation followed by calcination. The driving force for monolayer dispersion to happen spontaneously is that the Gibbs free energy of the whole system would decrease. When a compound disperses onto a support as a monolayer, the entropy of the whole system would increase considerably ( $\Delta S >> 0$ ). Meanwhile the strength of surface bonds formed between atoms, ions or molecules of the monolayer-dispersed compound and the surface of support is usually comparable to that of the bonds in bulk compound, so the change of energy and enthalpy of the whole system would be not much ( $\Delta H \approx \Delta E \approx 0$ ) in the process of monolayer dispersion. Therefore, the change of free energy of the whole system is negative ( $\Delta G = \Delta H - T\Delta S < 0$ ), and the monolayer-dispersion is a thermodynamically spontaneous process. So far dispersion thresholds of many systems have been determined by XRD, XPS, ISS, Raman spectroscopy, and so on(13).

The dispersed compound is in a monolayer state when the loading is below its dispersion threshold, and the surplus compound exists in an independent phase to form a mixture with the support covered by the dispersed compound when the loading is above its threshold. Therefore, performances of the system in many respects would appear a turn at the threshold. This idea has been proved by the experimental results of EXAFS, TPD, DTA-TG, surface acidity, specific surface area, porosity, adsorption and catalytic behavior(13). We can term this phenomenon "threshold effect".

Zeolites possess enormous internal surface and uniform pores and channels. Many oxides and salts can also disperse to the internal and external surfaces of zeolites on an atomic-molecular scale with respective dispersion thresholds(15,16). The dispersion process can also be accomplished by heat dispersion or impregnation followed by calcination.

Literature shows that oxide loading plays an important and subtle role in the improvement of para-selectivity in methylation of toluene over the zeolite modified with some oxides(5-12). In this paper, the dispersion behavior of five oxides,  $B_2O_3$ ,  $MgO$ ,  $Sb_2O_3$ ,  $P_2O_5$  and  $ZnO$  on HZSM-5 has been studied and their dispersion thresholds have been determined. It has been found that there are obvious threshold effects in performances of the catalysts, including their specific surface areas, surface acidity, activity and para-selectivity in methylation of toluene.

## Experimental

**Catalyst Preparation.** HZSM-5 zeolites with  $\text{SiO}_2/\text{Al}_2\text{O}_3$  of 38 and 50 were supplied by Catalyst Plant of Nankai University and noted as HZSM-5 [38] and HZSM-5 [50] respectively. The mixing and heating method was adopted in the preparation of  $\text{B}_2\text{O}_3/\text{HZSM-5}$  and  $\text{Sb}_2\text{O}_3/\text{HZSM-5}$  samples in order to emphasize the spontaneity of oxide dispersion on the zeolite. The heating conditions are  $400^\circ\text{C}$  for 6 hours for  $\text{B}_2\text{O}_3/\text{HZSM-5}$  and  $500^\circ\text{C}$  for 2 hours in  $\text{N}_2$  for  $\text{Sb}_2\text{O}_3/\text{HZSM-5}$ . The  $\text{MgO}/\text{HZSM-5}$ ,  $\text{ZnO}/\text{HZSM-5}$  and  $\text{P}_2\text{O}_5/\text{HZSM-5}$  catalysts were obtained by impregnating HZSM-5 with  $\text{Mg}(\text{NO}_3)_2$ ,  $\text{Zn}(\text{NO}_3)_2$  and  $\text{H}_3\text{PO}_4$  solutions, respectively, and followed by calcination at  $500^\circ\text{C}$  for 3 hours. The BET surface areas of the samples were determined by nitrogen adsorption method.

**Determination of Dispersion Threshold.** The thresholds of  $\text{Sb}_2\text{O}_3$ ,  $\text{MgO}$  and  $\text{ZnO}$  on HZSM-5 were determined by using X-ray diffraction quantitative phase analysis method(13,14). The thresholds of  $\text{MgO}$ ,  $\text{B}_2\text{O}_3$  and  $\text{P}_2\text{O}_5$  on HZSM-5 were obtained by XPS measurements(17), carrying out on a VG ESCA LAB5 Electron Spectrometer with AlK $\alpha$  excitation and a working pressure of  $10^{-6}$  Pa.

**Temperature Programmed Desorption (TPD) of  $\text{NH}_3$ .** The samples were pretreated at  $500^\circ\text{C}$  in  $\text{N}_2$  stream for one hour and then adsorbed  $\text{NH}_3$  at  $100^\circ\text{C}$  for 30min. The TPD procedure were carried out at a heating rate of  $12^\circ\text{C}/\text{min}$  from  $100$ - $500^\circ\text{C}$ .

**Alkylation of Toluene with Methanol.** The reaction was performed in a fixed-bed continuous flow micro-reactor. The catalyst (40-60 mesh) was placed in a glass reactor and pretreated with  $\text{N}_2$  stream at  $450^\circ\text{C}$  for 2 hours. The reaction was carried out in He stream, and the feed was injected into the catalyst bed with a micro-feeder. After reaction for one hour, the products of the reaction were analyzed by GC equipped with a TCD detector.

## Results and Discussion

**Spontaneous Dispersion of Oxides on HZSM-5 and Their Dispersion Thresholds.** The experiment results show that  $\text{B}_2\text{O}_3$ ,  $\text{Sb}_2\text{O}_3$ ,  $\text{MgO}$ ,  $\text{ZnO}$ ,  $\text{P}_2\text{O}_5$  can disperse onto the surface of HZSM-5 by heating mechanical mixture (for  $\text{B}_2\text{O}_3$  and  $\text{Sb}_2\text{O}_3$ ) or by impregnation followed by calcination method (for  $\text{MgO}$ ,  $\text{ZnO}$  and  $\text{P}_2\text{O}_5$ ). Figure 1 shows XRD patterns of the  $\text{MgO}/\text{HZSM-5}$  with different content of  $\text{MgO}$ . It can be seen that only when the content of  $\text{MgO}$  in the sample is higher than a certain level, do the peaks of crystalline  $\text{MgO}$  appear. According to the principle of spontaneous monolayer dispersion, these oxides may have dispersed onto the internal and external surface of the zeolite. The amount of residual crystalline oxides can be determined from the peak area of residual crystalline oxide in the XRD pattern(13,14). Figure 2 gives a plot of the relative crystalline  $\text{MgO}$  XRD peak intensity ratio ( $I_{\text{MgO}}/I_{\text{HZSM-5}}$ ) versus the total contents of  $\text{MgO}$  in the samples, from which the dispersion threshold of  $\text{MgO}$  on HZSM-5,  $0.12\text{g MgO/g HZSM-5}$ , can be derived. Similar to  $\text{MgO}/\text{HZSM-5}$ , the dispersion thresholds of  $\text{ZnO}$  and  $\text{Sb}_2\text{O}_3$  on HZSM-5 were obtained by XRD quantitative phase analysis, respectively, as shown in Table 1.

Since  $\text{B}_2\text{O}_3$  is generally present in vitrescence state and the crystalline phases of

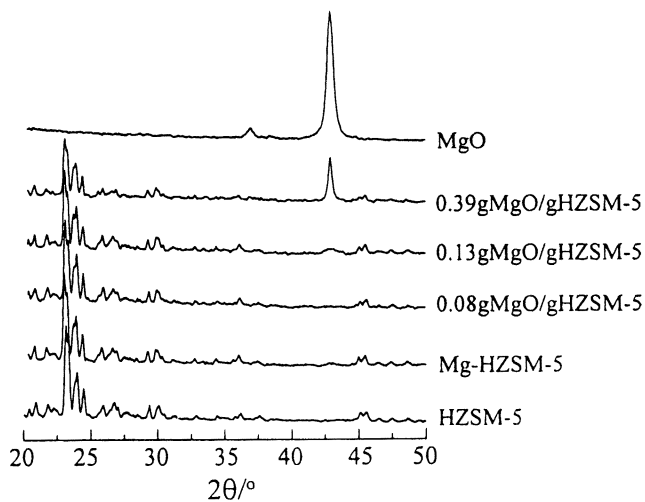


Figure 1. The XRD patterns of MgO/HZSM-5

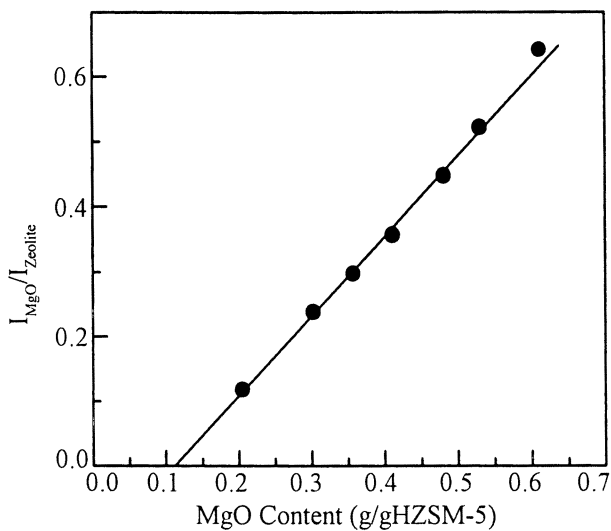


Figure 2. Relationship between the relative intensity of crystalline MgO and total content of MgO in MgO/HZSM-5

P<sub>2</sub>O<sub>5</sub> beyond its dispersion capacity are quite complicated, XPS technique was employed to determine their dispersion thresholds.

As an example, Figure 3 gives the XPS peak intensity ratio  $I_{\text{B}1s}/I_{\text{Si}2p}$  as a function of the total B<sub>2</sub>O<sub>3</sub> contents in the samples. It is observed that the intensity ratio  $I_{\text{B}1s}/I_{\text{Si}2p}$  increases sharply at the beginning, and then turns to rise slowly with B<sub>2</sub>O<sub>3</sub> content in the samples. The boron oxide content at the turning point corresponds the dispersion threshold of B<sub>2</sub>O<sub>3</sub> on HZSM-5(17). The dispersion thresholds of B<sub>2</sub>O<sub>3</sub> on HZSM-5[38] and HZSM-5[50] are the same value of 0.11g B<sub>2</sub>O<sub>3</sub>/g HZSM-5. When the B<sub>2</sub>O<sub>3</sub> content is below the threshold, B<sub>2</sub>O<sub>3</sub> is in monolayer dispersion state, surface concentration of B<sub>2</sub>O<sub>3</sub> on HZSM-5 or XPS peak intensity ratio  $I_{\text{B}1s}/I_{\text{Si}2p}$  grows up steeply with B<sub>2</sub>O<sub>3</sub> loading increase. As the loading of B<sub>2</sub>O<sub>3</sub> exceeds the threshold, the surplus B<sub>2</sub>O<sub>3</sub> appears as a bulk phase (vitrescence state), then the  $I_{\text{B}1s}/I_{\text{Si}2p}$  increase becomes slowly.

The dispersion thresholds of P<sub>2</sub>O<sub>5</sub> and MgO on HZSM-5 have also been determined by XPS and shown in Table I. The threshold value obtained by XRD and XPS for the MgO/HZSM-5 are the same. It confirms the reliability of the methods.

The BET specific surface area of the zeolite used is about 370m<sup>2</sup>/g. The thresholds converted to the number of metal atom of the oxides per nm<sup>2</sup> and per Si(Al) atom are also listed in Table I. Their values are consistent with atomic scale dispersion.

It is worth to note that the overwhelming majority of the dispersion oxide is on the internal surface of the zeolite since the external surface is only a very small part of the total surface. For example, if the mean size of HZSM-5 crystallites is about 1 μm, its external surface area is only about 3.5 m<sup>2</sup>/g HZSM-5, i.e. about 1% of its total surface area. For the B<sub>2</sub>O<sub>3</sub>/HZSM-5 catalysts, in terms of a close-pack model (13,14), the utmost capacity of B<sub>2</sub>O<sub>3</sub> on the external surface of the zeolite is about 0.002g B<sub>2</sub>O<sub>3</sub>/g HZSM-5, namely, only about 2 percent of the dispersion threshold (0.11gB<sub>2</sub>O<sub>3</sub>/g HZSM-5). It means that more than 98% of the dispersed B<sub>2</sub>O<sub>3</sub> is located on the internal surface, i.e., inside the intra-crystalline pores of the zeolite. Similar results can also be obtained from the data of other oxide modified HZSM-5 catalysts. The atomic scale dispersion of oxides on the surface (mainly internal surface) of the zeolite will influence its shape-selective catalytic behaviors.

Table I Dispersion thresholds of the oxides on HZSM-5

System	method	Threshold (g/g HZSM-5)	M-atoms /nm <sup>2</sup>	M-atoms /Si(Al) atom
MgO/HZSM-5[38]	XRD	0.12	9.8	0.179
MgO/HZSM-5[38]	XPS	0.12	9.8	0.179
ZnO/HZSM-5[38]	XRD	0.11	4.4	0.082
Sb <sub>2</sub> O <sub>3</sub> /HZSM-5[38]	XRD	0.25	2.8	0.10
Sb <sub>2</sub> O <sub>3</sub> /HZSM-5[50]	XRD	0.25	2.8	0.10
B <sub>2</sub> O <sub>3</sub> /HZSM-5[38]	XPS	0.11	5.2	0.19
B <sub>2</sub> O <sub>3</sub> /HZSM-5[50]	XPS	0.11	5.2	0.19
P <sub>2</sub> O <sub>5</sub> /HZSM-5[38]	XPS	0.21	4.8	0.177

Note: [38] and [50] are notes of SiO<sub>2</sub>/Al<sub>2</sub>O<sub>3</sub> of the zeolite.

### The Effect of Oxide Loading on Catalytic Methylation of Toluene over HZSM-5.

The activity and para-selectivity for toluene methylation over the HZSM-5 catalysts modified with these oxides have been investigated.

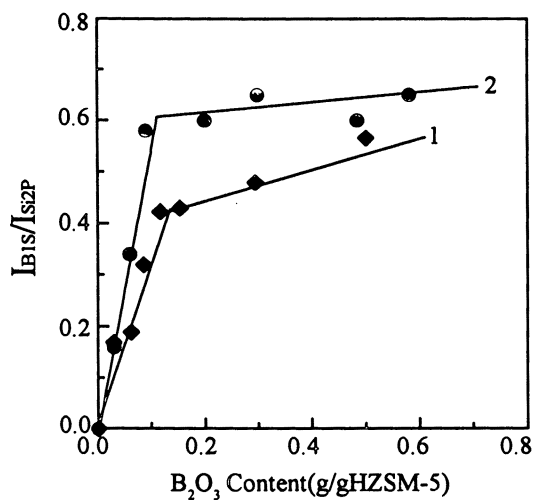


Figure 3. XPS intensity ratio  $I_{B1s}/I_{Si2p}$  versus  $B_2O_3$  content in the samples. 1.  $B_2O_3$ /HZSM-5(38); 2.  $B_2O_3$ /HZSM-5(50).

Figure 4 shows the effect of  $B_2O_3$ -loading on the activity and selectivity of toluene methylation over two  $B_2O_3$ /HZSM-5 catalyst systems. The selectivity for para-xylene increases rapidly up to >90% when  $B_2O_3$  loading rises up to close the threshold, 0.11 g  $B_2O_3$ /g HZSM-5, and then keeps almost constant when  $B_2O_3$  loading increases subsequently. On the contrary, the activity decreases down to 15-20% as  $B_2O_3$  loading goes up to the threshold, and varies little hereafter. The para-selectivity of  $B_2O_3$ /HZSM-5[50] is a little bit higher than that of  $B_2O_3$ /HZSM-5[38], and the activity of the former is a little bit lower than the latter, but both have turning point close to the dispersion threshold.

The situations of other systems are similar to that of  $B_2O_3$ /HZSM-5 catalysts. Figure 5 and 6 give the similar curves for MgO/HZSM-5 and  $Sb_2O_3$ /HZSM-5 systems, respectively. All the oxide modified HZSM-5 catalysts have 'threshold effect' on the para-selectivity and activity of toluene methylation reaction. Table II summarizes some results of the toluene methylene reaction over unmodified HZSM-5 and HZSM-5 modified with various oxides at loadings close to or over their dispersion thresholds. In Table II, we can find that near-equilibrium proportion (almost no shape-selectivity) of paraxylene and higher toluene conversion are obtained for unmodified HZSM-5 catalysts, but all the oxide-modified HZSM-5 catalysts show very high para-selectivities (80-100%) and low activities. Since all the oxide-modified HZSM-5 catalysts show the highest para-selectivity and the lowest activity at their loadings close to their dispersion thresholds, the effects of shape-selective catalysis can be attributed to that the dispersed oxides make the channels of the zeolite narrow, and the acidity of the external and internal surface of the zeolite changes.

Table II Reaction results of the toluene methylation over unmodified and modified HZSM-5

Catalyst	loading (g/g)	T (°C)	WHSV (h <sup>-1</sup> )	Tol/MeOH (mole)	C%	S <sub>px</sub> %	S <sub>xylene</sub> %
HZSM-5[38]	0	500	10.1	1	47.5	23	79
	0	450	6.9	1	45.9	25	84
	0	450	6.9	2	40.2	25	82
HZSM-5[50]	0	500	10.1	1	45.8	27	83
	0	450	6.9	2	41.2	28	81
	0	450	6.9	1	39.6	26	80
$B_2O_3$ /HZSM-5 [38]	0.08	500	10.1	1	22.6	85	89
	0.12	500	10.1	1	20.8	92	90
$B_2O_3$ /HZSM-5 [50]	0.16	500	10.1	1	16.6	94	93
$Sb_2O_3$ /HZSM-5 [38]	0.24	450	6.9	2	10.8	95	94
$Sb_2O_3$ /HZSM-5 [50]	0.29	450	6.9	2	7.5	100	100
MgO/HZSM-5 [38]	0.10	450	6.9	1	18.8	90	90
MgO/HZSM-5 [38]	0.20	450	6.9	1	15.3	94	93
$P_2O_5$ /HZSM-5 [38]	0.20	450	6.9	1	13.1	90	95
ZnO/HZSM-5 [38]	0.12	450	6.9	2	17.6	80	88

Note: The reaction products were analyzed after reaction for 1 hour.

C%: conversion of toluene; S<sub>px</sub>%: percent of para-xylene in all xylene isomers;

S<sub>xylene</sub>%: selectivity of xylene in products.

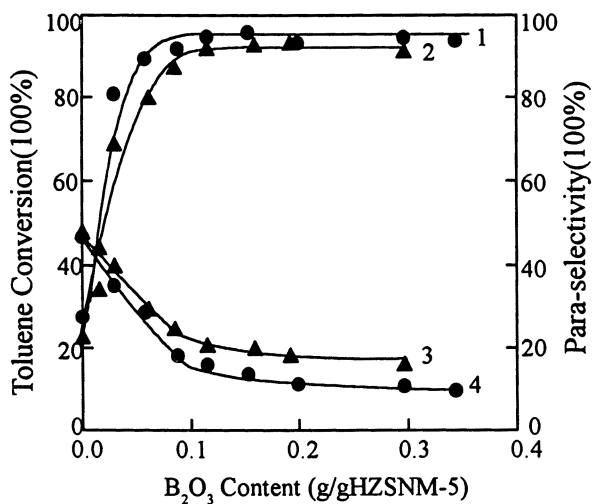


Figure 4. Effect of B<sub>2</sub>O<sub>3</sub> content on the activity and para-selectivity in toluene methylation. Para-selectivity for (1) B<sub>2</sub>O<sub>3</sub>/HZSM-5(50) and (2) B<sub>2</sub>O<sub>3</sub>/HZSM-5(38); toluene conversion for (3) B<sub>2</sub>O<sub>3</sub>/ZSM-5(38) and (4) B<sub>2</sub>O<sub>3</sub>/HZSM-5(50).

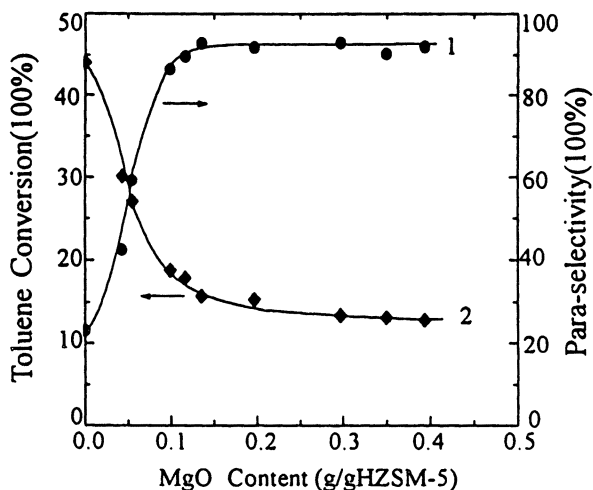


Figure 5. Effect of MgO loading on the activity and para-selectivity in toluene methylation. (1) para-selectivity. (2) toluene conversion.



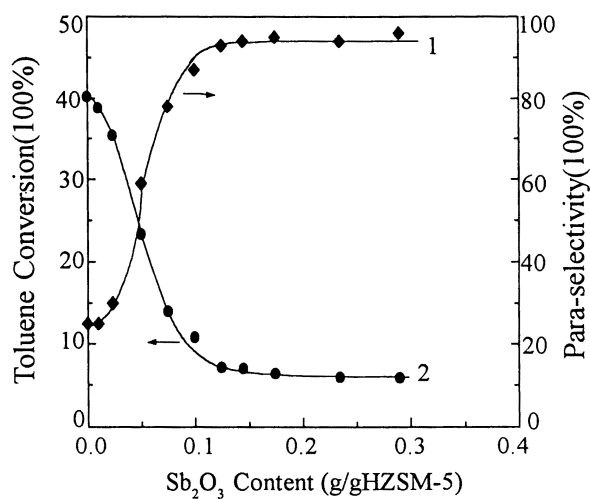


Figure 6. Effect of Sb<sub>2</sub>O<sub>3</sub> loading on the activity and para-selectivity in toluene methylation. (1) para-selectivity. (2) toluene conversion.

In addition to the threshold effects on catalytic property, we can also observe the effects on the specific surface area and surface acidity of the catalysts as reported in the following parts.

### **Threshold Effect Displayed in the Specific Surface Areas of the Catalysts.**

Figure 7, as a typical example, shows the surface area as a function of MgO loading on MgO/HZSM-5 catalysts. The measurement results show that the surface area of the zeolite catalysts decreases rapidly with the oxide loading increase to its dispersion threshold, because the oxide has entered the pores and channels of the zeolite to make its internal surface decrease. When the loading is above the threshold, the surface area decrease becomes slow, since the excess oxide presents as an independence phase outside the zeolite pores. The turning point is at about the threshold. Other oxide modified zeolite catalysts also show similar results of surface area.

**The Threshold Effect on Surface Acidity of the Catalysts.** The surface acidity of samples was characterized by  $\text{NH}_3$  TPD. Figure 8 gives the  $\text{NH}_3$  TPD spectra of  $\text{B}_2\text{O}_3$ /HZSM-5 samples and HZSM-5. It can be seen that there are two kinds of acid sites on the surface of HZSM-5. One is strong acidic sites with TPD peak at  $420^\circ\text{C}$ , and the other is weak acidic sites with TPD peak at  $250^\circ\text{C}$ . With the increase of  $\text{B}_2\text{O}_3$  loading, strong acid sites disappear rapidly whereas the number of weak acid sites decreases slowly and their strength weakens bit by bit. This measurement result is in agreement with that reported by Ducan and Douglass(18). As the loading is above its threshold(curve 4), the surface acidity of samples does not change any more. In short, results of surface acidity for  $\text{B}_2\text{O}_3$  also display the threshold effect obviously.

Since the change of strong acid sites is much more remarkable than that of the weak ones as the  $\text{B}_2\text{O}_3$  loading is low, and there are few strong acid sites remained as the oxide loading reaches only a half of the threshold, it is reasonable to consider that  $\text{B}_2\text{O}_3$  molecules prefer to combine with the strong acid sites or to cover them. However, not all of  $\text{B}_2\text{O}_3$  sit on the acid sites of the zeolite, since it only needs about  $0.03\text{g B}_2\text{O}_3/\text{g HZSM-5}$  to occupy all of Brønsted acid sites of HZSM-5 [38]. Therefore, a considerable part of  $\text{B}_2\text{O}_3$  should be dispersed on other sites of the zeolite.

Figure 9 and 10 show the TPD results of MgO/HZSM-5 and  $\text{Sb}_2\text{O}_3$ /HZSM-5, respectively. The surface acidity of  $\text{P}_2\text{O}_5$ /HZSM-5 and ZnO/HZSM-5 catalysts also show obvious threshold effect, though details of its change would be different from system to system.

The dispersed oxides make the surface acidity of the zeolite decrease. It is one of the reasons for the decrease of activity of the catalysts.

### **Conclusion**

Oxides such as  $\text{B}_2\text{O}_3$ , MgO,  $\text{Sb}_2\text{O}_3$ , ZnO and  $\text{P}_2\text{O}_5$  can disperse in atomic scale on the surface of HZSM-5 zeolite owing to the decrease of free energy of the whole systems in the process. There are dispersion thresholds for the oxides on the zeolite. When the loading of an oxide on the zeolite is close to its dispersion threshold, the oxide modified HZSM-5 catalyst will have the highest para-selectivity and lowest activity for the reaction of methylation of toluene. This common rule can be termed 'threshold effect'. This modification effect can be attributed to that the dispersed

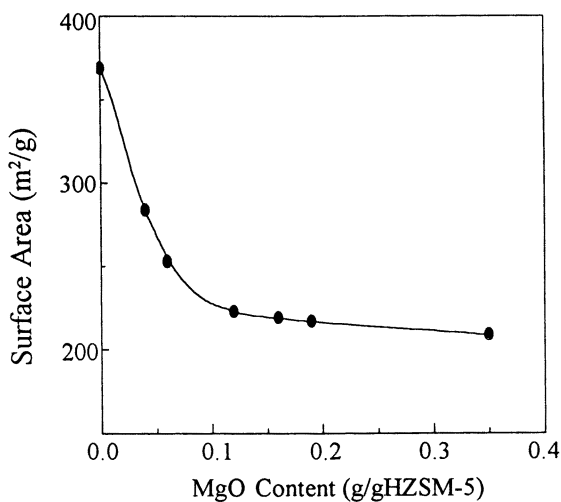


Figure 7. The specific surface area of MgO/HZSM-5 versus MgO loading

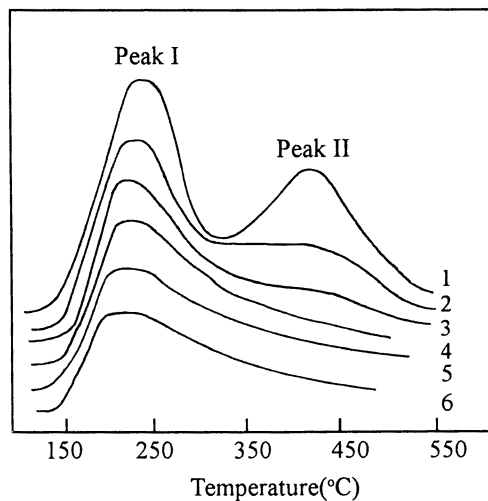


Figure 8.  $\text{NH}_3$ -TPD results of HZSM-5(38) and  $\text{B}_2\text{O}_3/\text{HZSM-5}$

1. HZSM-5; 2, 3, 4, 5 and 6 are 0.03, 0.06, 0.12, 0.19 and 0.29g  $\text{B}_2\text{O}_3/\text{g}$  HZSM-5, respectively.

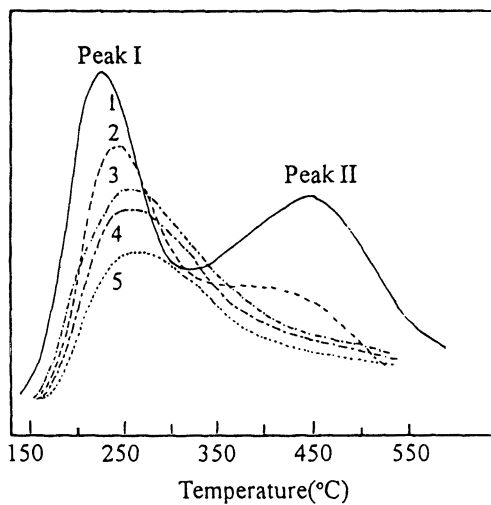


Figure 9. NH<sub>3</sub>-TPD results of MgO/HZSM-5

1. HZSM-5; 2, 3, 4 and 5 are 0.03, 0.10, 0.20 and 0.30g MgO/g HZSM-5, respectively.

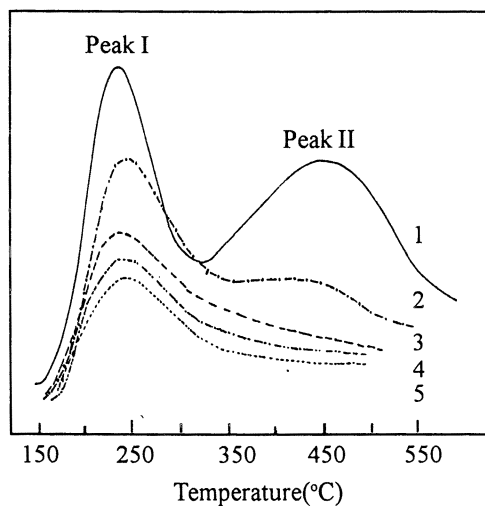


Figure 10. NH<sub>3</sub>-TPD results of Sb<sub>2</sub>O<sub>3</sub>/HZSM-5

1. HZSM-5; 2, 3, 4 and 5 are 0.14, 0.24, 0.29 and 0.35g Sb<sub>2</sub>O<sub>3</sub>/g HZSM-5, respectively.

oxides makes the channels of HZSM-5 to become narrow and the surface acidity and number of acid sites on the external and internal surface of the zeolite decrease. Spontaneous dispersion of oxides on surface of zeolites and the threshold effect might be of universal significance for other shape-selective zeolite catalysts.

### Acknowledgment

The project is supported by the National Science and Technology Committee of China and National Natural Science Foundation Committee of China.

### References

1. Kaeding, W.W.; Chu, C.C.; Young, L.B., *J. Catal.*, **1981**, *67*, 159
2. Hibino, T.; Niwa, M; Murakami, Y., *J. Catal.*, **1991**, *128*, 551
3. Zeng, Z. H., *Shape-selective catalysis*, 1<sup>st</sup> ed., Chinese Petrochemical Press, 1994, 200
4. Young, L.B.; Butter, S.A.; Kaeding, W.W., *J.Catal.*, **1982**, *76*, 418
5. Cavallaro, S.; Pino, L.; Tsiakaras, P; Giordano, N; Bao, B. S., *Zeolites*, **1987**, *77*, 408
6. Butter, S.A., US Patent No.4499321, 1985
7. Li, G.Y.; Zhao, J.C., *Petrochem. Technol.(China)*, **1987**, *16*,274
8. Zhao, J.C.; Li, G.Y.; Din, Y.Q., *J.Catal.(China)*, **1988**, *9*,152
9. Kim, J.H.; Namba, S.; Yashima, T., *Bull. Chem. Soc. Jpn.*, **1988**, *61*, 1081
10. Kim, J. H.; Namba, S.; Yashima, T., in Karge, H. G. and J, Weitcamp. J. (Editors), *Zeolites as Catalysts, Sorbents and Detergent Builders*, Elsevier, Amsterdam, Stud. Surf. Sci. Catal., 1989, *46*, 21
11. Chen, N.Y.; Kaeding, W.W., Dwyer, F.G., *J.Amer. Chem.Soc.*, **1979**, *101*, 6783
12. Kaeding, W.W.; Young, L.B.; Chu, C.C., *J.Catal.*, **1984**, *89*, 267
13. Xie, Y.C.; Tang, Y.Q., *Adv. in Catal.*, **1990**, *37*, 1
14. Xie, Y.C.; Yang, N.F.; Liu, Y.J.; Tang, Y.Q., *Scientia Sinica (Series B)*, **1983**, *26*, 337
15. Xie, Y.C.; Wang, C.B.; Tang, Y.Q., *Acta Physico-Chimica Sinica.*, **1993**, *9*, 735
16. Xie, Y.C.; Wang, C.B.; Tang, Y.Q., *Acta Chemica Sinica*, **1993**, *51*, 774
17. Gui, L.L.; Liu, Y.J.; Guo, Q.L.; Huang, H.Z.; Tang, Y.Q., *Scientia Sinica, (Series B)*, **1985**, *28*, 1234
18. Duncan, T.M.; Donglass, D.C., *Chem. Phys.*, **1984**, *82*, 339

## Chapter 14

# Direct Synthesis of *para*-Diethylbenzene over Modified HZSM-5 Zeolites

Wang Xiangsheng and Guo Hongchen

Institute of Industrial Catalysis, State E. C. Open Laboratory of Comprehensive Utilization for Carbonaceous Resource, Dalian University of Technology, Dalian, Peoples Republic of China

The direct synthesis of *para*-diethylbenzene (PDEB) was achieved commercially via ethylation of ethylbenzene over EA catalysts (modified ZSM-5 zeolites). The preparations of EA catalysts by modifying micron-sized ZSM-5 zeolites and the performances of EA catalysts in industrial units are discussed. It is observed, that the PDEB selectivity of HZSM-5 can be enhanced by strengthening the channels' geometric constraints, decreasing the amount of strong acid sites and eliminating the external surface acid sites of H-type zeolites. And that with combined modifications, an all-sided adjustment of said parameters of HZSM-5 zeolites could be reached, which favors the preparation of commercial catalyst by allowing good activity and durability. Combined modifications also works well in elevating the PDEB selectivity of nano-sized ZSM-5 zeolite, the promising candidate for a new generation of *para*-selective catalyst.

Since the pioneering work of Kaeding (1), there are a good many of papers dealing with the synthesis of PDEB over ZSM-5 zeolite (2-8). *para*-Diethylbenzene (PDEB) is a commercially important chemical. It can be directly used as a desorbent in the process of separation of xylenes. It may also serve as starting material for the producing of resin bridging agent and other novel polymers. In the past, the needs for PDEB were solely met by the well-known UOP simulated-moving-bed separation system (9), which utilizes a diethylbenzene mixture, namely the by-product of the ethylbenzene-synthesizing process, as its feedstock to produce PDEB with a purity of higher than 95%. However, this situation has gradually changed since the first unit for the direct synthesis of PDEB succeeded in commercialization in 1989(10). Currently the direct synthesis of PDEB can be performed by carrying out either the disproportionation of ethylbenzene (8) or the alkylation of ethylbenzene with ethylene or with 95% v/v industrial alcohol (3, 7). In both cases, the reactions are catalyzed by a modified Mobil high siliceous zeolite ZSM-5. Compared with the separation

approach, the synthetic route allows a lower construction cost and a higher equipment independence.

The direct synthesis of PDEB, together with the previously industrialized process (11) for the synthesis of *para*-methylethylbenzene (PET), are all based on the *para*-selective catalysis characteristic of ZSM-5 zeolite. In these processes, ZSM-5 zeolite needs to be endowed with an ability of identifying the minor differences among the diethylbenzene (DEB) isomers chemically and/or dimensionally, and therefore is capable of restricting the formation and the diffusion of the *ortho*- and *meta*- isomers, but favoring those of the *para*-isomer. This is quite different with the case such as ZSM-5 zeolites used in the well-known Mobil/Badger EB Process (11) and Mobil MTG Process (11). These latter processes are based on the generally termed shape-selective catalysis characteristic of ZSM-5 zeolite, where the catalysts are only required to be able to limit the heavy end of the product spectra and to hinder the formations of the coking intermediates, namely to impose a 'product selectivity' to the reactions. Obviously, the application of ZSM-5 zeolite to catalyze a *para*-selective reaction is more difficult than to catalyze a said shape-selective reaction.

It is generally agreed that (1, 12-13), during the synthesis of PDEB, the elimination of *ortho*-DEB is relatively easy because its bulky intermediate is too large to be formed within the 10 number ring ZSM-5 channels. This phenomenon is called 'restricted transition state selectivity'. During the ethylation of ethylbenzene, PDEB is of the sole product primarily formed on the weak acid sites. *meta*-DEB is the secondary product originated from the isomerization of PDEB on strong acid sites. During the disproportionation of ethylbenzene, *meta*-DEB can be produced directly from ethylbenzene. The formation of *meta*-DEB is favored thermodynamically. But the diffusive coefficient of *meta*-DEB in ZSM-5 channels is far smaller compared with that of PDEB. This difference leads to another type of selectivity termed 'configurational diffusion selectivity'. The acid sites on the external surface of ZSM-5 zeolite do not have any selectivity towards PDEB. They are responsible for the formation of *meta*- and *ortho*-DEBs. It is then obvious that in order to directly synthesize PDEB with HZSM-5 zeolite, modification is definitely necessary to be employed to precisely adjust the acidity, diffusivity, and to passivate the external surface of the zeolitic crystals. Besides, the use of large crystallite ZSM-5 zeolites has been proved helpful in enhancing the PDEB selectivity because, compared with their small crystallite analogs, the large crystallites have fewer external surface sites for nonselective reactions, and have stronger geometric constraints on the bulky, slowly diffusive *meta*- and *ortho*-isomers (1).

In the literatures pertaining to *para*-selective catalysis, various modification methods have been proposed to enhance the *para*-selectivity of HZSM-5 zeolites. Briefly, the proposed methods include steaming, oxide-impregnation, chemical vapour deposition (CVD) silica, and even the isomorphous substitution of the framework Al atoms of ZSM-5 with heteroatoms such as Sb, As, etc. One can refer to literatures (1-8, 12-13, 14-16) for details. Based on these researches, several modified large-crystal HZSM-5 zeolite (i. e.,  $\geq 1\mu\text{m}$ ) have been successfully commercialized to produce PDEB, and the fundamental of the *para*-selective catalysis has also been discussed. However, there is virtually no open report regarding the commercial PDEB catalysts. Moreover, controversies still exist in understanding the roles of the geometric constraints (the diffusivity), the acidity, and the external surface of the zeolite.

In this chapter, we intend to discuss the synthesis of PDEB via the alkylation of

ethylbenzene with ethylene and industrial alcohol over a modified HZSM-5 zeolites mainly based on our previous work. The emphasis is aimed at the modification of large-crystal HZSM-5 zeolites ( $\geq 1\mu\text{m}$ ) and the applications of commercial PDEB catalysts. In order to gain insight into the catalysts, the sorption properties/diffusivity, the acidity and the external surface of the catalysts, are discussed. Finally, we also intend to make a brief introduction of our most recent research in nano-crystal ZSM-5 catalyst. Nano-crystal ZSM-5 zeolite is a potential allowing to prepare *para*-selective catalyst with higher reactivity and better durability.

### Preparation of HZSM-5 Catalyst and Its Selectivity in the Ethylation

For the purpose of practical use, NaZSM-5 zeolites were used in combination with binder, in the form of extrudate. The preferred binder is  $\gamma$ -alumina. The binder content (wt%) and the pellet size of final catalysts were fixed according to the reactor scale and the reaction condition adopted. Thus a HZSM-5 catalyst could be prepared conveniently by ion-exchanging the said NaZSM-5 pellets with a solution containing proton source, for example, the solutions of  $\text{HNO}_3$ ,  $\text{HCl}$  and  $\text{NH}_4\text{NO}_3$ . High-purity ethylbenzene and ethylene were used here to investigate the performances of different HZSM-5 catalysts. The reaction results are summarized in Table 1-4.

Table 1 indicates an obvious crystal size effect on the *para*-selectivity of the HZSM-5 catalysts. Under the reaction condition used, the  $S_{\text{PDEB}}$ , % value with nano-crystal size HZSM-5 (20-50 nm) is only about 30%. The increase in the crystal size of

**Table 1. The *para*-Selectivity of Different HZSM-5 Zeolites**

<i>Template</i>	<i>Crystal size</i>	<i>Si/Al ratio</i> <sup>d</sup>	<i>Crystallinity % (XRD)</i>	<i>n-h/c-h</i> <sup>e</sup>	<i>DEB %</i> <sup>f</sup>	<i>S<sub>PDEB</sub></i> <sup>g</sup>
BA <sup>a</sup>	20-50 nm	12.68	82	1.16	21.09	30.61
EDA <sup>b</sup>	0.5-0.7 $\mu\text{m}$	22.85	119	-	20.70	32.40
without <sup>c</sup>	1-2 $\mu\text{m}$	17.09	95	1.87	20.48	38.11
without	2-4 $\mu\text{m}$	11.78	92	2.80	19.25	39.46
BA	4-6 $\mu\text{m}$	23.83	100	3.40	20.22	40.75

Reaction condition:  $340^\circ\text{C}$ ,  $\text{WHSV}_{\text{EB}}=5.2\text{h}^{-1}$ ,  $\text{EB}/\text{C}_2^-=5$  (molar ratio of ethylbenzene vs. ethylene),  $\text{N}_2/\text{C}_2^-=50/50$  (v/v).

a: butylamine, b: ethylenediamine, c: without organic template, but seeded with BA directed ZSM-5 crystals, d: by chemical analysis, e: the sorption capacity (wt %) ratio of hexane vs. cyclohexane, measured gravimetrically at 5h for n-h and 12h for c-h under the condition of  $25 \pm 0.1^\circ\text{C}$ , flowing state, f: the area percentage of DEB in liquid product, g: the selectivity of PDEB in DEB.

the HZSM-5 catalysts results in an increase in the  $S_{\text{PDEB}}$ , % value. The HZSM-5 with a crystal size of 4-6  $\mu\text{m}$  can be seen having a  $S_{\text{PDEB}}$ , % value of higher than 40%.



**Table 2. Thermodynamic Equilibrium of DEB isomers (I)**

<i>Temp.</i> , °C	<i>para</i>	<i>meta</i>	<i>ortho</i>
200	31.3	53.7	15.0
300	29.8	52.7	17.5
400	28.5	52.0	19.5

**Table 3. The Effect of Temperature on the Selectivity of HZSM-5(4-6 $\mu$ m)**

<i>Tempure</i> °C	<i>DEB</i> %		<i>S<sub>PDEB</sub></i> %		<i>By-P/DEB</i> <sup>a</sup>	
	<i>30 min</i>	<i>60min</i>	<i>30min</i>	<i>60min</i>	<i>30min</i>	<i>60min</i>
240	1.11	0.08	74.77	–	0.30	3.00
280	6.22	1.69	58.36	69.23	0.38	0.66
320	19.81	18.20	44.62	48.57	0.74	0.46
360	20.62	19.95	34.04	32.93	1.58	1.45
400	6.38	8.17	14.73	18.73	10.38	7.27

Reaction condition:  $WHSV_{EB}=5.2h^{-1}$ ,  $EB/C_2^-=5$  (mole),  $N_2/C_2^-=50/50$ (v/v)

a: the ratio of by-products vs. DEB (area ratio).

**Table 4. The Effects of  $WHSV_{EB}$  and  $EB/C_2^-$  on the Selectivity of HZSM-5(4-6 $\mu$ m)**

	<i>WHSV<sub>EB</sub></i> $h^{-1}$ <sup>a</sup>			<i>EB/C<sub>2</sub><sup>-</sup></i> , molar ratio <sup>b</sup>		
	<i>2.6</i>	<i>5.2</i>	<i>10.4</i>	<i>2</i>	<i>5</i>	<i>14</i>
DEB %	14.67	19.95	20.09	19.57	19.95	16.61
<i>S<sub>PDEB</sub></i> %	26.79	32.93	48.30	31.22	32.93	32.26
By-P/DEB	2.88	1.45	0.86	1.58	1.45	1.96

a: reaction condition: 360°C,  $EB/C_2^-=5$  (mole),  $N_2/C_2^-=50/50$ (v/v).

b: reaction condition: 360°C,  $WHSV_{EB}=5.2h^{-1}$ ,  $N_2/C_2^-=50/50$ (v/v).

According to Table 2, the  $S_{PDEB}$ , % value of the nano-catalyst is quite near the equilibrium value, while those of the micro-level catalysts are all beyond the equilibrium value. On the other hand, the difference in crystal size influencing the sorption performance of the catalysts has been confirmed (Table 1). Reasonably, the increase of the sorption capacity ratio of normal hexane and cyclohexane, i.e., the relative sorption capacity n-h/c-h, with crystal size is an indication of the strengthening of the channel geometric constraints of the larger crystallites. The increase of the channel geometric constraints enhances the said configurational diffusion selectivity, which might be one of the basic reason why the larger crystallites

of HZSM-5 produce less *meta*- and *ortho*-DEBs, and increase the  $S_{\text{PDEB}}$ , % value, as compared with the smaller ones.

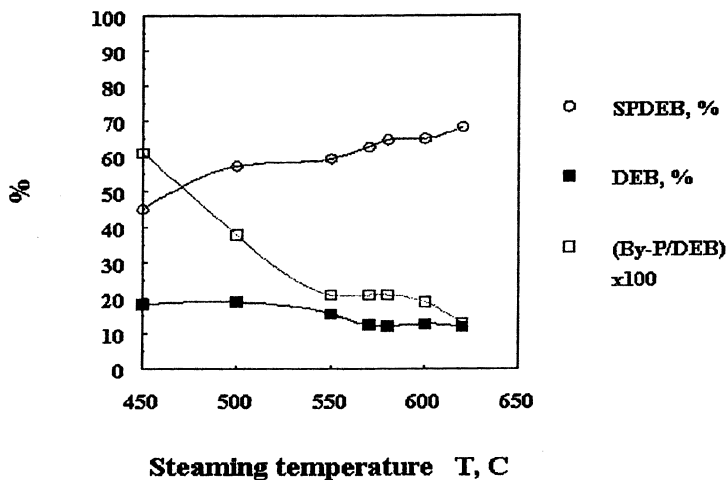
It has been indicated that the reaction condition also has an influence on the  $S_{\text{PDEB}}$ , % value of HZSM-5 catalysts (1). The influence may be seen from the reaction results obtained from HZSM-5 zeolite with the crystal size of 4–6  $\mu\text{m}$  ( Table 3 and 4). Generally speaking, reaction temperature is the primary factor. The higher the temperature, the lower the  $S_{\text{PDEB}}$ , % value, and vice versa. Next comes  $\text{WHSV}_{\text{EB}}$ . Contrariwise, the increase of the  $\text{WHSV}_{\text{EB}}$  is accompanied by an increase in the  $S_{\text{PDEB}}$ , % value. However, it can be inferred that even under optimal conditions, the  $S_{\text{PDEB}}$ , % value of a HZSM-5 catalyst would not be expected to go beyond ca. 60%, namely twice the thermodynamic equilibrium value. Thus, according to Keating's definition (1), HZSM-5 catalysts are generally non-*para*-selective catalysts. Meanwhile, it should also be remembered that to adjust the  $S_{\text{PDEB}}$ , % value of a HZSM-5 catalyst by temperature and the  $\text{WHSV}_{\text{EB}}$  may frequently be restricted because of the problems in engineering and in the performance of the catalysts (reactivity and durability). Therefore, the modification of HZSM-5 catalysts is a good idea. In the following paragraphs, the effects of some commonly used modification methods on the performances of HZSM-5 catalysts are summarized.

### High Temperature Steaming

To HZSM-5 catalyst pellets, said steaming treatment can easily be achieved by forcing, at a temperature of no less than 500°C, the steam-gas or its mixture with inert gas ( for example,  $\text{N}_2$  ) to pass through the catalyst bed for a period of time. Steaming treatment can improve the acid distribution of the catalysts. It can also reduce the pore dimension, increase the channel tortuosity and consequently strengthen the channel geometric constraints of the catalysts. All these effects are commonly attributed to the removal of the Al atoms from zeolitic lattice during steaming. A detailed study on the Al removal in steamed HZSM-5 catalysts has been reported by Kerr ( 19 ). The investigations on steaming conditions have also been reported (20–22), which disclosed the primary effect of the steaming temperature.

The reaction performance of a steamed HZSM-5 zeolite ( 1–2  $\mu\text{m}$ , Si/Al ratio is 17.) in the alkylation of ethylbenzene with ethanol ( 95% v/v ) is depicted in Figure 1. In this case, the steaming treatment was carried out with pure steam-gas at  $\text{WHSV}_{\text{H}_2\text{O}} = 3 \text{ h}^{-1}$  for 3 h, with the steaming temperature varied from 450°C to 620°C. This figure indicates that the most notable changes in performance of the catalysts caused by steaming are the boost of the  $S_{\text{PDEB}}$ , % value and the decline of the By-P/DEB ratio. In fact, at 450°C the steamed catalyst displays no change in product distribution, compared with its mother zeolite. Beyond it, however, the  $S_{\text{PDEB}}$ , % value increases steadily while the By-P/DEB ratio declines first rapidly when the temperature varies from 450°C - 550°C, and then slowly at higher temperatures. At relatively moderate temperatures, the steaming treatment seems to have no harm to the catalyst's alkylation activity. At elevated temperatures, however, the catalyst's alkylation activity is reduced as suggested by the visible decrease of the DEB, % value. There is no doubt that the use of the appropriate steaming treatment can not only benefit the direct synthesis of PDEB, but also favor the suppression of side-reactions.

**Figure 1. The Effect of Steaming on the Reaction Performance of HZSM-5 (1-2  $\mu\text{m}$ , Reaction Condition: 340°C,  $\text{WHSV}_{\text{Feed}}=8 \text{ h}^{-1}$ , EB/EtOH = 8 in Molar Ratio)**

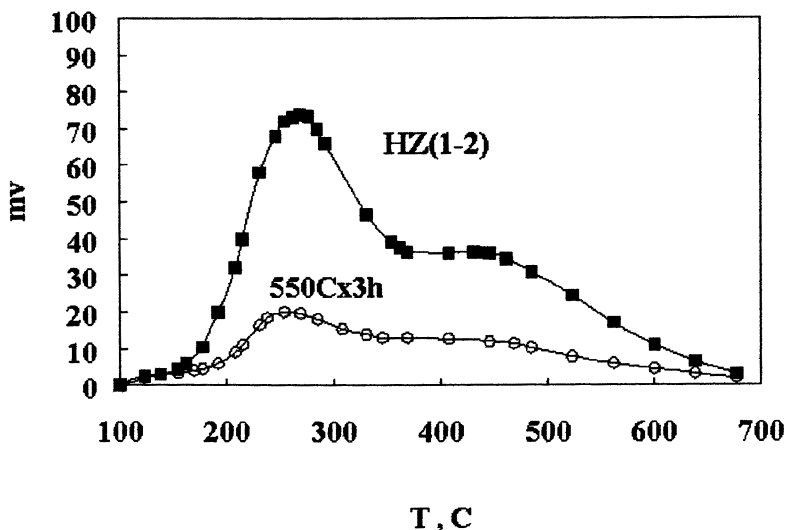


Another positive function the steaming treatment produced, although less perceivable, is to slow down the coke-depositing rate, and thereby increase the catalyst's durability. The effect of steaming condition on the average coke content of the toluene disproportionation catalysts has been studied by Ashton et al. (19).

From Figure 2 and Table 5 it is easy to see that the steaming treatment mainly results in the decreases in the catalyst's total acid amount and the overall acidic strength, and the increases in the sorption capacity ratio and the relative diffusivity of n-h and c-h, viz.  $D_n/D_c$ . The changes of the sorption and diffusion parameters confirmed that the channel geometric constraints are enhanced in the steamed sample. This enhancement together with the changes in acidity may well be the causes leading to the improvements of the catalyst's reaction performances. In our previous publication (21), the relationships of reaction properties with acidity and diffusivity in a series of steamed catalysts were studied in detail.

Generally speaking, in order to prepare a *para*-selective catalyst for the alkylation of ethylbenzene with ethylene, it is very helpful to treat the HZSM-5 zeolite with steaming method. In our opinion, the optimum steaming temperature range is ca. 500- 600°C. So treated, the catalyst will most probably exhibit a *para*-selectivity of ca. 60-70%, and become a *para*-selective catalyst as Keating termed (1). Although higher *para*-selectivity may be reached by steaming treatment, the expansion of the catalyst's activity would be high, so this treatment usually serves as a pre-modification method (1, 3, 8).

**Figure 2. NH<sub>3</sub> TPD Profiles of H-Type and Steamed HZSM-5 (1-2 μm)**



**Table 5. Diffusivity Data of Catalysts with or without Steaming Treatment <sup>a</sup>**

Catalyst	Sorption Capacity, wt%			$D/r^2$ , $S^{-1}$		Dn/Dc
	n-h	c-h	n-h/c-h	n-h $\times 10^3$	c-h $\times 10^6$	
HMFI(1-2μm)	8.91	4.76	1.87	1.1422	15.85	72.06
550°C, 3h	8.85	4.52	1.96	2.0360	18.75	108.59

a; in  $D/r^2$ , D stands for the diffusion coefficient, while  $r$  the radius of the spherical crystallite. The  $D/r^2$  value was calculated based on the Fick' second law and the measurements of the uptake rates of n-h and c-h by gravimetric method.

### Cations or Anions- impregnating

Impregnation with various cations or anions-containing solution provides rich opportunities to raise the *para*-selectivity of HZSM-5 zeolites. After being impregnated, dried and calcined, the cations or anions are converted into their corresponding oxides and then 'cover' on the surface of the catalysts ( including the interior part and the exterior part). These guest species have two chief functions, one is to cover the surface acid sites, the other is to narrow the channels and the pore openings. There are a great deal of literatures ( 25) relating to the impregnation of

HZSM-5 zeolites, and the effects of the modification on the physicochemical properties and catalytic performances of the catalysts. With regard to the *para*-selectively catalytic ethylation of ethylbenzene, P, Mg, La or the mixture of rare-earth elements impregnated HZSM-5 catalysts prove to be more effective.

**Impregnation onto a virgin HZSM-5.** Table 6 lists the reaction results of La, Mg, Fe, P single-oxide impregnated HZSM-5 catalysts. It can be seen that the cations- or anion-impregnation can significantly increase the *para*-selectivity of HZSM-5 zeolite.

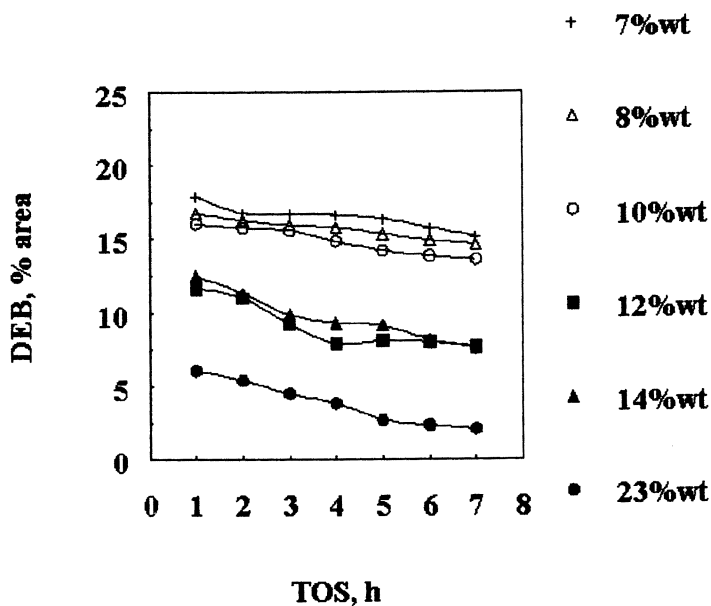
**Table 6. The Ethylation over HZSM-5 Impregnated with Different Oxides (2-4 $\mu$ m, Si/Al = 17) \***

Modification		Reaction properties		
modifier	Loading, wt%	DEB%, area	S <sub>PDEB</sub> %	By-P/DEB
without	—	20.94	45.56	0.41
La <sub>2</sub> O <sub>3</sub>	7	16.64	80.89	0.25
	12	9.67	96.90	0.18
	14	9.31	100	0.13
	23	3.85	100	0
MgO	5	15.51	90.26	0.16
	8	9.26	97.30	0.10
	10	7.44	100	0.09
	15	3.87	100	0.10
Fe <sub>2</sub> O <sub>3</sub>	4	20.24	65.98	0.30
	6	16.12	70.63	0.25
	8	14.98	74.95	0.22
P <sub>2</sub> O <sub>5</sub>	5	20.11	55.89	0.33
	10	18.33	64.19	0.28
	15	16.07	77.22	0.22

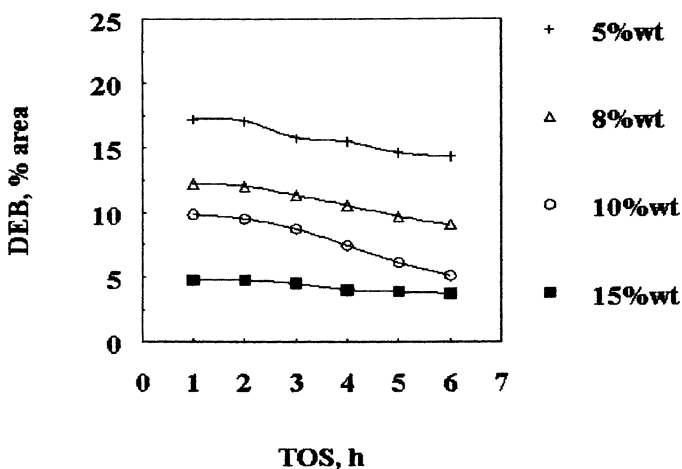
\* Reaction condition: 370°C, WHSV<sub>EB</sub> = 6h<sup>-1</sup>, EB/C<sub>2</sub> = 5-6 (mole), N<sub>2</sub>/C<sub>2</sub> = 50/50 (v/v); La<sub>2</sub>O<sub>3</sub>, MgO, Fe<sub>2</sub>O<sub>3</sub> are introduced by their corresponding nitrates, P<sub>2</sub>O<sub>5</sub> is introduced by 85% phosphorous acid, all the chemicals used are in A. R. Purity.

Relatively speaking, the increments of the *para*-selectivity against the oxide loading are less notable in the case of P<sub>2</sub>O<sub>5</sub>-modified HZSM-5 catalysts, while in the case of MgO-modified HZSM-5 catalysts, they are more pronounced. Similar to the steaming method, the impregnation method is also propitious to eliminate the side-reactions, as the By-P/DEB parameter would indicate. Whereas, there are disadvantages with impregnation modification, i.e., the loss of the catalytic activity and the retrogression of the catalyst durability. The latter can be seen from Figure 3 and 4. Fortunately, these disadvantages can be partly avoided by choosing the appropriate modifier and by limiting the oxide loading.

**Figure 3. The Reaction Stability of HZSM-5 Zeolites Impregnated with Different Amount of  $\text{La}_2\text{O}_3$  (Reaction Condition see Table 6.)**



**Figure 4. The Reaction Stability of HZSM-5 Zeolites Impregnated with Different Amount of  $\text{MgO}$  (Reaction Condition see Table 6.)**



**Impregnation onto a Pre-modified HZSM-5** The pre-modification method employed here is steaming combined with metal ion-exchanging. The pre-modified HZSM-5 (1 $\mu$ m, Si/Al = 17) is denominated 'DGA'. The catalytic properties of DGA and P<sub>2</sub>O<sub>5</sub> (originated from 85% phosphorous acid) impregnated DGA are summarized in Table 7. The NH<sub>3</sub>TPD profiles and the sorption capacities of this series of catalysts are given in Figure 5 and Table 8.

Table 7 indicates that DGA catalyst has a DEB % value of about 15%. During the time scale concerned, the DEB % value of DGA is rather stable. The S<sub>PDEB</sub> % value of DGA is about 84%. After being further modified by P<sub>2</sub>O<sub>5</sub>, the S<sub>PDEB</sub> % value increases steadily and obviously with the increase of the P<sub>2</sub>O<sub>5</sub> loading, which is accompanied by the decreases of the DEB % value. However, the decreases are gentle, and in each P<sub>2</sub>O<sub>5</sub>-impregnated sample, the reaction stability of DGA catalyst can be seen well succeeded. This virtue is important to the making of the practical catalysts.

**Table 7. The Effect of P<sub>2</sub>O<sub>5</sub>-Impregnation on the Performance of Catalyst DGA\***

Modification		TOS, h						
		1	2	3	4	5	6	7
DGA	DEB %	15.27	15.15	15.03	15.10	14.94	15.20	15.16
	S <sub>PDEB</sub> %	83.58	83.40	84.12	84.32	85.00	84.67	84.52
2	DEB %	15.30	15.02	15.00	15.10	14.77	14.80	14.91
	S <sub>PDEB</sub> %	88.32	89.57	89.36	89.73	89.85	88.98	89.62
4	DEB %	15.32	15.20	15.45	15.59	15.41	15.06	14.48
	S <sub>PDEB</sub> %	91.58	90.99	92.85	92.58	93.15	93.35	93.48
6	DEB %	14.55	14.40	14.38	14.04	14.09	13.76	13.85
	S <sub>PDEB</sub> %	95.50	95.26	95.77	95.21	95.41	96.15	96.03
8	DEB %	13.25	13.81	13.61	13.47	13.86	13.59	12.85
	S <sub>PDEB</sub> %	95.26	95.68	96.42	96.02	95.10	95.61	95.82
10	DEB %	12.70	12.32	12.10	12.05	11.73	11.38	11.34
	S <sub>PDEB</sub> %	97.56	97.70	97.60	97.60	97.50	97.73	97.77
12	DEB %	11.23	11.65	12.12	11.99	11.62	10.92	11.34
	S <sub>PDEB</sub> %	98.30	98.34	98.46	98.60	98.90	98.25	98.50

\* DGA is a HZSM-5 (SiO<sub>2</sub>/Al<sub>2</sub>O<sub>3</sub>  $\approx$  34, 1 $\mu$ m) modified by steaming and metal ion-exchanging; reaction condition: 340°C, WHSV<sub>EB</sub> = 5h<sup>-1</sup>, EB/C<sub>2</sub><sup>o</sup> = 6 (mole), N<sub>2</sub>/C<sub>2</sub><sup>o</sup> = 5.

NH<sub>3</sub>TPD measurements disclose that the further P<sub>2</sub>O<sub>5</sub>-impregnation has resulted in the remarkable decreases of the acid amount and the acid strength of DGA in the cases of P<sub>2</sub>O<sub>5</sub>-loading being no more than 6%wt. When the P<sub>2</sub>O<sub>5</sub>-loading exceeds 6%wt, no further change in acidic distribution could be observed in fact. On the other hand, the measurements of the sorption capacity indicate that the impregnation of P<sub>2</sub>O<sub>5</sub> onto DGA leads to a continual rise of the n-h/c-h ratio throughout the P<sub>2</sub>O<sub>5</sub>-loading range investigated. In both the low P<sub>2</sub>O<sub>5</sub>-loading region, ca. less than 4%wt and the high P<sub>2</sub>O<sub>5</sub>-loading region, ca. more than 10%wt, the

Figure 5.  $\text{NH}_3$ TPD Profiles of  $\text{P}_2\text{O}_5$ -impregnated DGA Catalyst Series

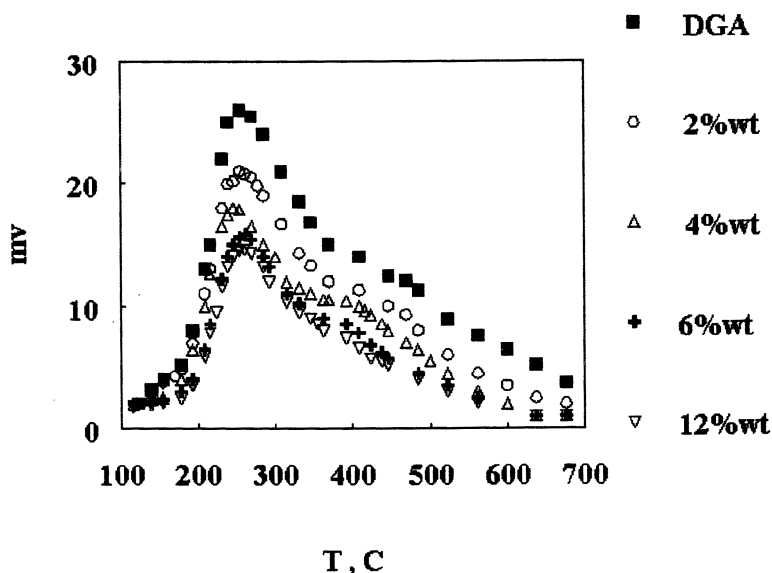


Table 8. The Sorption Capacity of the  $\text{P}_2\text{O}_5$ -impregnated DGA

$\text{P}_2\text{O}_5$ , wt%	—	2	4	6	8	10	12
$S_{\text{PDEB}}$ , %	84.12	89.36	92.85	95.77	96.42	97.60	98.46
n-h/c-h	2.14	2.28	2.71	3.86	4.20	4.55	4.61

increments of the n-h/c-h ratio are smaller, while in between them, the increments of the n-h/c-h ratio are bigger. From these phenomena, it may be concluded that, when the  $\text{P}_2\text{O}_5$ -loadings were lower, phosphorous species were randomly deposited to the interior and the exterior parts of the zeolitic surface. In those cases the phosphorous species had relatively stronger effect on the depressing of surface acidity. As the  $\text{P}_2\text{O}_5$ -loading being increased and the zeolitic channels getting narrower, more and more phosphorous species were forced to be deposited onto the neighborhood of pore openings as well as the external surface of the catalyst. In these cases, the influence of the phosphorous species on surface acidity ceased to increase, but the outdoor phosphorous species were still able to adjust the effective pore size by partly shielding off the pore openings of the zeolite, the pore size adjustment seems to get weak when the  $\text{P}_2\text{O}_5$ -loading is too high, ca. beyond 10%wt.

Generally speaking, the above-mentioned changes in the catalysts' physicochemical properties are quite general in HZSM-5 catalysts modified by cations- or anions-impregnation. These changes coincide with the change of the catalysts' *para*-selectivity, which seems to indicate that the enhancement of the



catalysts' *para*-selectivity is a synergic effect of the acidity and geometric constraints. The same connection can be observed with the steamed catalysts. With regard to the impregnation method, the reason why the impregnation of a pre-modified HZSM-5 differs from the direct impregnation of a virgin HZSM-5 is not very clear, although the similar bi-oxides impregnated (in succession) HZSM-5 zeolites as *para*-selective catalysts have already been recommended in literatures (1-3, 22-24). On the other hand, it has been observed that, in addition to the property of the resulting oxide itself, the state of the agent in aqueous solution, the concentration, PH value of the solution, and the impregnation condition such as temperature and times, are all important to the modification effects. In case of a high oxide-loading being needed, like the aforementioned cases in which at least 6%wt P<sub>2</sub>O<sub>5</sub>-loading are needed in order to obtain a PDEB selectivity of no less than 95%, it is better to accomplish the impregnation at ca. more than two times. Such an operation will benefit the catalyst's activity and durability. However, the complicated modification process will increase the cost of catalyst and decrease the preparation repeatability if it is employed to produce commercial catalyst.

### External Surface Reaction with Organosilicon Compound

A good way leading to this type of modification is to use the chemical vapor deposit (CVD) SiO<sub>2</sub> method which was first proposed by Niwa et al. (14-16). The CVD method may be interpreted as follows: at a suitable temperature, the vapor of the organosilicon compound such as tetramethyl ortho-silicate (0.89nm) and tetraethyl ortho-silicate (0.96nm) is carried to contact with the catalyst by inert gas like N<sub>2</sub> and He. In catalyst bed, the organosilicon molecules react with the surface acid sites and then bond with surface Al atoms probably in the form of (RO)<sub>3</sub>Si-O-Al≡. Here, R stands for alkyl groups. After being calcined, these surface species are converted into numerous inert silica molecules which cover right on the acid sites and deactivate them. The core of the CVD method is the uses of the bulky organosilicon compounds which are too large to enter the channels of HZSM-5. The CVD method has two effects on the catalyst modified: one is the selective elimination of the external acid sites, the other is the precise controlling of the pore openings' size. Obviously, the CVD method can enhance the *para*-selectivity of HZSM-5 zeolite by eliminating the non-selective acid sites, and by strengthening the geometric constraints of the pore openings.

Another simple way to reach the similar modification effect is to carry out said surface reactions in liquid phase, which is accordingly called chemical liquid deposit (CLD) silica. Details of the CLD method may be seen in ref. (25-27).

The use of the improved, *in situ* CVD methods to prepare *para*-selective catalysts (based on large crystal ZSM-5 zeolites) for the direct synthesis of PDEB by the disproportionation and the ethylation of ethylbenzene, have been reported by IKAI WANG, et al. (4, 8) and Halgeri, et al. (5-7). In these CVDs, a little amount of water, either directly fed or indirectly produced, was used to speed the decompositions of the organosilicon molecules. The use of water molecules might have resulted in the deposit of SiO<sub>2</sub> into the zeolitic channels because the decomposition product might contain small organosilicon species which could enter the channels of HZSM-5. In this aspect, these *in situ* CVD methods are special.

In our previous study (28), a SiO<sub>2</sub>-depositing method similar to the CVD method proposed by Niwa, et al. was used to modify a HZSM-5 zeolite. The modified catalysts (by using tetraethyl ortho-silicate) were characterized by sorption capacity (adsorbates including H<sub>2</sub>O, n-h, c-h), N<sub>2</sub>-BET specific area measurement, NH<sub>3</sub>TPD, 1, 3, 5-trimethylbenzene cracking reaction, and the ethylation of ethylbenzene with ethanol. The amount of SiO<sub>2</sub> deposited by the method employed varied from 0.43%wt to 1.45%wt. The characterizations showed that, in the whole SiO<sub>2</sub>-loading range, virtually no changes could be observed in the deposited catalysts with respect to the sorption capacities of H<sub>2</sub>O, n-h and the specific area of the catalysts. However, several changes did occur to the catalysts: (1). The uptake rate of c-h obviously decreased when the SiO<sub>2</sub>-loading increased from 0%wt to 0.43%wt, and to 1.41%wt; (2). There was no significant difference among the catalysts with SiO<sub>2</sub>-loading of 0%wt, 0.43%wt, 1.03%wt and 1.31%wt, respectively. But when the SiO<sub>2</sub>-loading increased from 0%wt to 0.43%wt, a visible decrease in the intensity of the high-temperature desorption peak appeared. It is interesting that, when the SiO<sub>2</sub>-loading increased from 0.43%wt to 1.31%wt, the intensity of said high-temperature desorption peak ceased to get weak, instead, the intensity of the low-temperature desorption peak began to drop visibly; (3). The cracking of 1, 3, 5-trimethylbenzene (TMB) indicated that, under the condition of 500°C, WHSV<sub>TMB</sub> = 2.4 h<sup>-1</sup>, carrier gas N<sub>2</sub> flow rate equaled 40 ml/min and TOS = 60 min, the cracking activity of the deposited catalysts decreased from 54.12% to 2.82% and to 1.76% when the SiO<sub>2</sub>-loading increased from 0%wt to 0.40%wt and to 1.45%wt; (4). The ethylation of ethylbenzene with ethanol further indicated that, under the condition of 340°C, WHSV<sub>EB+EtOH</sub> = 6h<sup>-1</sup>, EB/EtOH = 10 (molar ratio) and TOS = 120min, the PDEB selectivity of the deposited catalysts increased from 38.56% to 51.02% and to 58.02% when the SiO<sub>2</sub>-loading increased from 0%wt to 0.53%wt and to 1.05%wt. In the same sequence, only a minor decrease of the ethylbenzene conversion could be observed.

The above-mentioned experiment demonstrates that, during the course of SiO<sub>2</sub>-depositing onto HZSM-5 zeolite, the tetraethyl ortho-silicate molecules preferentially react with the strong acid sites, as a result, the surface strong acid sites were deactivated preferentially and the intensity of the high-temperature peak in the TPD profiles decreased first. The deposit of SiO<sub>2</sub> takes place solely on the external surface of HZSM-5 zeolite, this explains why the changes in the acidity of different samples were not that big like in the cases of steamed or oxide impregnated HZSM-5 zeolites. When the strong acid sites on the external surface disappeared, the deposit of SiO<sub>2</sub> began to occur onto the relatively weaker acid sites. In the aforesaid examples, as the SiO<sub>2</sub>-loading increased, the number of the acid sites on the external surface decreased rapidly, which was confirmed by the reduction of the 1, 3, 5-trimethylbenzene cracking activity. On the other hand, the pore opening size decreased gradually, which could be observed by the change of the c-h uptake rate. The relatively rapid disappearance of the 1, 3, 5-trimethylbenzene cracking activity at a low SiO<sub>2</sub>-loading of ca. 1.45%wt, suggests that the quotient of the external acid sites in the case of large-crystal HZSM-5 zeolite is rather small, but the catalytic activity of these acid sites should not be ignored, as the cracking activity of HZSM-5 zeolite would indicate. To eliminate these non-selective acid sites, approximately 2-3%wt SiO<sub>2</sub>-loading is enough. From the relatively slow decrease in c-h uptake rate, it is reasonably believed that the CVD method allows a precise pore size adjustment. Finally, the similarities of the H<sub>2</sub>O, n-h sorption capacity, and the similarity of the N<sub>2</sub>-

BET specific area among the samples having different SiO<sub>2</sub>-loading, suggest that the blockage of the pore openings in said SiO<sub>2</sub>-loading range does not occur to a pronounced degree. To summarize the experiment, the effects of the CVD silica method on the physicochemical properties of HZSM-5 zeolite are primarily the elimination of the external acid sites and the reduction of the pore opening size. On the other hand, the effect of the CVD silica method on the catalytic performance of HZSM-5 zeolite is mainly the enhancement of the catalyst's *para*-selectivity. In a HZSM-5 deposited with 1.05%wt SiO<sub>2</sub>, the external acid sites of the resulting catalyst were substantially suppressed. Its PDEB selectivity increased from 38.56% to 58.02%, while its ethylbenzene conversion decreased very little. Generally speaking, one feature concerning CVD silica modification is that the method has relatively small effect on the activity of the modified catalyst. The elimination of the external acid sites and the strengthening of the geometric constraints as a result of the adjustment of the pore opening size are the ultimate causes of its *para*-selectivity increase.

The deposit of SiO<sub>2</sub> onto HZSM-5 by said CLD silica method was also studied. In this case, the mother catalyst was pre-modified by steaming method and the ethylation was carried out by using ethylbenzene and ethylene instead. The catalytic performances of this series of catalysts are listed in Table 9. Obviously, CLD

**Table 9. The Effect of CLD SiO<sub>2</sub> on the Performance of WZ (TOS = 4h) \***

<i>Catalyst</i>	<i>DEB%, area</i>	<i>S<sub>PDEB</sub>%</i>	<i>By-P/DEB</i>
WZ	17.51	65.11	0.23
WZ+3%wt SiO <sub>2</sub>	14.59	77.31	0.22
WZ+5%wt SiO <sub>2</sub>	14.69	78.91	0.21

\*WZ is a HZSM-5 catalyst (Si/Al = 17, 1-2μm) steamed at 550°C, 3h; the weight per cent of SiO<sub>2</sub> here stands for the amount of tetraethyl ortho-silicste added to the CLD solution (expressed by SiO<sub>2</sub>%wt); reaction condition: 340°C, WHSV<sub>EB</sub> = 5.2h<sup>-1</sup>, EB/C<sub>2</sub><sup>-</sup> = 5 (molar ratio), C<sub>2</sub><sup>0</sup>/C<sub>2</sub><sup>-</sup> = 20/80 (v/v).

silica method is also effective with respect to the elevation of the catalyst's PDEB-selectivity. For example, when the SiO<sub>2</sub> added reaches 3%wt, the deposited catalyst displays some 10 per cent increment in PDEB selectivity on the basis of its mother catalyst WZ. When the SiO<sub>2</sub> added reaches 5%wt, however, there is no further notable increase in the catalyst's *para*-selectivity. This may be interpreted as that, when the SiO<sub>2</sub> added is excessive, the excessive part of the organosilicon compound can not be able to take part in the surface reaction because, as the aforesaid study would suggest, the external acid sites may be completely suppressed already. So, the real SiO<sub>2</sub>-loading may not increase in this case actually. This phenomenon may be a reflection of the limit of CLD or CVD silica method, owing to which the pore opening size of the catalyst modified can not be expected to be adjusted narrow enough to completely stop the diffusion of the *meta*-DEB, so the *para*-selectivity of the catalyst modified is not likely to be elevated to a very high level solely by said CVD or CLD

silica method. From Table 9, it can also be noted that the deposit of silica onto the external surface of the catalyst has little effect on suppressing the side-reactions. This may be another feature of CVD or CLD.

### Combined Modifications

The foregoing discussions reflect that the *para*-selectivity of a modified HZSM-5 catalyst relates to its acidity ( especially, acid strength), diffusivity or channel geometric constraints (channel tortuosity and pore opening size) and external non-selective acid sites. By using the aforementioned modifications, these parameters can be adjusted, but the degrees will mainly depend on the method used. On the other hand, it would be found that, by using a combined modifications, one can have relatively more freedom in adjusting all these parameters so as to make the *para*-selective catalyst more effective. A combined modifications is the combination of the basic modification methods which include the above-mentioned high-temperature steaming, cations- or anions-impregnation, and the deposit of silica onto a catalyst's external surface (CVD or CLD ). In Table 10, the physicochemical properties and the PDEB selectivity values of a HZSM-5 (1-2 $\mu$ m, Si/Al = 17) as well as its modification products, obtained by different combined modifications, are condensed. The goal of these investigations is to search for those promising combinations of the modification methods for the preparations of commercial PDEB catalysts which are expected to be suitable for use in the ethylations of ethylbenzene with ethylene and ethanol. For economic reason, a commercial PDEB catalyst should have not only a very high *para*-selectivity, but also a reasonable DEB spatio-temporal yield, an acceptable one-cycle operation time as well as a long enough life-span. These parameters are primarily decided by the catalyst's activity, anti-deactivation ability, coke-burning performance and thermal/hydrothermal stability ( including mother ZSM-5 zeolite and modifiers). In Table 11, the different modes of the combined modifications used in the preparations of HZ-A to HZ-D are summarized.

**Table 10. The Effect of Combined Modifications on the Properties of HZSM-5 (1-2  $\mu$ m) \***

<i>catalyst</i>	<i>n-h/c-h</i>	<i>Dn/Dc</i>	$S_{TPD \geq 377^\circ C}$ , <i>mm<sup>2</sup></i>	<i>external acid sites, mmol/g</i>	<i>DEB, %</i>	$S_{PDEB}$ <i>%</i>
HZ	1.87	72	620	0.08	21.11	48.84
HZ-A	1.96	108	270	—	15.99	65.48
HZ-B	2.03	—	290	0.02	20.50	73.34
HZ-C	2.24	—	240	0.02	18.60	78.57
HZ-D	4.89	335	250	0.03	12.66	98.17

\* HZ stands for HZSM-5 (1-2  $\mu$ m, Si/Al = 17), others are modification products of HZ sampled after different modification combination;  $S_{TPD \geq 377^\circ C}$  stands for the high-temperature peak area of the  $NH_3$ TPD profiles, which was calculated from  $T \geq 377^\circ C$ , sample net weight:  $0.2 \pm 0.0005g$ ; 'external acid sites' was measured by an improved Hammett indicator method by using cyclohexylamine as probe molecule.

**Table 11. The Modes of Combined Modifications for HZ Catalyst Series\***

<i>Catalyst</i>	<i>Modification Mode</i>
HZ-A	steaming
HZ-B	steaming→acid-dipping + CLDSiO <sub>2</sub>
HZ-C	steaming→acid-dipping + CLDSiO <sub>2</sub> →Ra <sup>+n</sup> -impregnation
HZ-D	steaming→acid-dipping + CLDSiO <sub>2</sub> →Ra <sup>+n</sup> -impregnation→impregnation

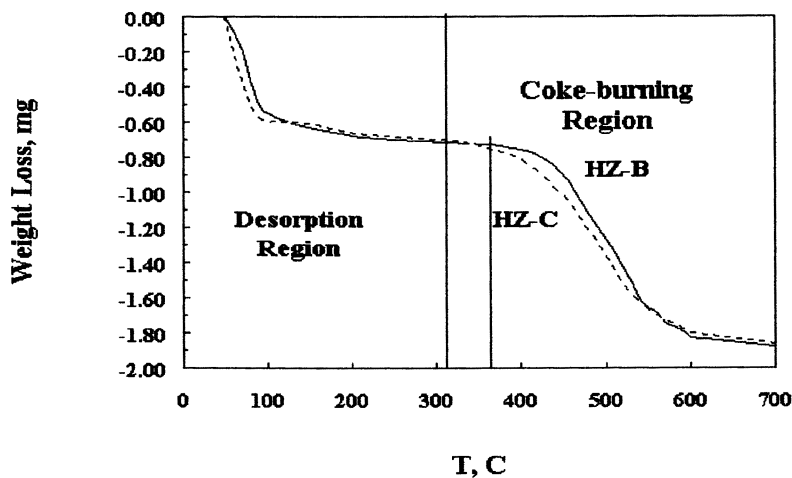
\* Ra<sup>+n</sup> stands for a mixture of rare-earth cations, mainly La<sup>+3</sup> and Ce<sup>+4</sup>.

In Table 10, it can generally be found that the herein listed combined modifications have caused not only the significant decreases in both of the total acid strength (measured by the amount of the strong acid sites,  $S_{\text{TPD}\geq 377^{\circ}\text{C}}$ , mm<sup>2</sup>) and the external acid site number of HZ, but also the significant increases in both of the catalyst's relative sorption capacity (n-h/c-h) and the relative diffusivity (Dn/Dc). These result in a notable increase in the *para*-selectivity of HZ. Specifically speaking, from HZ to HZ-A, the decrease in the acid strength is quite significant. Whereas the increase of the channel's geometric constraints is relatively small. A complementary experiment showed that the external surface cracking activities of HZ and HZ-A are 1.89% and 1.94% (molar conversion of *meta*-cymene at conditions of 270°C, WHSV = 4h<sup>-1</sup>, Reactant/N<sub>2</sub> molar ratio = 1:5) respectively, which suggests that the amount of the external non-selective acid sites has little change. Thus, in HZ-A, the decrease of the catalyst's acid strength is the main cause of its PDEB selectivity enhancement( from 48.84% to 65.48% ). From HZ-A to HZ-B, on the other hand, the changes in the channel's geometric constraints and the acid strength are trivial, but a great decrease in the number of the HZ-B's external non-selective acid sites can be observed. This may be the main cause of the increase of HZ-B's PDEB selectivity (from 65.48% to 73.34%). Accordingly, the increases of the catalysts' PDEB selectivity in the cases of HZ-C and HZ-D can be attributed mainly to the significant increases in the catalysts' channel geometric constraints. When HZ-D is compared directly with HZ, one can clearly find that, in a very high *para*-selective catalyst, the enhancement of the catalyst's *para*-selectivity is virtually reached by the synergic effect of the strengthening of the channel's geometric constraints, the reduction of the acid strength, and the elimination of the external non-selective acid sites. In this set of examples, while the main purpose is focused on the enhancement of the PDEB selectivity, special attentions are paid to the improvements of the catalyst's activity and anti-deactivation ability ( as would be seen in acid-dipping + CLDSiO<sub>2</sub> step ), and to the improvement of the catalyst's coke-burning performance ( as would be seen in Ra<sup>+n</sup>-impregnation step ). The modification effects can be seen from Table 12-13 and Figure 6. The foregoing results serve as an illustration of the usefulness of the combined modifications in the preparation of catalyst with commercial purpose.

**Table 12. The Activity and Durability of Catalyst HZ-D \***

<i>TOS, h</i>	<i>T</i> °C	<i>DEB</i>	<i>SPDEB%</i>
2	340	13.22	97.90
4	340	13.86	98.15
6	340	12.66	98.17
8	340	12.28	98.21
10	340	12.14	98.30
14	340	11.22	98.28
20	340	10.72	98.37
24	340	10.23	98.35
28	340	9.80	98.44
36	340	9.42	98.23
40	340	9.00	98.55
50	340	8.15	98.61
55	340	8.10	98.54
60	348	8.12	98.02
65	348	8.30	98.13

\* Reaction condition:  $WHSV_{EB}=6.5h^{-1}$ ,  $EB/C_2=5$  (molar ratio),  $C_2^o/C_2^=20/80$  (v/v).

**Figure 6. The TG Coke-burning Curves of HZ-B and HZ-C**

**Table 13. Coke-burning Analysis by TG\***

Catalyst	Ra <sub>2</sub> O <sub>3</sub> , %wt	Coke Content, wt%	Coke-burning Temperature, °C	
			Initial	Final
HZ-B	–	3.20	365	620
HZ-C	1.2	3.00	315	600

\* (1). The coking condition:  $\text{WHSV}_{\text{EB}} = 5\text{h}^{-1}$ ,  $\text{EB}/\text{C}_2 = 6$  (molar ratio), 340°C for 6h followed by  $\text{WHSV}_{\text{EB}} = 5\text{h}^{-1}$ ,  $\text{EB}/\text{C}_2 = 2.5$  (molar ratio), 360°C for 11h. After that the samples were purged *in situ* by N<sub>2</sub> under 360°C for 8h. (2). Ra<sub>2</sub>O<sub>3</sub> stands for a mixture of rare-earth oxides (mainly La, Ce). (3). TG analysis condition: sample net weight: 44–45mg, heating rate = 10°C/min, performed in flowing air.

### Direct Synthesis of PDEB in Units of Industrial Scale

The first PDEB-producing unit in the world was put into use in 1989 in Yanshan Petrochemical Co., Beijing, China. It was in fact a 200tPDEB/a pilot equipment constructed for the ethylation of ethylbenzene with ethylene. Its catalyst, denominated as EA-01, was developed in our laboratory for the purpose of producing PDEB with a 95% *para*-selectivity. Based on EA-01, Other two PDEB-synthesizing catalysts, viz. EA-02 and EA-03, have been developed in order to utilize industrial ethanol and low-purity ethylene as ethylation agents. The preparations of EA catalysts were characterized by applying special tailored combined modifications to a large-crystal (1–2µm), high-silica-alumina-ratio (Si/Al atomic ratio was around 20) zeolite having ZSM-5 topological structure. The practices of these catalysts suggested that the commercially direct syntheses of PDEB with EA catalysts are successful, and that the choices of the reaction conditions can be very important to the performances of these *para*-selective catalysts.

**Performances of EA Catalysts** The EA-01 was practiced in a 200tPDEB/a unit with a two-section fixed bed reactor. Under industrial reaction condition of ca. 300–400°C, 0.1–0.4 MPa,  $\text{EB}/\text{C}_2$  molar ratio equaled 2–3,  $\text{N}_2/\text{C}_2$  molar ratio equaled 3–5, EA-01 displayed a catalytic performance of PDEB average selectivity no less than 95%, EB initial conversion more than 30% (mol.), one-cycle operation time no less than 30 days if the shut-down EB conversion was considered as 9% (mol.). Because of the adoption of said rare-earth cations mixture as modifier, EA-01 showed excellent regeneration performance. Therefore, after initial 5 cycle trial, the pilot unit was kept on running to produce 95% PDEB as *para*-xylene-separation desorbent. By adjusting the combined modifications used for EA-01, a new PDEB industrial catalyst, named EA-02, was developed in our laboratory to produce 96–97% PDEB in the case of ethylation of ethylbenzene with industrial ethanol (95% v/v). Catalyst EA-02 was commercialized in 1992, in a 600tPDEB/a industrial unit with a two-section fixed bed reactor in Dalian Additives Plant, Liaoning, China. The use of industrial ethanol as ethylation agent proved beneficial to the PDEB synthesis in two ways: first, it permits the factory to be built in area where ethylene source is absent; second, it can simplify the feeding system and increase one-cycle operation time of the catalyst. In 1995,

another highly selective PDEB-synthesizing catalyst EA-03 was born in our laboratory and successfully industrialized in a 1000tPDEB/a unit with a one-section fixed bed reactor ( height/diameter ratio equals 1) in Jiangsu Danhua Chemical Group Co., Jiangsu, China. Catalyst EA-03 was developed by following a novel combined modifications so that it was endowed with a 98-99% PDEB selectivity and significant ethyne-poisoning resistibility. The basic features of the EA catalyst series are condensed in Table 14. The ethyne-poisoning resistibility of catalyst EA-03 is demonstrated in Table 15.

**Table 14. The Characteristics of EA Catalyst Series**

<i>Catalyst</i>	<i>EA-01</i>	<i>EA-02</i>	<i>EA-03</i>
Geometric Shape, mm	φ1, cylinder	φ1, cylinder	φ1, shamrock
Compactedness, g/cm <sup>3</sup>	0.6	0.6	0.5
Crush Strength (radial), kgf/cm	20	20	20
Porosity	0.15	0.13	0.10
Sorption Capacity, n-h/c-h	9.15/5.18	8.50/3.91	7.56/1.54
Specific Area, m <sup>2</sup> /g	290	270	191

**Table 15. Reaction Data of Fresh EA-03 Catalyst in 1000tPDEB/a Industrial Unit Under Ethyne-containing Ethylene Feed\***

<i>TOS, h</i>	<i>Temperature</i> °C	<i>Ethyne, ppm</i>		<i>Catalytic Performance</i>	
		<i>In feed gas</i>	<i>In vent gas</i>	<i>DEB%, area</i>	<i>S<sub>PDEB</sub>%</i>
4	370	112530	5600	9.83	98.81
10	360	5210	3800	9.26	99.04
20	360	4800	4180	9.14	98.53
50	362	2100	1150	8.81	98.70
80	365	2590	1450	7.67	98.90
100	360	860	753	6.19	99.22
120	360	4516	2100	8.15	99.34
140	370	1828	720	8.46	99.51
160	370	1911	832	7.29	99.13
180	370	2473	1540	8.31	99.04
200	376	1505	590	7.37	98.46
212	380	1505	467	6.78	99.31
220	375	1183	331	7.02	99.64
232	380	2365	893	7.26	99.54
240	380	4473	2364	6.37	98.42
252	385	360	20	7.67	99.43
310	385	510	89	6.42	99.54

\*WHSV<sub>EB</sub> = 5-7 h<sup>-1</sup>. C<sub>2</sub>= % in ethylene feed is maintained 50-80%v by controlled compensation and discharge, the major balance gases in circulating ethylene are ethane (18-45%v) and C<sub>3</sub>-C<sub>5</sub> light hydrocarbons ( 2-5%v).



### Effects of Reaction Conditions on Performances of Highly Selective Catalysts

Reaction conditions have remarkable influences on the performances of highly selective EA catalyst series. From Table 16-18 (laboratory test,  $C_2^-/C_2^0 = 80/20$  v/v, ethyne  $\leq 5$  ppm), it can be easily seen that, reaction temperature is the most important factor to the performance of catalyst EA-03, which has notable influence not only on catalyst's PDEB selectivity, but also on catalyst's activity, anti-coking ability as well as side-reactions-suppressing ability. It has been observed that in industrial unit the catalyst losses its activity rapidly if the starting temperature is lower than 330°C.  $WHSV_{EB}$  is the next factor worthy of regarding. At low  $WHSV_{EB}$ , the catalyst's DEB% value is higher but  $S_{PDEB}\%$  value is relatively lower as a result of a longer reaction time for the further isomerization of PDEB into *meta*-DEB. On the other hand, at higher

**Table 16. Effect of Temperature on Performance of EA-03\***

$T, ^\circ C$	Product Distribution, area %				Coke, wt%
	<i>B</i>	DEB%	$S_{PDEB}\%$	By-P/DEB	
300	0.81	5.07	98.70	0.16	1.84
320	1.49	5.94	98.85	0.25	1.24
340	2.50	9.43	98.02	0.27	0.83
360	4.94	12.36	97.63	0.40	0.67
380	7.85	14.81	95.14	0.53	0.75
400	9.07	10.55	92.91	0.86	0.90

\* $WHSV_{EB}=5.2h^{-1}$ ,  $EB/C_2^-=5$ , TOS = 1h.

**Table 17. Effect of  $WHSV_{EB}$  on Performance of EA-03\***

$WHSV_{EB}$ $h^{-1}$	Product Distribution, area %				Coke, wt%
	<i>B</i>	DEB%	$S_{PDEB}\%$	By-P/DEB	
2.6	8.33	16.34	94.10	0.51	0.44
5.2	4.94	12.36	97.63	0.40	0.67
10.4	0.91	5.69	99.26	0.16	0.91

\*360°C,  $EB/C_2^-=5$ , TOS = 1h.

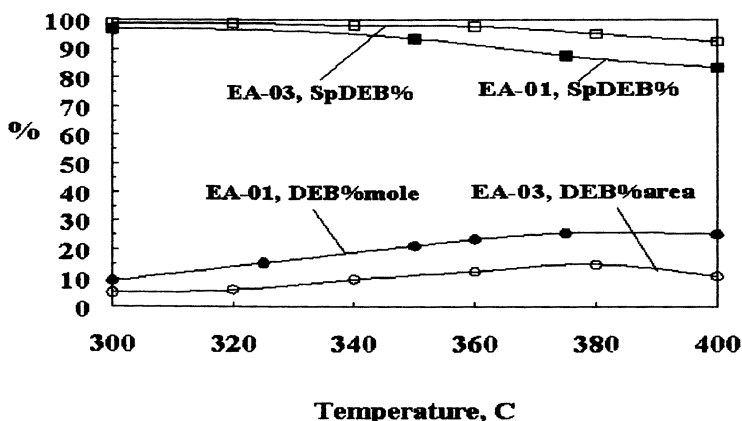
**Table 18. Effect of  $EB/C_2^-$  on Performance of EA-03\***

$EB/C_2^-$ , Mol, %	Product Distribution, area %				Coke, wt%
	<i>B</i>	DEB%	$S_{PDEB}\%$	By-P/DEB	
2	2.14	21.35	98.22	0.10	1.19
5	4.94	12.36	97.63	0.40	0.67
14	6.85	7.44	98.13	0.92	0.54

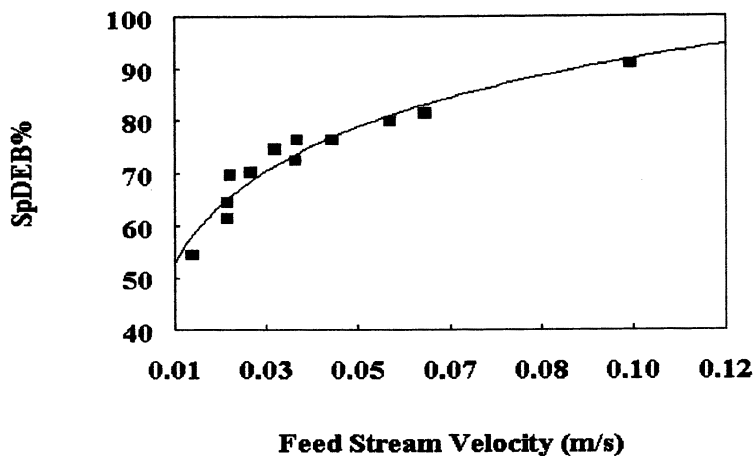
\*360°C,  $WHSV_{EB}=5.2h^{-1}$ , TOS = 1h.

WHSV<sub>EB</sub>, the catalyst's PDEB selectivity is higher but DEB% value becomes lower owing to insufficient reaction times for the desired ethylation. At higher WHSV<sub>EB</sub>, an increase of the coking rate can also be observed with catalyst EA-03 which is mainly due to a more serious polymerization of un-ethylated ethylene molecules. To highly selective catalyst EA-03, the major effect of EB/C<sub>2</sub><sup>-</sup> molar ratio is on the catalyst's DEB% value and coke-depositing rate. However, to less highly selective catalysts such as EA-01 and EA-02, the increase in EB/C<sub>2</sub><sup>-</sup> molar ratio leading to a decrease in PDEB selectivity has been observed because of a slowdown of feed stream velocity and therefore a longer residual time for the isomerization of PDEB. Generally speaking, to achieve smooth operation in case of an industrial unit, it is helpful to control the starting reaction temperature, WHSV<sub>EB</sub> and EB/C<sub>2</sub><sup>-</sup> molar ratio to moderate high levels. During the operation, one can little by little increase the reaction temperature and reduce the WHSV<sub>EB</sub> value to maintain the catalyst's activity. Besides, it has been observed that the influences of reaction condition on the PDEB selectivity of catalysts depend much on the catalysts' *para*-selectivity: the higher the *para*-selectivity they have, the less their PDEB selectivity, i.e. S<sub>PDEB</sub>% value, would be influenced by the reaction condition. The effects of temperature on the PDEB selectivity of different *para*-selective catalysts can be seen from Figure 7. In some cases, reaction pressure can be employed to adjust the catalyst's activity. Similar to the WHSV<sub>EB</sub> and the EB/C<sub>2</sub><sup>-</sup> molar ratio, reaction pressure also has influence on the catalyst's PDEB selectivity. Ultimately, the influences of WHSV<sub>EB</sub>, EB/C<sub>2</sub><sup>-</sup> molar ratio and reaction pressure on PDEB selectivity can be boiled down to the relationship of feed stream velocity (in m/s unit, this parameter has a relationship with the trans-section area of the reactor) with PDEB selectivity. Figure 8 illustrates the effect of said feed stream velocity on the PDEB selectivity of EA-01 catalyst.

**Figure 7. Effects of Temperature on the Performance of Different *para*-Selective Catalysts**



**Figure 8. A Correlation of the Feed Stream Velocity with the PDEB Selectivity of Catalyst EA-01**



### **Nano-sized ZSM-5 Zeolite as Catalyst for Ethylation of Ethylbenzene with Ethylene: A Most Recent Study**

The inherent advantage of micron-sized large crystal ZSM-5 zeolites in easily acquiring high shape selectivity has facilitated their commercial uses in *para*-selective catalyses. This virtue is a synergic effect of relatively long channels and small external surface of such zeolites. In the same time, however, micron-sized large crystal ZSM-5 zeolites often carry through the *para*-selective catalyses at rather low activity and with a short one-cycle operation time. These drawbacks, mainly due to the less accessibility of the innermost surface of the large crystallites after their channels' geometric constraints are accordingly strengthened, can be more serious in the cases where very high *para*-selectivity is required.

On other hand, recent patent literatures (29-30) disclose that very small ZSM-5 zeolitic crystal of 0.1 $\mu\text{m}$  could be converted, by using so-called trim-selection method, into high *para*-selective catalysts for the disproportionation of toluene ( up to 99.7% *para*-xylene selectivity) with significantly improved activity and durability. These results illumine a new way to the tackling of the problems existing in present high *para*-selective catalysts: that is, the use of very small or ultra small crystal zeolites to preparing the new generation of *para*-selective catalysts.

Most recently, we have investigated the catalytic performances of an H-type and systematically modified nano-crystal ZSM-5 zeolitic catalysts (20-50nm) in ethylation of ethylbenzene with ethylene. It has been observed that the nano-crystal

Figure 9. Effect of Crystal Size on Deactivation Rates of HZSM-5 Catalysts

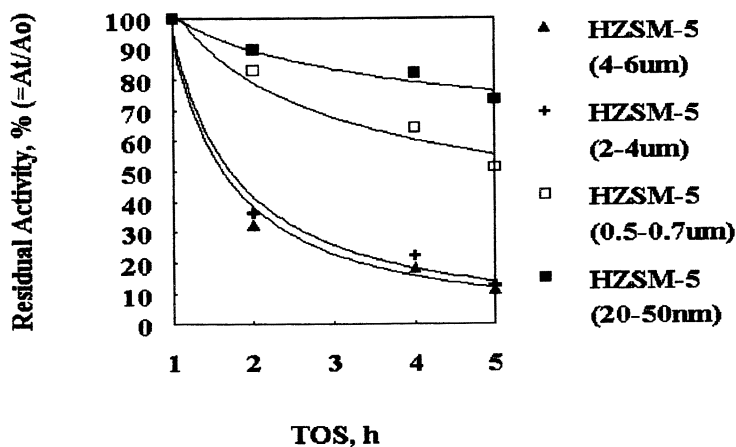


Table 19. Coking Analysis of HZSM-5 Zeolites with Different Crystal Sizes \*

HZSM-5 Catalyst	Coke, wt%	C/H, atomic ratio	Residual activity %	Activity loss/g coke
20-50nm	10.03	0.51	73.69	2.62
0.5-0.7 $\mu$ m	8.08	0.51	49.49	6.25
2-4 $\mu$ m	8.78	0.48	12.49	9.97
4-6 $\mu$ m	10.93	0.60	11.30	8.12

\* Reaction condition: 330°C,  $WHSV_{EB} = 8.7h^{-1}$ ,  $EB/C_2 = 3$  and  $N_2/C_2 = 50/50$

HZSM-5 has very good anti coking-deactivation ability, as indicated in Figure 9 and Table 19. The research also showed that the ultra fine ZSM-5 zeolite is difficult to be *para*-selectivated. However, by using a special tailored combined modification method, we have elevated the PDEB selectivity of the nano-sized zeolite from 29%(H-type) to 95%, the modified nano-sized ZSM-5 zeolite has a DEB% value ( reaction activity) of 20% at condition of 360°C,  $WHSV_{EB} = 5.2h^{-1}$ ,  $EB/C_2 = 5$  and  $N_2/C_2 = 50/50$ , only 1-2% lower than its H-type precursor. This study indicates that the nano-crystal ZSM-5 zeolite is a promising potential in preparing more efficient catalyst for *para*-selective reactions.

## References

1. Kaeding, W. W., *J. Catal.*, 95, 512(1985).
2. Pan Lurang, Li Hexuan, *PETROCHEMICAL TECHNOLOGY*, 21, 289 (1992) .
3. Wang Guiru, Li Shuwen, Wang Xiangsheng, Guo Hongchen, *Chinese* 1, 110, 628, Oct. 25, 1995; *Appl. Apr.* 18, 1994.
4. I. Wang, C. L. Ay, B. J. Lee. And M. H. Chen, *Proc. 9<sup>th</sup> Int. Congr. Catalysis*, Calgary 1988, P 324.
5. Y. S. Bhat, J. Das, A. B. Halgeri, *Appl. Catal. A*, 115, 257(1994).
6. Y. S. Bhat, J. Das, A. B. Halgeri, *Appl. Catal. A*, 130, L1-L4(1995).
7. A. B. Halgeri, *Appl. Catal. A*, 115, N4(1994).
8. Wang et al. U. S. Pat. 4 950 835, Aug. 21, 1990.
9. Neuzil et al., U. S. Pat. 4, 051, 192, Sept. 27, 1977.
10. Liu Jing, *PETROCHEMICAL TECHNOLOGY*, 19, 351 (1990) , N1.
11. N. Y. Chen, W.E. Garwood and F.G. Dwyer, "Shape Selective Catalysis in Industrial Applications," 36, Marcel Dekker, Inc. (1989).
12. J.-H. Kim, S. Namba and T. Yashima, *Appl. Catal.*, A83, 51(1992).
13. J.-H. Kim, S. Namba and T. Yashima, *Appl. Catal.*, A100, 27(1993).
14. M. Niwa, S. Kato, T. Hattori and Y. Murakari, *J. Chem. Soc. Faraday* I,80,3135(1984).
15. M. Niwa, Y. Kawashima and Y. Murakari, *J. Chem. Soc. Faraday Trans. I*,81, 2757(1985).
16. M. Niwa, S. Kato, T. Hattori and Y. Murakari, *J. Phys. Chem.*, 90, 6233(1986).
17. Kerr, G. T., *J. Catal.*, 15, 200(1969).
18. Zeng Zhaohuai, Li Yuguang, Mo Tinghuan, *CHINESE JOURNAL OF CATALYSIS*, 7, 190 (1986)
19. Ashton, A. G., Batmanian, S., Dwyer, J., et al., *J. Mol. Catal.*, 34,73(1986).
20. Han Cuiying, Wang Xiangsheng, *ACTA PETROLEI SINICA ( PETROLEUM PROCESSING SECTION )*,1 (1985) 29.
21. Wang Guiru, Xu Zhenquan, Yu Guiyan, et al., *PETROCHEMICAL TECHNOLOGY*, 16, 616 (1987) .
22. Cai Guangyu, Wang Qingxia, Zhou Zhiyuan, et al., *PETROCHEMICAL TECHNOLOGY*, 19, 791 (1990) .
23. Li Shuwen, Wang Xiangsheng, *JOURNAL OF FUEL CHEMISTRY AND TECHNOLOGY*, 13, 211 (1985) .
24. Chen Lianzhang, Bao Zhongying, Wang Xiangsheng, *JOURNAL OF FUEL CHEMISTRY AND TECHNOLOGY*, 12, 112 (1984) .
25. Z. Gao, Y. Yue and Y. Tang, *CN Pat. NO. 95111520(1995)*.
26. Y.-H. Yue, Y. Tang and Z. Gao, *Stud. Surf. Sci. Catal.* 105, 2059(1997).
27. Y. Liu, Z. Gao, *ACTA PETROLEI SINICA ( PETROLEUM PROCESSING SECTION )*, 12, 35 (1996) .
28. Dong Fei, Wang Guiru and Wang Xiangsheng, *Chinese Journal of Chemical Engineering*, (1995) 3 (4) 208
29. CHANG, *WO 93/17788* Sept. 16, 1993.
30. CHANG, *WO 93/17987* Sept. 16, 1993.

## Chapter 15

# Enhanced *para* Selectivity in Alkylation and Isomerization Reactions over Silylated ZSM-5 Zeolite

B. S. Rao, R. A. Shaikh, and A. V. Ramaswamy

Catalysis Division, National Chemical Laboratory, Pune 411 008, India  
(telephone and fax: +91 (212) 334761; e-mail: bsrao@dalton.ncl.res.in)

Controlled silylation of ZSM-5 by chemical vapor deposition (CVD) of tetraethyl orthosilicate, results in gradual alteration in the external surface and pore mouth. These samples are characterized by XRD, MAS-NMR, TPD of ammonia, FTIR and sorption techniques. The selectivity enhancement of 1,2,4-trimethylbenzene in the methylation of xylene, *p*-diethylbenzene in ethylbenzene disproportionation and *p*-xylene in *m*-xylene isomerization is attributed to the product shape selectivity, arising out of modification of ZSM-5.

Selectivity is one of the most important aspects to be considered in any catalytic process. Often the activity and selectivity are referred to together. The activity is associated with many aspects such as the reaction, reactants, reaction parameters, catalysts, inhibitors, etc. However, selectivity is associated with the catalyst and can be controlled by several ways such as structural, chemical, compositional changes, kinetic and energy considerations. New exploration in molecular sieve synthesis and increasing assemblage of novel structures has revealed catalytic chemistry and structure-activity relationship. A property frequently referred to in the catalytic behavior of zeolites is the shape selectivity, first coined by Weisz and Frilette (1). This property is more pronounced in medium pore pentasil zeolites. The dual pore system and the unique structure of ZSM-5 have enabled revolution in shape selective reactions (2,3), impressive commercial applications in petroleum refining (4) aromatics petrochemicals processing (5) and synthetic fuels (6,7). Molecular sieves represent a rich diversity of pore and channel sizes and shapes, channel

dimensions and connectivity and active site type concentration (8,9). The morphology and their crystallite size can also be varied (10,11). The zeolite sizes often match with those of the organic molecular dimensions. It is, therefore, possible to discriminate molecules on the basis of size. Only molecules whose dimensions are less than the critical diameter of the zeolites (pore diameter) can enter the pores and have access to internal catalytic sites to undergo reactions, then diffuse out and appear as product. A number of comprehensive reviews and critical discussions on the subject (12,13) with reference to the distinguished four categories of shape selectivity viz., reactant selectivity (14), product selectivity (15), restricted transition state selectivity (16) and to some extent, molecular traffic control (17), have appeared on medium pore zeolites like ZSM-5. This property of shape selectivity can further be enhanced by changes in the acidity, channel tortuosity, surface passivation and pore mouth narrowing (18-24). Even though wide pore zeolites like mordenite are reported to be shape selective (25), we restrict our discussions to the medium pore zeolites and to the product shape selectivity which often can be confused with transition shape selectivity.

The product shape selectivity (26), which is the subject of this report, can be achieved by the modification of the catalyst or the reaction conditions. Khouw and Davis (27) have discussed shape and size selectivity as well as primary and secondary selectivity in zeolites which are relevant to this and will be discussed at the appropriate place. In zeolites, the product shape selectivity (28,29), occurs when some of the products formed within the pores are too bulky to diffuse out as observed product. They are either converted to less bulky molecules or deactivate the catalyst by blocking the pores. This type of selectivity is not only dependent on pore size but also on the crystal size of the catalyst particle (30-32). In the product, a substance having diffusion coefficient considerably higher than the others diffuses fast. For example, the diffusion coefficient of p-xylene in ZSM-5 is approximately  $10^4$  times higher than that of m- or o- xylene, hence it diffuses fast. Xylene isomerization and dewaxing are the best examples for product shape selectivity. In addition to crystallite size variation, the product shape selectivity can be enhanced by several modifications. The modifications include cation exchange (33), metal impregnation (34), liquid phase silylation (35) or CVD (36,37). We report here the modifications of ZSM-5 by controlled chemical vapor deposition of silicon alkoxide, and the catalytic activity and selectivity of the modified samples in the alkylation, disproportionation and isomerization reactions.

## Experimental

The CVD of silicon alkoxides like tetra ethylorthosilicate (TEOS) is well known and described by several authors (36,37). Niwa, et al., have reported in length the CVD technique and the mechanism of silylation (21,23). This method consists of depositing the desired substance in the form of vapor and calcining further to achieve the material of interest. Well-characterized ZSM-5 ( $S_0$ , Table I) was silylated as per the procedures described by Niwa, et.al. (21,23). The unmodified ZSM-5 was taken in a fixed bed reactor. The sample was activated at 773 K for 8 h in a flow of air. The temperature was slowly brought down to the reaction

temperature in a flow of dry nitrogen. A solution containing 5-7% (TEOS) in toluene and methanol in desired mole ratio was contacted with the sample until a silica breakthrough was noticed in the reactor effluent. This was slowly heated to 623 K in a flow of nitrogen to drive off and decompose the organic. The sample was calcined at 823 K for 10 h. This sample is denoted as S<sub>1</sub>. Ethylbenzene disproportionation was studied as a probe reaction. The reaction was stopped and the catalyst was regenerated and cooled to a temperature around 473 K and further silylation was carried out to increase the silica deposition. The same procedure was repeated until the desired selectivity for p-diethylbenzene was obtained. Five samples designated as S<sub>1</sub>, S<sub>2</sub>, S<sub>3</sub>, S<sub>4</sub>, and S<sub>5</sub> were thus prepared. These samples were characterized by sorption methods, XPS and MASNMR techniques. The unit cell composition of the parent sample, amount of deposited silica and acidity changes by TPD are included in Table I along with the sorption data.

**Table-I: Amount of Silica deposited and equilibrium Sorption uptake of Silylated Catalysts (% , wt/wt).**

Sorbate	S <sub>0</sub>	S <sub>1</sub>	S <sub>2</sub>	S <sub>3</sub>	S <sub>4</sub>	S <sub>5</sub>
<b>Silica deposited</b>	0.0	1.80	4.60	5.60	9.90	12.5
<b>Acidity</b> <b>Weak +</b>	2.10	2.20	2.35	2.59	2.00	2.33
<b>(amount of medium</b>						
<b>desorbed</b> <b>strong</b>	0.75	0.80	0.84	0.87	0.92	0.83
<b>NH3 wt %)</b>						
<b>n-Hexane</b>	11.50	11.10	10.50	10.60	9.50	8.70
<b>Cyclohexane</b>	2.00	1.50	1.10	0.46	0.40	0.35
<b>Ethylbenzene</b>	10.9	10.20	9.80	9.50	7.84	6.40
<b>Water</b>	7.70	7.63	6.59	6.90	5.76	5.70
<b>P-Xylene</b>	13.60	13.20	12.40	12.80	10.80	9.20
<b>P-Ethyltoluene</b>	11.80	11.30	10.60	10.30	9.00	7.90
<b>P-Diethylbenzene</b>	9.70	9.10	8.80	8.10	7.90	7.70

Conditions: P/Po=0.5, Temp. 298K, Equilibrium time = 2h.

Parent sample H/ZSM-5, SAR = 260

Unit cell composition Na<sub>0.04</sub> [(SiO<sub>2</sub>)<sub>95.27</sub> (Al<sub>2</sub>O<sub>3</sub>)<sub>0.73</sub> ]11H<sub>2</sub>O

Catalytic evaluations were made in a down flow, all metal Catalyst unit supplied by M/s Geomecanique, France. About 10 g of the catalyst was used in the study. The catalyst was activated in air for 4 h. at 773 K in N<sub>2</sub> and then brought down to reaction temperature. Both gaseous and liquid products were collected at regular intervals and analyzed in a Shimadzu 15A GC fitted with a FID detector. Xylene Master capillary column (supplied by Shimadzu Corp.) was used for xylene isomers and a special column containing a mixed phase with Apiezon-L was used for



diethylbenzene isomer separation. Gaseous products were analyzed on porapak Q column (3 m long). Percent conversion and selectivity were calculated on the basis of yields of the individual components in the gas and in the liquid product.

## Results and Discussion

### Characterization of the samples

The modified samples were characterized by different techniques such as :

**XRD:** X-ray diffraction patterns did not show any change with progressive modification with silica deposition from the parent zeolite, as can be seen from Figure 1. This shows that crystallinity is well maintained.

**SEM:** The scanning electron micrographs did reveal changes in some samples. For 5.6 % silica deposited sample ( $S_3$ ) a few silica aggregates, and in case of sample with 12.5% deposition ( $S_5$ ) an accumulation like debris on the external surface were observed.

The details of XRD and SEM are reported earlier (37)

**XPS:** Since it is difficult to evaluate the contribution of the  $Al_{2s}$  peaks to the composite  $Al_{2s}$ -energy loss peak, using  $Al_{2p}$  peak the surface concentration of aluminium was evaluated. The  $SiO_2/Al_2O_3$  ratio was found to be 71,112,181,300 and >500 for samples  $S_1$  to  $S_5$  respectively, whereas the bulk ratio is 260 for  $S_0$  and increase up to 290 for  $S_5$  (37a). Therefore, the XPS studies clearly indicate that the parent sample  $S_0$  is highly enriched with aluminium and with progressive silylation the surface was enriched with silica.

**MAS-NMR:**  $^{27}Al$  MAS-NMR did not indicate any octahedral aluminium (-52 ppm) in any of the samples. Even after the acetyl acetone treatment there is no evidence of the peak around -52 ppm corresponding to the non-framework aluminium.

**FT-IR:** FT-IR Studies indicated both Lewis and Bronsted acid sites. Bronsted sites increased with progressive silylations at the expense of Lewis sites (38).

**TPD:** TPD of ammonia showed reduction in the weaker acid sites with silylation (38). Similarly, the sorption studies revealed a continuous decrease in the sorption volume with gradual silylation, which indicates the changes in the channels and in the pores (Table I).

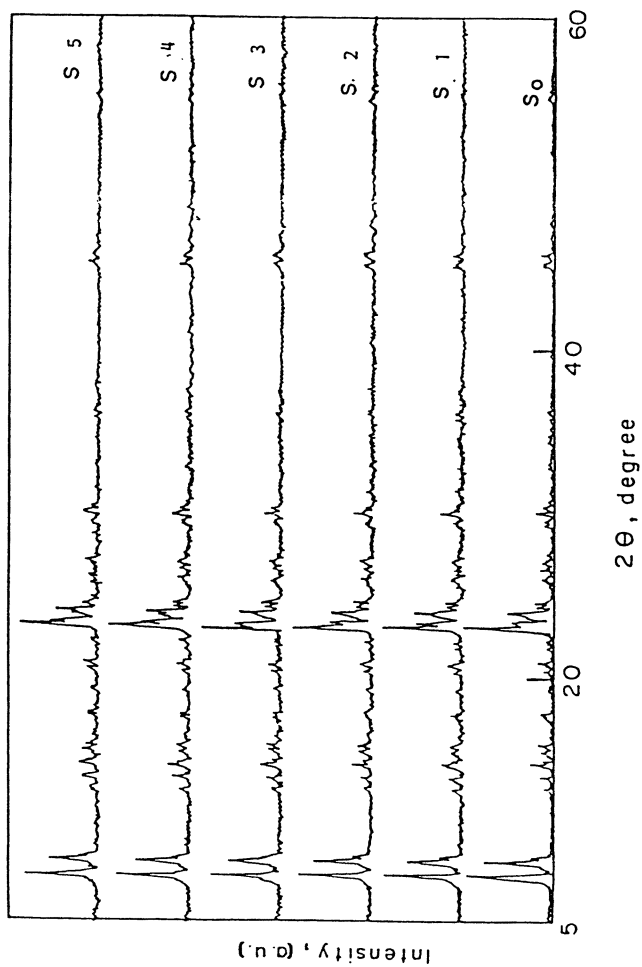


Figure 1. XRD profiles of silylated samples

The general observation is that with the progressive silylation the surface of the zeolite is first passivated reducing the surface acidic sites, as evidenced by the reduction in non-selective reactions, and gradually blocking the channels and pores. Modified catalysts are used in three types of reactions to correlate the activity - selectivity and the percent silica deposited. As pointed out earlier, the product shape selectivity and restricted shape selectivity is sometimes confused. The restricted transition state selectivity occurs when space within the zeolite is not sufficient to allow the larger or several transition state intermediates to form. This type of shape selectivity is independent of crystal size and activity of the catalyst, but depends on pore and cavity dimensions and on zeolite structure. For example, in transalkylation of dialkylbenzenes, the alkyl group is transferred from one molecule to another. The reaction is bimolecular and involves diphenylmethane type transition-state in case of molecules like xylene. The transition state complex can dissociate to smaller molecules, which can easily diffuse outside the zeolite channels or this can block the whole pore. Therefore, activity generally declines with time, unless hydrogenation activity is present. In toluene disproportionation reaction, a molecule each of benzene and xylene are formed by restricted transition-state due to steric hindrance inside the zeolite channel. However, in case of medium pore zeolites the formation of transition-state is very much restricted except for few molecules due to channel dimensions. But dealkylation can proceed. This dealkylated product can again react or realkylate with one of the reactants or the decomposed product to form the desired product as dictated by the reaction conditions. So, dealkylation, realkylation are also possible in medium pore zeolites. The disproportionation of toluene and ethylbenzene is interesting. It is possible to achieve benzene to xylene molar ratio of one, in case of toluene disproportionation, under optimum conditions with modified catalyst, indicating a predominance of transition state shape selectivity. However, in ethylbenzene reaction there is always an excess of benzene, which can only be explained by the dealkylation. The formation of diethylbenzene can be by dealkylation-realkylation as well as disproportionation (38). The thermodynamics indicate dealkylation to be more prominent than the disproportionation.

### **Alkylation of xylenes with methanol**

The smallest 1,2,4 trimethylbenzene, also known as pseudocumene is an important starting material for the production of trimellitic acid/anhydride which is used in the manufacture of plasticisers, polyesteramides, epoxy resins, etc. (39). This is produced by the selective methylation of xylene. Not much literature is available on the catalytic methylation of xylenes except that of Namba, et al. (40). They reported very high selectivity (>99%) for 1,2,4 TMB during their methylation studies of individual xylene isomers over HZSM-5 zeolite. This was correlated to the shape selectivity and the ortho - para orientation of the alkylation reactions. De Simone (41) has claimed, with a crystalline borosilicate molecular sieve impregnated with Mg, as high as 92% yield of TMB in the aromatic fraction. Anuj Raj, et al. (42) have interpreted the selectivity in case of isomorphously substituted Al, Ga, Fe-MEL zeolites to the weaker acid sites. These zeolites compete with isomerization activity

by suppressing the alkylation reaction. Xylene reacts with methanol in presence of an acid catalyst to form tri- and tetra-alkylbenzenes. The selectivity of 1,2,4 TMB among the polyalkylbenzenes varies with the catalyst modification while the yield of the product depends on the strength and number of acid sites. However, the selectivity to tri- and tetra-methylbenzenes depends on the pore mouth narrowing by CVD of silica. The modification narrows the pore mouth and passivates the surface active sites. Table II summarizes the data on the conversions and selectivity to 1,2,4 TMB obtained on HZSM-5 samples with different levels of silylation. In  $S_1$  silica deposited is less, hence conversion of xylene and selectivity of TMB and TTMB are similar to that of the parent unsilylated sample.

**Table II : Methylation of xylene**

Catalyst	$S_0$	$S_1$	$S_2$	$S_3$	$S_4$	$S_5$
SiO <sub>2</sub> , %	0.0	1.8	4.6	7.6	9.9	12.5
Temp. °C	450	450	450	450	450	450
WHSV, h <sup>-1</sup>	2.5	2.5	2.5	2.5	2.5	2.5
Xyl/MeOH	4	4	4	4	4	4
Conv.Xyl.,%	32.7	29.3	17.2	14.6	5.2	4.7
$\Sigma$ -tmb(a), %	60.2	37.5	29.9	54.1	76.9	-
$\Sigma$ -tmb(b), %	22.0	24.9	30.2	22.6	-	-
124tmb/a	50.5	62.0	64.6	83.3	98.9	-
1245ttm/b	40.9	42.8	57.5	97.6	-	-
p-xyl/ $\Sigma$ -xyl.	22.3	22.4	22.6	22.5	24.1	24.3

tmb = Trimethylbenzene, ttm = tetramethylbenzene.

However with increase of the degree of silylation gradual reduction in the formation of 1,3,5 and 1,2,3 TMB is noticed and selectively 1,2,4 TMB is formed at a silica level of 9.9%. At about 12.6% silica deposition no TMB formation was observed. Similarly the TTMB formation and selectivity of 1,2,4,5 TTMB was maximum at 5.6% deposition of silica. Thus, the cut off level for the selective formation of 1,2,4 TMB and 1,2,4,5 TTMB are 9.9 and 5.6 % silica. However unconverted xylene was noticed even at 12.6% silica. As described earlier the narrowing of the effective pore-mouth without much variation in the micropore volume is achieved by silylation, due to which the formation/reactions of molecules of higher molecular dimensions are restricted and p-isomers, being the smallest among the isomers of any compound diffuse out, can appear in large quantities in the product. Thus, the selective formation of 1,2,4 TMB and 1,2,4,5 TTMB is related to the modification of ZSM-5 by silylation. The p-xylene is in equilibrium concentration with other isomeric xylenes at this level of silica deposition indicating a need for higher level of modification for selective p-xylene formation by isomerization.

### Ethylbenzene disproportionation

P-diethylbenzene is a specialty chemical used as a desorbent in Parex process for the separation of para-xylene. Usually in the ethylbenzene disproportionation reaction or in the ethylation of ethylbenzene isomeric mixture of diethylbenzenes is produced. Two molecules of ethylbenzene react forming diethylbenzene and benzene over zeolite or any acid catalyst. The activity of the catalyst depends on the silica-alumina ratio of the catalyst. In this context, it is of great interest to study the reaction of ethylbenzene to form benzene and ethyl moiety, and preferential migration of ethyl group to another available reactant, in this case another ethylbenzene molecule. The competition for accepting the alkyl group and transforming to diethylbenzene depends on the nature of the catalyst and the reaction conditions. Generally, dealkylation is accompanied by disproportionation and the ratio of benzene to diethylbenzene is a measure of this. When a modified catalyst, such as the silylated ZSM-5 is used, side reactions are controlled and the selectivity towards p-isomer increases. The selectivity is governed by the diffusivity of the molecules inside the crystal. As already mentioned decrease in crystal size decreases the p-selectivity and also the diffusivity of the molecules decreases with the increase in effective minimum dimensions of the molecule. Table III presents the experimental data from modified ZSM-5 with varied Si deposition on the reaction of ethylbenzene.

**Table III : Disproportionation of ethylbenzene**

Catalyst	S <sub>0</sub>	S <sub>1</sub>	S <sub>2</sub>	S <sub>3</sub>	S <sub>4</sub>	S <sub>5</sub>
SiO <sub>2</sub> , %	0.0	1.8	4.6	7.6	9.9	12.5
Temp. °C	350	350	350	350	250	350
WHSV, h <sup>-1</sup>	3.5	3.5	3.5	3.5	3.5	3.5
Conv.EB, %	37.3	35.4	33.0	30.3	29.2	20.6
Sel.DEB, %	41.3	42.5	43.1	43.6	43.5	51.9
Sel. p-DEB, %	38.0	68.4	78.1	95.2	99.8	99.8
B/DEB, ratio	1.9	1.7	1.6	1.65	1.6	1.3

The main products are benzene and diethylbenzene isomers, with small amounts of toluene, and C9 aromatics. With increase in silylation, fall in conversion and increase in p-selectivity is noticed from the data. However, it should be noted that the adsorption of ammonia does not indicate a loss in acidity. Therefore, it can be inferred that the decrease in conversion is due to the reacting molecule accessibility to the active sites inside the channels due to poremouth narrowing. The removal of the active sites on the external surface also helps in restricting the secondary reaction of paradiethylbenzene isomerisation.

### Isomerisation of metaxylene:

Xylene isomerisation is one of the industrial reaction where medium pore zeolites play an important role. The p-xylene demand increases every year by 6-8% and to meet this demand either new plants have to be set up or the existing processes should improve the p-xylene selectivity. Selective toluene disproportionation and use of modified catalysts are some of the methods for enhancing p-xylene yields. But isomerisation of xylenes always leads to equilibrium compositions. Improvements on the catalyst have resulted in enhancement of paraselectivity, but not as much as that in the case of paradiethylbenzene. The modifications carried out for the other two earlier described reactions are not sufficient to enhance the p-selectivity in this reaction. Hence, further deposition of silica was done following the same CVD technique to obtain samples S<sub>6</sub> and S<sub>7</sub> with 15.4 % and 16.2 % silica respectively. Some of our recent results on the isomerization of m-xylene on the modified ZSM-5 are summarized in Table IV.

**Table IV: Isomerization of m-xylene**

Catalyst	S <sub>0</sub>	S <sub>5</sub>	S <sub>6</sub>	S <sub>7</sub>
SiO <sub>2</sub> , %	0.0	12.5	15.4	16.2
Temp. °C	375	375	375	375
WHSV, h <sup>-1</sup>	5	5	5	5
H <sub>2</sub> /HC, mole	1	1	1	1
Conv. m-xyl., %	51.5	43.4	36.6	30.2
p-/o-xylene	0.9	1.05	1.50	1.74
Sel. p-xylene, %	48.0	54.2	69.8	87.6

The results indicate an increase in p-xylene concentration in the product and decrease in the o-xylene formation. The reduction in the conversion of m-xylene is in direct proportion to the decrease in the formation of o-xylene, which is controlled by the diffusivity due to pore mouth narrowing. Secondly, the secondary reaction of o-xylene formation from p-xylene is also controlled due to the passivation of the external surface of the catalyst sample.

The results presented in Tables II-IV indicate that modification of ZSM-5 by chemical vapor deposition of silicon alkoxide improves the selectivity of the desired product. This is due to the passivation of the surface active sites. This passivation reduces the side reactions occurring on the surface sites. The silylation narrows the pore mouth opening, thereby facilitating the diffusivity of p-isomer in xylene isomerization, 1,2,4 and 1,2,4,5 methylbenzenes in xylene methylation and p-diethylbenzene in ethylbenzene disproportionation. Even though, a high selectivity

for the desired product is obtained, it may be noted that the percent silicon deposition varies from compound to compound and reaction to reaction. Thus, it is possible to achieve 88 % selectivity in p-xylene 98 % selectivity in p-DEB, 97 % selectivity in 1,2,4 TMB and 97 % selectivity in 1,2,4,5 TTMB with 16.2 %, 9.9 %, 9.9 % and 7.6 % deposition of SiO<sub>2</sub> respectively. As pointed by Khou and Davis (27) the primary selectivity can be associated with the para-product formation by pore narrowing and diffusion phenomenon, whereas the secondary selectivity is due to the passivation of the external surface of the catalyst which prevents the secondary reaction so that the primary product selectivity is maintained.

#### Acknowledgement:

The authors thank Mr. C.V. Kavedia and Dr. A.P. Budhkar for their help rendered during the experimentation and analysis.

#### References:

1. Weisz, P.B., Frilette, V.J., Maatman, R.W., and Mower, E.B., *J. Catal.*, 1, 307 (1962).
2. Chen, N.Y., Garwood, W.E. and Dwyer, F.G.; *Shape Selective Catalysis in Industrial Applications*, Marcell Dekker, New York
3. Weitkamp, H., Ernst, S., Dauns, H. and Gallei, E.; *Chem. Ing. Tech.*, **1986**, 58, 623.
4. Chen, N.Y. and Degnan, T.F.; *Chem. Eng. Prog.*, **1988**, 84, 32.
5. Haag, W.O., Olson, D. H. and Weisz, P.B.; in H. Gruenewald (Ed.), *IUPAC: Chemistry for the Future*, Pergamon Press, Oxford, 1984, pp 327-336.
6. Meisel, S.L., McCullough, J.P., Lechthaler, C.H. and Weisz, P.B.; *Chemtech*, **1976**, February.
7. Chang, C.D.; *Hydrocarbons from Methanol*, Marcel Dekker, New York, NY, Basel, 1983, pp 1-129.
8. Koningsveld. H.van.; *Stud. Surf. Sci. Catal.*, **1991**, 58, 35.
9. Davis, M.E.; *Chem. Ind.*, **1992**, 137.
10. Olson, D.H., Haag, W.O., *ACS Symp. Ser.* **1984**, 248, 275.
11. Haag, W.O., Chen, N.Y.; in L.L. Hegedus (Ed.) *Catalyst Design-Progress & Perspectives*, John Wiley & Sons, New York, NY, 1987 Ch. 6.
12. Venuto, P.B., *Microporous Materials*, **1994**, 2, 297.
13. Corma, A.; *Chem. Rev.* **1997**, 97, 2373.
14. Chen, N.Y., Garwood, W.E., *Catal., Rev. Sci. Eng.*, **1986**, 28, 1.
15. Chen, N.Y., Kaeding W.W. and Dwyer .F.G. *J. Am. Chem. Soc.* **1979**, 101, 6783.
16. Csicsery, S.M.; *J. Catal.*, **1971**, 23, 124.
17. Derouane, E.G. and Gabelica, Z.; *J. Catal.*, **1981**, 67, 218.
18. Yan. Y., Verbiest, J. Hulsters, P. De. and Vansant, E.F.; *J. Chem. Soc. Faraday Trans.* **1986**, 1, 82, 963.

19. Dossi, C. Schafer, H. and Schatler, W.M.H.; *J. Mol. Catal.*, **1989**, 52, 193.
20. Ozin, G.A., Godber, J., Hugues, F., Nazar, L.F.; *J. Mol. Catal.*, **1983**, 21, 313.
21. Niwa, M., Kato, S., Hattori, T. and Murakami, Y; *J. Chem. Soc. Faraday Trans.* **1984**, I, 80, 3135.
22. Murakami, Y; *Stud. Surf. Sci. Catal.*, **1988**, 44, 177.
23. Niwa, M. Murakami, Y.; *J. Phys. Chem. Solids* **1989**, Vol. 50, No. 5, 487.
24. Hibino, T., Niwa, M. and Murakami, Y.; *J. Catal.*, **1991**, 128, 551.
25. Cusmano, J.A.; *Chem Tech.* **1991**, 22, 482.
26. Weisz, P.B.; *Stud. Sci. Catal.*, **1981**, 7A, 3.
27. Khouw, K and Davis, M. E.; *ACS Sym. Ser.* **1991**, 517, 206.
28. Hartford, R.W., M. Kojima, and O'Connor, C.T.; *Ind. Eng. Chem. Res.*, **1989**, 2812.
29. Chutoransky. D., Dwyer. F.G.; *Adv. Chem. Ser.* **1973**, 121, 540.
30. Veruyn, J.P.; *Eur. Pat. Appl.* **1986**, 219, 354.
31. Amelse, J.A.; *Proc. 9<sup>th</sup>. Int. conf. (Eds. R. von Ballmoos, B. Higgins, M.M.J. Treacy) Butterworth-Heinemann, Montreal, 1993, 457.*
32. Vasant, E.F.; Peeters, G., and Michelena, I. J.; *J. Chem. Res., Res.*, **1978**, 90, 1165.
33. Kim, J.H., Namba, S. and Yashima, T.; *Zeolites*, **1991**, 11, 59.
34. Tadimitsu, K.; E.P. Application No. 93116800.9, assigned to Mitsui Toatsu Chemicals, Inc. Tokyo.
35. Niwa, M., Kawashima, Y. and Murakami, Y., *J. Chem. Soc. Faraday Trans.*, I, **1985**, 81, 2757.
36. Vasant, E.F., "Pore Size Engineering in Zeolites", Pub. John Wiley & Sons, New York 1990.
37. Shaikh, R.A., Hegde, S.G., Belhekar, A.A. and Rao, B.S.; *Proc. 1<sup>st</sup>. Indo-Pacific Catalysis Sym., (IPCAT-1), Jan. 1998.*
- 37a. Shaikh, R.A., Ph.D. Thesis, 1995 (unpublished work).
38. Amelse, J.A.; *Stud. Surf. Sci. Catal.*, **1988**, 38, 165.
39. Frank, H.G. and Staderhofer, J.W., "Industrial Aromatic Chemistry", Pub. Springer verlag, Berlin, Heidelberg, 1988, p. 292.
40. Namba, S., Inaka, A. and Yashima, T., *Zeolites*, **1983**, 3, 106.
41. De Simone R.E., US Patent 4,665,254 (1987) assigned to Amoco Corp.
42. Anuj Raj, Reddy, S., Kumar, R.; *J. Catal.*, **1992**, 138, 518.



## Chapter 16

# Interaction of P with HY Zeolite and Its Influence on Catalytic Transformation of Ethylbenzene

Huiping Tian, Zuguang Teng, Jianqiu Zhang, Weilin Zhang,  
Yingrui Fu, and Zhongbi Fan

Division 14, Research Institute of Petroleum Processing, 18 Xueyuan Road,  
Beijing 100083, Peoples Republic of China

Phosphorous was used as a binding material in forming 40-60 mesh HY zeolite particles. *o*-Xylene and ethylbenzene transformations were carried out at 400-460 °C over these P-doped HY samples. Phosphorous inserted into framework of HY zeolite as chain terminators by means of Al defects and framework rearrangement. The number of Bronsted sites increased by Phosphorous doping, leading to a rise in acidity. P-doped HY zeolite had an enhanced *o*-xylene isomerization activity, an improved ethylbenzene cracking activity and a notable oligomerization performance of ethylbenzene cracking products, while *o*-xylene disproportionation was prohibited by Phosphorous doping. These catalytic properties were explained by taking into account the influence of Phosphorous on the effectiveness of surface acid sites.

HY zeolite as an active component of FCC (fluid catalytic cracking) catalysts can catalyze several types of reactions besides cracking, e.g., isomerization [1], disproportionation [2], and oligomerization [3]. These reactions led to a wide variation of FCC product quality. In spite of great advances in the science of HY zeolite modification, such as dealumination and rare earth ion exchange for heavy feedstock processing, the goal of FCC catalyst researchers to make satisfied balance among these reactions in order to improve proficiently product quality of a FCC process has remained elusive. From last decade, Phosphorous has been adopted in FCC catalysts to enhance attrition resistant performance and reduce catalytic coke formation [4,5,6]. Studies performed in recent years over P-containing FCC catalysts showed that Phosphorous could adjust in the above mentioned reactions via its interaction with both matrix and Y zeolite [7]. Sauer et al. [8] reported the influence of Phosphorous on

zeolite acidity. Peltre et al. [9] studied distribution of Al, P and Si in faujasite type molecular sieve. The state of Silicon in SAPO-37 and its correlation with acidity and catalysis were conducted by Man et al. [10]. In this paper, interaction of P with HY zeolite and its influence on catalytic conversion of o-xylene and ethylbenzene were studied. The state and distribution of Phosphorous and its effect on catalytic sites were discussed.

## Experimental

P-doped HY zeolite (P-HY) was prepared by mechanical mixing method. A commercial HY zeolite ( $\text{SiO}_2/\text{Al}_2\text{O}_3=5.01$ ) was dealuminated in  $\text{H}_4\text{EDTA}$  solution [7,11] to different  $\text{SiO}_2/\text{Al}_2\text{O}_3$  ratios, then mixed with  $\text{NH}_4\text{H}_2\text{PO}_4$  in a mortar. The mixture was ground, pelletized and crushed to 40-60 mesh particles. These samples were calcined in air at 773 K for 2.0 h prior to being used in characterization or catalytic experiments.

P-HY was analyzed by means of X-ray diffraction for physical phase determination (XRD, D/max-III A), X-ray fluorimetry for elemental determination (XRF, 3013 model),  $\text{N}_2$  adsorption-desorption for surface area determination (BET, ASAP2400), and infrared measurement of adsorbed pyridine for acidity determination (IR, IFS113V).

$^{31}\text{P}$  MAS-NMR measurement was performed on DMX-300 at 121.495 MHz using excitation pulse of 5  $\mu\text{s}$  and relaxation delays of 10 s. The magic-angle spinning rate was 4.2 kHz.

The catalytic conversion of o-xylene and ethylbenzene over P-HY was carried out at 683 K using pulse method. 100-200 mg P-HY sample with 70  $\text{m}^2$  surface area was used for each measurement. The carrier gas was high-purity  $\text{N}_2$  at a flow rate of 100 mL/min.

## Results and Discussion

**State of Phosphorous and Physicochemical Properties of P-HY samples.** Figure 1 shows  $^{31}\text{P}$  MAS-NMR spectra of P-HY samples. The peak at 0 ppm is designated to amorphous Phosphorous in oxygen environment. The peak at -15 and -20 ppm is attributed to P atoms having two and three adjacent Al atoms in zeolite framework, respectively [7]. The peak at -3 ppm located between the above two types of peak, indicated amorphous  $\text{AlPO}_4$ . Variation of these peaks illustrated the difference of P-Al interaction. Amorphous  $\text{AlPO}_4$  existed only in high P content samples or high Al content samples, while the amount of framework P atoms increased with degree of dealumination of HY zeolite or blending ratio of P to HY. It was inferred that Phosphorous might interact with HY via dealumination and Si, Al, P rearrangement, as showed in Figure 2. Therefore, Al defect and framework rearrangement were

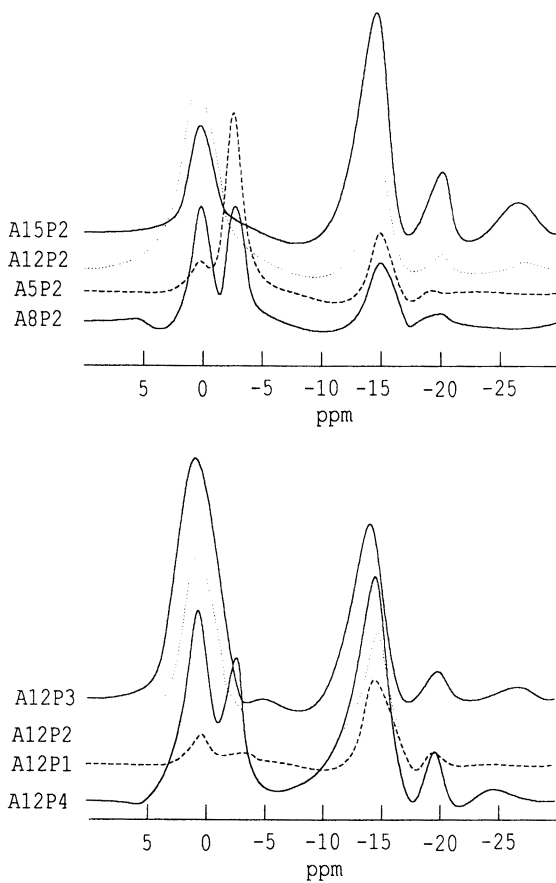


Figure 1.  $^{31}\text{P}$  MAS-NMR spectra. AxPy was sample No., in which x stood for  $\text{SiO}_2/\text{Al}_2\text{O}_3$  molar ratio and y stood for Phosphorous weight percentage.

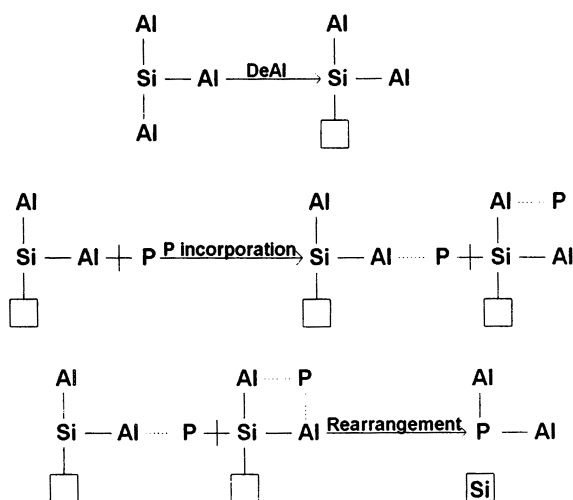


Figure 2. Mechanism of P interaction with HY zeolite.

considered to be the two important factors in P insertion into the framework. It was observed that steam-dealuminated HY had a countable amount of Al defect and was not sensitive to P considerable insertion [7].

The physicochemical properties of P-HY samples are listed in Table I and II. It was seen that increasing P content or decreasing Al content favored P incorporation into zeolite framework. Although the acidity of amorphous Phosphorous was removed by calcination [12], the acidity of P-HY samples slightly increased by Phosphorous doping due to larger increment of the number of Bronsted sites than decrement of the number of Lewis sites. It seemed that some of Lewis sites were converted into Bronsted sites by Phosphorous doping. In the case of P-HY samples having equal P content and varied SiO<sub>2</sub>/Al<sub>2</sub>O<sub>3</sub> ratio (A5P2, A8P2, A12P2, A15P2), the number of Lewis sites decreased with reduction of SiO<sub>2</sub>/Al<sub>2</sub>O<sub>3</sub> ratio, while the number of Bronsted sites increased due to increasing insertion of P into framework. This led to a rise in acidity. So, the insertion of Phosphorous into framework compensated the negative effect of dealumination on the acidity.

**Table I . Surface Area and Acidity of P-HY Samples.**

<i>P-HY</i>	<i>Surface Area</i> (m <sup>2</sup> /g)	<i>Acidity (10<sup>-3</sup>mmol/m<sup>2</sup>)</i>	
		<i>L-site</i>	<i>B-site</i>
A5P2	678	0.221	0.811
A8P2	585	0.188	0.855
A12P2	462	0.173	0.931
A15P2	355	0.141	1.070
A12P1	485	0.227	0.701
A12P3	440	0.114	1.182
A12P4	416	0.072	1.394

**Table II . Composition of P-HY Samples.**

<i>P-HY</i>	<i>Chemical Composition (wt%)</i>			<i>Framework Composition (mole%)</i>		
	<i>SiO<sub>2</sub></i>	<i>Al<sub>2</sub>O<sub>3</sub></i>	<i>P<sub>2</sub>O<sub>5</sub></i>	<i>Si</i>	<i>Al</i>	<i>P</i>
A5P2	73.5	24.5	2.0	0.721	0.273	0.006
A8P2	82.3	15.7	2.0	0.814	0.179	0.007
A12P2	86.0	12.0	2.0	0.848	0.142	0.010
A15P2	88.5	9.5	2.0	0.874	0.112	0.014
A12P1	86.9	12.1	1.0	0.849	0.142	0.009
A12P3	85.1	11.9	3.0	0.846	0.142	0.012
A12P4	84.3	11.7	4.0	0.853	0.131	0.016

**Catalytic Conversion of o-Xylene and Ethylbenzene.** Table III presents data for the catalytic patterns of o-xylene over P-HY samples at 683 K. Since the yield of C<sub>1</sub> and C<sub>2</sub>

was less than 0.2 mole%, dealkylation of o-xylene was not evident during the evaluation. o-Xylene was mainly converted into toluene, m-,p-xylene and trimethylbenzene. It was known that o-xylene was transformed into m- and p-xylene by isomerization, or toluene and trimethylbenzene by disproportionation [13]. The yield of toluene plus trimethylbenzene was larger than that of m-,p-xylene, indicating ease of o-xylene disproportionation. Moreover, it was observed in preliminary experiments that toluene from o-xylene disproportionation might further disproportionate at 713 K or higher temperatures.

**Table III. Transformation of o-Xylene at 683 K (mole%).<sup>a</sup>**

<i>P-HY</i>	<i>Toluene</i>	<i>m-,p-Xylene</i>	<i>Trimethylbenzene</i>
A5P2	4.73	4.10	4.70
A8P2	4.46	4.46	4.24
A12P2	4.35	4.42	4.30
A15P2	4.20	5.21	4.16
A12P1	4.76	3.64	4.75
A12P3	3.95	5.64	3.94
A12P4	3.41	6.18	3.36

<sup>a</sup>C<sub>1</sub> and C<sub>2</sub> yield was less than 0.2 mole%.

Since the variance of yield of toluene plus trimethylbenzene did not match that of m-,p-xylene, different surface sites were proposed for these reactions. As generally accepted [14,15,16], alkylbenzene isomerization and disproportionation reactions were mainly conducted on Bronsted and Lewis sites, respectively. m-, p-Xylene yield, corresponding to isomerization activity, and toluene and trimethylbenzene yield, representing disproportionation activity, are respectively plotted against Bronsted and Lewis sites in Figure 3. Linear curves reflected effectiveness of the acid sites. Based on this phenomenon, a possible mechanism was proposed in Figure 4.

Table IV lists results of ethylbenzene conversion. Ethylbenzene cracked into toluene, benzene and light hydrocarbons. C<sub>3</sub><sup>+</sup> fraction was mainly from oligomerization of C<sub>1</sub> and C<sub>2</sub>. Cracking of short chain alkylbenzene was hardly proceeded via the formation of a carboanion [17]. The carbonium mechanism by means of Bronsted sites was acceptable, that was showed in Figure 5. In fact, ethylbenzene cracking activity and oligomerization of ethylbenzene cracking products were both proportional to the number of Bronsted sites (Figure 6). Since the toluene yield was less than 1.0 mole%, disproportionation of toluene via C<sub>1</sub><sup>+</sup> spillover mechanism as suggested in Figure 4 was not detected.

**Comment.** The acidic sites of Si, Al based zeolites consisted of bridged hydroxyl groups as Bronsted sites and their dehydrated positions as Lewis sites. P insertion into zeolite framework created new acidic sites. Since P atoms were neighbored by only

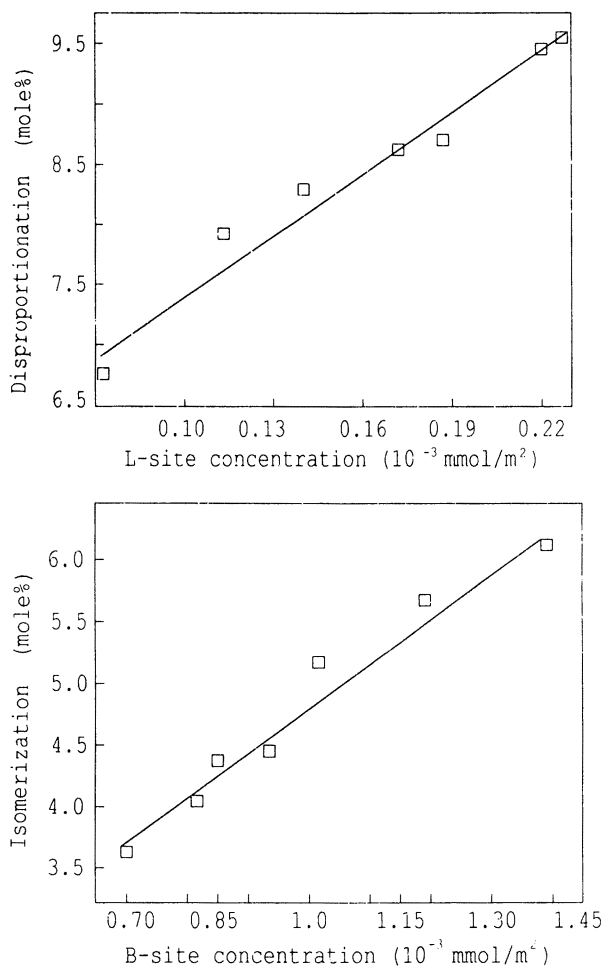


Figure 3. Influence of acidity on o-xylene conversion.

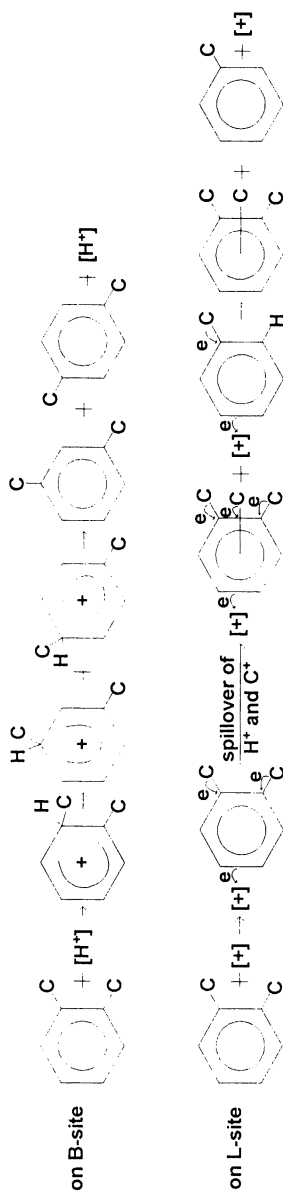


Figure 4. Mechanisms for catalytic conversion of o-xylene on B-site and L-site. [H\*] stood for B-site, [L\*] for L-site.



**Table IV. Transformation of Ethylbenzene at 683 K (mole%).**

<i>P-HY</i>	$C_1+C_2$	$C_3^+$	<i>Benzene</i>	<i>Toluene</i>
A5P2	0.71	0.39	2.83	0.13
A8P2	0.73	0.41	2.93	0.15
A12P2	0.76	0.43	3.05	0.18
A15P2	0.83	0.48	3.29	0.21
A12P1	0.69	0.37	2.68	0.11
A12P3	0.88	0.54	3.56	0.25
A12P4	0.88	0.55	3.67	0.26

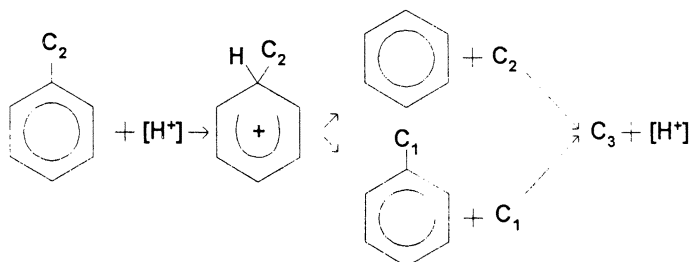


Figure 5. Mechanism of ethylbenzene cracking.

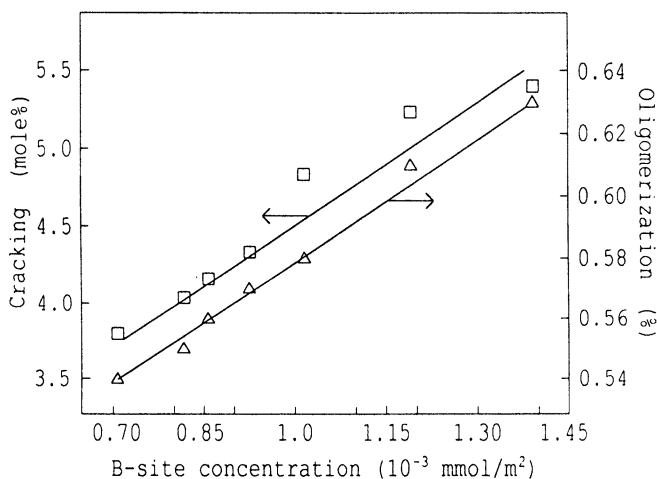


Figure 6. Influence of acidity on ethylbenzene conversion. Cracking activity was the conversion of ethylbenzene, and oligomerization activity was the ratio of  $C_3^+$  to  $C_1$  and  $C_2$ .

two or three Al atoms (Figure 1), it was deduced that Phosphorous was incorporated into framework as the terminator of the framework chain. That was to form a phosphoric acid-like group, leading to an increase of the zeolite acidity [8,18]. In the

case of SAPO-37, however, most of P atoms were surrounded by four Al atoms [9]. This resulted in a neutral framework and weak acidity [10]. So, P-doped HY zeolite was different from HY and SAPO-37 in acidity and acid-based catalytic performance. By modification using the above technique, a way to improve desired product selectivity in a complex system such as a FCC process is pointed out.

## Conclusion

Phosphorous was inserted into zeolite framework as chain terminators during doping with HY. This enhanced Bronsted acidity and inhibited Lewis acidity. In catalysis application, o-xylene isomerization and ethylbenzene cracking were improved by P-doping while o-xylene disproportionation decreased.

## References

1. Souverijns, W.; Parton, R.; Martens, J.A.; Froment, G.F.; Jacobs, P.A. *Catal. Lett.* 1996, 37(3,4), 207.
2. Vizayalakshmi, S.; Patwardhan, S.R.; Vyas, S.N. *Indian Chem. Eng., Sect. A* 1995, 37(4), 162.
3. O'Connor, C.T.; Kojima, M. *South Afr. J. Chem. Eng.* 1989, 1(1), 23.
4. Kumar, R. US5378670.
5. Wu, Z.; Liu, Q.; Yang, S.; Lu, Y.; Lui, D.; Zhang, W.; Yang, Q.; Zhou, J. CN1076714A.
6. Fan, Z.; Zhou, S.; Wu, Z.; Liu, Q.; Lu, Y.; Liu, D.; Ji, H.; Zhang, W.; Yang, J.; Chen, Y. CN1062157A.
7. Teng, Z. Thesis of Science Degree, Research Institute of Petroleum Processing, Beijing, China, 1997.
8. Sauer, J. *Stud. Surf. Sci. Catal.* 1989, 52, 87.
9. Peltre, M.J.; PMan, P.; Briend, M.; Derewinski, M.; Barthomeuf, D. *Catal. Lett.* 1992, 16, 123.
10. Man, P.; Briend, M.; Peltre, M.J.; Lamy, A.; Beaunier, phosphorous.; Barthomeuf, D. *Zeolites* 1991, 11, 563.
11. Kerr, G.T. *J. Phy. Chem.* 1968, 72(7), 2594.
12. Purcell, K.F.; Kotz, J.C. *Inorganic Chemistry*; W.B.Saunders Company: Philadelphia, 1977; pp 501.
13. Ward, J.W.; Hansford, R.C. *J. Catal.* 1969, 13, 364.
14. Hofmann, H.; Kolb, G. *Stud. Surf. Sci. Catal.* 1994, 88, 257.
15. Sobrinho, E.V.; Cardoso, D.; S-Aguiar, E.F.; Silva, J.G. *Appl. Catal. A* 1995, 127(1-2), 157.
16. Iwamoto, R.; Nita, K.; Hidaka, S.; Inamura, K.; Iino, A. *Acid-Base Catal.*; VCH publisher: New York, 1989; pp 313.
17. Meusinger, J.; Vinek, H.; Dworeckow, G.; Goepper, M.; Lercher, J.A. *Stud. Surf. Sci. Catal.* 1991, 69, 373.
18. Pauling, L. *The Nature of the Chemical Bond*, 3rd ed.; Cornell University Press: Ithaca, 1960; pp 103.

## Chapter 17

# Recent Progress in Selective Catalytic Conversion of Polycyclic Hydrocarbons over Zeolite Catalysts

Chunshan Song

Applied Catalysis in Energy Laboratory, and Department of Energy and Geo-Environmental Engineering, Pennsylvania State University, 209 Academic Projects Building, University Park, PA 16802

This paper is an account of our recent work which demonstrates that high-value chemicals can be obtained from polycyclic hydrocarbons by shape-selective conversion over certain 12-MR or 10-MR zeolite catalysts or zeolite-supported metal catalysts. We are studying shape-selective alkylation of naphthalene into 2,6-dialkyl-naphthalene, ring-shift isomerization of sym-octahydrophenanthrene into sym-octahydroanthracene, shape-selective alkylation of biphenyl into 4,4'-dialkylbiphenyl, conformational isomerization of cis-decalin into trans-decalin, selective hydrogenation of naphthalene into either cis- or trans-decalin, and regio-selective hydrogenation of heteroatom-containing aromatic compounds. The products of such selective reactions are value-added chemicals, specialty chemicals, monomers of advanced polymer materials such as high-performance polyesters and liquid crystalline polymers, or components of advanced thermally stable aviation jet fuels for high-Mach aircraft.

Since the pioneering studies reported by Paul B. Weisz and coworkers at Mobil in 1960, shape selective conversion of acyclic and monocyclic compounds over various zeolites have been studied extensively, as summarized in many reviews (1-7). However, until recently, little attention has been paid to shape-selective catalytic conversion of polycyclic aromatic hydrocarbons (PAH).

The needs for research on selective PAH conversion have been discussed recently (8-10). Briefly, recent years have witnessed significant growth of existing aromatic polymer materials and rapid development of advanced aromatic polymer materials such as engineering plastics, polyester resins and fibers, polyimides, and liquid crystalline polymers (LCPs). Table 1 shows some of these new polymer materials. The advanced polymer materials of interest include thermoplastic polyethylene naphthalate (PEN), polybutylene naphthalate (PBN), thermotropic LCPs, and heat-resistant polymers (Table 1), in addition to well-known polyethylene terephthalate (PET), polybutylene terephthalate (PBT), polycarbonate (PC), and polyphenylene oxide (PPO). All these polymers require a one- to four-ring aromatic monomer with a specific structure (more linear ones in most cases). Therefore, shape-

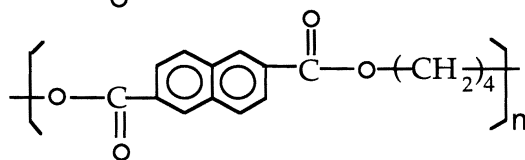
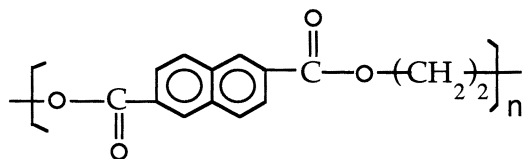
selective PAH conversion research can be applied for making chemicals from 1- to 4-ring compounds that are rich in some industrial process streams (byproduct tars from coal carbonization or gasification, oil refinery streams, etc.). This article is an account of our recent research on selective conversion of polycyclic hydrocarbons.

### Selective Synthesis of High-Value Chemicals

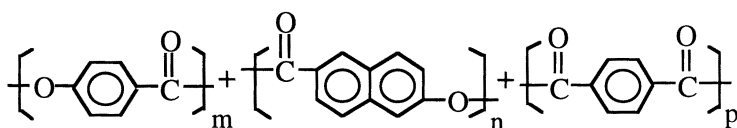
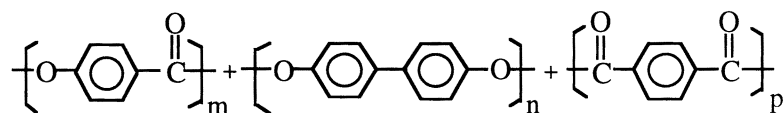
Our attention on chemicals has focused on shape-selective catalytic synthesis of value-added chemicals from polycyclic aromatic compounds that are rich in coal liquids and some refinery streams. We are studying ring-shift isomerization of phenanthrene derivatives to anthracene derivatives (11-13), shape-selective alkylation of naphthalene (14-19), shape-selective alkylation of biphenyl (19,20), conformational isomerization of cis-decahydronaphthalene (11,21), and shape-selective hydrogenation of naphthalene (22,23), and as described below.

**Table 1.** Structures of Some Important Aromatic Polymers

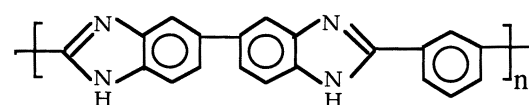
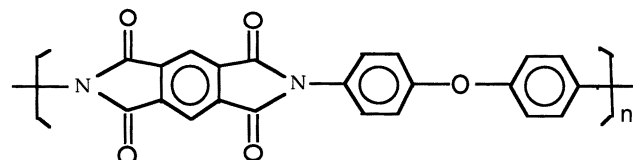
#### Thermoplastic Polyesters



#### Thermotropic Polyester LCPs

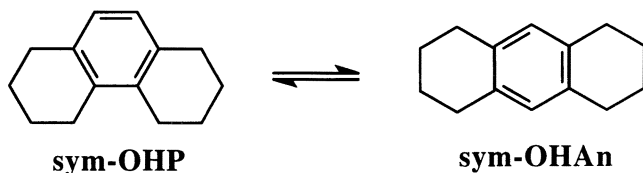


#### High-Temp Heat-Resistant Polymers



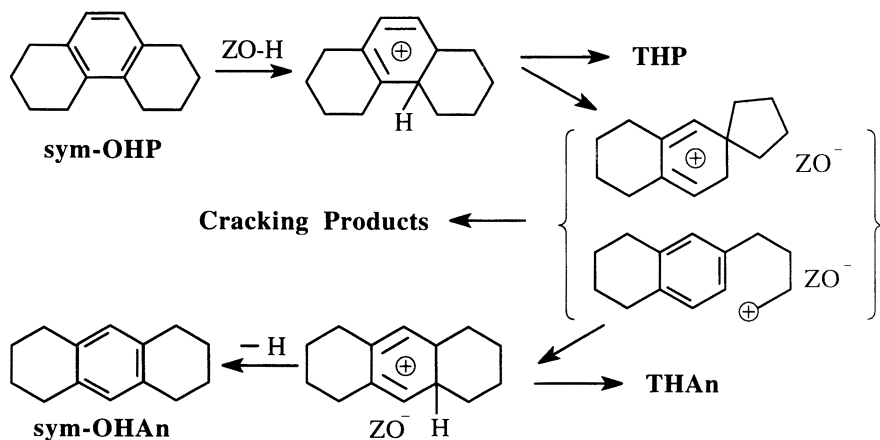
**Ring-Shift Isomerization.** Phenanthrene and its derivatives are rich in various coal-derived liquids such as coal tars, but their industrial use is still very limited. On the other hand, anthracene and its derivatives have found wide industrial applications (8,9). We have found that some mordenite and ion-exchanged Y zeolite catalysts selectively promote the transformation of sym-octahydrophenanthrene (sym-OHP) to sym-octahydroanthracene (sym-OHAn), which we call ring-shift isomerization (11), as shown in Scheme I. This reaction is in distinct contrast to the well-known ring-contraction isomerization which results in methylindane-type products. Table 2 shows some representative results (13). The properties of the Y-zeolite and mordenite catalysts in Table 2 are described elsewhere (11).

### Scheme I.



The reaction mechanism for the ring-shift isomerization has not yet been clarified. We proposed a possible mechanistic explanation of sym-OHP to sym-OHAn conversion on zeolite (11), as shown in a modified version in Scheme II. The first requirement would be the appropriate adsorption of sym-OHP on the catalyst surface. After the adsorption, the reaction is likely initiated by the protonation of the central aromatic ring in sym-OHP on Bronsted acid sites. However, the protonated intermediate could lead to several different products due to ring-opening cracking, alkyl chain isomerization, and subsequent cracking. In fact, the cracking reactions occur extensively on H-Y at  $\geq 250^\circ\text{C}$ , as can be seen from Table 2. Therefore, the second step is dependent upon whether or not the positive charge is stabilized. For the ring-shift isomerization, the cationic intermediate should be stabilized by nearby anionic sites.

### Scheme II.



Since zeolite acidity is associated with the aluminum ions, certain level of density of acid sites is required for effective ring-shift isomerization. From the above considerations, good zeolite catalysts should possess appropriate pore structure and the desired density and strength of the acidic sites for ring-shift isomerization of sym-OHP. This suggests that highly Al-deficient zeolite may not be suitable for this reaction. The fact that a hydrogen mordenite HML8 displayed higher selectivity than many others examined at 250 °C in both aliphatic and aromatic solvents suggests that it has the characteristics closer to those required for the reaction.

The selectivity and activity of the catalysts also depend on the reaction conditions. Under mild conditions, some zeolites can afford over 90% selectivity to sym-OHAN with high conversion of sym-OHP (11,13). This could provide a cheap route to anthracene and its derivatives, which are valuable chemicals in demand, from phenanthrene that is rich in liquids from coal. Possible uses of sym-OHAN include the manufacturing of anthracene (for dyestuffs), anthraquinone (pulping agent), and pyromellitic dianhydride (the monomer for polyimides such as Du Pont's Kapton) (8).

**Table 2.** Ring-Shift Isomerization of sym-OHP over Zeolite Catalysts in the Presence of Mesitylene Solvent

Catalyst ID	Run Conditions	OHP Conv (%)	Yields (% of OHP)			%Select Ring-shift
			Sym-OHAN <sup>a</sup>	THAN	THP	
HY	250°C-1 h	72.7	22.1	3.4	5.3	31.1
LaHY	250°C-1 h	73.4	21.8	3.6	5.5	30.7
NiHY	250°C-1 h	51.5	46.9	1.2	4.5	87.9
HML8	250°C-0.5 h	50.3	48.8	1.0	1.7	93.1
HML8	250°C-2 h	51.9	49.3	1.3	1.7	91.9
HML8	200°C-0.5 h h	13.1	14.7	0.1	1.4	91.2
HML8	300°C- 0.5 h	55.4	42.7	2.1	3.7	75.6
HM30A	250°C-1 h	55.1	42.9	2.1	2.5	76.2

a) The feed originally contained 91% sym-OHP, 2.9% sym-OHAN, and 6.1% others.

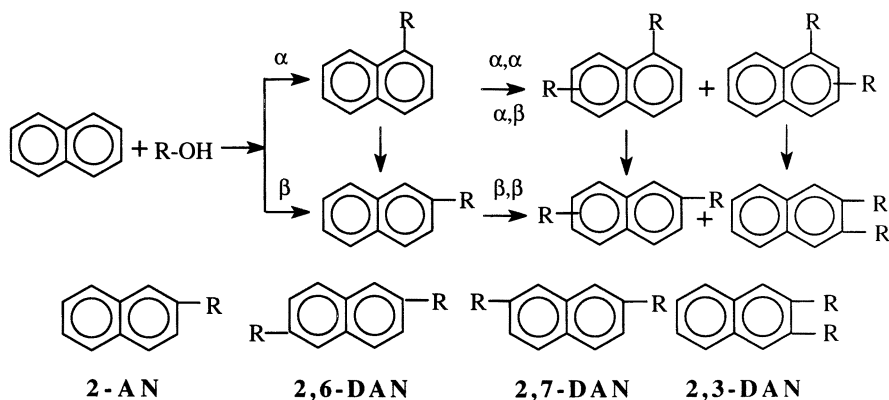
### Shape-selective alkylation of naphthalene.

Until recently, only limited attention has been paid to shape selective alkylation of two-ring aromatics such as naphthalene and biphenyl. Due to the demand for monomers for making the advanced polymer materials such as PEN and PBN, 2,6-dialkyl substituted naphthalene (2,6-DAN) is needed now for making the monomers for PEN, PBN and LCPs. In some refinery streams such as LCOs and in tars or liquids derived from coal, naphthalene and its derivatives are major components. Shape-selective alkylation over molecular sieve catalysts can produce 2,6-DAN.

There are ten possible DAN isomers. The  $\beta,\beta$ -selective alkylation over molecular sieve catalysts (Scheme III) can produce 2-alkylnaphthalene, 2,6-, 2,7-, and 2,3-DAN. The key challenge is to obtain 2,6-DAN with high selectivity, which means increasing the ratio of 2,6/2,7-DAN. Several recent papers described shape-selective isopropylation. Katayama and coworkers (24) reported preferential formation of 2,6-diisopropylnaphthalene (2,6-DIPN) using mordenite. On the other hand, Moreau and coworkers have observed that 2,6- and 2,7-disubstituted products are formed in equal yields with a ratio of around 1 when using mordenite and Y-zeolite catalysts for

isopropylation with isopropyl bromide and for cyclohexylation with cyclohexyl bromide (25).

### Scheme III



The results from our laboratory show that by using partially dealuminated mordenite catalysts, regioselective alkylation of naphthalene can be achieved with over 65% selectivity to 2,6-DIPN by using isopropanol (14) with 2,6-DIPN/2,7-DIPN ratio of about 3 or using propylene (15-19) as the alkylating agent with 2,6-DIPN/2,7-DIPN ratio of >2. Compared to parent mordenites, the partially dealuminated proton-form mordenites are more effective as shape-selective catalysts for isopropylation of naphthalene. The results on the effects of dealumination have been reported recently (15-19, 24, 26). It has been indicated that 2,6-DIPN is slightly smaller than 2,7-DIPN (14). Horsley and coworkers (27) have shown by computer simulation that the diffusion of 2,6-DIPN inside mordenite pore channel is easier than that of 2,7-DIPN, accounting at least partially for the observed selectivity of mordenite for 2,6-DIPN and higher 2,6-DIPN/2,7-DIPN ratio. We also found some simple and effective methods for enhancing the shape selectivity by using water and dealuminated mordenite (15,17,18). Table 3 shows some typical results for naphthalene alkylation with isopropanol as the alkylating agent in the presence of mesitylene solvent (11).

**Table 3.** Isopropylation of Naphthalene with Isopropanol over Zeolites at 250°C

Catalyst ID <sup>a</sup>	Structure Type	Naph Conv (%)	Yield (% of Naph)		% Isomer Select.	
			IPN	MIPN	% 2-IPN	% 2,6-DIPN
HY	Y Zeolite	38.2	90.4	9.5	33.8	16.0
HM30A	Mordenite	27.6	84.1	15.9	88.6	67.0

a) The alkylation was conducted in the presence of mesitylene solvent.

Sugi and coworkers (28) have reported detailed results on the effect of SiO<sub>2</sub>/Al<sub>2</sub>O<sub>3</sub> ratio of mordenite on naphthalene isopropylation with propylene. They analyzed not only the bulk of the reaction products, but also the products trapped in the pores of mordenite after the isopropylation. The results reveal that inside the mordenite pore channel 2,6-DIPN was formed in a much higher selectivity than 2,7-DIPN, but the external surface sites contribute more to the non-selective reactions as

well as coke formation. The same group also reported (29) that the impregnation of cerium is an effective method for the deactivation of external acid sites of hydrogen mordenite, which leads to improved selectivity to 2,6-DIPN, up to 70%. We have shown that the reactivity of 2,6-DIPN is substantially lower on dealuminated mordenite than on parent mordenite (16).

The selective naphthalene methylation has also been reported in literature (30, 31). Fraenkel and coworkers (30) first published on selective naphthalene methylation over ZSM-5 type catalysts in 1986, but 2,6- and 2,7-isomers were not separated. Komatsu and Yashima (31) recently reported on the selective formation of 2,6-dimethylnaphthalene (2,6-DMN) from methylation of 2-methylnaphthalene with methanol on HZSM-5 and metallosilicates with MFI structure. They demonstrated that isomorphous substitution of Al by other elements such as B and Fe and deactivation of external surface (by using basic nitrogen compound) can increase the selectivity to 2,6-DMN. They concluded that in order to obtain 2,6-DMN in high selectivity, it is effective to weaken the acid strength while keeping the pore dimension of MFI structure constant (or, wider, if possible), which can be achieved by using Fe-MFI as a catalyst. Their results probably represent the level of selectivity in 2-MN methylation that has been achieved and reported in open literature so far using HZSM-5 and metallosilicates with MFI structure. Based on the literature, it is difficult for methylation of naphthalene over medium-pore zeolites to reach the same level of selectivity achieved in isopropylation to 2,6-DAN with mordenite catalysts.

**Shape-selective Alkylation of Biphenyl.** Biphenyl and its derivatives are present in some refinery streams and in coal-derived liquids, although at concentrations lower than those of naphthalene derivatives. Shape-selective alkylation of biphenyl can produce 4,4'-dialkyl substituted biphenyl (4,4'-DAB), the starting material for monomer of some LCP materials represented by Xydar. Partially dealuminated proton-form mordenite can be used as shape-selective catalyst for isopropylation of biphenyl (Scheme IV).

Lee and Garces first published (32) on the effect of dealumination of mordenite on selective biphenyl isopropylation in 1989. They have demonstrated the beneficial effect of dealumination for selective formation of 4,4'- diisopropylbiphenyl (4,4'-DIPB). Sugi and coworkers have carried out a series of studies on biphenyl isopropylation over mordenites (33,34). They have reported on the influence of propylene pressure (35), effects of  $\text{SiO}_2/\text{Al}_2\text{O}_3$  ratio of mordenites, on shape-selectivity and coke deposition (36), and impact of cerium exchange of sodium mordenite (37). It was shown in our report that dealumination of some commercial mordenites by acid treatment first increases then decreases their activity, but increases their selectivity toward 4,4'-DIPB in isopropylation with propylene (19).

#### Scheme IV

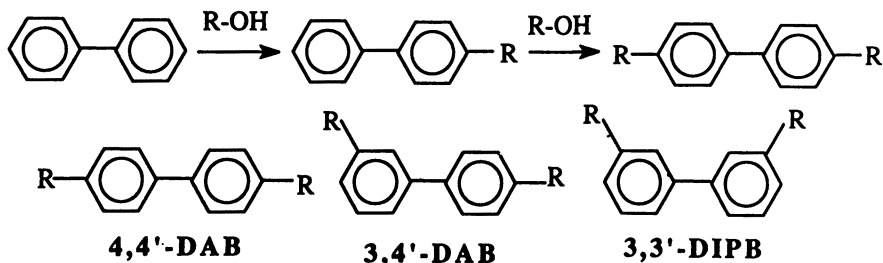




Table 4 shows some typical results for selective biphenyl isopropylation over dealuminated mordenites (20). More recently, we have found that addition of water to dealuminated mordenite is a simple method to inhibit deactivation of the partially dealuminated mordenite catalysts without losing activity and selectivity (20). Kikuchi and coworkers have shown that biphenyl can be selectively alkylated not only with mordenite (38) but also with SAPO-11 catalysts (39). In both cases, deactivation of external surfaces was shown to increase the selectivity to 4,4'-DIPB. In their report on mordenite, they demonstrated that deactivation of external acid sites on mordenite by treatment with tributylphosphite is effective for improving selectivity to 4,4'-DIPB.

**Table 4.** Isopropylation of Biphenyl with Propylene over Zeolites at 250°C

Catalyst ID <sup>a</sup>	Conv mol %	Product (mol%)			DIPB Isomer Selectivity, mol%			
		MIPB	DIPB	TrIPB	3,3'-	3,4'-	4,4'-	other
HM14	49	74	25	0.5	3.9	17	66	13.8
HM21	60	64	33	1.5	3.0	15	72	10.8
HM38	71	54	42	3.0	2.7	13	72	12.2
HM71B	46	62	37	1.1	1.3	11	83	4.9
HM230	23	67	32	0.5	0.9	10	87	2.5

a) Trailing digit indicate the SiO<sub>2</sub>/Al<sub>2</sub>O<sub>3</sub> molar ratio of the mordenite catalysts.

**Conformational Isomerization.** Commercial decalins obtained from naphthalene hydrogenation are almost equimolar mixtures of cis-decalin and trans-decalin. In the course of studying sym-OHP isomerization using decalin as solvent, we accidentally found that cis-decalin isomerizes to trans-decalin over ion-exchanged Y zeolite and mordenite catalysts (11) at low temperatures (250°C), as shown in Scheme V. This reaction would require a temperature of above 400°C in the absence of a catalyst (40).

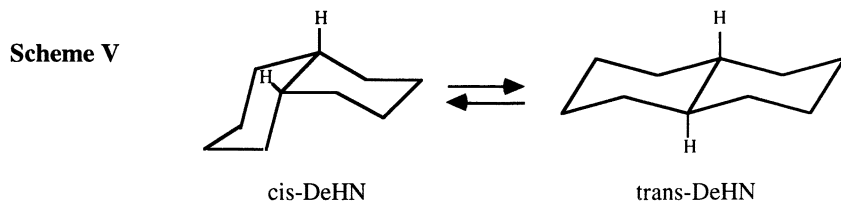


Table 5 shows some recent results from our laboratory (21). The catalytic reactions were mainly conducted at 200-250 °C for 0.15-8 h under an initial pressure of 0.79 MPa N<sub>2</sub> or H<sub>2</sub> using six catalysts: a hydrogen Y zeolite, a lanthanum ion-exchanged Y zeolite, a hydrogen mordenite, and three noble metal loaded mordenites.

Selected results are given in Table 5. Pt- and Pd-loaded mordenites displayed the highest selectivity towards trans-DeHN (nearly 100%), with a trans-DeHN/cis-DeHN ratio of about 13 under H<sub>2</sub> at 200°C; however, they are less effective under N<sub>2</sub>. Pre-reduction of Pt/HM30A could improve its catalytic effectiveness in N<sub>2</sub> atmosphere.

**Table 5.** Conformational Isomerization of cis-Decalin over Zeolite Catalysts at 200-250°C for 2 h under 0.79 MPa N<sub>2</sub> or H<sub>2</sub>

Catalyst <sup>a</sup>	Reaction Conditions	% trans-Decalin	% cis-Decalin	% Other Products	trans-D/cis-D Ratio
Decalin	Feed	48.34	50.62	1.04	0.95
LaHY	200°C - N <sub>2</sub>	48.29	50.73	0.98	0.95
LaHY	250°C - N <sub>2</sub>	65.15	18.82	16.03	3.9
HM30A	250°C - N <sub>2</sub>	53.02	31.60	15.38	1.7
Pt/HM30A	200°C - N <sub>2</sub>	62.40	33.46	4.14	1.9
Pd/HM30A	200°C - N <sub>2</sub>	54.50	42.43	3.07	1.3
Pt/HM30A	200°C - H <sub>2</sub>	92.34	7.25	0.41	12.7
Pd/HM30A	200°C - H <sub>2</sub>	92.31	7.23	0.46	12.8

a) Pt and Pd loading was 6 wt%.

By using mordenite-supported platinum or palladium catalysts, it is possible to achieve over 90% conversion with 95% selectivity at 200°C (21). trans-Decalin has substantially higher thermal stability at temperatures above 400°C (40). Possible applications of this process are high-temperature heat-transfer fluids and advanced thermally stable jet fuels, which can be used both as heat sinks and as fuels for high-Mach aircraft (41,42).

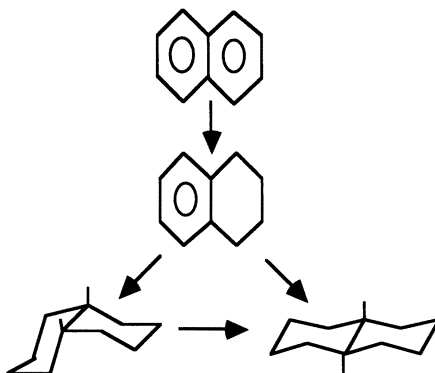
### Shape-Selective Hydrogenation of Naphthalene.

Complete hydrogenation of naphthalene in conventional processes produces mixtures of cis- and trans-decalin. Our work on selective naphthalene hydrogenation is motivated from the accidental finding (11) on zeolite-catalyzed isomerization of cis-decalin and from the need to tailor the formation of desired isomers from two-ring compounds. Our previous studies on naphthalene hydrogenation showed that certain catalysts show higher selectivity towards cis-decalin or trans-decalin. More recently, we found that mordenite and Y zeolite-supported Pt and Pd catalysts can selectively promote the formation of cis-decalin or trans-decalin (22), as shown in Scheme VI.

Table 6 shows some representative results (22). Catalytic selectivity was found to depend on both the metal and the zeolite. Consequently, the catalyst composition could be tailored for selective production of either cis-DeHN or trans-DeHN. For example, Pt/HY showed especially high selectivity (80%) for cis-DeHN and unlike all other catalysts tested, did not promote the isomerization of cis-DeHN. On the other hand, equilibrium between the DeHN isomers was achieved with Pd/HM21, giving ca. 93% trans-DeHN at 200 °C. In general, Pd catalysts showed higher initial selectivity for trans-DeHN than Pt catalysts. Also, the isomerization of cis-DeHN to trans-DeHN was more rapid on Pd catalysts. Selectivity for trans-DeHN appeared to increase with the fraction of weak acid sites on the zeolite (measured gravimetrically,

using TPD of n-butylamine). No correlation between metal crystallite sizes (determined from XRD line-broadening) and DeHN isomer selectivity was found.

Scheme VI



**Table 6.** Selective Hydrogenation of Naphthalene over Zeolite-Supported Pt and Pd Catalysts in Tridecane Solvent

Catalyst <sup>a</sup>	Conditions	% cis-Decalin	% trans-Decalin	trans/cis ratio
Pt/HY	200 °C- 1 h	82.3	15.1	0.2
Pt/HM38	200 °C- 1 h	29.9	70.1	2.3
Pd/HY	200 °C- 1 h	27.1	72.9	2.7
Pd/HM38	200 °C- 1 h	18.4	81.6	4.4

a) Pt and Pd loading was 6 wt%.

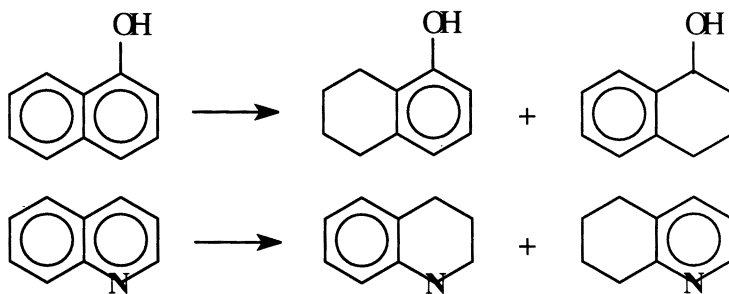
Now we can produce cis-decalin, with over 80% selectivity (or over 80% trans-decalin) at 100% conversion by using some zeolite-supported catalysts at 200°C (22). cis-Decalin may have potential industrial application as the starting material for making sebacic acid. Sebacic acid can be used for manufacturing Nylon 6,10 and softeners.

There is also an industrial need for selective production of tetralin, a hydrogen-donor solvent, from naphthalene. Partial passivation of some zeolite-supported noble metal catalysts by sulfur can make them highly selective for the production of tetralin during metal-catalyzed hydrogenation of naphthalene at low temperatures (23). In addition, recent work in our laboratory has shown that the selectivity in hydrogenation of polyaromatic compounds such as naphthalene and phenanthrene depends on the type of metal and the type of supports as well as the metal-support combinations and reaction conditions (43-45).

**Regio-Selective Hydrogenation.** More recently we have begun to explore regio-selective hydrogenation of heteroatom-containing aromatic compounds. Examples of such compounds are 1-naphthol and quinoline shown in Scheme VII. Partial hydrogenation of 1-naphthol can give 1,2,3,4-tetrahydro-1-naphthol (THNL-1) and 5,6,7,8-tetrahydro-1-naphthol (THNL-2). Under fuel hydrotreating conditions, hydrogenolysis of C-O bond can also take place. It is of interest to see whether we

can selectively produce THNL-1. Similarly, for partial hydrogenation of quinoline, either 1,2,3,4-tetrahydroquinoline (THQ-1) or 5,6,7,8-tetrahydroquinoline (THQ-2) can be produced. It is interesting to clarify how can one of the two isomers be produced selectively under practically useful conditions for catalytic processing. The hydroaromatic products of regio-selective hydrogenation have some unique applications. One example is their potential as hydrogen donors or radical scavengers for stabilizing fuels at high temperatures (46,47). We are conducting experimental work on regio-selective hydrogenation over various metal catalysts supported on zeolites, alumina and titania. As in the case of naphthalene hydrogenation described above, the type of metal and support were found to be important for achieving regio-selectivity (for example, to THNL-1).

**Scheme VII**



### Concluding Remarks

Selective catalytic conversion of PAHs can be very useful for making polycyclic specialty chemicals that have potential industrial applications. Because of the presence of two or more isomers of polycyclic compounds, the challenge is to direct the reaction along a very specific pathway to the desired isomer. Substantial progress has been made in the applied fundamental research in the past several years. In many cases, further improvement in catalyst selectivity and stability is needed, and many fundamental questions concerning mechanistic aspects remain to be answered by future study.

This article is an account of recent research conducted in our laboratory on selective conversion of polycyclic compounds. An excellent general review of research on shape-selective alkylation of polycyclic aromatics and isomerization of alkylated aromatics has been published recently by Sugi and Kubota (48). In addition to experimental research, computational analysis has also begun to shed light on selective conversion of polycyclic compounds (49).

### Acknowledgments

The author is very grateful to Prof. Harold H. Schobert for his encouragement and support for catalytic research, to his former coworkers Drs. Andrew D. Schmitz, Wei-Chuan Lai, Shawn D. Lin, and K. Madhusudan Reddy for many helpful discussions, and to Prof. Paul B. Weisz of PSU and Dr. Werner O. Haag of Mobil for their encouragement. The author also wishes to thank Dr. Michael Ford of Air

Products & Chemicals Inc. and Prof. John W. Larsen of Lehigh University for helpful discussions on the possible mechanism of sym-OHP ring-shift isomerization, and Dr. Juan M. Garces of Dow Chemical Company and Prof. Y. Sugi for general discussions on PAH conversion over zeolites. Various portions of our research were supported through funding or donations of special samples from the U.S. Department of Energy/Federal Energy Technology Center, U.S. Air Force/Wright Laboratories, Air Products and Chemicals Inc., and PQ Co.

### Literature Cited

1. Weisz, P. B. *Pure & Appl. Chem.*, **1980**, 52, 2091.
2. Venuto, P. B. *Micropor. Mater.*, **1994**, 2, 297.
3. Csicsery, S.M. *Stud. Surf. Sci. Catal.*, **1995**, 94, 1.
4. Haag, W. O. *Stud. Surf. Sci. Catal.*, **1994**, 84, 1375.
5. Weitkamp, J.; Weiß, U.; Ernst, S. *Stud. Surf. Sci. Catal.*, **1995**, 94, 363.
6. Suib, S. L. *Am. Chem. Soc. Sym. Ser.*, **1993**, 517, 1.
7. Chen, N. Y.; Garwood, W. E.; Dwyer, F. G. *Shape-Selective Catalysis in Industrial Applications*. 2nd Edition, Marcel Dekker, New York, **1996**, 282 pp.
8. Song, C.; Schobert, H. H. *Fuel Process. Technol.*, **1993**, 34, 157.
9. (a) Song, C.; Schobert, H. H. *Chem. Ind.*, **1996**, 7, 253; (b) Song, C.; Schobert, H. H. *Fuel*, **1996**, 75, 724.
10. Sugi, Y.; Toba, M., *Catal. Today*, **1994**, 19, 187.
11. Song, C.; Moffatt, K. *Micropor. Mater.*, **1994**, 2, 459.
12. Song, C. U.S. Patent, **1996**, No. 5,523,505.
13. Lai, W.-C.; Song, C.; van Duin, A.; de Leeuw, J.W. *Catal. Today*, **1996**, 31, 145.
14. Song, C.; Kirby, S. *Micropor. Mater.*, **1994**, 2, 467.
15. Schmitz, A.; Song, C. *Am. Chem. Soc. Div. Fuel Chem. Prepr.*, **1994**, 39, 986.
16. Schmitz, A.; Song, C. *Catal. Today*, **1996**, 31, 19.
17. Schmitz, A.; Song, C. *Catal. Lett.*, **1996**, 31, 59.
18. Song, C.; Schmitz, A., Extended Abstracts, Program. 11th Internat. Congress on Catalysis, Baltimore, Maryland, June 30-July 5, 1996, Po-164.
19. Schmitz, A.; Song, C. *Am. Chem. Soc. Div. Fuel Chem. Prepr.*, **1995**, 40, 918.
20. Song, C.; Schmitz, A. 15th North Am. Catal. Soc. Meet., Technical Program, Chicago, May 18-22, **1997**, p.159.
21. Lai, W.-C.; Song, C. *Catal. Today*, 1996, **1996**, 31, 171.
22. Schmitz, A.; Bowers, G.; Song, C. *Catal. Today*, **1996**, 31, 45.
23. Song, C.; Schmitz, A. *Energy & Fuels*, **1997**, 11, 656.
24. Katayama, A.; Toba, M.; Takeuchi, G.; Mizukami, F.; Niwa, S.; Mitamura, S. *J. Chem. Soc. Chem. Comm.*, **1991**, 39.
25. Moreau, P.; Finiels, A.; Geneste, P.; Joffre, J.; Moreau, F.; Solofo, J. *Catal. Today*, **1996**, 31, 11.
26. Fellmann, J.D.; Saxton, J.; Wentreck, P.R.; Derouane, E.G.; Massioni, P. U. S. Patent, **1991**, No. 5,026,942.
27. Horsley, J.A.; Fellmann, J.D.; Derouane, E.G.; Freeman, C.M. *J. Catal.*, **1994**, 147, 231.
28. Kim, J.-H.; Sugi, Y.; Matsuzaki, T.; Hanaoka, T.; Kubota, Y.; Tu, X.; Matsumoto, M. *Micropor. Mater.*, **1995**, 5, 113.
29. Kim, J.-H.; Sugi, Y.; Matsuzaki, T.; Hanaoka, T.; Kubota, Y.; Tu, X.; Matsumoto, M.; Nakata, S.; Kato, A.; Seo, G.; Pak, C. *Appl. Catal. A: General*, **1995**, 131, 15.
30. Fraenkel, D.; Cherniavsky, M.; Ittah, B.; Levy, M. *J. Catal.*, **1986**, 101, 273.
31. Komatsu, T.; Aoki, Y.; Namba, S.; Yashima, T. *Stud. Surf. Sci. Catal.*, **1994**, 84, 1821.
32. Lee, G.S.; Maj, J. J.; Rocke, S. C.; Garces, J. M. *Catal. Lett.*, **1989**, 2, 243.

33. Sugi, Y.; Matsuzaki, T.; Hanaoka, T.; Takeuchi, H.; Arakawa, H.; Tokono, T.; Takeuchi, G. *Shokubai*, **1989**, 31, 373.
34. Sugi, Y.; Matsuzaki, T.; Hanaoka, T.; Takeuchi, K.; Tokono, T.; Takeuchi, G. *Stud. Surf. Sci. Catal.*, **1991**, 60, 303.
35. Sugi, Y.; Tu, X.-L.; Matsuzaki, T.; Hanaoka, T.; Kubota, Y.; Kim, J.-H.; Matsumoto, M.; Nakajima, K.; Igarashi, A. *Catal. Today*, **1996**, 31, 3.
36. Sugi, Y.; Matsuzaki, T.; Hanaoka, T.; Kubota, Y.; Kim, J.-H.; Tu, X.; Matsumoto, M. *Catal. Lett.*, **1994**, 26, 181.
37. Sugi, Y.; Matsuzaki, T.; Hanaoka, T.; Kubota, Y.; Kim, J.-H.; Tu, X.; Matsumoto, M. *Catal. Lett.*, **1994**, 27, 315.
38. Matsuda, T.; Urata, T.; Saito, U.; Kikuchi, E. *Appl. Catal. A: General*, **1995**, 131, 215.
39. Matsuda, T.; Kimura, T.; Herawati, E.; Kobayashi, C.; Kikuchi, E. *Appl. Catal. A: General*, **1996**, 136, 19.
40. Lai, W.-C.; Song, C.; Schobert, H.H.; Arumugam, R. *Am. Chem. Soc. Div. Fuel Chem. Prepr.*, **1992**, 37, 1671.
41. Edwards, T.; Harrison, W. E.; Schobert, H. H. *33rd AIAA/ASME/ASME/SAE Joint Propulsion Conference and Exhibit*, July 6-9, **1997**, Seattle, WA, paper no. AIAA 97-2848.
42. Song, C.; Eser, S.; Schobert, H.H.; Hatcher, P.G. *Energy Fuels*, **1993**, 7, 234 .
43. Lin, S.D.; Song, C. *Catal. Today*, **1996**, 31, 93.
44. Reddy, K. M.; Song, C. *Catal. Today*, **1996**, 31, 137.
45. Reddy, K. M.; Song, C. *Mater. Res. Soc. Sym. Proc. Ser.*, **1997**, 454, 125.
46. Song, C.; Lai, W.-C.; Schobert, H. H. *Ind. Eng. Chem. Res.*, **1994**, 33, 548.
47. Yoon, E.; Selvaraj, L.; Song, C.; Stallman, J.; Coleman, M. M. *Energy Fuels*, **1996**, 10, 806.
48. Sugi, Y.; Kubota, Y. *Catalysis-Specialist Periodical Report*, **1997**, 13, 55.
49. Song, C.; Ma, X.; Schmitz, A. D.; Schobert, H. H. *Appl. Catal. A: General*, **1999**, in press.

## Chapter 18

# Influences of Bulkiness of Reagents in the Alkylation of Biphenyl over H-Mordenite

K. Nakajima<sup>1</sup>, T. Hanaoka<sup>2</sup>, Y. Sugi<sup>3,5</sup>, T. Matsuzaki<sup>2</sup>, Y. Kubota,  
A. Igarashi<sup>4</sup>, and K. Kunimori<sup>1</sup>

<sup>1</sup> Institute of Materials Science, University of Tsukuba, Tsukuba 305–8577, Japan

<sup>2</sup> National Institute of Materials and Chemical Research, Tsukuba 305–8565, Japan

<sup>3</sup> Department of Chemistry, Gifu University, Gifu 501–1193, Japan

<sup>4</sup> Department of Chemical Engineering, Kogakuin University,  
Tokyo 192–0015, Japan

The alkylation of biphenyl (BP), 4-alkylbiphenyls (4-ABP), and *p*-terphenyl (TP) with ethene, propene, and 1-butene was examined to understand the influence of bulkiness of reagents over H-mordenite (HM). The selectivity was highly dependent on the nature of alkene. The ethylation of BP to ethylbiphenyls (EBP) and diethylbiphenyls (DEBP) was non-regioselective. The ethylation of BP to EBP isomers was controlled kinetically. 4-EBP was ethylated preferentially among the isomers, although the formation of 4,4'-DEBP was less selective. The least bulky 4,4'-DEBP was also ethylated to polyethylbiphenyls (PEBP) at higher rates than the other DEBP isomers. These results show that HM pores are too loose for shape selective formation of the least bulky isomers, 4-EBP and 4,4'-DEBP, in the ethylation of BP and 4-EBP and that HM pores have enough space for the further ethylation of 4,4'-DEBP.

The isopropylation and the *sec*-butylation of BP and the isopropylation of TP yielded selectively the least bulky alkylates. The high selectivities are due to shape selective catalysis inside the pores. These discrepancies between the ethylation of BP and other alkylations depend on the difference of steric interaction among substrates and acid sites in the pores.

Attempts to control product distribution of the alkylation of polynuclear aromatics by zeolites have attracted the attention of many researchers (1-13). To synthesize target isomers selectively, it is essential to understand what occurs at acid sites inside the pore and on the external surface. We have found that the isopropylation of BP over

dealuminated HM gave high yield and selectivity of 4,4'-diisopropylbiphenyl (4,4'-DIPB) (1-6). The high selectivity of 4,4'-DIPB was explained by the steric restriction of the transition state inside HM pores (2). It is interesting to investigate steric interaction among substrates and catalytic active sites inside the pores. Although the ethylation of BP over HM was described by Takeuchi and his co-workers and us (11,12), details have not been clarified yet. In this work, the alkylations of biphenyls and *p*-terphenyl with ethene, propene, and 1-butene were examined to obtain the information of steric interaction at the transition state on shape selective catalysis.

## EXPERIMENTAL

**Reagents.** Dealuminated H-mordenite (HM,  $\text{SiO}_2/\text{Al}_2\text{O}_3=206$ ) was obtained from Tosoh Corporation, Tokyo, Japan, and calcined in an air stream at 450 °C before use. Some physicochemical properties of HM were shown in previous papers (6,10). BP, 4,4'-DIPB, 4-methylbiphenyl (4-MBP) and TP were purchased from Tokyo Chem. Ind. Co. Ltd., Tokyo, Japan. 4-Isopropylbiphenyl (4-IPBP), 3- and 4-EBP, and 4,4'-DEBP, and 4,4'-diisopropyl-*p*-terphenyl (4,4'-DIPT) were supplied from Nippon Steel Chemicals Co. Ltd., Tokyo, Japan. 3,3', 3,4', 2,4', 3,4-, and 2,4-DEBP were synthesized by the nickel catalyzed coupling of corresponding ethylphenyl magnesium bromide and bromoethylbenzene. Ethene, propene, and 1-butene were purchased from Tomoe Shokai Co. Ltd. Tokyo, Japan.

**Alkylation.** The ethylation of BP was carried out in a 100-ml autoclave. A standard set of reaction was included: BP 200 mmol, HM 1 g, ethene pressure 0.8 MPa, reaction temperature 250 °C, and reaction period 0.5 h. The reaction procedures for the ethylation of 4-ABP, the isopropylation of BP, 4-ABP, and TP and the *sec*-butylation of BP were done according to the conditions shown in footnote of Figures.

**Product analysis.** The products of the alkylation were analyzed with a Hewlett-Packard Model 5890 series II Gas Chromatograph using an Ultra-1 capillary column (25 m X 0.2 mm), and identified with a Hewlett-Packard Model 5890 series II Gas Chromatograph, equipped with a 5971A Mass Selective Detector System using the same columns. The yield of every product was calculated on the basis of BP consumed for the reaction. The selectivities of each alkylbiphenyl (ABP) and dialkylbiphenyl (DABP) isomers are based on total ABP and DABP isomers.

## RESULTS AND DISCUSSION

**Ethylation of biphenyl.** Figure 1 shows the dependence of temperature on the yield of bulk products in the ethylation of BP. The data were taken in early stages of the reaction. The feature of the formation of EBP and DEBP isomers in the ethylation was quite different from that of the isopropylation. The yield of 2- and 3-EBP increased with temperature, but the yield of 4-EBP was saturated at higher temperatures. The ratio of 2- and 3-EBP changed with the reaction temperature show that the less bulky 3-EBP participated in the alkylation at higher temperature as described below. The formation of DEBP isomers varied with temperature: the yields of 2,4-, 3,4-, 2,4', and 3,4'-DEBP increased with raising temperature. However, the feature of 4,4'-DEBP was quite different from the other isomers: the yield decreased slightly with the



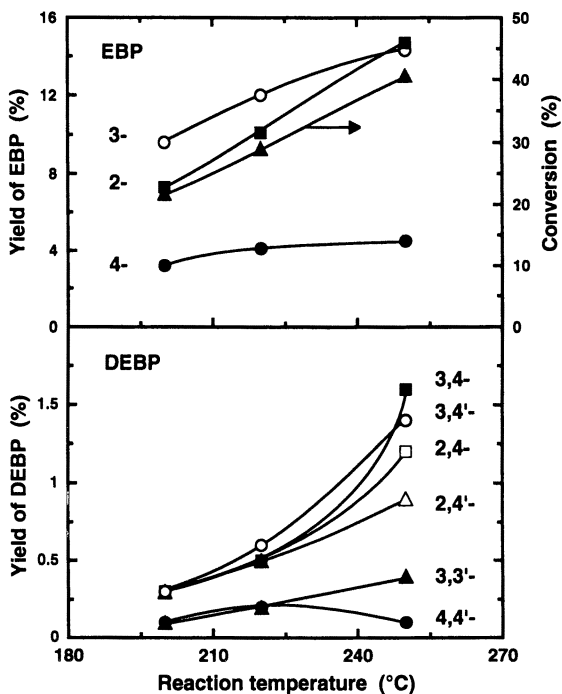


Figure 1. Effect of reaction temperature on the yield of EBP and DEBP isomers in bulk products in the ethylation of BP. Reaction conditions: BP, 200 mmol; HM, 1 g; ethene, 0.8 MPa; period, 0.5 h.

temperature. These results show that 4-EBP and 4,4'-DEBP have higher reactivities for further ethylated biphenyls than the other isomers, and that 4,4'-DEBP is the principal precursor of polyethylbiphenyls (PEBP). Similar non-regioselective alkylation was described over silica-alumina and HY in the literature (13).

The profile of the ethylation to EBP isomers at 220 °C was shown in Figure 2. The selectivities of EBP isomers were nearly in the ratio 4-EBP : 3-EBP : 2-EBP = 1 : 2 : 2 at an early stage. This means that the ethylation of BP to EBP isomers is controlled kinetically. The high selectivity of 2-EBP suggests that the nucleophilic attack to 2-position is predominated over other positions due to its high electron density. However, these three isomers act differently at higher conversion. The yield of 4-EBP reached maximum at 40-50% of the conversion, and decreased with the further reaction. The yields of 3-EBP increased at early and middle stages, but it was saturated at late stage. The formation of 2-EBP increased monotonously during the reaction. These results suggest that these three isomers have different reactivities for the ethylation to DEBP isomers according to their bulkiness. The least bulky isomer 4-EBP is consumed at the highest rates. Although 3-EBP has lower reactivity than 4-EBP, the ethylation occurs at higher conversion after the most of 4-EBP disappears. 2-EBP is not ethylated under the conditions.

The yield and the selectivity of DEBP isomers are shown in Figure 3. The yield of 2,4-, 3,4-, 3,4'-, and 2,4'-DEBP increased with increasing the conversion. However, the yield of 4,4'-DEBP increased only in the initial stages. It reached maximum at 40-60 % of the conversion, and then, decreased at higher conversion. The combined selectivity of DEBP isomers with 4-ethyl group, *i.e.*, 2,4-, 3,4-, 3,4'-, 2,4'-, and 4,4'-DEBP, kept 80 % during the reaction. However, the selectivities of 4,4'-, 3,4'-, and 2,4'-DEBP, which are less bulky isomers, decreased with increasing the conversion. Particularly, the behavior of 4,4'-DEBP was quite different from the other isomers: the yield was quite low and it decreased more rapidly than the other isomers do. This is quite similar to the behavior of 4-EBP discussed above. These results show that the most of DEBP isomers was formed from 4-EBP, and that 4,4'-DEBP were ethylated preferentially to PEBP at higher rate than the other isomers. The appearance of 3,3'-DEBP shows that the participation of 3-IPBP, and a part of 3,4'- and 3,4-DEBP are possibly formed from 3-EBP. These results correspond well to those from Figure 1 as discussed above.

The ethylation of 4-EBP at 220 °C gave similar feature to the ethylation of BP except for no formation of 3,3'-DEBP (Figure 4). The yield of 2,4-, 3,4-, 3,4'-, and 2,4'-DEBP isomers increased with the conversion. However, the yield of 4,4'-DEBP increased initially, whereas decreased at higher conversion. Figure 5 shows the ethylation of 3-EBP at 220 °C. The yields of 3,4'-, 3,3'-, and 3,4-DEBP, and other three isomers (D<sub>1</sub>, D<sub>2</sub> and D<sub>3</sub>)<sup>1</sup> increased with increasing the conversion. Among these isomers, the least bulky 3,4'-DEBP from 3-EBP, was consumed preferentially, and its selectivity decreased with the conversion.

Figure 6 shows the rates of the ethylation of BP, 3- and 4-EBP, and 4,4'-DEBP. The rates of these ethylations were at the same level except the case of 3-EBP. The case of the reaction may be comparable among these compounds regardless of the

<sup>1</sup> The structure of these isomers was not identified yet. These are three of 2,3-, 2,3'-, 2,5- and 3,5-DEBP isomers.

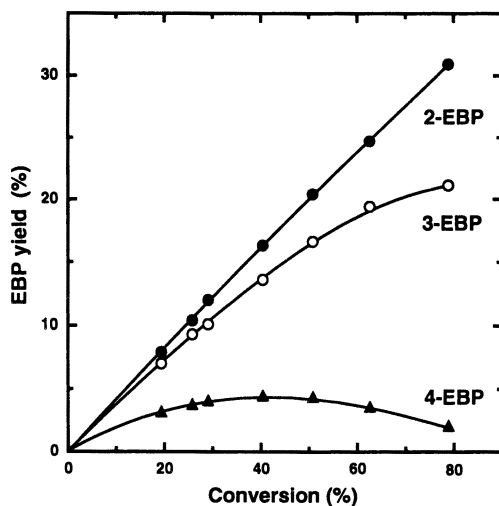


Figure 2. Profile of formation of EBP isomers in the ethylation of BP. Reaction conditions: BP, 200 mmol; HM, 1 g; ethene, 0.8 MPa; temperature, 220 °C.

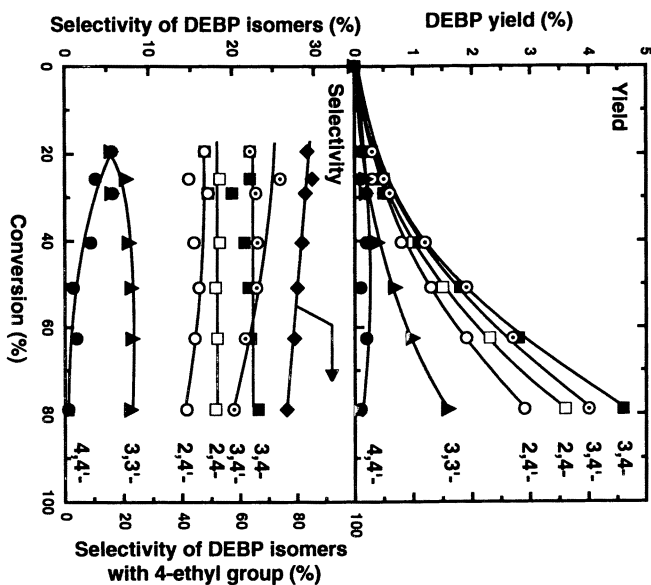


Figure 3. Profiles of the formation of DEBP isomers in the ethylation of BP. Reaction conditions are the same as in Figure 2.

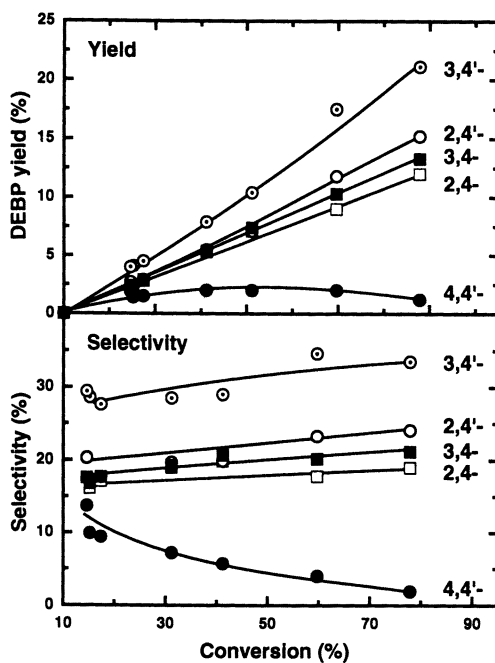


Figure 4. Profiles of the ethylation of 4-EBP. Reaction conditions: 4-EBP, 100 mmol; HM, 1 g; ethene, 0.8 MPa.

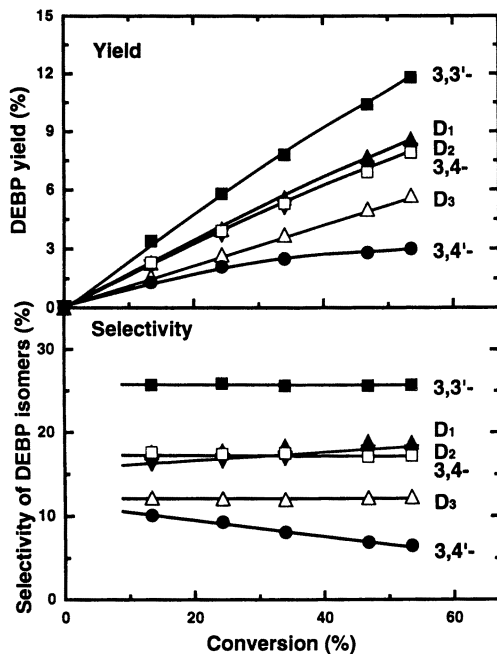


Figure 5. Profiles of the ethylation of 3-EBP. Reaction conditions: 3-EBP, 100 mmol; HM, 1 g; ethene, 0.8 MPa.

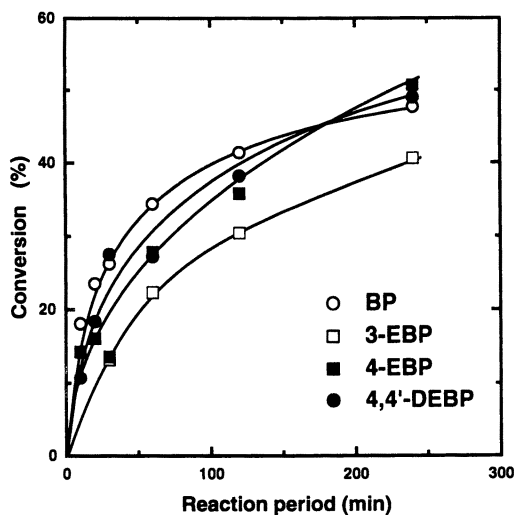


Figure 6. Rate of the ethylation of BP, 3- and 4-EBP, and 4,4'-DEBP. Reaction conditions: 3- and 4-EBP, 4,4'-DEBP, 100 mmol; HM, 1 g; ethene, 0.8 MPa; temperature, 220 °C. ethylation of BP: BP, 200 mmol; HM, 2 g. ethene, 0.8 MPa; temperature, 220 °C.

substitution with ethyl group. These results show that steric restriction of the transition state for the ethylation of BP and 4-EBP in HM pores is too loose for shape selective catalysis, and that HM pore has enough space for the further ethylation of 4,4'-DEBP. The explanation of these results by the diffusivity is less plausible because the least bulky isomers, 4-EBP and 4,4'-DEBP does not come preferentially to bulk products.

**Alkylation with different alkenes.** Figure 7 shows the difference of the selectivities of the least bulky isomers in the alkylation of BP. The selectivities of 4,4'-DIPB kept constant during the isopropylation of BP under moderately high propene pressure (4). The distribution in encapsulated products resembled to that in bulk products (2). The reaction proceeded exclusively in HM pore, and was governed by steric interaction of substrate, and acid sites with the pores. The profile of the *sec*-butylation of BP under 0.5 MPa of 1-butene is similar to those of the isopropylation: 85 % of the selectivity of 4,4'-di-*sec*-butylbiphenyl (4,4'-DSBB) was kept during the reaction. The selectivity for the isopropylation of TP was also shown in Figure 7. The profile was quite similar to the case of BP: highly selective formation of 4,4'-DIPT was also observed. Takeuchi and his co-workers obtained similar results on the isopropylation of TP (11). On the other hand, the ethylation of BP yielded 4,4'-DEBP in low yield as discussed above, and the selectivity decreased with increasing the conversion. From these results, the selectivity of the least bulky alkylates increased in the order: ethylation of BP << isopropylation of BP  $\approx$  isopropylation of TP  $\approx$  *sec*-butylation of BP. These discrepancies between the ethylation of BP and other alkylations depend on the difference of steric interaction among substrates and acid sites in HM pores.

**Isopropylation and ethylation of 4-alkylbiphenyls.** The isopropylation and the ethylation of 4-alkylbiphenyls (4-ABP) (alkyl = methyl, ethyl, and isopropyl) were examined to elucidate the steric interaction at the transition state in HM pores. 4-Methyl-4'-isopropylbiphenyl (4,4'-MIPB), 4-ethyl-4'-isopropylbiphenyl (4,4'-EIPB), and 4,4'-DIPB, were obtained selectively from corresponding 4-ABP in the isopropylation (Figure 8). The selectivity of 4,4'-DABP increased in the order: 4,4'-MIPB < 4,4'-EIPB < 4,4'-DIPB. As described previously (1-6), the selectivity of 4-IPBP was *ca.* 70 % in the early stage of the isopropylation of BP. Moreover, in the isopropylation of TP (4-phenylbiphenyl), the selectivity of 4-isopropyl-*p*-terphenyl was higher than 90% in the early stage of the reaction. These results show that the 4-substituent enhanced shape selective catalysis in the order: none < methyl < ethyl < isopropyl  $\approx$  phenyl. This is the order of bulkiness of substrates. On the other hand, the selectivity of 4,4'-DABP in the ethylation was much lower than that in the isopropylation, and no significant difference was observed among the substrates. The selectivity level of 4,4'-EIPB was quite different between the isopropylation of 4-EBP and the ethylation of 4-IPBP: the selectivity of 4,4'-EIPB in the ethylation of 4-IPBP was much lower than that in the isopropylation of 4-EBP. These results show that the influence of bulkiness of alkenes on the shape selectivity is more extensive than that of 4-substituents.

## CONCLUSION

In order to elucidate the mechanism of shape selective catalysis of HM, the alkylation of biphenyls was examined with ethene, propene, and 1-butene. The alkylation was highly

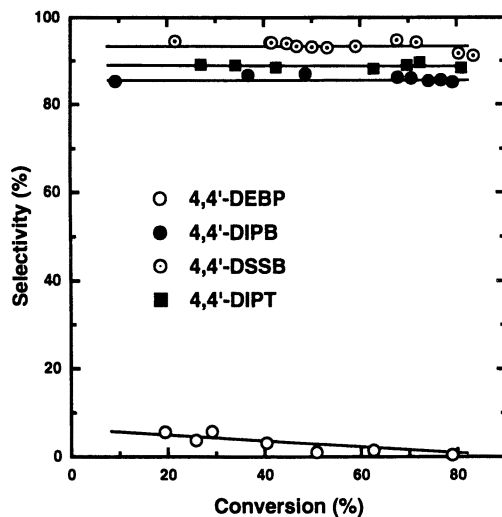


Figure 7. Selectivity of 4,4'-DABP and 4,4''-DIPT in the alkylation of BP and TP. Reaction conditions: isopropylation of BP and TP: BP or TP, 400 mmol; HM 2 g; temperature, 250 °C; propene, 0.8MPa. *sec*-butylation of BP: BP, 400 mmol; HM, 2 g; temperature, 250 °C; 1-butene, 0.5 MPa. ethylation of BP: *see* Figure 2.

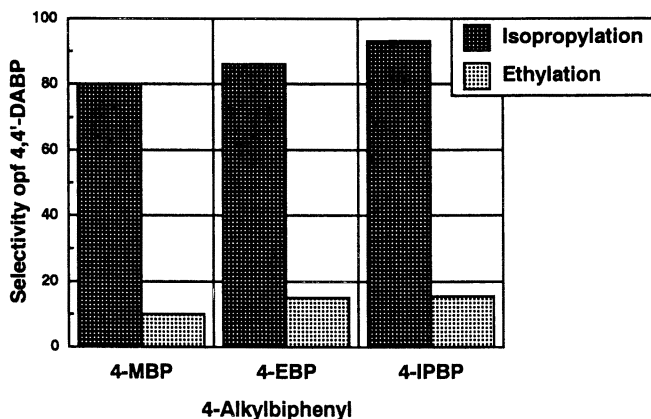


Figure 8. The isopropylation and the ethylation of 4-alkylbiphenyl. Reaction conditions. Isopropylation: substrate, 100 mmol. HM, 1 g. temperature, 250 °C, propene, 0.8 MPa, period, 4 h. Ethylation: substrate, 100 mmol; HM, 1 g; temperature, 220 °C; ethene, 0.8 MPa; period, 0.5 h.

dependent on the nature of alkene. The ethylation of BP was non-regioselective, and gave complex mixture of EBP and DEBP isomers. The ethylation of BP to EBP isomers was controlled kinetically to yield 4-EBP in low selectivity. 4-EBP is ethylated preferentially to DEBP isomers. The formation of 4,4'-DEBP was also less selective than the other isomers. Among DEBP isomers, 4,4'-DEBP was ethylated to PEBP at higher rates than the other isomers. These results show that steric restriction of the transition state with the pores for the ethylation of BP and 4-EBP is too loose for shape selective catalysis, and that HM pore has enough space for the further ethylation of 4,4'-DEBP.

The isopropylation and the *sec*-butylation of BP and the isopropylation of TP occurred shape selectively to yield the least bulky alkylates: the selectivity increased in the order: ethylation of BP << isopropylation of BP  $\approx$  isopropylation of TP  $\approx$  *sec*-butylation of BP. These discrepancies between the ethylation of BP and other alkylations depend on the difference of steric interaction among substrates and acid sites in HM pores.

The isopropylation of 4-ABP occurred shape selectively, and 4-substituents enhanced the selectivity of 4,4'-DABP in the order: none < methyl < ethyl < isopropyl  $\approx$  phenyl. This is the order of bulkiness of substrate. However, the selectivity of 4,4'-DABP in the ethylation of 4-ABP was much lower than that for the isopropylation in line with the alkylation of BP. These results showed that the influence of bulkiness of alkenes on the shape selectivity was more extensive than that of 4-substituents.

The primary factor for shape selective catalysis is the steric interaction at the transition state composed of BP, alkene, and acid sites inside the HM pores, and the steric restriction by 4-substituted group affects secondarily to improve the shape selectivity.

### Acknowledgement

A part of this work was supported by the Original Industrial Technology R&D Promotion Program from the New Energy and Industrial Technology Development Organization (NEDO) of Japan. The authors thank Nippon Steel Chemicals Co. Ltd., Tokyo, Japan for the gift of ethylbiphenyls.

### Literature Cited

1. Sugi, Y.; Toba M. *Catal. Today* **1994**, *19*, 187.
2. Sugi, Y.; Kubota, Y. in *Catalysis*, Spivey, J. J., Ed.; Specialist Periodical Report, Royal Soc. Chem., London, 1997, Vol. 13.; Chapter 3; pp 55-84.
3. Matsuzaki, T.; Sugi, Y.; Hanaoka, T.; Takeuchi, K.; Arakawa, H.; Tokoro, T.; Takeuchi, G. *Chem. Express* **1989**, *4*, 413.
4. Tu, X.; Matsumoto, M.; Matsuzaki, T.; Hanaoka, T.; Kubota, Y.; Kim, J. -H.; Sugi, Y. *Catal. Lett.* **1993**, *21*, 71.
5. Sugi, Y.; Matsuzaki, T.; Hanaoka, T.; Kubota, Y.; Kim, J.-H.; Tu, X.; Matsumoto, M. *Catal. Lett.* **1994**, *26*, 181.
6. Sugi, Y.; Matsuzaki, T.; Tokoro, T.; Hanaoka, T.; Takeuchi, K.; Tu, X.; Takeuchi, G. *Sekiyu Gakkaishi* **1994**, *37*, 376.
7. Lee, G. S.; Maj, J. J.; Rocke, S. C.; Garces, J.M. *Catal. Lett.* **1989**, *2*, 243.



8. Katayama, A.; Toba, M.; Takeuchi, G.; Mizukami, F.; Niwa, S.; Mitamura, S. *J. Chem. Soc. Chem. Commun.* **1991**, 31.
9. Song, C.; Kirby, S. *Micropor. Mater.* **1994**, *2*, 467.
10. Kim, J. -H.; Sugi, Y.; Matsuzaki, T.; Hanaoka, T.; Kubota, Y.; Matsumoto, M.; Tu, X. *Micropor. Mater.* **1995**, *5*, 113.
11. Takeuchi, G.; Okazaki, H.; Yamae, M.; Kito, K. *Appl. Catal.* **1991**, *76*, 49.
12. Tu, X.; Matsumoto, M.; Maeda, T.; Sugi, Y.; Matsuzaki, T.; Hanaoka, T.; Kubota, Y.; Kim, J. -H. *Micropor. Mater.* **1995**, *3*, 593.
13. Takeuchi, G.; Shimoura, Y.; Hara, T. *Appl. Catal. A: General* **1996**, *137*, 87.

## Chapter 19

# Encapsulated Products inside Pores of H-Mordenite in the Isopropylation of Biphenyl

K. Nakajima <sup>1</sup>, T. Hanaoka <sup>2</sup>, Y. Sugi <sup>3,5</sup>, T. Matsuzaki <sup>2</sup>, Y. Kubota, A. Igarashi <sup>4</sup>, and K. Kunimori <sup>1</sup>

<sup>1</sup> Institute of Materials Science, University of Tsukuba, Tsukuba 305-8577, Japan

<sup>2</sup> National Institute of Materials and Chemical Research, Tsukuba 305-8565, Japan

<sup>3</sup> Department of Chemistry, Gifu University, Gifu 501-1193, Japan

<sup>4</sup> Department of Chemical Engineering, Kogakuin University, Tokyo 192-0015, Japan

Selective formation of 4,4'-diisopropylbiphenyl (4,4'-DIPB) was observed in the isopropylation of biphenyl (BP) over H-mordenite (HM). The selectivity of 4,4'-DIPB was dependent on the SiO<sub>2</sub>/Al<sub>2</sub>O<sub>3</sub> ratio, and it was low for HMs with the lower ratio. Encapsulated products showed that the selectivities of 4,4'-DIPB inside the pores were higher than 85% for all HMs.

The selectivity of 4,4'-DIPB was influenced by propene pressure in the isopropylation of BP over highly dealuminated HM. The selectivity was up to 90% under 0.8 MPa of propene pressure, whereas the decrease of the selectivity occurred under 0.1 MPa. The selectivities of 4,4'-DIPB in encapsulated products for the isopropylation of BP was more than 90 % under all pressures. These results suggest that the formation of 4,4'-DIPB occurred in the pores. The low selectivity of 4,4'-DIPB over HM with low SiO<sub>2</sub>/Al<sub>2</sub>O<sub>3</sub> ratio is due to non-regioselective isopropylation at the external acid sites. The high selectivity of 4,4'-DIPB under high propene pressure is due to the prevention of the adsorption of 4,4'-DIPB on acid sites because of preferential adsorption of propene. The isomerization of 4,4'-DIPB under low pressures occurred on external acid sites where no propene was adsorbed.

Polynuclear aromatics such as biphenyl and naphthalene have attracted the attention of many researchers as a key component of advanced materials such as heat-resistant and liquid crystalline polymers. Shape selective alkylation using zeolite is a promising way for manufacturing symmetrically dialkylated polynuclear aromatics (1,2). HM has been

found to be the potential catalyst for shape selective isopropylation of BP with propene (1-7). Especially, highly dealuminated HM gave high catalytic activity and high selectivity of 4,4'-DIPB, while catalyst performances were low for HMs with the low  $\text{SiO}_2/\text{Al}_2\text{O}_3$  ratio (4-6). It is still unclear where the reaction occurs because the selectivity of 4,4'-DIPB is changed much by many factors such as reaction conditions and the nature of the catalyst.

In this paper, we describe relationships between encapsulated products inside the pores and bulk products in the isopropylation of BP and in the isomerization of 4,4'-DIPB, and discuss the mechanism of shape selective catalysis.

## Experimental

**Catalysts and Reagents.** H-Mordenites (HM,  $\text{SiO}_2/\text{Al}_2\text{O}_3 = 10, 15, 20, 25, 30, 73, 110, 128, 206,$  and 220) were obtained from Tosoh Corporation, Tokyo, Japan, and calcined at 550 °C in an air stream just before use. BP and 4,4'-DIPB were purchased from Tokyo Kasei Kogyo Co., Ltd., Tokyo, Japan, and 4-isopropylbiphenyl (4-IPBP) from Aldrich Chem. Co., Inc., Milwaukee, WI, USA. These reagents were used without further purification.

**Isopropylation.** The isopropylation of BP was carried out in a 100-ml SUS-316 autoclave under propene pressure. The autoclave containing BP and HM was purged with nitrogen before heating. After reaching reaction temperature, propene was introduced to the autoclave, and the pressure was kept constant throughout the reaction. After cooling the autoclave, the bulk products were diluted with toluene as a solvent. The products were analyzed by a Hewlett-Packard 5890 II Gas Chromatograph equipped with a Ultra-1 capillary column (25 m x 0.2 mm) and identified by a Hewlett-Packard 5978 series II Gas Chromatograph with a 5971A Mass Selective Detector. The yield of each product is calculated on the basis of consumed BP, and the selectivities of each IPBP and DIPB isomers are expressed based on total amounts of IPBP and DIPB isomers, respectively.

The analysis of encapsulated products in the catalyst used for the reaction was carried out as follows. The catalyst was filtered off, washed well with 200 ml of acetone, and dried at 110 °C for 12 h. The resulting catalyst was dissolved using a 3 ml of aqueous hydrofluoric acid (47%) at room temperature. This solution was basified with solid potassium carbonate, and the organic layer was extracted three times with 20 ml of dichloromethane. After removal of the solvent *in vacuo*, the residue was dissolved in 5 ml of toluene, and 10 mg of naphthalene was added to the resulting mixture as an internal standard. The GC analysis was done according to the procedure for bulk products.

Thermogravimetric analysis (TG) of HM was carried out after the reaction with the temperature programmed rate of 10 °C/min in an air stream by TG-DTA 2000 (MAC Science Co. Ltd., Tokyo, Japan). The weight loss due to adsorbed water was corrected by blank measurement of corresponding HM before being used for the reaction.

## Results and Discussion

**Effect of  $\text{SiO}_2/\text{Al}_2\text{O}_3$  ratio of HM.** The isopropylation of BP with propene over HMs yielded mixtures of IPBP, DIPB, and triisopropylbiphenyls (TriIPB) (1-5). Figure

1 shows the effect of  $\text{SiO}_2/\text{Al}_2\text{O}_3$  ratio of HM on the compositions of bulk products and of encapsulated products in the pores under 0.8 MPa of propene. In the bulk products, the percentage of IPBP and DIPB isomers increased with increasing the ratio. TriPB was also observed in a small amount for all catalysts. On the other hand, the percentages of BP in encapsulated products were much lower than that in bulk products except for the case of HM(10)<sup>1</sup>. DIPB isomers were predominant in the encapsulated products, particularly with highly dealuminated HMs, whereas TriPB isomers were not observed in the encapsulated products with any catalysts. These results show that the isopropylation of BP proceeds rapidly to yield IPBP and DIPB, but not TriPB. The absence of TriPB in encapsulated products was due to steric restriction of the pores against the isopropylation of DIPB. The conformation of DIPB isomers, especially 4,4'-DIPB, to form TriPB should not be allowed in the pores. The low percentages of IPBP and DIPB isomers over HMs with the low  $\text{SiO}_2/\text{Al}_2\text{O}_3$  ratio are due to deactivation by severe coke-deposition inside the pores.

Figure 2 shows the effects of  $\text{SiO}_2/\text{Al}_2\text{O}_3$  ratio of HM on the selectivities of 3,4'- and 4,4'-DIPB under 0.8 MPa of propene. In bulk products, the selectivity of 4,4'-DIPB increased with  $\text{SiO}_2/\text{Al}_2\text{O}_3$  ratio, whereas that of 3,4'-DIPB was low and almost constant for all catalysts. Highly selective formation of 4,4'-DIPB was observed for dealuminated HMs, especially for HM(206). However, the selectivity of 4,4'-DIPB with HM(10) was particularly low, and other DIPB isomers were obtained with high proportions. The features of encapsulated products are quite different from that of bulk products. The selectivities of 4,4'-DIPB were higher than 85 % with all HMs, even with HM(10). The results show that shape selective isopropylation occurs inside all HM pores. Therefore, the low selectivity of 4,4'-DIPB in bulk products for HM(10) is not due to the lack of shape selectivity of the pores. It should be explained by non-regioselective isopropylation on the external acid sites which are still active in spite of coke-deposition.

The high selectivities of 4,4'-DIPB in both bulk and encapsulated products for dealuminated HM show that the isopropylation occurs preferentially inside the pores, and that the external acid sites do not work as principal catalytic sites. Highly shape selective catalysis for the formation of 4-IPBP and 4,4'-DIPB is ascribed to the steric restriction at the transition states at microporous environments of the HM pores to produce the least bulky products.

It is important to elucidate the participation of external acid sites. Table 1 shows the isomerization of 4,4'-DIPB over HM(25) and HM(206) under 0.8 MPa of propene pressure. The isomerization of 4,4'-DIPB was very slow with both catalysts, and 4,4'-DIPB was found as an exclusive encapsulated product inside the pores. These results suggest that DIPB isomers were scarcely changed to other products during the reaction at the external acid sites after they were formed. Therefore, at least, under high propene pressure, the low selectivity of 4,4'-DIPB for HMs with the low  $\text{SiO}_2/\text{Al}_2\text{O}_3$  ratio is not due to the isomerization of 4,4'-DIPB, but to non-regioselective isopropylation at external acid sites. Details of the isomerization will be discussed in the next section.

<sup>1</sup> The number in parenthesis expresses the  $\text{SiO}_2/\text{Al}_2\text{O}_3$  ratio of HMs.

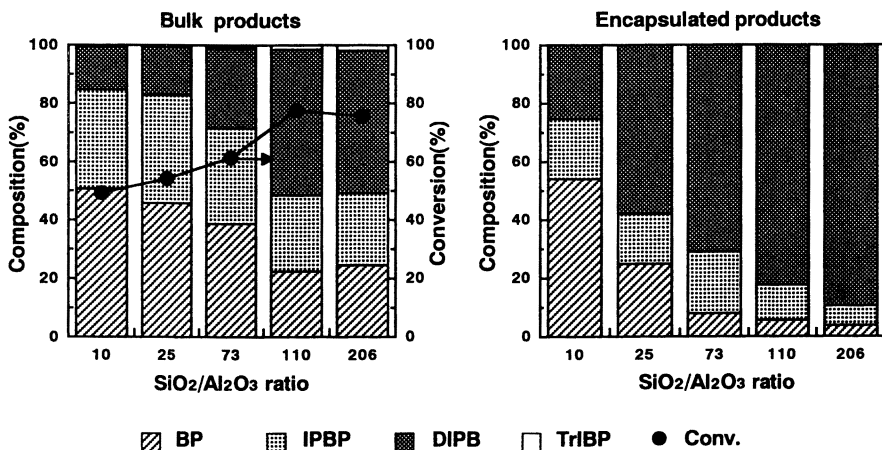


Figure 1. Effects of the SiO<sub>2</sub>/Al<sub>2</sub>O<sub>3</sub> ratio of HM on bulk and encapsulated products in the isopropylation of BP. Reaction conditions: BP, 200 mmol; HM, 1 g; propene, 0.8 MPa; temperature, 250 °C; period, 4 h.

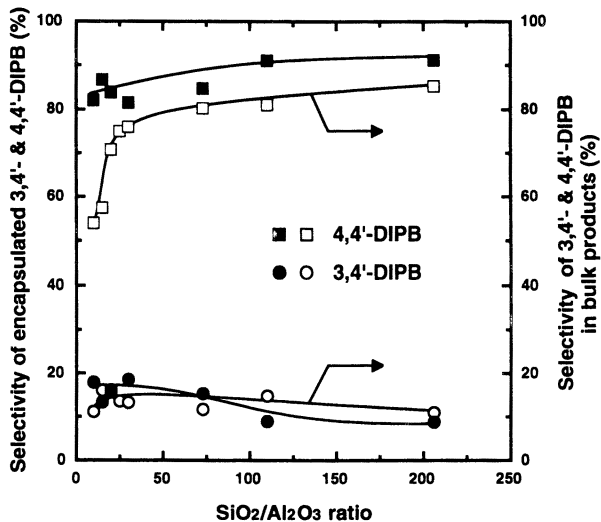


Figure 2. Effects of the SiO<sub>2</sub>/Al<sub>2</sub>O<sub>3</sub> ratio of HM on the selectivity of 3,4'- and 4,4'-DIPB in bulk and encapsulated products in the isopropylation of BP. The reaction conditions are the same as Figure 1.

Figure 3 shows TG profiles of HMs used for the isopropylation of BP. The amounts of cokes observed as a peak around 600 °C decreased with increasing the  $\text{SiO}_2/\text{Al}_2\text{O}_3$  ratio. Volatile organic compounds, which are ascribed to isopropylated biphenyls encapsulated inside the pores discussed above, were also found at 300-350 °C for dealuminated HMs ( $\text{SiO}_2/\text{Al}_2\text{O}_3 > 70$ ). These results are explained by preferential removal of strong acid sites by the dealumination (8,9). The coke-deposition easily occurs on strong and dense acid sites by the dehydrogenation of alkylated aromatics (10-12). It is considered that the most of the volatile compounds inside HM pores with the low  $\text{SiO}_2/\text{Al}_2\text{O}_3$  ratio was converted to coke-deposits, and that major parts of acid sites in the pores could not act as catalytic active sites by choking pore entrance. Highly dealuminated HMs, such as HM(206), effectively catalyze shape selective isopropylation of BP without the inhibition by coke-deposition.

**Effects of propene pressure on the isopropylation.** The formation of 4,4'-DIPB over HM(220) was much influenced by propene pressure as shown in Figure 4. The selectivities were as high as 80 % under all pressure conditions at early stages, and kept almost constant during the reaction under higher pressures than 0.3 MPa. However, the decrease of the selectivity was observed under lower pressures than 0.2 MPa. The decrease of the selectivity of 4,4'-DIPB corresponded to the increase of that of 3,4'-DIPB. The yields of 3,4'- and 4,4'-DIPB were in linear relations to the yield of combined DIPB isomers under higher pressure than 0.3 MPa as shown in Figure 5. These results show that the isopropylation occurs in steady state under high propene pressures. However, the yield of 4,4'-DIPB under such a low pressure as 0.1 MPa was deviated downwards from the linear plot under higher pressures, and the amount of 4,4'-DIPB decreased after reaching the maximum at higher conversion. On the contrary, the upward deviation occurred for the yield of 3,4'-DIPB. The increase of the yield of 3,4'-DIPB corresponded to the decrease of that of 4,4'-DIPB.

The change of the selectivities of 4,4'-DIPB is not due to the change of shape selectivity of the pore, but to its isomerization to 3,4'-DIPB, because 3,4'-DIPB is thermodynamically more stable isomer than 4,4'-DIPB (13).

**Isomerization of 4,4'-DIPB under propene pressure.** The behavior of 4,4'-DIPB during the reaction is one of the essential factors for product distributions. Figure 6 shows the stability of 4,4'-DIPB under propene pressures over HM(220). Without propene or under low propene pressure, 4,4'-DIPB was isomerized significantly to 3,4'-DIPB accompanying IPBP isomers formed by the dealkylation. However, the formation of 3,4'-DIPB decreased with the increase of propene pressure. These tendencies correspond well with the influences of propene pressure in the isopropylation of BP. The inhibition of the isomerization under high propene pressure shows that propene is adsorbed more preferentially than 4,4'-DIPB. Adsorbed propene prevents the adsorption of 4,4'-DIPB, and retards its isomerization. However, the adsorption of 4,4'-DIPB predominates over that of propene under low propene pressure to result in the enhancement of its isomerization.

Further isopropylation of 4,4'-DIPB under the conditions was observed only in small amounts even under high propene pressure; *i.e.*, the isopropylation of 4,4'-DIPB is prevented inside the pores. This is one of the reasons why shape selective

Table 1. The isomerization of 4,4'-DIPB under propylene pressure

Catalyst	Composition of 4,4'-DIPB (%)	
	Bulk products	Encapsulated products
HM(25)	96	99
HM(206)	94	98

Reaction conditions: 4,4'-DIPB, 100 mmol; HM, 1g; propene, 0.8 MPa; temperature, 250 °C; period, 4 h.

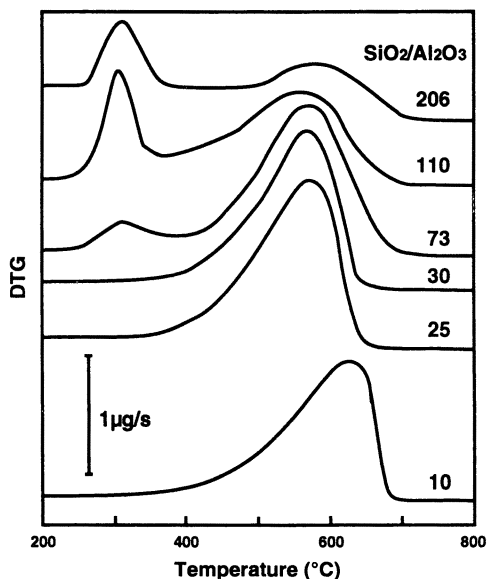


Figure 3. Thermogravimetric profiles of H-mordenite used for the reaction under air atmosphere. TG conditions: H-mordenite, 10 mg; programmed rate, 10 °C/min. The reaction conditions are the same as Figure 1.

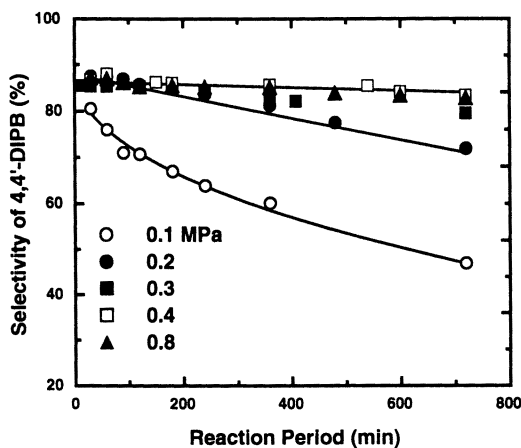


Figure 4. Effects of propene pressure on the selectivity of 4,4'-DIPB in the isopropylation of BP. Reaction conditions: BP, 400 mmol; HM(220), 2 g; propene, 0.1-0.8 MPa; temperature, 250 °C.

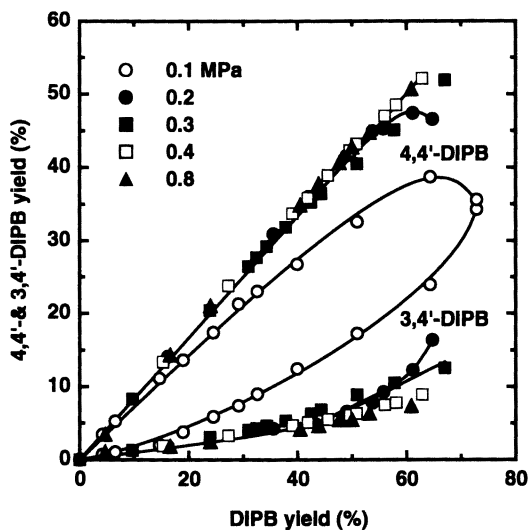


Figure 5. Effects of propene pressure on the yield of 3,4'- and 4,4'-DIPB in the isopropylation of BP. Reaction conditions were the same as Figure 4.



isopropylation occurs in the catalysis over HM. HM pore allows the formation of 3- and 4-IPBP, and 3,4'- and 4,4'-DIPB, while the formation of TriPB is forbidden in the pores. The higher steric restriction of 3,4'-DIPB compared with that of 4,4'-DIPB results in the lower selectivity for 3,4'-DIPB because molecular diameter of the former isomer is larger than that of the latter. Relatively high amount of TriPB was observed in the isomerization of 4,4'-DIPB under 0.1 MPa. TriPB is formed by the isomerized DIPB isomers at the external surface because of low propene pressure.

**Effect of propene pressure on encapsulated products inside the pores.** Figures 7 and 8 show the effect of propene pressure on the selectivities of 4,4'-DIPB in bulk and encapsulated products in the isopropylation of BP and the isomerization of 4,4'-DIPB over HM(206). The selectivity of 4,4'-DIPB encapsulated inside the pores in the isopropylation was almost constant under all pressures, whereas that of bulk products decreased under low propene pressure as discussed above. The effects of the pressure on the isomerization of 4,4'-DIPB showed similar tendency to the isopropylation of BP. The selectivity of 4,4'-DIPB in encapsulated DIPB isomers was almost constant under any pressure condition similar to the case of the isopropylation. On the other hand, 4,4'-DIPB itself isomerized significantly to 3,3'- and 3,4'-DIPB over HM(206) in the absence of propene, whereas no significant isomerization of 4,4'-DIPB occurred in the presence of sufficient propene pressure. These results indicate that the isomerization does not occur inside the pores, but at the external acid sites.

Preferential adsorption of propene on acid sites is considered to inhibit the isomerization of 4,4'-DIPB under high pressures. However, the adsorption of 4,4'-DIPB should predominate over that of propene under the low pressure, and thus, the isomerization of 4,4'-DIPB occurs at external acid sites.

## CONCLUSION

Shape selective formation of 4,4'-DIPB was observed in the isopropylation of BP over dealuminated HMs. The selectivity of 4,4'-DIPB was dependent on the  $\text{SiO}_2/\text{Al}_2\text{O}_3$  ratio of HM, and it was low for HMs with the lower ratio. However, encapsulated products showed that the selectivities of 4,4'-DIPB inside the pores were higher than 85% for all HMs regardless of the ratio. These results show that shape selective catalysis occurs inside the pores for all HMs in spite of the fact that non-regioselective isopropylation is predominant in bulk products for HMs with the lower ratio. This means that acid sites inside the pores do not always act as principal active sites for the isopropylation. Especially on HMs with the lower  $\text{SiO}_2/\text{Al}_2\text{O}_3$  ratio, coke-deposition occurs on these acid sites *via* the dehydrogenation of isopropylated biphenyls, and blocks the pores.

The effects of propene pressure on the isopropylation of BP were investigated over highly dealuminated HMs. The selectivity of 4,4'-DIPB was up to 90% under 0.8 MPa of propene pressure, whereas the decrease of the selectivity occurred under 0.1 MPa. The isomerization of 4,4'-DIPB occurred extensively in the absence of propene or under low pressures, but decreased with increasing the pressure. The selectivities of 4,4'-DIPB in encapsulated products for the isopropylation of BP and for the isomerization of 4,4'-DIPB was more than 90 % under all pressures. These results show that the decrease of the selectivity of 4,4'-DIPB during the isopropylation of BP is not ascribed to non-

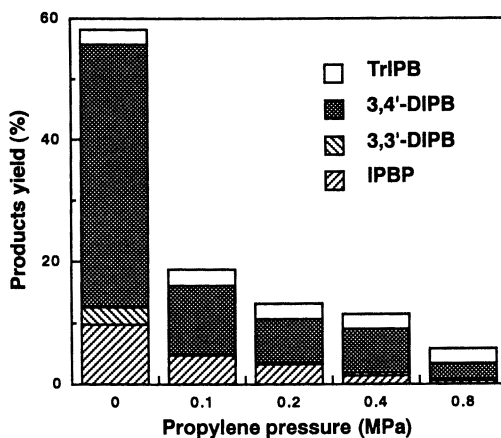


Figure 6. The isomerization of 4,4'-DIPB under propene pressure. Reaction conditions: 4,4'-DIPB, 100 mmol; HM(220), 1 g; propene, 0-0.8 MPa; temperature, 250 °C; period, 4 h.

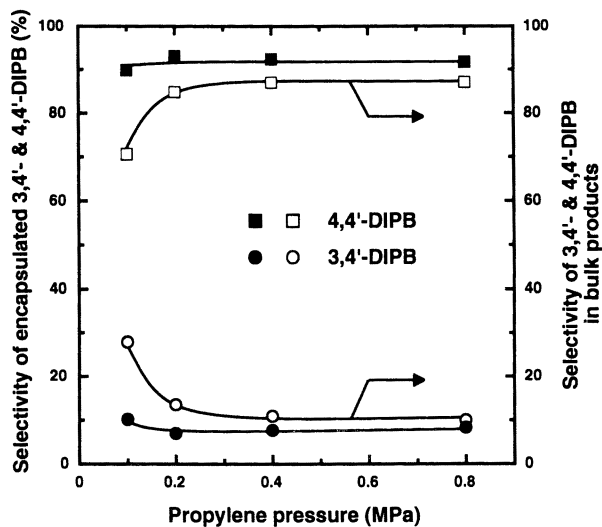


Figure 7. Effects of propene pressure on the selectivity of 3,4'- and 4,4'-DIPB in encapsulated and bulk products in the isopropylation of BP. Reaction conditions: BP, 200 mmol; HM(206), 1 g; propene, 0.1-0.8 MPa; temperature, 250 °C; period, 4 h.

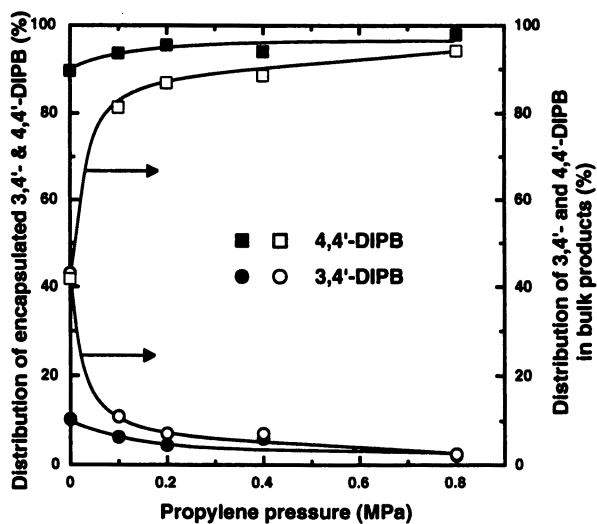


Figure 8. The selectivity of 3,4'- and 4,4'-DIPB in encapsulated and bulk products in the isomerization of 4,4'-DIPB. Reaction conditions were the same as Figure 6.

regioselective reaction in the pores, but to the isomerization at external acid sites. Preferential adsorption of propene on acid sites prevents the isomerization of 4,4'-DIPB under high pressures. However, the adsorption of 4,4'-DIPB should predominate over that of propene under the lower pressure, and thus, the isomerization of 4,4'-DIPB occurs at external acid sites.

### Acknowledgement

A part of this work was supported by the Original Industrial Technology R&D Promotion Program from the New Energy and Industrial Technology Development Organization (NEDO) of Japan.

### Literature Cited

- 1) Sugi, Y.; Toba M. *Catal. Today* **1994**, *19*, 187.
- 2) Sugi, Y.; Kubota, Y. in *Catalysis*, Spivey, J. J., Ed.; Specialist Periodical Report, Royal Soc. Chem., London, 1997, Vol. 13.; Chapter 3; pp 55-84.
- 3) Matsuzaki, T.; Sugi, Y.; Hanaoka, T.; Takeuchi, K.; Arakawa, H.; Tokoro, T.; Takeuchi, G. *Chem. Express* **1989**, *4*, 413.
- 4) Sugi, Y.; Matsuzaki, T.; Hanaoka, T.; Kubota, Y.; Kim, J. -H.; Tu, X.; Matsumoto, M. *Catal. Lett.* **1994**, *26*, 181.
- 5) Sugi, Y.; Matsuzaki, T.; Hanaoka, T.; Kubota, Y.; Kim, J. -H.; Tu, X.; Matsumoto, M. *Catal. Lett.*, **1994**, *27*, 315.
- 6) Sugi, Y.; Matsuzaki, T.; Tokoro, T.; Hanaoka, T.; Takeuchi, K.; Tu, X.; Takeuchi, G. *Sekiyu Gakkaishi* **1994**, *37*, 376.
- 7) Lee, G. S.; Maj, J. J.; Rocke, S. C.; Garces, J. M. *Catal. Lett.* **1989**, *2*, 243.
- 8) Matsuda, T.; Kikuchi, E. *Stud. Surf. Sci. Catal.* **1994**, *83*, 295.
- 9) Karge, H. G.; Weitkamp, J. *Chem. Ind. Tech.* **1986**, *58*, 946.
- 10) Sawa, M.; Niwa, M.; Murakami, Y. *Appl. Catal.* **1989**, *53*, 169, and their earlier papers cited in.
- 11) Guisnet, M.; Magnoux, P. *Appl. Catal.* **1989**, *54*, 1.
- 12) Bhatia, S.; Beltramini, J.; Do, D. D. *Catal. Rev. Sci. Eng.* **1989-90**, *31*, 431.
- 13) Weitkamp, J.; Neuber, N. *Stud. Surf. Sci. Catal.* 1991, **60**, 291.
- 14) Takeuchi, G.; Okazaki, H.; Kito, T.; Sugi, Y.; Matsuzaki, T. *Sekiyu Gakkaishi* **1991**, *34*, 242.

## Chapter 20

# Modification of Mordenite Catalyst for Selective Synthesis of 2,6-Diisopropylnaphthalene by Alkylation

T. Matsuda <sup>1</sup>, N. Takahashi <sup>1</sup>, and E. Kikuchi <sup>2</sup>

<sup>1</sup> Department of Materials Science, Kitami Institute of Technology,  
Kitami, Hokkaido 090-8507, Japan

<sup>2</sup> Department of Applied Chemistry, School of Science and Engineering,  
Waseda University, Shinjuku-ku, Tokyo 169-8555, Japan

The catalytic performances of dealuminated H-mordenite (HM) for alkylation of 2-isopropylnaphthalene with propene were investigated in comparison with those of HM modified with tributylphosphite (TBP). HM catalyst produced 2,6-diisopropylnaphthalene (DIPN) more selectively than 2,7-DIPN, and the 2,6-DIPN selectivity was enhanced by dealumination. However, undesirable reactions of propene were promoted on the dealuminated HM. Modification of HM with TBP improved the 2,6-DIPN selectivity, due to poisoning of external acid sites. The modified HM exhibited a low selectivity for 2,6-DIPN formation compared with the dealuminated HM, although no appreciable difference was observed in the activity for 1,3,5-triisopropylbenzene cracking. We deduce from these results that the increased 2,6-DIPN selectivity by dealumination can be attributed not only to a reduced contribution of external acid sites but also to a change in acidic property.

Regiospecific functionalization of polynuclear aromatic hydrocarbons such as naphthalene and biphenyl is drawing attention as one of key steps in developing advanced materials. Among polynuclear aromatic hydrocarbons, the most valuable compound is 2,6-dialkylnaphthalene, which is the raw material for polyethylene naphthalate and liquid crystals. Methylation of naphthalene and methyl naphthalenes using various zeolite catalysts were investigated by Fraenkel et al. (1), Weitkamp et al. (2) and Komatsu et al. (3). A high selectivity for the formation of slim isomers, 2,6- and 2,7-dimethylnaphthalenes, was obtained with MFI zeolites. We showed in our previous papers (4, 5) that methyl naphthalene was selectively disproportionated to 2,6 and 2,7-isomers on MFI zeolite. The activities of MFI zeolites for methylation and for disproportionation, however, were markedly low and MFI zeolites produced 2,7-isomer in a slightly higher proportion than 2,6-isomer.

It has been shown by several research groups (6-9) that HM catalyst produced 2,6-diisopropylnaphthalene (DIPN) selectively by alkylation of naphthalene with propene and with 2-propanol. HM was also effective for alkylation of biphenyl to produce 4,4'-diisopropylbiphenyl (10-13). Dealumination of HM was reported to improve the selectivity for the formations of symmetric polynuclear aromatic

hydrocarbons such as 2,6-DIPN and 4,4'-diisopropylbiphenyl (13-16). The improved selectivity has been explained by a reduced contribution of external acid sites. Indeed, poisoning of external acid sites by silanation (7), by adsorption of water (17), and by deposition of Ce oxide (18) was found to enhance the selectivity of HM for 2,6-DIPN formation. It was shown in our previous paper (19) that the modification of HM with tributylphosphite (TBP) improved the selectivity for 4,4'-diisopropylbiphenyl formation, due to the selective reaction of external acid sites and TBP. The present study describes the catalytic performances of HM modified with TBP for the alkylation of 2-isopropyl-naphthalene with propene in comparison with those of HM with different  $\text{SiO}_2/\text{Al}_2\text{O}_3$  ratios.

## Experimental

**Catalysts.** Na-mordenite with  $\text{SiO}_2/\text{Al}_2\text{O}_3$  ratio of 18 was obtained from Tosoh Corp, and was exchanged 5 times with 0.1 M  $\text{NH}_4\text{Cl}$  solution at 343 K for 6 h. Thus obtained  $\text{NH}_4$ -mordenite was calcined at 813 K for 4 h to form H-mordenite (HM). HM(57) were prepared by dealumination of HM(18) using 5 M HCl solution under reflux for 6 h. Dealumination of HM(57) under the same condition yielded HM(82). The values in parentheses represent the bulk  $\text{SiO}_2/\text{Al}_2\text{O}_3$  ratios, which were determined by chemical analysis using ICP-ICAP 575 Mark II. X-ray photoelectron measurements were carried out using JPS 90-MX spectra meter. The surface  $\text{SiO}_2/\text{Al}_2\text{O}_3$  ratio was determined from the intensities of Si(2p) and Al(2p).

Treatment of HM with tributylphosphite (TBP) involved the following procedures. Under nitrogen atmosphere, 10 g of HM was added to 50 ml of TBP solution and stirred for 3 h at 423 K. The product was filtered and washed with acetone to remove excess TBP, followed by calcination at 673 K for 2 h. HM treated with TBP will be abbreviated to TBP-HM.

The acidity of HM was determined by means of  $\text{NH}_3$  temperature-programmed desorption (TPD). In each TPD experiment, 0.5 g sample placed in a cell was evacuated at 813 K for 1 h, and  $\text{NH}_3$  was adsorbed at 373 K for 1 h, followed by evacuation for 1 h. The sample was heated from 373 to 1023 K at a rate of 10 K/min in a stream of He (60 ml/min). A thermal conductivity detector was used to monitor the desorbed  $\text{NH}_3$ .

**Catalytic studies.** Alkylation of 2-isopropyl-naphthalene (2-IPN) with propene was carried out at 523 K and at 2 MPa using a suspension of catalyst in tridecane as a liquid medium. The slurry phase reactor was a stainless steel autoclave, having an internal volume of 250 ml, equipped with a stirrer. The reactor containing 2.0 g catalyst, 20 ml (115 mmol) 2-IPN, and 100 ml tridecane was heated to 523 K in  $\text{N}_2$  atmosphere. The gas mixture of 5% propene and 95%  $\text{N}_2$  was fed to the reactor from the bottom through a nozzle at the flow rate of 100 ml/min (STP). Liquid and gaseous products were analyzed by means of FID gas chromatography using TC-17 glass capillary separation column, and TCD gas chromatography with unibeads 1S separation column, respectively. The activities of HM and TBP-HM catalysts for cracking of cumene and 1,3,5-triisopropylbenzene (1,3,5-TIPB) were determined at 623 K using a pulse technique.

## Results and Discussion

**Catalytic Performances of HM.** The catalytic activity and selectivity of HM with different  $\text{SiO}_2/\text{Al}_2\text{O}_3$  ratios were compared. Typical results are summarized in Table 1. Here, the data of alkylation were collected after 6 h run. 2-IPN was predominantly alkylated to DIPN on all of the catalysts. The activity and product distribution, however, varied from one catalyst to another. There are ten isomers of

DIPN and these isomers can be classified into three groups based on the position of isopropyl groups. DIPN having isopropyl groups at  $\beta$ -positions are of the smallest molecular dimension, and those at  $\alpha$ -positions are of the largest. Under reaction condition employed, HM catalysts did not produce 1,2-, 1,8-, and 2,3-DIPN isomers at all, irrespectively of the  $\text{SiO}_2/\text{Al}_2\text{O}_3$  ratio, due to the steric hindrance of isopropyl groups. The selectivity for 2,6- plus 2,7-DIPN ( $\beta$ - $\beta$  selectivity) and the 2,6-DIPN/2,7-DIPN ratio increased with increasing  $\text{SiO}_2/\text{Al}_2\text{O}_3$  ratio, although the alkylation activity was lowered. HM(82) exhibited the  $\beta$ - $\beta$  selectivity of 95% and the 2,6-DIPN/2,7-DIPN ratio of 3. The produced DIPN isomers were hardly alkylated to TIPN on HM(82). These results are in accordance with the reported results (13,14).

Figure 1 shows the selectivities of HM(18) for 2,6- and 2,7-DIPN formations as a function of the conversion level. The selectivities for these isomers were independent of the conversion levels. HM(57) and HM(82) exhibited the same tendency as HM(18). As shown in Table 1, isomerization of 2-IPN to 1-IPN was negligible on all of the catalysts tested. These results indicate that the isomerization reactions hardly occurred under the reaction condition employed. Sugi and co-workers (20) reported that the selectivity of HM for 4,4'-diisopropylbiphenyl (DIPB) formation by alkylation of biphenyl was improved under high propene pressure in a batch system. They suggested that adsorption of propene on acid sites inhibited the isomerization of 4,4'-DIPB produced. In this study, alkylation was performed in a continuous flow of propene. Propene will be preferentially adsorbed on acid sites, irrespectively of reaction period, due to the constant partial pressure of propene during reaction, resulting in suppression of isomerization reaction. The effect of isomerization of the produced DIPN can be excluded to consider the differences in the  $\beta$ - $\beta$  selectivity and the 2,6-DIPN/2,7-DIPN ratio shown in Table 1.

It was reported in the previous paper (4) that the selectivity of MFI zeolite for the formation of 2,6-dimethylnaphthalene by disproportionation of 2-methylnaphthalene was strongly influenced by the action of external acid sites. To study the activity of external surface, cracking of cumene and 1,3,5-TIPB were performed at 623 K. HM catalysts exhibited almost a similar activity for cumene cracking, independently of the  $\text{SiO}_2/\text{Al}_2\text{O}_3$  ratio.  $\text{NH}_3$ -TPD studies indicated that the acid amount of HM decreased with increasing  $\text{SiO}_2/\text{Al}_2\text{O}_3$  ratio. It is generally known that the acid strength of HM is enhanced by dealumination. The strong acidity of HM(82) seems to be responsible for its high activity for cumene cracking. In contrast, the catalytic activity of HM for 1,3,5-TIPB cracking was markedly lowered by an increase in  $\text{SiO}_2/\text{Al}_2\text{O}_3$  ratio. Cracking of 1,3,5-TIPB proceeds mainly on the external acid sites because the molecular dimension of 1,3,5-TIPB is large compared with the pore size of HM, and diffusion into the pore channel of HM is prohibited. It is obvious from these results that the external surface of HM became inactive after dealumination using HCl solution.

Figure 2 shows the relationship between the bulk and surface  $\text{SiO}_2/\text{Al}_2\text{O}_3$  ratios. In the case of HM(18), no appreciable difference was observed between the surface and bulk  $\text{SiO}_2/\text{Al}_2\text{O}_3$  ratios, determined by XPS and chemical analysis, respectively. On the other hand, there was great discrepancy in the surface and bulk  $\text{SiO}_2/\text{Al}_2\text{O}_3$  ratios of dealuminated HM. Dealumination using HCl solution yielded a silica-rich surface: the surface  $\text{SiO}_2/\text{Al}_2\text{O}_3$  ratio of HM(82) was determined to be 160 by XPS. The low activity of HM(82) for cracking of 1,3,5-TIPB was attributed to its high-silica external surface. These results indicate that contribution of external acid sites, which catalyzed non-selective alkylation to give the mixture of DIPN isomers, was reduced by dealumination, resulting in high  $\beta$ - $\beta$  selectivity and 2,6/2,7 ratio. Horsley and co-workers (21) showed by computer simulation that diffusion of 2,6-DIPN into the pore channel of HM was easier than that of 2,7-DIPN, suggesting that molecular dimension of 2,6-DIPN was small compared with that of 2,7-DIPN.

**Table I. Catalytic performances of HM with different SiO<sub>2</sub>/Al<sub>2</sub>O<sub>3</sub> ratios**

Catalyst	HM(18)	HM(57)	HM(82)
%Conversion of 2-IPN	50.4	38.9	21.1
Yield/%			
naphthalene	0.3	0.4	0.3
1-IPN	0.7	0.8	0.3
DIPN	42.4	35.1	20.0
TIPN	2.9	0.3	0.1
$\beta$ - $\beta$ selectivity	84.0	91.1	95.5
2,6-DIPN/2,7-DIPN	1.6	2.6	3.0
Amount of reacted C <sub>3</sub> /mmol	69.3	63.2	43.3
C <sub>3</sub> consumed by alkylation /mmol	55.5	41.1	23.2
Carbon balance based on	91.9	94.2	98.3
%Conversion of cumene	99.8	92.7	83.7
%Conversion of 1,3,5-TIPB	85.8	5.9	2.4

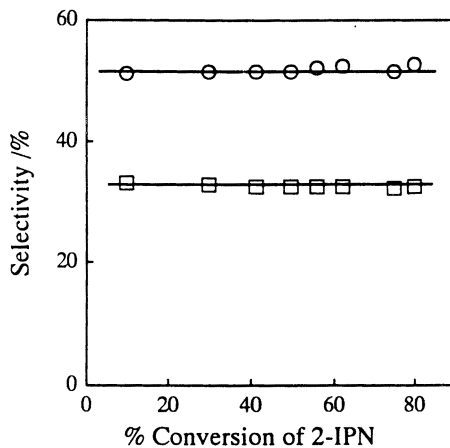


Figure 1. Selectivity of HM(18) for 2,6-DIPN(O) and 2,7-DIPN(□) as a function of conversion levels.



Furthermore, HM was reported to adsorb 2,6-DIPN selectively from the mixture of DIPN isomers (9). These results account for the higher 2,6-DIPN selectivity and 2,6-DIPN/2,7-DIPN ratio observed on HM(82).

In this reaction, it is very important to mention the consumption of propene by alkylation since propene is more reactive than 2-IPN. Hence, we studied the alkylation selectivity of propene. Typical results are demonstrated in Table 1. The amount of propene consumed by alkylation was calculated from the amount of DIPN and TIPN produced, and the total amount was determined by integrating the conversion curve of propene. The alkylation selectivity of propene was lowered by an increase in  $\text{SiO}_2/\text{Al}_2\text{O}_3$  ratio. The selectivities of HM(18), HM(57), and HM(82) were determined to be 80%, 65%, and 54%, respectively. HM(57) and HM(82) catalysts produced the gaseous products such as  $\text{C}_2$ , propane, and  $\text{C}_4$ , while the formation of these products was not detectable on HM(18). The previous paper showed (12) that in the alkylation of biphenyl, reduction of acid strength enhanced the alkylation selectivity of propene: the selectivity was dependent on the level of proton exchange, and propene was selectively consumed by alkylation on HM(20) having a level of proton exchange lower than 55%. The results obtained in this study are also understood by taking acid strength into consideration. In contrast, carbon balance based on naphthalene ring increased from 91.9 % to 98.3% by increasing  $\text{SiO}_2/\text{Al}_2\text{O}_3$  ratio from 18 to 82. Lee and co-workers (10) reported that the  $\text{SiO}_2/\text{Al}_2\text{O}_3$  ratio had to be higher than 50 to prevent coke deposition in alkylation of biphenyl with propene. Since coke deposited on large pore zeolites is usually aromatic hydrocarbons having 2-4 nuclei, the improved carbon balance observed on HM(82) may be caused by suppression of coke formation.

**Catalytic Performances of TBP-HM.** As mentioned above, the external acid sites strongly affects the selectivity of HM for 2,6-DIPN formation. We demonstrated in the previous papers (16,19) that the external acid sites of HM was deactivated by the treatment with TBP, and consequently biphenyl was selectively alkylated to 4,4'-DIPB on TBP-HM. Hence, alkylation of 2-IPN with propene was performed using TBP-HM catalysts. Table 2 summarizes the catalytic activities and selectivities of TBP-HM. Here, the data of alkylation were collected after 6 h run.

The catalytic activities of HM(18) and HM(57) for alkylation of 2-IPN were lowered, and the  $\beta$ - $\beta$  selectivity and the 2,6-DIPN/2,7-DIPN ratio were improved by TBP treatment. The formation of TIPN was restricted on these catalysts. TBP-HM(57) showed almost the same  $\beta$ - $\beta$  selectivity and the 2,6-DIPN/2,7-DIPN ratio as HM(82). TBP-HM(18) and TBP-HM(57) were less active for 1,3,5-TIPB cracking than the parent HM catalysts, while no appreciable difference was observed in the activity for cumene cracking. TBP treatment did not change the  $\text{NH}_3$ -TPD spectra at all. These results support the selective poisoning of external acid sites by TBP. It is obvious from these results that elimination of external acid sites enhanced the selectivity for 2,6-DIPN formation. In contrast, the catalytic properties of HM(82) for alkylation and for cracking were hardly affected by the TBP treatment, indicating that the external surface of HM(82) had no sites to react with TBP and the alkylation reaction on the external surface was negligible. We deduce from these results that 2-IPN is alkylated into the pore channel of HM with the  $\beta$ - $\beta$  selectivity of 95 % and the 2,6-DIPN/2,7-DIPN ratio of 3. As shown in Tables 1 and 2, TBP treatment did not vary the carbon balance based on naphthalene ring and the alkylation selectivity of propene, suggesting that TBP-HM had the same acidic property as the parent HM.

TBP-HM(18) is expected to give the similar selectivity for 2,6-DIPN formation to HM(82) and TBP-HM(57). The  $\beta$ - $\beta$  selectivity and the 2,6-DIPN/2,7-DIPN ratio of TBP-HM(18), however, was low compared with those of HM(82) and TBP-HM(57). Furthermore, 20% of 1,3,5-TIPB was converted on this catalyst. These results indicate that the external surface of HM(18) was active even after the TBP

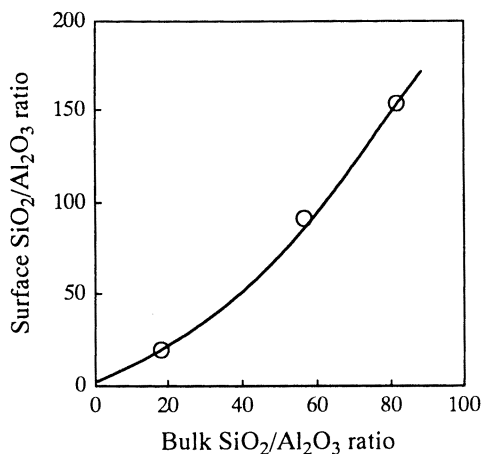


Figure 2. Relation between the bulk and the surface SiO<sub>2</sub>/Al<sub>2</sub>O<sub>3</sub> ratios.

**Table II. Effect of TBP treatment on catalytic performances of HM with different SiO<sub>2</sub>/Al<sub>2</sub>O<sub>3</sub> ratios**

Catalyst	TBP-HM(18)	TBP-HM(57)	TBP-HM(82)
%Conversion of 2-IPN	41.9	27.6	23.0
Yeild/%			
naphthalene	0.3	0.1	0.1
1-IPN	1.1	0.2	0.2
DIPN	36.5	26.0	22.2
TIPN	1.0	0.1	0.1
β-β selectivity	86.6	94.5	96.2
2,6-DIPN/2,7-DIPN	2.0	3.0	3.0
Amount of reacted C <sub>3</sub> /mmol	54.0	44.3	40.9
C <sub>3</sub> consumed by alkylation /mmol	44.3	30.1	25.8
Carbon balance based on	92.9	95.5	98.4
%Conversion of cumene	98.6	90.1	84.9
%Conversion of 1,3,5-TIPB	20.6	2.1	1.9

treatment, although TBP treatment was effective to completely poison the external surface of HM(57). This can be explained as follows: TBP is a bulky compound and can not react all of the external acid sites on HM(18) because the acid site density of HM(18) is large. TBP-HM without calcination exhibited no activity for the alkylation, probably due to pore blocking. The catalytic activity of TBP-HM was generated by calcination at 673 K, which decomposed TBP molecules and eliminated carbonaceous deposits formed during the TBP treatment. Hence, TBP treatment and calcination procedures were repeated for several times to deactivate the external surface completely. Figure 3 shows the  $\text{NH}_3$ -TPD spectra of HM(18) and that treated with TBP for 3 times. No appreciable difference was observed in the acidity between these two catalysts. As shown in Figure 4, the catalytic activity for cumene cracking was independent of the frequency of TBP treatment, in accordance with the TPD results. In contrast, the activity for 1,3,5-TIPB decreased markedly with increasing frequency of treatment. After treatment for 2 times, TBP-HM(18) became almost inactive for 1,3,5-TIPB cracking. These results indicate that the external acid sites of HM(18) were completely deactivated when TBP treatment was performed for 2 times and more.

Figure 5 shows the catalytic activity and selectivity of HM(18) for alkylation of 2-IPN as a function of frequency of TBP treatment. The  $\beta$ - $\beta$  selectivity and the 2,6-DIPN/2,7-DIPN ratio increased and the conversion level decreased with increasing treatment times, and reached to constant values after 2 times treatments. This activity change can be understood by taking a reduced contribution of external acid sites and/or modification of pore windows, by which diffusion of 2-IPN into the pore channel is restricted. Despite of its less acidic property, silica-alumina was more active for this reaction than HM(18), indicating that the alkylation activity of HM(18) was affected by diffusion of 2-IPN into the pore. In the case of diffusion-controlled reaction, the catalytic activity is markedly influenced by the presence of external acid sites. The low alkylation activity of TBP-HM seems to be mainly related to a reduced contribution of external surface. TBP-HM(18) treated for 3 times gave the  $\beta$ - $\beta$  selectivity of 90 % and the 2,6-DIPN/2,7-DIPN ratio of 2.5. These values were low compared with those of HM(82) and TBP-HM(57). We suggest from these results that HM with a low  $\text{SiO}_2/\text{Al}_2\text{O}_3$  ratio did not exhibit a high selectivity for 2,6-DIPN formation as obtained with HM having a high  $\text{SiO}_2/\text{Al}_2\text{O}_3$  ratio even when external acid sites were poisoned.

It is well known that shape selectivity of HM is affected not only by the external acid sites but also by modification of pore windows. In the cases of alkylation and disproportionation of toluene, modification of pore windows causes the restriction of diffusion of *o*- and *m*-xylenes produced in the pore, and consequently these isomers are converted to *p*-xylene with smaller molecular dimension, resulting in a high selectivity for *p*-xylene formation. If modification of pore windows by TBP treatment and dealumination is operative for the improved 2,6-DIPN/2,7-DIPN ratio, 2,7-DIPN has to isomerize to 2,6-DIPN. It has been reported (22) that isomerization of dimethylnaphthalene proceeds through the  $\alpha$ - $\beta$  shift of a methyl group, while the shift of a methyl group between  $\alpha$ - $\alpha$  and  $\beta$ - $\beta$  positions is prohibited. Hence, dialkyl naphthalene isomers can be classified into four groups. 2,6-, 1,6-, and 1,5-isomers are in one group among which the isomers are interconvertible. 2,7-, 1,7-, and 1,8-isomers are in another group. According to this, 2,6-DIPN/2,7-DIPN ratio can not be improved by modification of pore windows. 2,7-DIPN can be isomerized to 2,6-DIPN by transalkylation. Reaction space of HM, however, is too small to proceed the transalkylation in the pore.

It was shown in the previous paper (23) that 2,6-isomer group was more selectively formed than 2,7-isomer group by disproportionation of 2-methylnaphthalene on HM catalyst, while MFI zeolite produced 2,7-group in a slightly higher proportion than 2,6-group. The selectivity of HM for 2,6-group

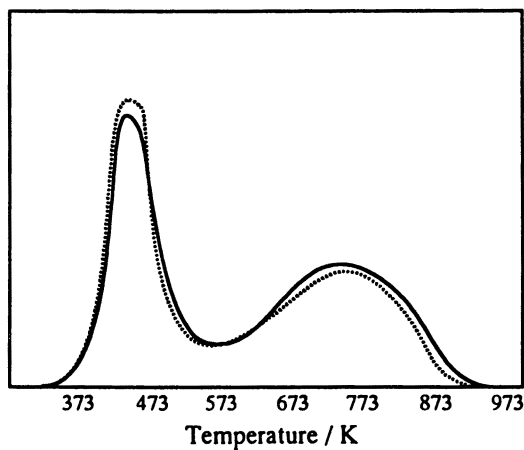


Figure 3.  $\text{NH}_3$ -TPD spectra of HM(18) and TBP-HM(18) treated at 3 times. — HM(18), ..... TBP-HM(18).

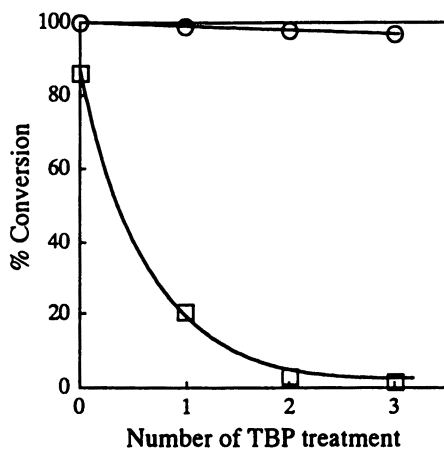


Figure 4. Effect of TBP treatment on the catalytic activity of HM(18) for cracking of cumene(O) and 1,3,5-TIPB(□).

against 2,7-group increased with increasing  $\text{SiO}_2/\text{Al}_2\text{O}_3$  ratio and the degree of proton exchange. This change was found to be related to the average acid strength of HM. We deduce from these results that the high selectivity of dealuminated HM for the formation of 2,6-DIPN can be attributed not only to the reduced contribution of external acid sites but also the change in acidic property.

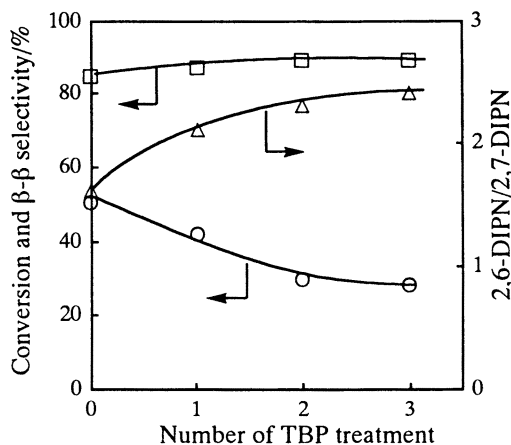


Figure 5. Effect of TBP treatment on the catalytic properties of HM(18) for alkylation of 2-IPN. ○, conversion; □,  $\beta$ - $\beta$  selectivity; △, 2,6/2,7 ratio.

## Conclusion

Slurry phase alkylation of 2-IPN with propene was carried out using HM catalysts. The  $\beta$ - $\beta$  selectivity and the 2,6-DIPN/2,7-DIPN ratio were improved by dealumination of HM with HCl. The dealuminated HM exhibited 95%  $\beta$ - $\beta$  selectivity and the 2,6-DIPN/2,7-DIPN ratio of 3. Dealumination, however, lowered the alkylation selectivity of propene, which was calculated from the total amount of reacted propene and the amount of propene consumed by alkylation. In the cases of HM with low  $\text{SiO}_2/\text{Al}_2\text{O}_3$  ratios, treatment with TBP was effective to enhance the 2,6-DIPN selectivity, due to selective poisoning of external acid sites. On the other hand, the catalytic activity and selectivity of highly dealuminated HM were not affected by TBP treatment at all. HM with low  $\text{SiO}_2/\text{Al}_2\text{O}_3$  ratio exhibited a low selectivity for 2,6-DIPN formation compared with highly dealuminated HM even after the complete deactivation of external surface by TBP treatment. We suggest from these results that the improved 2,6-DIPN selectivity by dealumination can be attributed not only to the reduced contribution of external acid sites but also the change in acidic property.

## Acknowledgment

This work was supported in part by a Grant-in-aid for Scientific Research on Priority Areas from the Japanese Ministry of Education, Science, Sports and Culture.

## Literature Cited

1. Fraenkel, D.; Cherniavsky, M.; Ittash, B.; Levy, M. *J. Catal.* **1986**, *101*, 273.
2. Neuber, M.; Karge, H.G.; Weitkamp, J. *Catal. Today* **1988**, *3*, 11.
3. Komatsu, T.; Aoki, Y.; Namba, S.; Yashima, T. *Stud. Surf. Sci. Catal.* **1994**, *84*, 1821.
4. Matsuda, T.; Yogo, K.; Kikuchi, E. *Chem. Lett.* **1990**, 1085.
5. Matsuda, T.; Yogo, K.; Nagaura, T.; Kikuchi, E. *Sekiyu Gakkaishi* **1990**, *33*, 214.
6. Katayama, A.; Toba, M.; Takeuchi, G.; Mizukami, F.; Niwa, S.; Mitamura, S. *J. Chem. Soc. Chem. Commun.* **1991**, 39.
7. Moreau, P.; Finiels, A.; Geneste, P.; Solofo, J. *J. Catal.* **1992**, *136*, 487.
8. Song, C.; Kirby, S. *Microporous Materials* **1994**, *2*, 467.
9. Kikuchi, E.; Sawada, K.; Maeda, M.; Matsuda, T. *Stud. Surf. Sci. Catal.* **1994**, *90*, 391.
10. Lee, G.S.; Maj, J.J.; Rocke, S.C.; Garces, J.N. *Catal. Lett.*, **1989**, *2*, 243.
11. Matsuzaki, T.; Sugi, Y.; Hanaoka, T.; Takeuchi, K.; Arakawa, H.; Tokoro, T.; Takeuchi, G. *Chem. Express* **1989**, *4*, 413.
12. Matsuda, T.; Urata, T.; Kikuchi, E. *Appl. Catal. A General* **1995**, *123*, 205.
13. Schmitz, A.; Song, C. *Catal. Today* **1996**, *31*, 19.
14. Kim, J.H.; Sugi, Y.; Matsuzaki, T.; Hanaoka, T.; Kubota, Y.; Tu, T.; Matsumoto, M. *Microporous Materials* **1995**, *5*, 113.
15. Sugi, Y.; Matsuzaki, T.; Hanaoka, T.; Kubota, Y.; Kim, J.H.; Tu, T.; Matsumoto, M. *Catal. Lett.* **1994**, *26*, 181.
16. Matsuda, T.; Urata, T.; Saito, K.; Kikuchi, E. *Appl. Catal. A General* **1995**, *131*, 215.
17. Schmitz, A.; Song, C. *Catal. Lett.* **1996**, *40*, 59.
18. Kim, J.H.; Sugi, Y.; Matsuzaki, T.; Hanaoka, T.; Kubota, Y.; Tu, T.; Matsumoto, M.; Nakata, S.; Kato, A.; Seo, G.; Pak, C. *Appl. Catal. A General* **1995**, *131*, 15.
19. Matsuda, T.; Kikuchi, E. *Stud. Surf. Sci. Catal.* **1994**, *83*, 295.
20. Sugi, Y.; Tu, X.L.; Matsuzaki, T.; Hanaoka, T.; Kubota, Y.; Kim, J.H.; Matsumoto, M.; Nakajima, K.; Igarashi, A. *Catal. Today* **1996**, *31*, 3.
21. Horsley, J.A.; Fellmann, J.D.; Derouane, E.G.; Freeman, C.M. *J. Catal.* **1994**, *147*, 231.
22. Suld G.; Stuart, A.P. *J. Org. Chem.* **1964**, *29*, 2939.
23. Kikuchi, E.; Mogi, Y.; Matsuda, T. *Collect. Czech. Chem. Commun* **1992**, *57*, 909.

## Chapter 21

# Isopropylation of Naphthalene over Solid Acid Catalysts

Makoto Toba <sup>1</sup>, Atsuhiko Katayama <sup>2</sup>, Genki Takeuchi <sup>2</sup>, Shu-ichi Niwa <sup>1</sup>,  
Fujio Mizukami <sup>1</sup>, and Shuichi Mitamura <sup>2</sup>

<sup>1</sup> National Institute of Materials and Chemical Research,  
1-1 Higashi Tsukuba, Ibaraki 305-8565, Japan

<sup>2</sup> Research and Development Laboratories, Nippon Steel Chemical Company, Ltd.,  
46-51 Nakabaru Sakinohama, Tobata, Kitakyushu 804-0002, Japan

Catalytic activities and product distributions in the isopropylation of naphthalene over various solid acid catalysts were investigated and reaction pathways were discussed. In the catalysts employed here except both ZSM-5 and mordenites, the isopropylation occurs at  $\alpha$ -positions of naphthalene nucleus in the first step, and then, isopropyl groups at  $\alpha$ -positions rearranged to  $\beta$ -positions through the isomerization which obeyed the Fries rule and the transalkylation. In the isopropylation of naphthalene over mordenite, selective alkylations were observed to yield 2,6-diisopropylnaphthalene, and the isomerization did not occur. ZSM-5 which has enough acidity for the isopropylation to occur, showed low activity because the pores of ZSM-5 are too small to allow the entrance of naphthalene molecules.

Dialkylnaphthalenes are noted as the raw materials to produce polyethylenenaphthalate (PEN) polymers. The most conventional method of synthesis of dialkylnaphthalenes is the alkylation of naphthalene using acid catalysts. Both homogeneous (1-3) and heterogeneous (4, 5) catalysts are used as

acid catalysts. However, it is more convenient to use heterogeneous catalysts because the separation of catalysts from reaction mixture is easy and catalysts are recyclable. In addition to having these advantages, heterogeneous catalysts, especially crystalline catalysts, enable regioselective alkylation because of their inherent crystal structures. Actually, high regioselective methylation of toluene occurs over ZSM-5 (6). However, catalytic activities and product distributions in the alkylation of polynuclear aromatics over various solid acid catalysts (7~10) differ from those in the alkylation of mononuclear aromatics because molecular sizes of polynuclear aromatics are different from those of mononuclear aromatics.

In this work, we examined the effect of pore structure and acidity on catalytic activities and product distributions in the isopropylation of naphthalene, and discussed the reaction paths to produce isopropyl-naphthalene isomers.

## Experimental

**Catalyst preparation.** Mordenite ( $\text{SiO}_2/\text{Al}_2\text{O}_3=10.9, 19, 23, 25.3$ ), Y-zeolite ( $\text{SiO}_2/\text{Al}_2\text{O}_3=5.6$ ), USY-zeolite ( $\text{SiO}_2/\text{Al}_2\text{O}_3=5.9, 14.1$ ), L-zeolite ( $\text{SiO}_2/\text{Al}_2\text{O}_3=6.0$ ), H ferrierite ( $\text{SiO}_2/\text{Al}_2\text{O}_3=16.8$ ) and H offretite/erionite ( $\text{SiO}_2/\text{Al}_2\text{O}_3=7.7$ ) are from TOSOH Co., Ltd., Tokyo. H Y-zeolite ( $\text{SiO}_2/\text{Al}_2\text{O}_3=7.3$ ) is from Catalysts & Chemicals Co., Ltd., Tokyo. ZSM-5 was synthesized by the conventional method [11].

Amorphous silica/alumina, silica/zirconia and silica/niobia were synthesized using diols as organic ligands by complexing agent-assisted sol-gel method (12~14).

**Isopropylation of naphthalene.** Naphthalene (34.7 g, 0.27 mol), propene (16~19 g, 0.38~0.45 mol), the catalyst (7 g), and n-undecane (240  $\text{cm}^3$ ) were put in a 500  $\text{cm}^3$  autoclave and stirred at 513, 453 or 433 K. The reaction mixtures were analyzed by GC with 50 m capillary column of OV-17 at 453 K. The products were separated by distillation, crystallization and preparative gas chromatography and confirmed by GC-MS with above column, and  $^1\text{H}$  NMR and  $^{13}\text{C}$  NMR spectroscopy.

**Characterization of catalysts.** Ammonia TPD profiles were obtained with 300 mg samples and the conditions are as follows: Samples were degassed at 773 K and ammonia was adsorbed at 423 K. The heating and sweep gas (helium) flow rates during measurement of ammonia desorption were 10  $\text{Kmin}^{-1}$ , 30  $\text{cm}^3\text{min}^{-1}$ , respectively. The specific surface area was determined by the B.E.T. method [15] and t plot method [16] from  $\text{N}_2$  adsorption data at 77 K using an Omnisorp 100 of Omicron Tech. Corp.



## Results and discussion

**Specific surface area and acidity.** Specific surface areas of catalysts are shown in Table 1. H Y-zeolites have very large surface areas derived from micropores. Other zeolites such as mordenites, L-zeolites, ferrierite, offretite/erionite and ZSM-5 also have large surface areas derived from micropores. However, surface areas derived from meso- and macropore of active clay and amorphous mixed oxides are much larger than surface areas derived from micropore of those catalysts.

**Table 1. Properties of Catalysts**

<i>Catalyst<sup>a,b</sup></i>	<i>Specific surface area derived from micropore<sup>c</sup> (m<sup>2</sup>/g)</i>	<i>Specific surface area derived from meso- &amp; macropore<sup>d</sup> (m<sup>2</sup>/g)</i>	<i>Acid sites<sup>e</sup> (mmol/g)</i>
HM(10.9) <sup>f</sup>	466	142	2.68
HM(19) <sup>f</sup>	518	191	0.996
HM(23) <sup>g</sup>	524	20	0.784
HM(25.3) <sup>g</sup>	446	162	0.693
HY(5.6) <sup>f</sup>	829	226	0.703
HY(7.3) <sup>g</sup>	821	213	0.960
H USY(5.9) <sup>g</sup>	732	223	0.752
H USY(14.1) <sup>g</sup>	543	200	0.266
HL(6.0) <sup>g</sup>	289	257	0.492
HF(16.8) <sup>f</sup>	347	169	1.184
H O/E(7.7) <sup>f</sup>	480	260	0.743
H ZSM-5(70)	374	36	0.435
Active Clay	~0	166	0.0924
Silica-alumina(50)	239	328	0.114
Silica-zirconia(10)	168	399	0.198
Silica-niobia(25)	98	369	0.316

<sup>a</sup>HM, H mordenite; HF, H ferrierite; HO/E, H offretite/erionite.

<sup>b</sup>Values in the parentheses express SiO<sub>2</sub>/Al<sub>2</sub>O<sub>3</sub>, SiO<sub>2</sub>/ZrO<sub>2</sub> and SiO<sub>2</sub>/Nb<sub>2</sub>O<sub>5</sub> ratios.

<sup>c</sup>Obtained by the Brunauer-Emmett-Teller method and t plot method.

<sup>d</sup>Obtained by the Brunauer-Emmett-Teller method.

<sup>e</sup>Obtained by ammonia temperature programmed desorption (TPD).

<sup>f</sup>Prepared by ion change method with NH<sub>4</sub>Cl from commercial Na or K zeolites.

<sup>g</sup>Commercial zeolites.

Acid amounts of catalysts are shown in Table 1. With the exception of some zeolites, the acid amounts of zeolites are larger than those of amorphous mixed oxides and active clay.

**Isopropylation of naphthalene.** In the isopropylation of naphthalene, reaction paths to produce diisopropyl naphthalene (DIPN) isomers are classified into three reactions. As shown in Figure 1, the reactions are : (1) alkylation, (2) isomerization, and (3) transalkylation with the rearrangement of isopropyl groups being caused by dealkylation-alkylation and transalkylation. At first reaction in the isopropylation of naphthalene,  $\alpha$ -alkylation normally occurs in the initial stage since  $\alpha$ -positions are more reactive than  $\beta$ -positions. DIPN isomers which are produced by alkylation at first reaction are isomerized at second reaction. At this reaction, isopropyl groups are isomerized from  $\alpha$ -positions to adjacent  $\beta$ -positions obeying the Fries rule (17). The similar isomerization is observed in the isomerization of dimethylnaphthalene mixtures (17), that is, the isomerization of methyl groups from  $\alpha$ -positions to adjacent  $\beta$ -positions occurs more easily than that between other positions. At third reaction, 2,6- and 2,7- DIPN, most thermodynamically stable isomers, are produced by dealkylation-alkylation and transalkylation processes. The catalyst type and reaction conditions such as reaction temperature usually determine the type of reaction which occurs.

**Table 2 Catalytic isopropylation of naphthalene with propene**

Cat. <sup>ab</sup>	Naphthalene		DIPN		Distribution of DIPN (%) <sup>cd</sup>					
	Reaction	Conv.(%)	Yield(%)	1,4	1,3	1,5	1,6	2,6	1,7	2,7
HM(10.9)	1.5	22	3	-	-	-	-	-	-	-
	2	70	22	16	13	7	14	22	15	13
	6.5	88	36	3	23	2	8	34	11	19
HM(19)	1	17	2	3	5	3	5	52	4	30
	2	35	6	3	5	2	6	53	5	27
	6.5	62	16	5	7	1	8	48	5	26
HM(23)	1.5	25	3	7	6	3	8	44	8	24
	2	37	6	8	7	3	10	41	9	23
	6.5	58	14	9	7	3	9	38	8	26
HM(25.3)	2	36	6	5	7	3	5	52	4	24
	6.5	67	18	4	5	2	7	52	5	25
HY(5.6)	1	46	8	38	10	12	10	3	25	3
	2	94	45	10	34	5	13	11	13	14
	6.5	95	46	1	20	0	6	33	5	35
HY(7.3)	1	46	10	37	12	13	10	2	23	3
	2	95	44	14	32	8	15	9	14	8
	6.5	96	47	1	27	0	7	31	5	30
H USY(5.9)	1	29	2	33	8	16	12	3	25	4
	2	87	37	36	17	13	13	4	15	3
	6.5	96	43	19	30	10	16	7	12	6

**Table 2 Catalytic isopropylation of naphthalene with propene (continue)**

Cat. <sup>ab</sup>	Reaction period(h)	Naphthalene DIPN		Distribution of DIPN (%) <sup>cd</sup>						
		Conv.(%)	Yield(%)	1,4	1,3	1,5	1,6	2,6	1,7	2,7
H USY(14.1)	1	33	2	21	5	19	14	3	32	6
	2	75	17	32	5	15	16	5	23	5
	6.5	91	34	28	11	13	16	7	19	7
HL(6.0)	1	34	5	37	15	12	10	3	20	2
	2	92	43	32	23	10	11	4	16	3
	6.5	95	42	10	39	7	15	6	17	6
HF(16.8)	1	6	1	35	14	17	12	3	16	3
	2	88	36	13	31	10	16	9	13	7
	6.5	90	38	4	35	5	16	16	12	13
HO/E(7.7)	1	48	8	22	13	10	17	9	18	8
	2	84	32	22	14	10	18	9	18	8
	6.5	93	40	11	24	7	16	15	15	12
H ZSM-5(70)	8	1	-	-	-	-	-	-	-	-
Active Clay	1	27	6	31	16	14	10	3	17	8
	2	85	33	9	37	6	13	10	14	10
	6.5	86	34	2	38	2	11	19	11	16
SA(50)	1	48	13	31	17	13	12	5	17	5
	2	95	38	20	28	9	14	8	15	7
	6.5	96	38	6	37	5	14	14	13	12
SZ(10)	1	7	1	27	19	12	11	6	17	9
	2	75	27	11	32	8	15	9	17	8
	6.5	79	29	1	36	1	11	22	9	19
SN(25)	2	18	3	31	16	13	13	5	18	4
	6.5	78	29	31	18	12	12	5	17	4

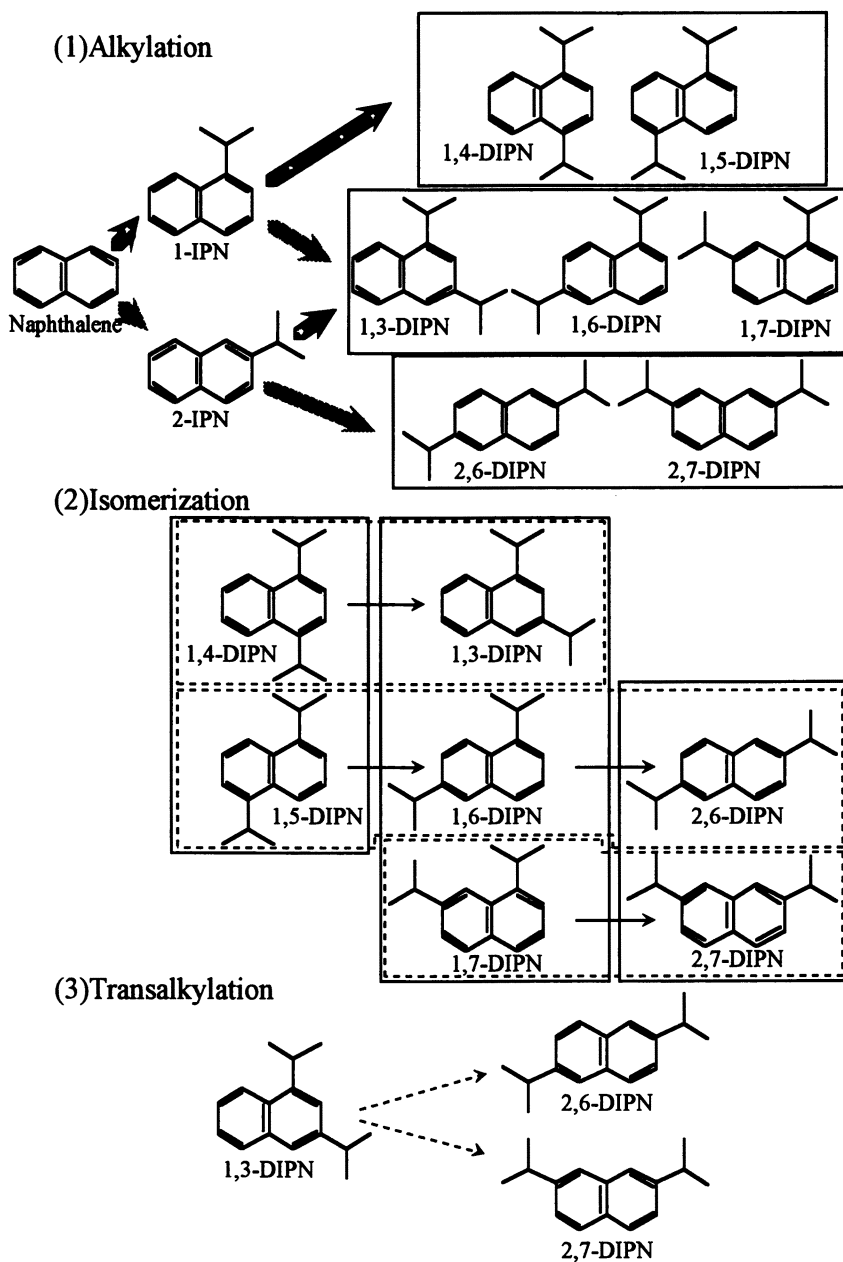
aHM, H mordenite; HF, H ferrierite; HO/E, H offretite/erionite; SA, silica-alumina; SZ, silica-zirconia; SN, silica-niobia.

bValues in the parentheses express SiO<sub>2</sub>/Al<sub>2</sub>O<sub>3</sub>, SiO<sub>2</sub>/ZrO<sub>2</sub> and SiO<sub>2</sub>/Nb<sub>2</sub>O<sub>5</sub> ratios.

cTrace amounts of other isomers were produced.

dMolecular size of DIPN: (calculated by M/M and M/D method with POLYGRAF which is the molecular simulation software from Bio Design Co., Ltd., USA): 1,4-DIPN, 0.73x1.07nm; 1,3-DIPN, 0.88x1.04nm; 1,5-DIPN, 0.71x1.16nm; 1,6-DIPN, 0.71x1.18nm; 2,6-DIPN, 0.65x1.32nm; 1,7-DIPN, 0.88x1.10nm; 2,7-DIPN, 0.65x1.25nm;

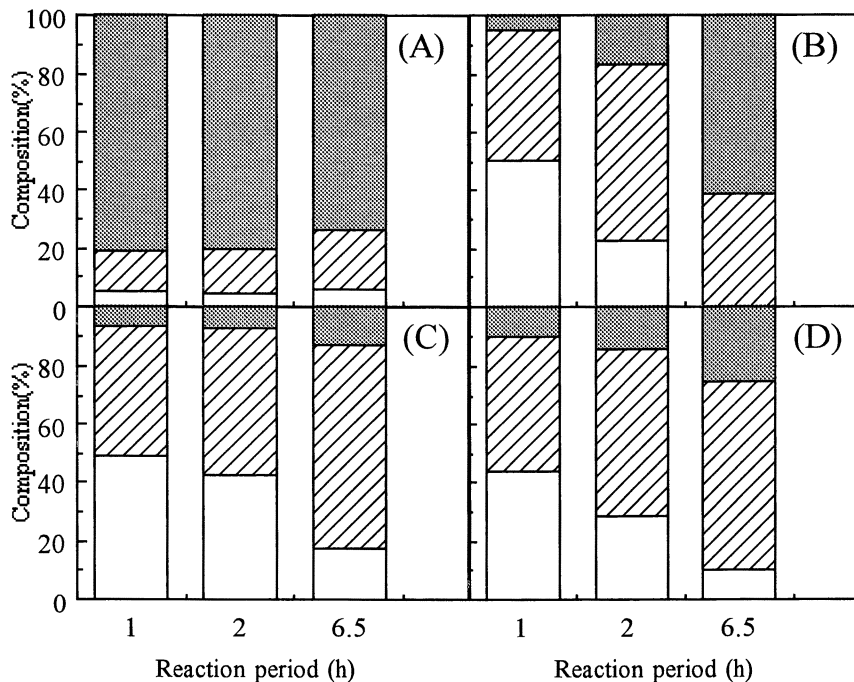
Table 2 shows the results of isopropylation of naphthalene with propene. Catalytic features of various catalysts are classified into five groups according to the reaction types producing DIPN isomers. The five groups are (1) H mordenite,



**Figure 1. The classification of reaction types in the isopropylation of naphthalene**

(2) H Y-zeolite, (3) H USY-zeolite, H L-zeolite and H offretite/erionite, (4) H ZSM-5, and (5) H ferrierite, active clay and amorphous mixed oxides. The representative distributions of IPN and DIPN isomers classified by positions of isopropyl groups are shown in Figure 2~4.

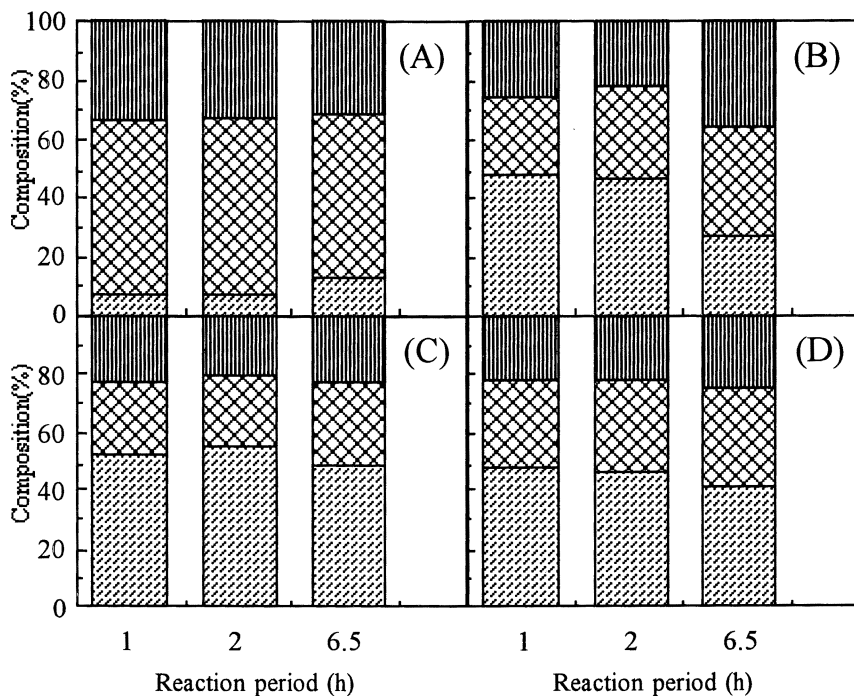
**Catalysis over H Mordenite (Group (1)).** The reaction features such as rates of naphthalene consumption and IPN or DIPN formations with H mordenite with Si/Al<sub>2</sub> ratio more than 19 are almost equal each other. Naphthalene is relatively slowly consumed in the isopropylation with H mordenite except with H mordenite (10.9) as shown in Table 2. In the initial stage, β,β-DIPN (2,6/2,7-DIPN), least bulky DIPN isomers, are preferentially produced in the isopropylation over H mordenite, and the proportions of these isomers are almost constant with reaction time (see Figure 2). As shown in Figure 3, the ratios of yield of three groups



**Figure 2. The time-course of DIPN groups in the isopropylation of naphthalene.**

(A) Mordenite, (B) Y-zeolite, (C) L-zeolite, (D) Amorphous silica-alumina

□ α,α-DIPN, ▨ α,β-DIPN, ▩ β,β-DIPN



**Figure 3. The time-course of DIPN groups in the isopropylation of naphthalene.**

(A) Mordenite, (B) Y-zeolite, (C) L-zeolite, (D) Amorphous silica-alumina

▨ (1,4- + 1,3-)DIPN, ▩ (1,5- + 1,6- + 2,6-)DIPN, ▮ (1,7- + 2,7-)DIPN

decrease in the order: (1,5- + 1,6- + 2,6-DIPN) group > (1,7- + 2,7-DIPN) group > (1,4- + 1,3-DIPN) group and this proportion are almost constant during reaction. However, in the isopropylation over H mordenite (10.9), considerable amounts of  $\alpha,\alpha$ - and  $\alpha,\beta$ -DIPN isomers are produced in the initial stage, and those isomers are converted into  $\alpha,\beta$ - or  $\beta,\beta$ -DIPN with reaction time. Another feature in the isopropylation of naphthalene with H mordenite is relatively high selectivity of 2,6-DIPN.

H mordenite has two kinds of channel as shown in Table 3. In the isopropylation over H mordenite, the active centers for catalysis are mainly present in the twelve-membered ring elliptical channel because naphthalene cannot enter the eight-membered ring channel. In the channel, the transition state of the alkylation is restricted to give the less bulky isomer such as  $\beta,\beta$ -isomers, because the  $\alpha,\alpha$ - and  $\alpha,\beta$ -isomers of DIPN have a larger molecular size than pore dimension of the twelve-membered ring channel as results of calculation with

POLYGRAF described in TABLE 2 (20) and propylene cannot attack the  $\alpha$ -positions of naphthalene. Therefore, the formation of  $\alpha,\alpha$ - and  $\alpha,\beta$ -DIPN isomers is prevented, and isomerization and transalkylation are not observed over H-mordenite. The specific reactivity of H mordenite ( $\text{Si}/\text{Al}_2=10.9$ ) seems to result from reaction at the acid sites on external surface, whereas with other H mordenites, the reaction primarily proceeds inside the pores.

However, the size effect of the H-mordenite channel does not explain why approximately twice as much 2,6-DIPN is formed than 2,7-DIPN (*see* Table 2), *i.e.*, both isomers have similar molecular dimensions. Molecular models indicate that 2,6-DIPN has a more linear structure than 2,7-DIPN, and therefore 2,6-DIPN would be more suited than 2,7-DIPN to move in the tight one-dimensional tunnels of H mordenite (21). In the UV-VIS spectra of 2-IPN adsorbed over HM, absorption at *ca.* 550 nm is observed; thereby possibly indicating that an activated complex which promotes the production of 2,6-DIPN is more easily formed between naphthalene, propylene, and the acid sites located at the wall of the H mordenite channels.

**Table 3 Pore sizes and proportions of surface areas derived from micro pores**

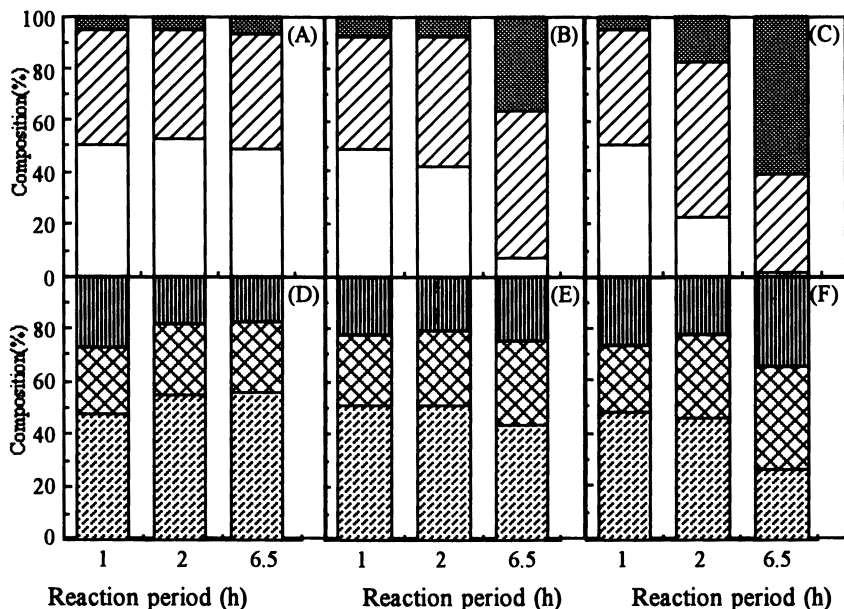
Zeolite	Pore Dimensions (nm) <sup>18)</sup>	Effective Pore Diameter (nm) <sup>19)</sup>	MS/TS
Mordenite	0.67x0.70, 0.29x0.57	0.62	0.62-0.96
Y-Zeolite	0.74	0.81	0.73-0.79
L-Zeolite	0.71	0.81	0.53-0.64
Ferrierite	0.43x0.55, 0.34x0.48	0.39	0.67
Offretite/Erionite	0.64, 0.36x0.52	0.60/0.43	0.65
ZSM-5	0.54x0.56, 0.51x0.55	0.55	0.91
Active Clay	-	-	0
Silica-alumina 50	-	-	0.42
Silica-zirconia 10	-	-	0.43
Silica-niobia 25	-	-	0.21

MS/TS = Surface area derived from micro pores / Total surface area

**Catalysis over H Y-zeolite (Group (2)).** Naphthalene is rapidly consumed in the isopropylation with H Y-zeolite as shown in Table 2. As shown in Figure 2, in the initial stage,  $\alpha,\alpha$ - and  $\alpha,\beta$ -DIPN isomers are preferentially produced.  $\alpha,\alpha$ -DIPN decreases and  $\beta,\beta$ -DIPN increases with reaction time. The yield of  $\alpha,\beta$ -DIPN increases with reaction time, reaches to maximum at the middle stage and then decreases with reaction time. From the comparison of the ratio of three groups at 1 h with that at 6.5 h, the yield of (1,4- + 1,3-DIPN) group decreases and those of (1,5- + 1,6- + 2,6-DIPN) and (1,7- + 2,7-DIPN) groups increases with reaction time as shown in Figure 3.

Figure 4 shows the effect of reaction temperature on catalytic isopropylation of naphthalene with H Y-zeolite. At 513 K,  $\alpha,\alpha$ -DIPN, especially 1,4-DIPN selectivity is initially high (37%), followed by isomerization to 1,3-DIPN, with approximately equal amounts of 2,6/2,7-DIPN being finally produced. At the low temperature of 433 K, high 1,4-DIPN selectivity is observed and subsequent isomerization only slightly occurs. These variations reflect the differences in activity and thermodynamic stability of the  $\alpha$ -positions of naphthalene.

The feature of isopropylation of naphthalene over H Y-zeolite indicates that H Y-zeolite has enough space in its pores for the alkylation of naphthalene and any alkylnaphthalene molecules can easily enter the pores since pore dimension of the channel of H Y-zeolite is larger than molecular sizes of DIPN isomers. Therefore, in the initial stage, 1,4-DIPN isomers are kinetically produced and then are isomerized to the more thermodynamically stable  $\alpha,\beta$ - and  $\beta,\beta$ -DIPN at high temperature (513 K). Another important feature is that (1,4- + 1,3-DIPN) group changes to (1,5- + 1,6- + 2,6-DIPN) and (1,7- + 2,7-DIPN) groups, especially to 2,6- and 2,7-DIPN with reaction time. This isomerization from (1,4- + 1,3-DIPN)



**Figure 4. Effect of reaction temperature on the composition of DIPN in the isopropylation of naphthalene over Y-zeolite.**

(A),(D) 433 K, (B),(E) 453 K, (C),(F) 513 K

□  $\alpha,\alpha$ -DIPN, ▨  $\alpha,\beta$ -DIPN, ■  $\beta,\beta$ -DIPN  
 ▩ (1,4- + 1,3-)DIPN, ⊞ (1,5- + 1,6- + 2,6-)DIPN, ▨ (1,7- + 2,7-)DIPN



group to 2,6- and 2,7-DIPN does not obey the Fries rule. This result indicates that the production of 2,6- and 2,7-DIPN results from dealkylation-alkylation and transalkylation processes. This phenomenon can possibly be attributed to the presence of a supercage in H Y-zeolite which promotes transalkylation.

**Catalysis over H L-zeolite (Group (3)).** Naphthalene is rapidly consumed in the isopropylation with H L-zeolite as shown in Table 2. As shown in Figure 2, in the initial stage,  $\alpha,\alpha$ - and  $\alpha,\beta$ -DIPN isomers are preferentially produced.  $\alpha,\alpha$ -DIPN decrease and  $\alpha,\beta$ -DIPN increases with reaction time. The yield of  $\beta,\beta$ -DIPN slightly increases with reaction time. As shown in Figure 3, the ratios of yield of three groups decrease in the order: (1,4- + 1,3-DIPN) group > (1,5- + 1,6- + 2,6-DIPN) group > (1,7- + 2,7-DIPN) group and this proportion are almost constant during reaction.

In the isopropylation over H L-zeolite, the active centers for catalysis are mainly present in the channel because most alkylnaphthalenes can enter the channel. The important feature of isopropylation of naphthalene over H L-zeolite is that the ratios of yield of (1,4- + 1,3-DIPN) group, (1,5- + 1,6- + 2,6-DIPN) group and (1,7- + 2,7-DIPN) group are almost constant during reaction. This result indicates that only alkylation and isomerization which obeys the Fries rule occur over H L-zeolite.

As shown in Table 3, pore dimension of H L-zeolite is almost as same as that of H mordenite and both zeolites have one-dimensional tunnels. However, the selectivity of DIPN isomers over H L-zeolite is much different from that over H mordenite. This difference is seemed to be caused by the channel shape (elliptical channel of H mordenite and round channel of H L-zeolite).

**Catalysis over H ZSM-5 (Group (4)).** As shown in Table 2, conversion of naphthalene at 8 hours is only 1% and the ratio of DIPN isomers could not be investigated by GC. Catalytic isopropylation of naphthalene with propene over H ZSM-5 hardly occurs because its pores are too small to allow the naphthalene molecules to enter and it does not have enough acid sites on external surface to form DIPN isomers. On the contrary, catalytic isopropylation of naphthalene with propene over H ferrierite easily occurs in spite of its small pores. The reactivity of ferrierite is caused by enough acid sites on its external surface in a similar manner as group (5).

**Catalysis over Amorphous Silica-alumina (Group (5)).** Naphthalene is rapidly consumed in the isopropylation with amorphous silica-alumina as shown in Table 2. As shown in Figure 2, in the initial stage,  $\alpha,\alpha$ - and  $\alpha,\beta$ -DIPN isomers are preferentially produced. 1-IPN and  $\alpha,\alpha$ -DIPN decrease and  $\alpha,\beta$ -DIPN and  $\beta,\beta$ -DIPN increase with reaction time. As shown in Figure 3, the ratios of yield of three groups decrease in the order: (1,4- + 1,3-DIPN) group > (1,5- + 1,6- + 2,6-DIPN)

group > (1,7- + 2,7-DIPN) group and this proportion are almost constant during reaction. A few reaction features of silica-niobia is different from those of other catalysts belong this group, that is, naphthalene is slowly consumed and subsequent isomerization only slightly occurs.

The feature of isopropylation of naphthalene over amorphous silica-alumina is very similar to that of H L-zeolite. The active sites of amorphous silica-alumina are present both inside and outside pores because any naphthalene molecules can contact with the surface both inside and outside pores. However, amorphous silica-alumina has low transalkylation reactivity because the acidity of silica-alumina is not enough to carry out transalkylation.

## Conclusions

Shapes and acidities of catalysts have enormous influence on activities and regioselectivities of DIPN isomers in the isopropylation of naphthalene. Thus, pore size determines whether reaction sites are inside pore or external surface. The main factor determining regioselectivity is pore shape if the isopropylation occurs inside pores, and is acidity if the isopropylation occurs at external surface. The isopropylation over H Y-zeolite and H L-zeolite mainly occurred inside their pores and gave  $\alpha,\alpha$ - and  $\alpha,\beta$ -DIPN isomers kinetically in the initial stage, and then these isomers isomerized to  $\alpha,\beta$ - and  $\beta,\beta$ -DIPN obeying the Fries rule with reaction time. In addition, the transalkylation easily occurred in the isopropylation over H Y-zeolite because of the existence of supercage. The isopropylation over some kinds of zeolites which have small pores, clays and mixed oxides occurred at external surface and gave  $\alpha,\alpha$ - and  $\alpha,\beta$ -DIPN isomers kinetically in the initial stage, and then these isomers isomerized to  $\alpha,\beta$ - and  $\beta,\beta$ -DIPN obeying the Fries rule with reaction time. Because of small amount of acid sites, the transalkylation did not occur in the isopropylation over these catalysts. In the isopropylation of naphthalene over H mordenite, selective isopropylation was observed to yield  $\beta,\beta$ -DIPN, especially 2,6-DIPN, and the isomerization did not occur. The regioselective formation of 2,6-DIPN was deduced to cause because of the synergism between the specificity of pore shape which is one-dimensional elliptical channel and the electronic effect caused by the formation of activated complexes.

## References

1. T. Bartik A. Simon, *Hung. J. Ind. Chem.*, **7**, 247 (1979).
2. Japan Tokkyo Kokai Koho 1989-61435.
3. G. Calik and T. H. Ozdamar, *Appl. Catal.*, **66**, 25 (1990).
4. Japan Tokkyo Kokai Koho 1991-88532.
5. A. V. Topchiev, M. V. Kurashev, and I. F. Gavrilenko, *Dokl. Akad. Nauk SSSR*, **139**, 124 (1961).

6. T. Yashima, Y. Sakaguchi, and S. Namba, In "Proceedings of the 7th international congress on catalysis" (T. Seiyama and K. Tanabe Eds.), Kodansha-Elsevier (1981).
7. Y. Sugi, T. Matsuzaki, T. Hanaoka, K. Takeuchi, T. Tokoro, and G. Takeuchi, *Studies in Surface Science and Catalysis*, **60**, T. Inui, S. Namba, and T. Tatsumi (Eds.) Kodansha-Elsevier (1991) 303.
8. G. S. Lee, J. J. Maj, S. C. Rocke, and J. M. Garces, *Catal. Lett.*, **2**, 243 (1989).
9. G. Takeuchi, H. Okazaki, M. Yamane, and T. Kito, *Appl. Catal.*, **76**, 25 (1991).
10. Japan Tokkyo Kokai Koho 1991-176429.
11. R. J. Argauer and J. R. Landolt, U. S. Pat. 3,702,886 (1972).
12. F. Mizukami, S. Niwa, M. Toba, T. Tsuchiya, K. Shimizu, S. Imai, and J. Imamura, *Studies in Surface Science and Catalysis*, **31**, B. Delmon, P. Grang, P. A. Jacobs, and G. Poncelet (Eds.) Elsevier (1987) 45.
13. M.Toba, S. Niwa, K. Shimizu, and F. Mizukami, *Nippon Kagaku Kaishi*, (**1989**) 1523.
14. M. Toba, F. Mizukami, S. Niwa, and K. Maeda, *J. Chem. Soc., Chem. Commun.*, (**1990**) 1211.
15. S. Brunaure, P. H. Emmett, and E. Teller, *J. Am. Chem. Soc.*, **60** (1938) 309.
16. J. H. deBoer, B. G. Linsen, Th van der Plas, and G. J. Zondervan, *J. Catal.*, **4** (1965) 649.
17. G. Suld and A. P. Stuart, *J. Org. Chem.*, **29** (1964) 2939.
18. N. Y. Chen and W. E. Garwood, *Catal. Rev., -Sci. Eng.*, **28**, 185 (1986).
19. D. W. Breck, "Zeolite Molecular Sieves", John Wiley & Sons, New York, (1974).
20. A. Katayama, M. Toba, G. Takeuchi, F. Mizukami, S. Niwa, and S. Mitamura, *J. Chem. Soc., Chem. Commun.*, (**1991**) 39.
21. S. M. Csicsery, *Zeolites*, **4**, 202 (1984).

## Chapter 22

# Computational Analysis for Shape-Selective Alkylation of Naphthalene over Zeolite Catalysts

Chunshan Song, Xiaoliang Ma, and Harold H. Schobert

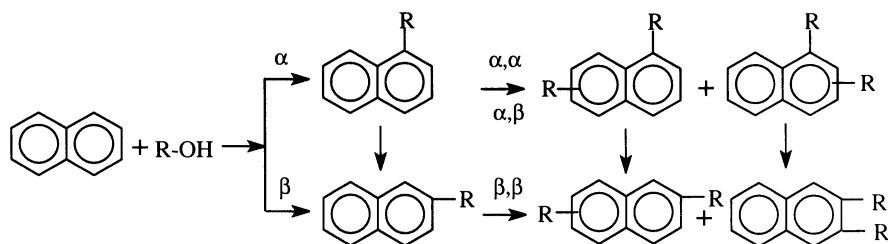
Applied Catalysis in Energy Laboratory, and Department of Energy and Geo-Environmental Engineering, Pennsylvania State University, 209 Academic Projects Building, University Park, PA 16802

This study is a computational analysis for shape-selective alkylation of naphthalene (including isopropylation, ethylation and methylation) by MINDO-PM3 calculations with MOPAC. There are 10 possible dialkylnaphthalene (DAN) isomers, with up to 3 from the so-called  $\beta$ ,  $\beta$ -selective dialkylation including 2,6-, 2,7- and 2,3-DAN. However, only 2,6-DAN is the desired product. We calculated the frontier electron density  $f_r(E)$  and molecular dimensions for alkylnaphthalene (AN) isomers and dialkylnaphthalene (DAN) isomers. The calculation shows that the 6-position in 2-AN has higher  $f_r(E)$  value than 7-position. The more reactive position for electrophilic substitution has higher  $f_r(E)$  value which represents the density of electrons in the highest occupied molecular orbital (HOMO). The formation of the cationic intermediate that leads to 2,6-DAN is favored energetically as compared to that for 2,7-DAN or 2,3-DAN. This suggests that during 2-AN alkylation inside a shape-selective channel, the formation of 2,6-DAN is favored electronically more than that of 2,7-DAN or 2,3-DAN, and thus the catalyst with lower acidity may favor 2,6-DAN. The results are consistent with experimental data in literature, and suggest that there is a restricted electronic transition-state selectivity to 2,6-DAN on some molecular-sieve catalysts with lower acidity, since both 2,6- and 2,7-DAN isomers are sterically permitted. In general, 2,6-DAN has a more linear structure with a similar or smaller critical diameter compared to 2,7-DAN, while 2,3-DAN always has a larger diameter than both 2,6- and 2,7-DAN.

Shape-selective catalysis plays an important role in environmentally benign synthesis of organic chemicals. Selective alkylation of benzene and alkylbenzenes over various zeolites has been studied extensively since the pioneering studies by Mobil researchers in the 1960's, as summarized in many excellent reviews (1-7). However, until recently, little attention has been paid to selective alkylation of two-ring aromatics such as naphthalene and biphenyl (8-11). Naphthalene and its derivatives are rich in some refinery streams and in liquids derived from coals via carbonization, gasification,

pyrolysis and liquefaction (11). Due to the demand for monomer for making the advanced polymer materials such as polyethylene naphthalate (PEN), polybutylene naphthalate (PBN) and liquid crystalline polymers (LCP),  $\beta$ -selective naphthalene alkylation for making 2,6-dialkyl naphthalene (2,6-DAN) has become an important subject (10-24).

Research in the area of shape-selective catalysis is dominated by experimental work so far and little has been reported on theoretical computational studies (11, 12, 24). However, with growing interest in selective conversion of polyaromatic compounds, the computational analysis may become a useful tool and provide some general guidelines. This is largely because the structural complexity and number of isomers increase dramatically from one-ring to multi-ring system. For example, dimethylbenzenes involve 3 isomers, and the desired isomer para-xylene is the product of selective methylation of toluene. In distinct contrast, there are as many as ten possible DAN isomers including  $\alpha,\alpha$ -,  $\alpha,\beta$ -, and  $\beta,\beta$ -disubstituted isomers, as shown in Figure 1.



**Figure 1.** Pathways for  $\alpha$ -alkylation (C-1) and  $\beta$ -alkylation of naphthalene (C-2).

As many as 3 products can be formed from the so-called  $\beta,\beta$ -selective dialkylation of naphthalene over molecular sieve catalysts. They are 2,6-, 2,7-, and 2,3-DAN<sup>o</sup>, as shown in Figure 2, but only the 2,6-DAN is the desired isomer. The challenge is to obtain 2,6-DAN with high selectivity and high 2,6/2,7-DAN ratio, but the key factors affecting the selectivity to 2,6-DAN have not been well established.

This work is an expansion of our recent preliminary work on computational analysis for diisopropylation of naphthalene (25). Several recent papers described experimental results of shape-selective isopropylation. Katayama et al. (10) reported that 2,6-DIPN and 2,7-DIPN have the same molecular diameter of 6.5 Å, but they observed preferential formation of 2,6-DIPN over mordenite catalyst. On the other hand, Moreau et al. (13) observed that 2,6- and 2,7-disubstituted products were formed in equal yields when using mordenite and Y-zeolite catalysts for isopropylation with isopropyl bromide and for cyclohexylation with cyclohexyl bromide. They reported that 2,6-DIPN and 2,7-DIPN have the same molecular diameter of 6.6 Å (13). The experimental results from our laboratory show that by using partially dealuminated mordenite catalysts, shape-selective alkylation of naphthalene can be enhanced with over 65% selectivity to 2,6-DIPN by using isopropanol with 2,6-DIPN/2,7-DIPN ratio of about 3 (14), or using propylene as the alkylating agent with 2,6-DIPN/2,7-DIPN ratio of >2 (15-17). Compared to parent mordenites, the partially dealuminated proton-form mordenites are more selective toward 2,6-DIPN against 2,7-DIPN. Apart from the structural changes in mordenite caused by dealumination, it was not clear whether the differentiation between the two isomers (2,6-DIPN and 2,7-DIPN) was caused by their difference in molecular dimension or in electronic property. For methylation of 2-methylnaphthalene (2-MN), Komatsu et al. (23) reported that poisoning the external

surface of ZSM-5 decreased the  $\alpha$ -substitution but does not increase the ratio of 2,6-dimethylnaphthalene (2,6-DMN) to 2,7-DMN; isomorphous substitution of ZSM-5 by Ga, B, or Fe can increase the 2,6/2,7-DMN ratio.

It is important to clarify the differences in molecular dimensions and electronic properties between the monoalkyl isomers and between the dialkyl isomers. Earlier calculation in our laboratory using PCModel program has indicated qualitatively that there are differences in molecular diameters between 2,6-DIPN and 2,7-DIPN (14). In order to develop a fundamental understanding of the shape selectivity in naphthalene alkylation, we performed a systematic computational analysis using MINDO-PM3 in MOPAC program for naphthalene, alkyl- and dialkylnaphthalene isomers involving isopropyl, ethyl and methyl substitution.

### Method of Calculation

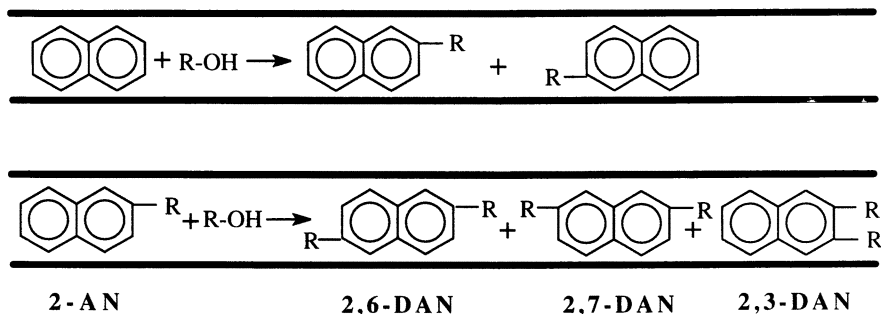
The molecular orbital package, MOPAC version 94 incorporated in CAChe software system, was used for computational analysis. The MOPAC program is based on quantum chemical principles, and calculates such chemical properties as electron density, HOMO, LUMO, heat of formation of molecules, radical and ionic intermediates, bond order, etc. In the present MOPAC calculation, we used the MINDO-PM3 semi-empirical parameters available in CAChe MOPAC developed by Stewart (26). For comparison, a molecular mechanics method using MM2 force field was also used to calculate the molecular dimension. The calculation was performed using a Power Macintosh computer system. The frontier electron density  $f_r(E)$  was calculated based on frontier orbital theory that was first developed by Fukui (27) and advanced by many researchers including Yonezawa and coworkers (28).

### Results and Discussion

**Molecular Dimensions.** The critical diameter is defined as the smallest diameter of a cylinder through which the molecule can pass through without distortion (14), and is calculated as the shortest distance between the two sides of a molecule. Table 1 summarizes the molecular dimensions of naphthalene, alkylnaphthalene and dialkylnaphthalene isomers for three different alkyl groups. In doing energy minimization, we found that there are two conformations of the isopropyl- and diisopropylnaphthalenes. Conformations A and B differ in dihedral angle ( $C_{ar3}-C_{ar2}-C_{\alpha}-H_{\alpha}$ ) between naphthalene ring and isopropyl C-H bond, as shown in Figure 3 for 2-IPN. Conformation A with dihedral angle of  $180^\circ$  has lower heat of formation and is slightly more stable. There are cases where the critical diameter shown in Table 1 is smaller than the diameter of the cylindrical cross section for certain conformations of some molecules with alkyl side chain, for which the size of such a cross-section is called cylinder diameter and is also shown in Table 1. Figure 4 illustrates the critical diameter, molecular length, and molecular thickness and cylinder diameter using two different conformations of 2,6-DIPN as examples. Figure 5 shows the steric structures of the more stable conformation (A) of 2,6-DIPN and 2,7-DIPN.

It is clear from Table 1 that  $\alpha$ -substitution creates molecules (1-AN and its DAN derivatives) with considerably larger critical diameters than the  $\beta$ -substitution (2-AN and its DAN derivatives). Similarly, the  $\alpha,\beta$ -disubstitution also creates molecules with larger critical diameters than the  $\beta,\beta$ -disubstitution. Among the  $\beta,\beta$ -DAN isomers, 2,3-DAN has a larger diameter than 2,6- and 2,7-DAN. 2,6-DAN has a similar or smaller diameter than 2,7-DAN in all of their corresponding conformations. 2,3-DAN has a different configuration compared to 2,6- or 2,7-DAN, which is due to steric repulsion

of the two adjacent alkyl groups. Consequently, 2,3-DAN has a larger critical diameter than either 2,6- or 2,7-DAN, regardless of the type of alkyl groups.



**Figure 2.** Shape-selective  $\beta$ -alkylation and  $\beta,\beta$ -dialkylation of naphthalene inside the pore channel of molecular-sieve catalysts.

**Table 1. Molecular Dimensions of Naphthalene and Alkylnaphthalenes**

Molecule	Steric Conform	Heat of Formation (kcal/mol)	Critical* Diameter (Å)	Molecular Length (Å)	Molecular Thickness (Å)	Cylinder** Diameter (Å)
Naphthalene		40.79	7.19	8.95	3.10	7.19
1-IPN	A	23.07	7.90	9.99	6.52	8.19
	B	24.14	8.28	9.52	6.52	8.55
2-IPN	A	22.11	7.21	11.03	6.52	7.21
	B	22.20	7.53	10.94	6.52	7.84
2,6-DIPN	A	3.44	7.21	13.14	6.52	7.21
	B	3.61	7.53	12.65	6.52	8.11
2,7-DIPN	A	3.44	7.26	13.14	6.52	7.26
	B	3.65	7.76	11.99	6.52	8.05
2,3-DIPN		3.20	8.97	10.71	6.03	8.97
1-EN		27.68	7.80	9.50	5.07	7.80
2-EN		26.81	7.19	10.62	5.07	7.19
2,6-DEN	A	12.59	7.19	12.90	6.44	8.05
	B	12.59	7.19	12.90	5.07	7.56
2,7-DEN	A	12.59	7.19	12.90	6.44	8.05
	B	12.59	7.19	12.90	5.07	7.56
2,3-DEN		12.78	7.25	10.86	6.37	7.25
1-MN		32.22	7.70	9.51	3.97	7.70
2-MN		31.37	7.19	9.87	3.97	7.19
2,6-DMN		21.81	7.19	10.84	3.97	7.19
2,7-DMN		21.92	7.19	10.84	3.97	7.19
2,3-DMN		22.83	7.30	9.89	3.97	7.30

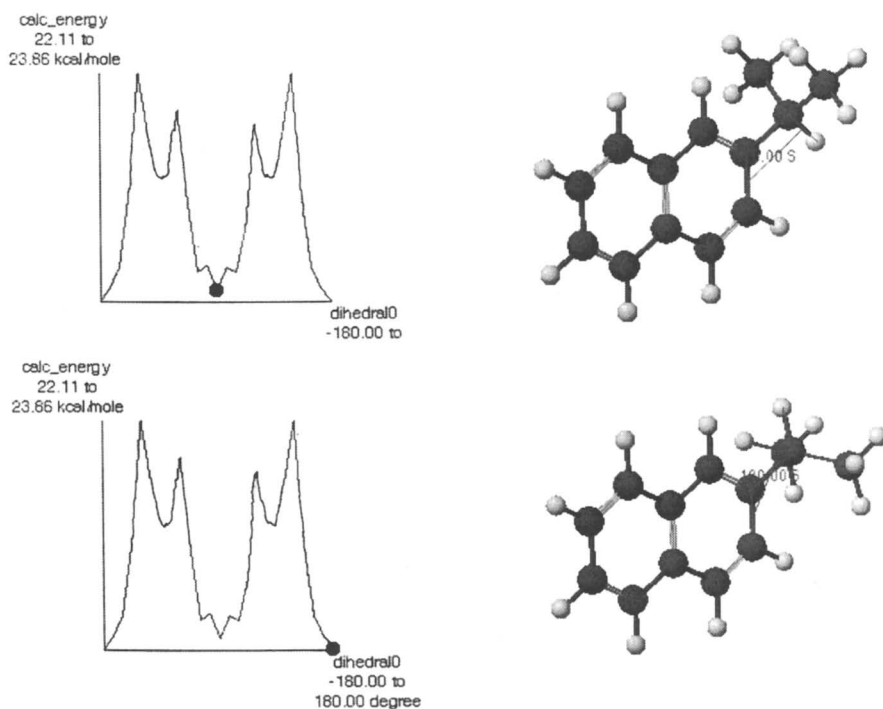
\* Van der Waals radius for H = 1.10 Å, for C = 1.55 Å.

\*\* Diameter for a largest possible cross-section circle of a molecular conformation.

**Table 2.** Comparison of Calculated Molecular Dimensions by MM2 and MOPAC

Method	Molecule	Critical Diameter (Å)	Molecular Length (Å)	Molecular Thickness (Å)	Source Reference
M/M and M/D with Polygraf	2,6-DIPN	6.5	13.2	n/a	(10)
	2,7-DIPN	6.5	12.5	n/a	(10)
MM+ with Hyperchem	2,6-DIPN	6.6	12.5	n/a	(13)
	2,7-DIPN	6.6	11.9	n/a	(13)
MINDO-PM3 With CAChe	2,6-DIPN	7.21	13.14	6.52	This work
	2,7-DIPN	7.26	13.14	6.52	This work
MM2 With CAChe	2,6-DIPN	7.19	13.19	6.56	This work
	2,7-DIPN	7.25	13.19	6.56	This work

n/a: not available with MM2 calculation method.

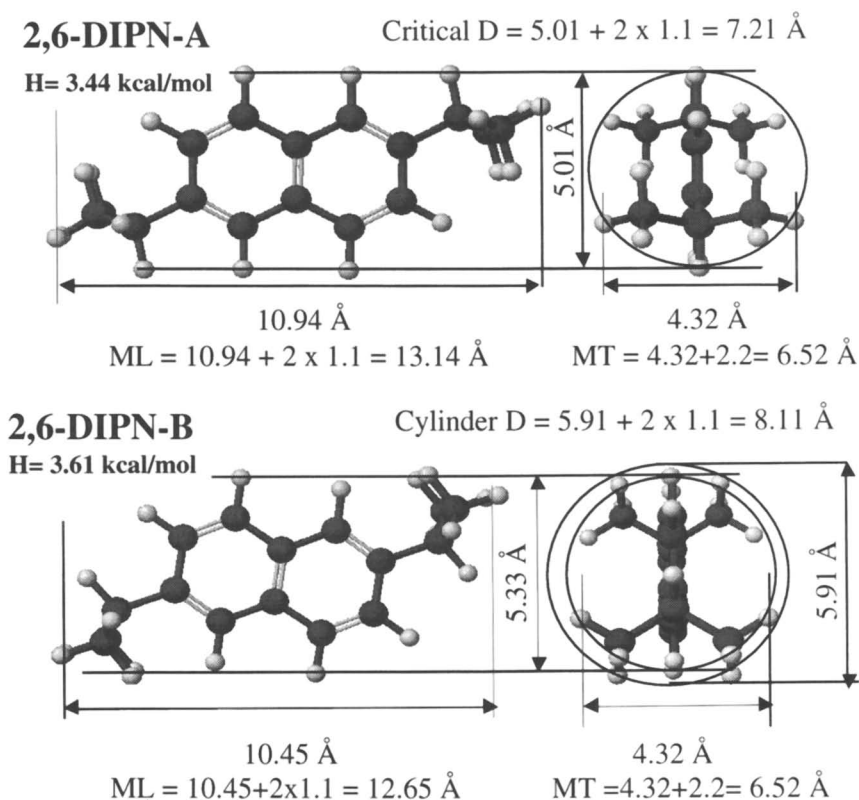


**Figure 3.** Energy minimization profiles for 2-DIPN with dihedral angle equal to 0° for conformation **B** (top) and 180° for conformation **A** (bottom).

In the case of isopropylation, both 2,6-DIPN and 2,7-DIPN are the products of the so-called  $\beta,\beta$ -selective dialkylation (Figure 2). The calculation shows that 2,6-DIPN



has a slightly smaller critical diameter (7.21 Å) than 2,7-DIPN (7.26 Å). The former is more linear than the latter, as can be seen from the steric structures shown in Figure 5.

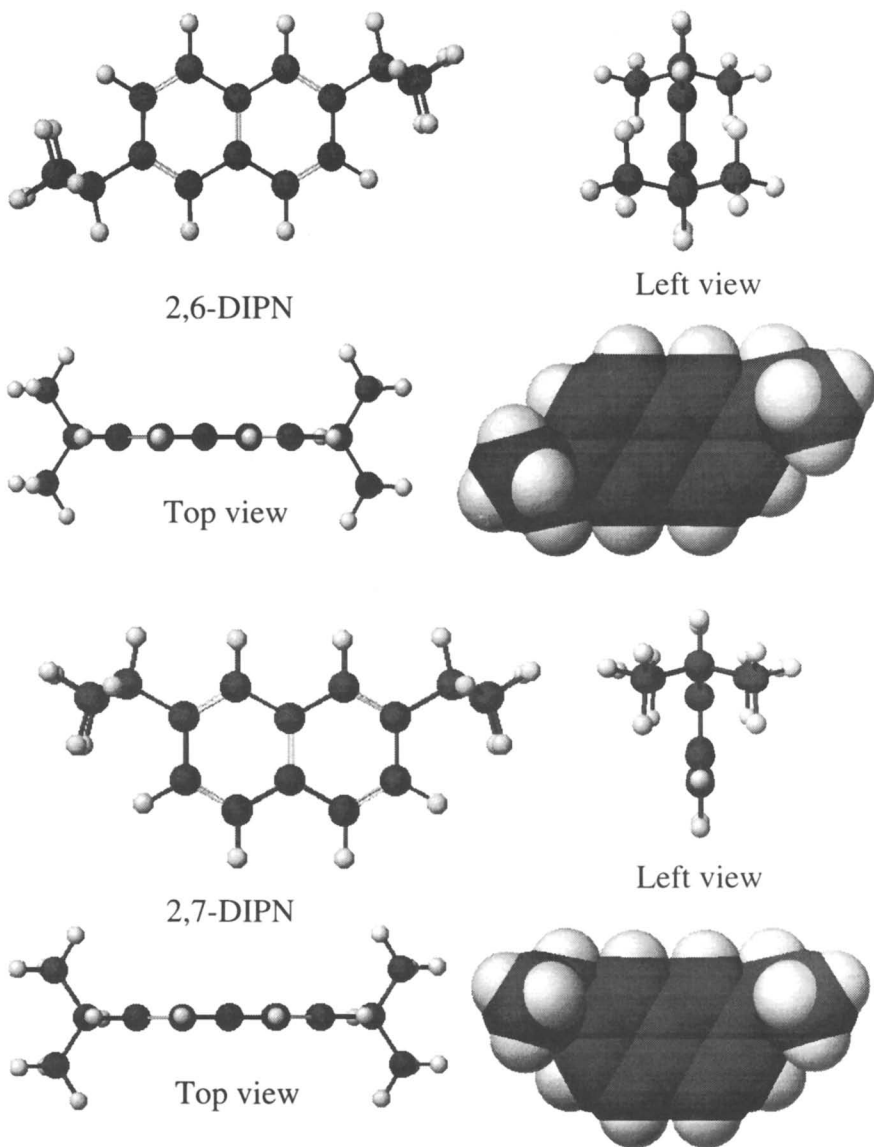


**Figure 4.** Illustration of critical diameter, length, thickness and cylinder diameter.

Table 2 compares the molecular dimensions calculated using MM2 and MOPAC methods. It is necessary to make the comparison since earlier work used M/M or M/D method (10) and MM<sup>+</sup> force field, an enhanced version of the MM2 force field (13). The results from MM2 method in the present work, however, show larger critical diameter values than those reported in previous studies (10, 13). In general, it is considered that MINDO-PM3 provides more accurate results than MM2 within the range of computational capability, since the latter determines molecular geometries using equations from classical Newtonian physics, but the former calculates both geometric and electronic properties of molecules by solving the Schrodinger equations using semi-empirical Hamiltonians. However, for calculating the molecular dimension, both methods give similar critical diameters, as can be seen from Table 2.

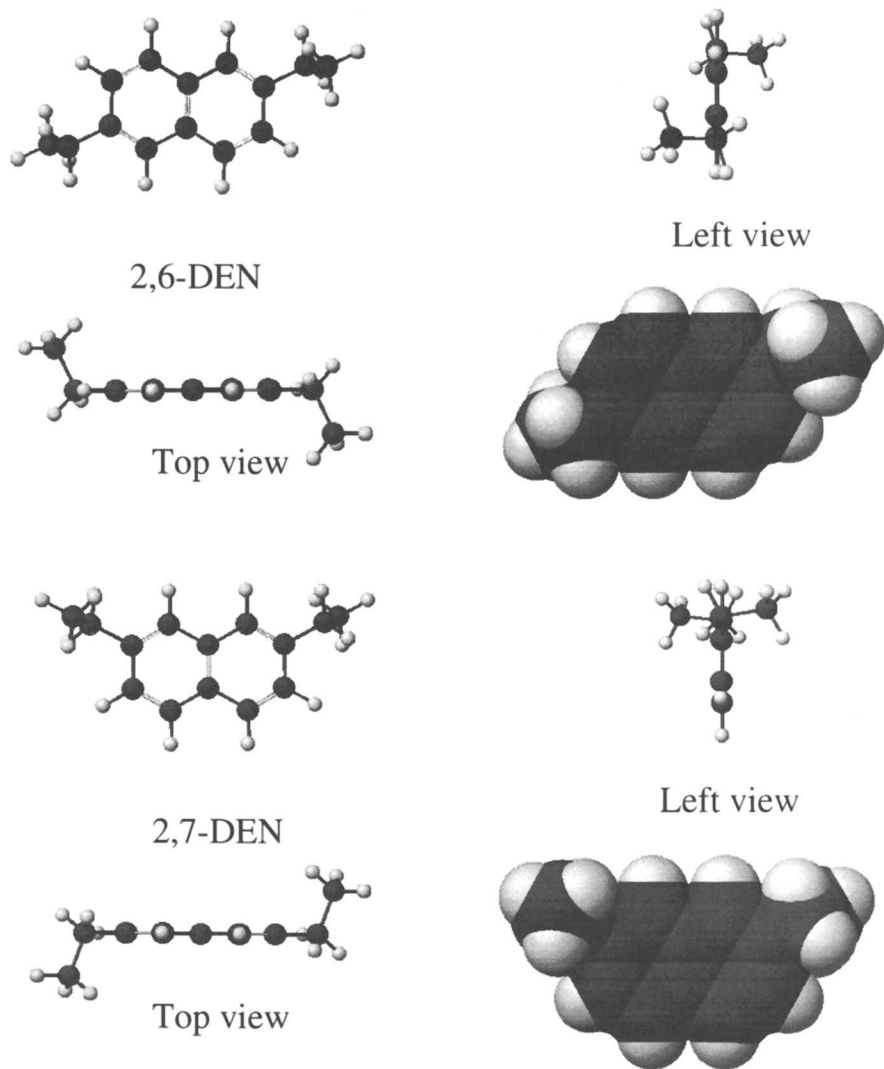
One of the variable in such calculations is the van der Waals radius of hydrogen atom. It should be a constant by definition (the internuclear distance or radius of closest approach of an atom to another with which it forms no bond) but there are different values of van der Waals radius for hydrogen atom in literature, 1.08 Å (26), 1.1 Å (18), and 1.2 Å (29) and the values for carbon are not always the same either. It is not

clear what value of radius for hydrogen was taken in previous calculations by Katayama et al. (11) and by Moreau et al. (13). We used the van der Waals radius values of 1.1 Å for hydrogen and 1.55 Å for carbon, which is consistent with a recent study in computer simulation by Horsley and co-workers (18).

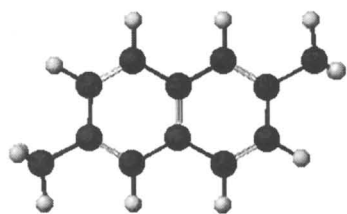


**Figure 5.** Steric structures including space-filling model of 2,6-DIPN (top) and 2,7-DIPN (bottom) in their more stable conformation A.

For diethylated and dimethylated naphthalene isomers, the situation of molecular dimension is somewhat different from that for diisopropylation. Figures 6 and 7 present the steric structures of the 2,6- and 2,7-isomers for DEN and DMN, respectively. For both 2,6- and 2,7-DEN, the conformation A in Table 1 corresponds to that with one ethyl group on each side of the ring in the left view in Figure 6. The conformation B corresponds to that with the two ethyl groups on the same side of the ring in the left view. For 2,6- and 2,7-DMN, however, they do not have such different conformations.



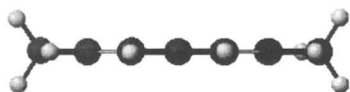
**Figure 6.** Steric structures of 2,6-DEN (top) and 2,7-DEN (bottom) in their conformation A.



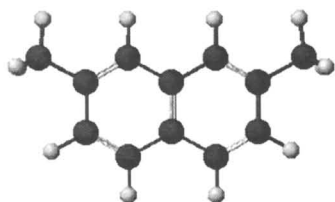
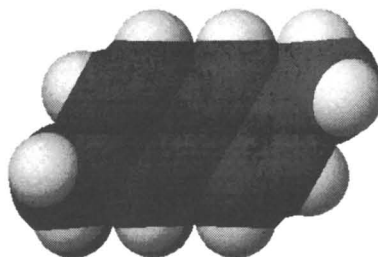
2,6-DMN



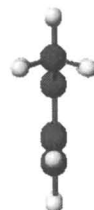
Left view



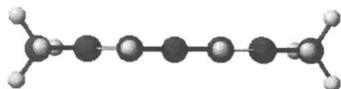
Top view



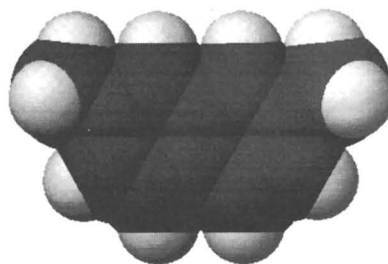
2,7-DMN



Left view



Top view



**Figure 7.** Steric structures of 2,6-DMN (top) and 2,7-DMN (bottom).

While there are significant differences in molecular dimensions between 1- and 2-alkyl isomers, the critical diameters of the 2,6- and 2,7-DEN (or DMN) isomers are identical, as shown in Table 1. However, the structure of 2,6-DEN in Figure 6 and that of 2,6-DMN in Figure 7 are clearly more linear than their corresponding 2,7-isomers.

**Frontier Electron Density.** Table 3 shows the frontier electron density value,  $f_r(E)$  for electrophilic substitution reaction which represents the density of electrons in the highest occupied molecular orbital (HOMO). According to the frontier molecular orbital theory (27,28), the most reactive position (the carbon atom on which electrophilic attack occurs most likely) has the highest frontier electron density. It is clear from Table 3 that the  $\alpha$ -carbon positions (1,4,5,8) are much more reactive than the  $\beta$ -carbon positions (2,3,6,7). Therefore,  $\alpha$ -substitution will occur preferentially when it is sterically permitted. This is consistent with experimentally observed high percentage of  $\alpha$ -isopropylation with HY (10, 14) and  $\text{SiO}_2\text{-Al}_2\text{O}_3$  (18), as shown in Table 4.

More importantly, the presence of an alkyl group at position 1 or 2 of naphthalene changes the frontier electron density at positions 6 and 7. In 1-IPN, position 7 has slightly higher  $f_r(E)$  value than position 6. However, the position 6 in 2-IPN has higher  $f_r(E)$  value than position 7. This suggests that during the isopropylation of 2-IPN inside a mordenite catalyst channel, the formation 2,6-DIPN is favored electronically than that of 2,7-DIPN. The same trend can be observed also for 1- and 2-ethyl naphthalene (2-EN) and for 1- and 2-MN.

**Table 3. Frontier Electron Density at Ring Carbons in Alkyl naphthalene**

Molecule ID	Carbon 1	Carbon 2	Carbon 3	Carbon 4	Carbon 5	Carbon 6	Carbon 7	Carbon 8
Naphthalene	0.347	0.153	0.153	0.347	0.347	0.153	0.152	0.347
1-IPN (A)	0.373	0.181	0.142	0.364	0.311	0.137	0.143	0.310
2-IPN (A)	0.373	0.193	0.110	0.335	0.329	0.177	0.122	0.339
2,6-DIPN	0.350	0.217	0.082	0.321	0.349	0.217	0.082	0.321
2,7-DIPN	0.366	0.159	0.134	0.325	0.325	0.135	0.159	0.366
2,3-DIPN	0.369	0.145	0.145	0.369	0.322	0.146	0.146	0.322
1-EN	0.370	0.183	0.142	0.366	0.308	0.135	0.143	0.307
2-EN	0.376	0.199	0.103	0.332	0.326	0.180	0.117	0.337
2,6-DEN	0.347	0.228	0.072	0.314	0.348	0.228	0.072	0.314
2,7-DEN	0.369	0.160	0.132	0.321	0.321	0.132	0.160	0.369
2,3-DEN	0.365	0.146	0.146	0.365	0.326	0.146	0.146	0.326
1-MN	0.374	0.191	0.140	0.372	0.297	0.128	0.142	0.294
2-MN	0.384	0.218	0.085	0.318	0.317	0.193	0.103	0.335
2,6-DMN	0.341	0.255	0.047	0.292	0.341	0.255	0.047	0.292
2,7-DMN	0.378	0.163	0.126	0.309	0.309	0.126	0.163	0.378
2,3-DMN	0.369	0.142	0.142	0.369	0.320	0.144	0.144	0.320

**Origin of Shape Selectivity to 2,6-DAN.** Shape-selective reactions require a close match between the pore dimension and the molecular dimension of the reactants, products, or transition state. The crystallographic calculation shows that the elliptical

pore channel of mordenite has a major diameter of 7.0 Å and a minor diameter of 6.5 Å (4, 7). It would appear that both 2,6- and 2,7-DIPN have a diameter that is larger than the pore diameter of mordenite. However, the effective apertures of mordenite and other zeolites have been estimated to be larger, especially at reaction temperatures, than values calculated from crystallographic measurements (18, 30, 31).

Our experimental results show that proper dealumination of mordenite can enhance the selectivity to 2,6-DIPN and increase the 2,6-DIPN/2,7-DIPN ratio (15-17), as shown in Table 4. Furthermore, Sugi and coworkers (19) studied in detail the effect of SiO<sub>2</sub>/Al<sub>2</sub>O<sub>3</sub> ratio of mordenite on naphthalene isopropylation with propylene. They analyzed not only the bulk of the reaction products, but also the products trapped in the pores of mordenite after the isopropylation. Inside the mordenite pore channel 2,6-DIPN was formed in a higher selectivity than 2,7-DIPN, and the 2,6/2,7 ratio inside the pore increased with increasing SiO<sub>2</sub>/Al<sub>2</sub>O<sub>3</sub> ratio of mordenite. An implication from these experimental results is that decreasing the mordenite acidity (reducing the number of acidic sites) by dealumination may increase the selectivity to 2,6-DIPN and 2,6/2,7 ratio.

**Table 4.** Literature Data for Naphthalene Isopropylation and Methylation

Catalyst ID	Si/Al Ratio	Naph Conv. %	Prod Mol%			DAN % Sel			Source Ref.
			AN	DAN	TrAN+	2,6-	2,7-	2,6/2,7	
<b>DIPN Rxn</b>									
HM14	28	76	63	32	4	33	19	1.76	(16)
HM38	76	73	60	34	4	39	19	1.99	(16)
HM71	142	74	60	37	2	51	22	2.29	(16)
HM74	148	47	75	23	0.6	55	25	2.24	(16)
HM3	20.6	16	55	34	11	41	38	1.08	(13)
US-HY	2.6	97	28	55	17	35	36	0.95	(13)
HY	7	96.1	≤ 50.4	49.6	NR	32.6	31.2	1.10	(10)
SiO <sub>2</sub> -Al <sub>2</sub> O <sub>3</sub>	2.98	23.4	91.9	8.1	0	36.8	36.8	1.0	(18)
SiO <sub>2</sub> -Al <sub>2</sub> O <sub>3</sub>	2.98	94.2	31.1	51.5	17.4	38.5	37.4	1.03	(18)
<b>DMN Rxn</b>									
		2-MN	1-MN						
ZSM-5	43	25.1	13.9	9.9		26.2	21.6	1.21	(23)
ZSM-5 <sup>a</sup>	43	9.4	0	8.6		46.0	37.7	1.22	(23)
Ga-MFI <sup>b</sup>	42 <sup>b</sup>	9.6	0	8.6		49.5	36.9	1.34	(23)
Fe-MFI <sup>c</sup>	37 <sup>c</sup>	10.5	0	9.5		56.0	31.4	1.78	(23)

**a:** ZSM-5 poisoned by 2,4-DMQ; **b:** Ga-MFI with Si/Ga ratio of 42 and poisoned by 2,4-DMQ; **c:** Fe-MFI with Si/Fe ratio of 37 and poisoned by 2,4-DMQ.

It is now clear that the  $\alpha$ -substitution occurs mainly on the external surface of mordenites during isopropylation. The data in Table 3 show that  $\alpha$ -positions have higher reactivity than all the  $\beta$ -positions, and thus are substituted more preferentially on acid sites that are not sterically restricted. Both dealumination by acid leaching (15-18) and surface coating (20) or surface poisoning (23) can decrease the external acid sites and thus improve the  $\beta$ -selectivity.

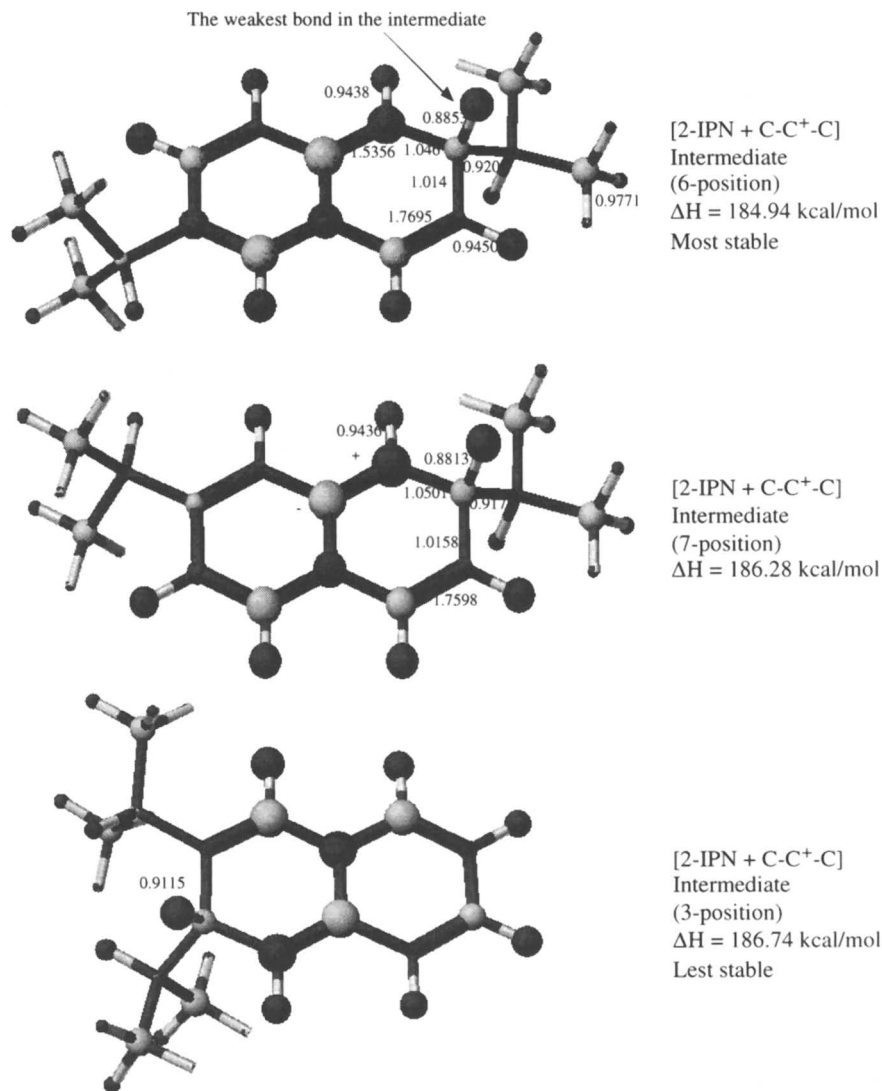
Both 2,6- and 2,7-DIPN are  $\beta,\beta$ -selective products. It was not clear from previous studies as to whether the enhanced selectivity to 2,6-DIPN was caused by steric difference or from electronic difference between 2,6- and 2,7-DIPN, apart from the decrease in acidity and structural changes in mordenite (22). Could a difference in molecular dimension cause the increase in 2,6-DIPN and 2,7-DIPN ratio? Judging from Table 1 and Figure 4, the more linear structure of 2,6-DIPN (with slightly smaller critical diameter) may make it easier to diffuse in the pore channel. Horsley and coworkers have shown by computer simulation (20) that the diffusion of 2,6-DIPN inside mordenite pore channel is easier than that of 2,7-DIPN, as reflected by the considerable difference in energy barrier values for diffusion of 2,6-DIPN (4 kcal/mol) and 2,7-DIPN (18 kcal/mol). This may partially account for the observed higher selectivity of mordenite for 2,6-DIPN. However, diffusion rate does not necessarily reflect the rate of reaction inside the pore. Moreau et al. (13) observed equal-molar yields of 2,6- and 2,7-DIPN over mordenites with isopropyl bromide as the alkylating agent, even after their CVD-modification which passivated external surface and thus enhanced overall selectivity to  $\beta,\beta$ -DIPN (2,6+2,7) by eliminating  $\alpha$ -substitution.

Therefore, in addition to diffusion, there may be other factors that also affect the selectivity towards 2,6-DIPN. Another question that arises is, which one of the two isomers (2,6-DIPN and 2,7-DIPN) is formed more easily inside the mordenite pore channel? In this regard, it is worth mentioning again that the ratios of 2,6-DIPN/2,7-DIPN inside the pore of the dealuminated mordenites were found to be higher than the bulk reaction products (19). The steric restriction can eliminate the  $\alpha$ -substitution inside the mordenite channel. By using the frontier molecular orbital theory we can compare the  $f_r(E)$  values of possible  $\beta$ -positions for electrophilic substitution inside the pore to identify the most reactive  $\beta$ -position with the highest frontier electron density (the  $\beta$ -carbon atom on which electrophilic attack occurs more easily).

Of the results in Table 3, the most important trend is the considerably higher frontier electron density in 6-position of 2-IPN (0.177) than that of 7-position (0.122). This means that the carbon at position 6 of 2-IPN has higher density of electrons in HOMO, and is therefore more reactive. The same trend in difference between the 6- and 7-positions can be seen for 2-EN and 2-MN in Table 3.

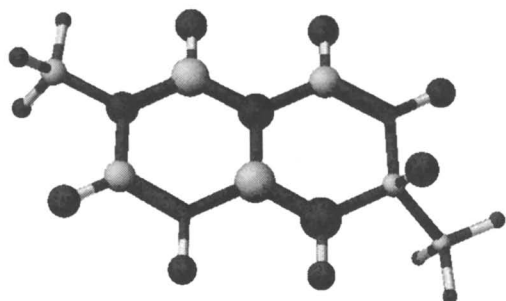
Figure 8 shows the cationic intermediates formed by attack of isopropyl cation on 6-, 7-, and 3-positions of 2-IPN. In Figure 8, the relative atomic diameter is proportional to the partial charge; the thickness of the connecting bond is proportional to the bond order. The data beside the bond indicate bond orders. Upon the attack by the isopropyl cation to 6-position, the positive charge is more concentrated on 1-position. The relative bond order indicates that the subsequent  $\beta$ -scission of the bond between carbon-2 and hydrogen (bond order: 0.8853) is more likely to occur, which leads to 2,6-DIPN, as compared to that of the bond between carbon-2 and carbon- $\alpha$ , which regenerates 2-IPN. From the data in Figure 8, the ease of formation in terms of energetics is 2,6-DIPN > 2,7-DIPN > 2,3-DIPN. Apparently, the formation of 2,6-DIPN is favored more than that of 2,7-DIPN, and that of 2,3-DIPN is the least favored. Our work showed that dealumination decreases the acidity of mordenite and reduces the number of strong acid sites as measured by TPD of n-butylamine (22). Based on Table 3 and Figure 8, dealumination could make the catalyst sites more selective towards 2,6-DIPN, since the 6-position of 2-IPN is more electron rich in the HOMO and attack there is factored. This consideration can help rationalize the experimental observation that much higher 2,6-DIPN selectivity was obtained with

isopropanol as the alkylating agent (14), since the byproduct water can partially passivate the stronger acid sites. In this context, stronger acid sites are not selective enough to distinguish between 2,6- and 2,7-DIPN. This consideration may account for why Moreau et al. (13) observed no preferential formation of 2,6-DIPN relative to 2,7-DIPN in mordenite and even with CVD-modified mordenite, because the alkylating agent isopropyl bromide can result in strong, non-selective acid sites in the system.

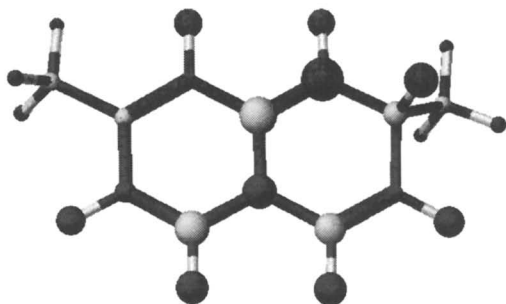


**Figure 8.** Energetics of cationic intermediates formed by attack of an isopropyl cation at the 6-, 7- and 3-positions of 2-IPN leading to 2,6-DIPN (top), 2,7-DIPN (middle) and 2,3-DIPN (bottom).

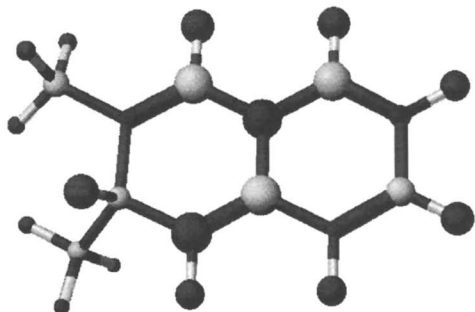




[2-MN + CH<sub>3</sub><sup>+</sup>]  
Intermediate  
(6-position)  
 $\Delta H = 205.055$  kcal/mol



[2-MN + CH<sub>3</sub><sup>+</sup>]  
Intermediate  
(7-position)  
 $\Delta H = 207.145$  kcal/mol



[2-MN + CH<sub>3</sub><sup>+</sup>]  
Intermediate  
(3-position)  
 $\Delta H = 206.353$  kcal/mol

**Figure 9.** Cationic intermediates formed by attack of a methyl cation at the 6-, 7- and 3-positions of 2-MN leading to 2,6-DMN (top), 2,7-DMN (middle) and 2,3-DMN (bottom).

Figure 9 shows the intermediates formed by attack of a methyl cation at the 6-, 7- and 3-positions of 2-MN. In this case, the ease of formation in terms of energetics is 2,6-DMN > 2,3-DMN > 2,7-DMN. This is somewhat different than that of isopropylation. The formation of 2,3-DAN is very limited in isopropylation but pronounced in methylation, probably due to the least favored energetics in the former

case. For methylation of 2-MN, Komatsu et al. (23) showed that the isomorphous substitution of ZSM-5 by Ga, B, and Fe can increase the selectivity to 2,6-DMN and 2,6-/2,7-DMN ratio. They suggested that weaker acidity may improve the selectivity to 2,6-DMN because of higher electron density of HOMO at C-6 than at C-7, although the electron density values were not reported. The same group also reported that such isomorphous substitution decrease the acidity and acid strength (32). In this context, the observed effect of acidity on dimethylation is similar in trend to that for diisopropylation discussed above.

It was reported that the selectivity of the alkylation of naphthalene may be explained by product selectivity (21) or rationalized by transition-state selectivity (19). In our earlier work, we considered both product selectivity and transition-state selectivity for isopropylation (14). The present results strongly suggest that, when the density of catalytically-active acid sites is lowered, the differences in frontier electron density and in the energetics of the cationic intermediates can lead to a preferred formation of the 2,6-oriented transition state from 2-IPN, which is favored by higher reactivity of the 6-position compared to that of 7-position in 2-IPN. The computational results suggest that there could be an electronic transition-state selectivity, among the two or more sterically-permitted transition states (for 2,6 and 2,7-DAN). The results reveal the importance of electronic factors for shape-selective PAH conversion, and it may be necessary to consider a restricted electronic transition-state selectivity, if there are two or more intermediates that can not be distinguished by the well-known spatial transition state selectivity. One can use the steric restriction to minimize any  $\alpha$ -substitution (on positions 1,4,5,8 and their DAN-derivatives). Since both 2,6- and 2,7-DAN isomers are sterically allowed, the selective formation of 2,6-DAN against 2,7-DAN may be enhanced by making use of the restricted electronic transition-state selectivity. The fact that 2,6-DAN has a more linear structure as compared to 2,7-DAN could make it easier to diffuse out of the pore channel, and therefore 2,6-DAN could be favored also in terms of product selectivity. These considerations partially account for the enhanced formation of 2,6-DIPN from 2-IPN inside mordenite channel and improved 2,6-DIPN selectivity upon proper dealumination of the catalyst.

Our experimental results suggest that reduced acidity through proper dealumination can make the acid sites more selective (22). Since dealumination reduces acidity and removes some strong acid sites (22), it is possible that the density, strength, and location of acid sites in properly dealuminated mordenites better match the requirements for selective formation of 2,6-DIPN than for 2,7-DIPN. Dealumination can cause not only the decrease in acidity as measured by base desorption, but also a small shrinkage of unit cell dimensions of mordenite (22). It should be noted that decrease in acidity does not mean a decrease in the acid strength of existing acidic sites.

Finally, it should be mentioned that the results of the frontier orbital analysis, although directly relevant to acid catalysis in homogeneous reaction, serve only as general guidelines for shape-selective catalysis inside the pore channel of a zeolite. The frontier orbital analysis indicates the 6-position is electronically favored over the 7-position in the electrophilic substitution of 2-IPN. However, there may be cases where the 7-position is more favored due to geometric structure of pore channel and location of acid sites in certain zeolites. For example, it has also been reported that zeolite L favors slightly more 2,7-DIPN rather than 2,6-DIPN (20). Therefore, both the electronic factors (this work) and the characteristics of zeolite structure related to molecular dimensions should be taken into account when considering the shape selectivity of naphthalene alkylation. Frontier orbital theory was first proposed and developed by Fukui and his coworkers (27,28). The present data for frontier electron density of 1- and 2-positions of naphthalene are in good agreement with earlier data (28). We have found no other reports on values of frontier electron density of alkyl- and dialkyl-naphthalenes by MOPAC or other methods such as *ab initio*, and thus we can not compare our results with literature data or discuss their relative accuracy.

## Concluding Remarks

MOPAC calculations can provide very useful insights into shape-selective alkylation. Due to higher frontier electron densities of  $\alpha$ -positions (carbons 1, 4, 5, and 8) than those of  $\beta$ -positions (carbons 2, 3, 6, and 7) in naphthalene, selectivity for  $\beta$ -substitution of naphthalene is not favored electronically as compared to  $\alpha$ -substitution. This calls upon the use of a shape-selective catalyst to impose steric restrictions to enhance the  $\beta$ -substitution and limit the  $\alpha$ -substitution.

The presence of an alkyl group on 1- or 2-position of naphthalene changes the relative order of frontier electron density in 6-, 7- and 3-positions. For  $\beta$ -selective isopropylation of 2-IPN, formation of 2,6-DAN is favored more than that of 2,7-DAN, because 6-position of 2-IPN has a higher frontier electron density and thus higher reactivity than the 7-position towards electrophilic substitution. Decreasing the catalyst acidity (reducing the number of strong acid sites) can make it more selective towards 2,6-DAN. The computational results suggest that there could be a restricted electronic transition-state selectivity towards an intermediate whose formation is electronically favored, among two or more sterically-permitted transition states for different products. The computational results reveal the importance of electronic factors for shape-selective PAH conversion, since 2,6- and 2,7-DAN (and 2,3-DAN in the cases of methylation) isomers are sterically allowed. Therefore, it may be necessary to distinguish the electronically-favored transition-state selectivity from (or within) the well-known sterically-restricted transition state selectivity. The fact that 2,6-DAN has a more linear structure (as compared to 2,7-DAN) makes it easier to diffuse out; 2,3-DAN has a larger diameter than 2,6- and 2,7-DAN and is therefore subject to more diffusional limitation.

The results of calculations by MOPAC are consistent with the experimental results for mordenite-catalyzed selective isopropylation, and MFI-catalyzed selective methylation of naphthalene that have been reported in literature. Therefore, it is very useful to explore molecular modeling technique to shed more light on the shape selective alkylation of naphthalene.

## References

1. Weisz, P. B. *Pure & Appl. Chem.*, **1980**, 52, 2091.
2. Venuto, P. B., *Micropor. Mater.*, **1994**, 2, 297.
3. Chen, N. Y.; Garwood, W. E.; Dwyer, F. G. *Shape-Selective Catalysis in Industrial Applications*. 2nd Edition, Marcel Dekker, New York, **1996**, 282 pp.
4. Csicsery, S. M. *Stud. Surf. Sci. Catal.*, **1995**, 94, 1.
5. Haag, W. O. *Stud. Surf. Sci. Catal.*, **1994**, 84, 1375.
6. Weitkamp, J.; Weiß, U.; Ernst, S. *Stud. Surf. Sci. Catal.*, **1995**, 94, 363.
7. Suib, S. L. *Am. Chem. Soc. Sym. Ser.*, **1993**, 517, 1.
8. Fraenkel, D.; Cherniavsky, M.; Ittah, B.; Levy, M. *J. Catal.*, **1986**, 101, 273.
9. Lee, G.S.; Maj, J. J.; Rocke, S.C.; Garces, J. M. *Catal. Lett.*, **1989**, 2, 243.
10. Katayama, A.; Toba, M.; Takeuchi, G.; Mizukami, F.; Niwa, S.; Mitamura, S. *J. Chem. Soc. Chem. Comm.*, **1991**, 39.
11. Song, C.; Schobert, H. H. *Fuel Process. Technol.*, **1993**, 34, 157; Song, C.; Schobert, H.H. *Chem. Ind.*, **1996**, 7, 253; Song, C.; Schobert, H. H. *Fuel*, **1996**, 75, 724.
12. Sugi, Y.; Toba, M., *Catal. Today*, **1994**, 19, 187.
13. Moreau, P.; Finiels, A.; Geneste, P.; Solofo, J. *J. Catal.*, **1992**, 136, 487; Moreau, P.; Finiels, A.; Geneste, P.; Joffre, J.; Moreau, F.; Solofo, J. *Catal. Today*, **1996**, 31, 11.

14. Song, C.; Kirby, S. *Micropor. Mater.*, **1994**, 2, 467.
15. Schmitz, A.; Song, C., *Am. Chem. Soc. Div. Fuel Chem. Prepr.*, **1994**, 39, 986; Schmitz, A.; Song, C., *Am. Chem. Soc. Div. Fuel Chem. Prepr.*, **1995**, 40, 918.
16. Schmitz, A.; Song, C. *Catal. Today*, **1996**, 31, 19.
17. Schmitz, A.; Song, C. *Catal. Lett.*, **1996**, 40, 59.
18. Horsley, J.A.; Fellmann, J.D.; Derouane, E.G.; Freeman, C.M. *J. Catal.*, **1994**, 147, 231.
19. Kim, J.-H.; Sugi, Y.; Matsuzaki, T.; Hanaoka, T.; Kubota, Y.; Tu, X.; Matsumoto, M. *Micropor. Mater.*, **1995**, 5, 113.
20. Kim, J.-H.; Sugi, Y.; Matsuzaki, T.; Hanaoka, T.; Kubota, Y.; Tu, X.; Matsumoto, M.; Nakata, S.; Kato, A.; Seo, G.; Pak, C., *Appl. Catal. A: General*, **1995**, 131, 15.
21. Kikuchi, E.; Sawada, K.; Maeda, M.; Mtsuda, T. *Stud. Surf. Sci. Catal.*, **1994**, 90, 391.
22. Song, C.; Schmitz, A. D.; Reddy, K. M., *Mat. Res. Soc. Sym. Proc. Ser.*, **1998**, in press.
23. Komtsu, T.; Araki, Y.; Namba, S.; Yashima, T., *Stud. Surf. Sci. Catal.*, **1994**, 84, 1821.
24. Song, C. *Stud. Surf. Sci. Catal.*, **1998**, 113, 163.
25. Song, C.; Ma, X.; Schmitz, A. D.; Schobert, H. H. *Am. Chem. Soc. Div. Petrol. Chem. Prepr.*, **1998**, 43, 280.
26. Stewart, J. J. P. *J. Comp. Chem.*, 10, 209 (1989); Oxford Molecular Group Inc., MOPAC Guide Version 3.8, **1995**.
27. Fukui, K.; Yonezawa, T.; Nagata, C. *J. Chem. Phys.*, **1957**, 27, 1247.
28. Yonezawa, T.; Nagata, T.; Kato, H.; Imamura, A.; Morokuma, K., *Ryoshi Kagaku Nyumon*, 3<sup>rd</sup> Ed., Kagaku Doujin Publisher, Kyoto, Japan, **1990**.
29. Dean, J. A., *Lange's Handbook of Chemistry*, 13th Ed., McGraw-Hill, New York, **1985**, p. 3-121.
30. Csicsery, S.M. *J. Catal.*, **1971**, 23, 124.
31. Kaeding, W.W.; Chu, C.; Young, B.; Weinstein, B.; Butter, S. A. *J. Catal.*, **1981**, 67, 159.
32. Kim, J.-H.; Namba, S.; Yashima, T., *Sekkiyu Gakkaishi*, **1996**, 39, 79.

## Chapter 23

# The Investigation on the Crystallinity of USY Zeolite during Hydrothermal Dealumination

Yuling Chen

Research Institute of Petroleum Processing, SINOPEC, CHINA, P. O. Box 914-14,  
Beijing 100083, Peoples Republic of China

Hydrothermal dealumination is an important way for improving hydrothermal stability and catalytic activity of Y-zeolite. The changes in relative crystallinity of zeolite E prepared by hydrothermal-chemical dealumination and zeolite A prepared by conventional hydrothermal dealumination were characterized by IR, XRD, TEM, etc.. It was illustrated that the crystallinity of product E was greater than that of its precursor, HY. As compared with zeolite A, the zeolite E possessed higher crystallinity ( $\cong 100\%$ ) and more developed secondary pore system which would benefit bottoms conversion.

At the end of 50's, Weisz and Frillette first put forward the concept of "Shape Selective Catalysis" to describe the peculiar selectivity of synthetic crystalline zeolites (1). Almost from its beginning, molecular sieve zeolites catalysis has had a strong dependency upon the catalyst structure. Using different type of zeolites and processing all kinds of raw material, the expected products can be obtained. It is generally accepted that in catalytic cracking the large molecular weight hydrocarbons are first cracked either thermally or catalytically on the amorphous matrix component and the cracked products can diffuse into the Zeolite crystalline surface of the catalyst and undertake further reactions. Catalytic cracking with zeolites catalyst would be induced in the definition of shape selectivity if the zeolites pores were large enough to admit the large hydrocarbon molecules(2). The zeolite characteristic prepared by hydrothermal dealumination is to having more amount of secondary pores which provide passage channel and is favorable to catalytic cracking of large hydrocarbon molecules. Therefore, to this day, the hydrothermal dealumination method for USY is still used in industry (3). However, the crystalline structure of Y-zeolite would be

seriously destroyed during conventional hydrothermal treatment, generally resulting in loss of crystallinity of around 30% and some times up to 40%. The products obtained were usually only at 60%-70% crystallinity (4). That is to say, crystalline structure partially collapsed and selective cracking of large hydrocarbon molecules obviously lowered when secondary pores were formed. In previous years, many researchers, home and abroad, put on effects trying to improve USY's crystallinity during hydrothermal dealumination (5).

This paper proposes a hypothesis of the existence of a pseudo-HY crystalline phase in hydrothermal-chemical dealumination process. The stable precursor can produce a secondary pore system during hydrothermal treatment while keeping entirely crystalline structure stable, and higher crystallinity can be obtained. Shape-selective cracking of large hydrocarbon molecules may occur on the obtained USY zeolite. The structure characteristic of the USY's precursors HY and  $\text{NH}_4\text{Y}$  were also studied with IR, XRD, TEM and others.

## Experimental

### Sample Preparation

**USY-I Prepared by Conventional Hydrothermal Dealumination**  $\text{Na}^+$  lattice cations in parent NaY were exchanged by  $\text{NH}_4^+$  to obtain  $\text{NH}_4\text{NaY}$ .  $\text{NH}_4\text{NaY}$  was calcined under self-steaming at  $650^\circ\text{C}$  to form  $\text{HNaY}$ . The  $\text{Na}^+$  in  $\text{HNaY}$  was exchanged further by  $\text{NH}_4^+$ . The precursor  $\text{NH}_4\text{Y}$  ( $\text{A}_0$ ) of USY-I (A) was obtained.  $\text{NH}_4\text{Y}$  was calcined under the same hydrothermal conditions again to form product USY-I (A).

Reaction steps:  $\text{NaY} \rightarrow \text{NH}_4\text{NaY} \rightarrow \text{HNaY} \rightarrow \text{NH}_4\text{Y}(\text{A}_0) \rightarrow \text{USY-I}(\text{A})$

**USY-II Prepared by Hydrothermal-Chemical Dealumination**  $\text{Na}^+$  lattice cations in parent NaY were exchanged by  $\text{H}^+$  to obtain  $\text{HY}(\text{E}_0)$ . The  $\text{HY}(\text{E}_0)$  was the precursor of USY-II(E). The  $\text{HY}(\text{E}_0)$  was calcined under self-steaming and  $\text{NH}_3$  at  $650^\circ\text{C}$  to form product USY-II(E).

Reaction steps:  $\text{NaY} \rightarrow \text{HY}(\text{E}_0) \rightarrow \text{USY-II}(\text{E})$

**Physicochemical Measurement** Chemical composition was analyzed by standard wet chemical methods. The crystallinity was measured by Japan Rigaku D/MAX-III A X-ray diffractometer at a scan rate of  $0.5^\circ$   $2\theta/\text{min}$  with  $\text{CuK}\alpha$ , Ni Filter. OH groups were measured at  $3200\text{-}3800\text{cm}^{-1}$  frequency by IFS-113V IR Spectroscope. Pore volumes were measured by nitrogen adsorption and desorption methods using ASAP2400 automatic adsorption instrument. The crystal collapse temperature was measured by DTA using Du Pont 2100 thermal analytical instrument. The photograph for secondary pores was given by H-800 type transillumination electronic microscope.

**Catalyst Testing** The activities and selectivity of catalyst samples were evaluated by microactivity test using VGO as feed ( $330\text{-}520^\circ\text{C}$ ), with reaction temperature of  $480^\circ\text{C}$ , weight hourly space velocity of  $16\text{ hr}^{-1}$  and catalyst to oil weight ratio of 4. The samples were deactivated at  $800^\circ\text{C}$  for 4 hrs with 100% steam before evaluation.

## Results and Discussion

**Changes of Crystallinities of  $E_0$  and  $A_0$  during Hydrothermal treatment** X-ray diffraction patterns of A and E at different stages of treatment are shown in Figure 1 and 2, respectively. The diffraction Intensities  $A < A_0$ , but  $E > E_0$  can be seen from Figure 1 and 2. The crystallinities calculated on the basis of the Intensities are shown in Table I. According to Table I the change of crystallinities is  $A < A_0$  in conventional hydrothermal methods. This is due to the damage of crystallinities during conventional hydrothermal dealumination as stated above. But the change of crystallinities is  $E > E_0$  in the hydrothermal-chemical method. It is an unusual change in crystallinities that the crystallinity of E is even greater than that of  $E_0$ . A reasonable explanation is that some of structure characteristic of  $E_0$  results in its stability during hydrothermal treatment and the mechanism of reactions from  $E_0$  to E is distinct from that from  $A_0$  to A. Therefore, there are the following results:  $E > E_0$  in crystallinities as well as high crystallinity of E up to 100%.

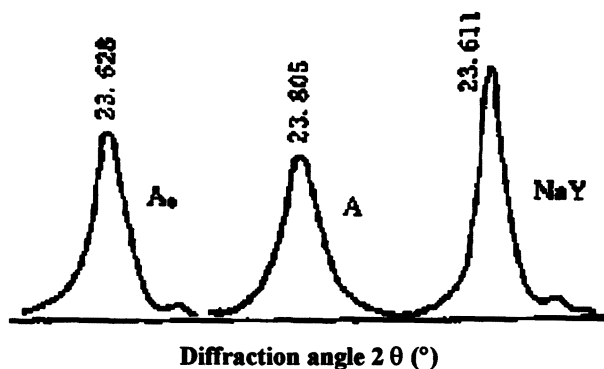


Figure 1. X-ray diffraction patterns of A at different stages

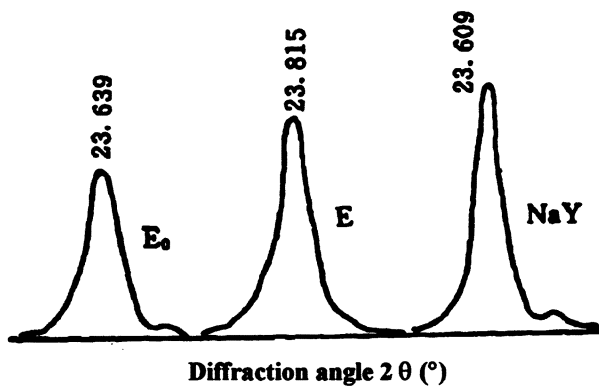


Figure 2. X-ray diffraction patterns of E at different stages

**Table I. The Crystallinity\* of the Precursors and the USY Products**

<i>Sample</i>	<i>Na<sub>2</sub>O wt.%</i>	<i>Crystallinity /%</i>	<i>Lattice Constant /nm</i>	<i>DTA <math>\rho</math>C</i>
NaY	13.5	100	2.468	880
NH <sub>4</sub> Y(A <sub>0</sub> )	1.1	85	2.460	—
USY- I (A)	1.1	70	2.449	1010
Pseudo- HY(E <sub>0</sub> )	4.8	80	2.460	—
USY-II (E)	4.8	100	2.448	1036

\*Relative to a pure synthetic NaY zeolite sample with an assigned crystallinity of 100%.

**Structure Characterization of E<sub>0</sub> and Pseudo-HY Zeolite** Few people have paid attention to the relation between the crystal structure of precursor and the crystallinity of final product USY by hydrothermal treatment. It is possible to form structural characteristic OH groups besides exchange of Na<sup>+</sup> lattice cations by H<sup>+</sup> cations and a small amount of dealumination while NaY zeolite reacts chemically with acid. The

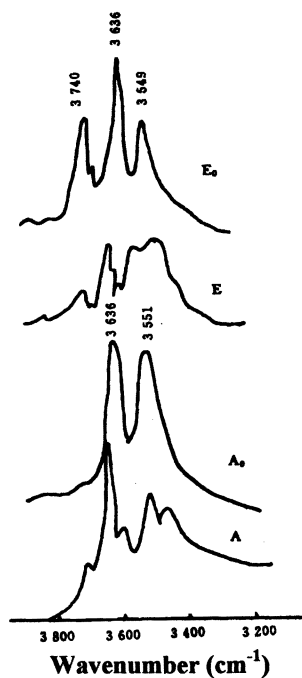


Figure 3. IR Spectra of Samples at Different Stages



characteristic structural OH groups might lead to the unusually stable crystalline structure of  $E_0$  during hydrothermal dealumination and the unusual change in crystallinities  $E > E_0$ , as shown in Figure 3. In infrared spectra precursor  $E_0$  still has  $3740\text{cm}^{-1}$  frequency of structural OH groups as contrasted with precursor  $A_0$ , similar in frequency to the strong band in various cations in Y-zeolite (6), besides absorption band characteristic of HY zeolite at  $3549$  and  $3636\text{cm}^{-1}$ . The only OH groups expected from structural considerations would be those terminating the giant lattice with a frequency near  $3740\text{cm}^{-1}$ (7). Hence the OH groups peculiar to stabilized zeolite might result from absorption band characteristic of precursor  $E_0$  at  $3740\text{cm}^{-1}$ . It is suggested to designate precursor  $E_0$  as "pseudo-HY zeolite" which might exhibit higher hydrothermal structural stability and transformation in crystal phase during hydrothermal- chemical dealumination. The relationship in crystal phase between precursor  $E_0$  and product E might be considered as a pseudo-crystal with a real crystal.

### The Performance of Pseudo-HY Zeolite

**Unit Cell Contraction Easy** Al in framework is usually replaced by Si for the ultrastabilization of Y-zeolite. After ultrastabilization the unit cell contraction occurs. Because the length of Si-O ( $0.161\text{ nm}$ ) bond is shorter than that of Al-O ( $0.174\text{ nm}$ ) bond the ultrastable structure is characterized by a significant contraction in unit cell dimensions of the order of 1% to 1.5% compared with the parent sodium Y-zeolite. Lattice constant of Y-zeolite with  $\text{SiO}_2/\text{Al}_2\text{O}_3$  ratio of 5 can generally reach  $2.450\text{ nm}$  or much less after ultrastabilization. The unit cell contraction is related to  $\text{Na}_2\text{O}$  content in Y-zeolite as shown graphically in Figure 4 (8). It illustrates the unit cell contraction of this same zeolite with varying levels of sodium content when stabilized

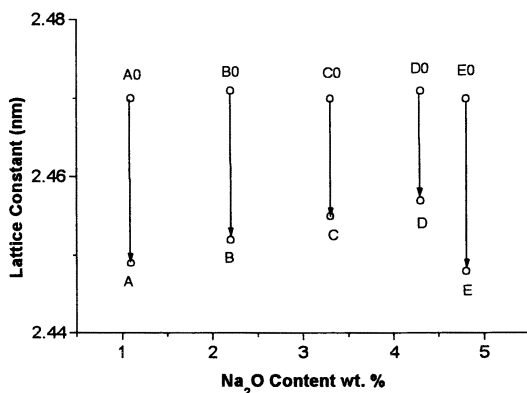


Figure 4. Unit Cell Contraction of  $\text{NH}_4^+$  or  $\text{H}^+$  exchanged Y-zeolite during stabilization as a function of sodium content

by self-steaming at  $650^\circ\text{C}$ . The degrees of unit cell contraction for precursors  $A_0$ ,  $B_0$ ,  $C_0$  and  $D_0$  decrease as the  $\text{Na}_2\text{O}$  contents increase. The unit cell contraction of

precursor  $A_0$  with 1%  $\text{Na}_2\text{O}$  content approaches 1% and the lattice constant  $a_0$  of product A reaches ultrastable range. The unit cell shrinkage with accompanying stabilization can be achieved when a certain amount of sodium is present especially during the conventional hydrothermal dealumination. However, the lattice constant of E from pseudo-HY zeolite  $E_0$  can reach ultrastable range 2.448 nm at 5 wt.%  $\text{Na}_2\text{O}$  content, in the meantime, the crystal structure still remains perfect, crystallinity high up to 100%, as shown in Table I and Figure 4. It is well known that it is difficult to exchange  $\text{Na}^+$  lattice cations on  $S_1$  position in faujasite by  $\text{NH}_4^+$  or  $\text{H}^+$ , therefore  $\text{Na}_2\text{O}$  content for precursor of USY can not reach 1 wt.% unless exchanges and calcinations can be carried out repeatedly (9).  $\text{Na}_2\text{O}$  contents in zeolite can only reach 4~5 wt.% through single step ion exchange. Obviously, an important reform of simplified process might take place for USY zeolite prepared by the hydrothermal-chemical method due to the characterization of pseudo-HY, which reduces loss, enhances yield and decreases cost for the product USY.

**Pretty Good hydrothermal Structure-Stability** Two suggested mechanisms of hydrothermal-chemical dealumination and conventional hydrothermal dealumination are proposed as shown in Figure 5, in which the dotted line frames represent the framework of zeolite. For the hydrothermal-chemical dealumination, two reactions may occur at the same time during the hydrothermal treatment of pseudo-HY zeolite: (1) dealumination and silicon insertion ultrastabilization, (2) transformation in crystal phase.

Sharply decreased damage in crystallinity of zeolite during hydrothermal - chemical dealumination and the unusual change in crystallinity  $E > E_0$  might be caused by the following: In reaction (1), it is possible that the coordination of dealumination rate and silicon migration rate makes the framework structure highly stable since OH groups characteristic of pseudo-HY appears. In reaction (2), pseudo-crystal of HY is transformed into crystal of USY by dehydration or dehydroxylation. In contrast with  $E_0$ , an absorption band of E at  $3740\text{cm}^{-1}$  sharply decreases as shown in Figure 3. Based on the above reactions, it is not difficult to understand the unusual change  $E > E_0$  in crystallinity and high crystallinity of E. Reaction (1) strengthens the framework structure of zeolite and the collapse of crystal structure is not significant during dealumination. As compared with precursor pseudo-HY zeolite  $E_0$ , the increase in XRD intensities of product USY-II zeolite E indicates the completion of phase transformation from a pseudo-crystal to a real crystal. Obviously, the formation of transitional crystal state, pseudo-HY, plays an important role in increasing the crystallinity of USY zeolite. The framework of precursor  $\text{NH}_4\text{Y}$  zeolite  $A_0$  is partially destroyed during hydrothermal treatment for silicon-migration rate might be less than dealumination rate. Thereby, there is the damage in the crystallinity of product USY-I zeolite A and the change of crystallinity  $A < A_0$  in conventional hydrothermal dealumination.

**Secondary Porosity and Crystallinity of E** In cracking reaction, secondary pore system of USY zeolite is important for cracking of large hydrocarbon molecules.

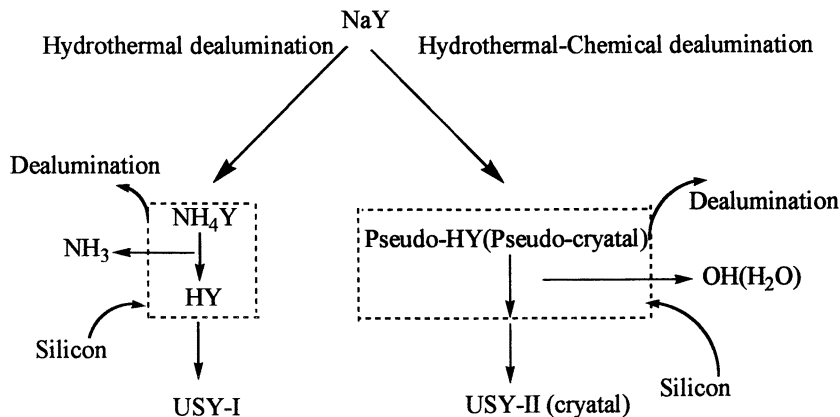


Figure 5. The reaction mechanism of conventional hydrothermal dealumination and hydrothermal-chemical dealumination

The formation of secondary pores depends on different dealumination method. Hydrothermal dealumination can make Y-zeolite produces more amount of secondary pores (10), and the diameters of cavities are about 5-10 nm by TEM (11). During conventional hydrothermal dealumination some aluminum atoms of the framework are leached out and some silicon atoms are also extracted from the framework. Thus crystal structure collapses partially and some  $\text{SiO}_2$  and/or  $\text{Al}_2\text{O}_3$  debris appear forming Secondary pores (12). The Secondary pores provide accessibility to reach active sites in micropores for reactant molecules. Although the secondary pore system is complex, in a very rough approximation, it can be considered that some defects of  $\beta$ -cage in the hydrothermal dealumination result in forming secondary pores by partial combination of the super-cage and the defected  $\beta$ -cage. The secondary pore system is not connected to the exterior of the crystals in a direct manner (13). Structure changes may be controlled in 2-3 super-cages. Dealumination destroyed the whole crystal structure only at a less extent (14). We suggest that some of active sites may be exposed to the formed secondary pores if the whole crystal structure retains almost undamaged during hydrothermal treatment. The formed secondary pores can take effect not only for providing a passage channel, but also for shape-selective cracking of large hydrocarbon molecules. Therefore, it is important to prepare the stable precursor "pseudo HY zeolite" which has much better structure-stability when it undergoes hydrothermal dealumination. The experimental results are good for keeping the whole crystal structure stable and for achieving the expectant goal. The amount of secondary pore for USY zeolite E with crystallinity up to 100% is not less than that for USY zeolite A with crystallinity 70% as shown in Table II. The data in Table II show that secondary pore volumes of samples E and A are  $0.098\text{cm}^3/\text{g}$  and  $0.086\text{cm}^3/\text{g}$ ,

Table II Pore Volume of USY

Sample	NaY	USY-I	USY-II
Total PV $\text{cm}^3 \text{g}^{-1}$	0.362	0.335	0.369
Micropore PV $\text{cm}^3 \text{g}^{-1}$	0.351	0.238	0.260
Mesopore PV $\text{cm}^3 \text{g}^{-1}$	0.011	0.097	0.109
Secondary PV <sup>a</sup> $\text{cm}^3 \text{g}^{-1}$	—	0.086	0.098
Secondary PV <sup>b</sup> ratio %	—	25.7	26.6

<sup>a</sup> Secondary PV = Sample Mesopore PV - NaY Mesopore PV

<sup>b</sup> Secondary PV Ratio % =  $\frac{\text{Secondary PV}}{\text{Total PV}} \times 100$

respectively. Distribution rates of secondary pore are 26.6% and 25.7%, respectively. Cavities with diameter of 4-10 nm has also been observed by TEM in USY zeolite E as shown in Figure 6, the little white dots in the photograph display the developed secondary pore.



Figure 6. TEM Photograph of Product E

**Shape-Selective Cracking of Heavy Oil** The USY zeolite E has higher crystallinity and more amount of secondary pores than USY zeolite A, therefore, it is more effective to crack large hydrocarbon molecules. Shape selective catalysis with zeolite has controlled selectivity by constraining the reactants which can be admitted to the catalytic sites, the products which can emit from zeolite pores and the product which can be formed within the zeolite cavities. Although progress continues to be made in

this research area, they are mainly subtle refinements of the original concepts(15). When n-C<sub>8</sub> was cracked by zeolite E and A, the cracking activities were not much different, 45.8% and 45.5%, respectively. So did with trimethylbenzene, 73.0% and 72.5%, respectively. But when heavy oil with b.p. range of 330-520<sup>0</sup>C was cracked by zeolite E and A, respectively, their cracking activities were much different as shown in Table III. From the Table III, the heavy oil conversion of USY zeolite E is 3.0% more than that of USY zeolite A. Especially gasoline yield of USY zeolite E is 5.5% more than that of USY zeolite A. The results can further show shape-selective cracking for large hydrocarbon molecules may occur in the secondary pores on the USY zeolite E with higher crystallinity. It is possible to predict that USY zeolite E will become an effective, economical and high activity component for shape-selective cracking of heavy oil.

**Table III Heavy Oil MAT**

Catalyst	Product distribution / wt. %					
	Gas	Coke	C <sub>5</sub> -204°C	204°C-330°C	204°C+Conv.	>330°C
USY-I(A)	13.3	2.8	57.9	17.8	74.0	8.2
USY-II(E)	14.1	2.8	63.4	14.5	80.3	5.2

### Conclusions

In the hydrothermal-chemical dealumination the USY zeolite E with crystallinity up to 100% possesses a developed secondary pore system and would become an effective, economical and high activity component for cracking of heavy oil.

### Acknowledgement

We would like to thank senior engineer Ying Rui Fu for the work of pure hydrocarbon reactions, and professor Zu Bi Chen, Cai Ying Li, Dr. wan Cheng Lu and Mr. wen bing Jiang for the help of the manuscript.

### Literature Cited

1. Weise P.B., FrlitteV.J., *J. Phys. Chem.*, **1960**, vol.64, PP382
2. J.S. Magee and M.M. Mitchell, Jr., *Studies in Surface Science and Catalysis*, Fluid catalytic Cracking: Science and Technology; Elsevier Science Publishers B.V.:Amsterdam,1993, vol.76; chapter13, pp499
3. Pine L.A., Maher P.J., Wachter W.A., *J. Catal.*,**1984**, vol.85, PP470
4. Kerr G.T., *J. Catal.*,**1969** vol.15(2), PP200

5. Eberly P.E. et al., US Patent 3506400(1970); 3591488(1971)
6. Scherzer J. et al., *J. Catal.*, **1973**, vol.28, PP101
7. John W. Ward, *Zeolite Chemistry and Catalysis*, ACS Monograph 171, American Chemistry Society: Washington, D.C., 1976; chapter3, PP.128,168
8. McDaniel C.V., et al., *Zeolite Chemistry and Catalysis*, ACS Monograph 171, American Chemistry Society: Washington, D.C., 1976; chapter4, PP.328
9. Chen Junwu, et al., *Catalytic Cracking Technology and Engineering*, ISBN 7-80043-537-7, China Petrochemical Press: Beijing, 1995, chapter3, PP154-179
10. Wang Shizhen, *Petroleum Processing*, **1991**, vol.22(1), PP330
11. Pellet R. J., Blackwell C. S., Rabo J. A., *Am. Chem. Soc. Preprint*, **1988**, vol.33(4), PP572
12. Lynch J, Dufresne P, Raatz F, *Zeolite*, **1987**, vol.7, PP333
13. P. E. Dai, D. E. Sherwood Jr., and B. R. Marttin, *Studies in Surface Science and Catalysis*, zeolites and microporous crystals; Elsevier Science B.V.: Amsterdam, 1994, vol.83, PP 489
14. Luan Zhaohua, et al., *Acta Petroleum Simica*, **1993**, vol.9(4), PP43-47
15. F.G.Dwyer, *Structure-Activity and Selectivity Relationships in heterogeneous Catalysis*, Elsevier Science Publishers B.V.:Amsterdam, 1991, vol. 67, PP179

## Chapter 24

# Evidence for a New Type of Shape Selectivity of Monodimensional Molecular Sieves: Tunnel-Shape Selectivity

M. Guisnet, S. Morin, and N. S. Gnep

Laboratoire de Catalyse en Chimie Organique, Unité Mixte de Recherche, 6503,  
Centre National de la Recherche Scientifique, Université de Poitiers,  
40 avenue du Recteur Pineau, 86022 Poitiers Cedex, France

While over an amorphous silica alumina, *m*-xylene isomerizes at similar rates into *o*- and *p*-xylenes as expected from the classical intramolecular mechanism, over HMCM-41 mesoporous aluminosilicates *o*-xylene is preferably formed. A bimolecular pathway involving *m*-xylene disproportionation followed by several rapid steps of transalkylation between trimethylbenzenes and *m*-xylene is shown to be responsible for this preferential isomerization into *o*-xylene. This particular behaviour of HMCM-41 aluminosilicates which cannot be attributed to the characteristics of their acidity (very similar to those of silica alumina) is proposed to be due to the presence of regular non-interconnected long channels : *m*-xylene molecules have to diffuse along the channels without any possibility of desorption before the exit, hence undergo successive reactions of disproportionation and transalkylation. This new mode of shape selectivity that we have called Tunnel Shape Selectivity would also be responsible for the particular behaviour of mordenites in alkane transformation and in coke formation.

Nearly 40 years ago, the term of "shape selective catalysis" was proposed to describe the selective cracking over a Ca A zeolite of *n*-alkanes to exclusively linear products (1). Afterwards, the discovery of medium-pore zeolites and particularly of the ZSM5 zeolite (MFI) has led to the development of various shape selective processes. The very low selectivity to carbonaceous deposits (coke) of acidic MFI zeolites, hence their high catalytic stability, has largely contributed to this development (2). This low selectivity to coke can be related to the difficulty of forming and trapping coke precursors at the narrow channel intersections of MFI zeolites (it is therefore a shape selectivity) (3).

The principles of shape selective catalysis have been comprehensively reviewed by various authors (4-9) :

- Reactant or product selectivity occur when only part of the corresponding reactant or product molecules are small enough to diffuse through the catalyst pores or at least when their rates of diffusion are very different.

- Restricted transition state selectivity occurs when certain reactions are prevented (or limited) because the space available near the active sites, in the cages, at the channel intersections etc. is too small to allow (easily) the formation of the corresponding transition states.

Whatever the size of their pore aperture all the molecular sieves (zeolites, SAPOs, mesoporous aluminosilicates etc.) can therefore present shape selective properties provided that the size of the reactant, intermediate or product molecules be close to those of the pore apertures, channels, cages or channel intersections.

This is well demonstrated for large pore monodimensional molecular sieves to which this paper is devoted. Thus acid mordenites are very selective for the synthesis by alkylation of 2,6-dialkylnaphthalene (10), of 4,4'-diisopropylbiphenyl (11) and of 2- phenyl long chain alkanes (12) i.e of the smallest isomers. However the high selectivity of mordenites does not seem to be due to the faster desorption of these isomers (product selectivity). Indeed the distributions of the products encapsulated in the pores and of the desorbed products were found to be quite similar (12, 13). This suggests that steric constraints affect the formation in the mordenite pores of the transition states leading to the bulkiest products. Transition state selectivity was also proposed to explain the limited formation of 1,3,5-trimethylbenzene by *m*-xylene disproportionation, of 1,3-dimethyl-5-ethylbenzene and 1-methyl-3,5-diethylbenzene by 1-methyl-2-ethylbenzene transalkylation over acid mordenite catalysts (5). However reactant selectivity is at the base of a dewaxing process using a mordenite catalyst : this catalyst allows a selective removal of straight chain and nearly straight chain paraffins from heavy petroleum fractions (5).

One important characteristic of monodimensional zeolites is that the diameter of their channels is close to the diameter of organic molecules which, therefore, cannot pass each other within the channels. This single file diffusion can be compared to the movement of pearls on a string (14). This mode of diffusion was proposed to be responsible for the particular behaviour of Pt mordenite catalysts in various reactions such as the isomerization of *n*-alkanes (15, 16), of methylcyclopentane (17) or the H/D exchange of cyclopentane (18).

The shape selective properties of monodimensional mesoporous molecular sieves such as MCM-41 are also well demonstrated. The combination of the mild acidity of HMCM-41 aluminosilicates and of large regular channels which allow the diffusion of bulky reactant and product molecules, makes them good candidates for the acid catalyzed synthesis of various Fine Chemicals (19, 20). Thus, within a series of acid catalysts, HMCM-41 gives the highest conversion and yield for the alkylation of 2,4-di-*t*-butylphenol with cinnamyl alcohol and is very efficient for the acylation of naphthol with 2,6-dimethylbenzoic acid (19). HMCM-41 materials exhibit also promising selectivity properties for catalytic cracking and especially for hydrocracking (20).



However, all the shape selective properties of monodimensional zeolite and mesoporous materials described in the literature are only related to the diameter of their channels (or the size of their pore apertures). We show here that not only this diameter but also the length of the channels of monodimensional molecular sieves can play a significant role in the selectivity of various reactions. This new type of shape selectivity that we have called "Tunnel Shape Selectivity" (21, 22) is related to the fact that the reactant molecules have to diffuse along the channels without any possibility of desorption before the exit of these channels, hence can undergo various successive reactions. Tunnel Shape Selectivity was firstly demonstrated in xylene isomerization over HMCM-41 samples (21). This reaction was shown to occur through a purely bimolecular mechanism via successive disproportionation and transalkylation steps whereas on an amorphous silica alumina having the same acidity a monomolecular mechanism was predominant. Other examples of Tunnel Shape Selectivity were observed for the transformation of n-alkanes and the formation of coke over mordenite catalysts.

### Transformation of Xylenes over MCM-41 Samples

In the large pore system of MCM-41 samples, the classical types of shape selectivity : reactant, product or transition state selectivity cannot be expected in the transformation of small reactant molecules such as xylenes into small product molecules : isomers and disproportionation products (trimethylbenzenes and toluene). This is why we were surprised to obtain a very particular selectivity in m-xylene isomerization over three HMCM-41 aluminosilicate samples with Si/Al ratios of 10, 30 and 100 (23). Indeed the initial para/ortho ratio was found to be equal to 0.4 with HMCM-41(10), 0.2 with HMCM-41(30) and 0.15 with HMCM-41(100) whereas with medium pore size zeolites, such as HMFI, values much higher than 1 are generally obtained and whereas with large pore zeolites, such as HFAU, HEMT, HMOR as well as with an amorphous silica alumina this para/ortho ratio was generally higher than 1 (Figure 1). An exception however, values slightly lower than 1 have been found with very dealuminated faujasite samples : 0.95 with HFAU(30) and 0.7 with HFAU(100) (24). These low values were explained by the participation in isomerization of a bimolecular mechanism besides the classical monomolecular mechanism (24).

We show here that, at least over HMCM-41(30) and (100), xylene isomerization occurs through a purely bimolecular mechanism. This particularity can be related to the presence of regular non-interconnected long channels in which xylene molecules undergo, before desorption, various successive reactions of disproportionation and transalkylation.

**Demonstration of the Bimolecular Mode of Xylene Isomerization.** The monomolecular isomerization mechanism involves, as limiting step, the transformation through methyl shift of benzenium ion intermediates resulting from xylene protonation.

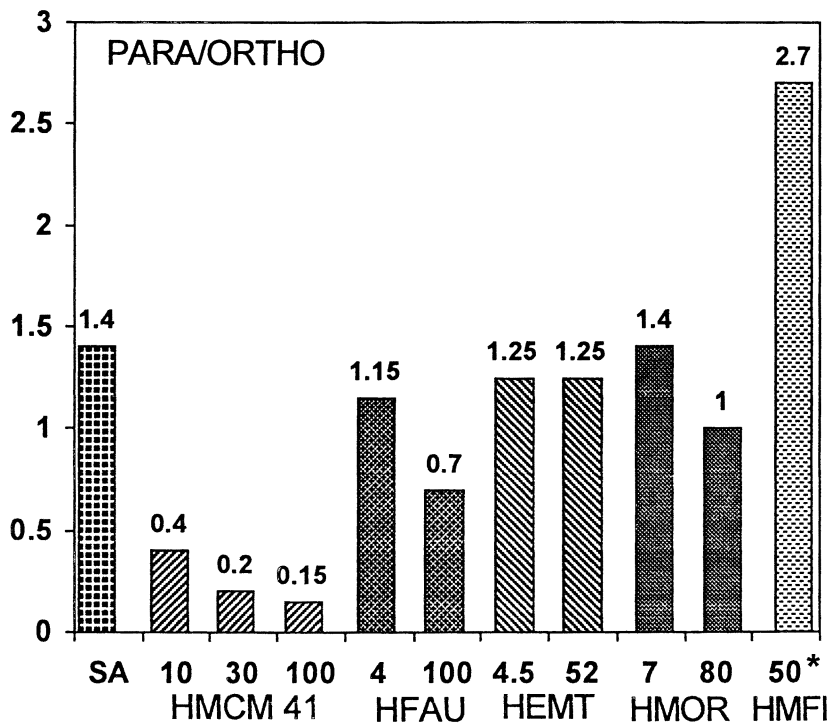
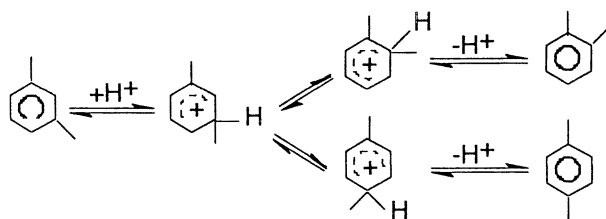
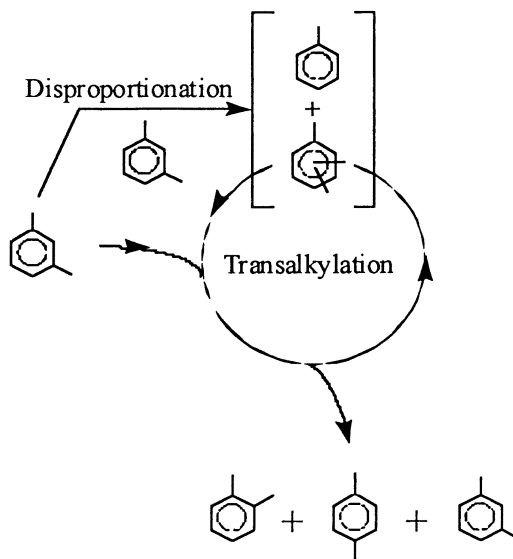


Figure 1. Isomerization of *m*-xylene over various acid molecular sieves and over an amorphous silica alumina (SA). Initial (extrapolated at zero conversion over the fresh catalysts) values of the *p/o* selectivity. \*Si/Al ratio.



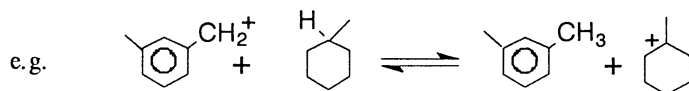
Therefore, in absence of diffusion limitations, no direct isomerization of *p*-xylene into *o*-xylene (or vice versa) can occur and as the steps leading from *m*-xylene to *o*- and *p*-xylenes are quite identical, these isomers should be formed at similar rates (25).

The bimolecular mechanism, firstly proposed to explain xylene isomerization in liquid phase at low temperature over a HFAU zeolite (26), involves consecutive disproportionation of xylenes and transalkylation between xylenes and trimethylbenzenes.



The selectivity of this bimolecular mechanism is completely different from that of the monomolecular one : direct isomerization of o-xylene into p-xylene (and vice versa) and preferential formation of o-xylene from m-xylene. The distribution of xylenes resulting from the bimolecular isomerization of m-xylene was estimated from a simple model (Figure 2) considering the distribution of trimethylbenzenes resulting from m-xylene disproportionation (Reactions 1) and estimating the rates of transalkylation (Reactions 2) from the measured rates of trimethylbenzene disproportionation. The following results were obtained : ortho : 41.5 % ; meta 47 % ; para : 11.5 % , hence a para/ortho ratio of 0.28.

The selectivity of xylene isomerization over the HMC41 samples is close to that expected from the bimolecular mechanism. There is a direct isomerization of ortho- into para-xylene (and vice versa) (23), and the para/ortho ratio obtained by m-xylene isomerization is between 0.15 and 0.4. Moreover this bimolecular isomerization process was confirmed by investigating the effect of methylcyclohexane addition to the reactant m-xylene. Indeed it has been shown on HFAU zeolites that branched alkanes inhibited xylene disproportionation without affecting their monomolecular isomerization (28). This inhibiting effect was attributed to the following hydride transfer reaction :



This reaction limits the concentration of benzylic carbocations which are involved as intermediates in disproportionation and transalkylation of methylaromatics hence the rate of these reactions (28). Figure 3 shows that the addition of methylcyclohexane to

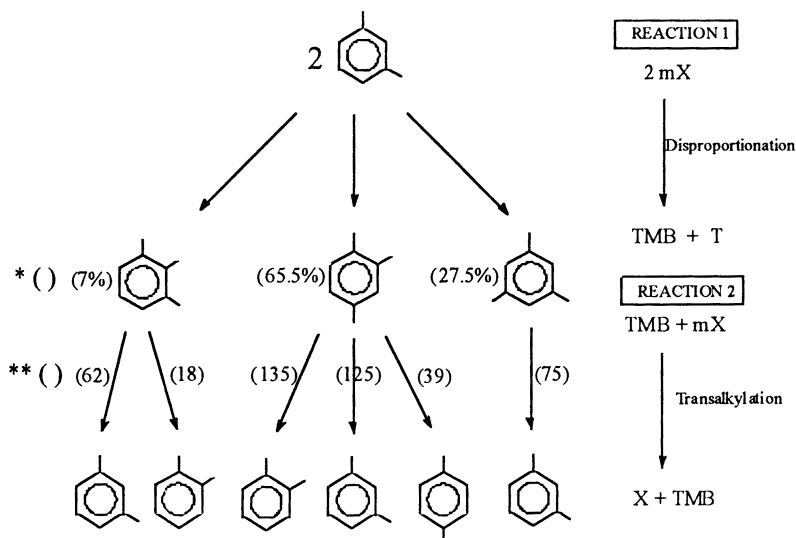


Figure 2. Bimolecular isomerization of m-xylene. Reaction scheme. \*Distribution of trimethylbenzenes resulting from reactions 1. \*\*Rates of reactions 2 over HFAU(4) ( $10^{-6} \text{ mol.s}^{-1}\text{g}^{-1}$ ) estimated from the rates and selectivities of trimethylbenzene disproportionation. Adapted from reference 27.

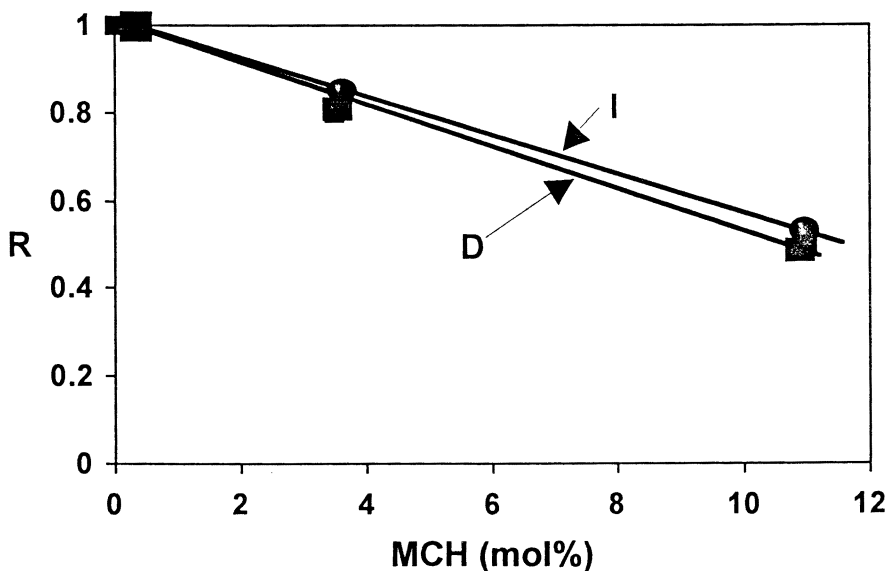


Figure 3. m-Xylene transformation over HMCM-41(30). Effect of the addition of methylcyclohexane (MCH) to m-xylene on the rates of isomerization I and of disproportionation D. R = ratio between the rates in presence and in absence of MCH.

m-xylene has a very significant inhibiting effect on m-xylene isomerization over the HMCM-41(30) sample. Moreover this effect is identical to the inhibiting effect observed for m-xylene disproportionation, which suggests that isomerization occurs totally through the disproportionation-transalkylation mechanism. This should not be the case for HMCM-41(10) for which the para/ortho ratio is higher than the one found with the bimolecular mechanism (0.28). From this value and from that obtained with HFAU for a purely monomolecular mechanism (1.18), the participation of the bimolecular mechanism in m-xylene isomerization over HMCM-41(10) was estimated to 85 %.

With this bimolecular pathway, different values of the disproportionation to isomerization rate ratio ( $D/I$ ) can be obtained. Indeed trimethylbenzenes resulting from disproportionation can undergo before desorption one or several successive reactions of transalkylation (shown to be faster than disproportionation (27)) with production of xylene isomers. Therefore, the differences between the  $D/I$  values of the HMCM-41 samples can be explained by differences in the number of transalkylation steps undergone by trimethylbenzene molecules. This number can be estimated from the disproportionation to bimolecular isomerization rate ratio and from the calculated selectivity of the bimolecular isomerization of m-xylene into itself (47 %). Figure 4 shows that the number of transalkylation steps passes from 3.4 with HMCM-41(10) to approximately 7 with HMCM-41(100) whereas it was only equal to 1 with a very dealuminated HFAU sample. The increase in the number of transalkylation steps with

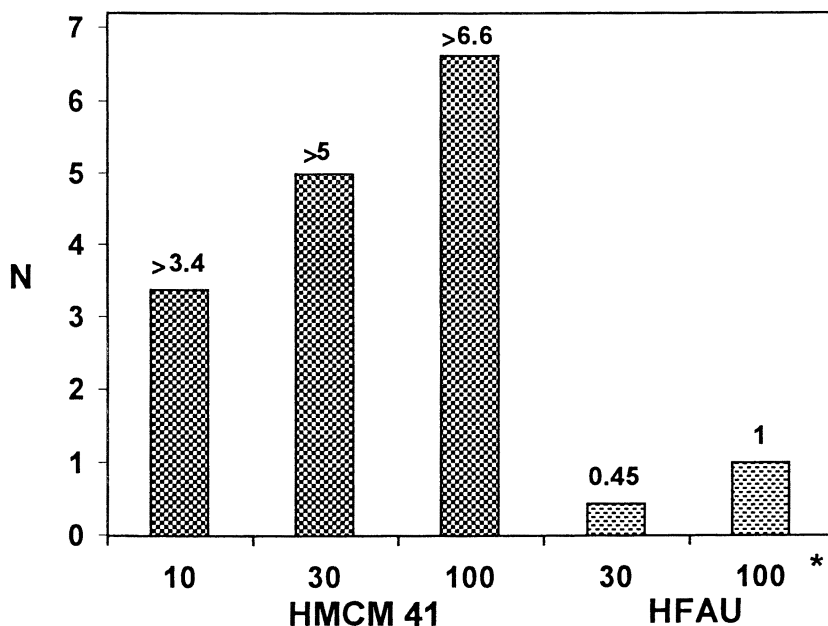
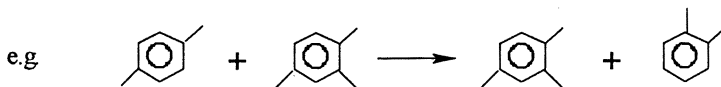


Figure 4. Number  $N$  of transalkylation steps in the bimolecular isomerization of m-xylene over HMCM-41 samples and over dealuminated HFAU zeolites. \*Si/Al ratio.

the Si/Al ratio of HMCM-41 samples could also be responsible for the decrease in the para/ortho ratio. Indeed not only m-xylene but also o- and p-xylenes can undergo transalkylation reactions and the transalkylation of trimethylbenzenes with p-xylene is faster than with o-xylene and moreover leads to a supplementary formation of this isomer :



**Origin of the particular behaviour of MCM-41.** The very high selectivity of HMCM-41 samples for bimolecular isomerization could be related to the characteristics of their acidity. Indeed these characteristics in particular weak protonic acidity, large concentration of strong Lewis sites (Table I) are very different from those of zeolites. However the acid properties of MCM41 samples are close to those of an amorphous silica alumina (Table I). (This is particularly clear for MCM41(10) (Figure 5)) which has a catalytic behaviour completely different : no direct ortho-para isomerization (23), para/ortho ratio obtained by m-xylene isomerization equal to 1.4 (Figure 1), strong inhibition of disproportionation by addition of methylcyclohexane to m-xylene reactant but no decrease in the isomerization rate (Figure 6). All these characteristics show that on silica alumina, isomerization occurs totally through the classical monomolecular mechanism.

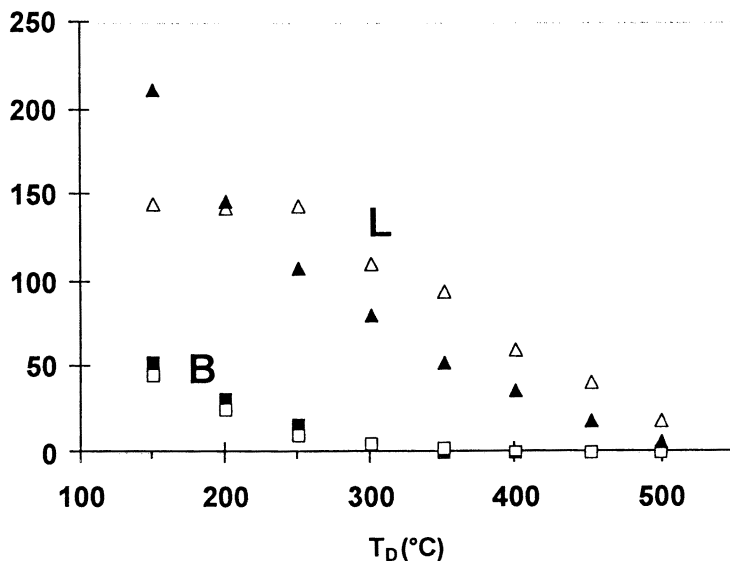


Figure 5. Concentrations ( $\mu\text{mol.g}^{-1}$ ) of Brønsted (B) and Lewis (L) sites of MCM41(10) (■, ▲) and silica alumina (□, △) samples on which pyridine remain adsorbed as a function of the temperature of desorption ( $T_D$ ) treatment.

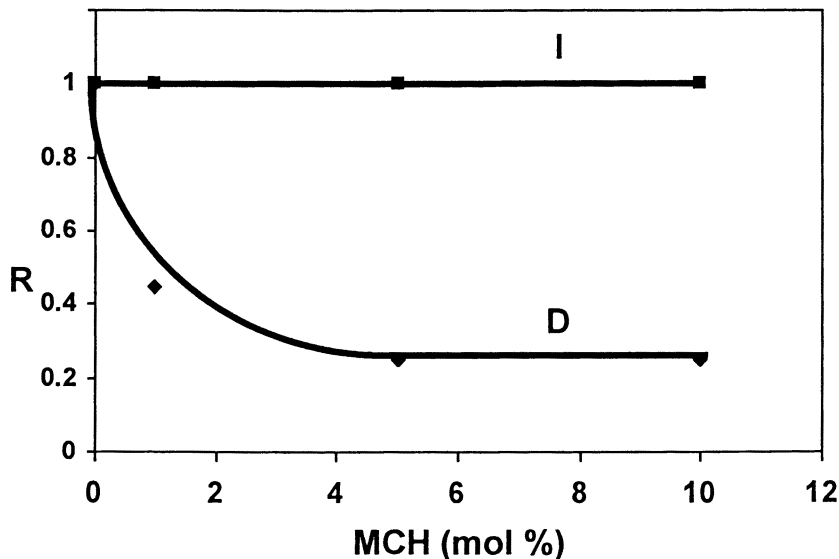


Figure 6. *m*-Xylene transformation over an amorphous silica alumina. Effect of the addition of methylcyclohexane (MCH) to *m*-xylene on the rates of isomerization I and of disproportionation D. R = ratio between the rates in presence and in absence of MCH.

It should however be emphasized that, whereas acid site densities of MCM41(10) and of silica-alumina calculated per gram of catalyst are very similar (Table I), the density per  $\text{m}^2$  is approximately 4 times lower for MCM41(10) than for silica alumina. However this difference in acid site density cannot explain the difference in catalytic behaviour. Indeed the bimolecular reactions (i.e. hydrogen transfer (29, 30)) are generally favoured by the acid site density although here the isomerization is only bimolecular on the catalyst with the lowest acid site density (MCM41(100) and only monomolecular on silica alumina which has the highest density per  $\text{m}^2$ .

Table I. Concentrations ( $\mu\text{mol.g}^{-1}$ ) of Brönsted ( $C_B$ ) and Lewis ( $C_L$ ) acid sites estimated by pyridine adsorption followed by FTIR (T of pyridine desorption =  $150^\circ\text{C}$ )

Sample	Silica-alumina	HMCM41(10)	HMCM41(30)	HMCM41(100)	HFAU(10)
$C_B$	45	53	21	19	465
$C_L$	145	210	85	70	160
$C_B/C_L$	0.31	0.25	0.25	0.27	2.9

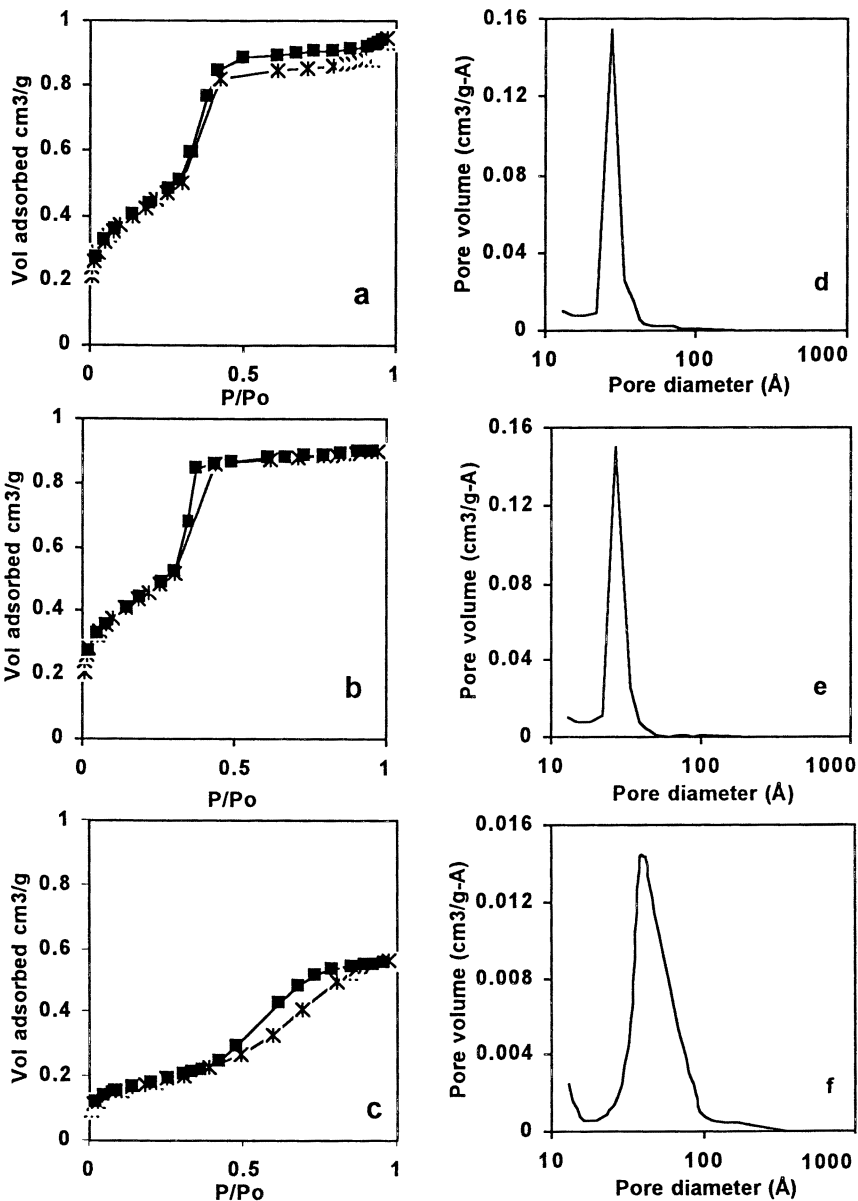


Figure 7. Isotherms of nitrogen adsorption at 77 K for HMC41(30), (a) HMC41(100) (b) and for silica alumina (c). Distribution of mesopores given by the BJH method (desorption step);  $dV/dD$  ( $\text{cm}^3/\text{g} \cdot \text{\AA}$ ) versus the pore diameter  $D$  ( $\text{\AA}$ ) for HMC41(30) (d), HMC41(100) (e) and silica alumina (f).



Therefore, the completely different behaviour of HMCM-41 samples and of silica alumina cannot be related to differences in acidity ; it is most likely due to differences in their pore systems. HMCM-41 samples present uniform non-interconnected mesopores with a diameter of approximately 30 Å whereas silica alumina has non-regular mesopores from 30 to 80 Å of diameter (Figure 7). When passing through the long channels of HMCM-41 samples, the molecules of m-xylene reactant would undergo various successive reactions of disproportionation and transalkylation with trimethylbenzene molecules with preferential formation of o-xylene molecules (Figure 8). This new mode of shape selectivity was called "Tunnel Shape Selectivity" (21, 22).

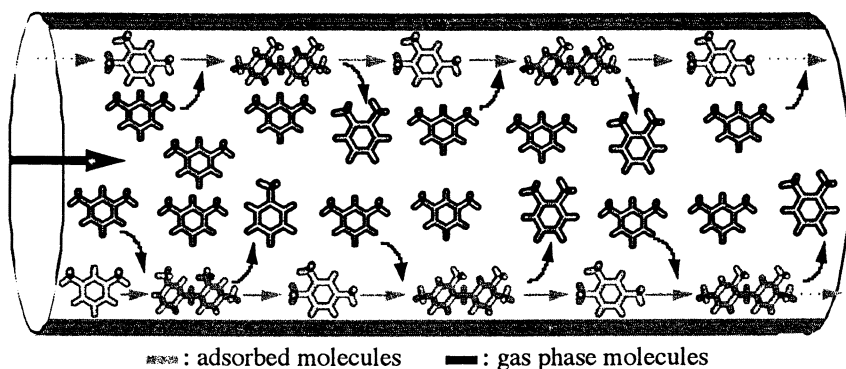


Figure 8. Bimolecular transformation of m-xylene in a section of the channel of a mesoporous MCM-41 aluminosilicate.

As previously shown (Figure 4) the number of transalkylation steps depends on the HMCM-41 samples, increasing with their Si/Al ratio. This can be related to the differences in their pore system shown by nitrogen adsorption (Figure 7) and by Transmission Electron Microscopy (TEM) (Figure 9). Whereas for all the samples, the sharp inflection at  $P/P_0 = 0.35$  characteristic of MCM-41 is observed, large differences are found between the adsorption desorption isotherms. With HMCM-41(100), sorption curves are typical of type IV isotherms without any hysteresis, corresponding to a very sharp distribution of mesopores of 28 Å diameter as furthermore confirmed by TEM. On the other hand hysteresis are observed with HMCM-41(30) and especially with HMCM-41(10) (23). In addition to the mesopores of 28 Å diameter observed with HMCM-41(100), these samples present non uniform larger mesopores as demonstrated by TEM (Figure 9). These larger mesopores created during the elimination of the surfactant by oxidative treatment decrease the length of the channels hence the number of successive reactions undergone by m-xylene molecules.

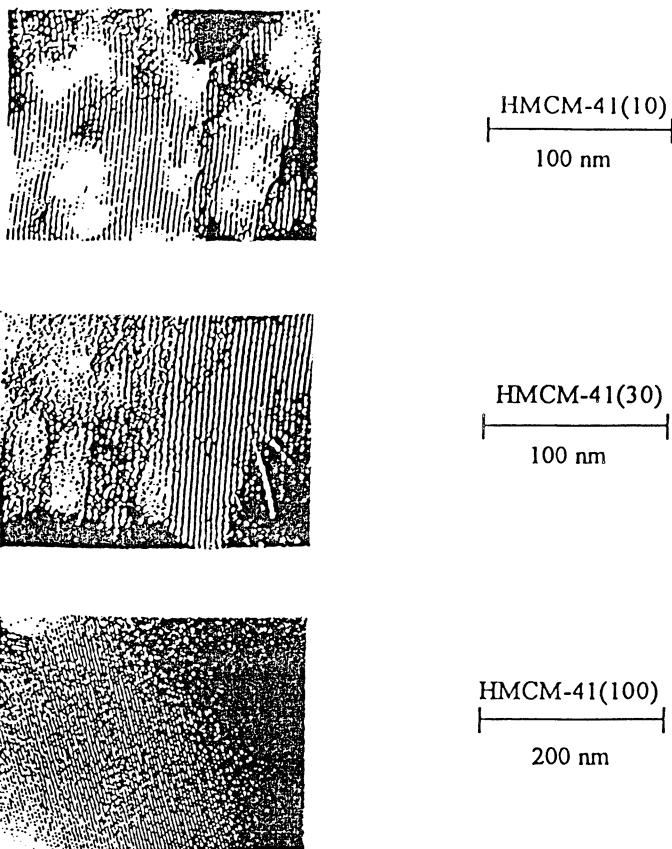


Figure 9. TEM micrographs of HMCM-41(10), (30) and (100) samples.

Curiously, this shape selective transformation of xylenes cannot be observed in the narrow pores of monodimensional zeolites such as mordenites. This is probably because steric constraints strongly limit the formation of the bulky intermediates of disproportionation and transalkylation reactions. Another explanation could be that these intermediates are very rapidly transformed into coke on the strong acid sites of these zeolites (31). However we shall show in the next sections that the tunnel shape selectivity plays most likely a significant role in the transformation of alkanes and in the formation of coke over mordenite catalysts.

### Transformation of n-Alkanes over Mordenite Catalysts

Large differences can be observed in the selectivity of a non dealuminated mordenite sample and of samples dealuminated by steaming then acid treatment. These latter samples present mesopores but have practically no extraframework aluminium species. Thus, in n-butane transformation at 250°C (22), the initial product

distribution is completely different with the non dealuminated (framework Si/Al ratio of 7) and the dealuminated samples (Figure 10). With the dealuminated sample the product distribution is the following : approximately 70 % (mol) of isobutane, 18 % of propane and 12 % of pentanes whereas with the non dealuminated samples (HMOR7) propane is extremely favored : 65 % (mol), only 25 % of isobutane and 10 % of pentane being formed. This completely behaviour of HMOR7 cannot be attributed to limitations in the desorption of branched alkanes. Indeed pyridine, which is bulkier than isoalkanes can accede to the protonic sites of the large channels of HMOR7 (32). The abrupt change in selectivity with the number of framework aluminium  $N_{Al}$  (hence of protonic sites  $N_{H^+}$ ) per unit cell (Figure 10) can no more be explained by an effect of the concentration of acid sites. Therefore, the particular selectivity of the non dealuminated sample is most likely due to the absence of mesopores in this zeolite, hence to the much longer diffusion pathway for organic molecules. While the reactant molecules diffuse through the channels, they can undergo many successive intermolecular reactions with consequently a preferential formation of propane (Tunnel Shape Selective Catalysis). Indeed butanes and pentanes which are very reactive compared to propane can be transformed into this product through the following scheme :

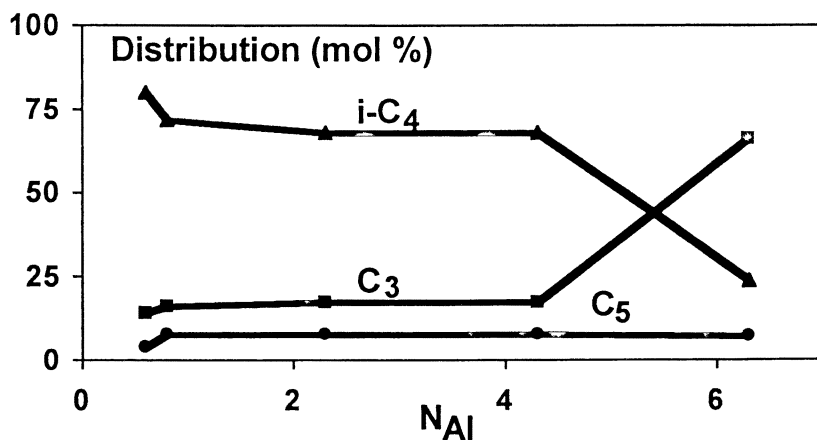
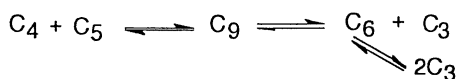


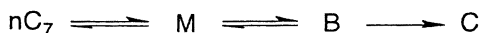
Figure 10. Distribution of the products of n-butane transformation at 250°C and under nitrogen over fresh HMOR samples vs.  $N_{Al}$ , the number of aluminium atoms per unit cell. Conversion values between 1 and 3 %. Adapted from reference 22.

Over bifunctional catalysts such as Pt supported on acidic zeolites, n-alkane hydroisomerization and hydrocracking occur through the following chemical and physical steps :

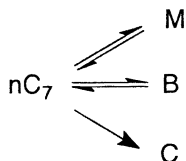
- a) Dehydrogenation of n-alkane molecules on the metal sites.
- b) Diffusion of alkene molecules to the acid sites from the metal sites where they are formed.
- c) Isomerization or cracking of alkenes over the acid sites.
- d) Diffusion of the alkene molecules produced from the acid to the metal sites.
- e) Hydrogenation of these alkenes over the metal sites.

From this reaction scheme, it can be expected that the activity, stability and selectivity of bifunctional zeolite catalysts are determined by two parameters : the balance between the hydrogenating and the acid functions (33, 34) and the pore structure of the zeolite (34, 35).

In the case of Pt HFAU catalysts it has been shown that the balance could be characterized by the ratio of the number of hydrogenating sites to the number of acid sites ( $nPt/nA$ ) (34). A successive reaction scheme of n-alkane transformation was shown to occur for high values of  $nPt/nA$  ( $\geq 0.03$ ). Thus, at 250°C, n-heptane ( $nC_7$ ) is successively transformed into monobranched isomers M, bibranched isomers B then into cracking products C (isobutane + propane) :



with consequently a high selectivity to isomerization compared to cracking (Figure 11). This can be explained by the fact that the number of acid sites encountered by the heptene intermediate molecules during their diffusion from a platinum site to another is such that only one transformation of heptene (branching isomerization or  $\beta$  scission) can occur before hydrogenation (34). For identical values of  $nPt/nA$ , the selectivity of PtHMOR catalysts is completely different from that of Pt HFAU catalysts (Figure 11). Even for  $nPt/nA = 0.05$ , the reaction scheme is apparently parallel : monobranched, bibranched isomers and cracking products appear as primary products.



As the cracking products are mainly composed of isobutane and propane they cannot result from the direct scission of linear  $C_7$  molecules. Therefore it can be suggested that the molecules of n-heptane which enter a mordenite channel can undergo several successive bifunctional transformations (into monobranched, bibranched isomers then cracking products) before desorbing from this channel. Again, the creation of

mesopores by dealumination changes completely the selectivity of Pt mordenite catalysts (Figure 11).

The possibility of a parallel scheme of *n*-alkane transformation presents a significant interest in the case of *n*-hexane isomerization, dimethylbutane isomers having the highest octane number. This is probably one of the reasons why monodimensional zeolites (MOR, MAZZ) are chosen as the acid component of commercial catalysts (36-38).

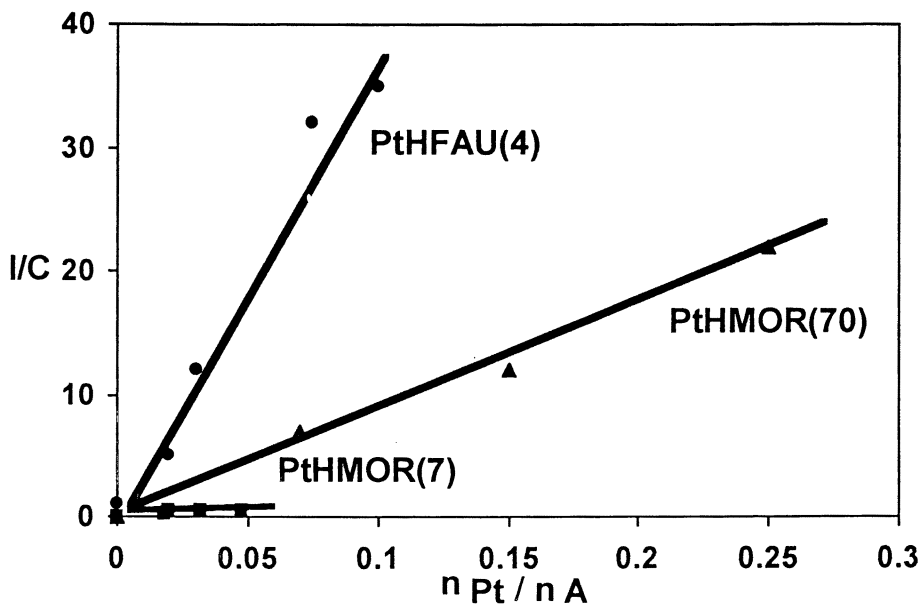


Figure 11. *n*-Heptane transformation at 250°C,  $p_{H_2} = 0.9$  bar,  $p_{nC_7} = 0.1$  bar over PtHMOR(7), PtHMOR(70) and PtHFAU(4). Ratio of the rates of isomerization and cracking (I/C) vs.  $n_{Pt}/n_A$ , the ratio between the number of accessible platinum sites to the number of acid sites.

### Coking and Deactivation of Mordenite Catalysts

A well-known particularity of zeolites with monodimensional pore systems is their fast deactivation by coke (39). This limits their use to commercial processes in which the reactant, product and intermediate molecules can only be transformed very slowly into coke. A typical example is the hydroisomerization of  $C_5$ - $C_6$  alkanes over bifunctional mordenite catalysts. In this reaction, alkenes, which are coke maker molecules, can only be formed very slowly by cracking because this reaction is more difficult than isomerization. Moreover, under the operating conditions, they would be immediately hydrogenated.

The very fast deactivation of monodimensional acid zeolites is mainly due to the pronounced deactivating effect of the coke molecules which are formed in their channels (40). Indeed one coke molecule deposited in a channel is able to block the access of the reactant molecules to all the active sites of this channel (deactivation by pore blockage).

This great sensitivity of monodimensional zeolites to deactivation by coke can be significantly decreased by creating mesopores which makes possible a quasi tridimensional diffusion of the reactant, intermediate and product molecules (41). Thus, in methanol conversion into hydrocarbons, the deactivating effect of coke was found to be 10 times less on a dealuminated mordenite having a large number of mesopores than on the non dealuminated sample. This positive effect of mesopores was also demonstrated in the synthesis of cumene (42), of long chain linear alkylbenzenes (12) etc.

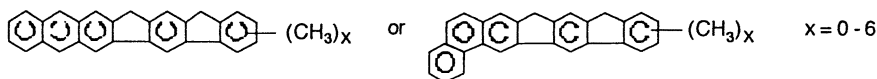
Another cause of this rapid deactivation is the fast formation of coke due to the fact that the molecules which enter a channel have to diffuse all along this channel before desorbing, hence can undergo several successive reactions leading to more and more condensed products. It is why, during n-heptane cracking at 450°C, the initial selectivity to coke of an acidic mordenite catalyst (HMOR) is very high : at one minute's reaction there is one molecule of n-heptane transformed into coke for only one molecule transformed into desorbed products. The selectivity of the fresh mordenite is probably much higher, for the deactivation of coking is faster than that of cracking (Table II). This means that a large part of the alkene molecules formed by cracking of n-heptane molecules in a HMOR channel undergo various reactions leading successively to more and more bulky molecules which finally remain blocked in the channels. This phenomenon is less pronounced with tridimensional zeolites as shown in table 2 for a HFAU zeolite having a cracking activity close to that of HMOR (43).

Table II. Initial Activities :  $a_0$  ( $10^{-3}$  mol n-Heptane Transformed into Cracking Products or into Coke  $h^{-1} g^{-1}$ ) and Deactivation Coefficients  $n$  estimated with the Voorhies equation :  $a = a_0 t^{-n}$ , the time-on-stream  $t$  being expressed in minutes

Zeolite :		HFAU	HMOR
Cracking	$a_0$	110	165
	$n$	0.6	1.4
Coke formation	$a_0$	30	160
	$n$	1.1	2.5
$a_0$ Coking/ $a_0$ Cracking		0.27	0.97

The compositions of coke are also completely different over HMOR and HFAU zeolites. Thus at low coke contents ( $\approx 2$  wt %), the coke of HFAU is mainly constituted of methylcyclopentapyrene molecules ( $C_nH_{2n-26}$  with  $n = 20-22$ ) whereas the coke of HMOR is constituted of very polyaromatic molecules insoluble in organic solvents. The atomic H/C ratio of these very polyaromatic molecules is close to 0.6, which suggests a quasi linear shape in agreement with a growth of coke molecules

along the mordenite channels (44). This growth of coke molecules along the mordenite channels is confirmed by the presence of molecules such as :



in the coke formed during o-xylene isomerization over mordenite at 350-450°C (45).

## Conclusion

In various hydrocarbon reactions catalyzed by acid monodimensional molecular sieves, a particular selectivity is observed which can be related to the length of their regular non-interconnected channels (Tunnel Shape Selectivity). Thus, m-xylene isomerization over mesoporous HMCM-41 aluminosilicates leads preferentially to o-xylene (para/ortho = 0.15-0.4) whereas with an amorphous silica alumina having similar acidity characteristics the para/ortho ratio is equal to 1.4. It is demonstrated that with silica alumina isomerization occurs through the classical intramolecular mechanism whereas with the monodimensional MCM-41 samples it occurs through a bimolecular mechanism involving successive disproportionation and transalkylation steps. This very particular behaviour of the HMCM-41 samples can be ascribed to their regular non-interconnected long channels in which xylene molecules undergo, before desorption, various successive reactions. This Tunnel Shape Selectivity cannot be observed in m-xylene transformation over monodimensional zeolites such as mordenites, probably because i) steric constraints limit the formation of the bulky intermediates of disproportionation and transalkylation steps in their narrow channels and ii) these intermediates are very rapidly transformed into coke on their strong acid sites. However, this new type of shape selectivity appears in reactions occurring with a slow coke formation such as n-butane transformation over HMOR catalysts or the hydroisomerization and hydrocracking of longer n-alkanes over bifunctional PtHMOR catalysts. Tunnel Shape Selectivity could also be responsible for the very fast formation of coke during n-heptane cracking over HMOR catalysts and for the particular shape of the corresponding coke molecules.

## Literature cited

- (1) Weisz, P.B.; and Frilette V.J., *J. Phys. Chem.* **1960**, *64*, p. 382.
- (2) Chen, N.Y.; Garwood, W.E. and Dwyer, F.G.; *Shape Selective Catalysis in Industrial Applications*; Chemical Industries; Marcel Dekker, Inc.: New-York and Basel, 1989, Vol. 36.
- (3) Rollman, L.D., *J. Catal.* **1977**, *47*, p. 113.
- (4) Weisz, P.B., *Chemtech* **1973**, *3*, p. 498.

- (5) Csicsery, S.M., in *Zeolite Chemistry and Catalysis*, Rabo, J.A., Ed.; ACS Monograph; American Chemical Society: Washington D.C., 1976, Vol. 171; pp. 680-713.
- (6) Csicsery, S.M., *Zeolites* **1984**, *4*, p. 202.
- (7) Derouane, E.G., in *Catalysis by Zeolites*; Imelik, B. et al., Eds.; Studies in Surface Science and Catalysis; Elsevier: Amsterdam, 1980, Vol. 5, pp. 5-18.
- (8) Haag, W.O. In *Proc. 6<sup>th</sup> Int. Zeolite Conference*, Olson, D. And Bisio, A., Eds.; Butterworth, Surrey, UK, 1984, pp. 466-478.
- (9) *Preprints Division of Petroleum Chemistry Symposium: Shape Selective Catalysis in Hydrocarbon Processing and Chemical Synthesis*; Song, C., Garces, J.M. and Sugi, Y., American Chemical Society, 1998, Vol. 43, pp. 218-306.
- (10) Schmitz, A.D.; Song, C., *Catal. Today* **1996**, *31*, p. 19.
- (11) Sugi, Y. and Toba, M., *Catal. Today*, **1994**, *19*, p. 187.
- (12) Magnoux, P.; Mourran, A.; Bernard, S. and Guisnet, M., in *Heterogeneous and Fine Chemicals IV*, Blaser H.U. et al., Eds.; Studies in Surface Science and Catalysis; Elsevier: Amsterdam, 1997, Vol. 108, pp. 107-114.
- (13) Sugi, Y.; Kubota, Y.; Nakajima, K.; Kunimori, K.; Hanaoka, T.; Matsuzaki, T.; Igarashi, A., *Preprints Division of Petroleum Chemistry Symposium: Shape Selective Catalysis in Hydrocarbon Processing and Chemical Synthesis*; Song, C., Garces, J.M. and Sugi, Y., American Chemical Society, 1998, Vol. 43, pp. 272-277.
- (14) Kärger, J.; Petzold, M.; Pfeiffer, H.; Ernst, S. and Weitkamp, J., *J. Catal.* **1992**, *136*, p. 283.
- (15) Carvill, B.T.; Lerner, B.A.; Adelman, B.J.; Tomczak, D.C. and Sachtler, W.M.H., *J. Catal.* **1993**, *144*, p. 1.
- (16) Liu, H.; Lei, G.D. and Sachtler, W.M.H., *Appl. Catal. A: General* **1996**, *137*, p. 167.
- (17) Lerner, B.A.; Carvill, B.T.; Sachtler, W.M.H., *Catal. Today* **1994**, *21*, p. 23.
- (18) Lei, G.D. and Sachtler, W.M.H., *J. Catal.* **1993**, *140*, p. 601.
- (19) van Bekkum, H. and Kloetstra, K.R., in *Mesoporous Molecular Sieves 1998*; Bonnevot, L. et al., Eds.; Studies in Surface Science and Catalysis; Elsevier: Amsterdam, 1988, Vol. 117; pp. 171-182.
- (20) Corma, A. and Kumar, D., in *Mesoporous Molecular Sieves 1998*; Bonnevot, L. et al., Eds.; Studies in Surface Science and Catalysis; Elsevier: Amsterdam, 1988, Vol. 117; pp. 201-222.
- (21) Morin, S., PhD Thesis, University of Poitiers, France, July 11<sup>th</sup> 1997.
- (22) Tran, M.T.; Gnep, N.S., Szabo, G. and Guisnet, M., *J. Catal.* **1998**, *174*, p. 185.
- (23) Morin, S.; Ayrault, P.; El Mouahid, S.; Gnep, N.S.; Guisnet, M., *Appl. Catal. A: General* **1997**, *159*, p. 317.
- (24) Morin, S.; Ayrault, P.; Gnep, N.S.; Guisnet, M., *Appl. Catal. A: General*, **1998**, *166*, pp. 281.



- (25) Guisnet, M.; Gnep, N.S., in *Zeolite Science and Technology*, Rodrigues, A.E. et al., Eds.; NATO ASI Series E, Martinus Nijhoff, The Hague, 1984, Vol. 80, pp. 571-582.
- (26) Lanewala, M.A. and Bolton, A.P., *J. Org. Chem.* **1969**, *34*, p. 3107.
- (27) Morin, S.; Gnep, N.S. and Guisnet, M., *J. Catal.* **1996**, *159*, p. 296.
- (28) Gnep, N.S. and Guisnet, M., *React. Kinet. Catal. Lett.* **1983**, *22*, p. 237.
- (29) Giannetto, G.; Sansare, S. and Guisnet, M. *J. Chem. Soc., Chem. Commun.* **1986**, p. 1302.
- (30) Corma, A; Fornes, V.; Martinez, A. and Orchilles, A.V. *ACS Symp. Ser.* **1998**, *368*, p. 542.
- (31) Morin, S.; Gnep, N.S.; Guisnet, M., *Appl. Catal. A: General* **1998**, *168*, p. 63.
- (32) Guisnet, M.; Ayrault, P. and Datka, J. *Polish J. Chem.*, **1997**, *71*, p. 1445.
- (33) Weitkamp, J., *Ind. Eng. Chem. Prod. Res. Dev.* **1982**, *21*, p. 550.
- (34) Guisnet, M.; Alvarez, F.; Giannetto, G. and Perot, G., *Catal. Today* **1987**, *1*, p. 415.
- (35) Martens, J.A.; Tielen, M. and Jacobs, P.A., in *Zeolite as Catalysts, Sorbents and Detergent Builders*, Karge, H.G.; Weitkamp, J., Eds.; Studies in Surface Science and Catalysis, Elsevier, Amsterdam, 1989, Vol. 46, pp. 49-60.
- (36) Belloum, M.; Travers, Ch. and Bournonville, J.P., *Rev. Inst. Fr. Petr.* **1991**, *46*, p.89.
- (37) Bolton, A.P., In *Zeolite Chemistry and Catalysis*, Rabo, J.A., Ed.; ACS Monograph; American Chemical Society: Washington D.C., 1976, Vol. 171, pp. 714-779.
- (38) Allain, J.F.; Magnoux, P.; Schulz, Ph.; Guisnet, M., *Appl. Catal. A: General* **1997**, *152*, p. 221.
- (39) Guisnet, M. and Magnoux, P., *Appl. Catal.* **1984**, *54*, p. 1.
- (40) Guisnet, M. and Magnoux, P., *Catal. Today* **1997**, *36*, p. 477.
- (41) Gnep, N.S.; Roger, Ph.; Cartraud, P.; Guisnet, M.; Juguin, B. and Hamon, C., *C.R. Acad. Sci., Serie II*, **1989**, *309*, p. 1743.
- (42) Meima, G.R.; van der Aalst, M.J.M.; Samson, M.S.V.; Garces, J.M. and Lee, J.G., in *Proc. 9<sup>th</sup> Int. Zeolite Conference*, van Ballmoss, R. et al., Eds.; Butterworth Heinemann, Boston, 1992, pp. 327-334.
- (43) Magnoux, P.; Cartraud, P.; Mignard, S. and Guisnet, M., *J. Catal.* **1987**, *106*, p. 242.
- (44) Magnoux, P., Ph.D Thesis, University of Poitiers, November 20, 1987.
- (45) Henrique, C.A.; Monteiro, L.; Magnoux, P.; Guisnet, M., *J. Catal.* **1997**, *172*, p. 436.

## Chapter 25

# Shape-Selective Solid Acid Catalysts Based on Tungstophosphoric Acid Supported on Mesoporous Silica

Yong Wang, Anthony Y. Kim, X. Shari Li, Li-Qiong Wang,  
Charles H. F. Peden, and Bruce C. Bunker

Pacific Northwest National Laboratory, MSIN: K8-93,  
P. O. Box 999, Richland, WA 99352

Solid acid catalysts comprising up to 70wt% tungstophosphoric acid (PW) dispersed on three mesoporous silicas with uniform pore size distributions of 18Å, 30Å, and 100Å, as well as on amorphous silica were synthesized. The effects of support pore size and catalyst preparation procedures on the chemical and physical properties of the synthesized catalysts were characterized using  $^{31}\text{P}$  magic angle spinning NMR, *in-situ* X-ray diffraction, and  $\text{N}_2$  physisorption. It was observed that right pore size of catalyst supports is important for PW dispersion via solution impregnation methods and PW is highly dispersed even at a 70wt% loading when the support pore size is  $\geq 30\text{Å}$ . Acid neutralization of silica supports and utilization of non-hydrolyzing organic polar solvents such as methanol are required to retain the Keggin structure of PW during sample preparation. The thermal stability of PW is enhanced when it is supported on silica supports. In addition, mesoporous silica with 30Å uniform pores exhibits improved PW stability to polar solvent leaching, probably as a result of steric hindrance of the silica support due to the compatible size between the pores of the silica support (30Å) and the cluster of PW (12Å). Mesoporous silica supported PW catalysts also show superior catalytic activities and provide shape selectivities in a probe reaction, the liquid phase alkylation of 4-*t*-butylphenol with styrene, because of the unique characteristics of mesoporous silica such as large surface area, ordered structure, and adjustable and uniform pore size distribution. The promising results with mesoporous silica supported PW catalysts indicate that they have potential applications in a variety of acid-catalyzed organic reactions involving large sized reacting, intermediate, and/or product molecules with desired shape selectivity to products and/or intermediates.

The chemical and petrochemical industries currently produce a wide range of organic compounds via alkylation, acylation, and isomerization by homogeneous acid catalysts such as  $\text{H}_2\text{SO}_4$ ,  $\text{H}_3\text{PO}_4$ ,  $\text{HF}$ ,  $\text{BF}_3$ , and  $\text{AlCl}_3$ . Although these homogeneous catalysts are efficient, they present many problems. The dissolved acids are difficult to separate from the product stream, making continuous operation, regeneration and reutilization of the catalysts difficult. Large amounts of catalyst are usually required, often leading to the generation of large quantities of acidic waste. In addition, the liquid acids are corrosive to the reactive system and are extremely hazardous to handle in a large-scale industrial setting. Therefore, solid superacid catalysts are currently under extensive investigation to replace homogeneous acid catalysts.

Among the solid superacid catalysts currently studied, a Keggin type tungstophosphoric acid (Figure 1B),  $\text{H}_3\text{PW}_{12}\text{O}_{40}$  (PW), is one promising candidate for the development of solid superacid catalysts. Catalysis by tungstophosphoric acid is a field of growing importance (1-6) since it has the strongest Brönsted acidity and highest thermal stability (about  $500^\circ\text{C}$ ) among heteropoly acids. The ideal Keggin-type tungstophosphoric acid anion,  $\text{PW}_{12}\text{O}_{40}^{3-}$ , has overall tetrahedral symmetry and is composed of a central  $\text{PO}_4$  tetrahedron surrounded by 12  $\text{WO}_6$  octahedra (7). These octahedra are arranged in four groups of three edge-shared octahedra,  $\text{W}_3\text{O}_{13}$ . These  $\text{W}_3$  triplets are linked by corner sharing to each other and to the central  $\text{PO}_4$ . In anhydrous  $\text{H}_3\text{PW}_{12}\text{O}_{40}$ , the three protons are located on the bridging oxygens (W-O-W) of the Keggin anion. Since there is almost no charge localization, the protons are very mobile resulting in strong Brönsted acidity. The advantages of tungstophosphoric acid as a catalyst include high activity at low temperatures, low volatility, low corrosivity, high activity and selectivity for a wide range of organic reactions, and lack of side reactions such as sulfonation, chlorination, nitration, etc., when compared to conventional mineral acids.

Bulk tungstophosphoric acid has low surface area (about  $1\text{-}5\text{ m}^2/\text{g}$ ) and is soluble in polar solvents. Supporting tungstophosphoric acid on high surface area solids would not only make product separation straightforward via heterogeneous catalysis, but also make the catalysts more active and effective in the reactions normally catalyzed by the surface of unsupported tungstophosphoric acid (8). Basic solids such as alumina and magnesia tend to decompose tungstophosphoric acid (5). Acidic or neutral substances are inert to tungstophosphoric acid and are suitable as supports with silica being used most often (9). Recently, tungstophosphoric acid supported on MCM-41-type mesoporous silica with  $30\text{Å}$  uniform pores has attracted interest as a promising solid acid catalyst for reactions involving large reactants and products (10-12). MCM-41 mesoporous silica, first reported by Mobil Oil in 1992 (13,14), is a novel material with high surface area ( $> 1000\text{ m}^2/\text{g}$ ), large pore volume, uniform pore size, and ordered structure. For example, one class of mesoporous materials contains a hexagonal honeycomb array of uniform mesopores whose diameter can be systematically varied from  $15$  to  $150\text{Å}$  (Figure 1A). The unique properties exhibited by mesoporous silica make them ideal for the development of solid superacid catalysts (Figure 1C). In particular, mesopores ( $>15\text{Å}$ ) of MCM-41

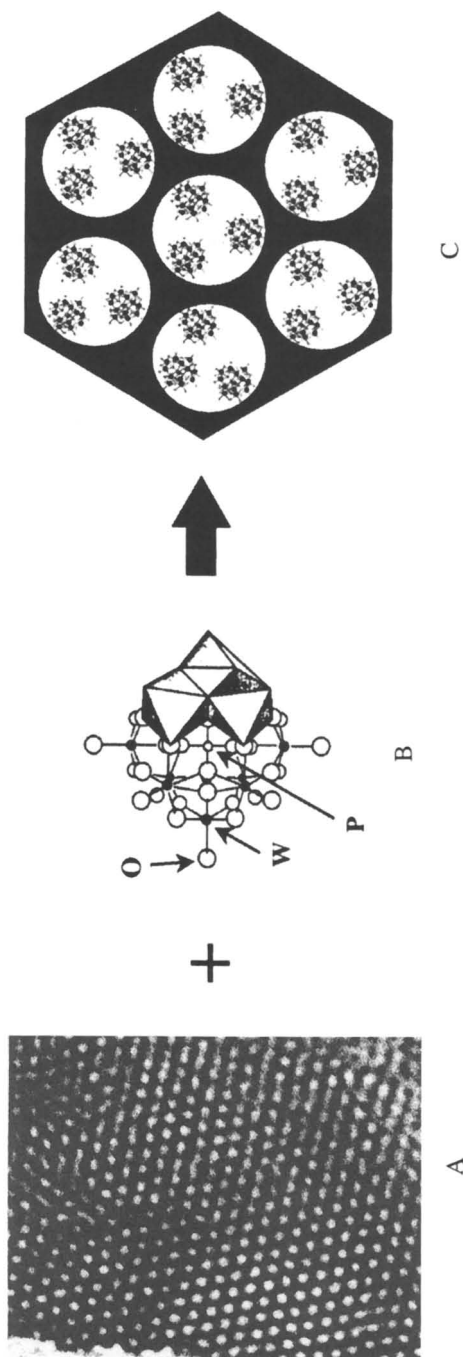


Figure 1. Dispersion of tungstophosphoric acids on mesoporous silica. A) TEM micrograph of hexagonal honeycomb structure of mesoporous silica with 30Å pore size; B) Keggin structure of the tungstophosphoric acid cluster; and C) a well dispersed solid acid catalyst.

silica are appropriate for the easy introduction of the relatively large cluster of tungstophosphoric acid (about 12Å), and their ordered structure and narrow pore size distribution provide strict selectivity of reacting and product molecules by their size and shape.

In this work, PW catalysts comprising up to 70wt% PW on three mesoporous silica (with 18Å, 30Å, and 100 Å pore size distribution) and on a premium amorphous Lyosil silica (15) were synthesized. The effects of support pore size and sample preparation procedures on the characteristics of the supported PW catalysts were studied. The synthesized catalysts were characterized using N<sub>2</sub> physisorption, <sup>31</sup>P magic angle spinning (MAS) NMR, and *in-situ* X-ray diffraction. Catalytic activities and shape selectivity of the supported PW catalysts were evaluated using the liquid phase alkylation of 4-*t*-butylphenol with styrene as a model reaction which involves large size reacting and product molecules.

## Experimental

**Sample Preparation.** Keggin structured tungstophosphoric acid (PW), H<sub>3</sub>PW<sub>12</sub>O<sub>40</sub>•xH<sub>2</sub>O, from Aldrich was used. Mesoporous silica with three different pore size distribution were synthesized, namely 18, 30, and 100 Å SiO<sub>2</sub>. 30 Å silica (MCM-41) was synthesized according to the literature procedure (13,14). Similar procedures were also used to synthesize the 18Å and 100Å SiO<sub>2</sub> except that cetyltrimethylammonium chloride was substituted with n-octyltrimethylammonium bromide for the synthesis of 18Å SiO<sub>2</sub> and trimethylbenzene was added as the micelle swelling agent for the synthesis of 100Å SiO<sub>2</sub>, respectively. A premium amorphous silica (Lyosil, surface area 581m<sup>2</sup>/g) (15) was also used as a catalyst support for comparison purposes. Some of the siliceous supports were first treated with 1M nitric acid solutions (10 ml 1M nitric acid per gram SiO<sub>2</sub>) at 90°C for 30 minutes, then dried at 100°C in vacuum overnight and calcined at 540°C for 1 hour. All of the supported PW catalysts, comprising up to 70 wt% PW, were prepared by impregnating a siliceous support with a PW aqueous solution or a PW methanol solution using the incipient wetness method (16). The catalysts were dried at room temperature in vacuum over P<sub>2</sub>O<sub>5</sub>.

**Experimental Techniques.** Pore size distributions and BET surface areas were determined from N<sub>2</sub> physisorption with a Quantachrome Autosorb 6-B Gas Sorption System, using the BJH (17) and multi-point BET (18) methods, respectively. Pore size distributions of the 18Å SiO<sub>2</sub> samples were determined from Ar physisorption.

The 120.78 MHZ <sup>31</sup>P NMR experiments were carried out with a Chemagnetics spectrometer (300 MHZ - 89 mm wide bore Oxford magnet) using a variable-temperature double-resonance probe. Single-pulse (SP) Bloch-decay with magical angle spinning (MAS) was used with <sup>1</sup>H decoupling. The samples were loaded into 7-mm Zirconia PENCIL™ rotors and spun at 3-5 kHz. Spectra were collected using a SP excitation Bloch-decay method with a 5-μs (90°) <sup>31</sup>P pulse, and a 30-s repetition delay. For all experiments, 164-ms acquisition time and a 25-kHz spectral window

were employed. The  $^{31}\text{P}$  chemical shifts were referenced to the 0 ppm signal from 85%  $\text{H}_3\text{PO}_4$ .

Thermal stabilities of the PW catalysts were studied under non-isothermal conditions at a heating rate of  $10^\circ\text{C}/\text{min}$  in air with an *in-situ* X-ray diffraction, which consists of a Siemens Model D500 diffractometer with  $\text{Co K}\alpha$  radiation equipped with a position sensitive detector and an Anton-Parr hot stage. X-ray diffraction measurements were also conducted using a Philips diffractometer with  $\text{Cu K}\alpha$  radiation.

Some supported PW catalysts were also evaluated in the extraction of PW with water at  $50^\circ\text{C}$ . 0.2 g supported catalyst was mixed with 5ml deionized water in a 20ml glass vial. The mixture was stirred at  $50^\circ\text{C}$  for a certain extraction period and then was filtered. PW dissolved into the deionized water was determined using a Milton Roy Spectronic 1001 spectrometry with the wavelength of 267.5 nm.

**Reaction Procedure.** Catalysts were evaluated with a probe reaction, the alkylation of 4-*t*-butylphenol (TBP, Aldrich, 99%) with styrene (Aldrich, 99+%), as reported in the literature (19). Alkylation was carried out in a 50ml three-neck flask with a condenser at a TBP/styrene molar ratio of 0.3 at  $105^\circ\text{C}$  under intensive stirring. The reactor was first charged with 6g TBP and 15g *n*-octane, and was heated to  $105^\circ\text{C}$ . Then 0.025g catalyst was added and the styrene supply was started. Styrene was added very slowly over a 20 to 50 minute period with a syringe pump in order to avoid its polymerization. Alkylate was treated by a  $\text{CHCl}_3/\text{H}_2\text{O} = 1:1.5$  mixture. The organic layer was analyzed and quantified using a Hewlett-Packard 5890 GC with a FID detector (J&W DB-5 30m x 0.53 mm capillary column). Products were identified using a Hewlett-Packard 5890 series II plus GC-MS with the same J&W DB-5 capillary column. Authentic GC calibration standards were synthesized and separated using a Harrison Chromatoron in our laboratory and qualified with the aforementioned GC-MS.

## Results and Discussion

**Characterization of PW Catalysts.** Mesoporous silicas with three uniform pore size distributions (18Å, 30Å, and 100Å) were chosen as the supports. For comparison purposes, a premium amorphous Lyosil silica was also used as a catalyst support. Table I shows BET surface area, pore volume, and pore diameter for the supports and supported catalysts with PW loading ranging from 20 to 70wt%. As expected, BET surface area and pore volume of the supported PW catalysts decrease as the PW loading increases. But even at higher PW loadings, supported catalysts still have rather large surface areas. It is noteworthy that the pore sizes of the 100Å and Lyosil silica supported PW catalysts decrease as the PW loading increases, while pore sizes of the 18Å and 30Å silica supported PW catalysts do not change with PW loading. It is also notable that all mesoporous silica supported PW catalysts retain the uniformity of their mesopores in the PW loading range investigated. Constant pore size of the MCM-41 supported PW catalysts independent of PW loading has also been reported by Kozhevnikov *et al* (10). We hypothesize that the rather large sized PW clusters

**Table I. Surface Area and Pore Characteristics of Supports and Catalysts**

<i>Sample</i>	<i>BET Surface Area m<sup>2</sup>/g</i>	<i>Pore Volume cc/g</i>	<i>Pore Diameter Å</i>
18Å SiO <sub>2</sub>	961	0.903	18
20wt%PW/18Å SiO <sub>2</sub>	721	0.647	18
50wt%PW/18Å SiO <sub>2</sub>	412	0.437	18
30Å SiO <sub>2</sub>	1045	0.966	30
20wt%PW/30Å SiO <sub>2</sub>	645	0.620	30
50wt%PW/30Å SiO <sub>2</sub>	455	0.403	30
70wt%PW/30Å SiO <sub>2</sub>	266	0.271	30
100Å SiO <sub>2</sub>	922	1.036	100
20wt%PW/100Å	579	0.549	40
50wt%PW/100Å	158	0.145	30
Lyosil SiO <sub>2</sub>	581	0.909	20-350
20wt%PW/Lyosil	415	0.634	20-140
50wt%PW/Lyosil	225	0.408	20-100
PW	2.49		

(12Å) can readily clog the pores during solution impregnation when support pore sizes are smaller than 30Å, while they have a better chance to coat the pores when the support pore size is sufficiently large such as the 100Å and Lyosil silicas. This explains why pore size of supported PW catalysts does not change when PW is supported on mesoporous silica with  $\leq 30\text{Å}$  pore sizes and the pore size distributions of supported PW catalysts shift to the smaller pore size range when PW is supported on Lyosil and 100Å silicas. The relationship between BET surface area and PW loading can also indirectly confirm the above hypothesis. As pore clogging takes place, the BET surface area reduction is proportional to the PW loading as with the 18Å silica supported PW catalysts (Figure 2A). In contrast, as the pores are coated with PW, the reduction of the square of BET surface area is proportional to the PW loading as with the 100Å silica supported PW catalysts (Figure 2B).

X-ray diffraction patterns of pure PW and 50wt% PW on four siliceous supports are compared in Figure 3. Except for the sample with 50wt%PW on 18Å silica, all supported PW catalysts are amorphous, indicating that PW is highly dispersed even at a 50wt% loading. This result can be explained by the large surface area of these supports (Table I). In fact, assuming that the cross sectional area of the PW cluster is slightly over  $113 \text{Å}^2$ , a monolayer PW on 30Å silica would require at least 80wt% PW loading. In contrast, PW crystalline phases already appear when PW is supported on silica with a lower BET surface area of  $300\text{m}^2/\text{g}$  at a 17wt% loading (9). The fact that the 50wt% PW/18Å SiO<sub>2</sub> sample shows some poor crystalline PW phases is probably due to the severe pore clogging during impregnation, resulting in formation of larger PW particles.

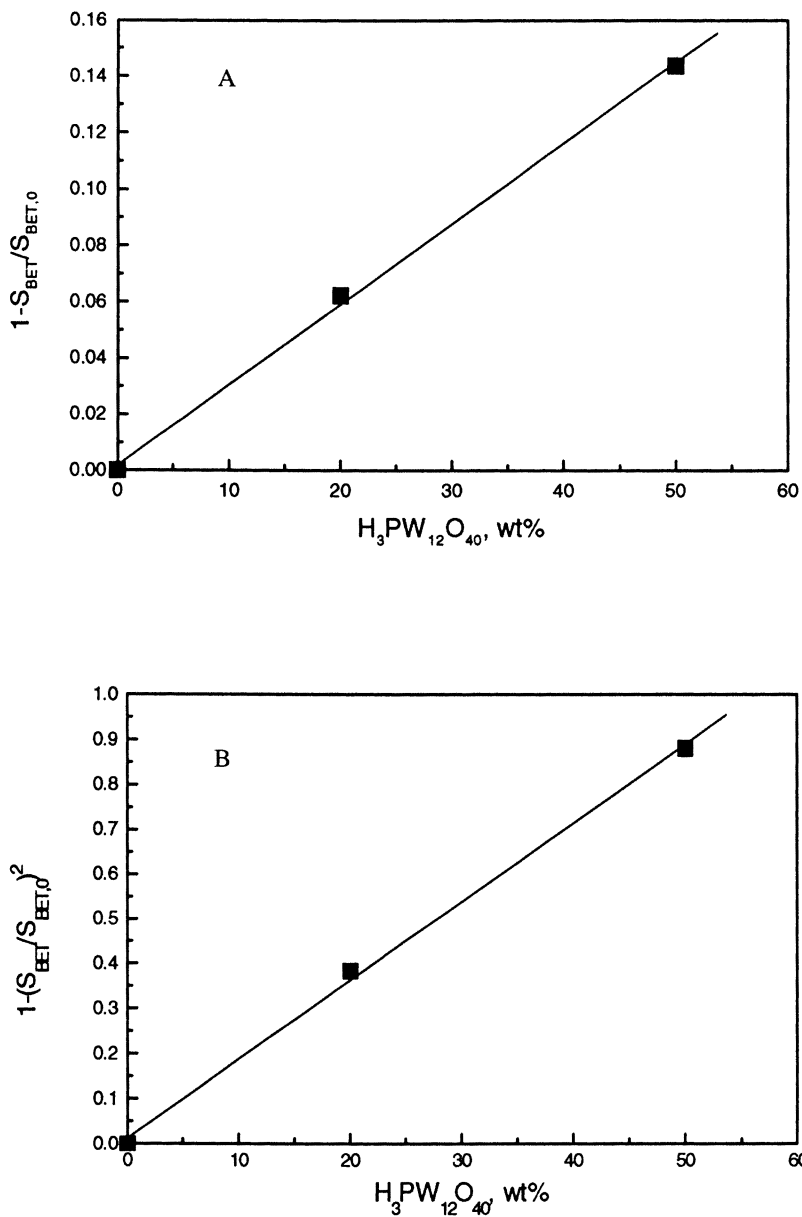


Figure 2. Surface area of supported PW catalysts as a function of PW loading. A) PW on 18Å SiO<sub>2</sub>; and B) PW on 100Å SiO<sub>2</sub>. (S<sub>BET</sub>: BET surface area of catalysts; and S<sub>BET,0</sub>: BET surface area of catalyst supports).



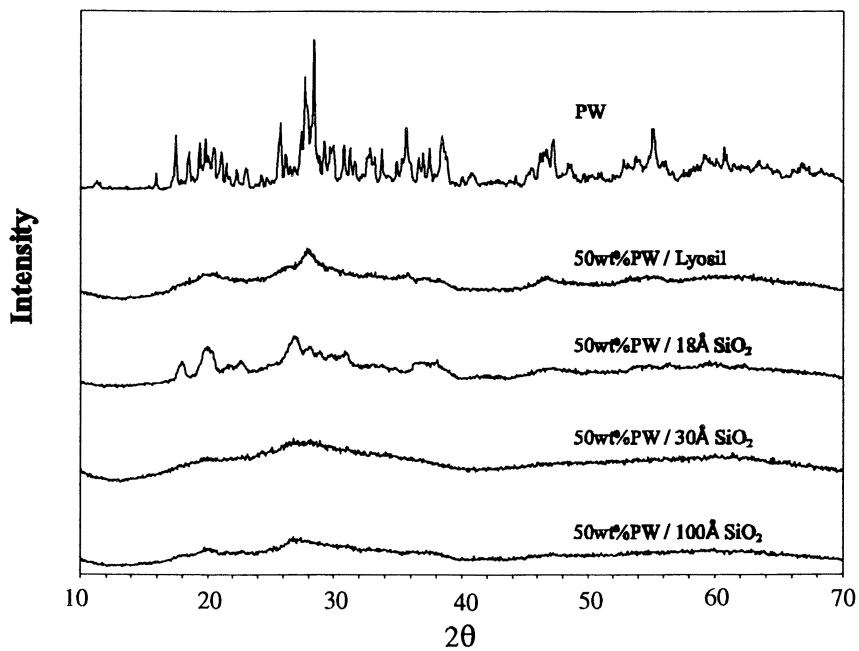
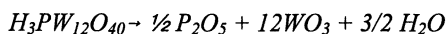


Figure 3. XRD patterns of bulk PW and 50wt% PW supported on amorphous and mesoporous silica.

Factors such as the surface properties of supports (5) and the pH of the sample preparation solution (20) play important roles in affecting the Keggin structure of PW.  $^{31}\text{P}$  NMR is the most convenient and revealing method for the assessment of the phosphorous environment in the phosphorous heteropoly compounds, and, in turn, the stability of the Keggin structure of PW. Figure 4 shows a series of  $^{31}\text{P}$  NMR spectra for PW supported on 30Å  $\text{SiO}_2$  catalysts. The spectra for the intact Keggin structure of PW should consist of one single line at about -15 ppm (7), depending on the amount of water of crystallization in the sample. The presence of the second resonance at ~ -13 ppm is assigned to the dimeric species  $\text{P}_2\text{W}_{21}\text{O}_{71}^{6-}$  according to (7,21), which are formed via decomposition of the Keggin structure of PW. As evidenced by small peak with the chemical shift at ~ -13 ppm in spectrum A, the hydroxyl groups on mesoporous silica tend to decompose the Keggin-type structure of PW even at a 50wt% acid loading. This is contrary to Kozhevnikov *et al*'s work (12), in which the Keggin structure of PW is retained when PW is directly supported on untreated MCM-41 if PW loading is > 30wt%. We attribute this discrepancy to the different surface properties of the MCM-41 silica potentially arising from differences in sample preparation. Decomposition of the PW Keggin structure was also found with the other three untreated siliceous supports even at a 50wt% loading. The intact Keggin structure was preserved when PW was supported on silica neutralized with 1N nitric acid such as the 50wt%PW/30Å  $\text{SiO}_2$  catalyst shown in spectrum B. However, at lower PW loadings such as 10wt%PW/30Å  $\text{SiO}_2$ , the Keggin structure of PW decomposes even with acid treated supports as confirmed by the chemical shift at ~ -13ppm (spectrum C). This may be caused by the dilute PW impregnation solution required to reach lower PW content in the supported PW catalysts, resulting in relatively higher pH of the PW impregnation solution. McGarvey and Moffat (20) have reported that water tends to hydrolyze PW, decomposing its Keggin structure, when the pH of aqueous PW solution is >1. In order to avoid using hydrolyzing solvents, methanol was also used as the solvent due to its high stability towards acids and the high solubility of PW therein. When methanol is used to impregnate acid-treated supports with PW, the intact Keggin structure was retained even at a 10wt%PW loading (spectrum D). It should be noted that all catalysts with decomposed Keggin structures, such as the ones shown in spectra A and C, are inactive in the probe reaction studied in this paper under the conditions investigated. Therefore, even with inert supports such as silica, neutralization of supports with acids and use of non-hydrolyzing polar solvents such as methanol are required to retain the Keggin structure when preparing supported PW catalysts with a solution impregnation method.

The thermal stability of PW and supported PW catalysts was studied using *in-situ* X-ray diffraction. Decomposition of PW is believed to be (1):



because supported PW catalysts are amorphous even at a 70wt% loading, the decomposition of PW was studied in this work by following the evolution of crystalline tungsten oxide. A single layer of sample with <5µm thickness was dispersed on the diffractometer sample heating strip in order to minimize the

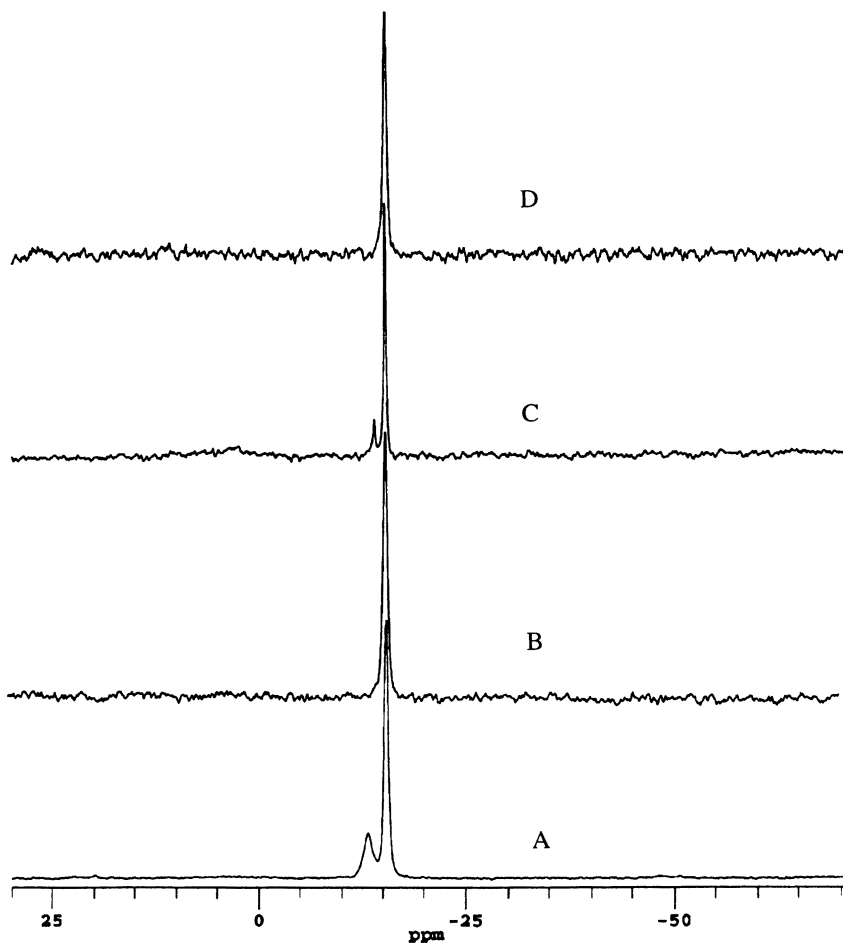


Figure 4.  $^{31}\text{P}$  MAS NMR Spectra: A) 50wt% PW/30Å  $\text{SiO}_2$  (water as solvent); B) 50wt% PW/acid treated 30Å  $\text{SiO}_2$  (water as solvent); C) 10wt% PW/acid treated 30Å  $\text{SiO}_2$  (water as solvent); D) 10wt% PW/acid treated 30Å  $\text{SiO}_2$  (methanol as solvent).

interparticle diffusion resistance for the reactions involving gaseous reactants or products (22). Figures 5A and 5B show typical *in-situ* X-ray diffraction results for bulk PW and 50wt%PW/30Å SiO<sub>2</sub> heated from 480 to 700°C at 10°C/min in air, respectively. Crystalline rhombohedral WO<sub>3</sub> appears at about 510°C in the bulk PW sample, which is consistent with the PW decomposition temperature range reported (1,5). With the 50wt%PW/30Å SiO<sub>2</sub> catalyst, diffraction lines (tentatively labeled as WO<sub>3</sub>) appear at about 585°C, indicating that the thermal stability of PW is enhanced by ~ 75°C when PW is supported on 30Å SiO<sub>2</sub>. The positions of these diffraction lines do not coincide with any crystalline species reported in the JCPDS files for compounds containing tungsten, oxygen, or tungsten, oxygen, and silica. However, these diffraction lines transform to those for the typical rhombohedral WO<sub>3</sub> structure when the sample was cooled to room temperature. We hypothesize that formation of the as yet un-identified metastable WO<sub>3</sub> species is promoted by SiO<sub>2</sub> at the high temperatures investigated here. In addition, similar enhancement of the PW thermal stability, although not as large an extent as with the 30Å SiO<sub>2</sub> supported PW catalyst, was also observed when PW is supported on 18Å, 100Å, and Lyosil silicas regardless of the PW loading.

The effect of thermal treatment on the stability of silica supported heteropoly acid catalysts have also been studied by other researchers (1,5,23,24) using TGA and/or DTA techniques. The main drawback with TGA and DTA is that sample quantity is usually an uncontrollable variable because it is directly related to experimental sensitivity and >1mg samples are typically employed, resulting in heat and mass transfer complications. This is probably why both enhanced (23) and unaffected (24) thermal stability of PW by silica supports have been observed with these techniques.

Silica has been identified as one of the most suitable supports for heteropoly acids (9). But due to the inertness of the silica surface to heteropoly acids, the acidic groups can be readily leached out of silica supports when water or organic polar solvents are present. In order to study whether the ordered structure and adjustable pore size of mesoporous silica can help prevent heteropoly acid leaching by water or organic polar solvents, supported PW catalysts were leach tested in water at 50°C over a 25 hour period. Water is chosen because it shows the highest degree of PW leaching of a number of polar solvents (25).

Figure 6 shows the relative amount of PW leached from 30Å, 100Å, and Lyosil silica supported PW catalysts with a PW content of 5wt%. In this case, mesoporous silica with a 30Å pore size apparently displays the lowest degree of PW leaching, presumably due to a steric hindrance to solvent leaching provided by compatible pore sizes between the support and the PW clusters. Although not as prominent as the ones with lower PW loadings, similar results were also observed for the supported PW catalysts with higher PW contents, which is consistent with the work of Izumi and Urabe (25). If leaching is being reduced in the mesoporous silica supported PW materials, then the 18Å support should display the best behavior if the PW is highly dispersed. However, an 18Å silica supported PW catalyst, not shown in the figure, does not display reduced PW leaching compared with the Lyosil supported PW catalyst. This result is likely due to the difficulty in dispersing 12Å PW clusters into

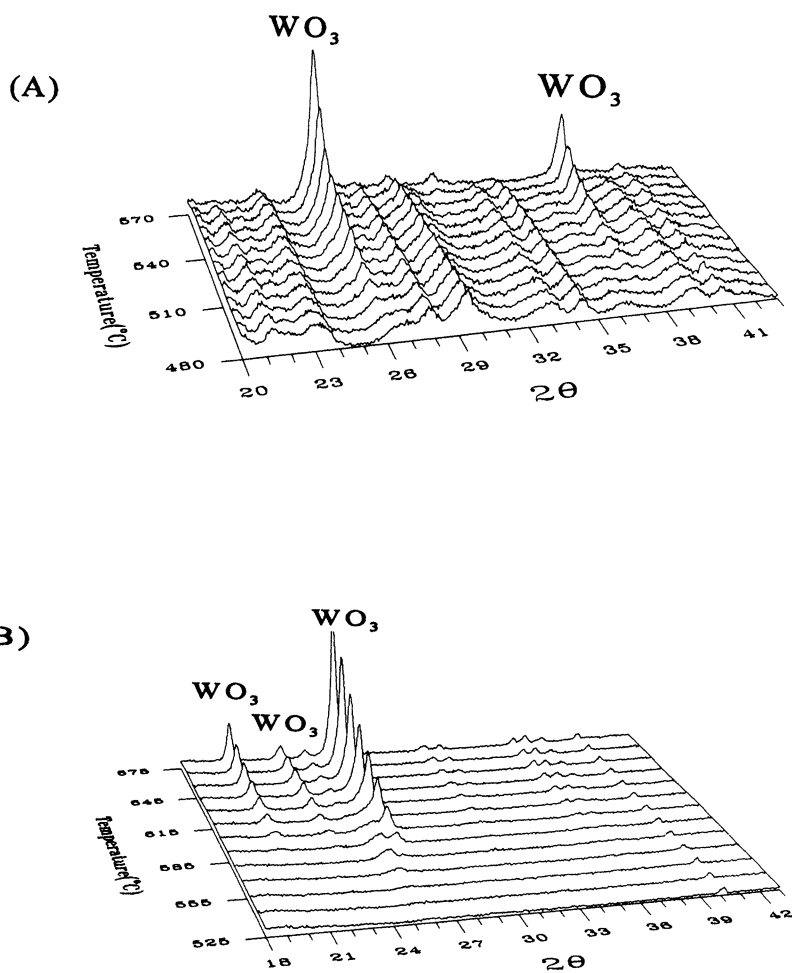


Figure 5. *In-situ* XRD patterns of: A) bulk PW; and B) 50wt% PW supported on mesoporous silica with 30Å pore size. (Heating rate = 10°C/min).

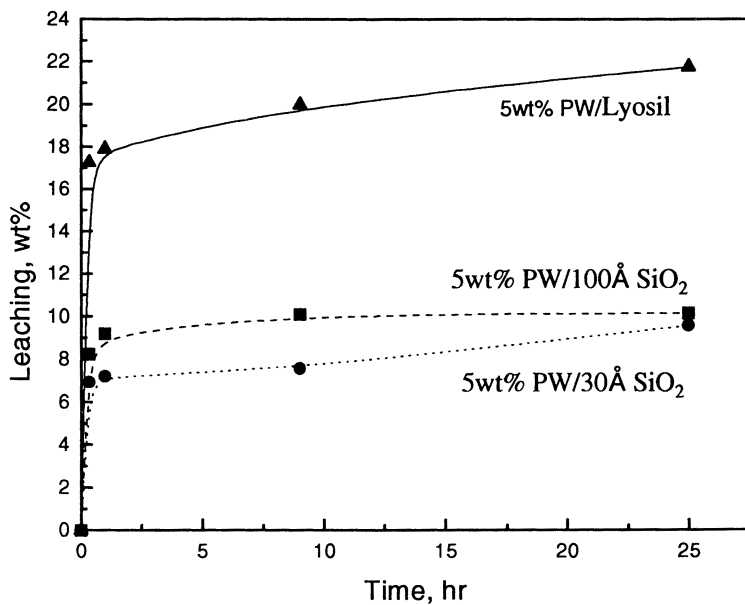


Figure 6. Leaching of PW supported on various silica by water at 50°C.

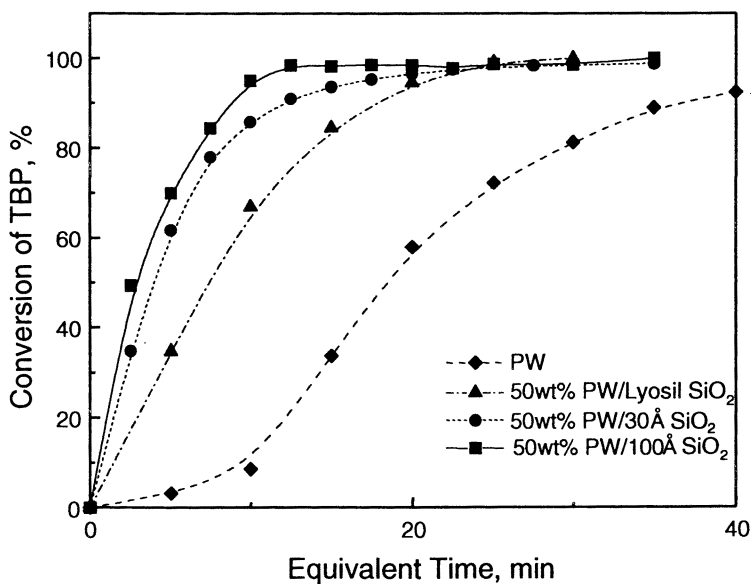


Figure 7. Alkylation of 4-*t*-butylphenol by styrene on various catalysts at 105°C (TBP/styrene molar ratio = 0.3, TBP: 6g, n-octane: 15g, and catalyst: 0.025g).



and compatible pore size (30Å). 18Å silica supported PW showed very low activity compared with other supported PW catalysts, presumably due to the poor dispersion of PW as aforementioned or the severe pore diffusion resistance to the bulky reactants.

## Conclusion

Several interesting features of mesoporous silica supported PW catalysts were noted in the present study. First, it was found that the pore size of mesoporous silica is very important for the efficient dispersion of PW anions. Because the size of PW clusters is quite large (typically about 12Å), it is almost impossible to disperse PW anions on mesoporous silica with a pore size smaller than 30Å. PW anions were found to clog the pores of these mesoporous silica supports instead. The dispersion of PW anions on supports was successfully achieved by using mesoporous silica supports with a pore size of 100Å. It was also found that it is essential to avoid using water as the solvent for PW in the impregnation process in order to eliminate the decomposition of Keggin structure due to hydrolysis. An organic solvent such as methanol can be used to circumvent this problem. In addition, the decomposition of the Keggin structure by a residual basicity of the mesoporous silica supports was observed. This can easily be avoided by pretreating the mesoporous silica support with an acidic solution.

A series of leaching tests indicate that PW anions are better retained (>90wt%) when supported on mesoporous silica with smaller pores. Silica supported PW catalysts also show improved thermal stability of PW with PW on 30Å SiO<sub>2</sub> being the most pronounced. Since mesoporous silica has a large surface area (about 1000 m<sup>2</sup>/g) compared to that of PW (about 5 m<sup>2</sup>/g), PW are still highly dispersed on mesoporous silica even at a 70wt% loading when the support pore size is ≥30Å. Therefore, it is not surprising to see superior catalytic activities of mesoporous silica supported PW in the tested alkylation of 4-*t*-butylphenol by styrene as well as added shape selectivity to mono alkylated product as opposed to multi alkylated products.

## Acknowledgments

This work was supported by the Laboratory Directed Research and Development Fund at Pacific Northwest National Laboratory, and was also partially funded by Office of Energy Research at U.S. Department of Energy. We thank professor William J. Thomson for the *in-situ* X-ray diffraction measurements at Washington State University. Pacific Northwest National Laboratory is operated for the U.S. Department of Energy by the Battelle Memorial Institute under Contract DE-AC06-76RLO 1830.

## References

1. Misono, M. *Catal.Rev.* **1987**, 29(2&3), 269.
2. Misono, M.; Nojirid, N. *Appl.Catal.* **1990**, 64(1),1.
3. Misono, M.; Okuhara, T. *ChemTech.* **1993**, 11, 23.
4. Basu, B.; Satappathy, S.; Bhatnagar, A.K. *Catal.Rev.* **1993**, 35(4), 483.
5. Kozhevnikov, I.V. *Catal.Rev.* **1995**, 37(2), 311.
6. Okuhara, T.; Mizuno, N.; Misono, M. *Advances in Catal.* **1996**, 41, 113.



7. Pope, M.T. *Heteropoly and Isopoly Oxometalates*; Springer: Berlin, 1983.
8. Wu, Y.; Ye, X.; Yang, X.; Wang, S.; Chu, W.; Hu, Y. *Ind.Eng.Chem.Res.* **1996**, *35*, 2546.
9. Izumi, Y.; Hasebe, R.; Urabe, K. *J.Catal.* **1983**, *84*, 402.
10. Kozhevnikov, I.V.; Sinnema, A.; Jansen, R.J.J.; Pamin, K.; Bekkum, H.van. *Catal.lett.* **1995**, *30*, 241.
11. Kresge, C.T.; Marler, D.S.; Rav, G.S.; Rose, R.H. US patent 5366945, 1994.
12. Kozhevnikov, I.V.; Kloetstra, K.R.; Sinnema, A.; Zandbergen, H.W.; Bekkum, H.van. *J.Mol.Catal. A: Chemical* **1996**, *114*, 287.
13. Beck, J.S.; Vartuli, J.C.; Roth, W.J.; Leonowicz, M.E.; Kresge, C.T.; Schmitt, K.D.; Chu, C.T.W.; Olson, D.H.; Sheppard, E.W.; McCullen, S.B.; Higgins, J.B.; Schlenker, J.C. *J.Am.Chem.Soc.* **1992**, *114*, 10834.
14. Kresge, C.T.; Leonowicz, M.E.; Roth, W.J.; Vartuli, J.C.; Beck, J.S. *Nature* **1992**, *359*, 710.
15. Lee, B.I.; Chou, K.T. *Mater. Lett.* **1992**, *14*, 112.
16. Satterfield, C.N. *Heterogeneous Catalysis in Industrial Practice*; McGraw-Hill: 1991.
17. Barrett, E.P.; Joyner, L.G.; Halenda, P.P. *J.Am.Chem.Soc.* **1951**, *73*, 373.
18. Brunauer, S.; Emmett, P.; Teller, E. *J.Am.Chem.Soc.* **1938**, *60*, 309.
19. Kozhevnikov, I.V.; Tsyganok, A.I.; Timofeeva, M.N.; Kulikov, S.M.; Sidelnikov, V.N. *React.Kinet.Catal.Lett.* **1992**, *46* (1), 17.
20. McGarney, G.B.; Moffat, J.B. *J.Molecular Catal.*, **1991**, *69*, 137.
21. Massart, R.; Contant, R.; Fruchart, J.; Ciabrini, J.; Fournier, M. *Inorg.Chem.* **1977**, *16*, 2916.
22. Wang, Y.; Thomson, W.J. *Thermochimica Acta* **1995**, *255*, 383.
23. Kasztelan, S.; Payen, E.; Moffat, J.B. *J.Catal.*, **1990**, *125*, 45.
24. Rocchiccioli-Deltcheff, C.; Amirouche, M.; Herve, G.; Fournier, M.; Che, M.; Tatibouet, J.M. *J.Catal.*, **1990**, *126*, 591.
25. Izumi, Y.; Urabe, K. *Chem.Lett.* **1981**, 663.

## Chapter 26

# Shape-Selective Catalytic Behavior of Pt-Porous Heteropoly Compounds in Skeletal Isomerization of *n*-Butane

Toshio Okuhara, Ryu-ichi Watanabe, and Yusuke Yoshinaga

Graduate School of Environmental Earth Science, Hokkaido University,  
Sapporo 060-0810, Japan

Effects of pore width of Pt-promoted porous materials including heteropoly compounds on selectivity in skeletal isomerization of *n*-butane have been studied. With 0.5wt%Pt-Cs<sub>2.5</sub>H<sub>0.5</sub>PW<sub>12</sub>O<sub>40</sub> which possesses mesopores with the width of about 5 nm, about 94%-selectivity was obtained in the presence of H<sub>2</sub> at 573 K. On the other hand, an ultramicroporous heteropoly compound, 0.5wt%Pt-Cs<sub>2.1</sub>H<sub>0.9</sub>PW<sub>12</sub>O<sub>40</sub>, of which the pore-width is 0.43 - 0.50 nm, gave mainly propane as well as isobutane. Pore-width of Pt-zeolites also affected greatly the selectivity; Pt-H-ZSM-5 and H-ZSM-5 produced mainly small molecules such as ethane and propane, while Pt-HY gave isobutane with 80%-selectivity. These results demonstrated that the pore width of the microporous materials is a crucial factor influencing the selectivity of skeletal isomerization of *n*-butane due to the shape selectivity by the constrained pores.

Shape selective catalysis as typically demonstrated by zeolites is of great interest from scientific as well as industrial viewpoints (1,2). Recently synthesized layered materials (3), microporous oxides and mixed oxides (4), and mesoporous silica (3) are also candidates for shape selective catalysts. Since heteropolyacids like H<sub>3</sub>PW<sub>12</sub>O<sub>40</sub> and its acidic salts are very strong acids and show high activities for various kinds of acid-catalyzed reactions (5), these materials have attracted much attention. Interestingly, porous heteropoly compounds were synthesized through partial substitution of Cs<sup>+</sup> for H<sup>+</sup> of H<sub>3</sub>PW<sub>12</sub>O<sub>40</sub> (5-10). We further synthesized a Pt-promoted Cs<sub>2.1</sub>H<sub>0.9</sub>PW<sub>12</sub>O<sub>40</sub>, which has only ultramicropores, having the width of about 0.5 nm (11). This bifunctional catalyst exhibits shape selectivity toward hydrogenation of alkenes and oxidation of hydrocarbons (11).

Skeletal isomerization of *n*-butane to isobutane is an important industrial

reaction, since isobutane is a feedstock for alkylation with butenes to C8 alkylates and synthesis of methyl *tert*-butyl ether. Cs<sub>2.5</sub>H<sub>0.5</sub>PW<sub>12</sub>O<sub>40</sub> was found to be active and selective than SO<sub>4</sub><sup>2-</sup>/ZrO<sub>2</sub> at 573 K (12). Furthermore, addition of Pt to Cs<sub>2.5</sub>H<sub>0.5</sub>PW<sub>12</sub>O<sub>40</sub> enhanced greatly the activity and selectivity for isomerization of *n*-butane in the presence of H<sub>2</sub> (13,14). It was reported that the skeletal isomerization of *n*-butane over Pt-Cs<sub>2.5</sub>H<sub>0.5</sub>PW<sub>12</sub>O<sub>40</sub> proceeds through a bifunctional mechanism, in which *n*-butane is dehydrogenated to *n*-butenes over Pt, and *n*-butenes are converted to *sec*-butyl carbenium ion intermediate (14). Furthermore, a unique function of proton has been proposed; protons present near the Pt particles play an important role in suppressing the hydrogenolysis on Pt, resulting in the selective skeletal isomerization (14).

To elucidate the factors controlling the selectivity of this reaction, we investigated the influence of the pore-width of porous catalysts on selectivity. The characteristics of Pt-promoted porous heteropoly compounds were examined by comparing the results with those of Pt-zeolites.

## Experimental

Pt-promoted Cs<sub>x</sub>H<sub>3-x</sub>PW<sub>12</sub>O<sub>40</sub> (x = 2.1, 2.2 and 2.5) were prepared by a titration method (11,15). For the former two, an aqueous solution of Pt(NH<sub>3</sub>)<sub>4</sub>(OH)<sub>2</sub> (0.03 mol·dm<sup>-3</sup>) was added to an aqueous solution of H<sub>3</sub>PW<sub>12</sub>O<sub>40</sub> (0.08 mol·dm<sup>-3</sup>) at room temperature. Then an aqueous solution of Cs<sub>2</sub>CO<sub>3</sub> (0.10 mol·dm<sup>-3</sup>) was added dropwise to the mixture at a rate of 0.1 cm<sup>3</sup>·min<sup>-1</sup> with vigorous stirring at room temperature. The obtained suspension was allowed to stand overnight at room temperature, and evaporated at 318 K to obtain solid. The Pt content of the solid was changed from 0.5wt% to 1.5wt% for Pt-Cs<sub>2.1</sub>H<sub>0.9</sub>PW<sub>12</sub>O<sub>40</sub>, and that of Pt-Cs<sub>2.2</sub>H<sub>0.8</sub>PW<sub>12</sub>O<sub>40</sub> was adjusted to 0.5wt%. These heteropoly compounds were pretreated in a flow of O<sub>2</sub> at 573 K for 2 h. These catalysts are denoted as, e.g., 0.5wt%Pt-Cs<sub>2.1</sub>. 0.5wt%Pt-Cs<sub>2.5</sub>H<sub>0.5</sub>PW<sub>12</sub>O<sub>40</sub> was prepared using aqueous solutions of H<sub>2</sub>PtCl<sub>6</sub>, H<sub>3</sub>PW<sub>12</sub>O<sub>40</sub>, and Cs<sub>2</sub>CO<sub>3</sub> by the same preparation method (14).

0.2wt%Pt-H-ZSM-5 was prepared by an ion-exchange method using NH<sub>4</sub>-ZSM-5 (from H-ZSM-5, SZ-820NAA, Tosoh Co.) and Pt(NH<sub>3</sub>)<sub>4</sub>(OH)<sub>2</sub> (Strem Chemicals). 0.2wt%Pt-HY zeolites was also prepared by the ion-exchange method using NH<sub>4</sub>-Y (from HY, JRC-Z-HY 4.8). These Pt-zeolites were calcined in air at 773 K for 4 h.

Nitrogen adsorption-desorption isotherms were measured after the catalyst was pretreated at 573 K in a vacuum with an automatic gas adsorption apparatus (BELSORP 28SA, BEL Japan, Inc.). Adsorption of various molecules having different size was measured by using a microbalance (Shimadzu TG-30) directly connected to a high vacuum system (16). Adsorption temperatures are 295 K for methanol, benzene, and 1,3,5-trimethylbenzene, 77 K for N<sub>2</sub> and 193 K for *n*-butane and isobutane. The relative pressure (p/p<sub>0</sub>) used is 0.2, since near monolayer adsorption would be obtained around this relative pressure (17).

Skeletal isomerization of *n*-butane was performed at 573 K with *n*-butane 5%, H<sub>2</sub> 50% (He balance) or *n*-butane 8%, H<sub>2</sub> 20% (He balance) after pretreatment in a flow of H<sub>2</sub> at 573 K for 2 h (14). The total flow rate was changed from 10 cm<sup>3</sup>·min<sup>-1</sup>

to  $40 \text{ cm}^3 \cdot \text{min}^{-1}$  and catalyst weight was  $0.2 \sim 2.0 \text{ g}$ . The products were analyzed with a TCD gas chromatograph (Shimadzu GC 8A) with a column, VZ-10.

## Results and Discussion

0.5wt%Pt-Cs2.1 gave a Type I isotherm of  $\text{N}_2$  adsorption and had  $61 \text{ m}^2 \cdot \text{g}^{-1}$  of BET surface area. Type I isotherm is usually observed for microporous materials (17). On the other hand, 1.0wt%, 1.5wt%Pt-Cs2.1 and 0.5wt%Pt-Cs2.5 showed Type IV isotherms which are applicable to mesoporous materials (17). Mesopore size distributions for these heteropoly compounds are provided in Fig. 1, where the distributions were derived from the desorption branch of the  $\text{N}_2$  isotherm by Dollimore-Heal method (18). Mesopores are defined as the pores having the width from 2 to 50 nm (19). It was found that no mesopore was present on 0.5wt%Pt-Cs2.1. Therefore, we can conclude that 0.5wt%Pt-Cs2.1 possesses only micropores.

On the other hand, 1.0wt%Pt-Cs2.1 and 1.5wt%Pt-Cs2.1 had mesopores with the widths of about 4.0 and 7.0 nm, respectively. Also for 0.5wt%Pt-Cs2.5, a relatively sharp peak due to mesopore was observed at about 5.0 nm. As was not shown in this figure, for 0.5wt%Pt-Cs2.2, only a small fraction of mesopores having the width less than 3.5 nm was detected (10). It was confirmed that when Pt-Cs2.5 was prepared from  $\text{Pt}(\text{NH}_3)_4(\text{OH})_2$ , the pore size was similar to that from  $\text{H}_2\text{PtCl}_6$ . This indicates that the effect of the Pt materials on the pore structure was little in the case.

Since the micropore size distribution cannot be reasonably determined from the  $\text{N}_2$  isotherm, we measured adsorption of molecules having different molecular size to estimate the micropore widths of these heteropoly compounds as well as Pt-zeolites. Table I compares the adsorption amounts measured by a microbalance connected directly to the ultrahigh vacuum system. The adsorption amounts were determined after the weight increases by the adsorptions with time became nearly zero. The adsorption amount is expressed by adsorption area calculated from the adsorption amount and molecular cross section area (see footnotes of Table I). The molecular cross section was estimated from the liquid density (17).

All samples shown in Table I adsorbed appreciably  $\text{N}_2$  (molecular size (MS) = 0.36 nm) and methanol (MS = 0.40 nm). On 0.5wt%Pt-Cs2.1, a considerable amount of  $\text{N}_2$  and a small amount of *n*-butane (MS = 0.43 nm) were adsorbed, but the adsorption amounts of benzene (MS = 0.59 nm) and 1,3,5-trimethylbenzene (MS = 0.75 nm) were negligibly small. This result strongly supports that 0.5wt%Pt-Cs2.1 has only ultramicropores and indicates that the pore-width is  $0.43 \sim 0.50 \text{ nm}$ . Ultramicropores are defined as pores having the width less than 0.7 nm (19). The adsorption areas of benzene and 1,3,5-trimethylbenzene on 0.5wt%Pt-Cs2.1 were about 3% of the total surface area, showing that the external surface area of 0.5wt%Pt-Cs2.1 is very small.

On 0.5wt%Pt-Cs2.5, all the molecules used in the present study were adsorbed appreciably and the adsorption areas are close to that of  $\text{N}_2$  (Table I). Thus, the pores of 0.5wt%Pt-Cs2.5 were larger than 0.75 nm if the micropores were present. As shown in Table I, 0.5wt%Pt-Cs2.2 has adsorption capacities of isobutane and

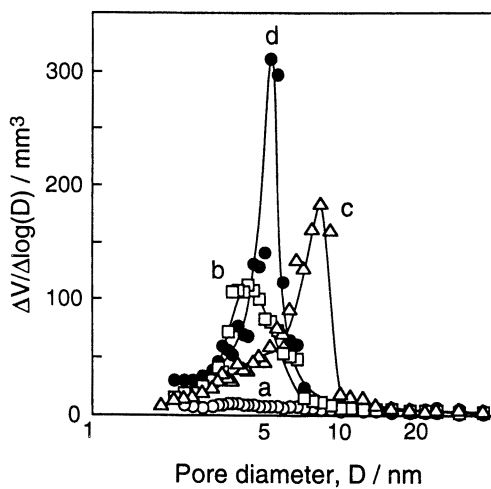


Figure 1. Pore size distribution curves for Pt-promoted heteropoly compounds derived from Dollimore-Heal method.

a: 0.5wt%Pt-Cs<sub>2.1</sub>H<sub>0.9</sub>PW<sub>12</sub>O<sub>40</sub>, b: 1.0wt%Pt-Cs<sub>2.1</sub>H<sub>0.9</sub>PW<sub>12</sub>O<sub>40</sub>, c: 1.5wt%Pt-Cs<sub>2.1</sub>H<sub>0.9</sub>PW<sub>12</sub>O<sub>40</sub>, d: 0.5wt%Pt-Cs<sub>2.5</sub>H<sub>0.5</sub>PW<sub>12</sub>O<sub>40</sub>.

**Table I. Adsorption of Various Molecules on Pt-promoted Porous Catalysts**

Catalyst	Adsorption area of molecules <sup>a</sup>					
	N <sub>2</sub> <sup>b</sup> [0.36]	MeOH <sup>c</sup> [0.40]	<i>n</i> -butane [0.43]	isobutane [0.50]	benzene [0.59]	1,3,5-TMB <sup>d</sup> [0.75]
0.5wt%Pt-Cs2.5 <sup>e</sup>	133	149	131	120	106	84
0.5wt%Pt-Cs2.2 <sup>f</sup>	72	118	25	22	20	4
0.5wt%Pt-Cs2.1 <sup>g</sup>	61	109	36 <sup>h</sup>	1	1	2
0.2wt%Pt-H-ZSM-5	405	621	457	442	319	54
0.2wt%Pt-HY	701	1050	563	520	541	10

<sup>a</sup>Calculated from the adsorption amount and molecular cross section area; m<sup>2</sup>·g<sup>-1</sup>. Molecular cross section areas used are 0.16 nm<sup>2</sup> (N<sub>2</sub>), 0.18 nm<sup>2</sup> (methanol), 0.32 nm<sup>2</sup> (*n*-butane and isobutane), 0.31 nm<sup>2</sup> (benzene), and 0.41 nm<sup>2</sup> (1,3,5-TMB). The figures in the brackets are molecular sizes in nm (20,21). <sup>b</sup>BET surface area, <sup>c</sup>Methanol. <sup>d</sup>1,3,5-trimethylbenzene. <sup>e</sup>0.5wt%Pt-Cs<sub>2.5</sub>H<sub>0.5</sub>PW<sub>12</sub>O<sub>40</sub>. <sup>f</sup>0.5wt%Pt-Cs<sub>2.2</sub>H<sub>0.8</sub>PW<sub>12</sub>O<sub>40</sub>. <sup>g</sup>0.5wt%Pt-Cs<sub>2.1</sub>H<sub>0.9</sub>PW<sub>12</sub>O<sub>40</sub>. <sup>h</sup>After 30 h. The value after 2 h was 8.

benzene, while the adsorption amounts were somewhat small. Although the pore structure of 0.5wt%Pt-Cs2.2 is thought to be rather complex, a part of the pores has the width more than 0.59 nm. When these micropores were analyzed with Ar adsorption isotherm developed by Saito and Foley (22), the obtained results were consistent with the above data as will be described elsewhere (23).

Figure 2 shows the time courses of skeletal isomerization of *n*-butane over 0.5wt%Pt-Cs2.5, 0.5wt%Pt-Cs2.2, and 0.5wt%Pt-Cs2.1 performed using 5% *n*-butane and 50% H<sub>2</sub> at 573 K. The value of W/F was 40 g·h·(mol of feed gas)<sup>-1</sup>, where W is catalyst weight (gram) and F is total flow rate (mol·h<sup>-1</sup>). The conversions on these catalysts decreased gradually at the initial stage of the reaction and reached nearly stationary states at 5 h. It was observed that the decreases in the conversion were smaller for 0.2wt%Pt-H-ZSM-5, 0.2wt%HY, and H-ZSM-5 than for the above heteropoly compounds. The conversion and selectivity were calculated on the basis of the data taken at 5 h of the reaction. While the starting material was different between Pt-Cs2.5 and Pt-Cs2.2 or Pt-Cs2.1, it was confirmed that the influence of the Pt material for Pt-Cs2.5 was little after the pretreatment with O<sub>2</sub> (14).

Dependencies of the stationary conversion on W/F are plotted in Fig. 3. The conversions increased linearly with the W/F for all catalysts up to at least 33%-conversion which corresponds to 66% that in the thermodynamic equilibrium. The changes in the stationary selectivity as a function of the conversion are given in Fig. 4 for these Pt-porous catalysts. A slight decrease in the selectivity for 0.5wt%Pt-Cs2.5 was observed, which is consistent with the previous result (19). Also in other cases in Fig. 4, the decreases in the selectivity to isobutane were not significant, while the selectivities were greatly different depending on the catalyst. Considering the trends in Fig. 4, the selectivity can be compared at a certain conversion in these conversion ranges.

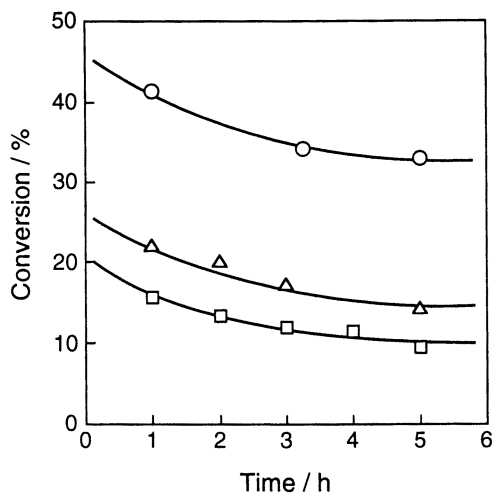


Figure 2. Time courses of *n*-butane isomerization at 573 K over Pt-promoted heteropoly compounds.  
 O: 0.5wt%Pt-Cs<sub>2.5</sub>H<sub>0.5</sub>PW<sub>12</sub>O<sub>40</sub>, Δ: 0.5wt%Pt-Cs<sub>2.2</sub>H<sub>0.8</sub>PW<sub>12</sub>O<sub>40</sub>, □: 0.5wt%Pt-Cs<sub>2.1</sub>H<sub>0.9</sub>PW<sub>12</sub>O<sub>40</sub>. Feed gas; *n*-butane: H<sub>2</sub> : He = 0.05: 0.50: 0.45, W/F = 40 g·h·(mol of feed gas)<sup>-1</sup>.

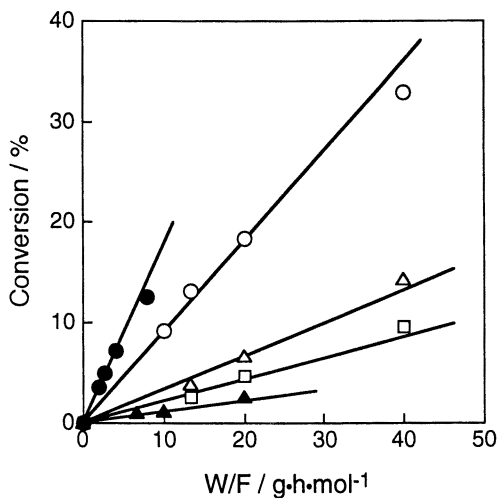


Figure 3. W/F dependence for *n*-butane skeletal isomerization at 573 K.  
 O: 0.5wt%Pt-Cs<sub>2.5</sub>H<sub>0.5</sub>PW<sub>12</sub>O<sub>40</sub>, Δ: 0.5wt%Pt-Cs<sub>2.2</sub>H<sub>0.8</sub>PW<sub>12</sub>O<sub>40</sub>, □: 0.5wt%Pt-Cs<sub>2.1</sub>H<sub>0.9</sub>PW<sub>12</sub>O<sub>40</sub>, ●: 0.2wt%Pt-H-ZSM-5, ▲: 0.2wt%Pt-HY. Feed gas; *n*-butane: H<sub>2</sub> : He = 0.05: 0.50: 0.45.

The catalytic data at stationary states at 573 K and 0.5 atm of H<sub>2</sub> are summarized in Table II. The catalytic activity estimated from the total reaction rate is in the order; 0.2wt%Pt-H-ZSM-5 > 0.5wt%Pt-Cs2.5 > 0.5wt%Pt-Cs2.2 > 0.5wt%Pt-Cs2.1 > 0.2wt%Pt-HY. The selectivity is in the order of Pt-Cs2.5 > 0.2wt%Pt-HY > 0.5wt%Pt-Cs2.2 > 0.5wt%Pt-Cs2.1 > 0.2wt%Pt-H-ZSM-5 > H-ZSM-5. Thus the rate for the isobutane formation is the highest for 0.5wt%Pt-Cs2.5 (Table II).

Table II demonstrates that the selectivity to isobutane greatly depended on the Cs content; 0.5wt%Pt-Cs2.1 (47.5%) < Pt-Cs2.2 (69.5%) < Pt-Cs2.5 (93.9%), where the figures in the parentheses are the selectivities to isobutane. Since the pore-width is in the order of 0.5wt%Pt-Cs2.1 < 0.5wt%Pt-Cs2.2 < Pt-Cs2.5, the different selectivity to isobutane is probably ascribed to the difference in the pore width. That is, the smaller micropores tended to produce the smaller molecules such as propane. It was previously reported that changes in the acid strength of the heteropolyacid were slight upon the substitution of Cs<sup>+</sup> for H<sup>+</sup> (1,24). Thus the difference in selectivity among these heteropoly compounds is not due to the acid strength.

The correlation between the selectivity to isobutane and the pore size of the catalysts is demonstrated in Fig. 5.

**Table II. Activity and Selectivity for Skeletal Isomerization of *n*-Butane over Pt-promoted Porous Catalysts in the Presence of 0.5 atm of H<sub>2</sub> at 573 K**

Catalyst	W/F <sup>a</sup>	Conv. (%)	Selectivity (mol%)					Rate <sup>b</sup>
			C1	C2	C3	<i>i</i> -C4	C5(+)	
0.5wt%Pt-Cs2.5 <sup>c</sup>	40	33.0	0.8	0.7	2.9	93.9	1.7	3.9
0.5wt%Pt-Cs2.2 <sup>d</sup>	40	14.2	2.0	3.0	20.1	69.5	5.4	1.2
0.5wt%Pt-Cs2.1 <sup>e</sup>	40	9.6	3.9	5.7	42.9	47.5	0	0.6
0.2wt%Pt-H-ZSM-5	8	12.5	20.2	34.1	23.2	22.5	0	1.8
0.2wt%Pt-HY	20	2.5	6.1	8.0	5.8	80.1	0	0.5
H-ZSM-5	20	15.3	0.8	3.7	74.7	15.2	5.6	0.6

<sup>a</sup>W/F = catalyst weight (g)/total flow rate (mol·h<sup>-1</sup>). <sup>b</sup>Rate for the formation of isobutane; 10<sup>-4</sup> mol·g<sup>-1</sup>·h<sup>-1</sup>. <sup>c</sup>0.5wt%Pt-Cs2.5H<sub>0.5</sub>PW<sub>12</sub>O<sub>40</sub>. <sup>d</sup>0.5wt%Pt-Cs2.2H<sub>0.8</sub>PW<sub>12</sub>O<sub>40</sub>. <sup>e</sup>0.5wt%Pt-Cs2.1H<sub>0.9</sub>PW<sub>12</sub>O<sub>40</sub>.

Pt-H-ZSM-5 gave mainly C1-C3 hydrocarbons and was less selective for the formation of isobutane (22.5%). Comparing the product composition of Pt-H-ZSM-5 with that of H-ZSM-5, methane and ethane formed over Pt-H-ZSM-5 would be hydrogenolysis products. Contrary to Pt-H-ZSM-5, Pt-HY was fairly selective (80.1% selectivity to isobutane) (Table II). Considering the different pore-opening size from ZSM-5 (0.53 x 0.56 nm) to HY (0.74 nm), it can be concluded that the pore width of the microporous catalysts is an important factor determining the product composition.

Effects of Pt loading amount on selectivity are shown in Table III. In this case,



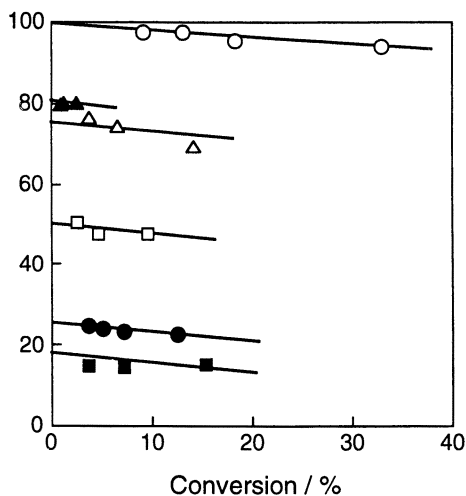


Figure 4. Selectivity to isobutane as a function of the conversion.  
 ○: 0.5wt%Pt-Cs<sub>2.5</sub>H<sub>0.5</sub>PW<sub>12</sub>O<sub>40</sub>, △: 0.5wt%Pt-Cs<sub>2.2</sub>H<sub>0.8</sub>PW<sub>12</sub>O<sub>40</sub>, □: 0.5wt%Pt-Cs<sub>2.1</sub>H<sub>0.9</sub>PW<sub>12</sub>O<sub>40</sub>, ●: 0.2wt%Pt-H-ZSM-5, ▲: 0.2wt%Pt-HY, ■: H-ZSM-5. Feed gas; *n*-butane: H<sub>2</sub> : He = 0.05: 0.50: 0.45.

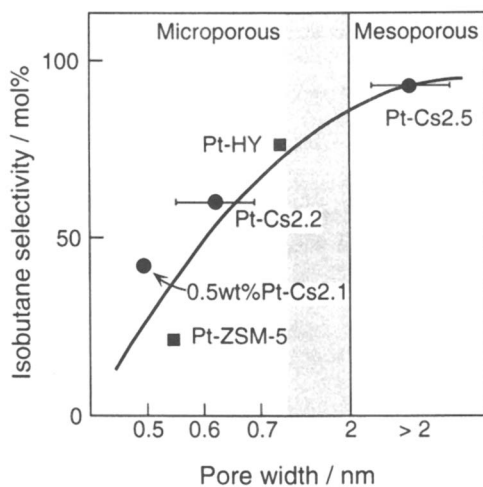


Figure 5. Effect of the pore width of the porous catalysts on selectivity to isobutane in *n*-butane skeletal isomerization (573 K).

the feed gas consists of 8% butane, 20% H<sub>2</sub> and 72% (He balance). Apparently, the selectivity to isobutane became higher as the Pt loading amount increased. 1.5wt%Pt-Cs2.1 and 1.0wt%Pt-Cs2.1 gave selectivities of 95% and 92%, respectively, while 0.5wt%Pt-Cs2.1 showed 42%-selectivity under these reaction conditions. Since 1.0wt% and 1.5wt%Pt-Cs2.1 were mesoporous similarly to 0.5wt%Pt-Cs2.5 as shown in Fig. 1, the higher selectivities of these mesoporous catalysts are reasonable.

Effects of pore width of zeolites on the selectivity for skeletal isomerization of *n*-butane have been pointed out by Storker et al. (25). They reported that HY zeolite was more selective to isobutane than a smaller pore zeolite like offretite, and presumed that the difference in selectivity is due to the shape selectivity. H-ZSM-5 was reported to be less selective to isobutane in the *n*-butane isomerization (26); the main products at 573 K were propane 78% and isobutane 24% at 23% conversion. Even at 473 K, the selectivity to isobutane over H-ZSM-5 was 28% (12). Ono and Kanae (27) claimed that cracking of *n*-butane catalyzed by H-ZSM-5 at 773 K proceeds through pentacoordinated carbocations to yield mainly methane, ethane, and hydrogen. However, this mechanism is probably inapplicable in this case, since methane and ethane were little formed at 573 K over H-ZSM-5 under these reaction conditions (Table II).

**Table III. Effect of Pt-loading Amount for Pt-Cs<sub>2.1</sub>H<sub>0.9</sub>PW<sub>12</sub>O<sub>40</sub> on Selectivity to Isobutane in Skeletal Isomerization of *n*-Butane at 573 K**

Catalyst	W/F <sup>a</sup>	Conv. (%)	Selectivity (mol%)				
			C1	C2	C3	<i>i</i> -C4	C5(+)
0.5wt%Pt-Cs2.1 <sup>b</sup>	40	5.9	7.0	7.6	42.9	35.4	7.0
1.0wt%Pt-Cs2.1 <sup>b</sup>	20	9.4	0.3	0.3	4.6	92.8	2.0
1.5wt%Pt-Cs2.1 <sup>b</sup>	20	21.1	0.4	0.4	4.0	94.8	0.4

Note: Reaction conditions; *n*-butane : H<sub>2</sub> : He = 0.08 : 0.20 : 0.72; catalyst 1~2 g; total flow rate 10 cm<sup>3</sup>·min<sup>-1</sup>.

<sup>a</sup>W/F = catalyst weight (g)/total flow rate (mol·h<sup>-1</sup>). <sup>b</sup>Cs<sub>2.1</sub>=Cs<sub>2.1</sub>H<sub>0.9</sub>PW<sub>12</sub>O<sub>40</sub>

Since 0.5wt%Pt-Cs2.1 has ultramicropores, of which the size is critical for the adsorption of isobutane (Table I), the diffusion of isobutane into or from the pores of 0.5wt%Pt-Cs2.1 may be restricted somewhat during the reaction. This would be responsible for the lower selectivity to isobutane. Therefore, the different selectivity on 0.5wt%Pt-Cs2.1 among the Pt-promoted Cs salts is most probably brought about by a product shape selectivity due to the constrained pores. For this reaction catalyzed by solid acids, two typical mechanisms have been proposed; monomolecular (28) and bimolecular mechanism (29,30). If the reaction takes place *via* bimolecular mechanism, C8 carbenium intermediates must be formed. The ultramicropores are too narrow to form the intermediates, which would be also responsible for the lower selectivities of 0.5wt%Pt-Cs2.1, H-ZSM-5, etc.

The above mechanisms would be related more importantly to the selectivity. When skeletal isomerization of *n*-pentane was performed on H-ZSM-5, the

selectivity was very high (31,32). The difference in the selectivity between *n*-butane and *n*-pentane can be ascribed to the mechanism; the former would proceed through bimolecular mechanism and the latter monomolecular mechanism because of the stability of carbenium ions. In the monomolecular mechanism, *n*-butane must proceed a primary carbenium ion, while *n*-pentane a secondary carbenium ion. Thus *n*-butane isomerizes preferentially through the bimolecular mechanism over H-ZSM-5. Since isobutane (and also isopentane) was readily adsorbed into the pore of Pt-H-ZSM-5 (Table I), the diffusion of isobutane is not restricted. Probably, the C8 carbenium ion intermediates formed in the micropores are unstable to decompose small molecules like propane.

Finally, the formation process of the pores of these heteropoly compounds will be described briefly. A schematic model for the microstructure of the Cs salts of heteropolyacid is shown in Fig. 6. The Keggin structure is called the primary structure, of which size is about 1.1 nm. The arrangement of the primary structure together with Cs<sup>+</sup> forms the secondary structure, which corresponds to the primary particles (microcrystallites). The microcrystallite size was determined to be about 10 nm (1,33). The space between the primary particles corresponds to pores. If one assumes that spherical particles with the size of 10 nm were closely packed, the pores formed have the width of about 4 nm. Thus the mesopores formed on 0.5wt%Pt-Cs2.5, etc. correspond to the space between the primary particles.

The micropores of 0.5wt%Pt-Cs2.1 may be formed through the different

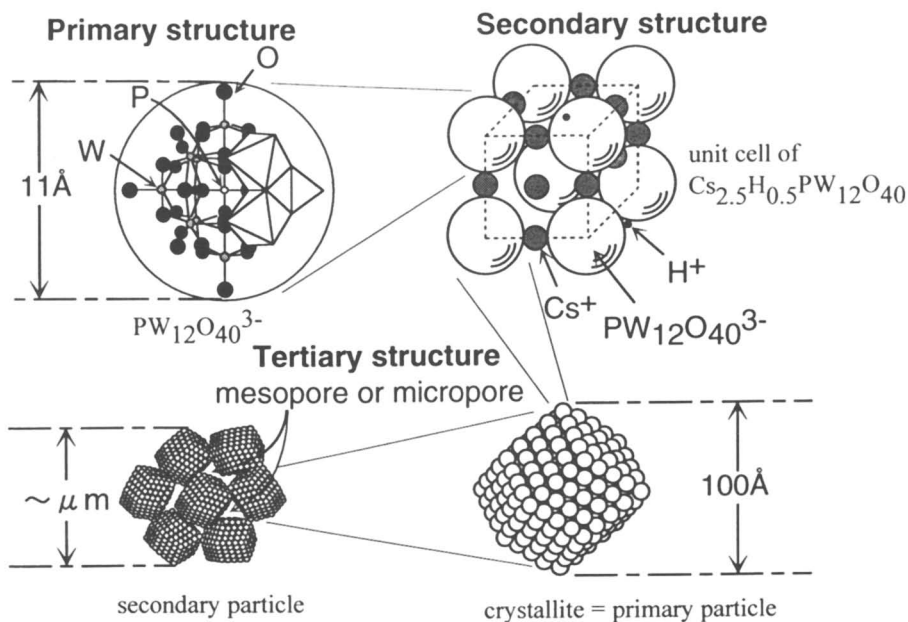


Figure 6. Model for the pores of heteropoly compounds.

process. We speculate that the micropores are spaces formed between the crystallites, that is, the pores correspond to voids formed by crystallographic mismatching (34).

## Conclusions

Bifunctional heteropoly compounds,  $\text{Pt-CsxH}_{3-x}\text{PW}_{12}\text{O}_{40}$ , catalyzed the skeletal isomerization of *n*-butane. The mesoporous salts such as  $\text{Pt-Cs}_{2.5}\text{H}_{0.5}\text{PW}_{12}\text{O}_{40}$  gave high selectivities to isobutane, but the microporous ones were less selective. Adsorption of various molecules revealed that microporous 0.5wt%Pt- $\text{Cs}_{2.1}\text{H}_{0.9}\text{PW}_{12}\text{O}_{40}$  has pores with the width less than the size of product isobutane. These restricted pores are responsible for the lower selectivities to isobutane in this reaction due to the product shape selectivity.

## Acknowledgement

This study was partly supported by Grant-in Aid for Scientific Research (No. 9555243) from the Ministry of Education, Science, Sports, and Culture, Japan.

## References

- (1) Csicsery, S. M. *Pure & Appl. Chem.* **1986**, *58*, 841.
- (2) Venuto, P. B. *Microporous Mater.* **1994**, *2*, 297.
- (3) Corma, A. *Chem. Rev.* **1997**, *97*, 2373.
- (4) Maier, W. F.; Martens, J. A.; Klein, S.; Heilmann, J.; Porton, R.; Vercruyse, K.; Jacobs, P. A. *Angew. Chem. Int. Ed. Engl.* **1996**, *35*, 180.
- (5) Okuhara, T.; Mizuno, N.; Misono, M. *Advan. Catal.* **1996**, *41*, 113.
- (6) Okuhara, T.; Nishimura, T.; Misono, M. *Proc. 11th Intern. Congr. Catal.* (eds. J. W. Hightower, W. N. Delgass, E. Iglesia and A. T. Bell), Elsevier, Amsterdam, 1996, 581.
- (7) Okuhara, T.; Nishimura, T.; and Misono, M. *Chem. Lett.* **1995**, 155.
- (8) Itoh, T.; Song, I.-K.; Inumaru, K.; Misono, M. *J. Phys. Chem.* **1997**, *48*, 9958.
- (9) MacMonagle, J. B.; Moffat, J. B. *J. Colloid Interface Sci.* **1984**, *101*, 479.
- (10) Okuhara, T.; Nakato, T. *Catal. Surveys from Japan* **1998**, *2*, 31.
- (11) Yoshinaga, Y.; Seki, K.; Nakato, T.; Okuhara, T. *Angew. Chem. Int. Ed. Engl.* **1997**, *36*, 2833.
- (12) Na, K.; Okuhara, T.; Misono, M. *J. Chem. Soc. Faraday Trans.* **1995**, *91*, 367.
- (13) Na, K.; Iizaki, T.; Okuhara, T.; Misono, M. *J. Mol. Catal. A* **1997**, *115*, 449.
- (14) Na, K.; Okuhara, T.; Misono, M. *J. Catal.* **1997**, *170*, 96.
- (15) Yoshinaga, Y.; Okuhara, T. *J. Chem. Soc. Faraday Trans.* **1998**, *94*, 2235.
- (16) Inumaru, K.; Okuhara, T.; Misono, M. *J. Phys. Chem.* **1991**, *95*, 4026.
- (17) Gregg, S. J.; Sing, K. S. W. *Adsorption, Surface Area, and Porosity*, 2nd Ed., Academic Press, London, 1982.
- (18) Dolloimore, D.; Heal, G. R. *J. Colloid Interface Sci.* **1970**, *33*, 508.

- (19) Rouquerol, J.; Avnir, D.; Fairbridge, C. W.; Everett, D. H.; Haynes, J. H.; Pernicone, N.; Ramsay, J. D. F.; Sing, K. S. W.; Unger, K. K. *Pure & Appl. Chem.* **1994**, *66*, 1739.
- (20) Breck, D. W. *Zeolite Molecular Sieves*, Wiley, New York, 1974.
- (21) Vauham, E. E. W.; Lussier, R. J. *Proc. 5th Intern. Conf. Zeolites*, Heyden and Son, London, 1980, pp 94.
- (22) Saito, A.; Foley, H. C. *Microporous Mater.* **1995**, *3*, 531.
- (23) Yamada, T.; Johkan, K.; Okuhara, T. *Microporous and Mesoporous Mater.* in press.
- (24) Nishimura, T.; Okuhara, T.; Watanabe, H.; Misono, M. *J. Mol. Catal.* **1992**, *74*, 247.
- (25) Storker, M.; Hemmersback, P.; Reader, J. H.; Grepstad, J. K. *Appl. Catal.* **1986**, *25*, 223.
- (26) Shigeishi, R.; Gorforth, I.; Harris, I.; Dwyer, J. *J. Catal.* **1991**, *30*, 423.
- (27) Ono, Y.; Kanae, K. *J. Chem. Soc. Faraday Trans.* **1991**, *87*, 663.
- (28) Gates, B. C. *Catalytic Chemistry*, 1992, John Wiley & Sons, Inc., New York.
- (29) Cheung, T.; D'Tri, J. L.; Gates, B. C. *J. Catal.* **1995**, *151*, 464.
- (30) Wan, K.; Khouw, C. B.; Davis, M. E. *J. Catal.* **1996**, *158*, 311.
- (31) Fujimoto, K.; Maeda, K.; Akimoto, K. *Appl. Catal.* **1992**, *91*, 81.
- (32) Liu, Y.; Koyano, G.; Na, K.; Misono, M. *Appl. Catal. A.* **1998**, L263 - L265.
- (33) Okuhara, T.; Watanabe, H.; Nishimura, T.; Misono, M. In *Acid-Base Catalysis II*, ed. Hattori, H.; Misono, M.; Ono, Y., Kodansha-Tokyo, **1994**, 419.
- (34) Yamada, T.; Yoshinaga, Y.; Okuhara, T. *Bull Chem. Soc. Jpn.* in press.

## Chapter 27

# A Proposed New Concept for Design of Sulfur-Resistant Noble Metal Catalysts Based on Shape-Selective Exclusion and Hydrogen Spillover

Chunshan Song

Applied Catalysis in Energy Laboratory, and Department of Energy and Geo-Environmental Engineering, Pennsylvania State University, 209 Academic Projects Building, University Park, PA 16802

The aims of this article are to briefly discuss the present understanding of the way in which noble metal catalysts are used for fuel hydrogenation, and to propose a new way of thinking for designing noble metal catalysts for low-temperature hydrotreating. A new concept is proposed for design of sulfur-resistant noble metal catalysts for hydrotreating at low temperatures on the basis of shape-selective exclusion, hydrogen spillover, and differentiation of sulfur resistance.

The world will continue to rely heavily on liquid transportation fuels, and it has become more important to make cleaner fuels that are environment friendly both in their production and in their utilization. Deep hydrogenation and deep desulfurization of distillate fuels, particularly diesel fuels, are receiving considerable attention due to the increasingly more stringent environmental regulations on transportation fuel composition (1-4). Hydrogenation of aromatic compounds is exothermic, and is therefore favored at lower reaction temperatures. However, conventional supported Ni-Mo and Co-Mo sulfide hydrotreating catalysts become active only at relatively high temperatures. While noble metals are active for hydrogenation at low temperatures, their use as catalysts will become attractive only if their sulfur resistance can be greatly enhanced.

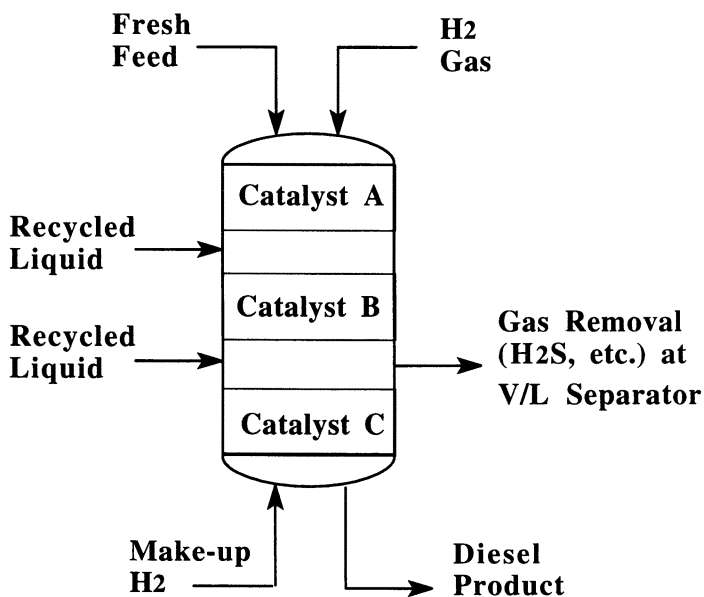
Herein we propose a new approach for the design of noble metal catalysts for hydrotreating of sulfur-containing distillates to produce clean distillate fuels such as diesel fuels, jet fuels and gasoline. This work is motivated by the need for efficient low-temperature catalytic hydrotreating processes, and, in part, a desire to apply our recent experimental observations (5-8) on the hydrogenation of naphthalene over noble metal catalysts that withstand added benzothiophene.

### Current Status of Application of Noble Metal Catalysts

In current processing schemes multiple catalyst beds are used to achieve deep desulfurization and deep hydrogenation. Hydrodesulfurization occurs in the first stage over a Ni-Mo or Co-Mo catalyst, followed by intermediate byproduct gas removal, and finally, hydrogenation over the noble metal catalyst operates in the bottom bed

where the concentrations of catalyst poisons (organosulfur and  $H_2S$ ) are very low (2, 3). Commercial examples of this technology are the Shell Middle Distillate Hydrogenation process, and the SynSat process developed by Criterion/Lummus (2-4). There are no reports of noble metal catalysts that can operate without such intermediate  $H_2S$  removal (3). Because of its importance, sulfur resistance of noble metal catalysts has been the subject of several recent publications (1, 5, 6, 9-12).

Figure 1 shows the SynSat process based on the published information (2-4). SynSat process is considered to be an innovation across the boundary between catalysis and reactor engineering (2). SynSat employs several different catalyst beds within a single reactor shell with intermediate by-product gas ( $H_2S$  etc.) removal, and optional counter current gas flow. Catalysts **A** and **B** in Figure 1 are metal sulfide catalysts such as sulfided Ni-Mo. Catalyst **C** is noble metal loaded on acidic support. There is an intermediate gas removal between the beds of Catalysts **B** and **C**. Nearly all the sulfur compounds must be converted on beds **A** and **B** and removed as  $H_2S$  before the fuel feed reaching noble metal catalyst bed **C**. Noble metal catalysts that can operate in a stacked-bed reactor with a NiMo catalyst without intermediate  $H_2S$  removal have not been reported (3). Published information is also available in open literature on the related two-stage processes developed by Shell, Haldor-Topsøe, and IFP (3, 4). A recent report by Shell Research and Technology Center (3) showed that commercial noble metal-based catalysts for deep hydrogenation of fuels operate in a regime where the large majority of the metal sites are poisoned by sulfur, even when sulfur tolerance has been improved by choosing modern support functions and metals. Thus these catalysts are currently used only after fuel deep desulfurization over Ni-Mo or Co-Mo catalysts followed by complete removal of poisonous gases, as is the case in the Shell Middle Distillate Hydrogenation process and in the SynSat process.

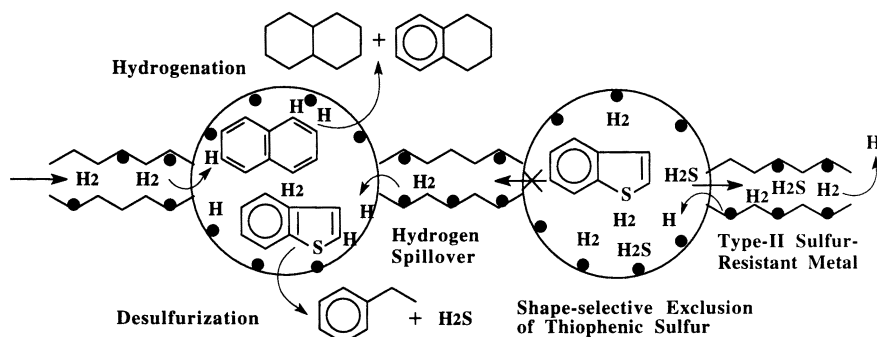


**Figure 1.** SynSat process with Criterion/Lummus catalytic hydrotreating reactor technology, with intermediate by-product gas removal, liquid recycle, and optional counter-current  $H_2$  gas flow.

## Proposed New Concept for Design of Sulfur-Resistant Noble Metal Catalyst

We have been exploring low-temperature hydrogenation based on noble metal catalysts (5-8). Based on our preliminary experimental results, here we propose a new concept for design of novel sulfur-resistant noble metal catalysts for more efficient hydrotreating of sulfur-containing distillates to produce clean transportation fuels.

The proposed design concept invokes some unique zeolites as supports for noble metals and utilizes (1) shape-selective exclusion, (2) hydrogen spillover, and (3) two types of sulfur resistance. Unique zeolite supports can be used to prepare bimodal distributions of noble metal particles. Some metals are located in small pores (**Sm**: pore opening less than about 5 Å); whereas, others will be contained in large pores (**La**: pore opening larger than 6 Å). Preferably, the two pore systems inter-connect, or are at least uniformly distributed so that they are in close proximity. Diffusion of organosulfur compounds such as thiophenic molecules into the small-pores would be inhibited by size (shape-selective exclusion). The large pores (large micropore or mesopore range) would preferably allow fast diffusion and reaction of bulky polycyclic aromatic and sulfur compounds. The thiophenic molecules could enter the large pores, but not the small pores. However, H<sub>2</sub> molecules can readily enter both types of pores, dissociatively adsorb on metal contained within, and be transported between pore systems by spillover. When the metal in the large pores becomes inactivated by adsorbed sulfur, spillover hydrogen could recover the poisoned metal sites by elimination of R-S-R and R-S-H. It is also of interest to classify sulfur resistance as either type I, resistance to organic sulfur compounds, or type II, resistance to inorganic H<sub>2</sub>S (5). The metal species, particularly those in small pores, should have higher type II sulfur resistance. Figure 2 shows a simplified representation of the proposed new concept.



**Figure 2.** Simplified representation of the proposed new concept for catalyst design based on shape-selective exclusion with molecular-sieve structure, hydrogen spillover, and two types of sulfur resistance. The black dots indicate metal particles on internal surface.

The proposed concept for the design of noble metal catalysts with high resistance to sulfur, if established with success, could result in a new class of materials for low-temperature catalytic hydrotreating, which includes but is not limited to deep hydrogenation and deep hydrodesulfurization of diesel fuels. The noble metal catalysts with substantially enhanced sulfur resistance (much higher than current commercial catalysts) will allow hydrotreating at substantially lower temperatures



under lower pressure which can lead to major improvement in refining efficiency and economics. Such new type of catalysts could be used for new processing schemes or in existing processes by combination with Ni-Mo or Co-Mo catalysts in stacked-beds within a singled reactor shell.

The proposed concept may be explored for making either bimodal catalyst (with both **Sm** and **La** pores) or hybrid catalysts (mixture of one catalyst possessing mostly **Sm** pore with another having largely **La** pore). Such catalyst is expected to significantly improve refining efficiency and economics for producing clean distillate fuels (gasoline, diesel and jet fuels) from various low-quality feedstocks such as naphtha, straight-run distillate oils, FCC naphtha, LCO from FCC, gas oil, coker distillates, visbreaker distillates, and blends of two or more of these. The following is a brief summary of experimental observations that lend support to our proposed new concept towards catalyst design.

**Role of Acidic Zeolite Supports.** Certain noble metals are more active at low temperatures for aromatics hydrogenation when supported on zeolites than their counterparts supported on alumina or titania. Noble metal catalysts loaded on zeolites or other acidic supports can afford higher hydrogenation activity and better sulfur-resistance than  $\text{Al}_2\text{O}_3$  or  $\text{TiO}_2$  supports. We observed this trend for naphthalene and phenanthrene hydrogenation over microporous zeolites (5-7) and mesoporous aluminosilicate molecular sieve (8). It is not difficult to imagine the better dispersion of metals on higher-surface-area zeolites than on lower-surface area alumina or titania. The higher activity of the former may be attributable partly to the better metal dispersion on zeolites and partly to the electron deficiency of metals supported on acidic materials. The concept of electron deficiency was first proposed by Dalla Betta and Boudart (11) and has been accepted by many researchers (1,11,12-14).

Some promising results were reported for supported on USY (9,10) or HY (11) in flow reactor test, and for Pt and Pd on HY or H-mordenite in batch test (5). Several proposals have been given to explain the weakened metal-sulfur interaction: electron transfer from the metal to the acidic support, creating electron-deficient metal species (13,14); formation of metal-proton adducts (14); or interaction between the metal and cations in the zeolite (15).

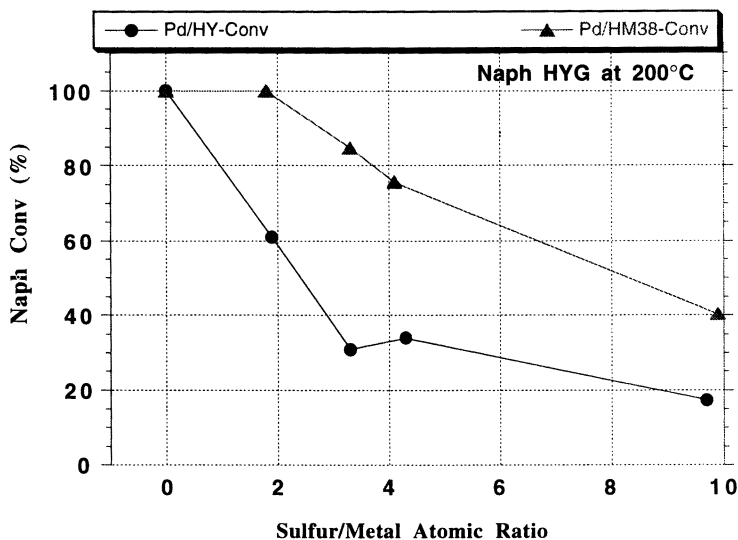
**Effect of Metal Type and Zeolite on Hydrogenation.** Activity and selectivity vary among different noble metals for hydrogenation (5-9). For hydrogenation of a model fuel containing 20% naphthalene at 200°C over the catalysts prepared in our laboratory listed in Table 1, the palladium (Pd) supported on Y zeolite or mordenite are more active than platinum (Pt) on the same supports at the same loading level (5). For a given metal, some zeolites are better than other zeolites as supports for achieving higher hydrogenation activity (5,7,9). For example, among the catalysts listed in Table 1, Pd/HM38 is more active than Pt/HM38. Several catalyst companies in the world are making noble metal-based deep hydrogenation catalysts supported on acidic supports such as amorphous silica-alumina and Y zeolites (16).

**Table 1.** Laboratory-Prepared Zeolite-Supported Catalysts Containing 2 wt% Metal

Catalyst ID	Support Zeolite Type	Tot. Pore Vol cc/g	Tot. Surface Area $\text{m}^2/\text{g}$	Micropore Area $\text{m}^2/\text{g}$	Mesopore Area $\text{m}^2/\text{g}$
Pd/HY	Y zeolite	0.296	538.0	529.6	8.4
Pd/HM38	Mordenite	0.351	539.4	356.4	183.0
Pt/HY	Y zeolite	0.370	589.3	562.9	26.4
Pt/HM38	Mordenite	0.368	541.6	363.4	178.2

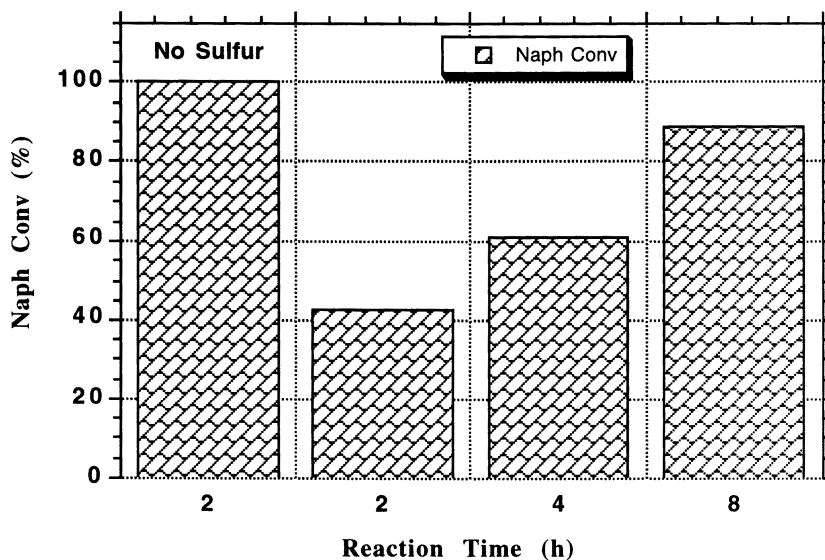
**Effect of Zeolite Structure and Metal on Sulfur Resistance.** It has been known that Y zeolite-supported noble metals can have higher sulfur tolerance than alumina-supported ones (1). This has been attributed to electron deficiency of metals on zeolites (1,12), but even the commercial Y zeolite-supported noble metal catalysts are not sulfur-resistant enough (3). It is also known that different metals may have different sulfur resistance (1,5,10).

Our recent work revealed the importance of the zeolite structure and metal type for improving sulfur resistance (5). For example, among the catalysts listed in Table 1, the mordenite-supported Pd catalyst has been found to be much more resistant to sulfur poisoning than the zeolite Y-supported Pd; both catalysts were prepared by the same method at the same metal loading level. As shown in Figure 3, even when the amount of added sulfur is more than twice the metal atoms, higher sulfur resistance was obtained with Pd supported H-mordenite (Pd/HM38) than with that on Y zeolite (Pd/HY) (5). Therefore, Pd supported on mordenite can be more active and more sulfur-resistant than the same metal supported on Y-zeolite at the same loading level, even in the presence of large amount of added sulfur up to sulfur-metal ratio of  $\geq 10$ . This observation shows the importance of zeolite structure on the sulfur resistance of a supported metal. There are also differences in mesopore surface areas between HM38 and HY supported catalysts, as shown in Table 1. While the contribution of mesopore areas in HM38 can not be neglected, the Pt supported on the same HM38 is much less sulfur-resistant. Therefore, both the structure of zeolite and the type of metal are important for superior performance.



**Figure 3.** Naphthalene conversion over Pd/HM38 and Pd/HY catalysts at 200°C under 1000 psig  $H_2$  in a sealed batch reactor for 2 h in the presence of added benzothiophene. Plotted based on data in ref. 5.

**Two Types of Sulfur Resistance.** In batch HDS tests where the  $H_2S$  product remains within the reactor and in contact with the catalyst, we observed gradual recovery of activity of some Pd catalysts poisoned by benzothiophene, while Pt catalysts did not show significant recovery in activity with increasing residence time (6). Figure 4 illustrates this trend. In other words, some supported Pd catalysts recovered its activity for hydrogenation when the sulfur in benzothiophene was converted to  $H_2S$ . These experimental observations led us to propose that noble metals may have two different types of sulfur resistance: tolerance to organic sulfur (I) and inorganic sulfur (II). The thiophenic organosulfur compounds have stronger poisoning effect than inorganic  $H_2S$ .



**Figure 4.** Naphthalene conversion over Pd/TiO<sub>2</sub> catalyst at 200°C under 1500 psig H<sub>2</sub> in a sealed batch reactor for 2-8 h in the absence and presence of added benzothiophene (4200 ppm). Plotted based on data in ref. 6.

**Shape-Selective Exclusion and Hydrogen Spillover.** The consideration on two types of sulfur resistance becomes more useful to us when we conceived the hypothesis of shape-selective exclusion of organic sulfur compounds from type **Sm** pores. There are significant structural differences between mordenite and Y zeolite. Pd on the mordenite HM38 shows particularly good resistance to sulfur poisoning. A possible explanation is that a significant fraction of the Pd particles are in mordenite side-pockets (hypothesis). Bulky organosulfur compounds such as benzothiophene can not enter into the small diameter side-pocket channels; consequently, metal particles contained within the side-pocket channels are protected from type I

poisoning by a molecular sieving mechanism. These considerations for our experimental results (5) are incorporated into our proposed concept as follows.

Because of pore size limitation, it is possible to prevent the thiophenic sulfur from diffusing into type **Sm** pores. In other words, type I sulfur-resistance maybe improved if the metals can be placed into the pores that thiophenic compounds can not enter. Transition metals can be introduced into very small micropores, and evidence has been reported in recent literature (14). Spillover of hydrogen on solid catalyst surface is a known phenomenon that has been reviewed recently (17). It is possible for hydrogen generated on metal sites in **Sm** pores to spillover to surface in **La** pores. However, if the metal in **Sm** is too weak to H<sub>2</sub>S, then it will not be very useful, because hydrodesulfurization by hydrogen atom spillover from type **Sm** to type **La** pores produces H<sub>2</sub>S, which is sufficiently small compared to any fuel molecules. It would be extremely difficult to prevent H<sub>2</sub>S from entering type **Sm** pores. This suggests that type II sulfur tolerance can not be improved easily by altering the catalyst pore structure. However, it may be influenced by other factors, such as metal-zeolite interaction. In our design concept, the important role of type **Sm** pores is to have and keep certain metal sites active even when they are exposed to H<sub>2</sub>S. Fortunately, the experimental results (Figure 3) have indicated that certain metals on some supports have higher type II sulfur resistance than others under low-temperature hydrotreating conditions.

Highly sulfur-tolerant hydrogenation with accompanying hydrodesulfurization can be realized when certain metal particles are dispersed in both small and large pores. The catalyst itself can foster continuous regeneration of organosulfur-poisoned metal sites in type **La** pores (through hydrogen spillover from sites in type **Sm** pores, Figure 2) and thus allow low-temperature deep hydrogenation of aromatics and hydrodesulfurization. This is partially supported by our work on low-temperature hydrotreating (5,6).

During naphthalene hydrogenation at 200°C over some zeolite-supported noble metal catalysts in the presence of added benzothiophene, unambiguous evidence on benzothiophene hydrodesulfurization has also been obtained (5), as shown in Table 2. Through detailed analysis, we have found that the added benzothiophene has been converted to ethylbenzene and even ethylcyclohexane during naphthalene hydrogenation over Pd/HM38 with 373 ppm sulfur. Thus hydrodesulfurization has been achieved using Pd supported on mordenite, even at 200°C. Proper combination of noble metal (e.g., Pd) and zeolite (e.g., partially dealuminated mordenite) was found to be important for high activity and improved sulfur resistance.

**Table 2.** Products from Added Benzothiophene (BTP) over Zeolite-Supported Catalysts during Naphthalene Hydrogenation at 200°C under 1000 psig H<sub>2</sub>.

Catalyst (2 wt% metal)	Pd/HM38	Pd/HM38	Pd/HY	Pd/HY	Pt/HM38	Pt/HM38
S in feed, ppm	373	1098	373	1095	500	895
S/M atom ratio	3.3	9.9	3.3	9.7	8.3	14.5
BTP Conv (%)	100	91.9	88.2	81.2	93.3	83.4
Prod Sel (%)						
Ethylcyclohexane	36.1	11.6	25.3	6.4	17.6	7.5
Ethylbenzene	63.9	36.0	26.8	18.9	25.9	13.5
Dihydro-BTP	0	52.4	48.0	74.7	56.5	79.0
Mass Balance	100	78.3	77.8	76.8	71.9	79.7

**Active Metal Sites: Monometallic or Bimetallic?** The proposed concept is not limited to single catalysts or to monometallic catalysts. The system may consist of either a bimodal catalyst or a hybrid of two catalysts. The metal species loaded onto the zeolite support can be either monometallic or bimetallic species. For design of a suitable bimetallic catalyst, one feasible idea is to introduce the second metal which is either itself more sulfur resistant than the first metal or can make the resulting bimetallic species more sulfur resistant. The second metal should be a transition metal which is active as metal or as metal compound for activation of  $H_2$  (18,19); it may or may not be a noble metal. It is known that introduction of a second metal can have beneficial effect on enhancing catalytic activity or sulfur resistance (1,10,13,14,20). One important issue in our proposed approach is to place in type **Sm** pores the metal species that have higher type II sulfur resistance.

### Concluding Remarks

A new concept has been proposed for design of sulfur-resistant noble metal catalysts for low-temperature hydrotreating. The new concept invokes zeolite as support, shape-selective exclusion, two types of sulfur resistance, and hydrogen spillover. We have shown that some molecular sieve supports can improve the sulfur-resistance of noble metals in hydrotreating applications.

Our own recent work on hydrogenation of naphthalene over mordenite- and Y zeolite-supported noble metal catalysts in the presence of benzothiophene suggests that there maybe at least one practical way to use the proposed concept for exploring new catalyst design. That is to load noble metal-based monometallic or bimetallic species which has relatively higher type-II sulfur tolerance into both the main channel and the side pocket of a mordenite. To facilitate the diffusion and mass transfer, the mordenite should be properly dealuminated before loading the metal. The metal precursor (monometallic or bimetallic) should be properly introduced into both type **La** and type **Sm** pores by careful preparation.

The proposed concept may have immediate bearing on research into sulfur resistant catalysts in general, as indicated in our preliminary communication (21). By dividing sulfur resistance into two types, the concept suggests that type I tolerance can be dramatically enhanced by structural design making use of shape-selective exclusion, and type II tolerance may be improved by modifying electronic properties of metal species to weaken the metal-sulfur interaction or bonding. Application of the new concept may involve both type **Sm** micropore and larger micropore or mesopore (**La**) in either a single bimodal catalyst (possessing metal in both **Sm** and **La** pores) or hybrid of two catalysts in which one contains metal in mostly type **Sm** pores and the other possesses metals in largely type **La** pores.

It must be noted that the proposed design concept is still in the hypothetical stage and needs to be tested and verified in an experimental program. Many fundamental and practical questions need to be answered by future research with continuous flow tests coupled with detailed characterization of the catalysts before and after the reactions.

Although the proposed concept is not yet fully established, a promising direction of research has been identified. We hope to apply this concept in further experimental and characterization studies for developing new catalysts for low-temperature hydrogenation, desulfurization, and denitrogenation of distillate fuels. The proposed concept may also have some implications on the design and development of nitrogen-resistant hydrotreating catalysts (21).

## Acknowledgments

The author is grateful to Prof. H. H. Schobert for his encouragement and support, and to Drs. A.D. Schmitz, S.-D. Lin, W.-C. Lai, and K.M. Reddy for helpful discussions on catalytic hydrogenation. A different version of this article is being considered for publication in the American Chemical Society magazine *Chemtech* in 1999.

## Literature Cited

- (a) Cooper, B. H.; Donnis, B. B. L., *Appl. Catal. A.*, **1996**, 137, 203; (b) Khan, R. M.; Reynolds, J. G. *Chemtech*, **1996**, 26, 56; (c) Unzelman, G. H. *Fuel Reformulation*, **1993**, 38; (d) Kreucher, W. M. *Chem. Ind.*, **1995**, 601.
- (a) Maxwell, I. E. *CATTECH*, **1997**, 1, 5; (b) ABB Lummus Global Inc. *Hydrocarbon Process.*, **1997**, 76 (2), 37.
- (a) Stork, W. H. J. *Am. Chem. Soc. Sym. Ser.*, **1996**, 634, 379; (b) Absi-Halabi, M.; Stanislaus, A.; Qabazard, H. *Hydrocarbon Process.*, **1997**, 76 (2), 45.
- (a) Suchanek, A. *Am. Chem. Soc. Div. Petrol. Chem. Prepr.*, **1996**, 41, 583; (b) Lucien, J. P.; van den Berg, J. P.; Germaine, G.; van Hooijdonk, H. M. J. H.; Gjers, M.; Thielemans, G. L. B. "Shell Middle Distillate Hydrogenation Process", in *Catalytic Hydroprocessing of Petroleum and Distillates*. Oballa, M. C.; Shih, S. S. Eds.; Marcel Dekker: New York, NY, 1994, pp. 291-313; (c) Cooper, B. H.; Sogaard-Anderson, P.; Nielsen-Hannerup, P. "Production of Swedish Class I Diesel Using Dual-Stage Process", in *Catalytic Hydroprocessing of Petroleum and Distillates*. Oballa, M. C.; Shih, S. S. Eds.; Marcel Dekker: New York, NY, 1994, pp. 279-290; (d) Marchal, N.; Kasztelan, S.; Mignard, S. "A Comparative Study of Catalysts for the Deep Aromatic Reduction in Hydrotreated Gas Oil", in *Catalytic Hydroprocessing of Petroleum and Distillates*. Oballa, M. C.; Shih, S. S. Eds.; Marcel Dekker: New York, NY, 1994, pp. 315-327.
- Song, C.; Schmitz, A. D., *Energy Fuels*, **1997**, 11, 656.
- Lin, S.D.; Song, C. *Catal. Today*, **1996**, 31, 93.
- Schmitz, A. D.; Song, C. *Catal. Today*, **1996**, 31, 45.
- Reddy, K. M.; Song, C. *Mat. Res. Soc. Sym. Proc. Ser.*, **1997**, 454, 125.
- Sugioka, M.; Sado, F.; Matsumoto, Y.; Maesaki, N. *Catal. Today*, **1996**, 29, 255.
- Yasuda, H.; Yoshimura, Y., *Catal. Lett.*, **1997**, 46, 43.
- Navarro, R.; Pawelec, B.; Fierro, J.L.G.; Vasudevan, P.T.; Cambra, J.F.; Arias, P.L., *Appl. Catal. A.*, **1996**, 137, 269.
- Dalla Betta, R. A.; Boudart, M. *Proc. 5th Int. Congr. Catal.*, **1972**, p.1329.
- Stanislaus, A.; Cooper, B. H. *Catal. Rev. - Sci. Eng.*, **1994**, 36, 75.
- Sachtler, W. M. H.; Zhange, Z., *Adv. Catal.*, **1993**, 39, 129.
- Mojie, B. L.; Kappers, M.J.; Muijsers, J.C.; Niemantsverdriet, J.W.; Miller, J.T.; Modica, F.S.; Koningsberger, D.C., *Stud. Surf. Sci. Catal.*, **1994**, 84, 909.
- Rhodes, A. K. *Oil Gas J.*, **1997**, 95, 41.
- (a) Satterfield, C. N. *Heterogeneous Catalysis in Industrial Practice*, McGraw-Hill, New York, 2nd Ed., **1991**, Chapter 6, p.194; (b) Conner, W. C.; Falconer, J. *Chem. Rev.*, **1995**, 95, 759.
- Song, C.; Schobert, H. H.; Matsui, H. *Am. Chem. Soc. Div. Fuel Chem. Prepr.*, **1991**, 36, 1892.
- Ueda, K.; Matsui, H.; Song, C.; Xu, W. *J. Japan Petrol. Inst.*, **1990**, 33, 413.
- Wada, T.; Kaneda, K.; Murata, S.; Nomura, M., *Catal. Today*, **1996**, 31, 113.
- Song, C. *Am. Chem. Soc. Div. Petrol. Chem. Prepr.*, **1998**, 43, 573.

# Author Index

- Bhaumik, Asim, 73  
Bunker, Bruce C., 353  
Chang, Clarence D., 96  
Chen, Nai Y., 39  
Chen, Yuling, 322  
Davis, Burtron H., 145  
Dhar, Murali G., 130  
Duan, Nian-Gao, 80  
Fan, Zhongbi, 236  
Fu, Yingrui, 236  
Garcés, Juan M., 1  
Gnep, N.S., 334  
Guisnet, M., 334  
Hanaoka, T., 260, 271  
Hongchen, Guo, 201  
Igarashi, A., 260, 271  
Inui, Tomoyuki, 115  
Katayama, Atsuhiko, 292  
Kikuchi, E., 282  
Kim, Anthony Y., 353  
Kim, J.-H., 162  
Kim, Jong-Ho, 181  
Kokotailo, George 145  
Komatsu, T., 162  
Kubota, Y., 260, 271  
Kunieda, Takehisa, 181  
Kunimori, K., 260, 271  
Li, X. Shari, 353  
Long, Xiangyun, 188  
Ma, Xiaoliang, 305  
Ma, Ying, 80  
Matsuda, T., 282  
Matsuzaki, T., 260, T., 271  
Mitamura, Shuichi, 292  
Mizukami, Fujio, 292  
Morin, S., 334  
Nakajima, K., 260, K., 271  
Niwa, Miki, 181  
Niwa, Shu-ichi, 292  
Okuhara, Toshio, 369  
Peden, Charles F., 353  
Ramaswamy, A.V., 225  
Rao, B.S., 225  
Rao, T.S.R. Prasada, 130  
Ray, N., 130  
Schobert, Harold H., 305  
Shaikh, R.A., 225  
Song, Chunshan, 1, 248, 305, 381  
Sugi, Y., 260, 271  
Sugi, Yoshihiro, 1  
Suib, Steven L., 80  
Takahashi, N. 282  
Takeuchi, Genki, 292  
Tang, Youqi, 188  
Tatsumi, Takashi, 73  
Teng, Zuguang, 236  
Tian, Huiping, 236  
Toba, Makoto, 292  
Tungate, Fred L., 145  
Venuto, Paul B., 66  
Viswanadham, N., 130  
Wang, Jin-Yun, 80  
Wang, Li-Qiong, 353  
Wang, Yong, 353  
Wang, Yuguo, 145  
Watanabe, Ryu-ichi, 369  
Weisz, Paul B., 18  
Xia, Guan-Guang, 80  
Xiangsheng, Wang, 201  
Xie, Youchang, 188  
Yashima, T., 162  
Yoshinaga, Yusuke, 369  
Zhang, Jianqiu, 236  
Zhang, Weilin, 236  
Zhao, Biying, 188

# Subject Index

## A

- Acid catalysts, solid. *See* Naphthalene isopropylation over solid acid catalysts; Tungstophosphoric acid (PW) on mesoporous silica
- Acid catalytic surface  
comparison of product distributions from variety of reactant charges, 32, 34*f*  
internal events, 29, 32  
methanol conversion, 33*f*
- Acid monodimensional molecular sieves. *See* Tunnel shape selectivity
- Acid montmorillonite, hydrocarbon conversion, 32, 33*f*
- Acid sites, effect on external surface of zeolite crystallites, 167, 174
- Acid strength  
effect in methylation of 2-methylnaphthalene, 175, 177  
effect on MFI catalysts in ethylation of ethylbenzene, 168, 170
- Acylation, synthesis of organic chemicals, 10*t*
- Alcohol dehydration reactions, reactant shape selectivity, 6
- Alkane dehydrocyclization with Pt-silicalite catalysts  
amounts of benzene and toluene with PtSi-1-A and PtSi-1-B, 149  
aromatic selectivity from conversion of 3-methylheptane, 156–157  
C<sub>8</sub> aromatic distribution from *n*-octane conversion with PtSi-2-B, 154–155  
catalyst preparation, 146  
conversion of 2-methylheptane with Pt-Si-3B, 150–151  
conversion of 3-methylheptane with Pt-Si-3B, 149–150  
conversion of *n*-octane and 3-methylheptane over acidic Pt-Si-1-A, 147  
conversion of *n*-octane and 3-methylheptane over non-acidic Pt-Si-1-B, 147–148  
conversion of *n*-octane with Pt-Si-2-B at 620°C, 151, 152*t*  
conversion of *n*-octane with Pt-Si-3B, 149–150  
experimental procedures, 146  
feed rate of *n*-octane, 154  
high selectivity of aromatization of hexane with Pt-KL zeolite catalysts, 157  
hydrogenolysis by multiple adsorptions of ethylbenzene, 157  
possible role of shape selectivity, 145  
preparing catalysts with dispersed platinum in channels of ZSM-5, 154  
product distribution from conversion of 3-methylheptane over Pt-Si-2-B at 620°C, 156  
relative intensities of 2θ for silicalite and PtSi-2 catalysts, 154*t*  
structures leading to ethylbenzene and *p*-xylene, 157–158, 158  
X-ray diffraction (XRD) for crystalline material analysis, 148  
XRD data for PtSi and silicalite catalysts, 151, 154  
XRD of silicalite, PtSi-2-A and PtSi-2-B, 153*f*
- Alkanes  
chemical and physical steps of *n*-alkane hydroisomerization and hydrocracking, 347  
coking and deactivation of mordenite catalysts, 348–350  
distribution of products of *n*-butane transformation, 346*f*  
*n*-heptane transformation at 250°C, 348*f*  
transformation over mordenite catalysts, 345–348  
*See also* Oxidation of alkanes; Tunnel shape selectivity
- Alkylations  
4-*t*-butylphenol (TBP) using tungstophosphoric acid (PW) supported on silica, 365*f*, 366–367  
naphthalene and biphenyl, shape-selective opportunity, 56  
shape-selective of biphenyl, 253–254  
shape-selective of naphthalene, 251–253  
synthesis of organic chemicals, 10*t*  
xylenes over methanol, 230–231  
*See also* Biphenyl alkylation over H-mordenite; 2,6-Diisopropylnaphthalene synthesis by alkylation
- Alkylbenzenes, linear, opportunity in shape-selective catalysis, 56
- 4-Alkylbiphenyls  
isopropylation and ethylation, 267, 268*f*  
*See also* Biphenyl alkylation over H-mordenite
- Aluminosilicates. *See* Tunnel shape selectivity
- Amorphous silica-alumina, isopropylation of naphthalene, 302–303
- Antimony oxide. *See* Methylation of toluene
- Aromatic hydrocarbons, polycyclic (PAH)  
selective formation with dealuminated H-mordenite, 282–283



See also 2,6-Diisopropyl-naphthalene synthesis by alkylation; Polycyclic hydrocarbon conversion over zeolites

Aromatic polyester technology, isomerization of xylenes, 51–52

Aromatization of natural gas, non-oxidative condition, 57

Aromatization reactions. See Cracking and aromatization reaction of *n*-heptane

## B

Beckmann rearrangement

caprolactam production, 54–55

effect of solvent, 55, 56*t*

performance of various zeolites, 55

Benzene, oxidative hydroxylation to phenol, 53

Benzoylation, synthesis of organic chemicals, 10*t*

Biphenyl

alkylation opportunity in shape-selective catalysis, 56

isopropylation with propylene at 250°C, 254*t*

shape-selective alkylation over zeolites, 253–254

Biphenyl alkylation over H-mordenite

alkylation reaction procedures, 261

alkylation with different alkenes, 267

effect of reaction temperature on ethylbiphenyl (EBP) and diethylbiphenyl (DEBP) isomers in ethylation, 262*f*

ethylation, 261, 263, 267

experimental, 261

isopropylation and ethylation of 4-

alkylbiphenyls, 267, 268*f*

mechanism elucidation, 267, 269

product analysis, 261

profiles of ethylation of 3-EBP, 263, 266*f*

profiles of ethylation of 4-EBP, 263, 265*f*

profiles of formation of DEBP isomers in

ethylation, 263, 264*f*

profiles of formation of EBP isomers in

ethylation, 263, 264*f*

rate of ethylation of BP, 3-EBP, 4-EBP, and

4,4'-DEBP, 263, 266*f*, 267

selectivity of least bulky isomers in BP

alkylation, 268*f*

Biphenyl isopropylation over H-mordenite

catalysts and reagents, 272

effect of propene pressure on encapsulated products inside pores, 278, 279*f*, 280*f*

effect of SiO<sub>2</sub>/Al<sub>2</sub>O<sub>3</sub> ratio of H-mordenite (HM) on bulk and encapsulated products, 274*f*

effect of SiO<sub>2</sub>/Al<sub>2</sub>O<sub>3</sub> ratio of HM on

selectivity of 3,4'- and 4,4'-

diisopropylbiphenyl (4,4'-DIPB) in bulk and encapsulated products, 274*f*

effect of SiO<sub>2</sub>/Al<sub>2</sub>O<sub>3</sub> ratio of HM, 272–275

effects of propene pressure on isopropylation, 275

effects of propene pressure on selectivity of 4,4'-DIPB, 277*f*

effects of propene pressure on yield of 3,4'- and 4,4'-DIPB, 277*f*

experimental, 272

isomerization of 4,4'-DIPB under propene pressure, 275, 278, 279*f*

isomerization of 4,4'-DIPB under propylene pressure, 273, 276*t*

isopropylation reaction procedures, 272

shape selectivity of 4,4'-DIPB, 278, 281

thermogravimetric profiles of HM, 275, 276*f*

Body temperature, in vivo, shape-selective catalysis, 56–57

Boron, effect on HZSM-5 catalyst in methylation, 178

Boron oxide. See Methylation of toluene

Bromination of toluene, *p*-selective organic synthesis over zeolites, 69

Bulkiness of reagents. See Biphenyl alkylation over H-mordenite

*n*-Butane. See Pt-porous heteropoly compounds

Butene isomerization, selective skeletal, 44

3-Buten-1-ol, cyclization, 74, 76

4-*t*-Butylphenol, alkylation by styrene using tungstophosphoric acid (PW) supported on silica, 366–367

## C

Cage effect, alkane isomerization to multibranched isomers, 43–44

ε-Caprolactam technology

Beckmann rearrangement of cyclohexanone oxime over zeolites, 54

effect of acidity on catalyst performance, 54*t*

effect of solvent on Beckmann rearrangement, 55, 56*t*

performance of various zeolites, 55*t*

uses, 53–54

Catalysis, heterogeneous selectivity types, 3–4

Catalyst, description, 2

Catalytic cracking. See Cracking, catalytic

Catalytic oxidations, organic synthesis over zeolites, 70

Chabazite

*ab initio* molecular dynamics simulation of methanol activation, 103

window effect, 29

Chemical detection technologies, potential, 35, 36*f*

- Chemical industry, future, 32
- Chemical liquid deposition (CLD)  
 combined modifications for HZ catalyst series, 215–218  
 effect on performance of HZSM-5 catalyst, 214*t*  
 external surface reaction HZSM-5 catalyst with organosilicon compound, 212, 214–215
- Chemical sensors, potential, 35, 36*f*
- Chemical synthesis  
 applications of shape-selective catalysis, 9–11  
 shape-selective processes for organic chemical synthesis, 10*t*
- Chemical vapor deposition (CVD)  
 combined modifications for HZ catalyst series, 215–218  
 external surface reaction HZSM-5 catalyst with organosilicon compound, 212–214  
 silylation of ZSM-5 zeolites, 226–227  
 zeolite modification method, 181–182  
*See also* Para shape selectivity
- Chlorinations, synthesis of organic chemicals, 10*t*
- Clinoptilolite, non-shape-selective, 22
- Clogging, science-technology symbiosis, 27
- Coke  
 coke-burning analysis by thermogravimetric analysis, 218*t*  
 effect of formation on shape selectivity, 135–137  
 effect of foreign materials on shape selectivity, 132–133  
 effect of reaction conditions on performances of highly selective catalysts, 220–222  
 effect of reaction severity on coke amount and enhanced *p*-selectivity, 136*t*  
 effect on pore diameter of zeolite, 143*f*  
 enhanced shape selectivity due to coke formation, 137*f*  
 pore dimension modification, 131  
 pore dimension reduction, 136  
 thermogravimetric coke-burning curves of catalysts with combined modifications, 216, 217*f*
- Coking  
 analysis of HZSM-5 zeolites with different crystal sizes, 223*t*  
 initial activities and deactivation coefficients, 349*t*  
 mordenite catalysts, 348–350  
 reducing components transport rates, 27
- Combustion, shape-selective conversions over Pt incorporated Ca-A zeolite, 21*t*
- Computational analysis. *See* Naphthalene alkylation, computational analysis
- Conformational isomerization, decalins, 254–255
- Constraint index, definition, 29
- Cracking, catalytic  
 coking and deactivation of mordenite catalysts, 348–350  
 initial activities and deactivation coefficients, 349*t*  
 shape-selective cracking of heavy oil, 329–330  
 zeolite catalysts, 322–323  
*See also* Hydrothermal dealumination
- Cracking and aromatization reaction of *n*-heptane  
 amorphous materials, 132–133  
 coke, 132–133  
 density functional theory for micro and meso pore size distributions, 140, 142  
 dependence of concentration of aluminum types on steaming severity of ZSM-5, 133*t*  
 effect of amorphous materials in zeolites, 137–138  
 effect of coke formation on shape selectivity, 135–137  
 effect of coke on pore diameter of zeolite channels, 143*f*  
 effect of coke on pore size distribution of catalyst, 140*t*, 141*f*  
 effect of extra framework alumina on shape selectivity, 134–135  
 effect of foreign materials on shape selectivity, 132–133  
 effect of reaction severity on coke amount and enhanced *p*-selectivity, 136*t*  
 enhance shape selectivity due to coke formation, 137*f*  
 evidence for molecular traffic control mechanism, 138–143  
 experimental procedures, 132  
 extra framework aluminum, 132–133  
 molecular traffic control (MTC) in ZSM-5 channels, 139*f*  
 synthesis of ZSM-5 without aid of organic template, 133  
 typical product distribution in *n*-heptane aromatization, 134*t*
- Crystallinity of USY zeolite  
 changes during hydrothermal treatment, 324  
 crystallinity of precursors and USY products, 325*t*  
 sample preparations, 323  
 X-ray diffraction patterns of samples at different stages, 324*f*  
*See also* Hydrothermal dealumination
- Crystal size  
 analysis of HZSM-5 zeolites with different

crystal sizes, 223*t*  
 effect on deactivates rates of HZSM-5 catalysts, 223*f*  
 effect on *para*-selectivity of HZSM-5 catalysts, 203*t*  
 nano-sized HZSM-5 zeolite for ethylation of ethylbenzene, 222–223  
 Crystal structure, molecular sieves, 40  
 Cumene  
 phenol synthesis, 52  
 cracking, effect of tributylphosphite treatment on H-mordenite, 288, 289*f*  
 Cyclizations. *See* Regioselective cyclizations  
 Cyclodimerization, synthesis of organic chemicals, 10*t*  
 Cyclohexane  
 effects of TEMPO radical trap on oxidation, 87–88, 91  
 oxidation with different catalysts, 83–84, 88–89  
 product distribution, 86, 87*t*  
 relationships of rates and catalysts, 86–87  
*See also* Oxidation of alkanes  
 Cyclohexanone oxime, • -caprolactam technology, 53–56

## D

Dealumination. *See* Hydrothermal dealumination  
*cis*-Decalin  
 oxidation with different catalysts, 84, 86, 89–90  
 relationships of rates and catalysts, 86–87  
*See also* Oxidation of alkanes  
 Decalins, conformational isomerization, 254–255  
 Dehydrocyclizations  
*n*-hexane, 45  
 organic synthesis over zeolites, 70  
 synthesis of organic chemicals, 10*t*  
*See also* Alkane dehydrocyclization with Pt-silicalite catalysts  
 Density-functional theory (DFT)  
 carbene generation from methanol, 102  
 comparing heats of adsorption and activation barriers in C–C bond formation, 102–103  
 energetics of routes to dimethyl ether, 101–102  
 methanol-to-hydrocarbons reaction, 101  
 micro and meso pore size distributions, 140, 142  
 Desulfurization. *See* Noble metal catalysts  
 Dialkyl-naphthalenes  
 frontier electron density, 314  
 molecular dimensions, 307–314  
 origin of shape selectivity to 2,6-dialkyl-naphthalene (2,6-DAN), 314–319  
 synthesis, 292–293  
*See also* Naphthalene alkylation, computational analysis; Naphthalene isopropylation over solid acid catalysts  
 Dicyclopentadiene, liquid phase oligomerization, 49–50  
 Diethylbenzene. *See* Ethylation of ethylbenzene  
*para*-Diethylbenzene, *para*-selective alkylation product, 51  
*para*-Diethylbenzene synthesis (PDEB)  
 activity and durability of HZ-D catalyst, 217*t*  
 characteristics of industrial EA catalyst series, 219*t*  
 chemical liquid deposition (CLD) silica method, 212, 214–215  
 chemical vapor deposition (CVD) SiO<sub>2</sub> method, 212  
 coke-burning analysis by thermogravimetric analysis, 218*t*  
 coking analysis of HZSM-5 zeolites with different crystal sizes, 223*t*  
 combined modifications, 215–218  
 correlation of feed stream velocity with PDEB selectivity of EA-01 catalyst, 222*f*  
 diffusivity data of catalysts with or without steaming, 207*t*  
 direct methods, 201–202  
 direct synthesis at industrial scale, 218–222  
 effect of CLD SiO<sub>2</sub> on performance of WZ (HZSM-5 catalyst), 214*t*  
 effect of combined modifications on HZSM-5 properties, 215*t*  
 effect of crystal size on deactivation rates of HZSM-5 catalysts, 223*f*  
 effect of EB/C<sub>2</sub><sup>≡</sup> on EA-03 performance, 220*t*  
 effect of P<sub>2</sub>O<sub>5</sub>-impregnation on pre-modified HZSM-5 (DGA), 210*t*  
 effect of reaction conditions on EA catalyst performance, 220–222  
 effect of steaming on reaction performance of HZSM-5, 206*f*  
 effect of temperature on EA-03 performance, 220*t*  
 effect of temperature on performance of different *para*-selective catalysts, 221*f*  
 effect of temperature on selectivity of HZSM-5, 204*t*  
 effect of WHSV<sub>EB</sub> on and EB/C<sub>2</sub><sup>≡</sup> on selectivity of HZSM-5, 204*t*  
 effect of WHSV<sub>EB</sub> on EA-03 performance, 220*t*  
 elimination of *ortho*-diethylbenzene, 202  
 ethylation over HZSM-5 impregnated with

- different oxides, 208*t*
- external surface reaction with organosilicon compound, 212–215
- high temperature steaming, 205–207
- impregnation eliminating side reactions, 208
- impregnation onto pre-modified HZSM-5, 210–212
- impregnation onto virgin HZSM-5, 208–209
- impregnation with cations or anions, 207–212
- increases in *para*-selectivity of HZ series, 216
- modes of combined modifications for HZ catalyst series, 216*t*
- modification methods for *para*-selective catalysis, 202–203
- nano-sized ZSM-5 zeolite as catalyst for ethylation of ethylbenzene with ethylene, 222–223
- NH<sub>3</sub> TPD profiles of H-type and steamed HZSM-5, 207*f*
- NH<sub>3</sub> TPD profiles of P<sub>2</sub>O<sub>5</sub>-impregnated DGA series, 211*f*
- para*-selectivity of different HZSM-5 zeolites, 203*t*
- performance of EA catalysts, 218–219
- preparation of HZSM-5 catalyst and its ethylation selectivity, 203–205
- preparations of industrial EA catalysts, 218
- reaction data of fresh EA-03 catalyst in 1000tPDEB/a industrial unit, 219*t*
- reaction stability of oxide-impregnated HZSM-5 zeolites, 209*f*
- selective catalysis characteristics of ZSM-5 zeolite, 202
- sorption capacity of P<sub>2</sub>O<sub>5</sub>-impregnated DGA, 211*t*
- thermodynamic equilibrium of DEB isomers, 204*t*
- thermogravimetric coke-burning curves of HZ-B and HZ-C, 217*f*
- uses, 201
- using improved in situ CVD methods, 212
- See also* Ethylation of ethylbenzene
- Diethylbiphenyls (DEBP). *See* Biphenyl alkylation over H-mordenite
- Diffusion, shape selectivity and, 26–27
- Diffusivity measurement, science-technology symbiosis, 27
- 4,4'-Disisopropylbiphenyl (4,4'-DIPB). *See* Biphenyl isopropylation over H-mordenite
- 2,6-Diisopropyl-naphthalene synthesis by alkylation catalysts, 283
- catalytic performances of H-mordenite (HM), 283–286
- catalytic performances of HM with different SiO<sub>2</sub>/Al<sub>2</sub>O<sub>3</sub> ratios, 285*t*
- catalytic performances of tributylphosphite (TBP) modified HM (TBP-HM), 286, 288–290
- catalytic studies, 283
- effect of TBP treatment on catalytic activity of HM(18) for cracking of cumene and 1,3,5-triisopropylbenzene, 288, 289*f*
- effect of TBP treatment on catalytic performances of HM with different SiO<sub>2</sub>/Al<sub>2</sub>O<sub>3</sub> ratios, 287*t*
- effect of TBP treatment on catalytic properties of HM(18) for alkylation of 2-isopropyl-naphthalene (2-IPN), 288, 290
- experimental, 283
- NH<sub>3</sub>-TPD spectra of HM(18) and TBP-HM(18) treated at 3 times, 288, 289*f*
- relation between bulk and surface SiO<sub>2</sub>/Al<sub>2</sub>O<sub>3</sub> ratios, 284, 286, 287*f*
- selectivity of HM(18) for 2,6-DIPN and 2,7-DIPN as function of conversion levels, 284, 285*f*
- slurry phase alkylation of 2-IPN, 283, 290
- Diisopropyl-naphthalenes (DIPN)
- catalysis over amorphous silica-alumina, 302–303
- catalysis over H L-zeolite, 302
- catalysis over H mordenite, 298–300
- catalysis over H Y-zeolite, 300–302
- catalysis over H ZSM-5, 302
- catalytic isopropylation of naphthalene with propene, 295*t*, 296*t*
- molecular dimensions, 307–314
- origin of shape selectivity to 2,6-dialkyl-naphthalene (2,6-DAN), 314–319
- product or transition-state selectivity, 319
- reaction paths producing, 295–298
- shape-selectivity in synthesis, 305–307
- time course of DIPN groups in isopropylation of naphthalene, 298*f*, 299*f*
- See also* Naphthalene alkylation, computational analysis; Naphthalene isopropylation over solid acid catalysts
- Dimethylnaphthalene (DMN). *See* Methylation of 2-methylnaphthalene (2-MN)
- 2,4-Dimethylquinoline (2,4-DMQ), poisoning acid sites of catalyst, 167*t*
- Diphosphorus pentoxide P<sub>2</sub>O<sub>5</sub>
- impregnation onto premodified HZSM-5 catalyst (DGA), 210–212
- impregnation on virgin HZSM-5, 208–209
- NH<sub>3</sub> TPD profiles of P<sub>2</sub>O<sub>5</sub>-impregnated DGA catalyst series, 211*t*
- sorption capacity of P<sub>2</sub>O<sub>5</sub>-impregnated DGA, 211*t*
- See also para*-Diethylbenzene synthesis (PDEB)

Disproportionation  
ethylbenzene over silylated zeolites, 232  
*para*-xylene production, 25  
synthesis of organic chemicals, 10*t*  
transition-state shape selectivity of  
dialkylbenzenes, 8  
Durene, zeolite shape-selectivity, 97–98

## E

Encapsulated products. *See* Biphenyl  
isopropylation over H-mordenite  
Environmental science, potential, 35  
Erionite, first commercial shape-selective  
process using, 22–23  
Ethylation of ethylbenzene  
coking analysis of HZSM-5 zeolites with  
different crystal sizes, 223*t*  
effect of acid sites on external surface, 167  
effect of acid strength, 168, 170  
effect of contact time on fraction of  
diethylbenzene isomer, 166*f*  
effect of crystal size on deactivation rates of  
HZSM-5 catalysts, 223*f*  
effect of pore tortuosity, 167–168  
ethylation with ethanol on MFI catalysts, 165*t*  
experimental, 163–164  
generation of *para*-selectivity, 170  
nano-sized ZSM-5 zeolite as catalyst with  
ethylene, 222–223  
*para*-selectivity, 164  
*para*-selectivity of modified HZSM-5 zeolites,  
163  
poisoning acid sites on external surface with  
2,4-dimethylquinoline (2,4-DMQ), 167*t*  
primary product, 164–165  
relation between *para*-selectivity and acid  
strength of catalysts, 173*f*  
relation between *para*-selectivity and pore  
tortuosity of catalysts, 169*f*, 171*f*  
typical *o*-xylene uptake curves for modified  
HZSM-5 and Me-MFI catalysts, 169*f*  
typical profiles of NH<sub>3</sub>-TPD (temperature  
programmed desorption of ammonia) for  
HZSM-5 and Me-MFI, 171*f*  
*See also para*-Diethylbenzene synthesis  
(PDEB); MFI-type metallosilicates  
Ethylations. *See* Biphenyl alkylation over H-  
mordenite  
Ethylbenzene  
catalytic conversion over P-HY zeolites, 240–  
241  
disproportionation with silylated zeolites, 232  
influence of acidity on conversion, 244*f*  
mechanism of cracking, 244*f*  
styrene technology, 50–51

transformation over P-HY zeolites at 683 K,  
244*t*  
Ethylbiphenyls (EBP). *See* Biphenyl alkylation  
over H-mordenite  
External surface acidity  
inactivation by depositing silica from various  
silicon compounds, 183*f*  
inactivation dependent on selected molecule,  
182  
plot versus external surface area, 186*f*  
three-dimensional plot of selectivity against  
pore-opening size and, 184*f*  
External surface reactions  
chemical liquid deposition (CLD) method,  
212, 214–215  
chemical vapor deposition (CVD) method,  
212–214

## F

Ferrierite  
*ab initio* molecular dynamics simulation of  
methanol activation, 103  
isobutene selectivity, 44  
Fischer–Tropsch waxes, conversion to low pour  
point distillates, 42  
Fluid catalytic cracking (FCC) catalysts, HY  
zeolite active component, 236–237  
Frontier orbital density  
naphthalene alkylation, 314, 319  
*See also* Naphthalene alkylation,  
computational analysis  
Fuel cells, hydrogen, transportation, 57–58  
Fuels, high energy high density  
liquid phase oligomerization of  
dicyclopentadiene, 49–50  
liquid phase oligomerization of norbornene,  
49  
rocket fuel JP-10 synthesis, 49  
shape-selective catalysis advances, 48–50  
Future potential  
chemical sensors, 35, 36*f*  
selective chemical detection technologies, 35,  
36*f*  
shape selectivity catalysis, 32, 35

## G

Gmelinite, testing mineral samples, 20

## H

H-ferrierite. *See* Naphthalene isopropylation  
over solid acid catalysts

- H L-zeolite**  
 isopropylation of naphthalene, 302  
 properties, 294*t*  
*See also* Naphthalene isopropylation over solid acid catalysts
- H-mordenite**  
 isopropylation of naphthalene, 298–300  
 properties, 294*t*  
*See also* Biphenyl alkylation over H-mordenite; Biphenyl isopropylation over H-mordenite; 2,6-Diisopropylnaphthalene synthesis by alkylation; Naphthalene isopropylation over solid acid catalysts
- H offretite/erionite.** *See* Naphthalene isopropylation over solid acid catalysts
- H Y-zeolites**  
 isopropylation of naphthalene, 300–302  
 properties, 294*t*  
*See also* Naphthalene isopropylation over solid acid catalysts; Phosphorus with HY zeolites
- Half-cavities, zeolite MCM-22,** 46
- Heavy oil**  
 cracking abilities of USY zeolites, 330*t*  
 shape-selective cracking, 329–330
- n*-Heptane.** *See* Cracking and aromatization reaction of *n*-heptane
- Heterogeneous catalysis**  
 future, 32  
 general selectivity types, 3–4  
 use in U.S. chemical and petroleum industries, 1
- n*-Hexane**  
 oxidation with different catalysts, 84, 85*t*, 89  
 relationships of rates and catalysts, 86–87  
*See also* Oxidation of alkanes
- 5-Hexen-1-ol, cyclization,** 75
- cis*-4-Hexen-1-ol, cyclization,** 75, 77
- High-temp heat-resistant polymers**  
 structures, 249*t*  
*See also* Polycyclic hydrocarbon conversion over zeolites
- Hydrocarbon conversion.** *See* Polycyclic hydrocarbon conversion over zeolites
- Hydrocarbon processing**  
 applications of shape-selective catalysis, 11–12  
 selective catalytic processes, 11*t*
- Hydrocarbons**  
 future of industry, 32, 35  
 product distributions for acid catalyzed conversions of variety of reactant charges, 32, 34*f*  
 selectofoming process, 40
- Hydrocracking, combination with**  
 hydroisomerization, 42
- Hydrodesulfurization.** *See* Noble metal catalysts
- Hydrogen**  
 fuel cells for transportation, 57–58  
 on board production by steam reforming of gasoline fuel, 58
- Hydrogen spillover.** *See* Noble metal catalysts
- Hydrogenation**  
 effect of metal type and zeolite, 384  
 engineered shape selectivity in Pt-containing Na-mordenite, 21*t*  
 hydrotreating sulfur-containing distillates, 381  
 products from added benzothiophene over zeolite-supported catalysts during naphthalene, 387  
 regio-selective of 1-naphthol and quinoline, 256–257  
 role of acidic zeolite supports for aromatics, 384  
 shape-selective conversions over Pt incorporated Ca-A zeolite, 21*t*  
 shape-selective of naphthalene, 255–256  
 synthesis of organic chemicals, 10*t*  
*See also* Noble metal catalysts
- Hydroisomerization**  
 differences in C<sub>7</sub> isomer distribution, 42, 43*t*  
 selective conversion of paraffinic fraction, 41–42
- Hydrothermal dealumination**  
 catalyst testing, 323  
 conventional method for USY-I (A) preparation, 323  
 cracking abilities of zeolite USY-II (E) and A, 330*t*  
 crystallinity changes of E<sub>0</sub> and A<sub>0</sub> during hydrothermal treatment, 324  
 crystallinity of precursors and USY products, 325*t*  
 hydrothermal-chemical dealumination for E preparation, 323  
 hydrothermal structure-stability of pseudo-HY zeolite, 327  
 improving USY zeolite crystallinity, 322–323  
 IR spectra of A and E samples at different stages, 325*f*  
 performance of pseudo-HY zeolite, 326–328  
 physicochemical measurement, 323  
 pore volume of USY, 329*t*  
 reaction mechanism of conventional and hydrothermal-chemical dealumination, 328*f*  
 sample preparations, 323  
 secondary porosity and crystallinity of E, 327–329  
 shape-selective cracking of heavy oil, 329–330  
 structure characterization of E<sub>0</sub> and pseudo-

HY zeolite, 325–326  
 transmission electron microscopy (TEM)  
 photograph of E, 329f  
 unit cell contraction of  $\text{NH}_4^+$  and  $\text{H}^+$   
 exchanged Y-zeolite, 326–327  
 X-ray diffraction (XRD) patterns of A at  
 different stages, 324f  
 XRD patterns of E at different stages, 324f  
 zeolite characteristics, 322–323

## I

**Impregnation modification**  
 cations or anions, 207–212  
 combined modifications for HZ catalyst  
 series, 215–218  
 effect of  $\text{P}_2\text{O}_5$  impregnation on pre-modified  
 catalyst (DGA) performance, 210t  
 eliminating side reactions, 208  
 ethylation over oxide-impregnated HZSM-5,  
 208t  
 impregnation on pre-modified HZSM-5, 210–  
 212  
 impregnation on virgin HZSM-5, 208–209  
 $\text{NH}_3$  TPD profiles of  $\text{P}_2\text{O}_5$ -impregnated DGA  
 series, 211t  
 reaction stability of oxide-impregnated  
 HZSM-5 zeolites, 209f  
 sorption capacity of  $\text{P}_2\text{O}_5$ -impregnated DGA,  
 211t  
*See also para-Diethylbenzene synthesis*  
 (PDEB)  
**Industrial scale synthesis, para-diethylbenzene,**  
 218–222  
**Internal reactor heat production, potential for**  
 controlled oxidation, 35  
**Intersecting channels of different size openings**  
 characteristics, 41–42  
 examples, 40t  
**Inverse shape selectivity,** 9  
**In vivo shape-selective catalysis, body**  
 temperature, opportunities, 56–57  
**Iron(III) oxide. *See para-Diethylbenzene***  
**synthesis (PDEB)**  
**ISODEWAXING process, lube dewaxing by**  
 wax isomerization, 42  
**Isomerizations**  
 bimolecular of *m*-xylene, 339f  
 conformational of decalins, 254–255  
 demonstration of bimolecular mode of xylene,  
 336–341  
 number of alkylation steps for bimolecular  
 isomerization of *m*-xylene, 340f  
 ring-shift over zeolite catalysts, 250–251  
 selective skeletal butene, 44

selectivity of xylene isomerization over  
 HMCM-41 samples, 338, 340  
 synthesis of organic chemicals, 10t  
*m*-xylene over silylated zeolites, 233–234  
*m*-xylene over various molecular sieves and  
 amorphous silica alumina, 337f  
*p*-xylene production, 25  
 xylenes, 51–52  
*See also* Pt-porous heteropoly compounds

## Isopropylations

4-alkylbiphenyls, 267, 268f  
*See also* Biphenyl alkylation over H-  
 mordenite; Biphenyl isopropylation over H-  
 mordenite; Naphthalene isopropylation over  
 solid acid catalysts  
 Isopropylbenzene, phenol synthesis, 52  
 2-Isopropyl-naphthalene (2-IPN)  
 effect of tributylphosphite (TPB) treatment on  
 H-mordenite catalytic properties for  
 alkylation of 2-IPN, 288, 290  
*See also* 2,6-Diisopropyl-naphthalene synthesis  
 by alkylation

## K

Kinetics, shape-selective catalysis, 2–4

## L

$\text{La}_2\text{O}_3$  modified HZSM-5  
 impregnation on virgin HZSM-5, 208–209  
 reaction stability of impregnated zeolites with  
 different amount of  $\text{La}_2\text{O}_3$ , 209f  
*See also para-Diethylbenzene synthesis*  
 (PDEB)  
**Leaching acid**  
 leaching of tungstophosphoric acid (PW) on  
 various silica by water at 50°C, 365f  
 relative amount of PW from silica supported  
 PW catalysts, 363, 366  
*See also* Tungstophosphoric acid on  
 mesoporous silica  
**Linear alkylbenzenes, opportunity in shape-**  
**selective catalysis,** 56  
**Liquid phase alkylation technology, styrene,** 51  
**Lubrication oil, dewaxing,** 25

## M

Magnesium oxide. *See para-Diethylbenzene*  
*synthesis (PDEB)*; Methylation of toluene  
 Manganese based catalysts  
 four different octahedral molecular sieves

- (OMS), 81, 82*f*  
*See also* Octahedral molecular sieves (OMS);  
 Oxidation of alkanes  
 Meerwein–Ponndorf–Verley reduction,  
 synthesis over zeolites, 69–70  
 Mesoporous molecular sieves  
 characteristics, 47  
 organic synthesis, 71  
 Mesoporous silica. *See* Tungstophosphoric acid  
 (PW) on mesoporous silica  
 Metal catalysts, noble. *See* Noble metal  
 catalysts  
 Metal-incorporated silicoaluminophosphate  
 catalysts. *See* Methanol-to-olefin conversion  
 Metallosilicates. *See* MFI-type metallosilicates  
 Methanol conversion, acid catalytic surface, 33*f*  
 Methanol-to-gasoline (MTG), organic synthesis  
 over zeolites, 71  
 Methanol-to-hydrocarbons reaction  
 activation of methane by zeolitic protons, 103  
 alkyl substituted cyclopentenyl carbenium  
 ions in catalyst, 108, 110  
 autocatalysis and beyond, 104, 106–111  
 autocatalysis in presence of aromatics, 104,  
 106, 107  
 calculated transition state geometry for H–D  
 exchange between methane and acid zeolite  
 cluster, 103, 105*f*  
 carbene-carbenoid mechanisms, 100  
 carbocationic mechanisms, 100  
 carbonium ion formation as transition state,  
 103–104  
 chemisorption in methanol activation, 101  
 complex kinetics and diffusion disguise of  
 methanol-to-gasoline (MTG) mechanism,  
 106  
 computational methodology, 101  
 computational methods to decipher initial C–  
 C bond formation from methanol, 102  
 critical step of removing proton from methyl  
 group, 100  
 cyclopentenyl cation intermediates of olefin  
 condensation reactions, 111  
 density-functional theory, 101  
 diffusion disguise, 108  
 Fischer–Tropsch process, 96  
 general characteristics, 97  
 hydrocarbon product distributions from  
 various O-compounds over HZSM-5, 109*t*  
 induction period, 108, 111  
 influence of zeolite pore geometry on MTG  
 aromatics distribution, 99*f*  
 initial C–C bond formation, 98, 100  
 mechanistic considerations, 98, 100–111  
 MTG process, 96  
 oxonium-ylide mechanisms, 100  
 proposed carbon pool mechanism for  
 methanol conversion, 105, 106, 108  
 proposed mechanisms for dimethyl ether  
 formation, 101–102  
 radical mechanisms, 100  
 red oils, 108, 111  
 shape-selectivity in tri- and  
 tetramethylbenzenes from MTG, 99*t*  
 zeolite shape-selectivity, 97–98  
 Methanol-to-olefin conversion  
 alternative route to light olefin synthesis, 115–  
 116  
 catalytic performance  
 MeAPSO-34 and its homologues, 118–120  
 metallosilicates having MFI structure, 117–  
 118  
 modified H-ZSM-5, 117  
 narrow-pore size zeolites, 116–117  
 SAPO-34 (silicon in AlPO family) and its  
 homologues, 118  
 controlling factors to prepare Ni-APSO-34  
 (nickel incorporated  
 silicoaluminophosphates), 120  
 correlation between acid density of external  
 surface of crystals and amount of deposited  
 coke, 125*f*  
 correlation between acid density of internal  
 surface of crystals and selectivity to  
 ethylene, 124*f*  
 highly selective Ni-APSO-34 catalyst in  
 methanol, 120–125  
 high selectivity of C<sub>2</sub>–C<sub>4</sub> olefins from  
 methanol, 119  
 post modifications improving catalytic  
 performance, 123  
 preparation procedure of Ni-APSO-34, 122*f*  
 reactions using SAPOs and MeAPSOs as  
 catalysts, 118–120  
 reliable procedure for synthesis of Ni-APSO-  
 34, 120, 123  
 unique selectivity to ethylene formation on  
 Ni-APSO-34, 119  
 various Ni-APSO-34 catalysts, procedures and  
 properties, 121*t*  
 zeolitic catalysts, 116–118  
 Methylation of 2-methylnaphthalene (2-MN)  
 effect of 2,4-dimethylquinoline (2,4-DMQ),  
 174, 175*t*  
 effect of acid sites on external surface, 174  
 effect of acid strength, 175, 177  
 effect of boron added to HZSM-5 in presence  
 of 2,4-DMQ, acid strength, and pore  
 tortuosity, 178*f*  
 effect of contact time on fraction of  
 dimethylnaphthalene (DMN) isomer, 173*f*  
 experimental, 172



- methylation on HZSM-5, 172
- methylation on HZSM-5 in presence of 2,4-DMQ, 174, 176f
- reaction path, 172, 174
- selective formation of 2,6-DMN, 177–179
- shape selective formation of DMN, 170
- studies with shape-selective zeolite catalysts, 170, 172
- summary of reaction paths, 176f
- See also* MFI-type metallosilicates
- Methylation of toluene
- alkylation of toluene with methanol, 190
- catalyst preparation, 190
- determination of dispersion threshold, 190
- dispersion thresholds of oxides on HZSM-5, 192t
- effect of B<sub>2</sub>O<sub>3</sub> loading on activity and selectivity, 194, 195f
- effect of MgO loading on activity and selectivity, 194, 195f
- effect of oxide loading on reaction over HZSM-5, 192, 194–197
- effect of Sb<sub>2</sub>O<sub>3</sub> loading on activity and selectivity, 194, 196f
- experimental, 190
- oxide and salts forming monolayer or submonolayer, 189
- oxide improving *para*-selectivity, 189
- oxide-modified HZSM-5, 188–189
- plot of relative crystalline MgO X-ray diffraction (XRD) peak intensity ratio versus total MgO content, 191f
- product shape selectivity, 6–7
- results of reactions over unmodified and modified HZSM-5, 194t
- spontaneous dispersion of oxides on HZSM-5 and dispersion thresholds, 190, 192
- strength of surface bonds between monolayer-dispersed compound and support surface, 189
- surface area as function of MgO loading on MgO/HZSM-5, 198f
- temperature programmed desorption (TPD) of NH<sub>3</sub>, 190
- threshold effect in specific surface areas of catalysts, 197
- threshold effect on surface acidity of catalysts, 197
- TPD results of MgO/HZSM-5 and Sb<sub>2</sub>O<sub>3</sub>/HZSM-5, 199f
- TPD spectra of B<sub>2</sub>O<sub>3</sub>/HZSM-5 samples and HZSM-5, 198f
- X-ray photoelectron spectroscopy (XPS) peak intensity ratio as function of total B<sub>2</sub>O<sub>3</sub> content, 193f
- XRD patterns of MgO/HZSM-5 with different MgO content, 191f
- Methylations, xylenes over silylated zeolites, 230–231
- 2-Methylheptane
- conversion with Pt-silicalite catalysts, 150–151
- See also* Alkane dehydrocyclization with Pt-silicalite catalysts
- 3-Methylheptane
- aromatic selectivity of conversion with Pt on noncrystalline silica or non-acidic alumina support, 156–157
- conversion with acidic and non-acidic Pt-Si catalysts, 147–148
- conversion with PtSi-2B, 156
- conversion with Pt-silicalite catalysts, 149–150
- See also* Alkane dehydrocyclization with Pt-silicalite catalysts
- MFI-type metallosilicates
- effect of acid strength, 168, 170
- effect pore dimension estimation, 164
- ethylation of ethylbenzene, 163–170
- methylation of 2-methylnaphthalene (2-MN), 170, 172–179
- shape selectivity in alkylation, 162–163
- See also* Ethylation of ethylbenzene; Methylation of 2-methylnaphthalene (2-MN)
- Mobil TransPlus process, mixed xylenes, 52
- Molecular orbital calculations
- comparison of calculated molecular dimensions by MM2 and MOPAC, 309t, 310
- insights using MOPAC, 320
- MOPAC package for naphthalene alkylation, 307
- See also* Naphthalene alkylation, computational analysis
- Molecular sieves
- advances in industrial applications, 48–56
- crystal structure, 40
- intersecting channels of different size openings, 40t, 41–42
- MCM-36 possessing zeolitic properties, 47
- mesoporous, 47
- modification methods, 47–48
- mono-functional catalytic cracking of gas oils, 42
- new useful, 40–47
- non-intersecting channel system, 41t, 42–45
- pore dimensions, 4t
- schematic of zeolite pore and Brønsted acid site, 5f
- separations, 12
- shape-selective catalysis, 4–5
- unusual two, non-intersecting pore system, 45–47

*See also* Zeolites

Molecular traffic control (MTC)

evidence for mechanism in cracking and aromatization reaction, 138–143

MTC in ZSM-5 channels, 139f

*See also* Cracking and aromatization reaction of *n*-heptane

Monodimensional molecular sieves. *See* Tunnel shape selectivity

Mordenites

characteristics, 42

chemical and physical steps of *n*-alkane hydroisomerization and hydrocracking, 347

coking and deactivation of, 348–350

dealumination enhancing selectivity to 2,6-diisopropylnaphthalene (2,6-DIPN), 315, 319

distribution of products of *n*-butane transformation, 346

*n*-heptane transformation, 348f

*n*-heptane transformation at 250°C, 348f

high selectivity, 335

testing mineral samples, 20

transformation of *n*-alkanes, 345–348

*See also* Biphenyl alkylation over H-mordenite; Biphenyl isopropylation over H-mordenite; 2,6-Diisopropylnaphthalene synthesis by alkylation

## N

Naphthalene

conversion over Pd/HM38 and Pd/HY catalysts, 385f

conversion over Pd/TiO<sub>2</sub> catalyst, 386f  
isopropylation with isopropanol at 250°C, 252t

products from added benzothiophene over zeolite-supported catalysts during hydrogenation, 387

shape-selective alkylation, 8

shape-selective alkylation over zeolites, 251–253

shape-selective hydrogenation, 255–256

*See also* 2,6-Diisopropylnaphthalene synthesis by alkylation

Naphthalene alkylation

dealuminated H-mordenite for formations of symmetric polynuclear aromatic hydrocarbons, 282–283

opportunity in shape-selective catalysis, 56

*See also* 2,6-Diisopropylnaphthalene synthesis by alkylation

Naphthalene alkylation, computational analysis

calculation method, 307

cationic intermediates by attack of isopropylation at 6-, 7-, and 3-positions of 2-isopropylnaphthalene (2-IPN), 316–317

cationic intermediates by attack of methylation at 6-, 7-, and 3-positions of 2-methylnaphthalene (2-MN), 318–319

comparison of calculated molecular dimensions by MM2 and MOPAC, 309t, 310

dealumination of mordenite enhancing 2,6-DIPN selectivity, 315

dealumination reducing acidity, 319

energy minimization profiles for 2-DIPN with conformations A and B, 307, 309f

frontier electron density, 314

frontier electron density at ring carbons in alkylnaphthalenes, 314t

frontier orbital analysis favoring 6-position in 2-IPN, 319

illustration of critical diameter, length, thickness, and cylinder diameter, 307, 310f

literature data for naphthalene isopropylation and methylation, 314, 315t

molecular dimensions, 307–314

molecular dimensions of naphthalene and alkylnaphthalenes, 308t

MOPAC calculations providing insight, 320

origin of shape selectivity to 2,6-dialkylnaphthalene (2,6-DAN), 314–319

pathways for •-alkylation (C-1) and •-

alkylation (C-2) of naphthalene, 306f

product or transition-state selectivity, 319

shape-selective •-alkylation and •-, •-dialkylation of naphthalene inside pore channel of molecular sieve catalysts, 306, 308f

steric structures including space-filling model of 2,6-DIPN and 2,7-DIPN in conformation A, 307, 311f

steric structures of 2,6-diethylnaphthalene (2,6-DEN) and 2,7-DEN in conformation A, 312f

steric structures of 2,6-dimethylnaphthalene (2,6-DMN) and 2,7-DMN, 312, 313f

Naphthalene isopropylation over solid acid catalysts

catalysis over amorphous silica-alumina, 302–303

H L-zeolite, 302

H-mordenite, 298–300

H Y-zeolite, 300–302

H ZSM-5, 302

catalyst preparation, 293

catalyst types, 296, 298

catalytic isopropylation of naphthalene with propene, 295t, 296t

characterization of catalysts, 293  
 classification of reaction types, 297*f*  
 effect of reaction temperature on composition of diisopropylnaphthalene (DIPN) over Y-zeolite, 301*f*  
 experimental, 293  
 isopropylation reaction, 293  
 pore sizes and proportions of surface areas derived from micropores, 300*t*  
 properties of catalysts, 294*t*  
 reaction paths to DIPN isomers, 295  
 specific surface area and acidity, 294  
 time course of DIPN groups, 298*f*, 299*f*  
 1-Naphthol, regio-selective hydrogenation, 256–257  
 Natural gas, aromatization under non-oxidative condition, 57  
 Nickel-incorporated silicoaluminophosphate catalysts. *See* Methanol-to-olefin conversion  
 Noble metal catalysts  
 active metal sites, 388  
 current status of application, 381–382  
 effect of metal type and zeolite on hydrogenation, 384  
 effect of zeolite structure and metal on sulfur resistance, 385  
 laboratory-prepared zeolite-supported catalysts containing 2 wt% metal, 384*t*  
 naphthalene conversion over Pd/HM38 and Pd/HY catalysts, 385*f*  
 naphthalene conversion over Pd/TiO<sub>2</sub> catalyst, 386*f*  
 products from added benzothiophene (BTP) over zeolite-supported catalysts during naphthalene hydrogenation, 387*t*  
 proposed new concept for sulfur-resistant design, 383–388  
 role of acidic zeolite supports, 384  
 shape-selective exclusion and hydrogen spillover, 386–387  
 simplified representation for proposed new catalyst design, 383*f*  
 SynSat process with hydrotreating reactor technology, 382*f*  
 two types of sulfur resistance, 386  
 Non-intersecting pore system molecular sieves  
 characteristics, 42–45  
 dehydrocyclization of *n*-hexane, 45  
 distribution of hexane isomers from *n*-pentane, 45*t*  
 examples, 41*t*  
 hydroisomerization of *n*-heptane, 42, 43*t*  
 ISODEWAXING process, 42  
 paraffin hydroisomerization, 42–45  
 pore mouth and key-lock catalysis, 43–44  
 selective skeletal butene isomerization, 44  
 unusual catalytic properties, 44–45

Non-intersecting pore system molecular sieves, unusual two  
 molecular sieve MCM-38, 47  
 potential MCM-22 applications, 47  
 schematic of MCM-22, 46*f*  
 selective production of *o*-diethyl benzene, 46–47  
 synthesis of MCM-22, 45–46  
 zeolite MCM-22, 45–47  
 zeolite MCM-49, 47  
 Norbornene, liquid phase oligomerization, 49  
 Nucleophilic aromatic substitution, organic synthesis over zeolites, 69

## O

Octahedral molecular sieves (OMS)  
 manganese based, 80–81  
 schematic, 82*f*  
 synthesis, 81, 83  
*See also* Oxidation of alkanes  
*sym*-Octahydrophenanthrene (*sym*-OHP)  
 ring-shift isomerization over zeolite catalysts, 250–251  
*n*-Octane  
 C<sub>8</sub> aromatic distribution for aromatic products from conversion with PtSi-2B, 155*t*  
 conversion with acidic and non-acidic Pt-Si catalysts, 147–148  
 conversion with Pt-silicalite catalysts, 149–150  
 feed rate, 154  
 selectivity for ethylbenzene and styrene with PtSi-2B catalyst, 151, 152*t*  
*See also* Alkane dehydrocyclization with Pt-silicalite catalysts  
 Offretite, non-shape-selective, 22  
 Olefin synthesis. *See* Methanol-to-olefin conversion  
 Organic catalysis over zeolites and molecular sieves  
 commercial applications utilizing shape selective zeolites, 67, 68*t*  
 complexity of reaction system, 66  
 exploration and scoping potentials, 68–69  
 interaction of reactant, catalyst, and system, 67*f*  
 isomorphous substitution and variety of compositions, 67–68  
 light paraffin aromatization activity of Pt/KBaL zeolite, 70  
 Meerwein–Ponndorf–Verley reduction, 69–70  
 mesoporous materials, 71  
 methanol-to-gasoline reaction, 71  
 nucleophilic aromatic substitution of chlorobenzene, 69

scope of recent activity, 69f  
 selective catalytic oxidations, 70  
 Organic chemicals  
 applications of shape-selective catalysis, 9–11  
 shape-selective processes for synthesis, 10r  
 Oxidation, controlled, potential for internal reactor heat production, 35  
 Oxidation of alkanes  
 activity and selectivity of manganese oxide materials, 91  
 catalytic reaction conditions, 83  
 cyclohexane oxidation, 88–89  
 cyclohexane with different catalysts, 83–84  
*cis*-decalin oxidation, 89–90  
 decalin with different catalysts, 84, 85t, 86  
 effects of TEMPO radicals, 91  
 four octahedral molecular sieves (OMS), 81, 82f  
 hexane oxidation, 89  
*n*-hexane with different catalysts, 84, 85t  
 initial disappearance rates of TBHP over different catalysts, 88t  
 product distribution with different catalysts, 86, 87t  
 radical (TEMPO) effects on cyclohexane oxidation, 87–88  
 radical trap (TEMPO) effect on cyclohexane oxidation using OMS-2, 88t  
 rates of organic substrates conversion and disappearance of TBHP, 90  
 relationships of rates and catalysts, 86–87  
 synthesis of catalysts, 81, 83  
 Oxidations, catalytic  
 organic synthesis over zeolites, 70  
 synthesis of organic chemicals, 10r  
 titanium silicate molecular sieve, TS-1, 73–74  
 Oxide-impregnated HZSM-5 catalysts. *See para*-Diethylbenzene synthesis (PDEB)  
 Oxide-supported HZSM-5 catalysts. *See* Methylation of toluene

## P

P<sub>2</sub>O<sub>5</sub> diphosphorus pentoxide. *See para*-Diethylbenzene synthesis (PDEB)  
 Palladium. *See* Noble metal catalysts  
 Paraffin aromatization activity, organic synthesis over zeolites, 70  
 Paraffin hydroisomerization, non-intersecting channel system molecular sieves, 42–45  
*n*-Paraffin selective acid catalyst  
 fluidity improvements for removal of *n*-paraffins from paraffinic oil, 24f  
 superactive natural zeolite, 22–23  
 Parallel reactions, selectivity type, 3  
 Para-selectivity

ethylation of ethylbenzene, 164, 165t  
*See also para*-Diethylbenzene synthesis (PDEB)

Para shape selectivity  
 adsorption property and external surface acidity correlation, 181–182  
 chemical vapor deposition (CVD) zeolite modification method, 181–182  
 control of pore-opening size, 183f  
 dependence of selectivity on conversion, 184  
 enhancing *p*-xylene formation by CVD with silicon alkoxides, 182–184  
 evaluating degree of control in pore-size opening, 182  
 extent of modification, 182  
 formation of para alkylaromatics, 181  
 inactivation of external surface acidity, 183f  
 plot of external surface acidity against external surface area, 186f  
 relationship between rate constant of *o*-xylene adsorption and crystal size, 185, 186f  
 selectivity on synthesized HZSM-5 versus rate constant for *o*-xylene adsorption, 187f  
 shape-selectivity on synthesized ZSM-5, 184–185  
 three-dimensional plot of selectivity against external surface acidity and pore-opening size, 184f  
 4-Penten-1-ol, cyclization, 75  
 4-Penten-2-ol, cyclization, 75, 76  
 Petroleum  
 boiling and approximate carbon number ranges of typical products, 28f  
 potential of dewaxing fractions, 25  
 upgrading higher boiling distillates, 25  
 Petroleum industry, capabilities and flexibility of new processes, 25  
 Pharmaceutical industry, future, 32  
 Phenol technology, advances in synthesis, 52–53  
 Phosphorus with HY zeolites  
 catalytic conversion of *o*-xylene and ethylbenzene, 240–241  
 composition of P-HY samples, 240t  
 experimental, 237  
 influence of acidity on ethylbenzene conversion, 244f  
 influence of acidity on *o*-xylene conversion, 242f  
 mechanism of ethylbenzene cracking, 244f  
 mechanism of P interaction with HY zeolite, 239f  
 mechanisms for catalytic conversion of *o*-xylene on B-site and L-site, 243f  
<sup>31</sup>P MAS-NMR spectra of HY samples, 238f  
 state of P and physicochemical properties of P-HY samples, 237–240

- surface area and acidity of P-HY samples, 240*t*
- transformation of ethylbenzene at 683 K, 244*t*
- transformation of *o*-xylene at 683 K, 241*t*
- use of P in fluid catalytic cracking (FCC) catalysts, 236–237
- Platinum. *See* Noble metal catalysts; Pt-porous heteropoly compounds
- Polycyclic aromatic hydrocarbons (PAH)
- selective formation with dealuminated H-mordenite, 282–283
- See also* 2,6-Diisopropyl-naphthalene synthesis by alkylation; Polycyclic hydrocarbon conversion over zeolites
- Polycyclic hydrocarbon conversion over zeolites
- conformational isomerization, 254–255
- conformational isomerization of *cis*-decalin at 200–250°C, 255*t*
- isopropylation of biphenyl with propylene at 250°C, 254*t*
- isopropylation of naphthalene with isopropanol at 250°C, 252*t*
- regio-selective hydrogenation, 256–257
- research on selective polycyclic aromatic hydrocarbons (PAH), 248–249
- ring-shift isomerization, 250–251
- ring-shift isomerization of *sym*-octahydrophenanthrene (*sym*-OHP) with mesitylene solvent, 251*t*
- selective hydrogenation of naphthalene in tridecane solvent, 256*t*
- selective synthesis of high-value chemicals, 249
- shape-selective alkylation of biphenyl, 253–254
- shape-selective alkylation of naphthalene, 251–253
- shape-selective hydrogenation of naphthalene, 255–256
- structures of some important aromatic polymers, 249*t*
- Polyester based industry, limited *p*-xylene resource, 25
- Polyester technology, isomerization of xylenes, 51–52
- Polyethylbiphenyls (PEBP). *See* Biphenyl alkylation over H-mordenite
- Pore mouth and key-lock catalysis, alkane isomerization to multibranched isomers, 43–44
- Pore-opening size
- controlling by depositing silica from various silicon compounds, 183*f*
- evaluating degree of control, 182
- three dimensional plot of selectivity against external surface acidity and, 184*f*
- Pore size distribution
- effect of coke, 140–143
- tungstophosphoric acid (PW) at various loading on supports, 357–358
- Pore tortuosity, micropores of MFI catalyst structure, 167–168
- Pore volume
- secondary porosity and crystallinity of USY zeolite, 327–329
- USY zeolites, 329*t*
- Product shape selectivity
- alkylation of naphthalene, 319
- catalyst or reaction modification, 226
- definition, 6
- ethylation of ethylbenzene, 163
- examples, 6–7
- reactions over microporous molecular sieves, 7
- -selective naphthalene alkylation reactions, 8
- toluene methylation reactions, 7*f*
- Pt-porous heteropoly compounds
- activity and selectivity for skeletal isomerization of *n*-butane, 375*t*
- adsorption by microbalance connected to ultrahigh vacuum system, 371
- adsorption of various molecules on Pt-promoted porous catalysts, 373*t*
- compound preparation method, 370
- correlation between selectivity to isobutane and pore size of catalysts, 376*f*
- dependencies of stationary conversion on catalyst weight/total flow rate (W/F), 373, 374*f*
- difference in selectivity between *n*-butane and *n*-pentane, 377–378
- effects of pore width of zeolites on selectivity, 377
- effects of Pt loading amount on selectivity, 375, 377*t*
- experimental, 370–371
- isotherm of N<sub>2</sub> adsorption and surface area of porous materials, 371
- lower selectivity to isobutane, 377
- mesopore size distributions for heteropoly compounds, 372*f*
- model for pores of heteropoly compounds, 378–379
- nitrogen adsorption-desorption isotherms, 370
- pore size distribution curves for heteropoly compounds by Dollimore–Heal method, 372*f*
- procedure for skeletal isomerization of *n*-butane, 370–371
- selectivity to isobutane as function of conversion, 373, 376*f*

time courses of *n*-butane isomerization, 373, 374f  
 Pt-silicalite catalysts. *See* Alkane dehydrocyclization with Pt-silicalite catalysts

## Q

Quinoline, regio-selective hydrogenation, 256–257

## R

Reactant shape selectivity  
 alcohol dehydration reaction, 6f  
 concept, 181  
 definition, 5  
 examples, 6  
 Reaction complex size  
 relative size of *n*-hexane versus 3-methylpentane complexes with propyl carbenium ion, 30f  
 science-technology symbiosis, 27, 29  
 Reagent bulkiness. *See* Biphenyl alkylation over H-mordenite  
 Red oils, methanol-to-hydrocarbon reactions, 108, 111  
 Regioselective cyclizations  
 3-buten-1-ol, 74, 76  
 characterization and synthesis of titanium silicate molecular sieves (TS-1), 74  
*cis*-4-hexen-1-ol, 75, 77  
 generation of titanium hydroperoxo species in TS-1/H<sub>2</sub>O<sub>2</sub> system, 77  
 5-hexen-1-ol, 75  
 mechanistic aspects, 78  
 oxidative cyclization in oxidation of linalool, 78  
 4-penten-1-ol, 75  
 4-penten-2-ol, 75, 76  
 proposed reaction scheme for *cis*-4-hexen-1-ol cyclization, 77  
 reaction sequences for 4-penten-2-ol at 298 K and 333 K, 76  
 unsaturated alcohols, 74–75  
 unsaturated alcohols and cyclized products, 76  
 Regio-selective hydrogenation, 1-naphthol and quinoline, 256–257  
 Restricted transition state selectivity, 67  
 depressing formation of *o*-diethylbenzene, 165  
 electronic, 8–9  
 ethylation of ethylbenzene, 163  
 Ring-shift isomerization, over zeolite catalysts, 250–251  
 Rocket fuel, synthesis, 49

## S

Science-technology symbiosis  
 internal events of acid catalytic surface, 29, 32  
 measurement of diffusivity, 27  
 relationship between Thiele modulus and effectiveness factor, 27, 28f  
 relative size of *n*-hexane versus 3-methylpentane complexes with propyl carbenium ion, 30f  
 shape selectivity and diffusion, 26–27  
 shape selectivity by clogging, 27, 28f  
 shape selectivity due to size of reaction complex, 27, 29  
 shapes after segment rotations and typical parameters of distance and time passage, 31f  
 window effect, 29  
 Secondary shape selectivity, 9  
 Selective skeletal butene isomerization, 44  
 Selectivity, types in heterogeneous catalysis, 3–4  
 Selectoforming  
 fluidity improvements for removal of *n*-paraffins from paraffinic oil, 24f  
 removing *n*-paraffins from gasoline, 22–23  
 selective conversion of straight chain hydrocarbons, 40  
 Separations, applications of shape-selective catalysis, 12  
 Serial reactions, selectivity type, 3–4  
 Shape-selective catalysis  
 advances in industrial applications, 48–56  
 analogy to emergency of transistors, 18, 35  
 applications, 9–12  
 chemicals synthesis, 9–11  
 definition, 4–5  
 emergency of new synthetic zeolites, 23  
 engineered shape selectivity in Pt-containing Na-mordenite, 21t  
 environmentally benign chemical processing, 1–2  
 extending concept of shape-selective paraffin conversion, 23  
 first commercial shape-selective process using natural zeolites, 22–23  
 fluidity improvements for removal of *n*-paraffins from paraffinic oil, 24f  
 future objectives, 32, 35  
 hydrocarbon processing, 11–12  
 identification of potentials for industry, 22  
 new opportunities, 56–58  
 path toward technology, 20, 22  
 personal experience, 19–20  
 principles, 2–5, 334–335  
 representative molecular sieves, 4t

- rise of new technologies, 23, 25–26  
 schematic of zeolite pore and Brønsted acid site, 5*f*  
 science-technology symbiosis, 26–32  
 separations, 12  
 shape-selective conversions over Pt incorporated Ca-A zeolite, 21*t*  
 shape selective paraffins cracking over Ca-A zeolite, 21*t*  
 thermodynamics and kinetics, 2–4  
 use of molecular sieves, 4–5  
*See also* Tunnel shape selectivity; Zeolites
- Shape selectivity  
 bulky products, 9  
 catalytic behavior of zeolites, 225–226  
 clogging, 27, 28*f*  
 effect of coke formation, 135–137  
 effect of extra framework alumina, 134–135  
 effect of foreign materials, 132–133  
 effect of reaction severity on coke amount and enhanced *p*-selectivity, 136*t*  
 inverse, 9  
 product, 6–7, 131  
 reactant, 5–6  
 science-technology symbiosis, 26–27  
 secondary, 9  
 transition-state, 7–9  
 tunnel, 335–336  
 types, 5–9  
 types influencing para selectivity, 131  
*See also* Cracking and aromatization reaction of *n*-heptane; Para shape selectivity; Tunnel shape selectivity
- Shell middle distillate hydrogenation process, 382
- Silicalite catalysts. *See* Alkane dehydrocyclization with Pt-silicalite catalysts
- Silicoaluminophosphate catalysts  
 highly selective nickel-incorporated Ni-APSO-34 in methanol to C<sub>2</sub>, 120–125  
 methanol-to-olefin studies using SAPOs and MeAPOs catalysts, 118–120  
*See also* Methanol-to-olefin conversion
- Silylated ZSM-5 zeolite  
 alkylation of xylenes with methanol, 230–231  
 amount of silica and equilibrium sorption uptake of silylated catalysts, 227*t*  
 catalytic evaluations method, 227–228  
 chemical vapor deposition (CVD) of silicon alkoxides, 226–227  
 ethylbenzene disproportionation, 232  
 experimental, 226–228  
 Fourier transform infrared (FT-IR), 228  
 isomerization of *m*-xylene, 233–234  
 magic angle spinning nuclear magnetic resonance (MAS-NMR), 228  
 methylation of xylene, 231*t*  
 progressive silylation, 230  
 sample characterizations, 228–230  
 scanning electron micrographs (SEM), 228  
 temperature programmed desorption (TPD), 228  
 X-ray diffraction (XRD) technique and profiles, 228, 229*f*  
 X-ray photoelectron spectroscopy (XPS), 228
- Simultaneous reactions, selectivity type, 3
- Solid acid catalysts. *See* Naphthalene isopropylation over solid acid catalysts; Tungstophosphoric acid (PW) on mesoporous silica
- Spatioselectivity, 67
- Steaming treatment  
 combined modifications for HZ catalyst series, 215–218  
 decreasing catalyst's acid content and strength, 206  
 diffusivity data of catalysts with and without steaming, 207*t*  
 effect on reaction performance of HZSM-5, 206*f*  
 high temperature steaming, 205–207  
 NH<sub>3</sub> TPD profiles of H-type and steamed HZSM-5, 207*f*
- Styrene  
 alkylation of 4-*t*-butylphenol (TBP) using tungstophosphoric acid (PW) supported on silica, 366–367  
 dimerization, organic synthesis over zeolites, 69  
 oxidative dehydrogenation of ethylbenzene, 50–51
- Sulfur-resistance  
 effect of zeolite structure and metal, 385  
 types, 386  
*See also* Noble metal catalysts
- Superacid catalysts, solid tungstophosphoric acid (PW) promising, 354, 356  
*See also* Tungstophosphoric acid on mesoporous silica
- Superactive catalysts  
 erionite, 22–23  
 mordenite and gmelinite, 20
- Supercages, zeolite MCM-22, 46
- SynSat process, deep desulfurization and deep hydrogenation, 382
- T**
- Technology  
 resistance by specifications, 25–26  
 rise of novel, 23, 25–26  
 Technology Vision 2020, 1

- Temperature-programmed desorption of ammonia (NH<sub>3</sub> TPD)
- acid properties of catalysts, 164
- methylation of toluene, 190, 197
- NH<sub>3</sub> TPD profiles of H-type and steamed HZSM-5, 207*f*
- NH<sub>3</sub> TPD profiles of P<sub>2</sub>O<sub>5</sub>-impregnated pre-modified HZSM-5 (DGA) series, 211*f*
- results of MgO/HZSM-5 and Sb<sub>2</sub>O<sub>3</sub>/HZSM-5, 199*f*
- silylated ZSM-5 zeolites, 228
- spectra of B<sub>2</sub>O<sub>3</sub>/HZSM-5 samples and HZSM-5, 198*f*
- spectra of H-mordenite (HM) and tributylphosphite (TBP) modified HM, 288, 289*f*
- Terephthalic acid, oxidation of *p*-xylene, 41
- p*-Terphenyl (TP)
- selectivity in alkylation, 267, 268*f*
- See also* Biphenyl alkylation over H-mordenite
- 1,2,4,5-Tetramethylbenzene, zeolite shape-selectivity, 97–98
- Thermodynamics, shape-selective catalysis, 2–4
- Thermoplastic polyesters. *See* Polycyclic hydrocarbon conversion over zeolites
- Thermoplastic polymers, structures, 249*t*
- Thermotropic polyester liquid crystalline polymers (LCPs)
- structures, 249*t*
- See also* Polycyclic hydrocarbon conversion over zeolites
- Thiele modulus
- reaction complex size, 27, 29
- relationship to effectiveness factor, 30*f*
- Threshold effect, methylation of toluene, 197
- Titanium silicate molecular sieve (TS-1)
- cyclization of unsaturated alcohols, 74–75
- generation of titanium hydroperoxo species in TS-1/H<sub>2</sub>O<sub>2</sub> system, 77
- mechanistic aspects, 78
- selective oxidation catalyst, 73–74
- synthesis and characterization, 74
- titanium hydroperoxo species in aqueous H<sub>2</sub>O<sub>2</sub>, 74, 79
- See also* Regioselective cyclizations
- Toluene ethylation, para selectivities, 132
- Toluene methylation. *See* Methylation of toluene
- Toluene methylation reactions, product shape selectivity, 6–7
- Transalkylation
- synthesis of organic chemicals, 10*t*
- p*-xylene production, 25
- Transalkylation of dialkylbenzenes, transition-state shape selectivity, 8
- Transition-state selectivity
- acid-catalyzed disproportionation (transalkylation) of dialkylbenzenes, 8
- alkylation of naphthalene, 319
- restricted electronic, 8–9
- -selective naphthalene alkylation reactions, 8
- steric restrictions of pore geometry, 7
- m*-xylene disproportionation reactions, 7*f*
- Transmethylation, *m*-xylene disproportionation, 7
- Transportation, hydrogen fuel cells, 57–58
- Tributylphosphite (TBP) modified H-mordenite catalyst treatment, 283
- catalytic performances, 286, 288–290
- effect of TBP treatment on catalytic activity of HM for cracking cumene and 1,3,5-triisopropylbenzene, 288, 289*f*
- effect of TBP treatment on HM catalytic performance, 287*t*
- effect of TBP treatment on HM catalytic properties for alkylation of 2-isopropyl-naphthalene (2-IPN), 288, 290
- NH<sub>3</sub> TPD spectra of TBP-HM, 288, 289*f*
- See also* 2,6-Diisopropyl-naphthalene synthesis by alkylation
- 1,3,5-Triisopropylbenzene, effect of tributylphosphite treatment on H-mordenite, 288, 289*f*
- Tungstophosphoric acid (PW) on mesoporous silica
- alkylation of 4-*t*-butylphenol (TBP) by styrene, 365*f*, 366–367
- catalytic testing, 366–367
- characterization of PW catalysts, 357–366
- characterization techniques, 356–357
- dispersion of PW on mesoporous silica, 355*f*
- effect of thermal treatment on stability by TGA and DTA techniques, 363
- factors affecting Keggin structure of PW, 361
- in situ X-ray diffraction (XRD) patterns for bulk PW and 50wt% PW on silica, 364*f*
- Keggin structure of PW cluster, 355*f*
- leaching of PW from silica supported PW catalysts, 363, 366
- leaching of PW supported on various silica by water at 50°C, 365*f*
- <sup>31</sup>P MAS NMR spectra assessing phosphorus environment, 362*f*
- properties and supporting PW, 354, 356
- PW promising for solid superacid catalysts, 354
- reaction procedure for catalytic testing, 357
- sample preparation, 356
- selectivities of 90% conversion of TBP, 366*t*
- surface area and pore characteristics of supports and catalysts, 358*t*



surface area of supported PW catalysts as function of PW loading, 358, 359f

TEM micrograph of hexagonal honeycomb structure of mesoporous silica, 355f

thermal stability of PW and supported PW catalysts using in situ XRD, 361, 363

well dispersed solid acid catalyst, 355f

XRD patterns of bulk PW and 50wt% PW supported on amorphous and mesoporous silica, 358, 360f

**Tunnel shape selectivity**

bimolecular mechanism explaining xylene isomerization, 337–338

bimolecular transformation of *m*-xylene in section of channel of mesoporous MCM-41 aluminosilicate, 344f

chemical and physical steps of *n*-alkane hydroisomerization and hydrocracking, 347

coking and deactivation of mordenite catalysts, 348–350

concentrations of Brønsted and Lewis acid sites by pyridine adsorption followed by FTIR, 342t

concentrations of Brønsted and Lewis sites of MCM-41(10), 341f

demonstration of bimolecular mode of xylene isomerization, 336–341

distribution of products of *n*-butane transformation, 346f

effect of methylcyclohexane (MCH) addition to *m*-xylene on isomerization and disproportionation rates, 339f

effect of MCH addition to *m*-xylene on rates of isomerization and disproportionation, 342f

initial activities and deactivation coefficients for cracking and coke formation, 349t

isomerization of *m*-xylene over various acid molecular sieves and amorphous silica alumina (SA), 337f

isotherms of nitrogen adsorption at 77 K for HMCM-41(30), HMCM-41(100), and SA, 343f

monodimensional zeolite and mesoporous materials, 335–336

*m*-xylene transformation over amorphous SA, 342f

*m*-xylene transformation over HMCM-41(30), 339, 339f

*n*-heptane transformation, 347–348

number of transalkylation steps in bimolecular isomerization of *m*-xylene, 340f

origin of particular behavior of MCM-41, 341–345

reaction scheme, bimolecular isomerization of xylene, 339f

relation to length of non-interconnected channels, 350

selectivity of xylene isomerization over HMCM-41 samples, 338, 340

TEM micrographs of HMCM-41(10), (30), and (100) samples, 345f

transformation of *n*-alkanes over mordenite catalysts, 345–348

transformation of xylenes over MCM-41 samples, 336–345

## U

USY zeolites. *See* Hydrothermal dealumination

## V

Vapor phase process, styrene technology, 50–51

## W

**Window effect**

alkane isomerization to multibranched isomers, 43–44

science-technology symbiosis, 29

shapes after segment rotations and typical parameters of distance and time passage, 31f

## X

**X-ray diffraction (XRD)**

bulk tungstophosphoric acid (PW) and 50wt% PW supported on amorphous and mesoporous silica, 358, 360f

crystallinity changes of USY zeolites during hydrothermal treatment, 324–325

profiles of silylated ZSM-5 zeolites, 228, 229f

Pt-silicalite catalyst analysis, 148

in situ XRD patterns of bulk PW and 50 wt% PW on mesoporous silica, 364f

thermal stability of PW and PW-supported catalysts by in situ XRD, 361, 363

XRD of silicalite, PtSi-2-A and PtSi-2-B, 153f

*See also* Alkane dehydrocyclization with Pt-silicalite catalysts

***m*-Xylene**

disproportionation, transition-state selectivity, 7

isomerization with silylated zeolites, 233–234

*See also* Tunnel shape selectivity; Xylenes

*o*-Xylene

- catalytic conversion over P-HY zeolites, 240–241
- influence of acidity on conversion, 242*f*
- mechanisms for catalytic conversion on B-site and L-site, 243*f*
- transformation over P-HY zeolites at 683 K, 241*t*

*p*-Xylene

- isomerization of *m*-xylene, 233–234
- novel process for *para*-substituted aromatics, 25
- shape-selective catalytic alkylation of toluene, 188–189

*See also* Methylation of toluene

## Xylenes

- alkylation with methanol over silylated zeolites, 230–231
  - bimolecular isomerization of *m*-xylene, 339*f*
  - bimolecular transformation of *m*-xylene in section of channel of mesoporous MCM-41 aluminosilicates, 344*f*
  - demonstration of bimolecular mode of isomerization, 336–341
  - methylation, 231*t*
  - number of alkylation steps for bimolecular isomerization of *m*-xylene, 340*f*
  - product shape selectivity, 7
  - transformation of *m*-xylene over amorphous silica alumina, 342*f*
  - transformation of *m*-xylene over HMCM-41(30), 339*f*
  - transformation over MCM-41 samples, 336–345
- See also* Tunnel shape selectivity

**Z**

Zeolite Beta (BEA), selective conversion of paraffinic fraction, 41–42

## Zeolites

- analogy to emergency of transistors, 18, 35
  - -caprolactam technology, 53–56
- clinoptilolite, 22
- dependence of concentration of aluminum types on steaming severity of ZSM-5, 133*t*
- effect of amorphous materials, 137–138
- effect of coke on pore diameter, 143*f*

effect of coke on pore size distribution, 140–142

- emergency of new synthetic, 23
  - engineered shape selectivity in Pt-containing Na-mordenite, 21*t*
  - erionite, 22–23
  - exploration of non-acidic catalysis, 20
  - extending concept of shape-selective paraffin conversion, 23
  - first commercial shape-selective process using natural, 22–23
  - hydrocarbon processing, 11–12
  - influence of pore geometry on methanol-to-gasoline aromatics distribution, 99*f*
  - isopropylation of naphthalene over H ZSM-5, 302
  - MCM-22 synthesis, 45–46
  - MCM-49 synthesis, 47
  - monodimensional, 335–336
  - mordenite, 20
  - naphthalene alkylation reactions, 8
  - phenol production, 52–53
  - representative molecular sieves, 4*t*
  - schematic of MCM-22, 46*f*
  - schematic of pore and Brønsted acid site, 5*f*
  - selective dehydration of alcohols, 6
  - selective production of *o*-diethyl benzene, 46
  - selectoforcing, 22–23
  - shape-selective catalysis, 4–5
  - shape-selective conversions over Pt incorporated Ca-A zeolite, 21*t*
  - shape-selective paraffins cracking over Ca-A zeolite, 21*t*
  - shape selectivity determination, 162
  - shape-selectivity in MTG process, 97–98
  - sizes, 225–226
  - styrene technology, 50–51
  - synthesis of ZSM-5 without aid of organic template, 133
  - synthetic 4A and 5A, 19
  - technology emergence, 18, 35
  - testing mineral samples, 20
  - toluene methylation reactions, 7
  - window effect, 29
- See also* Cracking and aromatization reaction of *n*-heptane; *para*-Diethylbenzene synthesis (PDEB); Methanol-to-olefin conversion; Molecular sieves; Phosphorus with HY zeolites; Silylated ZSM-5 zeolite